CANADIAN THESES ON MICROFICHE

I.S.B.N.

THESES CANADIENNES SUR MICROFICHE

National Library of Canada
Collections Development Branch

Canadian Theses on
Microfiche Service

Ottawa, Canada
K1A 0N4

Bibliothèque nationale du Canada
Direction du développement des collections

Service des thèses canadiennes
sur microfiche

NOTICE

The quality of this microfiche is heavily dependent upon the quality of the original thesis submitted for microfilming. Every effort has been made to ensure the highest quality of reproduction possible.

If pages are missing, contact the university which granted the degree.

Some pages may have indistinct print especially if the original pages were typed with a poor typewriter ribbon or if the university sent us a poor photocopy.

Previously copyrighted materials (journal articles, published tests, etc.) are not filmed.

AVIS

La qualité de cette microfiche dépend grandement de la qualité de la thèse soumise au microfilmage. Nous avons tout fait pour assurer une qualité supérieure de reproduction.

S'il manque des pages, veuillez communiquer avec l'université qui a conféré le grade.

La qualité d'impression de certaines pages peut laisser à désirer, surtout si les pages originales ont été dactylographiées à l'aide d'un ruban usé ou si l'université nous a fait parvenir une photocopie de mauvaise qualité.

Les documents qui font déjà l'objet d'un droit d'auteur (articles de revue, examens publiés, etc.) ne sont pas microfilmés.

THIS DISSERTATION
HAS BEEN MICROFILMED
EXACTLY AS RECEIVED

LA THÈSE A ÉTÉ
MICROFILMÉE TELLE QUE
NOUS L'AVONS REÇUE

NL-339 (r. 82/08)

Canada

0-315-06011-5

National Library of Canada
Canadian Theses Division
Ottawa, Canada
K1A 0N4

Bibliothèque nationale du Canada
Division des thèses canadiennes

53932

PERMISSION TO MICROFILM — AUTORISATION DE MICROFILMER

• Please print or type — Écrire en lettres moulées ou dactylographier

Full Name of Author — Nom complet de l'auteur

TARK SCOTT HAMILTON

Date of Birth — Date de naissance
SEPT. 25 1981

Country of Birth — Lieu de naissance
U.S.A.

Permanent Address — Résidence fixe
5311 - 39 A AVE
EDMONTON ALBERTA

Title of Thesis — Titre de la thèse
Late Cenozoic Alkalic Volcanics of the Level Mountain Range, Northwestern British Columbia: Geology, Petrology and Paleomagnetism

University — Université
University of Alberta

Degree for which thesis was presented — Grade pour lequel cette thèse fut présentée
Doctor of Philosophy

Year this degree conferred — Année d'obtention de ce grade
1981

Name of Supervisor — Nom du directeur de thèse
DR. C. M. SCARFE

Permission is hereby granted to the NATIONAL LIBRARY OF CANADA to microfilm this thesis and to lend or sell copies of the film.

The author reserves other publication rights, and neither the thesis nor extensive extracts from it may be printed or otherwise reproduced without the author's written permission.

L'autorisation est, par la présente, accordée à la BIBLIOTHÈQUE NATIONALE DU CANADA de microfilmer cette thèse et de prêter ou de vendre des exemplaires du film.

L'auteur se réserve les autres droits de publication; ni la thèse ni de longs extraits de celle-ci ne doivent être imprimés ou autrement reproduits sans l'autorisation écrite de l'auteur.

Date
16 October 1981

Signature
Tark Scott Hamilton

NL-91 (4/77)

THE UNIVERSITY OF ALBERTA

LATE CENOZOIC ALKALINE VOLCANICS OF THE LEVEL MOUNTAIN RANGE, NORTHWESTERN BRITISH COLUMBIA: GEOLOGY, PETROLOGY AND PALEOMAGNETISM

(C) by

TARK SCOTT HAMILTON

A THESIS

SUBMITTED TO THE FACULTY OF GRADUATE STUDIES AND RESEARCH IN PARTIAL FULFILMENT OF THE REQUIREMENTS FOR THE DEGREE OF DOCTOR OF PHILOSOPHY

GEOLOGY

EDMONTON, ALBERTA

FALL 1981

THE UNIVERSITY OF ALBERTA

RELEASE FORM

NAME OF AUTHOR TARK SCOTT HAMILTON

TITLE OF THESIS LATE CENOZOIC ALKALINE VOLCANICS OF THE LEVEL MOUNTAIN RANGE, NORTHWESTERN BRITISH COLUMBIA: GEOLOGY, PETROLOGY AND PALEOMAGNETISM

DEGREE FOR WHICH THESIS WAS PRESENTED DOCTOR OF PHILOSOPHY

YEAR THIS DEGREE GRANTED FALL 1981

(SIGNED) Tark Scott Hamilton

PERMANENT ADDRESS:
5311 - 39A Ave.
EDMONTON, ALBERTA
T6L 2E3

DATED 16 October 1981

THE UNIVERSITY OF ALBERTA

FACULTY OF GRADUATE STUDIES AND RESEARCH

The undersigned certify that they have read, and recommend to the Faculty of Graduate Studies and Research, for acceptance, a thesis entitled LATE CENOZOIC ALKALINE VOLCANICS OF THE LEVEL MOUNTAIN RANGE, NORTHWESTERN BRITISH COLUMBIA: GEOLOGY, PETROLOGY AND PALEOMAGNETISM submitted by TARK SCOTT HAMILTON in partial fulfilment of the requirements for the degree of DOCTOR OF PHILOSOPHY.

.....

Supervisor

.....

.....

.....

.....

External Examiner

Date 16 October 1981

ABSTRACT

Level Mountain is a Late Cenozoic shield volcano located near 131°20'W,58°31'N in the Stikine Volcanic Belt of northern British Columbia. The volcanic plateau with an average elevation of 4500',(1372m), is younger than Upper Miocene in age and is comprised of up to four sequences of alkali basalt and ankaramite flows and tuffs. The central region of peaks and ridges rises to a maximum elevation of 7200',(2195m), and has a repetitive bimodal distribution of alkali basalt and peralkaline salic lavas and tuffs that spans the period from 4.5 million years b.p. to recent times. Feeble basaltic vents with spatter, bombs and scoria apparently postdate continental glaciation. A paleomagnetic study on two stratigraphic sections that span the entire range of volcanism samples the earth's major polarity reversals for the past 6 MY.

Petrochemically the lavas belong to the sodic alkali basalt series and are of continental affinity. Oxygen isotope values near 5.6°/$_{oo}$ $\delta^{18}O$ SMOW have been measured for unaltered rocks including basalts, salics, and ultramafic inclusions. This would seem to indicate that the mantle under northwestern British Columbia is normal with respect to oxygen and that the Level Mountain magmas are mantle derived. Corroborating evidence is available from the whole rock strontium isotope studies which show a total range of $^{87}Sr/^{86}Sr$ from .7025 to .7071. The presence of basic and

salic, undersaturated and ovesaturated, peralkaline and metaluminous rocks attests to the complexity of petrogenetic processes at Level Mountain. Although the two volumetrically important lava types appear to be primary and mantle derived, the presence of some rhyolites enriched in ^{18}O, granitic gneiss inclusions in basalts and tristanites and great variation in whole rock lead isotope ratios are probably all indicative of some degree of interaction between magmas and crustal rocks. Major and trace element geochemical variations and mineralogy indicate an upper mantle origin at shallower than 15 kbar pressure from an undersaturated ultramafic source that possessed an abundance of alkalis and incompatible elements. The mineralogy and chemistry of the major rock types indicate conditions of low oxygen fugacity and a dry gas phase composition for both peralkaline flows and basalts. The field relations of some comendite flows implies fluid behavior and seems to indicate a viscosity two to three orders of magnitude lower than would be predicted on the basis of silica content and whole rock chemistry. This could be partially reconciled if the gas phase had been halogen rich and dry.

Calculations of the volume and energetics of the volcanism of the Stikine Belt indicate that less than 15% of the modern heat flow is necessary to maintain the levels of volcanicity since Pliocene times.

ACKNOWLEDGEMENTS

This study was conceived with the help of Dr. J.G. Souther of the Geological Survey of Canada and Dr. C.M. Scarfe of the Department of Geology, The University of Alberta. Various aspects of the research led to collaboration with or guidance from several faculty members and graduate students including: Dr. K. Muehlenbachs for the Oxygen isotope study, Dr. H. Baadsgaard for Rb/Sr,Sr, and Pb isotope work, Dr. D.G.W. Smith on aspects of the mineralogy and microprobe work, Dr. M.E. Evans of the Department of Physics for help with the paleomagnetic study, and Dr. J.W. Nicholls of the University of Calgary for the use of his computer program ROCK and many enlightening discussions. Special help in the form of advice, techniques, and computations was obtained from: Dr. K. Schimann for the preparation and analysis of whole rock glasses, Dr. G. Hoye for help with the spinner magnetometers and the induction study, and Dr. C.M. Gold for help with data reduction of EDA microprobe results. Invaluable help with and training in various laboratory methods was unselfishly given by Alec Stelmach, Elizabeth Toth, Steve Launspach and Dave Tomlinson. As the research progressed and ideas began to unfold, discussions with fellow graduate students proved very rewarding including those with Drs. Karl and Monique Schimann, Dr. Brett Beddoe-Stevens, Steve Goff, John Casey, and Graham Nixon. Field assistance during the three

expeditions to Level Mountain was performed by Hans Rex, Doug Hamilton, Don Emerson, Gerry Hoye and Ken Ragan. A greatly expanded understanding of the general geology of the Dease Lake area came from discussions with Dr. H. Gabrielse of the G.S.C.and shared field experience with three exploration geologists: George Sievertz, Barry Price and Tony Mould. My sister, Margaret Hamilton contributed six weeks of her energies to help with the data organization and computing. Special thanks go to my wife Coreen for her typing of the first draft and continual forebearance. My thanks goes to all of these people for sharing in this research effort. Particular thanks are due to Dr. C.M. Scarfe for his guidance in all aspects of this project.

Logistical support and field equipment were provided by the Departments of Geology, Physics, Zoology, and the Boreal Institute for Northern Studies of the University of Alberta, Mattagami Lake Mines, and the Geological Survey of Canada. Financial assistance was provided by grants from The Boreal Institute for Northern Studies, D.E.M.R. research agreements 1135-D13-4-138176,2239-4-51/77,80-4-78 to Dr. Scarfe, N.R.C. grant # A8394 to Dr. Scarfe and by graduate assistantships and bursaries from the Department of Geology. The support of these institutions is greatfully acknowledged. My special thanks goes to Carl Simmons of Yukon Air Ltd. for his dependable field support and hospitality at Dease Lake.

Table of Contents

List of Tables

List of Figures

List of Plates

List of Maps

CHAPTER 1. INTRODUCTION

LEVEL MOUNTAIN VOLCANIC CENTRE

Level Mountain is a major, alkaline and peralkaline continental shield volcano in the Intermontane Belt of British Columbia (Souther, 1977a). The description and study of the Late Cenozoic volcanics is of considerable importance to the further understanding of regional tectonics and volcanism in Western Canada. Investigations into the tectonics of this region have been published by Souther (1970, 1977b), Monger and Souther (1972), Gabrielse and Souther (1962), White (1959), and St. Armand (1957). Contemporary and recent studies on the volcanism of the Intermontane Belt include the work of Casey (1980), Bevier (1977, 1978), Fiesinger and Nicholls (1977), and Souther (op. cit.).

The petrogenesis of alkaline volcanoes of bimodal character has been an open question and a topic for investigation by petrologists for many years, e.g. Daly (1933), Bowen (1938), Shand (1927), Chayes (1963, 1964), Gass and Mallick (1968), Gibson (1974), Bryan (1964, 1966, 1976), and Clague (1978). The controversy over the origin of peralkaline rocks is a long standing one whose beginnings stem from investigations of the volcanics of the Isle of Pantelleria Washington (1913, 1914). The conditions for the appearance of peralkaline ferromagnesian minerals have been studied experimentally by Ernst (1962), Marsh (1975), and

Edgar and Parker (1974) with many questions still left to be answered. The mineralogy and petrochemistry of natural and synthetic peralkaline systems has been treated by Nicholls and Carmichael (1969), Bailey (1974) and Bailey and MacDonald (1970, 1975).

OBJECTIVES

The present study was begun in the Fall of 1974. The intent of the study was to geologically map and sample the Level Mountain Volcanics and to relate them through petrological and geochemical studies to Mount Edziza and Late Cenozoic volcanism of the Stikine Volcanic Belt as a whole. In addition to the original aspects of the study, which included mapping, petrography, petrochemistry, and mineralogy, the problem of accurately defining the age and span of volcanism led to a paleomagnetic study and to attempts at radiometric dating. The questions on petrogenesis led to the acquisition of trace element and rare earth data in addition to analyses for oxygen, strontium and lead isotopes. Other questions regarding the petrogenesis of the peralkaline salic lavas prompted a series of one-atmosphere melting and crystallization experiments on natural compositions under conditions of controlled oxygen fugacity. Finally, attempts to relate the volcanism at Level Mountain to the regional picture of Late Cenozoic volcanism in Western Canada led to: a review of the existing literature on the geophysics and tectonics of the

Intermontane Belt, field trips to other areas of the Intermontane, and some physical calculations regarding the nature of the volcanism.

LOCATION, ACCESS, PHYSIOGRAPHY, AND CLIMATE

The Level Mountain Range, centered near 131°20'W-58°31'N, is the prominent physiographic feature of the Nahlin Plateau which is located in the Cassiar land district of northwestern British Columbia. The division between the Cassiar and Atlin mining districts crosses the plateau. The nearest road approach is to Telegraph Creek from the Stewart Cassiar Highway. Access to the area is best provided by helicopter from Dease Lake, 45 miles, (72 km), to the East.

The plateau is bounded by steep cliffs of columnar jointed basalt flows on the southern, western, and northeastern sides. The slopes to the northwest and southeast fall away more gently due to the influence of continental glaciation. The drainage from Level Mountain has a basically radial pattern, following the U-shaped glacial valleys that dissect the central region. The principal drainages are: Beatty Creek, Little Tahltan River, Egnell Creek, Dudidontu River, Kakuchuya Creek, Matsatu Creek, Megatushon Creek, Little Tuya River and Mansfield Creek. The southern and eastern watershed is part of the Stikine drainage system. The northern and western watershed is to the Nahlin River and the southwestern watershed is to the

Sheslay River.

The climate of the region is rather severe due to the elevation and almost constant winds of greater then 15mph (24kph). Precipitation in the general area, (Atlin, Telegraph Creek, Dease Lake), is 10-15 in. (25-38 cm) per year. Summer weather is usally brisk, less than 13°C, and partly cloudy to overcast. Breakup does not usually happen until June, and during this time the plateau becomes a mess of deranged drainage, bogs and fens for up to 3 weeks. Snow fields usually remain throughout the summer on north facing slopes and may not ablate or melt for several years. The rather severe conditions on the plateau are conducive to the formation of desert varnish, which is seen on most outcrops and joint faces. The general geomorphology of the plateau is characteristic of low precipitation subalpine areas. Soils on Level Mountain are thin and generally show poor development and limited lateral extent. The two dominant types are acid well drained regosols on the steep slopes and brunisolic grey luvisols on the plateau surface and in alpine valley bottoms. Cryoturbation generally obscures any horizon development (Fengor, 1981)

Tertiary Geomorphology

The Tertiary Geomorphology of the Stikine region was characterized by mature drainage systems and gentle topography with a maximum of 1000m of relief; more typical variation was on the order of 150m. Most of the major lowland valleys such as the Tahltan River and the Dudidontu

River are either exumed or resequent valleys. This is in marked contrast to the young consequent streams of the lava plateau. The major river systems of the area such as the Nahlin-Inklin, the Shesley and the Stikine are resequent but rejuvenated by Late Tertiary uplift of the entire region. Investigations by Johnson (1926) and Kerr (1936) indicate a net uplift on the order of 1000m since Mid-Tertiary time. Even more extensive uplift has been reported for the adjacent coast range region (Parrish, 1981). This uplift has not only affected the drainage and geomorphology but is probably also related to the major tectonic processes responsible for the widespread alkaline volcanism and normal faulting of Late Tertiary times. There is a contrast in the geomorphology of the Intermontane Belt from north to south that could be explained by different rates of uplift. In the Stikine region the Intermontane Plateau has been incised by youthful rivers. Tertiary valleys that had recently held Pleistocene glacial deposits have been exumed. In contrast to this, the Tertiary topography of the Cariboo region is still buried beneath glacial deposits and youthful lava plateaux. This is evident near Anahim Lake (Tipper 1969). In the Cariboo, the headward erosion of major rivers has not yet crossed the western boundary of the Intermontane Belt. The geomorphology of the southern Intermontane Belt has been more strongly influenced by the paths of Quaternary glaciation and subsequent streams than any of the area to the north or west (Fulton, 1975).

PREVIOUS WORK

There are few previous geological investigations in the Level Mountain Range. Single traverses over or around the plateau margin were made by Cockfield (1925) and Mathews (Watson and Mathews 1944). During "Project Stikine" and the preliminary mapping of the Dease Lake Sheet (Gabrielse and Souther, 1962) a long traverse was made by Root and Ostensoe in the summer of 1958 (Ostensoe, 1960). In these early investigations of the Level Mountain Volcanics, field names for rock types include basalts as well as andesite, rhyolite, and quartz latite giving a misleading impression toward calc-alkaline character. Ostensoe (1960) was the first to penetrate the central region, collect rock samples and perform petrographic analyses. His preliminary findings, including the report of titaniferous augite in the basalts and aenigmatite from a comendite demonstrate the alkaline nature of the Level Mountain Lavas.

Souther, of the Geological Survey of Canada, has done considerable regional mapping of the Late Tertiary and Quaternary volcanics of the Intermontane Belt. His studies have been highlighted by the work on Mount Edziza, the other major centre of the Stikine Volcanic Belt (Souther, 1966). His studies include detailed petrological (Souther, 1974), mineralogical (Yagi and Souther, 1974), and paleomagnetic work (Souther and Symons, 1974). His pioneering investigations into the volcanism and tectonics (Souther, 1977a, 1977b) have revealed the presence of peralkaline

lavas and the possibility that the Northern Stikine Volcanic Belt may represent a situation of incipient continental rifting (Souther, 1977b).

The type locality of the Level Mountain formation (Souther, 1971) is a continental shield volcano of uppermost Tertiary and Quaternary age centered near 131°20'W, 58°31'N. Alkalic lavas outcrop over an area of about 700 square miles (1812 square kilometers) in the form of a basaltic plateau with average elevation of 4500 feet (1372m). Capping the plateau is a geologically complex central region of glacially dissected ridges and vents with elevations to 7200 feet (2195m). The distal portions of the shield consist of flat lying flows, with primary dips less than 2°, of alkali basalt, ankaramite and tuffs. Four mappable stratigraphic units have been recognized on the plateau (Hamilton and Scarfe, 1977). The central region with its dissected stratocone and domes has a bimodal distribution, with peralkaline trachytes and comendites predominating over basalts.

Chapter 2. REGIONAL SETTING

HISTORICAL GEOLOGY OF THE INTERMONTANE BELT

Reviews of the historical geology of the Cordillera have been given by White (1959) and Monger et al (1972). The focus of those studies was the geological evolution of British Columbia since Paleozoic time. Souther (1970) divided B.C. into five major northwest trending geological evolutionary belts. From west to east these are: The Insular Belt, The Coast Crystalline Belt, The Intermontane Belt, The Omineca Belt, and the Eastern Marginal Belt. These physiographic/tectonic regions and the distribution of Mid-Tertiary and older volcanic rocks is given in Figure 2-1. The tectonic development of British Columbia and portions of Alaska has been discussed by St. Armand (1957). The Intermontane Belt (IMB) lies between 180 and 420 miles inland and parallel to the present day Pacific Coast. Intermittent but extensive volcanic activity since Paleozoic time has characterized the IMB. This distinction as a volcanic region continues on through Late Cenozoic and to Recent times (Souther, 1977a).

The IBM is characterized by subdued topography and a multitude of small isolated Tertiary basins, each with its own sequence of continental sediments, lavas, and a veneer of Quaternary glacial deposits. The basement is characteristically comprised of Mesozoic calc alkaline plutonic rocks as major batholiths, and structurally

Figure 2-1.
Physiographic belts of the Cordillera and the distribution of older volcanic rocks, adapted from Souther, 1970.

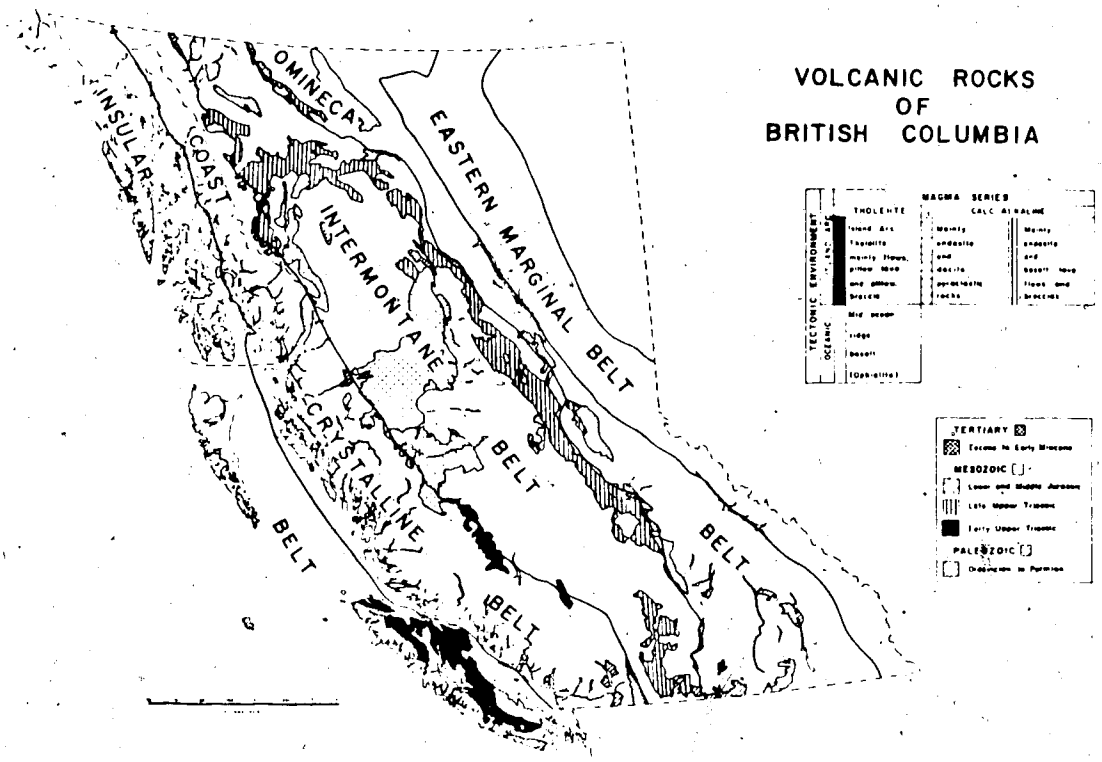

deformed marine sediments of Upper Paleozoic and Mesozoic age. Regional metamorphic rocks are rare and usually associated with the distinct margins of the IMB.

The volcanism of the IMB from Paleozoic to Middle Cenozoic times has been dominated by calc-alkaline intermediate magmas. The sedimentary section from Permian time onwards has been strongly influenced by local sources and basin development has been dominated by local tectonic movements (Monger et al, 1972). These two observations tend to indicate that for most of the past 250MY the IMB has been located near a major plate boundary, in the modern tectonic sense, or at least the IMB has been coincident with an active continental margin. Since the onset of the Mesozoic orogenies with their widespread plutonism, the western part of British Columbia has been locally emergent (Souther, 1967). Most of the IMB has been emergent since the close of Jurassic time. Volcanism of the Late Cretaceous appears to have been relatively extensive but erosion has taken its toll and even the major volcanic formations such as Ootsa Lake or Sloko are now represented by remnants of small areal extent that have been preserved in down-faulted regions (Souther, 1970). The volcanism of the Eocene and Oligocene was subaerial and calc-alkaline with dominant control by local eruptive centres and shallow crustal magma chambers with compositions ranging from basaltic andesite through andesite, dacite, and rhyolite. This period of volcanic activity was definitively more extensive in the central and

southern portions of the IMB than in the north. A hiatus in volcanic activity occurred between Oligocene and Middle Miocene time. This period has been interpreted as corresponding to the cessation of subduction along the western Canadian continental margin with the disappearance of the Kula plate (DeLong et al, 1978). This was the time of most extensive Tertiary basin development. The resumption of volcanism in Miocene time brought a pronounced change in the chemical nature of the lavas. From Miocene to Recent time the volcanism has been predominantly alkaline and characterized by both major lava plateaux and isolated centres. Repeated glaciation of both continental and alpine type has occurred since Upper Miocene time.

As one of the regions of most varied igneous and tectonic processes since the Paleozoic, the IMB is an important place to study the complex geological history of the continental margin and the evolution of the western North American crust and upper mantle. The traditional geosynclinal models, with their strong reliance on localized or regional vertical crustal movements, are being replaced by a patchwork tectonics of Cordilleran microplates (Yorath and Chase, 1981; Riddihough, 1977, 1981). It is currently being proposed that many of the Cordilleran terranes, including the Stikine, are in fact allochthonous and derived from more southerly latitudes, with docking times ranging from the Mesozoic to the Mid-Tertiary (Monger and Irving, 1980). With the possibility of a separate geological

evolution for adjacent areas of the Cordillera the value of a single historical geology and tectonic development is cast in doubt.

LEVEL MOUNTAIN AND LATE CENOZOIC VOLCANISM IN BRITISH COLUMBIA

The distribution of Miocene to Recent volcanism of the Intermontane Belt is presented in Figure 2-2. The Middle to Upper Miocene onset of this latest volcanic episode is preceeded by a hiatus of 10 to 15MY duration, and a fundamental change in the character of the lavas from calc alkaline to continental alkaline. Regional mapping by the G.S.C. (Operation Stikine) and reconnaissance by the author on the following sheets: Kettle River, Princeton, Nicola, Bonaparte Lake, Quesnel, Anahim Lake, Prince George, and Stikine River, demonstrate the two stage nature of Tertiary volcanism. This generalization holds from the Okanagan to the Cariboo and from the Omineca to the Stikine. The alkaline nature of the Miocene to Recent lavas of the Intermontane Belt is supported by whole rock chemical analyses presented in this study, as well as by independent conclusions by Souther (1977a) and Fiesinger and Nicholls (1977b). Souther (1977) has subdivided the Late-Cenozoic alkaline lavas of the Intermontane Belt into three belts: (i) Plateau Belt, central B.C., (ii) Anahim Volcanic Belt, western B.C., (iii) Stikine Volcanic Belt, northwestern B.C. Other volcanic belts (calc-alkaline) such as the Garibaldi

Figure 2-2.
Miocene to Recent volcanism of the Intermontane Belt; adapted from Souther, 1970, 1977.

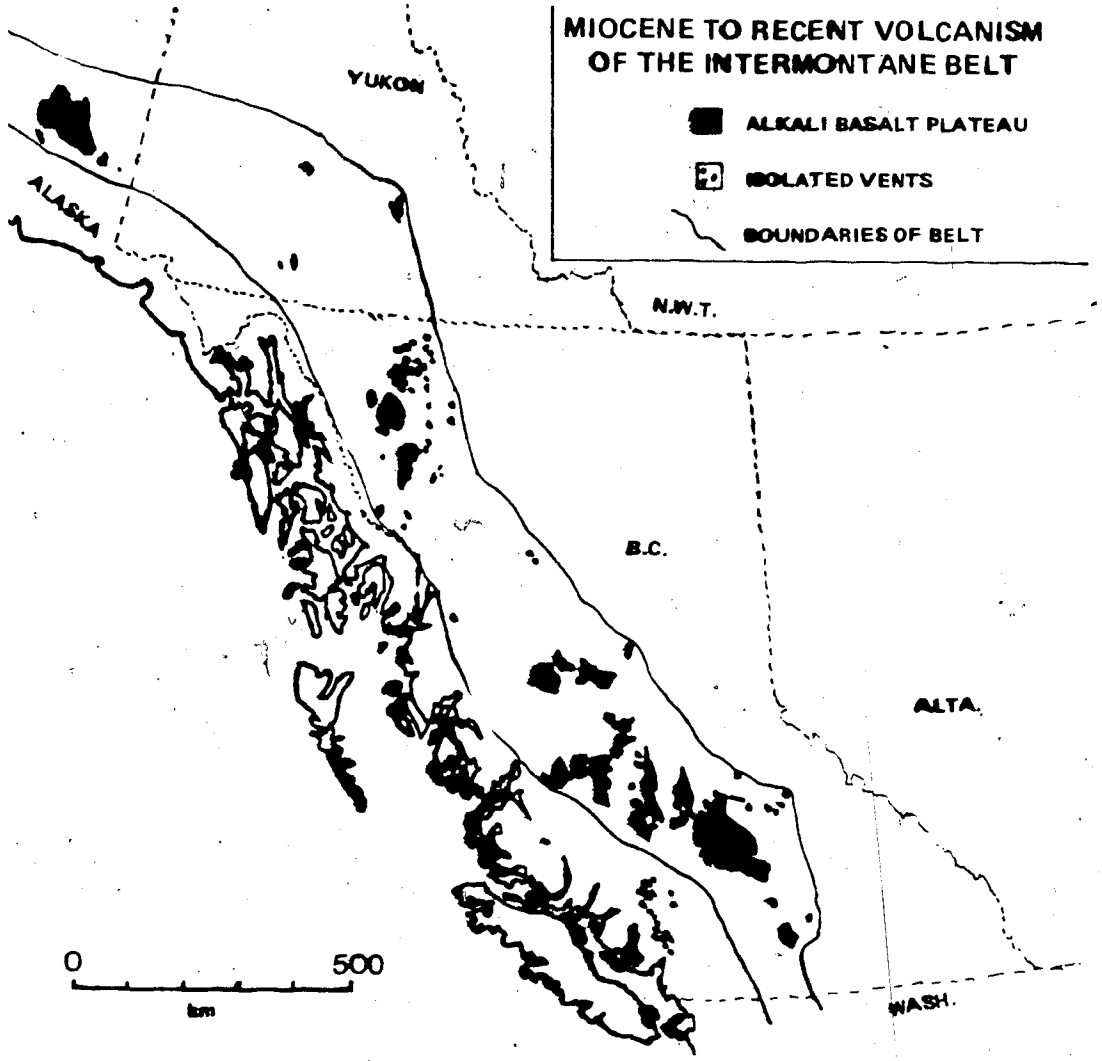

Belt and Wrangell Volcanic Belt are demonstrably related to active or fossil convergent plate boundaries and slabs of subducted crustal lithosphere (Green, 1977; Armstrong et al, 1977). It has been Souther's contention that the alkaline lavas and their distribution are similarly associated with major lithospheric tectonic features. For the Anahim volcanic belt this could be a tensional region associated with the tear fault edge of the subducted slab which was responsible for the Garibaldi Volcanic Belt (Bevier et al, 1979). For the Stikine Belt the feature might be related to a subducted ridge or incipient continental rifting (Souther, 1977b). Typically the alkaline volcanics of the world have one of two principle settings. The most abundant are permitted, discordant types associated with lithosphere in tension along ridge-spreading centres - rifts and transform faults. The other type is tectonically uncorrelated such as on oceanic islands, and isolated alkaline piles that are set in tectonically complex areas (Sorensen, 1970; MacDonald, 1974; Bailey, 1977). Unlike the second cycle calc-alkaline magmas that in some fashion involve remelting of crust (McBirney, 1969), the alkaline magmas are primary and reflect only the physical conditions and chemistry of the upper mantle (Sorensen, 1970; Wyllie, 1971). It is possible that the Stikine and Anahim Volcanic Belts are related to crustal tension associated with the shear geometry of the Pacific continental margin and the Queen Charlotte Fault system (Souther, 1977b). Another possibility is that the

Late Cenozoic volcanism of the Intermontane Belt is primarily related to thermal and compositional aspects of the upper mantle and only influenced to a lesser degree by variations in crustal fabric, thickness and composition.

The alkaline lavas of the IMB are predominantly fluid basalts that fill local Tertiary basins to create extensive plateaux and local shield edifices. Examples of the basaltic plateaux are the upper Kamloops Group (Bonaparte Sheet), the Quesnel Group (Campbell and Tipper, 1971) and the Stikine Group (Souther, 1970, 1977a). Examples of more localized shields and composite volcanoes, which include peralkaline trachytes and other salic lavas, are the Itchas, Ilgachuz, and Rainbow Mountain Ranges of the Anahim Volcanic Belt and Edziza and Level Mountain of the Stikine Volcanic Belt.

The distribution of lavas in the Stikine Volcanic Belt is given in Figure 2-3 which has been adapted from the 1":4mile geologic map of Project Stikine (map 1957b) and subsequent mapping by: Souther and Symons (1974), Hamilton and Scarfe (1977) and Casey (1980). Other than the spatial juxtaposition of the Edziza Volcanism with the Mess Creek Fault and the Level Mountain Volcanism with the Nahlin Fault, there is no apparent relation of Late Cenozoic Volcanism to Pre-Tertiary crustal structures. The wide disparity in age between the alkaline volcanics and the last activity on these old crustal structures (Gabrielse and Wheeler, 1961; Wheeler and Gabrielse, 1972; Souther and Armstrong, 1966) may demonstrate their spatial association

Figure 2-3.
Geological sketch map of the Stikine Volcanic Belt showing the distribution of Late Cenozoic alkaline lavas and ancient faults. Adapted in part from: Stikine River Map 9-1959, Souther, 1970; Casey, 1980. LEGEND:(a) - Kawdy Plateau, (b) - Heart Peaks, (c) - Nahlin Fault, (d) - Level Mountain, (e) - Tanzilla Plateau, (f) - Tahltan Plateau, (g) - Stikine River, (h) - Mount Edziza, (i) - Castle Rock, (j) - Klappan Range, (k) - Mess Creek Fault, (l) - Hoodoo Mountain, (m) - Iskut River.

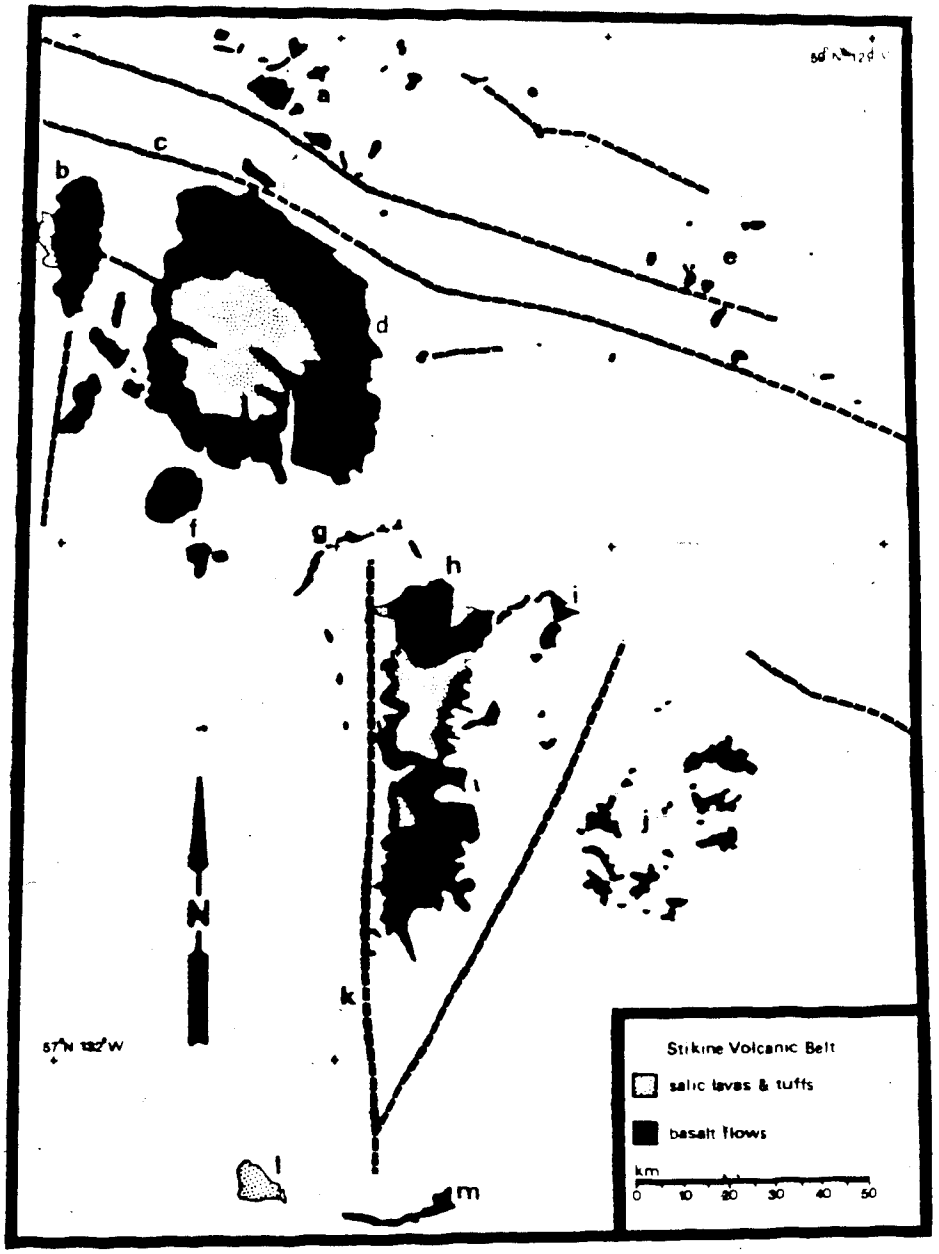

to be of no genetic significance. However, the Nahlin Fault may be a pervasive crustal structure (suture zone), formed as a result of the Mesozoic emplacement of the allochthonous Stikine terrane (Monger and Price, 1979). In that alkaline magmas are typically associated with extensional tectonics and fracture zones (MacDonald, 1974), the lavas of the northern Stikine Volcanic Belt (Heart Peaks, Kawdy Plateau, Level Mountain Range and Tanzilla Plateau) could be related in part to a Late Cenozoic reactivation of this old crustal weakness.

CHAPTER 3. GEOPHYSICS OF THE INTERMONTANE BELT AND THE TECTONIC SETTING OF THE LEVEL MOUNTAIN RANGE.

GEOPHYSICS AND REGIONAL TECTONICS OF THE INTERMONTANE BELT

In the past two decades over twenty papers of major consequence have been written on various geophysical studies in the Cordillera. The results of these studies will be presented as a series of four discussions, according to the type of geophysical information. The discussions will be (i) seismology, (ii) potential fields, (iii) time variant electromagnetism, and (iv) heat flow. A final summary will treat the overall interpretation and its shortcomings. Due to limited accessibility, particularily for any long term surveys or data acquisition, most of the geophysical information is concentrated in the southern Cordillera, (Clowes, 1981). The extension of these interpretations into the northern portion of the Intermontane Belt is made purely on geological and physiographic grounds. As there are no extensive geophysical surveys in the northern Cordillera extrapolations of geophysical data or conclusions from such studies to the crust and upper mantle of the Stikine should be regarded as highly speculative.

The seismicity of Western Canada has been treated by Milne (1963) and Milne et al (1978). The distribution of earthquakes greater than magnitude five is coincident with the Insular Belt. These major events give fault plane solutions consistent with compression in a NW-SE sense,

parallel to the Queen Charlotte - Fairweather transcurrent fault system. Milne et al (1978) have mapped the strain release in units of quantity of magnitude five events per 10,000km^2 per hundred years. On this plot, the zero contour of strain release lies mainly within the Coast Crystalline Belt. The smaller magnitude events show a pronounced regional bias to southern B.C. This reflects only the distribution of seismic observatories and the strong need for geophysical research in northern B.C. Presumably the true distribution of events of magnitude four and smaller is more uniform than mapped. Due to the transform fault nature of the continental margin, one might expect some dilational features on the continental side as a shear-gash fracture effect. The likely orientation for such features would depend on the local crustal fabric with respect to the general NE striking tensional axis. It is possible that the Stikine Volcanic Belt and Anahim Volcanic Belts of Souther (1977b) are just such crustal features. The presence of hot shallow upper mantle and warmer than average continental crust would tend to reduce earthquake-style strain release in the IMB, (Milne et al, 1978). Regardless of the explanation, the IMB appears to be a relatively aseismic region.

The best information on lithospheric structure comes from seismology. A single-end refraction profile across the southern Cordillera was performed by White et al (1968). Wiggens (1976) used refracted body waves from natural

seismic events and records from the Canadian Seismic Network to examine the upper mantle beneath the IMB. Roebroek and Nyland (1975) also looked at Vp data for natural events. Surface wave dispersion studies were performed by Wickens (1977) for eight stations in south and central B.C. to give a regional model for the crust and upper mantle. A more recent model incorporating S-wave, P-wave and surface wave data is presented by Wickens and Buchbinder (1980). The model obtained by White and Savage (1965) is given in Figure 3-1. Three important statements can be made about the Intermontane Belt: (i) the crust is thin (approximately 30km), (ii) the compressional wave velocity (5.9km/s) is rather low by contrast with adjacent crust and the Conrad discontinuity is shallower or not seen beneath the IMB, (iii) the upper mantle is shallow and has a lower compressional wave velocity (7.6km/s) than the mantle beneath the adjacent Pacific or the main North American continent to the East and South. The data of Sarkar and Wiggens (1976) indicate a low compressional wave velocity, approximately 7.8km/sec, and a high Poisson ratio for the upper mantle beneath the northern IMB. Roebrock and Nyland (1975) examined P wave residuals from over 1500 natural events for ray paths that bottomed beneath Western Canada. Their travel time residual versus epicentral angle (delta) plots for three sub-regions of the Cordillera show a large variation in the delta range from 14° to 17°. This would be expected for the presence of a 30 to 50km low velocity zone

Figure3-1.
Geophysical cross section of Cordillera taken from Lambert and Caner (1965) originally adapted from White and Savage (1965).

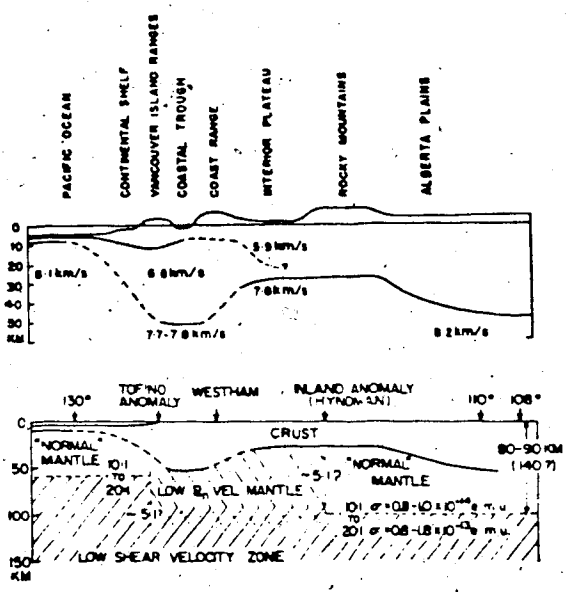

(LVZ); however, their data do not warrant so singular an explanation. They find no significant regionalisation of P wave velocity structure from north to south. However, their data does support some lateral variation including the evidence for modern subduction of the Juan de Fuca Plate. Wickens (1971) presents surface wave velocities for Canada, Figure 3-2. The regular westward decrease in Love wave phase velocity at 50km depth is probably indicative of a regional thermal or compositional gradient. Such a feature is in agreement with the White and Savage (1965) model. More detailed work by Wickens (1976) in the Cordillera demonstrates the following characteristics of the IMB: (i) thin crust and shallow Moho, (ii) no high velocity lid on upper mantle such as is found beneath the Alberta Plains or the Insular Belt. Nicholls et al (1981) have argued that a high velocity lid may still exist. If the difference between high velocity lid and low velocity zone were as small as 0.05 km/sec, and if the lid is sufficiently thin (<1.0km), it may escape resolution by low frequency data.

Regional gravity studies in the Cordillera have been made by Garland and Tanner (1957) and Stacey (1973, 1974). Kanasewich (1966) has used joint inversions of gravity and seismic data to generate consistent models for the crust and upper mantle of Western Canada. There is a widespread Bouger minimum over central B.C. and the IMB. From crustal seismology there is sufficient evidence to rule out the normal explanation of crustal thickening, Airy root, as the

Figure 3-2.
Love wave velocity structure at a depth of 50km from Wickens (1971).

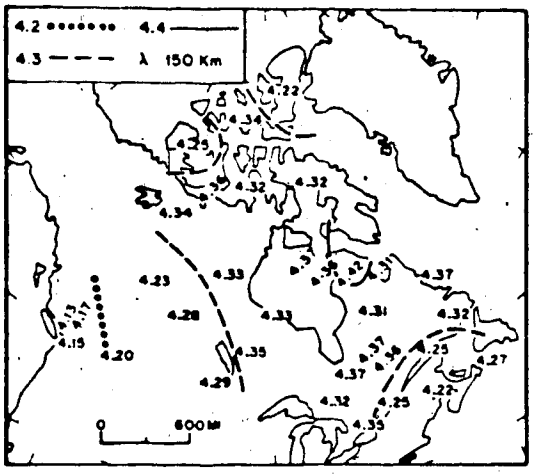

Figure 3-3.
Density variation in the Cordillera computed from joint inversion of gravity and seismic data; taken from Berry and Forsyth (1975). Contoured density in units of kg per cubic meter. Negative sign denotes low density regions for crust and possibly upper mantle. Roman numerals denote physiographic belts: I. Insular belt, II. Coast crystalline belt, III. Intermontane belt, IV. Hinterland belt, V. Omineca belt.

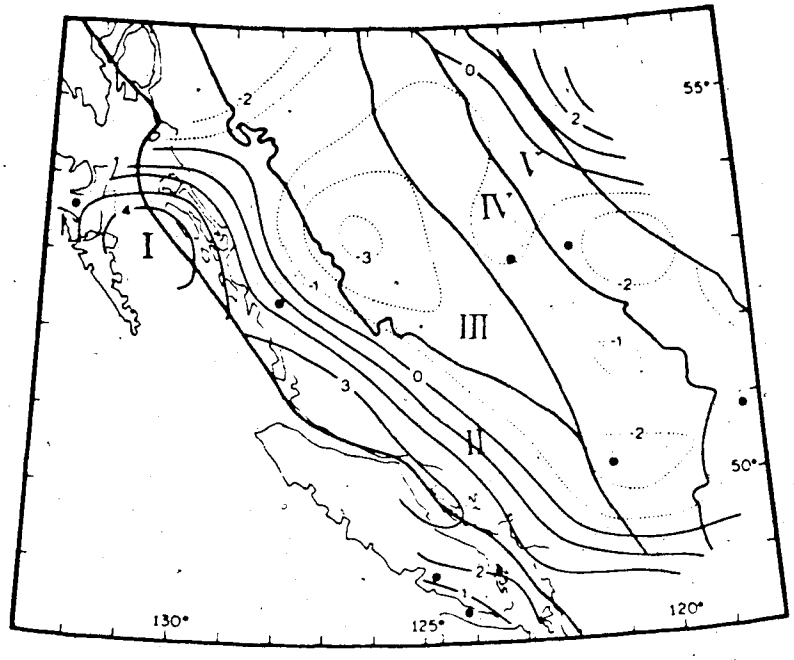

cause. A model for density variation in the crust and upper mantle is given in Figure 3-3 (taken from Berry and Forsyth, 1975), which shows the Bouger effect as a large low density region. Because this coincides with thinner crust, it implies a low density upper mantle which could have at least three explanations: (i) the absence of a high density lid on the upper mantle beneath the IMB, (ii) the presence of a thick LVZ with partial melting, or (iii) a less refractory upper mantle. This type of potential field information cannot distinguish among the three cases. Kanasewich presents a Pratt - type model which attempts to account for gravity anomalies with gross density variations. This model, in Figure 3-4, integrates all three possibilities mentioned above.

Caner (1969a,b) examined aeromagnetic profiles across the Cordillera and found long wavelength (greater than 150km) anomalies west of the Rocky Mountain Trench. He presents three possible explanations: (i) hot crust and consequently a shallow Curie-isotherm depth, (ii) small scale break up of magnetic (and geological) structures, and (iii) more silicic crust. It would be quite reasonable in the light of the present geological knowledge of the Cordillera to accept all three hypotheses.

Caner (1969a,b; 1970) has also performed time variant electromagnetic studies of the Canadian Cordillera by both geomagnetic depth sounding and magnetotellurics. The inversion of his electromagnetic data as a layered

Figure 3-4.
Model cross section of crust and upper mantle of the Cordillera based on joint inversion of seismic and gravity data; taken from Kanasewich (1966).

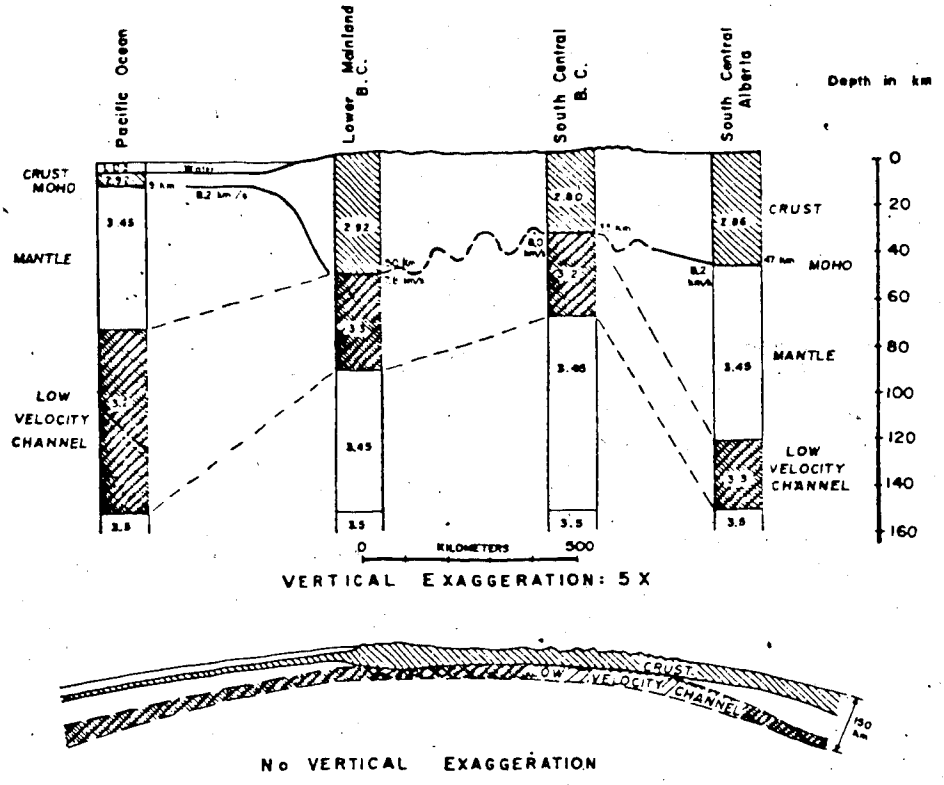

Figure 3-5.
Comparison of geoelectric sections for world rift areas with B. C. Data for Baikal from Gornostayev (1972), for East Africa from Banks and Ottey (1974), for Rhine Graben from Reitmayr (1975), for B. C. from Caner (1969, 1970, et al 1969). Data base includes magnetotellurics, geomagnetic depth sounding and aeromagnetics. Error bars indicate range of reported values. World rift areas have a zone of anomalously low resistivity (<50ohm-meters) at shallower than 30 km depth.

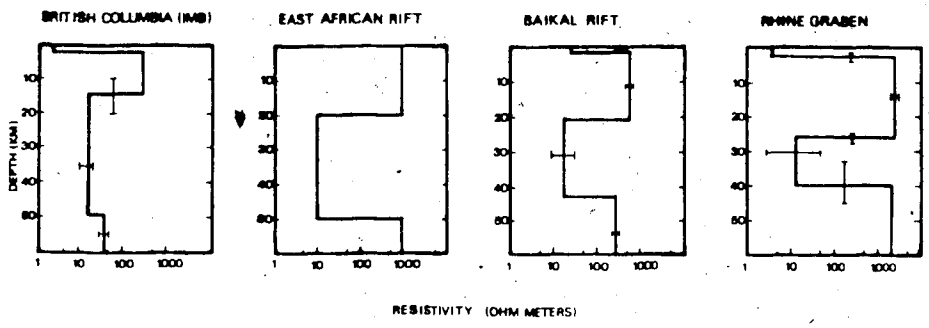

resisivity structure predicted lower crustal apparent resistivities of about 5ohm-meters, which led Caner to speculate that the lower crust is probably volatile rich (hydrated ?) and/or partially molten, and that the Moho is hotter than 750° with a moderately conductive upper mantle which could be partially molten. An alternate explanation for such a highly conductive lower crust would require temperatures above 900°C, which is considered less likely. A comparison of Caner's magnetotelluric sounding data for the Cordillera with rift areas of the world is given in figure 3-5. The geoelectric signature for the IMB is sufficiently similar to established rift areas to speculate that the IMB may be an incipient continental rift.

The western Cordillera of Canada and the IMB very probably has heat flow values on the order of 1.8 to 2.5 H.F.U. (μcal/cm^2/sec), (Jessop and Judge, 1971; Jessop and Souther, 1980), which would compare with the Cordilleran geothermal anomaly of the western U.S. (Roy et al, 1968). A value of 2.0 was given (Jessop and Judge, 1971) for Penticton with values of 2.0 and 2.3 in adjacent Washington. The prairies are characterized by values of 1.0 to 1.2 and the shield has values like 0.8. The more recently active volcanic regions of the IMB no doubt exhibit the highest heat flow. The cause of the high western heat flow values must lie within the mantle. Geologically unreasonable levels of radioactive elements would be required for crustal rocks to explain the observed heat flow. To some extent, higher

temperatures in the crust and mantle would be consistent with all of the previously discussed geophysical data. Increased temperatures have a lowering effect on compressional wave velocities (Anderson and Grew, 1977). The range of laboratory determinations for mafic rocks and minerals is reported to be -2.5×10^{-4} to -38.0×10^{-4} km/sec/°C. For garnet and forsterite this lowering effect shows moderate increases with temperature. Soga (1966) derived polynomial expressions for extending these data to higher temperatures which show the effect to be non-linear. If we use the value of -5×10^{-4} km/sec°C for the temperature dependence of velocity, the normal U.M. velocity of 8.5 km/sec and the anomalous U.M. velocity of 7.8 km/sec, we can calculate a hypothetical lateral temperature difference of 600°C. Although this sort of difference could exist on a lateral scale of hundreds of kilometers between normal and hot mantle, the actual difference is likely to be more on the order of 400°C or less. Roy et al (1968) report 35km isotherms of 860°C under the western U.S. and 460°C under the eastern U.S. Using 800°C as a temperature estimate for the Moho of the IMB, the 8.1km/sec normal mantle under the continent could be 600°C, but certainly not as low as 200°C. If instead of the -5×10^{-4} km/sec/°C velocity - temperature dependence given above, Hughes and Maurette's value for Dunite of 38×10^{-4} km/sec/°C is used, the model temperature difference would only be 78°C. With data of this quality one cannot distinguish between temperature and compositional

effects. As was suggested in the discussion of geomagnetic induction data, both temperature and composition effects are likely to play a part.

A single cross-section has been constructed to summarize the general geophysical characteristics of the Intermontane Belt and its setting within the Cordillera. This cross-section is shown in Figure 3-6. In summary, the geophysical data for the IMB indicates the following generalizations. The crust may have a shallow 0 to 3km upper layer of variable low velocity (3 to 4km/sec) sediments. Under the IMB the Conrad is shallower and discontinuous (poorly resolved). This coincides with possible upwelling of the Curie Isotherm (to 18km ?) and presumably higher than average continental heat flow values (2.0 H.F.U.). The compressional wave velocity of the IMB crust is only 5.9km/sec by contrast with the 6.1 km/sec of the Coast Crystalline Belt or the Eastern Marginal Belt. There is a lower crustal (below 10km) zone of high conductivity which could indicate volatile enrichment and/or partial melting. All of these observations are consistent with a hotter more salic crust for the IMB. The upper mantle of the IMB lacks a distinct high velocity lid such as is present 300km to the east or west. The upper mantle is characterized by lower compressional and Love wave velocities, but the occurrences of lateral-compositional variations cannot be distinguished from lateral-temperature variations. The most important generalization of these physical data is that the IMB is a

Figure 3-6.
Hypothetical cross-section for the crust and upper mantle beneath northern B. C. from seismic velocities and gravity data. The coast crystalline belt after Johnson et al (1972), IMB region from Wickens and Buchbinder (1980), Rocky Mountains from Mereu et al (1977), density variations after Stacey (1973) and Kanasewich (1966).

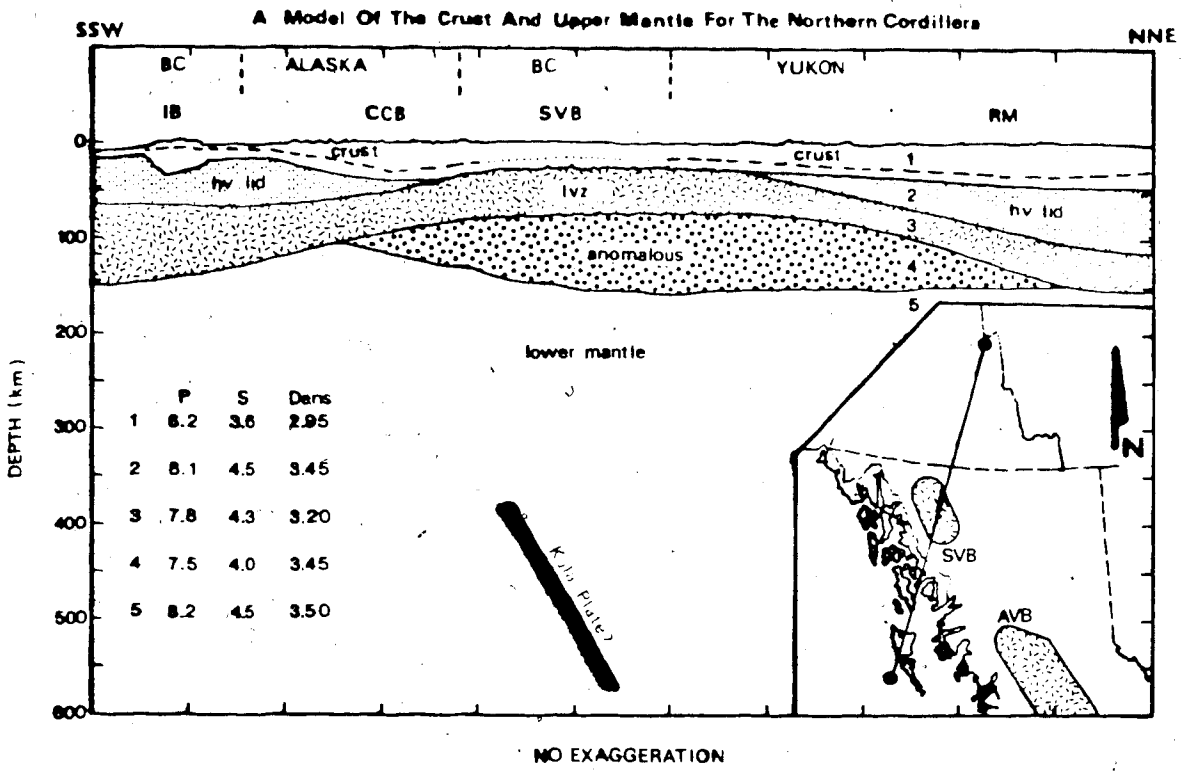

distinct geological region for the entire thickness of the continental crust and the upper 40km of the mantle. The compositional and thermal causes of volcanism in the IMB are certainly related to these pervasive geophysical peculiarities. Any realistic tectonic or geological theory for volcanism in the IMB must take into account at least several of these physical features.

INTERPRETATIONS OF AEROMAGNETIC DATA FOR THE NAHLIN PLATEAU

The Nahlin Plateau, including Level Mountain, has been mapped aeromagnetically on a 1:50,000 scale by the Department of Energy, Mines and Resources. The spatial resolution of the maps is sufficient to discern features of wavelength greater than 1.6km. The resolving capability of the maps for magnetic features on the basaltic plateau can be expressed as the average and maximum lateral gradients, of 250nT/km and 700nT/km, respectively. Preliminary geological interpretations have been made of prominent magnetic features, particularly where they relate to basement geology, structure and tectonics, and to Late Cenozoic basalts. Several anomalous features and general trends are portrayed in sketch-map form in Figure 3-7.

In these high latitudes, above 58°N, a geometrically regular vertically magnetized body of rock, having a susceptibility contrast to surrounding rocks, should display a vertically symmetric anomaly that is either a high or a low depending on the sense of the magnetization (up or

Figure 3-7:
Schematic interpretation of aeromagnetic maps for the Nahlin Plateau.

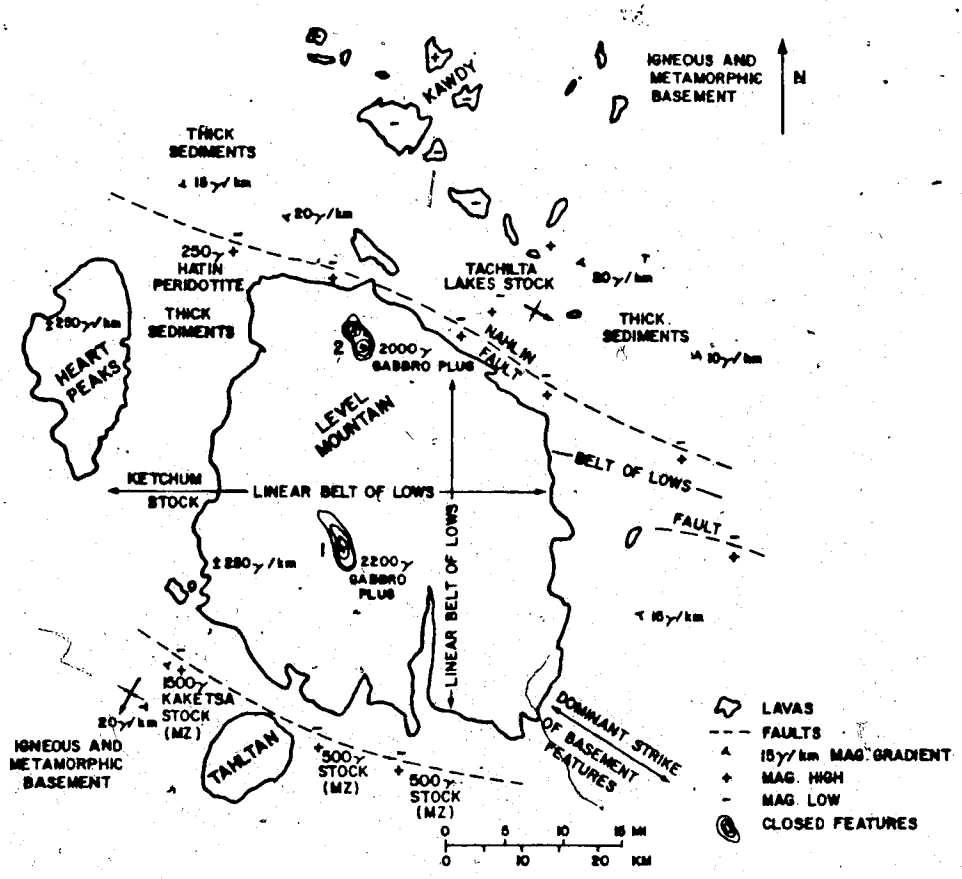

down). Prior to the Cenozoic there have been structural deformations and tectonic movements such that the present orientation of the rocks, with respect to the earth's main field, has changed with respect to the original position. There are three major types of apparent susceptibility signatures on the Nahlin Plateau: (i) highly magnetic, Late Cenozoic basaltic lavas, (ii) moderately magnetic crystalline rocks that make up the local basement (plutonics, older volcanics and metamorphics), and (iii) weakly magnetic sediments.

The dominant magnetic strike in the area is WNW-ESE which is in good general agreement with broad geological and structural trends mapped by the GSC (Gabrielse and Souther, 1962). Major basement faults such as the Nahlin Fault and the Snow Peak Fault are discernable in that they separate geological terranes of different magnetic expression. Recognition of these faults is based on alignment of paired high-low features (second vertical derivative zero crossings) and to a lesser extent on horizontal inflection of magnetic trends.

The marine sediments of the Nahlin Trough and the Dudidontu Lowlands, northwest of Level Mountain, are typified by horizontal gradients below 20 nT/km. Approximate calculations (by the methods of Peters, 1949) on the depth to the basement below these sedimentary areas indicate a sedimentary thickness on the order of 2km. There is also an indication of a different susceptibility for the basement

rocks on opposite sides of the Nahlin Fault, lending support to regional geological mapping (Gabrielse and Souther, 1962), which indicates the Nahlin Fault to be a major crustal structure.

The magnetic fabric of the igneous and metamorphic basement is dominated by subsymmetric features with wavelengths less than a few kilometers and intensities in the range 250 to 1500nT . The prominent igneous basement features appear to be non-vertically magnetized. At least five of these anomalies could be explained by bodies that were initially-vertically magnetized (in normal field) and were subsequently rotated to the southwest. This poses a tectonic question as to whether the bodies were originally vertically-magnetized and subsequently rotated down to the southwest, or whether there was a major shift in latitude (more than 15° to the north), of this block of crust afer the Jurassic. Symons (1978), on the basis of paleomagnetic evidence, has suggested crustal tilting 30° down to the west for a section of the Coast Range Batholith a few hundred kilometers to the south. This sort of simple tectonic rotation is by far the least demanding hypothesis energetically. Because the Cretaceous and Cenozoic outcrops of the Level Mountain Region are essentially horizontal, any hypothetical crustal tilting must have occured between Jurassic and Middle Cretaceous time. The possibility that the Stikine terrane is allochthonous and has been tectonically displaced prior to the Cenozoic cannot be ruled

out.

In addition to the east-west belt of lows discussed with respect to the continuation of the Ketchum stock under the Level Mountain Plateau, there is another north-south belt of lows parallel to Beatty Creek. This trend is neither parallel to regional structure nor to the Mesozoic intrusions. There exist two possible explanations of this feature: (i) this is a basement topographic high and the lavas are thin or (ii) a major portion of the plateau section here could be reversely magnetized. The second idea is unlikely in the light of the development of the lava plateau, discussed later, and in terms of the measured paleomagnetic section at the Little Tahltan Canyon, which shows most of the thickness of the plateau to be normally magnetized. The first explanation would make Beatty Creek a resequent stream. The Dudidontu to the west and the Tuya to the east are exumed or resequent. If the historical drainage density was similar to that of today, Beatty Creek is probably a resequent stream as well.

The remaining two magnetic features on the Level Mountain Plateau are magnetic highs with amplitude greater than 2000nT and wavelength 4 to 8km. These anomalies have been profiled, digitized and interpreted by the geometric techniques of Peters (1949), Vacquier et al (1951). The domical high indicated by a 1 on the aeromagnetic sketch map is the most prominent magnetic feature on Level Mountain as a whole. Its amplitude against the plateau expression is

2200nT and against true regional background is greater than 2500nT . It is elongate NNW-SSE with a maximum expression of 8km long by 4km wide. Depth rule estimate derivative methods (Peters, 1949), in addition to assumed susceptibility contrasts and 2-D modelling by use of a graticule after Grant and West (1965) and Peters (1949), indicate a depth to the top of the body of 3.46km (2.15miles) below ground surface (ie. 1630m below sea level). These features relate to hypabyssal mafic intrusions which are probably intimately related to Level Mountain volcanism. The two features occur on the Beatty Creek Sheet near the southern end of the Central Chain and on the Granite Lake Sheet on the Northern Level Mountain Plateau. Both assumed bodies are coincident with regions of dyke outcrop, and the first is possibly associated with a high level keystone graben which is indicated on the cross-section of the geological map. In surface outcrop the dykes are quite thin, meters to a few tens of meters, and the susceptibility contrast is not sufficient to account for even a few percent of the observed anomaly. If the initial discussion in this section (on the map resolution of magnetic features) is taken into account, estimates of the lateral extent of the more prominent anomaly indicate an upper surface area of 20km^2. If its thickness is assumed to be roughly the same as its lateral dimensions, the volume can be estimated as 100 to 160km^3, which is about the volume of an average pulse of surface volcanism for the plateau events. In a similar fashion, the

2000nT anomaly in the southwest corner of the Granite Lake Sheet has been interpreted to be due to two adjacent vertically-magnetized basaltic plugs that reach the plateau base (957m below plateau surface or 719m above sea level). The northwesterly of the two bodies has been estimated to have a volume of 80km^3 and the southeasterly a volume of 55km^3. In terms of petrogenesis, these hypabyssal stocks most likely represent high level magma chambers that fed the plateau eruptions. The estimated susceptibilities of these bodies, based on measurements of Level Mountain rocks, would indicate them to be basalt (gabbro) in composition. Neither of these bodies can be realistically considered to be the residue of protracted crystal fractionation, such as might be required to generate the observed salic volcanism. Their calculated volumes are too small by at least an order of magnitude to account for the observed volumes of salic magma and their location is substantially removed from the extensive salic piles.

CHAPTER 4. GENERAL GEOLOGY OF THE LEVEL MOUNTAIN RANGE

HISTORICAL GEOLOGY AND FIELD MAPPING

Field mapping and sampling of the Level Mountain Formation was performed by the author during the 1975, 1976, 1977 field seasons. Stratigraphic sections were examined, described, and correlated between the central glacially dissected ridges and also between the southern and western distal regions of the volcanic shield. Stratigraphic control and sampling elevations were determined by a hand-held altimeter (Thommens c), accurate to within 15 feet. Mapping was done on one inch to one mile air photos with approximately 400% ground coverage and on 1:12,500 scale topographic base maps. The 1:12,500 scale topographic maps were enlarged mosaics made from the 1:50,000 NTS sheets. The geologic cross-sections have been constructed along composite traverse lines with combined topographic and altimetric control. The geologic map of the Level Mountain Volcanic Centre, Map 1, was constructed from field maps and an air photo mosaic and transferred to a 1:63,000 scale topographic base. The actual traverse control on the mapping can be ascertained from the traverse and sampling map, Map 2. The numbered traverses indicate the sampled and measured sections. The northern and eastern portions of the shield have been interpreted by helicopter traverse, photo geologic methods and with aeromagnetic maps. The air photos (NAPL) were taken from an altitude of approximately 20,000 feet

with a six inch lens taken over the 19 year period from 1948 to 1967. The aeromagnetic maps are from EMR, 1979.

Basement Geology

Traverse and mapping in the basement rocks (Pre-Miocene) have been concentrated in three areas: (i) Dudidontu River Valley - Ketchum Lake, (ii) Egnel Creek, and (iii) Little Tahltan River Valley. The geology varies on a local scale of 2km or less with examples of marine sediments and metasediments, acid plutonic rocks, porphyritic andesine andesites and conglomerates derived therefrom, subaerially erupted pyroxene andesites and continental sediments. These units will be briefly descibed in the hope of making a contribution to the understanding of the complex geologic history of the area. The names and ages ascribed to the various basement units do not always coincide with the preliminary mapping by the GSC (Gabrielse and Souther, 1962). This reinterpretation of the geology is intended to synthesize existing information with field work done by the author. The description of units are presented in order of increasing age.

Continental Sediments - Sustut Group

Isolated sections of Early Tertiary fluvial and lacustrine clastic sediments occur along Classy Creek, Mansfield Creek, Tuya River and Nahlin River. Silts and shales predominate over sands and thin lenticular coal deposits are present along with some occurrences of mineralized and petrified wood (G. Sivertz, pers.comm.; T.

Mould, pers.comm.). The GSC reports fossils of Paleocene age from this unit in the Tuya River (Gabrielse and Souther, 1962). The unit was likely deposited along a series of separated Early Tertiary Basins in respose to some regional change in base level, similar to the Deadman River Formation on the Bonaparte Lake sheet (Campbell and Tipper, 1971) or the Hotnarko Sediments on the Anahim Lake Sheet (Tipper, 1969).

Sloko Volcanics

In the valley of Egnell Creek and in places on the Wrathall Plateau are outcrops of subaerially erupted calc-alkaline volcanics, see selected analyses in Table 4-1. The entire formation is up to 500 feet thick (152m) and formed predominantly of green and purple flows of pyroxene - andesite and pyroxene - hornblende andesites. The package of andesite flows is obliquely cut by dykes from 1 to 3m in width of the same material. Capping this pyroxene andesite package on the surface of the Wrathall Plateau are local occurrences of fine grained basaltic andesite, rhyodacite and rhyolite breccia. The rhyolite breccia occurs near the northern edge of the Wrathall plateau and appears to continue into a plug-like body which probably represents a vent area. This entire sequence of calc-alkaline volcanics has been subjected to zeolite facies metamorphism and to considerable alteration with fracture and joint mineralization and infilled vesicles. The groundmass of most rocks is devitrified and recrystallized to a matte of

Table 4-1. Sloko Volcanics Chemical Analyses, Norms and Trace Elements.

	10/15	15/19A	P2	8/31-85
SiO2	52.71	51.11	53.16	52.14
TiO2	1.52	1.81	1.50	1.22
Al203	15.30	16.73	15.89	15.45
Fe203	4.26	9.10	5.73	5.91
FeO	6.22	1.15	3.14	2.91
MnO	0.17	0.10	0.14	0.06
MgO	4.51	3.64	3.67	3.95
CaO	7.61	7.81	7.19	9.00
Na20	3.43	3.02	3.92	3.61
K2O	1.80	2.14	1.83	3.90
P2O5	0.42	0.65	0.65	1.56
H2O+	0.86	2.21	2.44	
H2O-	1.17	0.45	0.70	
S	0.03	0.08	0.07	
BaO				0.30
Q	4.44	6.91	6.70	
OR	10.64	12.65	10.81	23.05
(AB)	29.02	25.55	33.17	30.55
(AN)	21.03	25.77	20.36	14.43
PL	50.06	51.33	53.53	44.98
(WO)	5.83	2.89	4.62	8.59
(EN)	3.64	2.50	3.89	7.42
(FS)	1.85			
DI	11.32	5.39	8.61	16.01
(EN)	7.60	6.57	5.15	1.26
(FS)	3.86			
HY	11.46	6.57	5.15	1.26
(FO)				0.81
(FA)				
OL				0.81
MT	6.18		6.23	6.04
IL	2.89	2.45	2.85	2.32
HM		9.10	1.43	1.75
TN		1.27		
AP	1.02	1.54	1.59	3.70
PY	0.06	0.15	0.13	
CLASSIFICATION	BA	BA	BA	BA
MAP UNIT	Sloko	Sloko	Sloko	Sloko

Trace element analyses ppm (XRF)

	10/15	15/19A	P2
Ba	1201	1451	1514
Nb	16	24	29
Zr	148	253	262
Y	25	36	36
Sr	611	770	866
Rb	33	41	34
Zn	101	115	114
Cn	38	33	18
Ni	33	95	53
Cr	123	228	113

zeolites and clays or calcite and quartz. This unit has exposures along Egnell Creek, the Sheslay River and to the north and west of Ketchum Lake. Near the Dudidontu River, aphyric basaltic andesites outcrop with predominant colours of grey, red, and brown, with the brown material being very intensely altered and friable. Chemical analyses on specimens from Egnell, Wrathall and Dudidontu are presented in Table 4-1. Structural deformation of these volcanics appears to be mainly tilting 10° to 15° to the northeast and some block faulting. Some sulfide mineralization is locally present near the vent area and in exposures to the west and north of Ketchum Lake. This unit (Sloko) does not appear on the preliminary mapping of the Dease Lake sheet (Gabrielse and Souther, 1962). Instead, the Level Mountain Formation is mapped in its place. These rocks are older than the Level Mountain formation by tens of millions of years Level Mountain Formation and they are distinguishable on the basis of their field appearance of weathering in pastel colours, calc-alkaline mineralogy, major and trace element chemistry, their zeolite facies metamorphism and mild state of structural deformation. Judging from the appearance of the Eocene and Oligocene volcanism in the central and southern part of the Intermontane Belt, these Sloko rocks is older still. It is tentatively assumed to be Uppermost Cretaceous or Paleocene in age and roughly correlative with the Sloko Volcanics which have been discussed by Souther (1967, 1970) and Monger (1968).

Tahltan Group (Lower Cretaceous)

Outcrops of dense green, porphyric andesine andesite and indurated conglomerate, with the andesite as the predominant clasts, occur in the Little Tahltan River Canyon at about 3600 feet elevation. Outcrop of this material is also present on Kakesta Mountain to the southeast. The name given to this rock by exploration geologists in the area is Turkey Track Porphyry due to cumulophyric aggregates of andesine. These volcanic rocks and closely associated sediments are distinct from both the earlier amphibolite facies meta-andesites (Triassic) that outcrop on the southeastern side of the Heart Peaks and from the Sloko Volcanics (Upper Cretaceous-Paleocene) described above. Presumably this unit is representative of the lower Jurassic Stuhuni Group, although very similar material from the Tulsequah sheet is mapped as Cretaceous (Souther 71).

Sheslay Batholith (Coast Plutonic Complex, Triassic or Jurassic)

Outcrops of multiphase, intermediate to acid, calc-alkaline plutonic rocks are found in the vicinity of Ketchum Lake and to the southeast of Heart Peaks. Similar plutonics outcrop adjacent to the Sheslay River. Predominant lithologies are hornblende biotite granodiorite and quartz monzonite, but locally pods of diorite and pegmatite dykes are exposed east of Ketchum Lake. These plutonic rocks occur as a series of nested and cross-cutting stocks with average dimensions of about 0.4km. These intrusive rocks have

experienced hydrothermal alteration and potassium feldspathization in addition to both syn- and post-orogenic structural deformation. The most intense deformation is represented by NNW-SSE shear zones to the northeast of Ketchum Lake, with intensive chloritization and some assorted supergene copper mineralization. The general appearance of this plutonic complex is reminiscent of the earliest Mesozoic plutonism seen throughout the Intermontane Belt, such as the Thuya Batholith on the Bonaparte Lake sheet (Campbell and Tipper, 1971). These intrusive rocks have definite cross-cutting relationships with greenstones and low-grade regionally metamorphosed pelitic sediments to the east of Ketchum Lake. They also have cross-cutting relationships with amphibolite facies metavolcanics (Stuhini Group) along the east side of the Heart Peaks.

Marine Sediments and Submarine Volcanics

A sequence of shales and siltstones with green volcanic flows outcrops in the Little Tahltan Valley. This unit is folded about a NW - SE axis with high angle dips (greater than 50°). The northern and southern limits of this map unit are high angle faults. Other than the expected effects of burial diagenesis and minor calcite veining, the sediments are mineralogically unaltered. They could be Triassic in age and belong to the Stuhini Group, which would put them in map unit 4 as mapped by Gabrielse and Souther (1962), or they could belong to map unit 7 and be part of the deepwater facies of the Lower Middle Jurassic Inklin Formation.

Regional Metamorphics (Paleozoic)

Low-grade, regionally metamorphosed, pelitic sediments, chlorite schists, and greenstones outcrop east of Ketchum Lake. These rocks are crosscut by the Ketchum Stock as well as having fault contacts with the stock. These rocks are isoclinally folded and faulted about a NNW - SSE structural trend. The principal metamorphism appears to predate the structural deformation, while the structural deformation postdates the emplacement of the Ketchum Stock. This does not preclude that the metamorphic recrystrallization was related to the emplacement; however, the metamorphism appears to be regional rather than contact. These rocks do not fit easily into the map units of the Dease Lake sheet. It is the opinion of the author that these regional metamorphics, along with the amphibolite facies basic volcanics that outcrop the SE of Heart Peaks, represent metamorphosed paleozoics. They could be the same as map unit 13 (Gabrielse and Souther, 1962), which occurs an roadcuts along the Dease River in the northeast part of the Dease Lake sheet. The other possibility, although not a strong one in the light of contrasting compositions and lithologies, is that these are the metamorphosed equivalents of the Permo-Triassic Cache Creek-type rocks that outcrop to the north of Level Mountain across the Nahlin fault.

Within the basement geology of the Nahlin Plateau Region there is evidence for five or more episodes and directions of structural deformation, two distinct periods

and grades of metamorphism and five or more episodes of igneous activity. All the events took place in the past three hundred million years.

The Nahlin Fault is a major tectonic feature both in terms of surface outcrops (Gabrielse and Souther, 1962) and crustal structure, as can be seen from the 1:50,000 aeromagnetic maps. This major fault probably dates from Permo-Triassic time with movement continuing through the Late Jurassic. The Snow Peak Fault, also WNW in strike, is probably related to the Nahlin Fault, although it may be younger in part. The major WNW valley of the Tahltan River, which has a coincident aeromagnetic expression similar to the faults mentioned above, may also be a major upper level crustal structure. It has been hypothesized by Gabrielse, Souther and Monger (pers. comm.) that the Nahlin fault is a fossil transform relating to the accretion of a Stikine plate to the Cordillera in Mesozoic time. This could account for the pronounced differences in stratigraphy, structure, lithology, metamorphic grade and magnetic expression of the two sides of the fault. The location of the Level Mountain volcanics alongside this fault may indicate a zone of pervasive crustal weakness.

In three places minor faulting was observed, each with its own orientation. In the Little Tahltan River Valley, two high angle reverse faults striking N100°E were observed to cut marine sediments which are either Triassic (Stuhini Group) or Lower Middle Jurassic (Inklin Formation). The

faulting is probably Jurassic, although the sense is not clearly related to the major Triassic-Jurassic structures previously discussed. The Ketchum Stock and the pelites to the east are both faulted by a set of thrusts or high angle reverse faults with strike N165°E. These are probably Cretaceous in age. At Egnell Creek, high angle normal faults, of Eocene age (map unit 7 of Gabrielse and Souther, 1962) bound a downdropped block of Upper Cretaceous-Paleocene Sloko volcanics. None of these minor structural trends fits easily into a single crustal fabric or deformational scheme.

The only straightforward point that can be made in review of the Pre-Tertiary geology of the Level Mountain Region is that it has been an area of repeated tectonism, volcanism, and sedimentation, which is to say that the Stikine has long been associated with an active continental margin. The outcrops in the area attest to the complexity of shallow crustal geology as do the aeromagnetic maps. The basement rocks are predominantly calc-alkaline plutonics and clastic marine sediments, and aside from the few major faults, blocks of similar age and structural fabric probably do not extend more than a few kilometers.

PHYSICAL VOLCANOLOGY

The Level Mountain range is a low profile, continental shield volcano with two principle parts: a flat lying basaltic plateau and a composite stratocone cap of bimodal

composition. The plateau has pronounced cliff margins due to erosive action of continental ice. Alpine glaciation has deeply incised the central statocone to form a series of radial U shaped valleys with separating ridges (plate 4-1).

The Level Mountain shield is made up of sequences of thin fluid alkali basalt flows with occasional tuffs and localized fluvial or glacial sediments. The basalts generally display 2 to 3m thicknesses with prominent columnar jointing. These columnar jointed basalts are usually made up of 3 to 8 flows so closely spaced in time (hours to days) that they cooled as a single unit. Most of these cooling units have intermittent basal agglomerates or fire-red clays consisting of quenched basalt fragments, carbonized plant materials and wood at lower elevations, and baked soils and clays. These basal agglomerates have pervasive hydrothermal alteration with localized veins of calcite and zeolites. Collapsed lava tubes can be seen on the present day surface of the plateau and central ridges and occasionally in cliff exposures. All tubes in basalts had inside diameters less than 2m, see plate 4-2. Vesiculation occurs in the upper meter so of most basalt flows and bubble trains or pipe vesicles often extend through the flow. Blocky aa basalt flows were only observed in two localties: due east of Ketchum Lake on the western plateau margin and in the Little Tahltan River valley. In both cases the blocky lava flows overlie thick volcanoglacial or fluvioglacial units, plate 4-3, Basaltic

Plate 4-1.
Glacially dissected stratocone cap. View to the SE. Subhorizontal trachyte flows and tuffs (units 5 to 7) dominate the stratigraphic succession of the Kakuchuya-Dudidontu ridge. Alpine valley of Kakuchuya creek in foreground is downcut to the level of the basaltic shield.

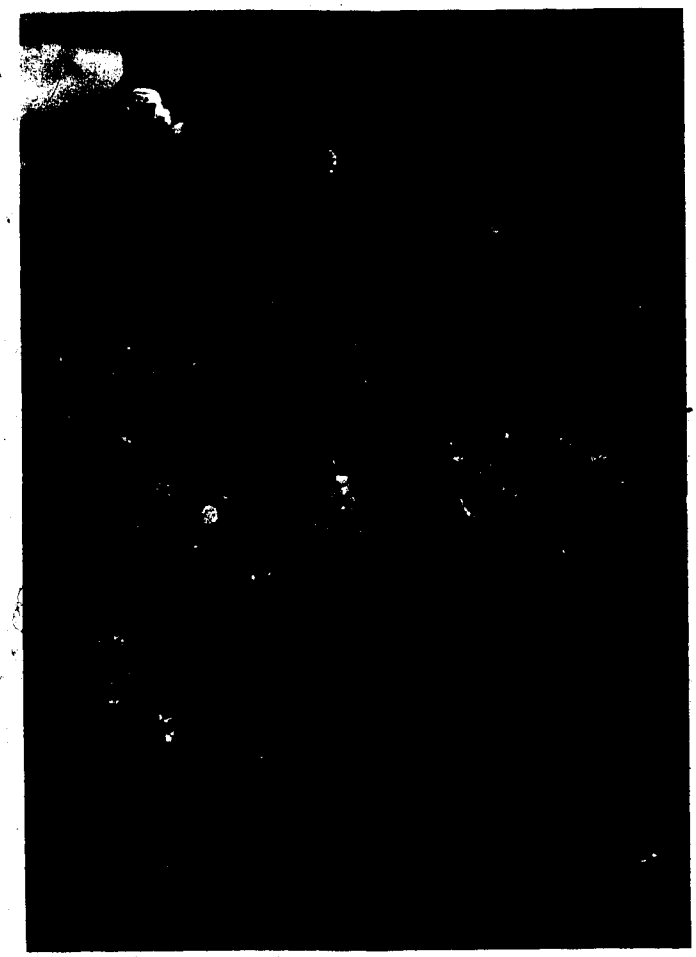

Plate 4-2.
Cross section of 2 meter high lava tube in a fine-grained alkali basalt-hawaiite. Map unit 4, Little Tahltan Canyon.

Plate 4-3.
150 meter thick pile of unconsolidated fluvioglacial and volcanofluvioglacial sediments exposed at the forks of the Little Tahltan River on the southern plateau margin. Steep dips of up to 70° and folding may have resulted from deposition on top of ice, with later slump to their present position.

dykes tend to be linear features. Too little is known about basement structures to say in each case whether basaltic dyke orientation is the result of basement fabric or high level volcano-tectonic control. Some of the more prominent dyke features, however, can be explained. The dykes in the region of Egnell Creek are parallel to Early Cenozoic faulting, where Sloko volcanics are preserved in a down-dropped block. The dykes on the northern plateau are coincident with a major aeromagnetic anomaly that is interpreted to reflect a hypabyssal gabbro body, possibly a crystallized shallow magma chamber. Tristanite dykes (1-3m wide) in the central chain make a linear feature from below the forks of Beatty Creek to Meszah Peak. This 10km trend is not parallel to folds or basement faults in the region (Gabrielse and Souther, 1962), yet it is difficult to imagine a single high level magma chamber of this dimension.

Three of the thicker flows of the upper plateau unit in the westen region formed tumulus structures. Reports by Watson and Mathews (1944) and a helicopter survey indicate several tuyas on the northeastern plateau surface. Tuyas are attributed to be the result of eruption into the base of an overlying ice sheet. Other volcano-glacial deposits include: (i) palagonite tuff breccia with basaltic balloons and baked lacustrine silts, plates 4-4 and 4-5 , (ii) fresh water pillow basalts, (iii) cold lahars (till and agglomerate), (iv) till cemented by pisolitic siliceous sinter, and (v) glacial erratics at the base of flows and tuffs. The most

Plate 4-4.
Palagonite tuff breccia of basaltic composition outcropping on the western plateau margin. Vitroclastic bombs and glass-rimmed balloons (to right of hammer) stand out in a poorly-bedded tuff.

Plate 4-5.
Basaltic volcano-glacial tuff contains boulders of granite not indigenous to the volcano, fragments of older fine-grained basalt (both to right of hammer), and baked lacustrine silts (to left).

recent volcanism appears to be feeble bombs (fusiform) and spatter at localized vents in the central region.

Several physical and textural peculiarities are present in the salic flows:

(i) peralkaline trachyte flows tend to be 2 to 4m thick with relatively high phenocryst content, yet judging from flow morphology, they are as fluid as basalts in the same section,

(ii) thicker units of comendite and trachyte have columnar jointing and in some horizons abundant lava tubes (see plate 4-6),

(iii) aphyric and vitrophyric units often show peculiar flow-banding and mottling. This is generally a purple and gold blebby banding parallel to the original flow surface. Glassy comendite dykes often have fresh cores and white crystalline edges. The glass is peralkaline, whereas the white crystalline margins are now metaluminous. These changes in texture and chemistry are probably due to crystallization, devitrification or alteration (Noble, 1967).

(iv) aphyric and fine-grained trachytes often show onion-skin exfoliation features. In some massive units this weathering feature is so pervasive that it masks the true flow bedding. It can be mistaken for structural deformation and steep dips. The appearance of the exfoliated lavas is like a metamorphic schist. The key to understanding these features are outcrops on the crest of alpine ridges where

Plate 4-6.
Infilled lava tube from a comendite trachyte of unit 7 on the SW face of Meszah Peak. Fluid features of these salic flows attest to their low viscosity upon eruption.

the exfoliation relates to periglacial and frost features,

(v) four rock bosses occur in the basal salic unit. All of these are thick, columnar-jointed, aphyric masses that presently sit in the bottom of alpine glacial valleys. They may be neck plugs or other hypabyssal volcanic features or they might be the result of eruption of salic magma into ice. On the whole, the salic rocks are physically much more variable in appearance, thickness, distribution, phenocryst content and chemistry than the basalts.

(vi) there is a high level trachytic stock on the north side of Meszah Peak. This stock has sub-vertical miarolitic cavities along two zones and well developed joint sets.

GEOMORPHOLOGY AND GLACIAL GEOLOGY

After the volcanic landforms, the most striking geomorphological features visible on Level Mountain are glacial or periglacial in origin. According to Bostock (1948) the Stikine plateau was covered by Pleistocene ice to an elevation of 6500 feet. The central, volcanologically complex, region has been dissected by alpine glaciation to form a series of radial U-shaped valleys with separating ridges (see figure 4-1). The ridges are sculptured by cirques which may have fed alpine glaciers or may have entirely postdated them. Many of the cirques have small tarns and moraines which adjoin or overlie the lateral moraines of alpine valley glaciation. The radial valley glaciers generally cut a sharper gradient through the Level

Figure
Interpretation of glacial geomorphology for Level Mountain.

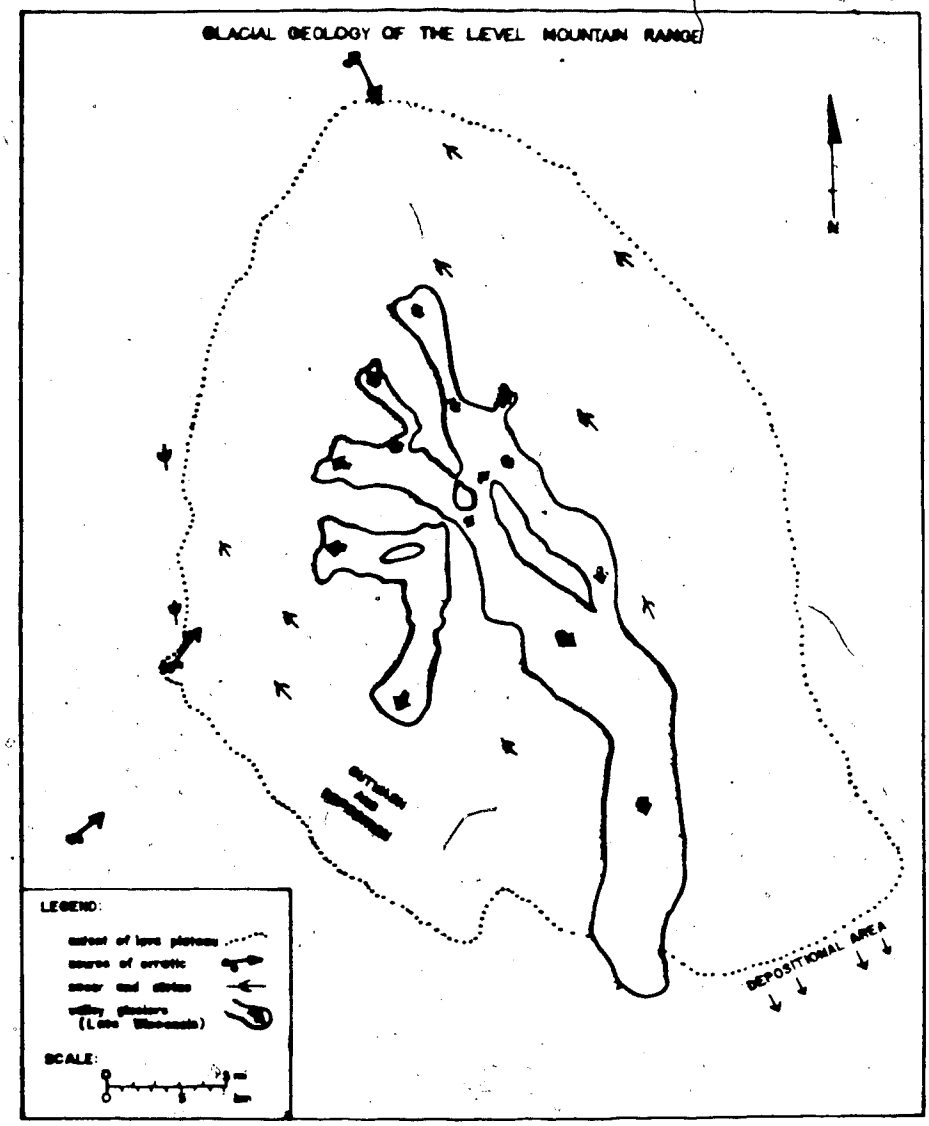

Mountain Formation than the small primary dips of the lavas. The differential hardness of basalts and trachyte flows as compared to alternating tuffs and agglomerates gave rise to a riegel and basin profile down the valleys. The basins often contain shallow, bedrock floored lakes: Dudidontu Valley, two lakes; Kakuchuya Valley, two lakes; North Beatty Valley, one lake. The remainder of the stepped valley bottoms are generally covered with till, alluvial and/or mass-wasting deposits that usually mask the geology (for example, the South Beatty Valley and the upper valley of the Little Tahltan). Both the alpine glacial valleys and the plateau margins display rock bosses, whalebacks, and drumlin-like hills. The aphyric and relatively homogeneous high level intrusives are more resistant to glacial erosion than the surrounding well jointed thin flows and tuffs. A hypabyssal trachyte stock, northeast of Meszah Peak, forms a whaleback with glacial striae and chatter marks. Massive sills or laccolithic type plugs in the Kakuchuya and Upper Beatty Valleys form rock bosses with asymmetric profiles, that step down the valley in the direction of ice flow, plate 4-7.

The upper regions of glacial valleys and the ridge crests have abundant examples of felsenmeer, sorted frost polygons, stony solifluction and patterned ground. On slopes the stone polygons are elongate down slope with vertical stone bands on the perimeters and interior regions of fines. Steep slopes on the central region, as well as on the

Plate 4-7.
Rock boss, sill of columnar jointed aphyric peralkaline phonolites in lower (western) end of Kakuchuya alpine valley. Valley wall to north comprises comendite, phonolite, hawaiite and alkali basalt flows of unit 5.

plateau margins, have sliplenses and terracettes. A landslide of modest proportion occurred during July, 1977, in the Little Tahltan Valley.

Stratified screes flank most of the domes along the central range, see plate 4-8. High gradient snow melt streams have cut through the scree to reveal steep initial dips and layering with different degrees of inclination. Most ridge crests and cliffs have frost wedging and crevassing. In thick columnar units near cliff faces these crevasses may be 2 to 3m wide and more than 10m deep. Frost shattering and exfoliation of salic flow tuffs gives rise to onion-skin textures and apparent cross-bedding. Sometimes exfoliation is so severe as to mask the horizontal nature of salic flows.

Small moraines or rock glaciers occur below the cirques. Lateral and end moraines are found at the mouths of most glacial valleys (Dudidontu and Little Tahltan). The lower reaches of the alpine valleys and the major extent of the plateau surface have mudfields and thufur (mud hummocks). Frost boils are abundant in mudfields and in seasonally dry ephemeral lakes (meltwater ponds). One small (4m high x 10m x 15m) pingo-like feature was found near Ketchum Lake in a bog-filled, shear feature of the Ketchum Stock. The entire southeastern plateau surface (south of Nalachaga Mountain) is covered with string bogs, with the pushed up ridges forming terraces of elongate bogs across the low sloping ground surface, plate 4-9. Steep slopes on

Plate 4-8.
Statified screes, cupola and headed dykes (top right) on phonolite dome in Dudidontu alpine valley. Dissected stratocone flank in near background. Coast range in far background.

Plate 4-9.
String bogs cover the low gradient plateau surface south of Nalachaga mountain, between Beatty and Mansfield creeks.

the plateau margin give rise to mudflows and landslides. A pronounced variability of dissection and patterning of the plateau surface is evident on the air photos. The plateau surface has oriented ridges of till, usually a meter or less in height, and parallel bands of abundant lakes and elongate ponds. This upper plateau unit also has basalts which contain erratics, or formed as tuyas, pillow basalts, palagonite tuff breccias, and lava flows that overly two till units (Pliocene). These features may be found at the canyon of the Little Tahltan Valley, and on the northeast plateau, where the Dudidontu River crosses the western plateau margin, on the western plateau margin above Ketchum La[illegible] and in the lower region of the Little Tahltan Valley. This episode almost certainly marks a major continental glaciation. Dating by fission track and Rb/Sr would indicate that this continental glacial episode occured around 4.5MYBP. The striae, till ridges and ablation till fields all indicate a southeastern direction of ice flow. This ties in nicely with major outwash and eolian deposits to the south and southeast of the Level Mountain Plateau. In contrast to this, a northerly ice movement is indicated by bedrock features in the lowlands west of the Level Mountain Plateau. Perhaps these features represent an earlier continental ice flow, or even a later one that was thin enough to have bypassed Level Mountain without again scouring the plateau surface. If this latter interpretation is correct, the time may have been correlative with the

valley glaciers which dissected the stratocone. This interpretation would make the penultimate continental glaciation stronger than the ultimate in the Level Mountain area.

STRATIGRAPHIC DEVELOPMENT OF THE LEVEL MOUNTAIN FORMATION

Plateau Building Stage

Volcanism at Level Mountain began in Upper Miocene time between six and seven million years ago. The topographic relief in the area was mild and the region presently covered by the lava plateau probably held two or [illegible] drainage systems similar to the lowland portion of the present day Dudidontu River. The first flows were rather volumetric and served to [illegible] those Mid-Tertiary valleys. The two major ancestral drainages probably ran north-south, one between the Little Tahltan River Canyon and Elm Lake and the other on the east side of Beatty Creek through Nalachaga Mountain toward Megatushon Creek. Regional drainage for these streams was probably to the north-northeast similar to the Dease system (to the East) and the exhumed Dudidontu Valley (to the west).

The basal flows rest uncomformably on three extensive Pre-Tertiary rock units: (i) marine sediments of Mesozoic and possibly some of Paleozoic age, (ii) intermediate to acid calc alkaline plutonics, and (iii) upper Cretaceous andesitic volcanics. Thick agglomerate sequences and

basaltic stream conglomerates are exposed in several places. Always low in the Level Mountain section, these represent the basal infilling of previous topographic lowlands. Along the bottom of the Little Tahltan Canyon a thick basaltic stream boulder conglomerate apparently underlies the lowest columnar ankaramite flows exposed laterally in the cliff section. This Late Tertiary conglomerate rests on a highly indurated Jurassic conglomerate whose predominant clasts are subangular fragments of prophyritic andesine andesite similar to those exposed on Kaketsa Mountain to the southwest. The boulders in the basal Level Mountain conglomerate are coarse-grained ankaramites, commonly sub-rounded and up to a few tens of centimeters in size. The rounding could easily be accomplished because the coarse ankaramites typically display spheroidal weathering or decompose to a pyroxene grus; however, clasts of this size, making up a unit 7 to 10m in thickness, could only be carried and deposited in a high energy and fairly major drainage system. Similar basal conglomerate/agglomerate outcrops occur where the north fork of the Beatty Creek incises the north-east flank of Wolf Bones Ridge and where the Megatushon downcuts through the plateau to the northeast (Ostensoe, 1960). The character and placement of these volcanically derived sediments and certain linear features on the 1:50,000 N.T.S. aeromagnetic maps (1979) have suggested the ancestral Tertiary north - south drainage reconstruction as discussed above.

After the existing topography was infilled, construction of the plateau edifice could commence. The lowest flows (plateau unit 1, Hamilton and Scarfe, 1977) of the plateau are massive ankaramites. These, as well as subsequent plateau events, were probably major fissure eruptions. The dyke features mapped on the Northern Plateau represent such fissures for unit 4, earlier vents have probably been covered. Each of the plateau units (I-IV, Hamilton and Scarfe, 1977) has up to eight major equivolumnal cooling units for an average total volume of 165km^3 per eruptive pulse. The flows and flow packages that compromise the plateau are essentially horizontal. Lateral correlations of 10km or more suggest dip rates of less than 1° and maximum uncertainin stratigraphy ties of a few hundred feet. Because the contacts of the first three plateau units are essentially exposed only in steep cliff sections, such as the Little Tahltan or Egnell Canyons, these three units have been lumped for display purposes on the geologic map.

Each plateau unit is composed of several cooling units and each cooling unit is in turn made up of one or more flows. These cooling units generally have a thin basal agglomerate or "fireclay" and a closely timed series of flows which may still retain their own basal crystal-rich horizons or upper vesicular regions, yet still cooled and crystallized as a single unit and show pervasive columnar joints, plate 4-10. The spacing on the columnar joints is

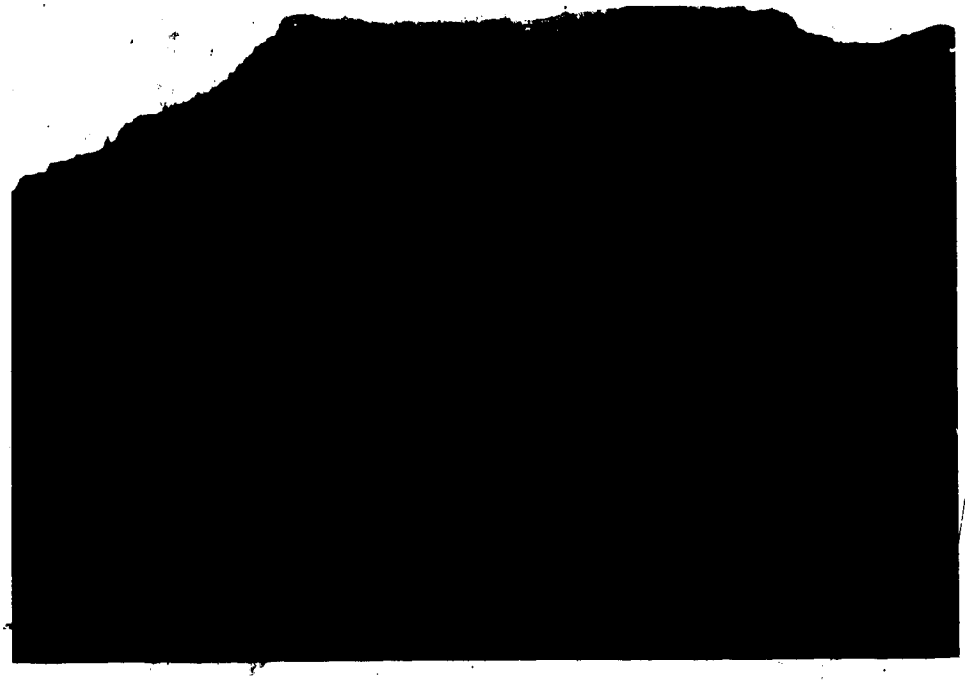

Plate 4-10.
Alkali basalts and hawaiites of map unit 4, southern plateau margin. Ledges develop in basal fireclays and rubbly vesicular flow tops between more resistant flows. 7m thick unit at base of cliff is comprised of 4 closely spaced flows which cooled as a single unit with pervasive columnar jointing.

LEAVE 68, 69, 70, OMITTED

IN PAGE NUMBERING

Plate 4-11.

View to NE of Meszah Peak, highest point of Level Mountain range. Resistant outcrops (units 7, 8 and 9) of peralkaline trachyte, benmoreite and hawaiite flows with comendite flows and ash flow tuffs. Dark scoria slope to right is flank of Gravel Top, a trachyte-benmoreite scoria cone. 2m wide discontinuous tristanite dyke crossing flank of cone points to Meszah Peak. Plateau surface (top right) is the drainage of Matsatu creek.

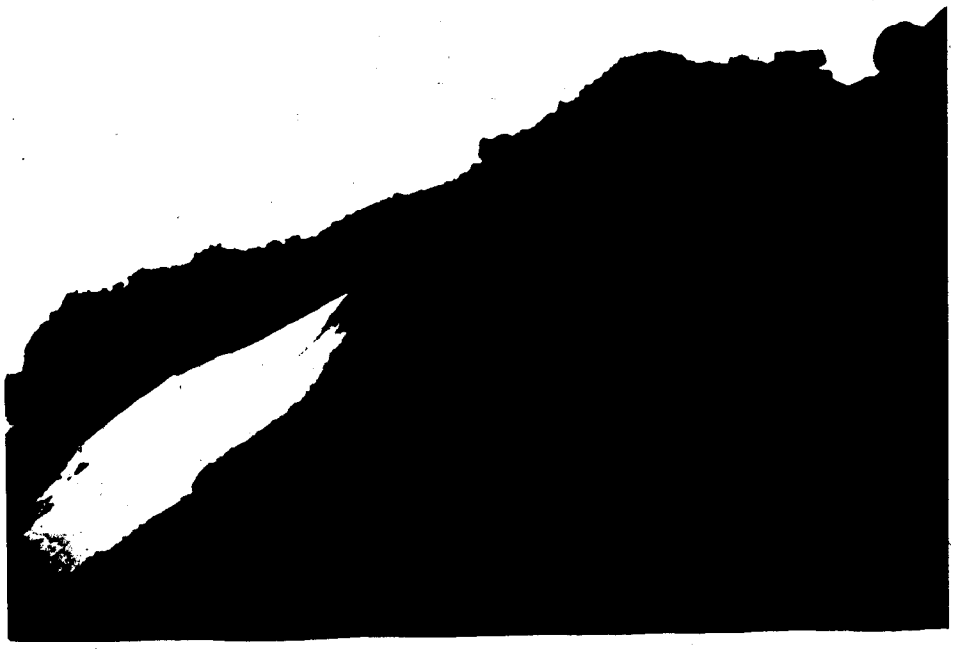

Plate 4-12.
View to SE of Gravel Top. Moderately well stratified trachyte-benmoreite scoria cone on crest of alpine ridge SE of Meszah Peak.

present the northwest margin of this feature has a series of linearly aligned post-glacial hawaiite dykes, sag ponds and keystone features. It is also likely that the central chain with its calc alkaline rhyolite domes (map unit 7c) is located on a subsided block as indicated in cross section. The most abundant salic lavas and tuffs of unit 7 are comendites which are markedly less peralkaline than are the pantellerite trachytes of units 5 and 6. Additionally, map unit 7 also contains domes and breccia pipes of calc-alkaline rhyolite, see plate 4-13, and areally limited flows and dykes of metaluminous tristanite. To stratigraphically tie the basal units of the central ridge requires that the ridge be a keystone graben which has been down dropped 200 feet or more with respect to the outcrops on Meszah Ridge or Wolf Bones Ridge. The limited occurrence of rhyolites and other calc-alkaline lavas in this central chain is probably related to a high level crustal magma chamber and to some degree of shallow tectonism. The coincidence of present alpine valleys with the one time active centres of extrusion may simply be related to the predominance of tuffs, high primary dips, and pronounced thermal alteration at these locations. However, the possibility of radial volcanotectonic grabens cannot be totally discounted.

The latest eruptive activity at Level Mountain has been a series of basalt flows, spatter and dykes that occurred in at least 3 separate episodes over the past million years.

Plate 4-13.

View to south from summit of Kakuchuya-Beatty dome. Dark comendite dyke in foreground above tarn. Domes of central chain are dominantly comendite and rhyolite tuffs with subordinate obsidian flows and ignimbrites. Low elevation background (top right) is southern plateau margin. Coast range in far background.

Selected hand specimens from this recent activity are shown in plate 4-14. These basalts are phenocryst-rich hawaiites with prominent plagioclase megacrysts in the dykes along the Egnell and Wrathall Plateau and inclusions of gneiss and troctolite on Meszah Peak. The volume of these is very subordinate by comparison with the plateau basalts and is more comparable to the basalts of units 5b and 6b. In that most of the erosion responsible for the radial glacial valleys is probably Pleistocene in age, up to 60% of these lavas may have been removed by glacial activity.

According to the paleomagnetic evidence for timing, no period in the history of Level Mountain has seen so little eruptive activity as the last million years. Although some eruptive features definitively postdate glaciation, their volume is so small that Level Mountain should be classed as dormant or extinct. A review of the energetics of Level Mountain volcanism, given in a subsequent section, supports this viewpoint.

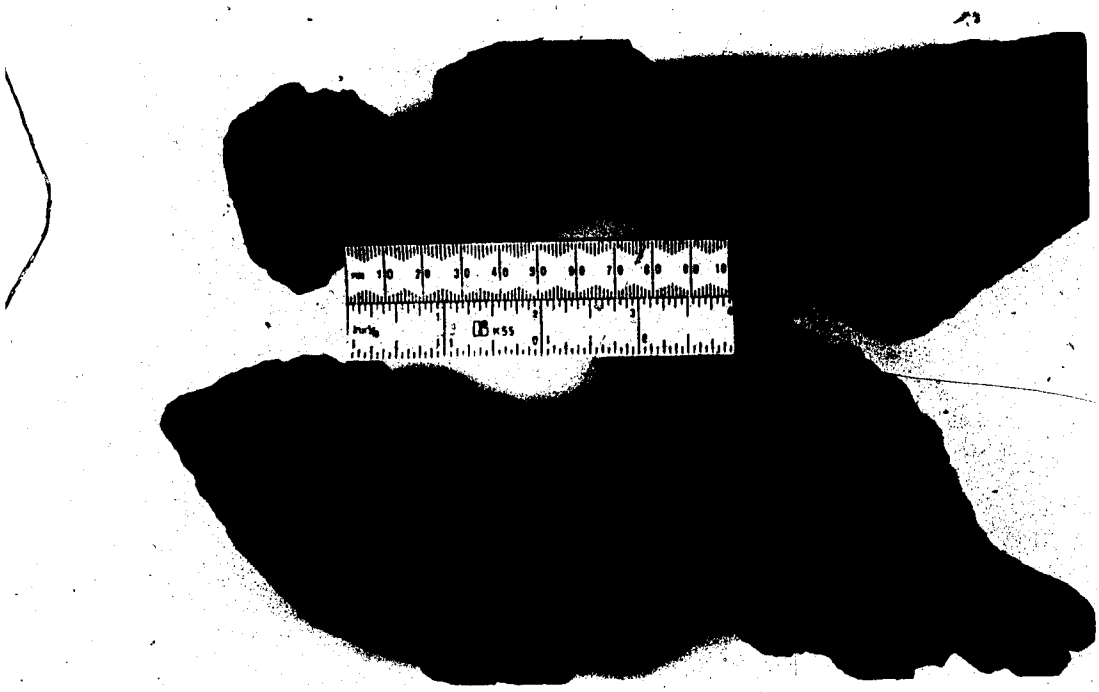

Plate 4-14

Hand specimens of recent hawaiites and basalts. Top left, breadcrust bomb; Top centre, vitroclastic scoria; Top right, polygonal "micro"-columnar jointed vesicular hawaiite; Bottom left, fusiform aerial bomb; Bottom right, ropy lava from hawaiite flow top.

CHAPTER 5. PETROGRAPHY OF THE LEVEL MOUNTAIN LAVAS

INTRODUCTION

In a discussion of the petography of the Level Mountain lavas it is important to describe all of the rock types, textures, mineralogies and crystallization sequences and to relate them in a reasonable genetic framework. A summary of petrographic data and representative modes are presented in Table 5-1. Modes include both phenocryst and groundmass phases. The petrochemistry, norms and detailed mineralogy for most of these samples are presented in subsequent sections. The petrographic discussion of major lava types emphasizes the flows and fine grained tuffs rather than the agglomerates. This primarily reflects a volume bias; however, very few samples were collected of the agglomerates, lahars and coarse grained pyroclastic rocks due to their dubious value as petrochemical or genetic indicators. The petrographic discussion is the result of observing over six hundred thin sections and reconnaissance microprobe work on over one hundred polished sections. The norms are more restricted as chemical analyses were limited to about two hundred and fifty rocks that were considered sufficiently fresh and representative. The important point to consider throughout the discussion of each lava type is that volumetrically there are only two major and important magmas, alkali basalt and peralkaline trachyte. Every other lava type ultimately bears some genetic relationship to one

Table 5-1 Petrography of the Level Mountain Lavas

A. Plateau Lavas

Beatty Creek

	Class	Map Unit	Ol	Cpx	Pl	Ox	AF	Gl/Alt	Texture	Xeno	Melt/Rxn
8/10-26/4517	ANK	4	29%	16%	42%	5%	2%	6%	protoclastic intersertal		
8/10-26/4515	AB	4	X	X	X	X		X	xenolithic intersertal	Ol + cpx	
8/10-26/4505	AB	4	X	X	An 50	X		X	intersertal/pilotaxitic	cpx	X
8/8-24/4335	ANK	3	26%	16%	48%	5%	1%	4%	protoclastic panidiomorphic		
8/9-25/4337	AB	3	X	Ti Aug	An 58	X		X	xenolithic intersertal	Granite	X
8/9-25/4330	ANK	3	27%	15%	36%	5%	tr	16%	panidiomorphic intersertal		
8/9-25/4325	ANK	3	23%	15%	41%	3%		17%	xenolithic panidiomorphic	Hornfels	

Little Tahltan East

8/20-2/4410	HAW	4	X		An 50			>70%	mesohyaline		
8/20-2/4307	HAW	4	X	X	X	X		X	panidiomorphic mesohyaline		
8/23-7/4120	HAW	3	10% Fo 77	Ti Aug	An 35	X		X	pilotaxitic ocellar		
8/23-7/4001	AB	3	17%	14%	56%	10%		3%	panidiomorphic pilotaxitic		
8/23-7/3960	ANK	3	27%	21%	41%	7%	tr	4%	xenolithic protoclastic	Ol + cpx	X
8/23-7/3940	Fe Bas	3	13%	16%	39%	32%			panidiomorphic pilotaxitic	cpx	X
8/23-7/3852	ANK	2	28%	27%	34%	8%		3%	panidiomorphic intersertal		
8/23-7/3825	ANK	2	X	Ti Aug	X	X		X	protoclastic seriate		
8/23-7/3785	ANK	2	22%	24%	42%	9%		3%	protoclastic panidiomorphic		
8/23-7/3765	ANK	2	20% Fo 87	Ti Aug	An 55	X		X	protoclastic		
8/23-7/3725	AB	2	15% Fo 85	Ti Aug	An 55	X		X	panidiomorphic seriate		
8/23-7/3710	ANK	1	21%	15%	45%	8%	1%	10%	subophitic ocellar		
8/23-7/3700	AB	1	10% Fo 85	Ti Aug	An 55	X		X	intersertal amygdaloidal		

Table 5-1 (continued) Petrography of the Level Mountain Lavas

Little Tahltan West

	Class	Map Unit	Ol	Cpx	Pl	Ox	AF	Gl/Alt	Texture	XENO	RXN/Melt
PAA 4560	AB	4	6	24	48	19	3	tr	protoclastic panidiomorphic		
PAB 4505	AB	4	X	X	X	X		X	xenolithic mesohyaline	SCARN	X
PAC 4465	HAW	4	X	X	X	X		X	protoclastic panidiomorphic		
PAD 4440	AB	4		X	X	X		X	xenolithic mesohyaline	Ol+Cpx+Sp	
PAE 4400	HAW/AB	4	X	Ti Aug	X	X	tr	X	pilotaxitic		
PAF 4370	HAW	4		Ti Aug	X	X	tr	X	protoclastic mesohyaline		
PAG 4340	HAW	9	X	26	49	13	1	2	panidiomorphic intersertal		
PAH 4300	HAW	4	X	X	X	X		X	subophitic	En 70	X
PAI 4230	AB	3	X	Ti Aug	X	X		X	intersertal		
PAJ 4200	AB	3	X	Ti Aug	X	X		X	panidiomorphic mesohyaline		
PAK 4170	AB	3	15	23	47	6		9	protoclastic panidiomorphic		
PAL 4155	AB	3		Ti Aug	X	X		X	ophitic		
PAM 4135	AB	3		Ti Aug	X	X		X	ophitic		
PAN 4125	AB	3	18	22	48	3		9	panidiomorphic intersertal		
PAO 4115	AB	3	X	Ti Aug	X	X		X	xenolitic protoclastic	Ol + Sp	
PAP 4100	AB	3	X	X	X	X		X	panidiomorphic intersertal		
PAQ 4065	AB	3	X	Ti Aug	X	X		X	cumulophyric mesohyaline		
PAR 4030	AB	2	20	24	47	2	1	6	xenolithic protoclastic	Ol + cpx	X
PAS 3880	HAW/AB	2	X	X	X	X		X	cumulophyric		
PAT 3860	HAW	2	X	X	X	X		X	vesicular altered		
PAU 3815	AB	2	X	X	X	X		X	panidiomorphic		
PAV 3780	HAW	2	X	X	X	X		X	panidiomorphic		
PAW 3700	AB	1		Ti Aug	X	X		X	ophitic		
PAX 3675	AB/HAW	1	14	20	38	5	1	22	protoclastic intersertal		
PAY 3650	AB	1	X	X	X	X		X	vesicular ocellar		

Egnell Canyon/Wrathall Plateau

KD-1 Dyke	AB	8	13%	28%	36%	13%		10%	xenocrystic protoclastic seriate	Ol + Pl	X
13-k	AB/HAW	4	19%	7%	49%	14%		11%	protoclastic pilotaxitic		
11-13 Tuff	AB	3	X		X			X	vitroclastic vesicular		
16/19d	AB	3	21%	15%	47% An62	14%		3%	protoclastic subophitic	Granite	X
Ol	ANK	2	24% Fo 90	28%	30% An66	7%	1%	10%	xenolithic protoclastic	Ol + Cpx	
P5	HAW	2		X	X	X		X	xenolithic pilotaxitic	Ol+Opx+Cpx	
Q1	AB	2	X	X	An 50	X		X	pilotaxitic		
R5	HAW	2	X	X	An 40	X		X	xenocrystic panidiomorphic	Pl+cpx(Gabbro)	X
S3	AB	2	10%	5%	55% An56	10%		10%	xenocrystic panidiomorphic	Fo95+En100	X
U1	AB	2	X		X	X		X	xenocrystic panidiomorphic	Opx	X

Table 5-1 (continued) Petrography of the Level Mountain Lavas

Western Plateau/Ketchum

Sample	Class	Map Unit	Ol	Cpx	Pl	Ox	AF	Gl/Alt	Texture	XENO	RXN/Melt
B	AB	3	X	Ti Aug	An 50	X		X	subophitic		
Cb	ANK	3	31% Fo 96	21% TiAug	28% An62	2%		11%	subophitic ocellar		
D	AB	3	X	X	An 55	X		X	intersertal		
F	AB	3		Ti Aug	X	X	tr	X	ophitic ocellar		
G	HAW	3		Ti Aug	An 30	X		X	ophitic		
H	ANK	3	23%	25%	36% An63	3		13%	xenocrystic subophitic	Fo83 + En89	X
J	HAW	3	X	X	X	X		X	xenocrystic ophitic	Ol + En	X
Pt Tuff Breccia	HAW	3			An 30	X		X	autoclastic hypohyaline	Seds + Lavas	

Dudidontu Falls

29/1a	AB	4	16%	11%	54%	16%		3%	xenocrystic		
29/1b	AB	4	X	X	X	X		X	cumulophyric ocellar		
29/1d	AB	3	X	Ti Aug	X	X		X	xenocrystic ophitic	Anorthoclase	X
29/1f	ANK	3	Fo 90	X	An 66	X		X	xenolithic pilotaxitic	Ol + Opx	X
29/1g	AB	3	X	Ti Aug	An 46	X		X	mesocrystalline		
29/1h	AB	3	X	X	X	X		X	ophitic		
29/1i	AB	3	X	X	X	X		X	ophitic		
29/1l	AB/ANK	3	23%		33%	1%		43%	mesohyaline		
29/1m	AB	3	X	Ti AUg	X	X		X	subophitic		

Table 5-1 (continued) Petrography of the Level Mountain Lavas

B. Stratocone Basic Lavas

Meszah Peak

Sample	Class	Map Unit	Ol	Cpx	Pl	Ox	AF	Gl/Alt	Texture	Xeno	Melt/ Rxn
PBT 7250	HAW	9			X	X		X	xenocrystic mesohyaline	gneiss	X
PBS 7200	HAW	9		X	An 55	X	X	X	xenocrystic mesohyaline	sanidine	
PBR 6625	HAW	9	5	20	40	15		20	xenolithic protoclastic	troctolite gabbro gneiss	X
PBQ 6580	HAW	9		X	X	X		X	panidiomorphic mesohyaline		
8/25-50/6397	HAW	8	X	X	X	X		X	xenolithic panidiomorphic	troctolite	X
8/25-50/6377	HAW	8	10%Fo60	24%	41%An45	22%		3%	pilotaxitic		
9/2-98/5830	HAW	8	X	X	An 40	X	X	X	xenolithic protoclastic	gabbro (Ol+Cpx+Ox)	X
PBJ 5690	HAW	6b	6	25	59	8		3	xenocrystic panidiomorphic	[illegible] Pl+Cpx	
PBI 5675	AB	6b	X	TiAug	X	X		X	protoclastic		
PBH 5655	AB	6b	X	X	X	X		X	protoclastic		
PBD 5460	HAW	5b	X	X	X	X		X	protoclastic mesohyaline		
PBC 5450	AB	5b	X					X	panidiomorphic mesohyaline		
PBB 5430	AB	5b	9	23	51	9		8	panidiomorphic		
PBA 5420	HAW	5b		X	X	X		X	xenocrystic	[illegible] Microcline	X
PBX 5385	HAW	5b	X	X	An 45	X		X	xenocrystic pilotaxitic	[illegible]	
9/2-98/5030	HAW	5b	Fo 65	X	An 50	X		X	xenolithic protoclastic	[illegible]	X

Dudidontu Ridge

	Class	Map Unit	Ol	Cpx	Pl	Ox	AF	Gl/Alt	Texture	XENO	RXN/Melt
25/3b	AB	8	X	X	An 58	X		X	pilotaxitic		
25/3a	HAW	8		X	X	X	tr	X	xenolithic	Granite	X
24/2f	HAW	5b	9%	19%	63%	29%		8%	xenolithic protoclastic	Ol+Pl+3cpx	
25/1k	AB	6b	X	X	An 64	X		X	pilotaxitic		
25/1i	HAW	6b		X	An 32	X	X	X	panidiomorphic pilotaxitic		
25/1h	AB	6b	X	X	X	X		X	xenocrystic protoclastic	Amorthoclase	
25/1g	HAW	6b	Fo 76	X	An 62	X	X	X	xenocrystic protoclastic	Fo89 + En83	X
25/1f	HAW	6b	X	X	An 35	X	X	X	xenocrystic protoclastic	Ol + Cpx	X
25/1a	HAW	5b	X	X	An 48	X		X	xenolithic pilotaxitic	Granite	X

Table 5-1 (continued) Petrography of the Level Mountain Lavas

C. Stratocone Salic Lavas

Dudidontu Headwaters

Sample	Class	Map Unit	Ox	Fa	Aeg Aug	Pl	Anocl	San	Aen	Rieb	Arf	Other	Q	Gl	Texture	Xeno	Melt / Rxn
25/6A	P.Trachyte	7b	X		X		X	X	X		X			X	pilotaxitic		
25/6B	C.Trachyte	7b	X		X	X	X							X	xenolithic pilotaxitic	(Pl+TiAug+Mt) Aeg	im
25/5b	P.Trachyte	7b	tr		5%	35%Ab83		35%	10%	1%	4%	Rosenb.	10%		eutaxitic/diktytaxitic		
25/5c	Pantellerite	7b	X			X		X	X						pilotaxitic		
25/5d	Pantellerite	7b	10%	trFa66	5%		50%	25%	5%	5%	tr		10%		autolithic intersertal	(Fa+Aeg+Anocl+Py)	
25/5e	Pantellerite	7b	3%		21%	Ab 83	12%	40%	7%				15%	2%	glomeroporphyritic orthophyric		
25/1d	P.Trachyte	6a	Ilm,Py		X		X	X	X	X	X		X		glomeroporphyritic patchy		
25/1c	Pantellerite	6a	Ilm	X	X			X	X	X	X		X		glomeroporphyritic patchy		
25/1b	Pantellerite	6a			X	Ab 84		X	X	X	X				patchy		
26/5	P.Trachyte	5a	X		X			X	X		X	Astr.		X	eutaxitic hyalopilitic		
26/4	Trachyte	5a	X		X	Ab 88	X							X	hyalopilitic		
24/2 o/c	Pantellerite	5a		Fa 65				X	X	X	X				porphyritic patchy		
24/2 c	C.Trachyte	5a	X		X	Ab 80		X						X	hyalopilitic		
24/1 hi	P.Trachyte	5a	10%		13%	tr	6%	60%					tr	10%	glomeroporphyeritic pilotaxitic		
24/1 lo	C.Trachyte	5a	X		X	X		X		X	X			X	glomeroporphyritic		
25/7	P.Trachyte	5a					X	X	X	X	X	Astr.			pilotaxitic patchy		
7/1	P.Trachyte	5a	1%		5%	X	7%	65%	10%	9%	3%			X	porphyritic pilotaxitic		

Meszah Peak

9/5-107/6600	Comendite	7c			X		X		X		X	Rosenb.	X	X	eutaxitic ignimbrite		
8/25-54/6345	Comendite	7c			X			X				Zircon	X		hypohyaline		
PBN 6340	C.Trachyte	7a	Ilm		X	X		X	X		X	Astr.			felsophyric intersertal		
8/26-56/6336	C.Trachyte	7a	X	X	X			X	X	X			X		eutaxitic		
8/26-56/6321	Pantellerite	7a	1% Ilm	1%	13%			44%	11%	13%		5% Astr.	12%		pilotaxitic patchy		
PBM 6160	C.Trachyte	7a	X	X	X			X	X	X					felsophyric intersertal		
8/25-52/5880	P.Trachyte	7a	1% Ilm	3%Fa80	3%	24%		40%	8%	13%			8%		miarolitic hypabyssal		
PBL 5835	C.Trachyte	7a	Ilm	X	X			X				Astr.	X		felsophyric intersertal		
PBY 5780	C.Trachyte	7a	Ilm		X	X	X	X	X	X					xenocrystic intersertal	Microcline	X
PBK 5745	C.Trachyte	7a	Ilm		X	X		X		X.		Astr.			felsophyric intersertal		
8/28-70/5620	P.Trachyte	6a	X	X	X	X	X	X	X	X	X	Kataph			protoclastic intersertal		
PBG 5580	P.Trachyte	6a	Ilm		X	X	X	X	X	X					protoclastic intersertal		
PBF 5545	P.Trachyte	6a	Ilm	X	X		X	X	X	X					protoclastic intersertal		
PBE 5475	P.Trachyte	6a	Ilm	X	X		X	X	X	X		Astr.	X		glomeroporphyritic pilotaxitic		
QBW 5000	Comendite	5a	Ilm		X		X	X	X	X		Astr.	X		autolithic patchy		

Table 5-1 (continued) Petrography of the Level Mountain Lavas

Central Chain

Sample	Class	Map Unit	Ox	Ol	Cpx	Pl	A.F.	Q/FOID	Other	Gl	Texture	Xeno	Melt/ Rxn
9/2-95/6040dyke	Phonolite	7c	Mt	Fa	AegAug		Anocl	Sodalite Leucite		X	porphyritic hypohyaline		
LMI20c	Tristanite	7c	10% Mt		20%AegAug	35%Ab65	2[illegible]San			10%	xenocrystic protoclastic	microcline	X
LMI20d	Trachybasalt	7c		X	TiAug	An42/Ab84	San		AegAug	X	protoclastic mixed	2 glasses	X
LMI20I	P.Phonolite	7c	5%Rut.			40%Ab83	35%San	5%Neph	10%Aen	5%glass	pilotaxitic		
LMIIIA	Tristanite	7c	1% Ilm		2%AegAug	7%Ab65	7%Anocl	tr 1% Bt	3%B.Hbl	79%	glomeroporphyritic eutaxitic		
LMIII30b	P.Phonolite	7c	Mt		AegAug		San	Sodalite Neph	Aen/Arf	X	pilotaxitic eutaxitic		
LMIII30f	Trachybasalt	7c	Mt		Hd,Aeg	Lab,Ab84	X		Rieb	X	mixed, lithophysae	Basalt+Trach	X
8/16-44/6250c (dyke)	Tristanite	7c	Mt		Cr.Di.	X	Anocl	X	Bt,B.Hbd	X	xenolithic pilotaxitic	gneiss	

Wolf Bones Ridge

8/8-23/5030	Trachybasalt	6a	X	Fo	TiAug,Hd	Ab 65	Anocl, San		Aen,Rieb	X	protoclastic porphyritic		

D. Stratocone Intermediate Lavas

Meszah Peak

Sample	Class	Map Unit	Ox	Ol	Cpx	Pl	A.F.	Q/FOID	Other	Gl	Texture	Xeno	Melt/ Rxn
8/26-55/6722	Benmoreite	8		Fo 65	NaHd	Ab65	San			X	xenolithic eutaxitic	granite gneiss	X
8/26-57/6750	Benmoreite	8	10% Mt	5% Fa	5%NaHd	50%Ab65	30%Anocl		Apatite		plotaxitic		
8/26-57/6630	Benmoreite	8	X	Fay	NaHd	X	X				xenolithic pilotaxitic	granite	X
PBP 6480	Benmoreite	8	X	Fay	Hd	X	X			X	pilotaxitic		
PBO 6440	Benmoreite	8	X	Fay	Hd	X	X			X	xenolithic pilotaxitic	granite	X
8/30-82/6150	P.Phonolite	7c	X	Fo 55		Ab65	Anocl	Neph Sodalite	Arf	X	porphyritic granophyric		
9/2-98/5840	Trachybasalt	7b	X	Fo 65	NaHd	Ab50	Anocl			X	mixed hyalopilitic ophitic	comendite glass	X
9/2-98/5830	Trachybasalt	7b	X	Fo 60		Ab60	Anocl			X	xenolithic mixed	ferrogabbro	X
9/1-86/5421L	P. Phonolite	5a	X				Anocl		Bt,Arf	X	eutaxitic hyalopilitic		
9/1-86/5421d	P. Phonolite	5a	X				Anocl		Bt,Arf	X	eutaxitic hyalopilitic		
PBU 5220	P. Phonolite	5a	Ilm	Fay	NaHd		San		Arf		protoclastic pilotaxitic		
PBV 5100	P. Phonolite	5a	Ilm	Fay	NaHd		Anoc/San		Arf		protoclastic pilotaxitic		

Dudidontu Dome

25/6A	P.Phonolite	7c	Mt		AegAug		Anoc/San	Neph	Aen,Arf		protoclastic pilotaxitic		
25/6C	Phonolite	7c	X					Leucite		X	vitroclastic		
26/4	Phonolite	5a	X			X		Leucite	Sphene/Ap	X	vitroclastic eutaxitic		

or both of these.

ANKARAMITES

Ankaramites and olivine-rich basalts (ANK in Table 5-1) are the least glassy of the Level Mountain lavas. Two textural varieties are common: pandiomorphic subophitic intersertal, see plate 5-1, and pandiomorphic protoclastic cumulophyric intersertal, see plate 5-2. The protoclastic cumulophyric variety may have phenocryst contents as high as 45% by volume, although 15 to 20% is more typical. The groundmass olivines and titaniferous augites of this type have an intergranular relationship to the felty plagioclase laths. Oxides are cubic to subdendritic. Intersertal areas are less common than in other basaltic flows. The common primary infillings are devitrified brown glass. The anakaramites have essential phenocryst olivine which is more forsteritic than Fo_{85}. Groundmass olivine may be as low in magnesium as Fo_{75}. The size distribution for olivines from phenocryst to goundmass is usually seriate with the largest phenocrysts being a few millimeters. The forsteritic phenocrysts are hypidiomorphic to allotriomorphic and may have concentric or patchwork optical zonation and occasional anhedral cores. Embayed olivines from the flows of plateau unit 2 frequently contain inclusions of brown spinel. Optical and microprobe analyses on these xenocrystic-appearing olivines and spinels reveal them to be chemically variable even within a single flow. Lamellar

Plate 5-1.
Ankaramite (H)(X.P.L., 2.97x2.07mm) with subophitic zoned titaniferous augite (sides) intersertal plagioclase An63, and subhedral olivine altered to iddingsite.

Plate 5-2.
Ankaramite (8/23-7/3785)(X.P.L., 2.97x2.07mm) protoclastic pandiomorphic with polycrystalline clots of olivine having brown spinel inclusions (xenocrysts). Groundmass contains euhedral plagioclase, titanomagnetite and olivine with intersertal augite and brown glass.

exsolved diopside sometimes accompanies forsteritic olivine in these xenocryst clots, see photomicrograph of sample PAR, shown in plate 5 3. The olivines of the ankaramites are considered to be in part xenocrystic fragments of the basaltic source region and in part of the earliest crystallizing phase. Although most ankaramites have olivine as the only phenocryst phase, the following multiphase assemblages have been observed: (ol, opx), (ol, opx, pl) (ol, pl), (ol, cpx, pl), and (ol, cpx). While phenocryst olivine and orthopyroxene may show fracture and imperfectly developed crystal forms, they do not show a mutual reaction relationship or textures indicative of clear cut sequential crystallization. Neither do they show a marked reaction relationship with the mesostasis. By contrast, whenever clinopyroxene phenocrysts occur they show pronounced reaction coronas. Plagioclases usually show reaction rims and fritted cores. The crystal forms and aggregate textures of the plagioclase and clinopyroxene phenocryst clots suggest rather that they are cognate plutonic xenocrysts. The clinopyroxene of the groundmass of the ankaramites is invariably titaniferous showing brown or purplish colours in plane polarized light and zonation to higher titanium contents at the crystal rims. The crystal form of the groundmass clinopyroxene within a given flow is usually constant, although overall the texture ranges from intergranular prismatic, to feathery acicular, to subophitic. Skeletal magnetites sometimes form as parallel

Plate 5-3.
Alkali basalt (PAR)(X.P.L., 2.97x2.07mm) Protoclastic xenocryst or cognate xenolith clots of olivine and lamellar exsolved diopside in a groundmass of labradorite, augite, titaniferous magnetite and glass.

poikilitic inclusions within subophitic augites.

Plagioclase feldspar compositions are in the labradorite to bytownite range with the groundmass plagioclase usually being An_{55} to An_{60}. Phenocryst feldspars tend to be tabular and twinned but not markedly zoned. Groundmass feldspar is lathlike to anhedral, normally zoned and often complexely twinned.

The predominant crystallization sequence is olivine (with or without diopsidic pyroxene and spinel), plagioclase, titanaugite, Fe-Ti spinel. This is reflected both in texture and serial size range. Olivine crystallization is pre-eruptive while the crystallization of other phases is usually not. Primary intersertal glass was 10% by volume or less. This is usually altered to blue green chlorite or mixtures of chlorite and zeolites. Vesicles are rare in ankaramites and where present have been infilled by calcite. The ankaramites are generally more chemically and mineralogically altered than the alkali basalts or hawaiites; but not sufficiently so as to mask their crystallization history or chemically distinctive nature.

ALKALI BASALTS

Alkali basalts (AB in Table 5-1) are the most variably textured lava type as well as the most abundant. Flows predominate over tuffs and the tuffs, once hypohyaline, are now severely altered. Flows may be very fine grained and nearly aphyric or phenocryst laden panidiomorphic seriate or

medium to coarse grained diabasic (sub-ophitic) in texture, see plate 5-4. The occurence of phenocrysts and phenocryst clots (xenolith clots?) is very common. For an example see plate 5-5. Forsteritic olivine, pale green diopside, bytownite to labradorite plagioclase and iron titanium oxides occur as phenocrysts. Of these olivine is the most common. Phenocryst clots of clinopyroxene and clinopyroxene-olivine are the most abundant aggregate types. Plagioclase and clinopyroxene phenocrysts usually show twinning and multiple concentric zonation. Chemical zonation is usually in the normal sense but reset and marked by a zone of fine inclusions. Non-zoned types in crystal aggregates usually show more optical homogeneity and often have triple-point textures. The groundmass has essential plagioclase, titaniferous augite, and iron titanium oxide, see plate 5-6. Intersertal brown glass or the alteration products calcite, chlorite and zeolites are also present. Olivine is not always present as a groundmass phase. When it does occur it shows a marked compositional break with the phenocryst olivine, such as Fo_{70} groundmass, contrasted with Fo_{90} phenocryst. Occasionally in the alkali basalts with a more intergranular groundmass, melilite rods were observed. The clinopyroxene of the mesostasis was invariably pink-brown titaniferous augite with ophitic or subophitic texture. Phenocryst clinopyroxene may be either titaniferous augite or green diopside. Plagioclase phenocrysts tend to be labradorite, An_{65} to An_{55}, while that of the mesostasis is

Plate 5-4.
Fine-grained alkali basalt (16/19D)(X.P.L., 2.97x2.07mm) with subophitic subhyalo-ophitic texture. Zoned (An55 to An45) and twinned euhedral plagioclase laths, titaniferous augite, basaltic glass and Fe-Ti oxides.

Plate 5-5.
Sample (PAL)(X.P.L., 2.97x2.07mm) Alkali basalt with microxenoliths of pyroxenite (diopside>hypersthene). Groundmass glass shows alteration to chlorite.

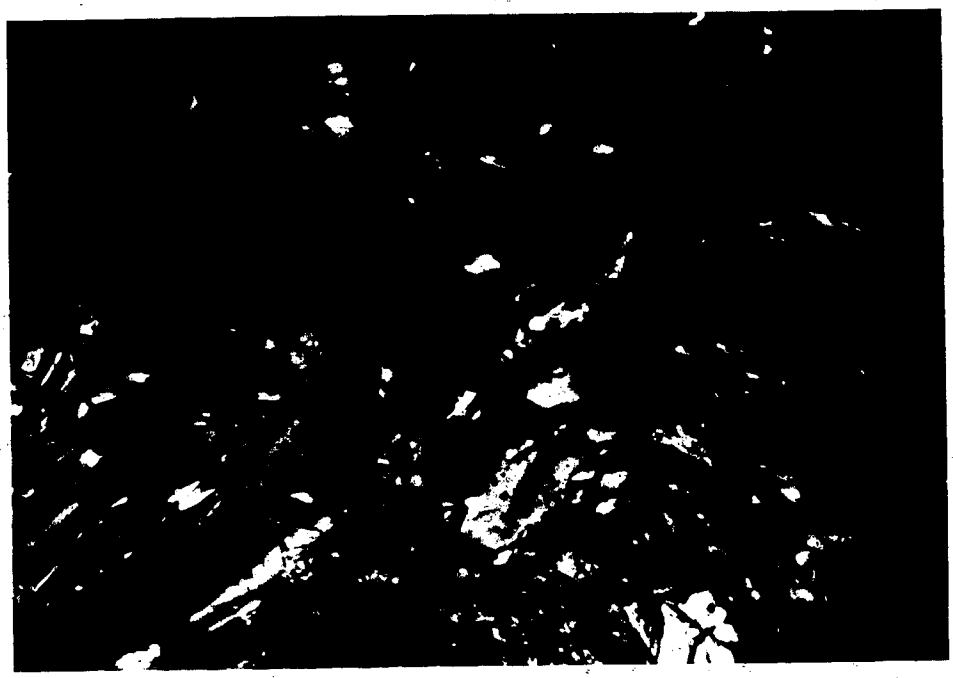

Plate 5-6.
Groundmass of alkali basalt (PAB)(X.P.L., 1.90x1.33mm) with subhedral olivine microphenocrysts, magnetite cubes, and laths of plagioclase with intersertal titaniferous augite.

more sodic, in the andesine range, An_{50} to as low as An_{35}.

It is the author's opinion that the only truly equilibrium phenocryst phases are olivine and plagioclase or olivine and clinopyroxene. The common embayment (resorption) of plagioclase and clinopyroxene and reaction coronas indicate disequilibrium. Even when these phenocrysts are concentrically zoned they are probably cognate xenocrysts and sometimes they are genuinely foreign. The normal crystallization sequence is olivine, plagioclase, clinopyroxene, and opaques, with eruption occurring while plagioclase is on the liquidus. The common occurrence of reset oscillatory zonation, concentric zonation and compositional differences between phenocryst and groundmass plagioclase indicates that the liquidus phase and its composition is very sensitive to thermochemical variables. The changes from phenocryst diopside to mesostasis titaniferous augite and the presence of phenocryst ilmenite and groundmass titanomagnetite are particularily indicative of changes in oxygen fugacity and in the partitioning of titanium into various sites. The remelting of phenocrysts seems to indicate changes in magmatic heat content as well.

HAWAIITES

Hawaiites (HAW in Table 5-1) tend to be protoclastic pandiomorphic mesohyaline and are more prone to be xenocrystic and xenophyric than the alkali basalts. The two types are obviously genetically related. Hawaiites tended to

be vesicular pandiomorphic cumulophyric seriate with a pilotaxitic mesostasis, see plate 5-7. The mesostasis is noticeably dominated by plagioclase (andesine) with variable amounts of titaniferous augite, iron-titanium oxides and brown glass. Olivine and alkali feldspar may be present in the mesostasis but neither is essential. Alteration of the groundmass glass is less pronounced than in the more basic lavas. The occurrence of large plagioclase phenocrysts, and tabular megacrysts to a few centimeters in size was most common in the hawaiites. Hawaiites often contain reverse and complexly zoned plagioclase and sometimes plagioclase phenocrysts of up to three distinct geneses. An example of the large, plagioclase-bearing type is shown in plate 5-8. Although groundmass plagioclase was usually andesine, the phenocryst (xenocryst?) compositions had an overall range from andesine to anorthite. Because hawaiites have many xenocryst phases, they can contain such diverse phenocryst types as enstatite and sanidine in a single flow. While the groundmass may represent an important "magma type", the reaction relationship to the phenocryst assemblages indicates the petrogenetic complexity of the hawaiite.

The occurrence of hawaiites spans the entire history of Level Mountain volcanism, although they are usually a subordinate lava type in terms of abundance. During the first three plateau periods they were subordinate to alkali basalt and ankaramite. The upper plateau unit 4, as sampled in the Little Tahltan Canyon, consists primarily of

Plate 5-7.
Vesicular hawaiite (8/20-2/4410)(X.P.L., 2.97x2.07mm) with seriate euhedral phenocrysts of Fo82 olivine and An50 plagioclase in mesohyaline mesostasis.

Plate 5-8.
(X.P.L., 2.97x2.07mm)Plutonic textured xenocrysts of plagioclase (An40) and microphenocryst of titaniferous augite from fine-grained hawaiite R5. Groundmass is oxide-rich with plagioclase, titaniferous augite and brown glass.

hawaiites. This may or may not be true of unit 4 as a whole. While hawaiite is the most abundant mafic lava type during the stratocone formation, it was quite subordinate in volume and areal extent to the peralkaline salic types.

Texturally and optically the hawaiites are more complex than the other mafic lavas. Judging from their variable and often disequilibrium phenocryst character and the relatively frequent occurrence of xenocrysts and xenoliths, the hawaiites are probably not a primary magma type. Their origin most certainly involves subsequent petrogenetic processes such as crystal fractionation, contamination, and magma mixing.

TRACHYBASALTS

Trachybasalts are the least volumetric and the most variable mineralogically and chemically of any rock type at Level Mountain, see Table 5-1, section D. They were usually pyroclastic and agglomeratic with phenocryst and fragment contents typically around 40% by volume. Mineralogically and chemically these rocks are gradational with alkali basalts and with the tristanites and trachytes. Trachybasalt agglomerates are found in the alpine glacial valley of the Dudidontu and at the eastern end of Wolf Bones Ridge. These "flows" contain about 30% altered glass and the phenocryst/xenocryst assemblage may include hyalosiderite olivine (Fo_{60} to Fo_{55},) hedenbergitic clinopyroxene, basaltic hornblende, plagioclase (labradorite to

oligoclase), anorthoclase, and magnetite. The occurrence of phenocrysts of basaltic hornblende is restricted to trachybasalts and tristanites. The olivine is usually in aggregates, sometimes with green hedenbergite, and always has a reaction corona of iron oxides. Large inclusions of apatite are common. The appearance of these mafic intermediate clots suggests that were derived by the disaggregation of an alkali ferrogabbro, conceivably a cognate plutonic member of the Level Mountain suite, see plate 5-9. Both agglomerates and flows contain resorbed phenocrysts of intermediate plagioclase and frequently have glomeroporphyritic aggregates of anorthoclase, pyrite, and aegerine augite or sodic ferrohedenbergite. Occasionally the clinopyroxene phenocrysts have cores of titaniferous augite and rims of green hedenbergite. The phenocrysts in trachybasalt are always in reaction with the groundmass. The mesostasis, when crystalline, is hyalopilitic to pilotaxitic with laths of andesine (An_{50} to An_{40}), sodic pyroxene and yellow-green glass. The chemical classification of these disequilibrium rocks is difficult. They may be over or undersaturated with respect to silica and may vary from anorthite to corundum normative. Following the nomenclature of Irvine and Baragar (1971) these rocks may have such diverse names as mugearite, benmoreite, tholeiitic andesite or peraluminous phonolite. Modal names would certainly include trachybasalt and the vulsinites and ciminites of Italy (Washington, 1896; Tilley et al, 1964). Textural and

Plate 5.9.
Fragmental trachybasalt flow (LMIII30f)(P.P.L., 2.97x2.07mm). Fragments include euhedral plagioclase, clinopyroxene and dark basaltic glass. The groundmass is eutaxitic with light and dark areas of different crystallinity. Interpreted to be a product of explosive magma mixing.

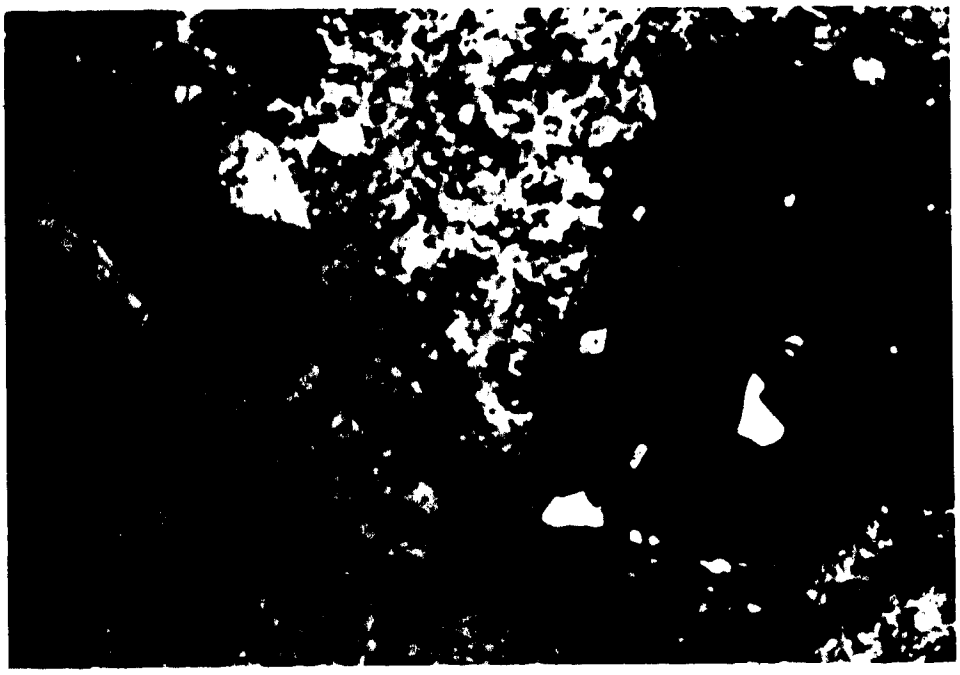

mineralogical evidence suggests that these lavas are the result of magma mixing of basic and salic types with incorporation of some cognate and foreign rock material from the crust. One trachybasalt flow had glassy inclusions which were presumably peralkaline due to their sparse phenocrysts of green sodic pyroxene, ilmenite and anorthoclase. Although the name trachybasalt is not an accepted term in the sodic alkaline basalt series, it is used to emphasize their peculiar character. In some areas of the world such as the French alkaline province (Brouse and Varet, 1966) and the Gregory Rift (Goles, 1976) the importance of intermediate magmas such as mugearites and benmoreites has been pointed out. Goles makes a special case for the petrogenesis of peralkaline salic lavas to be dependent on crystal fractionation from mugearite-benmoreite types. For Level Mountain, however, the petrographic evidence is strongly in favor of trachybasalts being a rather minor mixing derivative of the dominant basic and salic magma types.

TRACHYTES, PANTELLERITES, AND COMENDITES

Trachytes are the dominant rock type from the stratocone. In Table 5-1, P. Trachyte refers to peralkaline trachyte of pantelleric affinity and C. Trachyte refers to peralkaline trachyte of comenditic affinity. The two most common are porphyritic hypocrystalline pilotaxitic and porphyritic eutaxitic. Phenocrysts are usually zoned and rimmed or resorbed. Depending on the crystallinity of the

groundmass feldspars the textures range from orthophyric to felsophyric. The groundmass ferromagnesian minerals may be prismatic, subhedral lanceolate or poikilitic. A few outcrops of hypabyssal stocks, dikes and sills of this composition are more correctly termed peralkaline syenites and have aplitic to granophyric textures. The more holocrystalline examples contain free quartz in the groundmass.

Phenocryst types in order of abundance are alkali feldspar, plagioclase, sodic clinopyroxene, fayalitic olivine, aenigmatite, Fe-Ti oxides and rarely biotite. The occurrence of two to four phenocryst types is common in a single flow and usually this assemblage is prevalent for a sequence of flows. The alkali feldspars are the single essential phase of the trachytes. They may be euhedral or resorbed and fritted and often occur in glomeroporphyritic aggregates or fragmental plutonic textured clots with mafic phases and/or quartz, see plate 5-10. Plagioclase phenocrysts have a compositional range from oligoclase to albite and they may occur with alkali feldspars but are not essential by themselves. Iron rich olivine, in the range Fo_{35} (ferrohortonolite) to Fo_{10} fayalite, is one of the two most common ferromagnesian phenocrysts. It is usually euhedral and rimmed or altered and often in clots with feldspar, sodic pyroxene and iron titanium oxides. When altered, it commonly has rims of sodic pyroxene or riebeckite. Olivine is characteristically only a phenocryst

Plate 5-10.
Orthophyric, xenolithic pantellerite flow (25/5e)(X.P.L., 2.97x2.07mm). Cognate xenolith of plutonic textured alkali granite comprised of quartz, microcline and aegerine with an aenigmatite rim.

phase, although occasionally pure fayalite is part of the groundmass assemblage. Sodic clinopyroxene is the most common ferromagnesian mineral both as a phenocryst or part of the groundmass. Phenocrysts have optics in the range from sodic ferrohedenbergite to aegerine augite. They are usually pleochroic in shades of green. Phenocryst clinopyroxene may only be mildly sodic and be a pale clear green in plane polarized light. This type usually has a discrete rim with dusty titanomagnetite inclusions and a more acmitic composition. The other variation has an intense green colouration which dominates the high birefringence. This type (oikocryst) often has a peculiar leopard frog appearance due to the abundant rounded inclusions of titaniferous magnetite. This is probably a reaction texture where a pyroxene plus oxide assemblage is pseudomorphous after some prior ferromagnesian phenocryst phase, perhaps amphibole or garnet. While the phenocryst clinopyroxene may be fresh or altered, that of the groundmass is invariably fresh. The groundmass clinopyroxene tends to be more sodic when it is the dominant mafic of the mesostasis and is accompanied by titanomagnetite. Conversely, when the groundmass assemblage includes aenigmatite in addition to a sodic amphibole, the pyroxene is only mildly sodic and has nearly pure hedenbergite composition. Iron - titanium oxides, either ilmenite or titanomagnetite, are present as inclusions in fayalite or clinopyroxene. Titaniferous biotite was observed in a nepheline normative trachyte

(phonolite) dyke and flow of map unit 5. Aenigmatite is very prevalent as a groundmass phase, although occasionally it occurs as a phenocryst. The aenigmatite phenocrysts are euhedral and prismatic and may be the only ferroan phase or may be subsequent to sodic pyroxene. The deep red-brown pleochroism tends to mask the high birefringence (0.07). The groundmass aenigmatite may occur as subhedral prisms although subophitic or poikilitic masses are more common. A photomicrograph showing typical groundmass textures is given in plate 5-11.

The paragenesis of aenigmatite is a rather complex and controversial topic. The stability of aenigmatite has been studied experimentally by Ernst (1962), Marsh (1975), Lindsley et al (1971), and Thompson and Chisholm (1969). All of these investigations show that aenigmatite is present in a relatively restricted field in T-fO_2 space. When aenigmatite occurs as the only crystallizing ferroan silicate this can be interpreted to represent the joint conditions of peralkalinity and low fO_2. However, at Level Mountain the aenigmatite usually occurs in a mesostasis assemblage with phases that are far more oxidized such as alkali amphiboles. Usually iron-titanium oxides are absent. Since the two groundmass fractions are often only separated by tens of microns, this leads to conceptual problems in the interpretation of fO_2 conditions. Where the peralkaline trachytes are somewhat deuterically altered, a golden yellow astrophyllite may partially or wholly replace the

Plate 5-11.

(P.P.L., 0.48x0.33mm) Pilotaxitic groundmass of peralkaline trachyte (7/11). Dark green phenocryst (side of photo) and euhedral high relief prismatic green brown phase in groundmass are sodic pyroxenes. Deep reddish-black anhedral aenigmatite (centre), clear dark blue riebeickite, light pale green arfvedsonite, golden astrophyllite and clear laths and anhedra of alkali feldspar and quartz. The groundmass of these holocrystalline peralkaline trachytes is typically heterogeneous, as if there were steep diffusion gradients on a scale of a few tens of microns.

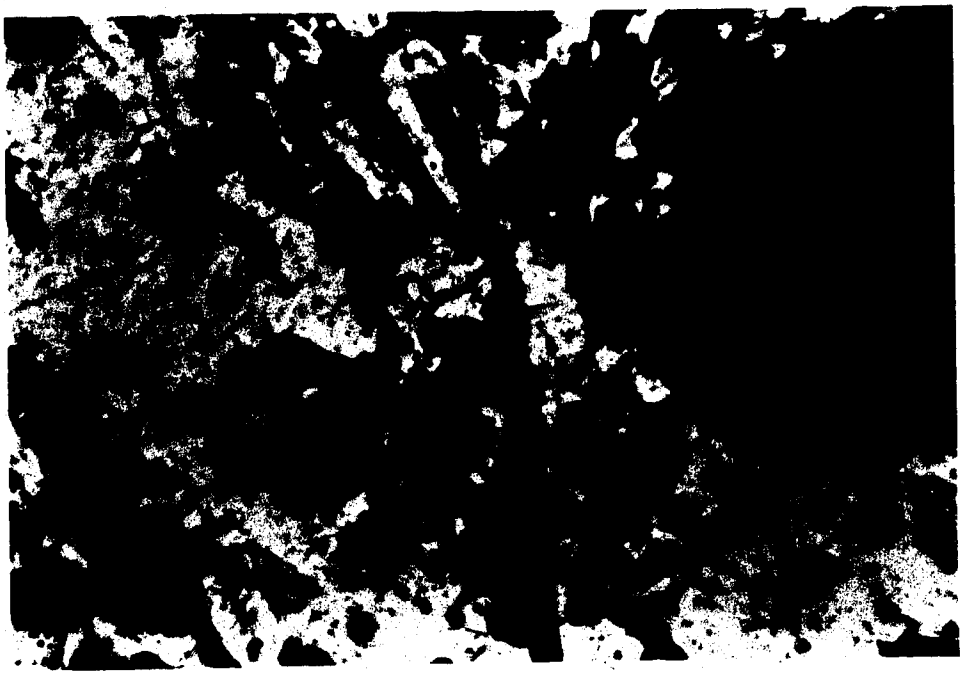

aenigmatite. The groundmass assemblage typically has two feldspars in sub-equal amounts. The plagioclase is oligoclase to albite and normally zoned. The alkali feldspar is sanidine, typically occurring as square cross sectional stubby prisms. Quartz may occur in rapikivi-type intergrowths in the eutaxitic trachytes or in the irregular spaces between feldspar laths. Possible groundmass mafic minerals include fayalite, sodic pyroxene, aenigmatite, alkali amphiboles (riebeckite, arfvedsonite), and astrophyllite. Rosenbuschite was recognized as a groundmass phase in a few flows (both by petrography and microprobe analysis). Common accessory minerals include baddeleyite or zircon. Occasionally the groundmass contained a cathodoluminescent phase with high contents of Ce and rare earths.

The pantellerites and comedites are transitional to the peralkline trachytes and are not so abundant. Owing to their similar mineralogy and chemistry these more silica rich peralkaline types are probably differentiates from the more common peralkaline trachyte magmas. Pantellerites at Level Mountain are almost exclusively holocrystalline, see photomicrograph shown in plate 5-12, while comendites occur as glassy dykes, flows, and tuffs. This situation is the converse for other peralkaline localities such as Pantelleria (Villari, 1974) or Fant-ale (Gibson, 1972, 1974) where the more strongly peralkaline pantellerites occur as pitchstones. The peralkaline eruptives of the Great Basin in

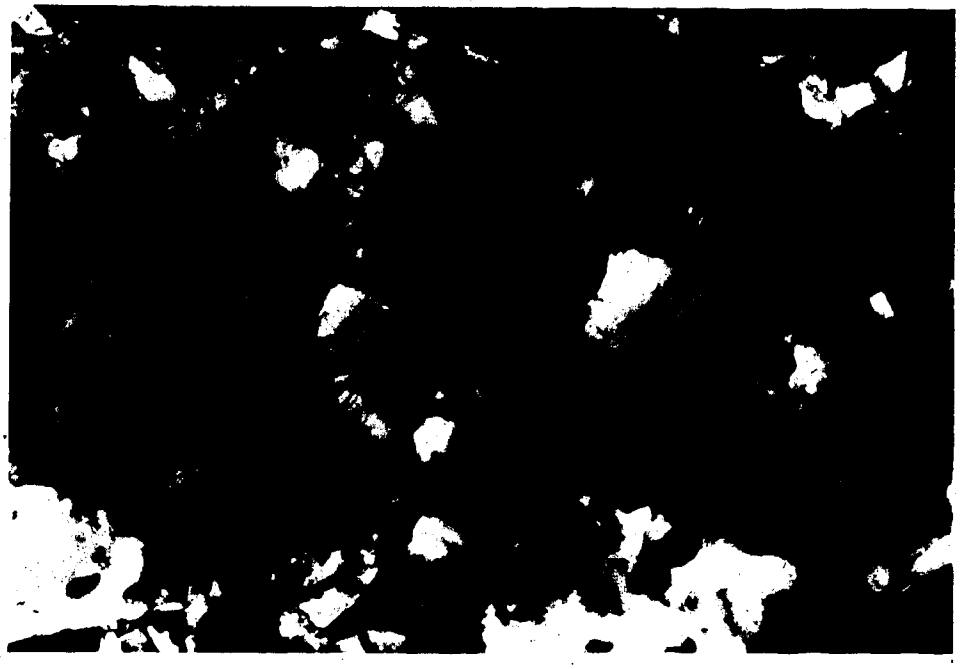

Plate 5-12.
(X.P.L., 0.60x0.42mm) Groundmass of holocrystalline pantelleritic trachyte (25/5b). White areas with sutures are quartz and microgranite. Sanidine shows straight edges or rectangular cross sections. Some riebeckite films gives quartz a bluish shade. High relief prisms with anomalous green and pink birefringence are rosenbuschite. Aenigmatite prisms are euhedral with deep reddish brown to black colouration that masks their birefringence.

the western U.S. tend to be comendite tuffs (Noble and Parker, 1974). Petrochemically the pantellerites and comendites are both peralkaline rhyolites.

Pantellerites have more than 12.5% mafic minerals in the norm. Comendites tend to have agpaitic indices very close to unity and higher quartz contents in the norm. There is a tendency for the comendites to be preferentially associated with oceanic islands and pantellerites with continental rifts. At Level Mountain the pantellerites were more coarsely crystalline, more ferromagnesian-rich counterparts of the eutaxitic trachytes. Common phenocryst assemblages were anorthoclase-aenigmatite or anorthoclase-fayalite. When fayalite occurred, it had reaction rims of riebeckite. Aenigmatite phenocrysts typically showed patchy oxidation to iron-titanium oxides. Aenigmatite and riebeckite were the most common groundmass mafics. Comendites tended to be aphyric or sparsely phenocrystic pitchstones or tuffs. The phenocryst assemblage was either anorthoclase, fayalite, and ilmenite or anorthoclase, sodic ferrohedenbergite, and ilmenite. In the few holocrystalline types there was essential groundmass quartz and opaques. The groundmass was almost entirely quartzofeldspathic with minor sodic pyroxene or riebeckite.

A summary of the typical crystallization history of these peralkaline salic magmas is given in table 5-2.

Table 5-2. Summary of Crystallization Sequences for Peralkaline Lavas

1. Fayalite + Anorthoclase on liquidus (dry)

2. Fayalite oxidizes to magnetite + SiO_2(melt) + heat (causing anorthoclase resorption)

3. Fayalite + Melt go to acmite clinopyroxene
   OR
   Soda-Iron Amphibole
   (with build up of pH_2O prior to eruption)

NOTE: Eruption may proceed after 1, 2, or 3.

4. Groundmass crystallization usually proceeds dry at low fO_2 conditions with fayalite or aenigmatite; or at locally determined fO_2 and H_2O content, due to diffusion lag and undercooling, to get aenigmatite, ferrohedenbergite, alkali amphibole.

5. With late deuteric alteration get astrophyllite.

PHONOLITES, TRISTANITES AND RHYOLITES

The relatively uncommon silica undersaturated lavas are restricted to map units 5 and 7 and the metaluminous lavas are restricted to map unit 7. Phonolites occur both as tuffs and glassy to fine-grained flows. The tuffs, usually yellow, white, or buff in appearance contained anorthoclase and sparse altered phenocrysts of analcime or sodalite. The flows were grey in appearance and relatively aphyric, with a groundmass of alkali feldspar, nepheline, opaque and glass. These rocks have normative nepheline in the range 4 to 6% with plagioclase in the oligoclase - albite range as the dominant feldspar. Petrographic examination of phonolite flows from map unit 5 in the Meszah Peak section revealed phenocryst amphibole and biotite. The phonolites could represent some fractional derivative of the more common basic undersaturated melts, such as alkali basalt and hawaiite, or could be a product of magma mixing of basalt and trachyte (particularly for the tuffaceous varieties which contain xenocryst clinopyroxene and plagioclase derived from basalt). Similar phonolites have been reported from alkaline centres such as St.Helena (Baker, 1969), the Auvergne (Varet, 1969), the Canary Islands (Tenerife) (Ridley, 1970), and the Azores (White, 1979). A review of the origin of phonolite lavas is given by Wright (1971).

Tristanite occurred as flows and dykes. Both quartz and nepheline normative varieties were noted as well as metaluminous and peraluminous types. The texture is

glomeroporphyritic pilotaxitic hypohyaline. The phenocryst assemblage includes andesine, anorthoclase, chrome diopside (confirmed by microprobe), basaltic hornblende, biotite, and titanomagnetite. The groundmass always shows a high degree of deuteric alteration. A xenolith of gneiss was found in one dyke, so the metaluminous nature may be in part due to crustal assimilation by a more typical trachytic melt. The low agpaitic index is not the only petrological peculiarity of the tristanites. These flows and dykes are markedly potassic which contrasts with the remainder of the salic rocks (sodic). The high water content could be inherent, as indicated by the hydrous phenocryst amphibole and mica. The length and spatial distribution of the tristanite dykes suggests that they could be related to high level volcano-tectonic features as previously discussed. These tristanite magmas undoubtedly have a complex genesis, perhaps as a mantle derived trachyte melt they suffered some high level crustal contamination, yet were able to retain early phenocrysts from depth. It does not seem satisfactory to derive the tristanites by crystal fractionation processes or by contamination of hawaiites or trachytes.

Rhyolites are mildly metaluminous and usually contain only phenocryst alkali feldspar and magnetite. Pyroclastics and glassy varieties are more common than any other salic lava type. Rhyolites find their greatest distribution along with minor occurrences of calc alkaline dacite during the period of unit 7. The rhyolite flows show extensive

hydrothermal alteration and occasionally sulfide mineralization. The rocks are usually fine grained and both devitrified glass or aplitic textures are common. One glassy comendite dyke has a fresh core, yet the hydrothermally altered white selvedges were rhyolite, see photomicrograph shown in plate 5-13. The rhyolites as flows and tuffs are often closely associated with comendites. For the most part these lavas and tuffs probably were comendites that have lost their slight peralkalinity through crystallization or alteration reactions as discussed by Noble (1967). The remainder are probably the composite offspring of trachyte differentiation and high level contamination.

INCLUSIONS: OCCURRENCE AND PETROGRAPHIC CHARACTERISTICS

The majority of lava flows on Level Mountain, irrespective of chemical type, are aphyric to fine-grained and relatively free of phenocrysts. It is reasonable to assume that these fine grained flows have been extruded at or near their liquidus temperatures. Ocasionally inclusions of both cognate and xenolithic character have been observed for a variety of Level Mountain lavas. Their distribution is rather widespread but their actual occurrence is certainly the exception rather than the rule. Where they are found, with the exception of one rhyolite vent area, they never comprise more than a few percent by volume of the host lava. A summary of petrography and modes for inclusions is given in Table 5-3. Plate 5-14 shows a photograph of some of the

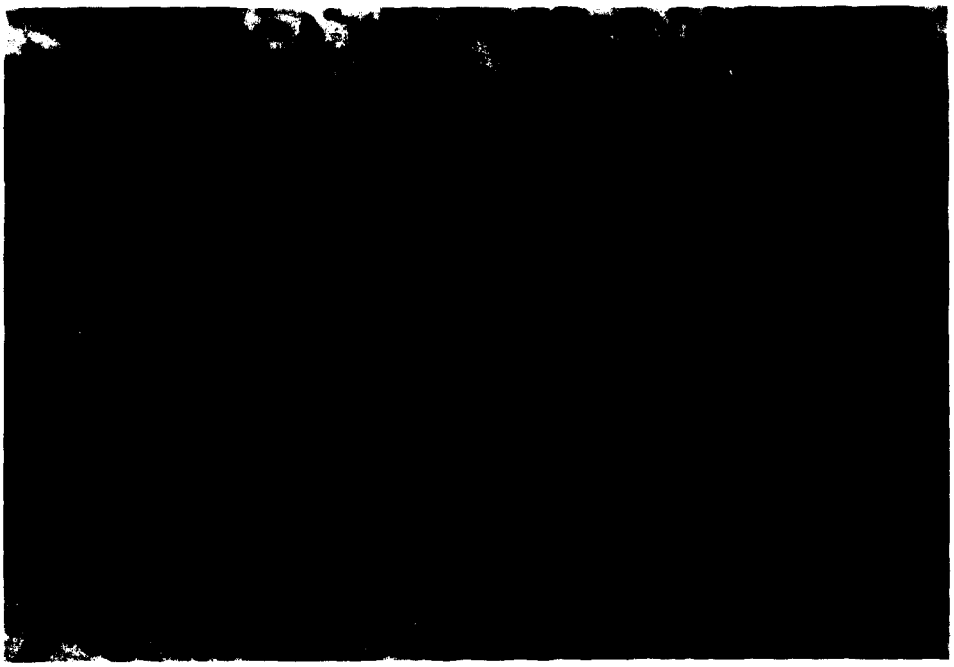

Plate 5-13.
(P.P.L., 0.78x0.55mm) Petrographically this dyke selvedge (LMI3) is a comendite, with white euhedral alkali feldspar, white anhedral quartz, patches of inky blue riebeckite and green arfvedsonite with a few percent pale tan devitrified glass. Chemically however this is a rhyolite.

Table 5-3 Petrography and Modes of Selected Inclusions from Level Mountain Lavas

Sample # Classification Host Flow Map Unit	TCL 1004-41 Lherzolite Alkali Basalt Stikine River	8/31-85 Peridotite Basalt Dyke Egnell Creek	MPM Troctolite/Gabbro 8/25-50/6397 Hawaiite 8	8/6-12 n Eucrite 8/6-12/5290 C. Trachyte 5a	8/14-39 n Scarn 8/14-39 P.Trachyte 6	8.16-44] Gneiss 8/16-44/6250 Tristanite dyke 7c
Phenocrysts	56% Ol (Fo 89) 9% Opx (En 89) 29% Cpx (Chrome-Diopside) 4% Spinel 1% Sulfide (Py 64 Pn 36) 1% Plagioclase (An 55)	62% Diopside 21% Olivine 3% Spinel 14% Plag	36% Fo 84 43% An 92 18% Brown augite 3% Opaque	5% Olivine (Fo 95) 20% Diopside 10% Amphibole 37% Plagioclase (An 95) 4% Opaque 16% Nepheline 8% Phlogopite	40% Epidote 55% Calcite 5% Magnetite	16% Plagioclase (An 27) 46% Microcline 31% Quartz 2% Amphibole 5% Opaque
Description	Oval 3 cm long. Equigranular. Spinel lherzolite with some shear along grain boundaries. Minor interstitial plagioclase, Fe-Ni sulfide and sphene. No melting or reaction textures.	Interlocking brownish green diopside with included forsteritic olivine (rounded) and anorthitic plagioclase. Brown spinels occur as inclusions in olivine.	Rounded nodules. Plutonic equigranular. Crystals to 0.5 cm. H_2O/CO_2 fluid inclusions in olivine. Olivines are rounded inclusions in plagioclase Augite. Augites show shattered planar shear features within crystals. Plagioclase anhedral unzoned with interlocking texture. Opaques are ilmenite with magnesioferrite exolved.	Armored yellow weathering irregular nodules. Pale green diopside which may contain Forsteritic olivine and Anhedral opaques. Green amphibole overgrowths on enhedral diopside. Anhedral plagioclase is sausseritized. Feldspathoid and mica appear to be of a later genesis. Apatite needles common.	Radial porphyroblasts of green epidote to 5 cm in irregular polycrystalline calcite.	Angular fragments of fine grained felsic gneiss. Altered amphibole and oxides in isolated layers. No sign of melting or reaction.

inclusion types.

Megacrysts, cumulophyric aggregates, clots ad intergrowths comprise the cognate types. In flows and dykes of alkali basalt and hawaiite, single plagioclase and pyroxene megacrysts were found that exceed five centimeters in size. The most typical example is an egg-shaped plagioclase - pyroxene intergrowth which has coarse grain size, interlocking plutonic texture, and a rounded shape with a size ranging from 2.5 to 8 centimeters. These vary from dominantly plagioclase to dominantly pyroxene. The pyroxene is usually black and of vitreous appearance with conchoidal fracture more frequently seen than cleavage. It is easily mistaken for basaltic glass. The density of these plagioclase - pyroxene inclusions varies from 2.64 to 3.24 grams per cubic centimeter which covers the range from neutral buoyancy to approximately 20% greater than their host basalts. The peralkaline trachyte flows of map units 5a and 6a occasionally contain lithophysae or cognate clots of alkali feldspar and sodic pyroxene with a very open texture and acicular intersertal crystals of alkali amphibole. The texture of these clots is usually diktytaxitic with actual voids between crystal faces. While the plagioclase-pyroxene eggs of the basalts might be plutonic autoliths or even accidentally incorporated fragments of the source region, the open trachytic clots are obviously of a high level origin. The voids and automorphic crystal shapes are probably indicative of crystallization in the presence of a

Plate 5-14.

Hand specimens of inclusions: top left, partially melted and disaggregated granite gneiss (light coloured) in dark hawaiite; top right, calc silicate nodule from trachyte host, with crystalloblastic calcite and epidote; centre left, granitic gneiss in vesicular tristanite, no reaction; centre, granitic gneiss (no melting) in hawaiite; right centre, embayed eucrite nodule with yellow-weathering,glassy-devitrified rim from a peralkaline trachyte flow; bottom, partially melted embayed and dissagregated granitic gneiss (white) in hawaiite(dark).

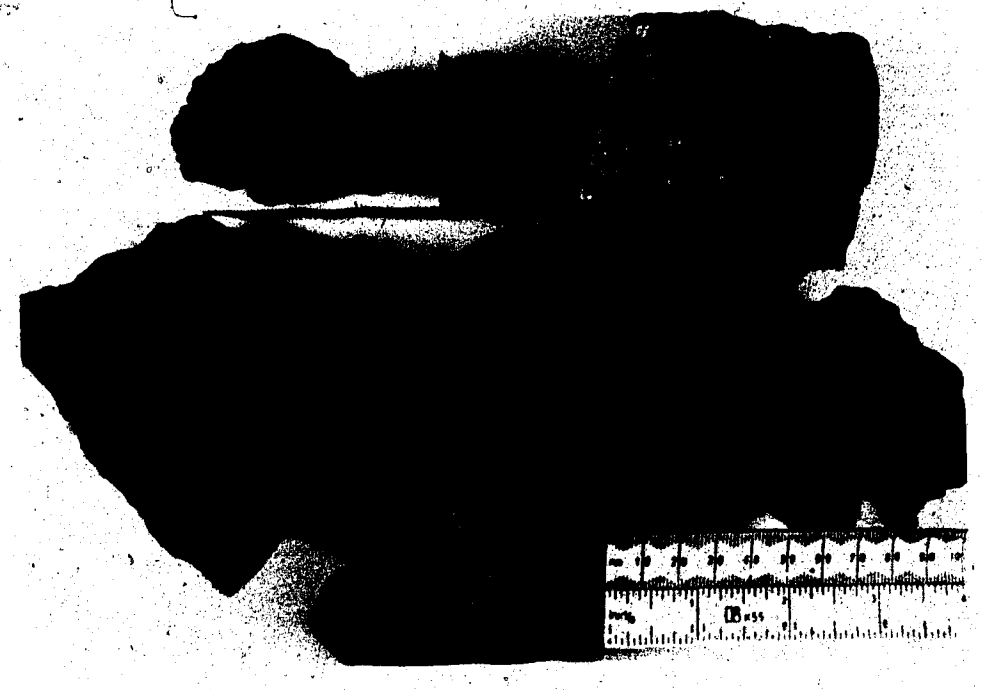

separate gas phase and reduced pressure.

The occurrence of incontrovertibly foreign inclusions has been used to indicate upper mantle origins of lavas and to estimate the compositional variation of the upper mantle (Sobolev, 1977). At Level Mountain the occurrence of foreign inclusions in fluid lavas is restricted to three petrochemical types: basalts, peralkaline trachytes and tristanites. The Hawaiites of map units 8-10 on Meszah Peak contain xenoliths of anorthosite, gabbro, and troctolite (allivalite), see photo in plate 5-15, as well as partially fused and quenched fragments of granite gneiss, see photo in plate 5-16. Both basalts and peralkaline trachytes have been found to contain alkaline ultramafic inclusions having diopside and spinel as the dominant phases with variable amounts of olivine, amphibole and feldspathoids, see plate 5-17. One dyke in the Egnell Canyon had xenoliths of augite peridotite. An altered ankaramite flow of map unit 5b, in the Kakuchuya Valley, was found to contain xenoliths of garnet wehrlite (cpx, ol, gt, and sp). Contemporaneous basalts from the Stikine Canyon and Castle Rock occasionally contain lherzolite nodules (Littlejohn and Greenwood, 1974). Deformation lamellae and kink bands in the olivine and pyroxene crystals of these ultramafic xenoliths may either be the result of explosive shock upon eruption (J. Krupica, pers.comm.) or deformation in the source region.

Inclusions of diorite and hornfelsic sediments were found in an alkali basalt flow of the Upper Plateau, unit 4,

Plate 5-15.
(X.P.L., 2.97x2.07mm)Plutonic textured troctolite (Allivalite) xenolith (MPM) sampled from hawaiite flow on Meszah Peak. Twinned plagioclase dominates with euhedral to subhedral olivine and diopside, note fractures in all grains.

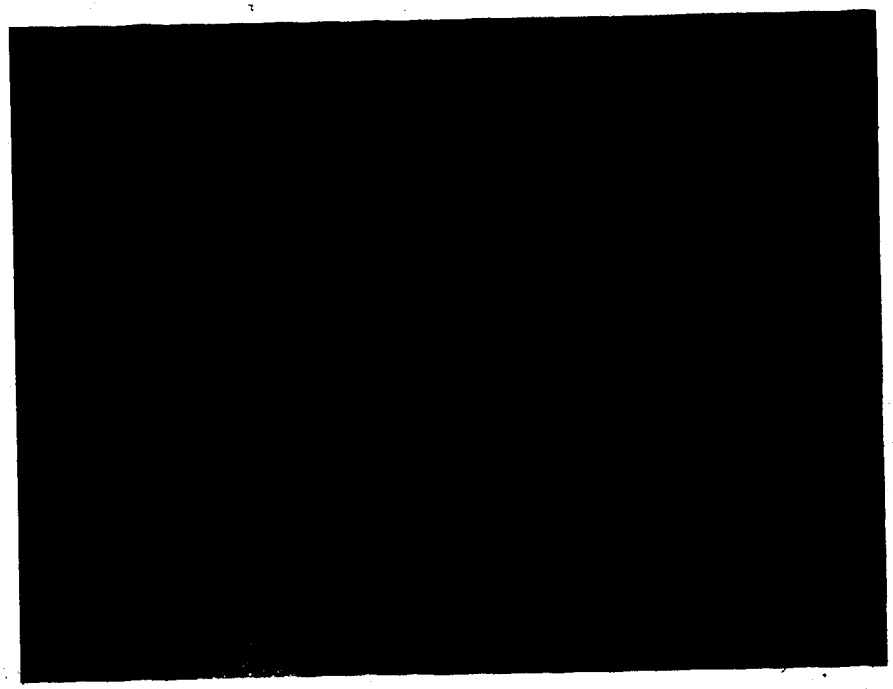

Plate 5-16.
(X.P.L., 2.97x2.07mm) Partially fused granitic gneiss fragment from hawaiite on Meszah Peak. Showing grain boundary reaction and interstitial rapikivi texture for quenched partial melts, seen as white and dark areas of quartz and feldspar intergrowths. Mineralogy includes plagioclase, alkali feldspar, quartz, biotite and glass.

Plate 5-17.
(P.P.L., 2.97x2.07mm) Alkali peridotite (8/31-85), with granular metamorphic-textured green diopside, fractured high-relief olivine, with overgrowths of tan to brown anhedral hornblende showing good amphibole cleavage, black anhedral spinel, saussuritized yellow and white low relief plagioclase and clear-granular patches of nepheline.

in the canyon of the Little Tahltan River. Granite inclusions from basalts at Mezsah Peak show petrographic evidence of partial melting, reaction and quench textures. Armoured ultramafic nodules were noted at three separate locations in peralkaline trachyte flows: in unit 6a on the east end of Wolf Bones Ridge, on the Dudidontu dome and on the ridge that separates the Dudidontu and Kakuchuya valleys. The nodules characteristically were about 1cm in size and rounded with a yellowish reaction rim up to 2cm in thickness. The texture was coarse grained and idiomorphic. The mineralogy was dominantly anorthitic plagioclase and brown titaniferous augite with inclusions of forsteritic olivine, brown apatite, opaques, amphibole, mica and accessory interstitial nepheline, see plate 5-18. These nodules are both alkaline and ultramafic having a composition intermediate between eucrite and essexite. It is uncertain whether these nodules are representative of source material, a fractionated source residua, or a reaction product. However their peculiar mineralogy, texture, and reaction rims rule them out as fractionates from the trachyte magma. The most abundant inclusions in the trachytes are phenocryst or xenocryst clots of alkali feldspar, with or without oligoclase and quartz. These frequently have sutured internal boundaries, resorption outlines and alkali-rich rims, all of which may be an indication that they are partially assimilated crust.

Plate 5-18.
(X.P.L., 2.97x2.07mm) Eucrite/essexite (8/6-12n) from peralkaline trachyte flow. Interlocking plutonic texture with twinned cleaved brown augite, light and dark grey feldspathoid, brown mica and black magnetite.

Although the inclusions are not volumetrically abundant at Level Mountain, they represent quite a variety of lithologies. They are associated with several magma types and the age of the flows that carry inclusions spans most of Level Mountain's history. Petrogenetically the inclusions indicate three things. Ultramafic nodules such as lherzolite, peridotite, wehrlite, troctolite, anorthosite, and eucrite-essexite are usually interpreted as being part of the Upper Mantle (Varne, 1970; Basu and MacGregor, 1979; Mercier and Nicolas, 1975). They are common inclusion types in alkalic magmas and the variety of inclusions in alkalic lavas is one of their hallmarks. That these occur in the Level Mountain basalts and peralkaline trachytes, in addition to other lavas of the Intermontane Belt, indicates a mantle source for these magmas.

The accidental inclusions of older crytalline rocks such as diorite, granite, and gneiss indicates the possibilities of crustal magma chambers and some crustal contamination to the primary alkalic magmas. These foreign rocks as well as hornfelsed sediments are found both in basalts and also in the low volume, late occurring, metaluminous types such as tristanite and rhyolite. A small degree of crustal contamination would likely have very different effects on basic and salic magmas dependent upon which phase(s) were on the liquidus. In a mildly nephelinitic alkali basalt, Si-Al contamination could enhance the crystallization of calcic plagioclase and

possibly make the magma hypersthene- or quartz-normative. While in the case of a comendite melt, the same Si-Al contamination could cause the magma to become metaluminous.

Many of the inclusions are clearly of a different texture but of sufficient chemical affinity to term them cognate. Into this class fall the pyroxene-plagioclase clots, the alkali gabbros and possibly the essexite - eucrite inclusions. These cognate types allude to a complex plutonic history in addition to the already complex surficial manifestations of volcanism.

SUMMARY OF PETROGRAPHY AND PETROGENESIS

The basaltic lavas are of alkaline affinity and mineralogically similar to the alkaline olivine basalt and sodic basalt types. The dominant phenocryst minerals which are likely candidates for low pressure crystal fractionation arguments include forsteritic olivine, calcic plagioclase and calcic pyroxene. The ankaramites and alkali basalts could be related by variable olivine and clinopyroxene fractionation or accumulation. Fractionation of olivine, clinopyroxene and plagioclase could explain the derivation of hawaiite from an alkali basalt primary melt. However, the complex zonation and reaction textures of the hawaiite phenocrysts suggest that the actual petrological processes may be more complex. The pronounced zonation and great variability of the plagioclase phenocrysts may partially account for the existence of both nepheline and hypersthene

normative compositions. Where calcic plagioclase and olivine are the dominant fractionating phases, a nepheline-normative hawaiite could result as has been demonstrated experimentally by Yoder and Tilley (1962). Variation in the composition of the fractionating plagioclase, plus the effect of clinopyroxene, could cause the trend for silica enrichment to dominate, producing the hypersthenic type. Due to the occurrence of xenoliths and xenocrysts, simple fractionating arguments should not be expected to account for all of the observed mineralogical or petrochemical variation.

The peralkaline trachytes and the more silica-saturated pantellerites and comendites seem to fall into two groups characterized by different phenocryst assemblages. Alkali feldspar and iron titanium oxide are ubiquitous phenocryst phases. Sodic palgioclase may be ancillary to anorthoclase but it has not been observed alone. Fayalitic olivine and sodic clinopyroxene are the dominant mafic types. Usually they do not occur together. When they do, the fayalite is in a reaction relationship with the liquid, while the pyroxene is not. Fractionation of alkali feldspar plus iron titanium oxide plus a mafic silicate would tend to lower the colour index and raise the peralkalinity. When the dominant mafic is fayalitic olivine, residual calcium would remain and the Na/K ratio would tend to be enhanced. The effect of this could perhaps be seen as a more calcic groundmass plagioclase with the occurrence of calcic groundmass mafics

such as clinopyroxene or amphiboles. If the dominant mafic was a sodic pyroxene, the more effective calcium removal would lead to the crystallization of groundmass aenigmatite. The effect of having two sodium bearing fractionating phases could enhance the subsequent role of potassium. In this case, the proportion of groundmass sanidine would likely be higher, and the groundmass plagioclase would likely be more sodic.

The derivation of the low volume intermediate magma types in the trachybasalt-mugearite-benmoreite range probably involves magma mixing. Phenocryst types, usually characteristic of either the basic or salic lavas, are sometimes found together in these disequilibrium textured lavas. Inclusions of one type of melt in the other have been observed in both senses. One flow from the central range was a mixture of basaltic and trachytic lava. In this instance eruption occured too swiftly for intimate admixture to result.

CHAPTER 6. CHEMICAL MINERALOGY OF THE LEVEL MOUNTAIN LAVAS

OVERVIEW OF THE MAJOR MINERAL GROUPS AND MICROPROBE ANALYSIS

All mineral analyses were performed on the University of Alberta ARL electron microprobe fitted with an Ortec system for energy dispersive analysis. Using the energy dispersive facility, a qualitative identification of component mineral phases and their constituent elements was made for over two hundred representative lavas. In a reconnaissance sense, the variations in major and minor element contents were compared for all mineral assemblages. Using anhydrous mineral standards and four hundred second counting times, over ninety quantitative analyses were produced for the major rock forming minerals and a few of the accessory phases. The method of data reduction was that of Smith and Gold (1979). All data were collected and interpreted quantitatively for twenty-one elements: Na, Mg, Al, Si, P, S, Cl, K, Ca, Sc, Ti, V, Cr, Mn, Fe, Co, Ni, Cu, Zn, plus Zr, and Ba. This list of elements covers the range of atomic numbers eleven through thirty plus forty and fifty-six. The wavelength dispersive crystal spectrometers were routinely used to verify the presence of minor elements and elements not on the list. Additionally, the output of the wavelength spectrometers were used in reconnaissance to examine the distribution of minor and trace elements and to examine the sense of chemical zonation. Oxygen, which is the most abundant mineral forming element, cannot be

quantitatively analysed by present energy or wavelength dispersive techniques and was calculated by difference. In an analysis expressed as element weight percent, the difference between the reported oxygen value and the theoretical amount of oxygen which would be associated with the metals in their appropriate valences is a measure of the reliability of the analysis.

In the following sections on systematic mineralogy the tables are arranged by mineral type and presented as element weight percent, as advocated by Pinsent and Smith (1975), and structural formulae calculated on the basis of n oxygens. There are several justifications for presenting mineral compositions from microprobe analyses as element weight percent, rather than as equivalent oxides. The first lies in the iterative form of the ZAF correction procedure for probe analyses, with direct comparison of element counts for standards and samples. Since oxygen is not directly analysed, or compared between sample and standards, it is the least reliable element and should not be convolved with the other elements. Inclusion of oxygen results in the spreading out of any error in totals or error in the fit to average atomic number. The compositional variations for most minerals of interest involve substitution of different metals into specific coordination sites within an oxygen framework. The parameter of importance in mineral geothermometry is the variation in a specific element, not its oxide, and that element's concentration (activity) into

specific coordination sites. The expression of mineral analyses as weight percent oxides is a carryover from the days of gravimetric analyses. Analyses in this form must always be recalculated before they can be used for thermochemical or petrogenetic arguments. The structure formula calculation was iterative with partition of iron to satisfy charge balance and stoichiometry. The sample numbers refer to rocks. The approximate rock type is given for ready comparison. Each mineral section closes with a comparison of analysed compositions to mineral compositions predicted by normative calculations on the host lavas, along with discussions of the relevant petrogenetic roles of the mineral.

OLIVINES

Representative olivine analyses are given in Table 6-1. Olivine compositions range from nearly pure forsterite (Mg_2SiO_4) to pure fayalite (Fe_2SiO_4) with greater than 97% of the compositional variation occurring in this two-component solid solution series. Minor element contents always include calcium and manganese in subequal amounts such that 1 to 2% molecular glaucochroite ($CaMnSiO_4$) is present in all structural formulae. In the hortonolite-ferrohortonolite range, molecular manganese exceeds calcium such that molecular tephroite (Mn_2SiO_4) must be present. A component of molecular monticellite may be present in the chrysolite-hyalosiderite compositions but is

Table 6-1 Microprobe Analyses of Olivines

Sample #	1	2	3	4	5	6	7	8	9	10	11	12	13	14	15	16	17	18	19
Si	18.8	18.6	18.5	18.3	18.5	18.0	17.7	17.6	17.4	16.1	16.1	15.5	16.0	16.3	16.0	15.7	16.0	14.9	15.1
Al	0.1	.2	0.1	.1	.1	.1	.2	.2	.6	.1	.1	.1	.2	.1	.1	.1	.1	.1	.1
Fe	12.9	13.4	16.5	17.7	20.6	21.3	26.8	27.5	25.8	28.9	28.2	31.1	38.2	37.6	36.3	41.4	40.0	42.2	44.8
Mn	0.2	.2	.2	.2	.2	.3	.3	.5	.3	.5	.6	.7	.7	1.1	1.3	1.2	1.1	1.4	2.1
Mg	27.3	25.8	25.2	24.3	23.0	22.3	18.6	17.9	16.2	15.1	14.9	12.7	11.8	11.6	10.8	9.3	9.7	6.0	5.2
Ca	0.2	.2	0.2	.2	.2	.3	.2	.3	.4	.3	.3	.3	.3	.3	.3	.4	.7	.4	.4
Ni	0.3	.2	.1	.1	.2	.2	.1	.1	.1	-	.1	.1	-	.1	-	-	-	-	-
Na	0.2	-	.4	.1	-	.1	-	-	-	.2	.2	.1	.3	.2	-	.4	.3	-	-
O	40.2	41.4	39.1	39.0	37.1	37.4	35.9	35.9	39.0	39.7	39.7	39.3	32.3	33.0	35.1	31.4	31.9	34.9	32.2

Structural Formulae as Cations per 4 Oxygens, Iron Oxidation Assigned by Stoichiometry, Sodium Ignored

Si^{4+}	.987	1.003	.987	.986	.992	.981	.994	.997	1.022	1.002	1.001	.997	.969	.992	1.002	.976	.994	1.007	1.001
Al^{3+}	.004	.001	.005	.004	.005	.008	.011	.009	.041	.003	.006	.007	.011	.004	.007	.008	.007	.006	.008
Fe^{3+}	.014	-	-	.024	-	.029	.001	-	-	-	-	-	.047	-	-	.039	-	-	-
Mg^{2+}	1.654	1.608	1.558	1.514	1.426	1.402	1.209	1.176	1.102	1.087	1.072	.942	.829	.815	.786	.668	.699	.468	.400
Fe^{2+}	.327	.365	.443	.457	.545	.556	.760	.784	.763	.874	.882	1.0083	1.120	1.150	1.143	1.254	1.255	1.435	1.496
Mn^{2+}	.004	.004	.006	.006	.007	.007	.010	.016	.010	.016	.018	.022	.024	.033	.041	.038	.033	.049	.070
Ca^{2+}	.008	.008	.004	.008	.007	.013	.009	.010	.015	.013	.011	.014	.009	.011	.011	.017	.014	.021	.018
Ni^{2+}	.006	.005	.003	.003	.004	.004	.003	.002	.001	-	.002	.002	-	.002	-	-	-	.002	-
Fo %	82.5	81.1	77.9	75.9	72.4	70.2	61.4	60.0	59.1	55.4	54.9	48.3	41.6	41.5	40.7	34.1	33.4	24.6	21.1

Key to Sample Numbers

1. PAR phenocryst from alkali basalt flow, unit 2, Little Tahltan River.
2. 8/20-2/4307 core (#9-rim) of zoned olivine phenocryst, hawaiite flow, unit 4, Little Tahltan River.
3. PAO phenocryst or xenocryst embayed and partially altered to iddingsite from altered alkali basalt flow, unit 3, Little Tahltan River.
4. PAX phenocryst from transitional alkali basalt-hawaiite flow, unit 1, Little Tahltan River.
5. 8/25-50/6397 phenocryst, transitional hawaiite-alkali basalt flow, unit 8, Meszah Peak.
6. PAO unzoned microphenocryst, altered alkali basalt flow, unit 3, Little Tahltan River.
7. 8/23-7/3940 phenocryst alkali basalt flow, unit 3, Little Tahltan River.
8. 8/25-50/6397 groundmass, transitional hawaiite-alkali basalt flow, unit 8, Meszah Peak.
9. 8/20-2/4307 run (#2=core) of zoned olivine phenocryst, hawaiite flow, unit 4, Little Tahltan River.
10. PAF phenocryst or xenocryst olivine in hawaiite flow, unit 4, Little Tahltan River.
11. PAC groundmass olivine from hawaiite flow, unit 4, Little Tahltan River.
12. PAF microphenocryst olivine in cumulophyric aggregate with titanomagnetite and apatite from hawaiite flow, unit 4, Little Tahltan River.
13. PBX microphenocryst from Ne hawaiite, unit 5b, Kakuchuya Valley.
14. PBO microphenocryst from transitional benmoreite trachyte, unit 4b, S.face, Meszah Peak.
15. 8/30-82/6150 phenocryst from comenditic trachyte, unit 6a, Badger Brook.
16. PBP microphenocryst from transitional benmoreite-trachyte, unit 7b, S.face, Meszah Peak.
17. PBP microphenocryst from transitional benmoreite-trachyte, unit 7b, S.face, Meszah Peak.
18. 8/7-19/5830 microphenocryst from comenditic trachyte, unit 6a, Wolf Bones ridge.
19. 8/26-56/6336 phenocryst from trachyte, unit 7a, south foot of Meszah Peak.

not essential.

Phenocryst olivine for the entire range of Level Mountain lavas is in the chrysolite-ferrohortonolite range. More forsteritic olivines occasionally occur in basalts as phenocrysts and in ultramafic nodules. Compositions near pure fayalite are restricted to the groundmass of peralkaline salic lavas and alkaline syenite sills. Their presence here is considered to be the combined result of a peculiar crystallization history and restricted conditions of fO_2 imposed by the composition and physical conditions of groundmass crystallization. Olivines, when present, are usually the most magnesian phenocryst mineral in a given lava or paragenesis. In terms of major and trace element variation trends, olivine fractionation should have pronounced effects on Mg, Mn and ni.

The microprobe analyses and estimates of olivine compositions compare favorably with petrographic determinations. The detailed comparison of actual olivine chemistry to norm calculations reveals several surprises. Normative olivine chemistry for nodules and basalts is usually reasonable and within 10% mol Fo. However while olivine phenocrysts are very common in the basalts, the chemical analyses of the basalts may be hypersthene or quartz normative (depending on the iron oxidation state). In this case pyroxenes are calculated instead of olivines. The comparison of olivine to whole rock chemistry and norms for salic lavas is very poor. While actual fayalitic olivine

exists as phenocrysts, microphenocrysts, or in the groundmass of salic lavas their norms show iron in oxides, acmite, ferrosilite, or hedenbergite.

CLINOPYROXENES

Clinopyroxenes, although not universally present, are the most widespread of the ferromagnesian minerals in Level Mountain lavas. Diopside and titaniferous augite dominate the basalts, while salic and intermediate lavas have ferroaugite-ferrosalite-ferrohedenbergite types. A collection of selected clinopyroxene analyses is presented in Table 6-2. The elements Ca, Mg and Fe account for greater than 94% of the X and Y site positions. The remainder are predominantly accounted for by Al, Ti, Na, and Mn. The distribution of the Level Mountain clinopyroxenes and their corresponding whole rocks is presented for the system Wo-En-Fs in Figure 6-1. The range of compositions covers: 40.3-45.5 Wo, 24.6-44.5 En, 11.9-34.1 Fs, all expressed as mol%. The clinopyroxene compositional variation is close to the diopside-hedenbergite join when represented in the tetrahedron diopside - hedenbergite - acmite - johannsenite. There is no good correlation between the normative diopside component and the actual Diopside content of pyroxenes in the rock.

Sodium and the acmite component are always more abundant than Mn and the johannsennite component for the entire range of compositions. Other elements which may be

Table 6-2 Microprobe Analyses of Clinopyroxenes

Sample #	1	2	3	4	5	6	7	8	9	10	11	12
Si	24.1	24.3	24.9	23.5	23.2	24.2	22.3	24.1	24.0	23.5	24.9	21.0
Ti	.7	.7	.3	.9	1.3	.7	1.1	.4	.3	.4	1.5	1.1
Al	1.5	1.4	.7	3.2	1.7	.8	1.6	1.1	.5	.8	.2	2.7
Cr	.2	.3	-	.2	-	-	-	-	-	-	-	.0
Fe	5.8	6.0	11.9	7.3	9.3	9.2	7.8	10.9	12.4	14.8	20.6	6.0
Mg	9.4	9.3	7.2	8.7	8.2	8.2	6.9	7.0	5.8	4.9	Zr 1.4	2.6
Mn	.1	.1	.6	.1	.2	.2	.2	.5	.7	.7	.3	.1
Ca	15.1	15.3	14.4	13.5	13.6	14.5	14.1	13.7	14.8	13.3	1.1	14.8
Na	.3	.4	.5	.4	.5	.4	.5	.4	-	.4	9.1	-
O	42.8	42.3	39.6	42.2	42.0	41.7	45.0	41.9	41.4	41.2	40.8	51.6

Formulae as cations per 6 oxygens

Si^{4+}	1.894	1.894	1.953	1.834	1.851	1.924	1.894	1.951	1.982	1.965		
Al^{3+}	.123	.115	.057	.258	.137	.067	.144	.089	.044	.066		
Ti^{4+}	.031	.033	.014	.041	.063	.033	.057	.021	.014	.019		
Fe^{3+}	.041	.051	.045	.078	.075	.059	.003	.018	-	.012		
Cr^{3+}	.011	.015	-	.006	-	-	-	-	-	-		
Mg^{2+}	.849	.834	.653	.789	.756	.751	.673	.659	.547	.475		
Fe^{2+}	.186	.183	.425	.264	.300	.307	.330	.425	.514	.608		
Mn^{2+}	.003	.003	.023	.005	.007	.010	.008	.019	.028	.030		
Ca^{2+}	.831	.834	.789	.740	.763	.809	.841	.776	.853	.779		
Na^{+}	.027	.037	.045	.038	.045	.040	.050	.043	-	.044		
Mg	44.5	43.8	33.8	43.3	39.8	38.8	36.3	34.7	28.2	25.0	0.0	18.0
Fe	12.0	12.4	25.5	16.0	20.1	19.4	18.4	24.4	27.9	34.1	93.3	18.6
Ca	43.5	43.8	40.8	40.6	40.1	41.8	45.3	40.9	43.9	40.9	6.7	63.4
Di	79.7	78.8	78.2	70.5	68.2	67.8	63.2	56.6	50.3	40.6	1.5	16.1
Hd	17.5	17.4	12.1	25.7	27.1	27.7	31.4	38.1	47.2	53.1	5.9	43.1
Ac	2.5	3.5	5.4	3.4	4.1	3.6	4.7	3.7	0.0	3.8	90.9	39.9 Cats
Jo	0.3	0.3	4.3	0.4	0.6	0.9	0.7	1.6	2.5	2.6	1.7	0.8

Key to Sample Numbers

1. PAR Titaniferous augite from alkali basalt flow, unit 2, Little Tahltan River.
2. PAO augite phenocryst from alkali basalt flow, unit 3, Little Tahltan River.
3. PBO Green augite phenocryst from transitional benmoreite-trachyte, unit 7b, S.face Meszah Pk.
4. 8/25-50/6397 phenocryst diopsidic augite, transitional hawaiite-alkali basalt flow, unit 8, W.shoulder, Meszah Pk.
5. PAX titaniferous augite phenocryst from transitional alkali basalt-hawaiite flow, unit 1, Little Tahltan River.
6. PBX Microphenocryst from Ne hawaiite, unit 5b, Kakuchuya Valley.
7. PAF Microphenocryst or groundmass augite from hawaiite flow, unit 4, Little Tahltan River.
8. 8/30-83/6150 phenocryst augite from comendite trachyte flow, unit 6a, Badger Brook.
9. PBY phenocryst bustamitic augite from alkaline trachyte flow, unit 6a, Badger Brook, Na in spectrum, lost in reduction.
10. 8/26-56/6336 phenocryst augite from trachyte, unit 7a, S.foot, Meszah Pk.
11. 9/5-107/6600 phenocryst acmitic pyroxene with micro inclusions of apatite and elpidite from comenditic pitchstone flow, 7b, east Meszah Pk.
12. 8/16-44/6250E Al-Cr-Ti augite enhedral microphenocryst from tristanite dyke, unit 7, central chain.

Figure 6-1.
Level Mountain lavas and clinopyroxenes in the pyroxene trapezoid (Wo:En:Fs) (atomic ratio).

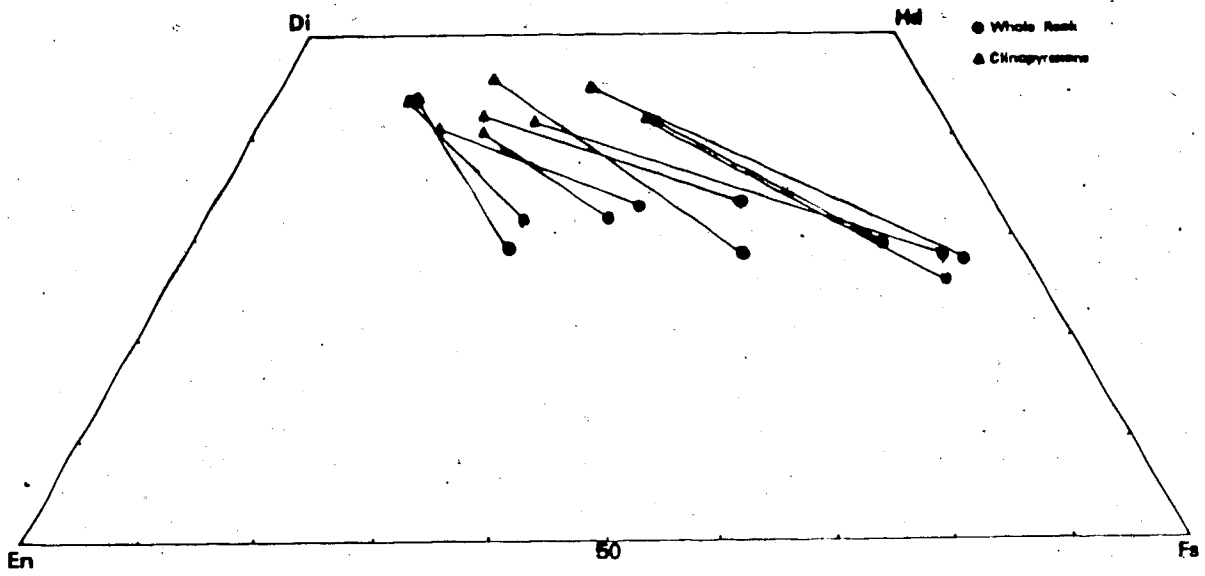

present include Al, Ti, Cr and ferric iron. Atomic aluminum exceeds titanium for all clinopyroxenes. The most titanium rich phase is always an oxide; however, the effect of clinopyroxene fractionation on titanium variation cannot be ignored. All phenocryst clinopyroxenes have more atomic aluminum than sodium, so clinopyroxene fractionation will cause an increase in the agpaitic index and the tendency towards peralkaline residua. Clinopyroxenes from intermediate and salic melts have a lower aluminum content than those from basaltic melts. The concentration of aluminum in basaltic melts is equivalent to or slightly lower than that in intermediate and salic melts. This antipathetic relation between aluminum concentration in the melt and aluminum concentration into the clinopyroxene suggests a difference in the chemical potential of aluminum into the clinopyroxene phase between the two dominant melt types. This may be related to differences in the assemblage of aluminum-bearing phases, to composition and concentration differences for other elements in the melts, or to fundamental differences in the pressure - temperature - oxidation conditions under which these different clinopyroxenes crystallized. As to the first speculation, clinopyroxene is never the most aluminous phenocryst phase in any of the Level Mountain lavas. It is always associated with a feldspar, plagioclase in the basalts and anorthoclase in the salics. As to the second speculation, the fundamental differences between basalts and salics are obvious but the

compositional effects on the changing role of aluminum in the melt structure and its activity in the crystallizing phases are not obvious. The third possibility (which implies a higher pressure origin for basalts than salic lavas) is the most likely. This possibilty is dealt with in a subsequent section including calculations on geothermometry and geobarometry.

An exception to the aluminum discussion above is the clinopyroxenes of the tristanites. These pale green, eight-sided, euhedral phenocrysts are rich in aluminum with moderate levels of chromium and titanium. The calcium and aluminum levels are comparable in the clinopyroxene and the whole rock. In a normative sense, these pyroxenes are dominated by hedenbergite, calcium-tschermakite and diopside.

In the salic rocks, clinopyroxene is the most significant calcium-bearing phase. The concentration of calcium in clinopyroxene is two orders of magnitude greater than calcium in coexisting alkali feldspar, and is also significantly higher than calcium in the whole rock. There is no straightforward relationship between sodium content of the melt and sodium content of clinopyroxene. In fact, the most variation in molecular acmite into clinopyroxene occurs for the high sodium salic melts (about 6.0% Na_2O) and is equally unrelated to peralkalinity. The aegerine-acmite type pyroxenes are generally restricted to the groundmass of peralkaline lavas. Analysis #11 is from the groundmass of a

eutaxitic pantellerite flow. In a formula sense, this sample is 91% acmite and 6% hedenbergite with 3% johannsennite and jadeite. A tracing of the spectrum of this unusual acmitic pyroxene is given in figure 6-2.

The typical phenocryst clinopyroxene of the peralkaline trachytes and related lavas is sodic ferrohedenbergite. These is a positive correlation between sodium content of the melt and manganese content of the clinopyroxene. However, this manganese expressed as molecular johannsennite does not follow the variation of hedenbergite or acmite components.

Clinopyroxenes occuring as phenocrysts are almost always zoned. In basalts the clinopyroxene cores are more magnesium rich, while rims and groundmass clinopyroxene were higher in iron and titanium. Zoned phenocrysts from salic melts showed higher iron, manganese and sodium contents for crystal margins. In the salic rocks the groundmass clinopyroxene may or may not be more sodium rich than coexisting phenocryst clinopyroxene. Here the presence of other sodic ferromagnesian phases play the deciding role.

FELDSPARS

A collection of representative feldspar analyses is given in Table 6-3 for plagioclases and 6-4 for alkali feldspars. The sample number and rock type are given, along with the weight percent elemental analysis and structure formula calculated on the basis of eight oxygens. For ease

Figure 6-2.
Energy dispersive XRay spectrum for Na-Fe-Si microphenocryst from comendite ignimbrite (9/5-107/6600). Note minor content of Zr, Ca, Ti, Mn. From Na/Si ratio, possible compositions include: aegerine, rosenbuschite and astrophyllite.

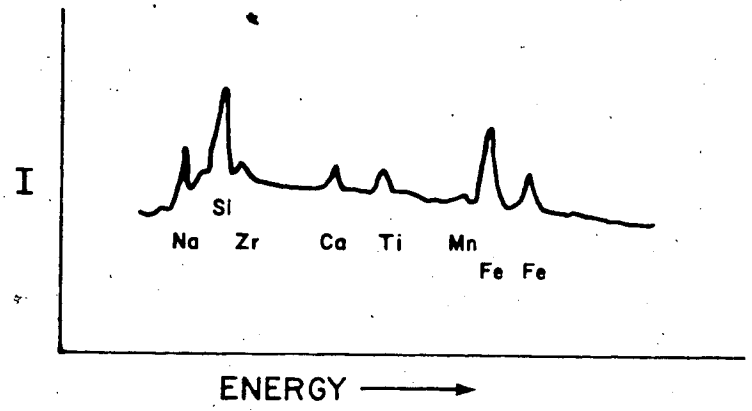

Table 6-3 Microprobe Analyses of Plagioclase Feldspars

Sample #	1	2	3	4	5	6	7	8	9	10	11	12	13	14	15
Si	24.8	25.6	25.4	25.3	25.7	25.9	25.6	26.3	25.0	26.3	25.9	26.8	29.5	29.0	29.1
Al	15.6	15.1	15.4	15.2	14.9	14.8	14.9	14.2	13.7	14.7	13.2	13.1	12.4	11.9	12.4
Fe	.5	.4	.7	.6	.6	.7	.8	1.0	.3	.4	.6	.9	.3	.3	.2
Ba	.08	.1	-	.08	-	-	-	.1	.0	-	-	.1	.7	1.2	.6
Ca	8.9	8.4	8.8	8.4	7.9	7.7	7.9	6.8	6.7	7.4	5.7	5.1	3.4	2.8	3.4
Na	3.3	3.1	3.2	3.7	3.6	3.6	3.9	4.3	4.3	3.9	4.8	4.6	5.5	5.8	6.1
K	.3	.2	.3	.2	.3	.4	.3	.5	.4	.4	.8	1.2	1.5	2.0	1.3
O	46.4	46.6	46.2	46.4	46.6	46.6	46.4	46.8	49.6	46.8	49.0	48.2	46.6	46.8	47.0

Structural Formulae as Cations per 8 Oxygens

Si^{4+}	2.397	2.471	2.437	2.434	2.478	2.490	2.458	2.527	2.527	2.490	2.590	2.630	2.777	2.781	2.762
Al^{3+}	1.567	1.519	1.532	1.524	1.497	1.487	1.487	1.420	1.444	1.449	1.371	1.334	1.209	1.188	1.216
Fe^{3+}	.023	-	-	.036	-	-	.036	.048	.015	.021	.006	.030	-	.015	.012
Na^{+}	.384	.360	.375	.432	.422	.423	.460	.511	.534	.605	.583	.550	.636	.682	.705
Ca^{2+}	.603	.568	.590	.565	.534	.521	.531	.458	.475	.494	.396	.353	.228	.191	.227
K^{+}	.018	.017	.019	.016	.021	.025	.018	.032	.029	.026	.056	.081	.103	.134	.088
Ba^{2+}	.002	.004	-	.002	-	-	-	.001	.001	-	-	.002	.014	.023	.012
Fe^{2+}	-	.020	.034	-	.031	.033	-	-	-	-	.024	.017	.013	-	-
An	59.9	59.9	59.0	55.7	54.7	53.8	52.7	45.7	45.7	43.9	38.3	35.8	23.2	66.2	68.3
Ab	38.1	37.9	37.6	42.5	43.2	43.7	45.6	51.0	51.4	53.8	56.4	55.8	64.9	18.5	22.0
Or	1.8	1.8	3.4	1.6	2.2	2.5	1.7	3.2	2.8	2.3	5.4	8.2	10.5	13.0	8.5
Cels	0.2	0.4	0.0	0.2	0.0	0.0	0.0	0.1	0.1	0.0	0.0	0.2	1.4	7.2	1.1
AF Na / WR Na+K	95.4 / 82.1	95.5 / 87.2	95.3 / 87.2	97.3 / 85.0	95.2 / 76.9	94.5 / 82.1	96.2 / 78.6	94.1 / 79.4	94.9 / 75.2	95.9 / 76.9	91.3 / 78.3	87.2 / 73.1	86.1 / 64.3	83.6 / 70.1	88.9 / 70.1
AF Na / WR Na+Ca	38.9 / 37.3	38.8 / 42.3	38.9 / 43.2	43.3 / 42.9	44.1 / 48.4	44.8 / 37.3	46.4 / 35.9	52.7 / 47.2	52.9 / 53.5	55.1 / 48.4	59.6 / 53.8	60.9 / 28.2	73.7 / 74.4	78.2 / 79.1	75.6 / 79.1
Label in Figures	2	8b	8a	3	7gnd	*	1	4	5	7 pheno	6	*	*	9a	9b

Key to Sample Numbers

1. PAR phenocryst from alkali basalt flow unit 2, Little Tahltan River.
2. 8/25-50/6397 megacryst, transitional hawaiite-alkali basalt flow, unit 8, Meszah Pk.
3. 8/25-50/6397 phenocryst, transitional hawaiite-alkali basalt flow, unit 8, Meszah Pk.
4. PAX phenocryst from transitional alkali basalt-hawaiite flow, unit 1, Little Tahltan River.
5. 8/20-2/4307 groundmass plag, hawaiite flow, unit 4, Little Tahltan River.
6. 8/23-7/3140 phenocryst from alkali basalt flow, unit 3, Little Tahltan River.
7. PAO microphenocryst altered alkali basalt flow, unit 3, Little Tahltan River.
8. PBX microphenocryst, Ne hawaiite, unit 5b, Kakuchuya Valley.
9. PAC phenocryst, hawaiite flow, unit 4, Little Tahltan River.
10. 8/20-2/4307 phenocryst, hawaiite flow, unit 4, Little Tahltan River.
11. PAF phenocryst, hawaiite flow, unit 4, Little Tahltan River.
12. B1 groundmass plag, ophitic alkali basalt, unit 3, Western Plateau.
13. 8/30-82/6150 phenocryst from comenditic trachyte, unit 6a, Badger Brook.
14. PBP microphenocryst from transitional bermorite-trachyte, unit 7b, S.face, Meszah Pk.
15. PBP microphenocryst from transitional bermorite-trachyte, unit 7b, S.face, Meszah Pk.

Table 6-4 Microprobe Analyses of Alkali Feldspars

Sample #	1	2	3	4	5	6	7	8	9	10	11	12	13	14	15	16
Si	30.8	30.9	29.8	30.6	30.3	30.5	30.6	30.3	29.4	29.6	32.5	32.7	32.8	32.2	32.6	32.4
Al	11.7	11.5	11.2	11.3	11.0	10.7	10.3	9.5	9.8	9.6	9.8	9.7	10.0	9.9	9.9	10.2
Fe	.6	.4	.5	.5	.5	.1	.4	.4	.4	.2	32	.4	.2	.5	.2	.2
Ba	.8	.4	.9	.8	1.1	.1	.7	-	-	-	-	-	-	-	-	-
Ca	2.0	2.0	1.9	1.7	1.6	.9	.7	-	.4	.2	-	-	.2	.2	.1	.3
Na	6.0	6.0	5.7	5.6	5.4	5.9	5.3	5.6	5.3	5.2	5.6	5.4	5.2	5.0	5.0	4.7
K	2.7	2.7	3.0	3.4	3.4	3.6	4.3	4.5	4.5	4.7	5.0	5.4	5.3	5.6	5.7	6.1
O	45.4	46.1	46.8	46.0	46.6	48.2	47.6	49.7	50.1	50.3	46.9	46.6	46.4	46.7	46.6	46.0
Structural Formulae as Cations per 8 Oxygens																
Si^{4+}	2.845	2.869	2.847	2.815	2.888	2.932	2.950	3.004	2.957	2.985	3.034	3.047	3.034	3.021	3.033	3.009
Al^{3+}	1.123	1.112	1.114	1.102	1.088	1.067	1.033	.977	1.025	1.004	.952	.940	.961	.965	.960	.988
Fe^{3+}	.062	.019	.026	.023	-	.004	-	.014	.020	.010	.001	-	-	-	.008	-
Ti^{4+}	.006	-	.006	.002	.005	-	.003	-	-	-	-	-	-	-	-	-
Na^{+}	.683	.679	.667	.642	.633	.689	.628	.679	.648	.647	.635	.610	.592	.572	.572	.537
Ca^{2+}	.129	.127	.128	.106	.108	.058	.050	-	.032	.017	-	-	.009	.011	.006	.020
K^{+}	.177	.182	.208	.231	.229	.248	.295	.321	.325	.338	.336	.344	.352	.380	.380	.404
Ba^{2+}	.014	.008	.018	.016	.209	.002	.014	-	-	-	-	-	-	-	-	-
Fe^{2+}	-	-	-	-	.023	-	[illegible]	.006	-	-	-	.019	.010	.023	-	.009
Ab	68.0	68.1	65.3	64.1	62.6	69.2	63	9	64.5	64.6	65.4	64.0	62.1	59.3	59.7	55.9
Or	17.7	18.3	20.4	23.5	23.9	24.8	29	.1	32.4	33.7	34.6	36.0	36.9	39.5	39.6	42.0
An	12.9	12.8	12.5	10.8	11.3	5.8	5.1	-	3.1	1.7	-	-	1.0	1.2	0.7	2.1
Cels	1.4	0.8	1.8	1.6	2.2	0.2	1.5	-	-	-	-	-	-	-	-	-
AF Na	79.4	78.8	76.2	73.5	73.4	73.6	68.0	67.9	66.6	65.7	65.4	64.0	62.7	60.1	60.1	57.1
WR $\frac{Na}{Na+K}$	70.4	70.4	70.1	70.1	64.3	62.7	64.3	50.7	61.8	49.7	64.7	67.3	53.7	51.5	54.3	57.1
AF Na	84.1	84.2	83.9	85.8	85.4	92.2	92.6	100.0	95.4	97.4	100.0	100.0	98.4	98.1	98.9	96.4
WR $\frac{Na}{Na+Ca}$	80.4	80.4	79.1	79.1	74.4	82.7	85.3	87.8	96.9	87.3	100.0	98.3	98.5	94.9	97.3	93.9

Key to Sample Numbers

1. PBO phenocryst from transitional benmoreite trachyte, unit 7b, S.face Meszah Pk.
2. PBO "
3. PBP "
4. PBP "
5. 8/30-82/6150 phenocryst from comenditic trachyte, unit 6a, Badger Brook.
6. 8/16-44/6250E phenocryst from tristanite dyke, unit 7c, Moose Mtn.
7. 8/26-56/6336 groundmass feldspar from trachyte, unit 7a, s.face Meszah pk.
8. 8/7-19/5830 phenocryst from comenditic trachyte flow, unit 6a, Wolf Bones Ridge.
9. 25/5-D phenocryst from crystalline pantellerite, unit 7b, Dudidontu-Kakuchuya Ridge.
10. 8/16-43/5990 phenocryst from rhyolite ignimbrite, unit 7a, central chain.
11. 9/5-107/6600 phenocryst from comendite eutaxitic tuff, unit 7b, E.shoulder Meszah.
12. 8/25-54/6345 microphenocryst from comendite pitchstone, unit 7b, E.shoulder Meszah Pk.
13. 8/27-66/5862 phenocryst from altered comendite dyke, unit 7b, N.end central chain.
14. 8/27-63/6788 phenocryst from altered comendite dyke, unit 7b, N.end central chain.
15. 9/2-95/5625 phenocryst from comendite pitchstone, unit 7b, E.shoulder Meszah Pk.
16. 8/27-62/6890 phenocryst from rhyolite (altered comendite dyke), unit 7b, central chain.

in labelling graphs and diagrams, the analyses and sample designations are referenced by column numbers. All analyses are for phenocrysts unless otherwise noted. In most instances, the within grain and grain to grain variations were qualitatively examined using short counts and small sweep scans. The actual analyses were done using a twenty micron square or larger sweep area on the most abundant compositions. The resulting analyses are taken to be more representative for crystal fractionation arguments than point analyses would be. The large scans and collected groups of twenty-five second counts were also done to avoid problems of sodium excitation or volatilization.

In a molecular sense, 98% of the feldspar compositions are accounted for by the anorthite, albite and orthoclase end members. The most important component beyond those mentioned is barium (as celsian).

Plagioclase compositions from microprobe analyses agree well with optical determinations. Phenocrysts from hawaiites often have multiply reset or reversed concentric zonation. The groundmass plagioclase of these disequilibrium rocks may be more sodic than either phenocrysts or whole rocks (see analysis from 8/20-2/4307, upper plateau unit).

Figure 6-3 shows plagioclase-whole rock pairs in the atomic system calcium-sodium-potassium. It is evident that potassium is only a minor constituent of the plagioclase and that the whole rock and the melt are enriched in potassium during plagioclase crystallization. The distribution of

Figure 6-3.
Level Mountain lavas and feldspars in Ca, Na, K atomic.

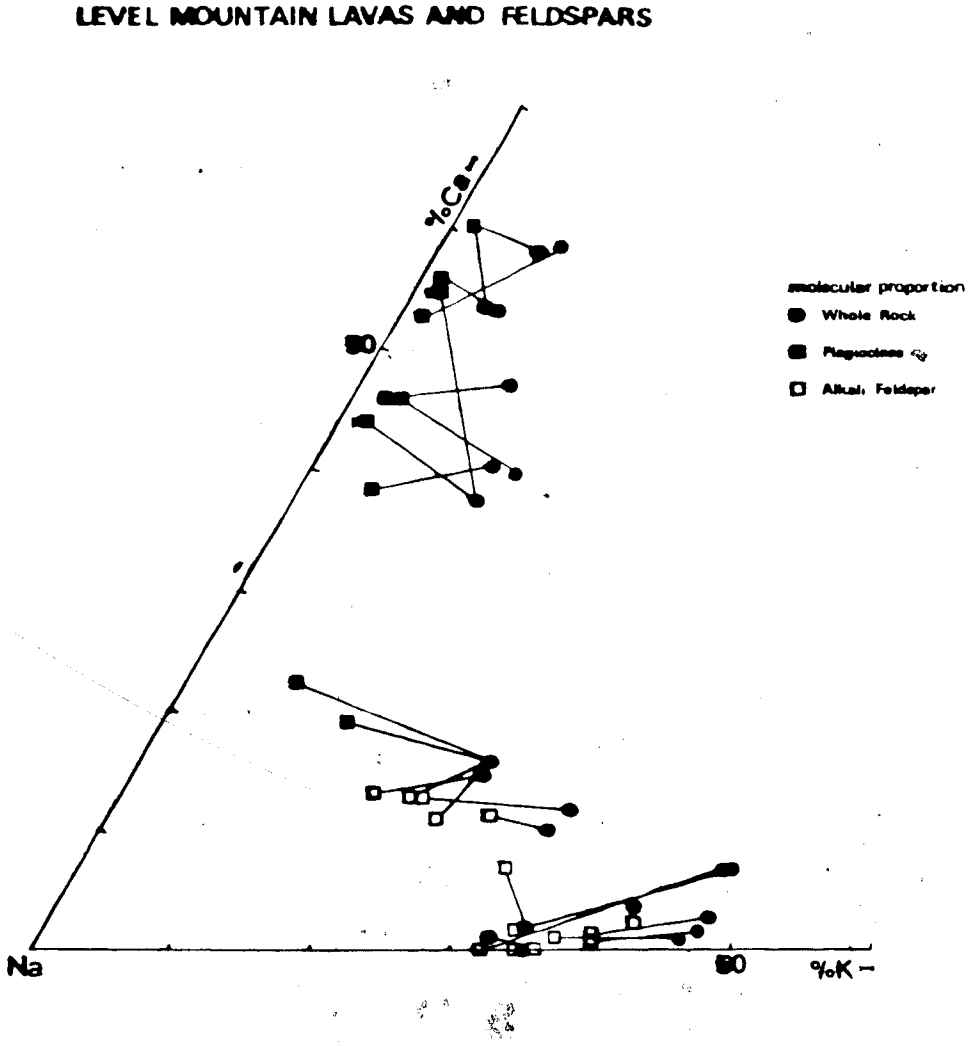

whole rocks as seen here could not be simply related by fractionation of their phenocryst plagioclase alone because the trend of whole rock variation is nearly perpendicular to the feldspar vector. plagioclase alone. Presuming the basalts to be related by fractionation, the controlling phase would have to be a calcium rich phase such as clinopyroxene, with only minor effect due to the feldspar.

Alkali feldspar analyses presented are for phenocrysts only. The anorthoclase phenocrysts tend to show patchy chemical zonation (in sodium, potassium) on a scale of 30 microns or less. The zonal differences in Ab and Or are slight and not nearly as pronounced as the difference in composition between phenocrysts and groundmass. The groundmass almost always has microlites of nearly pure sanidine. Groundmass alkali feldspar is always more potassium rich than phenocryst alkali feldspar. Anorthoclase phenocrysts may have rims that are either more sodic or more potassic than their cores. The presence of two distinct groupings is apparent in figure 6-3. The grouping with the higher calcium content represent the low volume metaluminous salic lavas. In this set the calcium of content of phenocrysts is not significantly lower than in the rock as a whole, and the sodium contents are higher. The second group are the alkaline and peralkaline salic lavas. With one exception, the phenocryst feldspars are more sodic and less calcic than their whole rock systems. The two groups could possibly be related by the addition of intermediate

plagioclase or sodic plagioclase and amphibole. Within either group, fractionation of the indicated feldspars cannot account for whole rock variations. For further elaboration of this and other fractionation arguments refer to the subsequent section on whole rock chemistry. The peralkaline group variation could be explained by the joint effect of alkali feldspar and a calcic phase (hedenbergite). The detailed compositional variation of alkali feldspar-phenocrysts and whole rocks has been examined by mol ratio plots involving sodium, potassium, aluminum, calcium and their various combinations. No obvious mathematical relations could be discerned. Nicholls and Carmichael (1969) made two rather definite statements relating alkali feldspar compositions and peralkaline residual glasses. Those statements were: (i) K/Na feldspar is greater than K/Na whole rock and (ii) feldspar compositional variation shows pronounced restriction with incresing agpaitic index. The first conclusion is only true for Level Mountain sample 25/5e, in fact the converse is generally true. Their second conclusion appears to hold for Level Mountain lavas.

Feldspars are the most abundant phenocrysts for all Level Mountain lavas but their compositions, if involved in fractionation at all, cannot alone account for trends in whole rock variation. There are three distinct whole rock-feldspar sets: (i) basalt-calcic plagioclase, (ii) peralkaline salic-sodic anorthoclase and (iii) intermediate

metaluminous-sodic alkali feldspar, with or without sodic plagioclase. In all three cases, the whole rocks show trends of calcium variation, while the feldspars do not have significantly different calcium levels from whole rocks. The most likely phases to account for the calcium variation would be calcic pyroxenes or possibly amphiboles.

IRON TITANIUM OXIDES AND RELATED MINERALS

Microprobe analyses of iron titanium oxides for representative Level Mountain lavas are presented in Table 6-5 for spinels and Table 6-6 for ilmenites. Analyses were obtained using a focussed beam spot, unless otherwise indicated. Structure formulae have been calculated for ilmenites on the basis of four oxygens. The spinel types have additionally been represented as percentage of end member molecules.

Spinels

The most abundant cations are iron and titanium; with essential aluminum and manganese in subordinate amounts. Magnesium and zinc are usually present in minor to trace amounts. Chromium and vanadium have mutually sympathetic presence and distribution and are limited to oxides from basaltic samples. Trace amounts of calcium, nickel and cobalt may be present but show no sensible variation. In ulvospinels from salic lavas, chlorine and sulfur often appear in trace amounts.

Table 6-5 Microprobe Analyses of Spinels

Sample #	1	2	3	4	5	6	7	8	9	10	11	12	13	14
Si	.1	.4	.1	.3	-	.3	.3	-	.4	.4	.1	.1	-	.2
Ti	17.3	16.7	15.6	15.3	14.5	14.0	13.4	13.5	15.9	14.5	3.7	2.6	1.2	.9
Al	.1	.2	.7	.4	.4	1.0	.2	1.0	1.1	.6	1.6	10.4	3.7	14.2
Cr	-	-	-	-	-	.2	-	-	1.5	-	.2	20.8	.5	19.6
V	-	.1	-	-	-	.1	-	-	.1	-	.3	.3	.5	.1
Fe	54.4	53.3	49.1	55.9	57.4	50.5	56.1	57.4	50.0	52.5	60.0	28.6	59.5	26.0
Mg	-	-	.9	.2	.5	2.1	.1	.8	1.8	.5	.3	5.8	2.1	6.5
Mn	.8	.7	.5	.8	.7	.5	1.4	.6	.3	.8	.1	.3	.2	.3
Zn	.2	.3	.1	-	.0	-	.2	.1	.1	.2	.2	.0	.1	.1
O	27.0	28.2	33.0	27.0	26.0	31.6	28.1	26.0	28.4	29.5	33.6	30.6	32.5	32.0

Structural formulae as cations per 4 oxygens

Si^{4+}	.010	.034	.005	.026	-	.025	.022	-	.027	.032	.004	.009	-	.009
Ti^{4+}	.788	.778	.763	.701	.657	.649	.626	.604	.728	.683	.186	.102	.056	.031
Al^{3+}	.009	.017	.065	.032	.036	.080	.020	.080	.057	.054	.143	.721	.305	.870
Cr^{3+}	-	-	-	-	-	.007	-	-	.040	-	.009	.745	.021	.625
V^{3+}	-	.002	-	-	-	.006	-	-	.004	-	.012	.009	.021	.005
Fe^{3+}	.425	.353	.391	.515	.633	.563	.676	.719	.391	.515	1.466	.287	1.540	.440
Fe^{2+}	1.700	1.774	1.668	1.676	1.597	1.449	1.576	1.481	1.565	1.610	1.130	.669	.852	.332
Mg^{2+}	-	-	.083	.020	.041	.187	.008	.070	.165	.050	.025	.444	.191	.654
Mn^{2+}	.032	.028	.021	.030	.027	.201	.058	.024	.012	.031	.005	.010	.010	.008
Zn^{2+}	.006	.011	.004	-	.002	-	.009	.004	.004	.006	.006	.002	.002	.002
Mt	15.8	17.9	12.5	22.3	28.5	12.5	28.7	30.0	24.1	36.1	68.1	6.4	72.8	15.0
Ulv	79.9	79.5	76.3	72.6	66.3	65.5	63.6	60.2	59.1	56.4	18.1	10.2	5.6	3.3
Sp	-	-	3.2	1.6	1.8	4.1	0.8	4.0	2.3	2.2	2.5	36.2	15.3	45.9
Cr	-	-	-	-	-	0.7	-	-	1.6	-	0.4	37.4	1.0	32.9
Other*	4.1	2.6	8.0	3.5	3.4	17.2	6.9	5.8	12.9	5.3	10.9	9.8	5.3	2.9

* Other = (Mft + Jac + Hc + Fr + Tr)

SAMPLE KEY

1. PBP benmoreite, Unit 8, microphenocryst.
2. PBE peralkaline trachyte, unit 6, microphenocryst.
3. PAF hawaiite, unit 4, microphenocryst.
4. 8/26-56/6336 trachyte, unit 7, microphenocryst.
5. PBO benmoreite, unit 8, phenocryst.
6. 8/20-2/4307 hawaiite, unit 4, microphenocryst.
7. PBY trachyte, unit 7, phenocryst.
8. PBP benmoreite, unit 8, phenocryst.
9. 8/23-7/3940 alkali basalt, unit 2, microphenocryst.
10. 8/30-82/6150 peralkaline trachyte, unit 6, phenocryst.
11. PAC hawaiite, unit 4, microphenocryst.
12. PAO alkali basalt, unit 3, chrome rich spinel in olivine xenocryst.
13. PAC hawaiite, unit 4, phenocryst with lamellae of parapseudobrookite.
14. PAO alkali basalt, unit 2, chrome rich spinel in olivine xenocryst.

Table 6-6 Microprobe Analyses of Ilmenites

Sample #	1	2	3	4	5	6	7	8	9	10
Si	0.3	0.3	0.1	0.0	0.5	0.2	0.0	0.3	0.2	0.3
Zr	0.2	0.2	0.0	0.0	0.1	0.1	0.0	0.2	0.0	0.2
Al	0.2	0.1	0.1	0.0	0.1	0.1	0.1	0.0	0.1	0.4
Ti	30.3	32.5	33.3	29.9	30.5	30.3	32.5	29.7	31.4	26.8
Fe	34.8	36.9	37.6	35.0	36.5	36.4	39.0	36.7	39.0	38.4
Mg	1.8	1.3	1.0	0.0	0.0	0.0	0.6	0.0	0.3	2.1
Mn	0.4	0.6	0.7	1.2	0.9	0.9	0.4	1.0	0.4	0.5
Ca	0.2	0.2	0.1	0.0	0.0	0.1	0.1	0.0	0.2	0.1
Na	0.0	0.1	0.2	0.0	0.0	0.0	0.1	0.0	0.2	Cr.2
O	31.2	27.7	27.1	33.9	30.8	31.8	27.3	32.0	28.3	29.1

Structural formulae as cations per 4 oxygens

Si^{4+}	.014	.017	.002	.000	.025	.008	.002	.016	.010	.016
Zr^{4+}	.003	.003	.000	.000	.001	.002	.000	.005	.000	.003
Al^{3+}	.010	.006	.006	.000	.005	.004	.005	.000	.007	.018
Ti^{4+}	.914	.938	.971	.979	.956	.963	.956	.947	.938	.807
Fe^{2+}	.750	.846	.895	.943	.952	.943	.896	.931	.891	.663
Fe^{3+}	.126	.084	.047	.039	.029	.050	.089	.073	.110	.327
Mg^{2+}	.104	.077	.060	.000	.000	.000	.033	.000	.016	.123
Mn^{2+}	.047	.015	.017	.034	.025	.025	.010	.028	.011	.013
Ca^{2+}	.005	.009	.002	.000	.000	.002	.003	.000	.006	.003
Na^{+}	.000	.008	.001	.000	.000	.000	.007	.000	.010	Cr^{3+} .006
Ilm	100.0	100.0	100.0	99.8	98.7	98.5	98.5	97.1	96.7	89.8
Hm	0.0	0.0	0.0	0.2	1.3	1.5	1.5	2.9	3.3	10.2

Key to Sample Numbers

1. 8/25-50/6397 hawaiite, unit 8, groundmass.
2. PBX hawaiite, unit 5.
3. PAR alkali basalt, unit 2, phenocryst.
4. 8/7-19/5830 pantellerite, unit 6, phenocryst.
5. 8/27-62/6890 rhyolite, unit 7, phenocryst.
6. 8/11-30/6111 comendite, unit 6, phenocryst.
7. PAX alkali basalt, unit 1, phenocryst.
8. PBS comendite, unit 5, phenocryst.
9. PAO alkali basalt, unit 3.
10. 8/25-50/6397 hawaiite, unit 8, phenocryst (xenocryst?).

Figure 6-4 shows the distribution of oxide analyses (both spinel and ilmenite type), in the system TiO_2-FeO-$0.5Fe_2O_3$. Four points do not fall close to the two equilibrium compositional joins, magnetite-ulvospinel and hematite-ilmenite. The two points below the magnetite-ulvospinel join are the PAO spinel samples previously discussed. The single point between the joins could be an unexsolved composition. In flow PAC a large magnetite phenocryst showed broad lamellae of unusual composition. These unusual lamellae plot on the FeO-TiO_2 join. Although it is dominantly a Ti-Fe composition, it is not a common mineral. On the basis of five oxygens there are 2.98 cations; giving $(Fe,M)Ti_2O_5$ as a possible formula, indicating the low oxidation end member of the pseudobrookite series. It is relatively common to have exsolution relations between magnetite and ilmenite in the Level Mountain lavas. This occurrence of a pseudobrookite could indicate a peculiar activity for titanium in this flow. Another possibility is that these lamellae, with a lower density and higher titanium content than ilmenite formed at a different (lower) pressure than the crystallization of most lavas.

Ilmenites

Ilmenites, while not universally present, have been found in every lava type at Level Mountain. Essential cations are iron, titanium and manganese. Trace and minor constituents include zirconium aluminum, and magnesium. The

Figure 6-4.
Level Mountain lavas and iron-titanium oxides Ti^{4+}-Fe^{2+}-Fe^{3+} cation proportions.

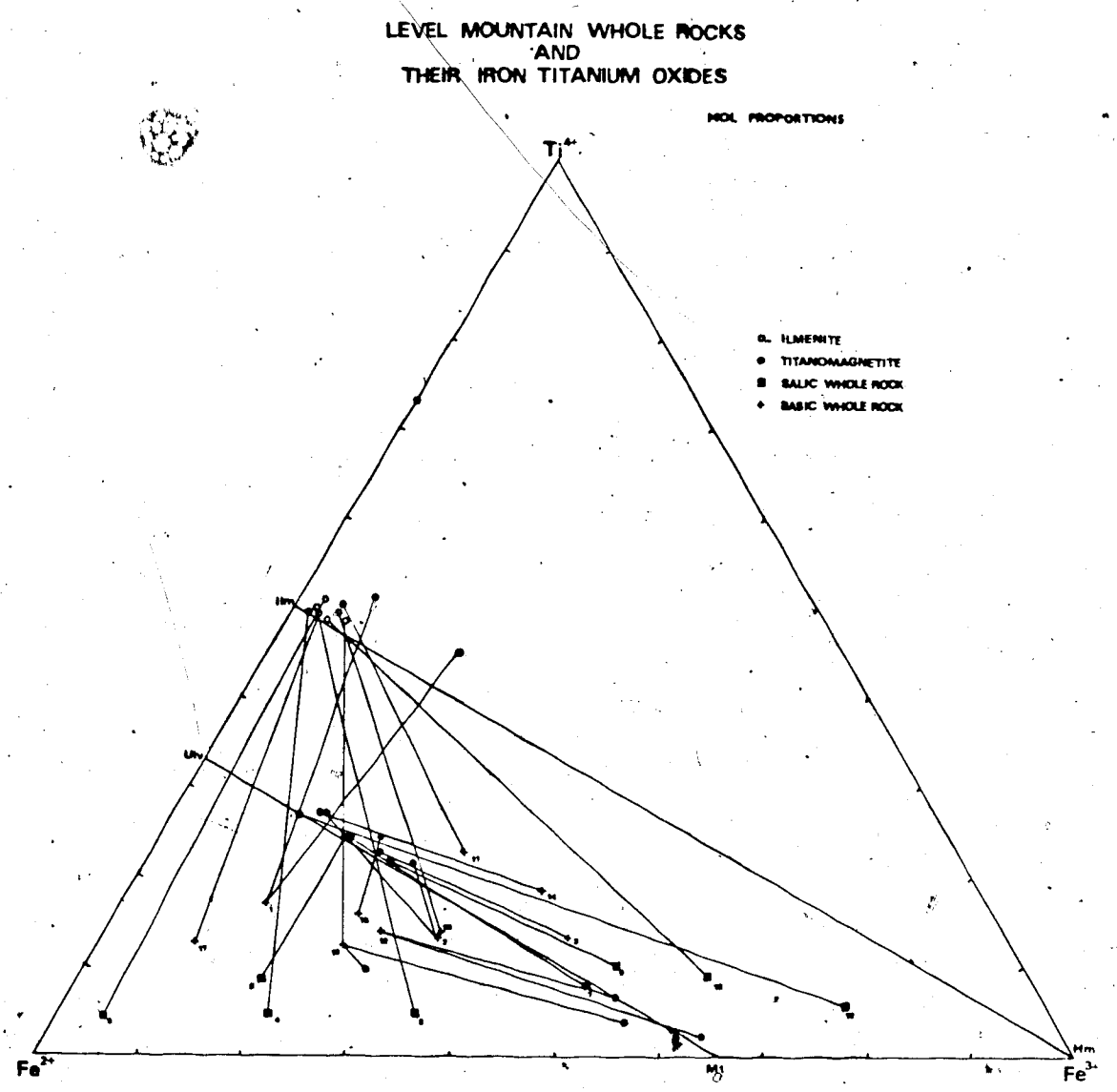

occurrence of traces of zirconium is most typical for ilmenites in the salic lavas, rather than in the basalts; so it would seem that the zirconium content in ilmenite reflects its content in the rock.

In salic lavas the ilmenites contain detectable niobium which was confirmed by wavelength dispersive analyses. It is thought that zirconium and niobium probably substitute for titanium as a perovskite type component. The levels of these minor elements vary from rock to rock, but seem to be present in small concentrations in several coexisting mineral phases.

The importance of these oxide minerals is twofold. Depending on the total iron-bearing mineral assemblage, an oxide phase can be used as an indication of oxygen fugacity, (Buddington and Lindsley, 1964; Carmichael and Nicholls, 1967). The prevalence of ilmenite, or the absence of oxides in the case of the peralkaline trachytes, indicates fairly low fO_2. The distribution of whole rock compositions with respect to $Fe^{2+}/(Fe^{2+} + Fe^{3+})$ is greater than for their oxides. Salic rocks have greater variation in oxidation state of iron and are generally lower in titanium than the basic or intermediate rocks. While the fractionation of magnetite and ilmenite may drive the iron oxidation ratio up or down, it almost invariably depletes the residual melt with respect to titanium. The basalts may have two exsolved oxide phases, while the salics tend more commonly to have one or none, as is common for the peralkaline compositions.

Basalts are usually driven to higher Fe^{2+} (lower fO_2) by oxide fractionation. The basalt PAO has three very different oxides. The ilmenite composition can be considered to be an ordinary phase for a rock of this composition, but the other two cannot. Petrographically these are xenocrysts and they are high in spinel content.

ALKALI FERROMAGNESIAN MINERALS

Aenigmatite

Aenigmatite, while an uncommon mineral in igneous rocks as a whole, is a characteristic phase in peralkaline lavas and their plutonic equivalents. Aenigmatite is a triclinic inosilicate, with a deep reddish-brown colour, and a composition that does not vary appreciably from its ideal formula: $Na_2Fe_5TiSi_6O_{20}$ (Deer, Howie and Zussman, 1978). Its occurrence, previously reported on Level Mountain (Ostensoe, 1960), confirms the peralkaline condition and indicates a low oxygen fugacity (Marsh, 1975). The best examples of this phase on Level Mountain occur on a whaleback outcrop north of Meszah Peak. There, striated blades of red-bronze coloured aeigmatite up to 1.2cm long were found in miarolitic cavities of a trachyte stock, see plate 6-1. An XRD pattern was obtained for this material with the calculated d spacings presented in Table 6-7, showing good agreement with published values (Thompson and Chisholm, 1969; Kelsey and McKie, 1964; Ernst, 1962). Although aenigmatite is common in the peralkaline lavas from Level

Plate 6-1.

S. E. M. photograph of aenigmatite prisms in a miarolitic cavity. Blocky pseudohexagonal crystals are sodic pyroxene, alkali feldspars are tabular. Note 400 micron scale bar below sample number. Operating conditions for Cambridge 150 Stereoscan S.E.M.: 20KV EHT, 3 amp filament current at saturation level, 0.15 picoamp beam current, prefocussed condenser setting of 2.5 amps at 90 volts, focussing condenser setting of 3.0 amps at 90 volts, working distance 12mm.

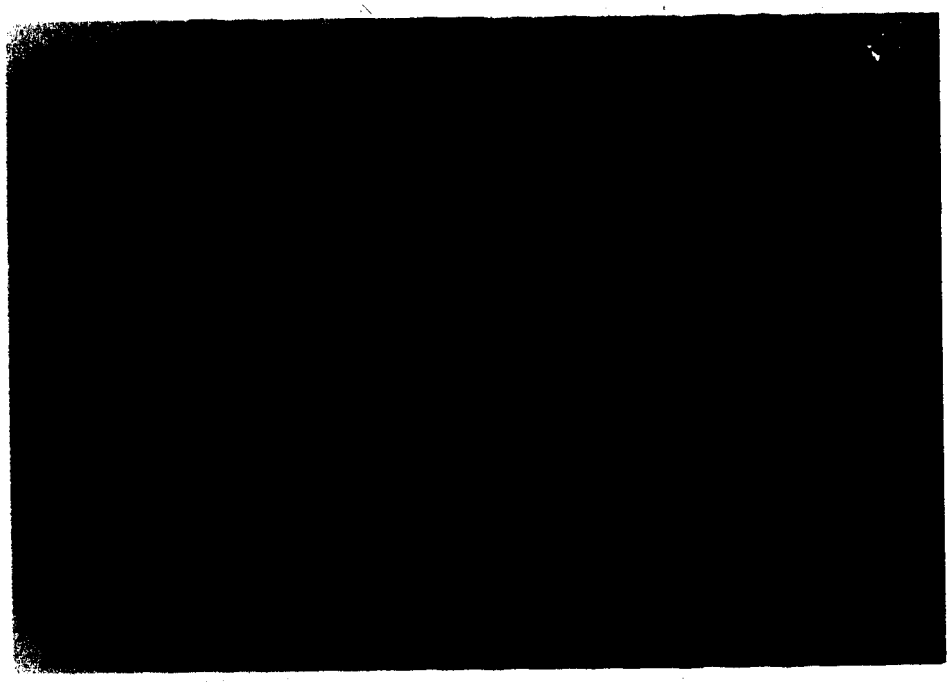

Table 6-7 XRD[1] Pattern for Aenigmatite 8/25-52/5880

d(A)	I/I1	hkl
8.088	35	001,010
7.400	1	$01\bar{1}$
6.366	1	$1\bar{1}1$
4.820	4	$011,11\bar{1}$
4.412	4	$0\bar{1}2,02\bar{1}$
4.201	3	$2\bar{2}1,20\bar{1}$
3.708	7	$02\bar{2}$
3.487	2	$\bar{2}30,\bar{2}31$
3.324	1	111
3.241	4	$1\bar{3}0,102$
3.153	100	$012,02\bar{1}$
3.062	1	$12\bar{2},3\bar{2}1$
2.945	11	$01\bar{3},03\bar{1}$
2.861	1	$\bar{3}31,10\bar{3}$
2.822	1	$\bar{1}22$
2.757	4	$\bar{3}22,1\bar{2}3$
2.710	18	$\bar{1}31,003$
2.657	2	$1\bar{1}3,300$
2.549	17	$2\bar{1}3,4\bar{2}0$
2.460	3	$1\bar{4}2,202$
2.416	7	$022,2\bar{3}3$
2.346	3	$1\bar{4}0,4\bar{4}0$
2.307	2	$301,4\bar{2}1$
2.220	1	$\bar{3}23,2\bar{1}3$
2.199	3	$132,0\bar{4}2$
2.120	13	$20\bar{4},3\bar{3}3$
2.073	3	$2\bar{5}2,3\bar{5}0,0\bar{4}3,0\bar{3}4$
2.009	4	$122,2\bar{5}0$
1.945	2	$221,2\bar{3}2$
1.913	2	$032,\bar{1}31$
1.814	2	
1.732	2	
1.682	2	
1.635	4	
1.625	8	
1.613	3	
1.590	1	
1.575	1	
1.559	2	
1.555	2	

1 Pattern made using CuKα radiation, from 2° to 60° 2θ, with slit settings of 0.5°-1.0°-0.5°, with an 8 second time constant at a scan rate of 0.5° 2θ per minute and a chart speed of 30 cm per hour.

Mountain, in the polished thin sections prepared for microprobe analysis aenigmatite was confined to the groundmass. In those samples, aenigmatite occurred in patches up to 20 microns in size, but texturally it was intergrown with other phases making it impossible to obtain good quality microprobe analyses. Energy dispersive spectra obtained with a focussed beam and twenty second counting times contained peaks for Na, Si, Ti, Mn, and Fe. Sometimes a low intensity Zn peak was noted but peaks for Mg, K, and Ca were absent, although small amounts of these elements are typically reported in the literature. For comparison, aenigmatite compositions from other peralkaline lavas are presented in table 6-8.

ACCESSORY AND ALTERATION MINERALS

Probe analyses of selected accessory and alteration phases are presented in Table 6-9. Apatite has been recognized as an accessory mineral in all lava types at Level Mountain. Usually apatite occurs as acicular inclusions in the primary phenocrysts. In the intermediate lavas, particularily benmoreites and phonolites however, apatite occurs in phenocryst aggregates along with hortonolite, andesine, and ulvospinel. Such an analysis from flow PBP is given in the table. Chlorine is present in the apatites particularily from the salic lavas. Flourine may be present as well but detection of the soft XRays from this element is beyond the analytical capability of the EDA

Table 6-8 Aenigmatites From Other Alkaline Volcanic Centers, Structural Formulae as Cations per 20 Oxygens

	P	N	R-44	E2
Si	5.87	5.90	5.83	5.43
Al	0.13	0.10	0.04	0.46
Fe^{3+}	0.00	0.00	0.13	0.11
	6.0	6.0	6.0	6.0
Al	0.02	0.01	0.00	0.00
Fe^{3+}	0.14	0.40	0.00	0.70
Ti	0.96	0.80	0.88	0.83
Mg	0.02	0.27	0.00	0.01
Fe^{2+}	4.65	4.36	4.82	4.30
Mn	0.14	0.12	0.10	0.09
Ca	0.07	0.03	0.03	0.08
	6.0	6.0	5.8	6.0
Ca	0.00	0.02	0.00	0.22
Na	2.04	2.05	2.12	1.78
K	0.01	0.02	0.00	0.00
	2.1	2.1	2.1	2.0
$\frac{100\ Ti}{Fe + Ti}$	16.72	14.35	15.03	13.93

Key to Sample Numbers

P - Pantelleria obsidian (Carmichael, 1962)
N - Nandewar, New South Wales, peralkaline trachyte (Abbott, 1967)
R44 - Rainbow Range, B.C., pantellerite (Bevier, 1978)
2 - Mt. Edziza, B.C., comendite (Yagi and Souther, 1974)

Table 6-9 Microprobe Analyses of Accessory Minerals from Level Mountain

PBP Chlorapatite

	Element Wt.%	Structural Formula	
Si	0.24	0.042	
Mg	0.16	0.032	
Fe	1.02	0.090	
Mn	0.16	0.014	8.0
Ca	39.93	4.87	
Na	0.06	0.01	
P	18.57	2.93	
Cl	0.08	0.01	
O	39.75	13.00	

8/27-63/6788 Zircon

	Element Wt.%	Structural Formula	
Si	15.80	1.013	
Zr	49.44	0.976	
Ti	0.06	0.002	2.0
Fe	0.28	0.009	
K	0.07	0.003	
O	34.37	4.000	

PAC Septechlorite

	Element Wt.%		Structural Formula		Recast Oxide Analysis	
Si	10.98		5.956		SiO_2	25.98
Ti	0.04		0.137		TiO_2	0.08
Al	1.21		0.681	8.0	Al_2O_3	2.52
V	0.05		0.015		V_2O_3	0.10
Fe	29.28	Fe^{3+}	1.334		Fe_2O_3	20.36
		Fe^{3+}	2.179		FeO	23.31
		Fe^{2+}	4.471		MnO	0.23
Mn	0.17		0.459	12.0	MgO	13.88
Mg	7.57		4.744		Na_2O	0.33
Na	0.22		0.147		H_2O	13.21
O	49.79		28.000			

Theoretical Formula clinochlore/cronstedite

$(Mg,Mn,Fe^{2+},Fe^{3+})_{12}(Fe^{3+},Al,V,Ti,Si)_8O_{20}(OH)_{16}$

system. The recognition of phosphorous and halogen bearing phases is important to understanding the minor element geochemistry and gas phase composition of the salic lavas.

Carbonate as a vesicle and fracture infilling is one of the most common alteration minerals. Carbonates from the basalts are usually calcite or aragonite and sometimes have noticeable levels of Sr as verified by atomic absorption analyses. The groundmass/intersertal carbonate from phonolites, tristanites and mixed flows is consistently high in Fe and Mn. In a molecular sense these are 85% calcite, 10% siderite, 5% rhodochrosite. Some of these high Fe-Mn calcites have inclusions of pyrite and are probably hydrothermal in origin.

Zirconium minerals are usually found as accessories in the peralkaline salic lavas. Baddeleyite microphenocrysts have been found in comendite pitchstones. Zircon is the most common Zr bearing mineral found as inclusions in pyroxenes and alkali feldspars as well as in the mesostasis. Butterman and Foster (1967) studied the pure ZrO_2 - SiO_2 system and found Baddeleyite to be stable below 1170°C which is at a lower temperature than the stability field for zircon. This would seem to indicate that the liquidus temperature for the baddeleyite bearing glassy comendites is lower than that for the other peralkaline flows which more commonly contain zircon.

The most abundant alteration mineral in basalts was petrographically chlorite, but probe analyses showed it to

be essentially iron silicate with minor Al, and hence more akin to septechlorite or septechamosite.

CHAPTER 7. PETROCHEMISTRY

INTRODUCTION TO THE WHOLE ROCK CHEMISTRY AND ANALYTICAL METHODS

More than one hundred and ten major element analyses were performed by electron microprobe EDA of whole rock glasses after the method of Schimann and Smith (1980). This type of whole rock analysis has previously been reported by Rucklidge et al (1970) and by Reed and Ware (1975). Data reduction was by the method of Smith and Gold (1979) and Smith (1976). Thirty XRF analyses, mostly on sample splits, were performed by Dr. J.G. Holland at the University of Durham after the method of Brown et al (1977). The XRF data additionally include minor and trace element concentrations. Other trace element data were collected by atomic absorption spectroscopy. Whole rock isotopic compositions for oxygen, strontium and lead were surveyed for the entire range of petrochemical variation.

All rock powders intended for major element analyses were measured for H_2O^- and loss on ignition. Total water analyses were made by the Penfield tube method. All whole rock powders were tested for the presence of carbonate. Those few samples, mostly older basalts, which tested positive were accurately measured for CO_2 in an evolution-absorption apparatus modified after Goldich et al (1959). The weight percent of ferrous iron was determined by acid dissolution of a known weight of sample and titration

with a standardized solution of $KMnO_4$. The sample weights were corrected for water content before calculating the weight percent of Fe^{2+}.

To prepare glasses for microprobe analysis, the whole rock powders after L.O.I. were transferred from crucibles to molybdenum pedestals and fused under reduced pressure in an image furnace. This apparatus was constructed by K. Schimann (Schimann and Smith, 1980). Probe analyses were made against anhydrous mineral standards with concentrations of standard elements in excess of sample concentrations. Minor elements were referenced to default values. The standards used, with their weight concentration of critical elements, are presented in table 7-1. Whole rock analyses were recast as oxides with iron calculated Sample homogeneity was verified by 50 second scans on different areas. as ferrous oxide. Those analyses with totals greater than 98% were considered acceptable. Most analyses had totals greater than 99%. The errors associated with these whole rock analyses can be limited to three kinds. The first, acciracy,, is related to concentration. The lower the concentration of an element in the sample the poorer the counting statistics. For instance, Si has three to four significant figures while Mn has only one to two. In the case of the energy dispersive analyses of glasses, the concentration of each element in the standard is greater than in any sample. Some replicate analyses (E.D.A.), and XRF analyses for comparison are presented in table 7-2. The variations between these analyses should be

Table 7-1. Anhydrous Mineral Standards

U. of A. Microprobe Code	Standard Name	Weight Percent of Elements Used as Standards
CCNM 0332	Franklin Willemite	53.716%Zn; 3.733%Mn
CCNM 0087	Wakefield Diopside	18.39%Ca; 11.233%Mg;(Alternate for Basalts: 25.878%Si)
CCNM 0279	Hohenfels Sanidine	30.230%Si; 9.930%Al; 10.050%K; 0.980%Ba
CCNM 0005	Albite Glass (Ab100)	8.770%Na
CCNM 0102	Fluorapatite	17.840%P
CCNM 0311	Tugtupite	7.580%Cl
CCNM 0152	Odegaarden Ilmenite	28.59%Ti; 38.69%Fe

taken as representative of errors for all whole rock analyses presented.

MAJOR ELEMENT GEOCHEMISTRY

Introduction

Eleven series of histograms have been prepared for the prominent lava types, figure 7-1. Along the abscissa are plotted the weight ranges for the eleven major chemical components. The number of samples in each range is plotted along the ordinate. Components (except H_2O) have been recast as oxide percent on a dry basis. Total iron is expressed as ferrous oxide. Basaltic [illegible] intermediate lava types have been classified according to Irvine and Baragar (1971). The distribution of Level Mountain lavas on Irvine and Baragar's normative classification plot follows the typical sodic alkali basalt series, see figure 7-2. Peralkaline salic lavas have been classified according to MacDonald (1947b). Source derivation tests have been performed for all Level Mountain lavas. Partial melting calculations for basalts used a pyrolite source (Green and Ringwood, 1967) and for salics used a clinopyroxene amphibolite from Three Valley gap. Results of these calculations appear in the tables of chemical analyses as %MELT.

For ready comparison of the overall chemical variation of Level Mountain lavas with other alkaline volcanic suites

Table 7-2. Analytical Comparison of Whole Rock Chemical Analyses

	25/5-E		24/1-HI		LMIII30b		AIYANSH		PAP	
	XRF[1]	EDA[2]	XRF[1]	EDA	XRF[1]	EDA	WET-CHEM[2]	EDA	EDA[3]	EDA
SiO2	67.03	67.27	64.13	64.52	63.66	63.87	46.58	48.06	47.92	47.95
TiO2	0.45	0.50	0.41	0.40	0.57	0.57	3.72	3.58	1.77	2.30
Al2O3	13.44	13.45	17.47	17.61	16.42	16.48	14.40	14.79	15.00	14.55
										0.06=Cr2O3
Fe2O3	7.53	7.57	4.10	3.59	3.23	2.89	2.27	3.49	4.22	4.36
FeO	0.21	0.21	0.94	0.94	3.11	3.11	12.76	10.45	7.42	7.15
MnO	0.17	0.20	0.14	0.10	0.26	0.26	.29	.18	.14	0.13
MgO	0.07	0.10	0.16	0.12	0.43	0.43	4.52	4.24	10.61	10.63
CaO	0.34	0.30	1.02	1.01	1.54	1.54	7.53	7.51	7.80	8.30
								0.10=BaO		
Na2O	5.89	5.92	6.15	6.14	5.16	5.17	4.12	4.18	1.57	2.16
K2O	4.59	4.92	5.33	5.34	5.26	5.27	1.87	1.79	1.54	1.16
P2O5	0.04	0.00	0.10	0.10	0.12	0.12	1.15	1.18	n.a.	0.39
S	0.01	0.00	0.00	0.00	0.02	0.05	n.a.	n.a.	n.a.	0.37=CO2
H2O+	0.23	0.30	0.06	0.06	0.23	0.21	0.16	n.a.	n.a.	0.43
TOTAL	100.00	100.74	100.01	100.01	100.01	99.97	99.32	99.55	97.99	99.94

1) XRF analyses by J.G. Holland after the method of Brown et al (1977)

2) Wet chemical analysis by J. Nicholls, separate sampling of same Lava Flow, Nicholls et al (in prep), original total 99.39 with .07 H2O

3) EDA Microprobe analysis of glass prepared for viscosity measurement by C.M. Scarfe, Scarfe and Hamilton (1980)

Figure 7-1.
Histograms of chemical composition for the various Level Mountain lavas. Number of samples versus oxide content (dry basis). Rock types: RHY - rhyolite; COM - comendite; PANT - pantellerite; TRACH - trachyte; BEN - benmoreite; TRIS - tristanite; PHO - phonolite; MUG - mugearite, HAW - hawaiite; AB - alkali basalt; ANK - ankaramite.

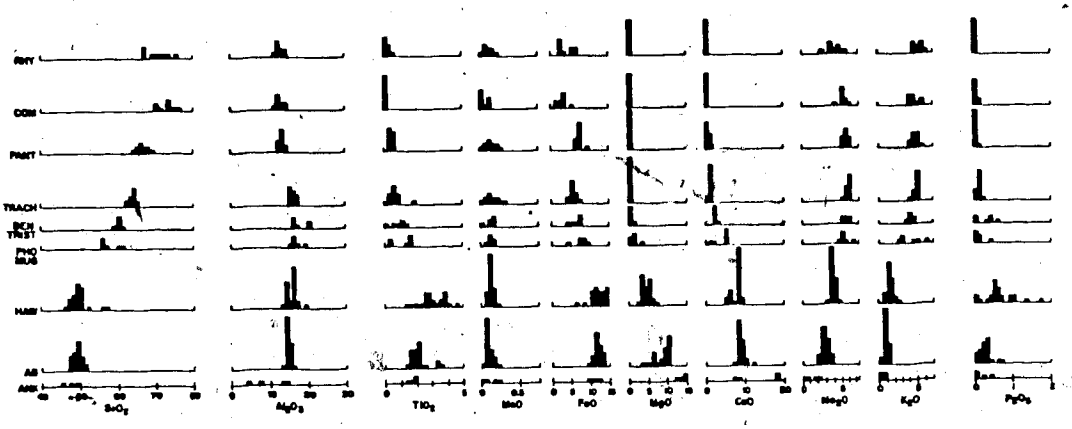

Figure 7-2.
Level Mountain lavas on the normative classification plot of Irvine and Baragar (1971).

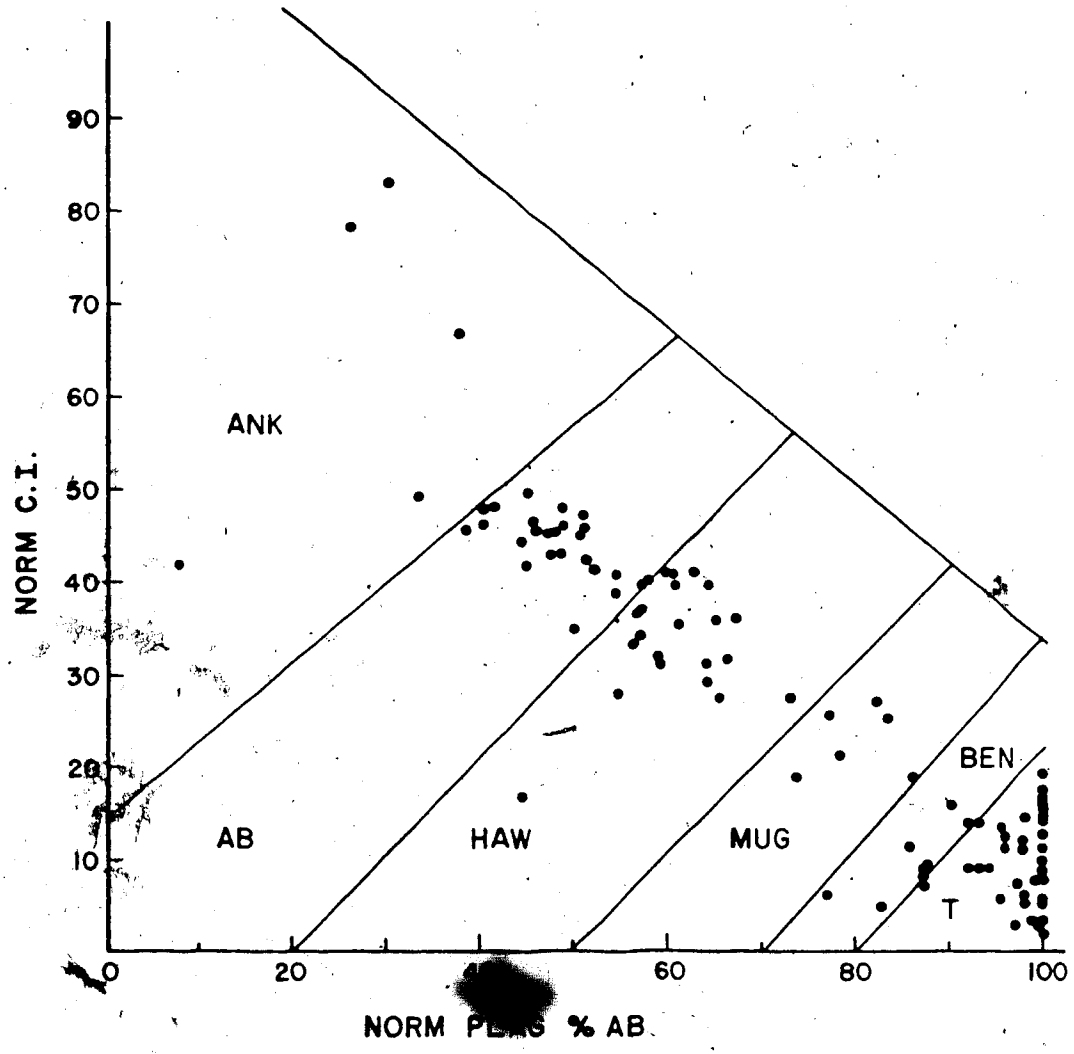

the familiar AFM and $CaO - Na_2O - K_2O$ plots, both mol ratio, are presented in figures 7-3 and 7-4 respectively. The dense clusters of points reflect the bimodal distribution of lava types with few intermediate compositions. The bimodal distribution and compositional gap is also well expressed in the atomic ratio plot (Fe+Mg)/Al versus (Na+K)/Al, figure 7-5. In this plot the intermediate lavas, which are thought to be formed by a combination of magma mixing and crustal contamination, are represented by squares, while the primary magma types are labeled with dots for salic and triangles for basalts. The next pair of figures 7-6 are atomic ratio plots of Si/Al versus agpaitic index. Note the similarity in overall range and distribution for Level Mountain lavas as compared with other major Cenozoic volcanic centres of the Intermontane Belt.

Ankaramites (Olivine Rich Basalts)

In the case of the ankaramites, which tended to be coarsely crystalline and altered, only four analyses were made, table 7-3. For the norm calculations on these oxidized samples, iron oxidation state has been adjusted according to the TiO_2 content (Irvine and Baragar, 1971). These lavas are higher in magnesium than the other Level Mountain basalt types, while the concentration of all other major elements considered is similar to, or lower than, in the basalts. Table 7-4 presents some representative ankaramite analyses from other localities. The only published ankaramite analyses from the Cenozoic of British Columbia are from

Figure 7-3.
AFM plot for Level Mountain lavas.

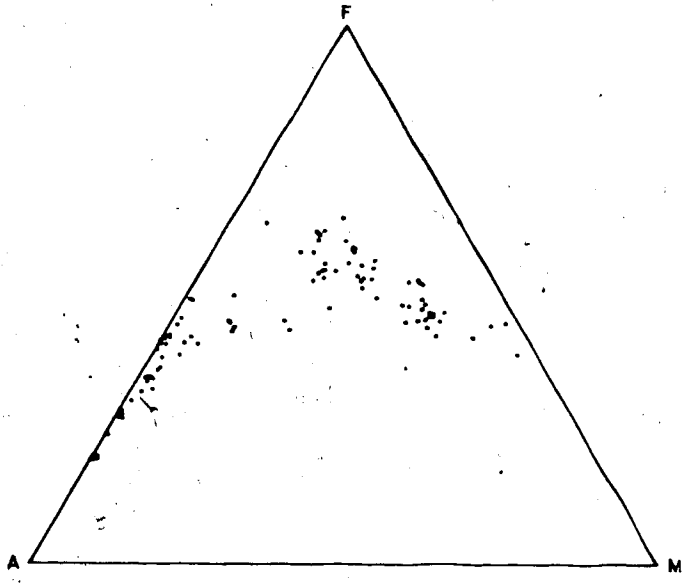

Figure 7-4.
Distribution of Level Mountain lavas in $CaO-Na_2O-K_2O$.

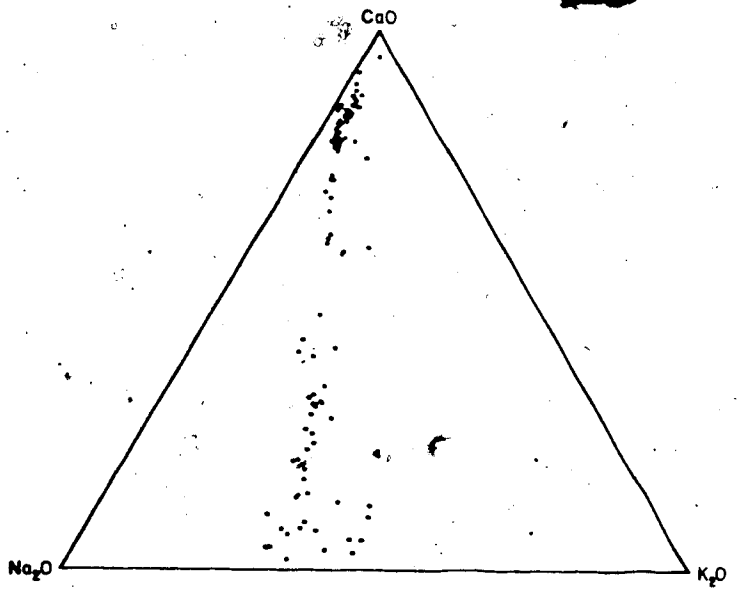

Figure 7-5.
Atomic ratio variation diagram for Level Mountain lavas.

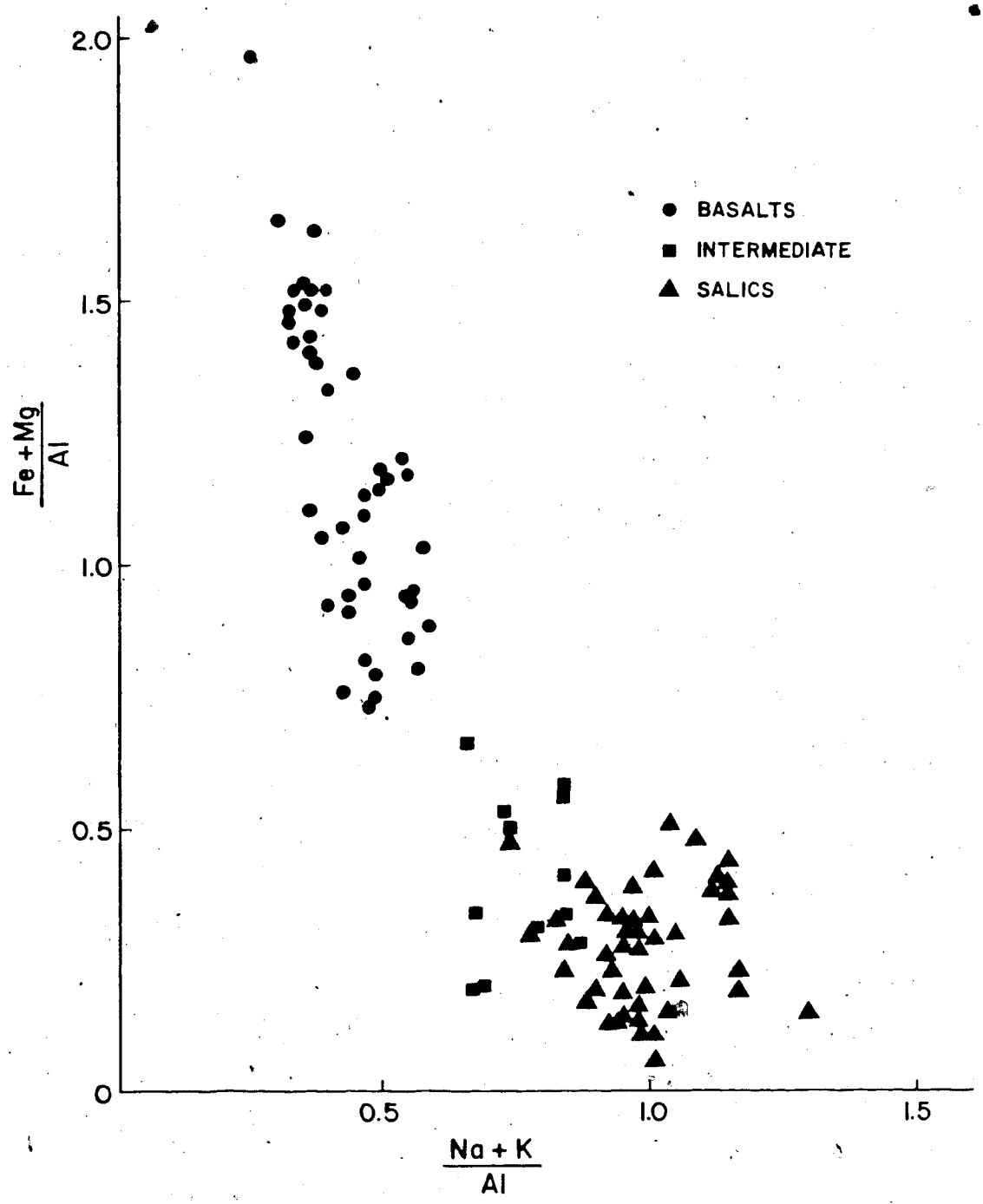

Figure 7-6.
Si/Al versus agpaitic index atomic ratio plots for Level Mountain lavas and other Late Cenozoic lavas of the Intermontane Belt. There are really two distinct trends here. For the basalts, Al variation is independent of Si/Al, while for salic lavas, Si/Al variation is largely independent of Al.

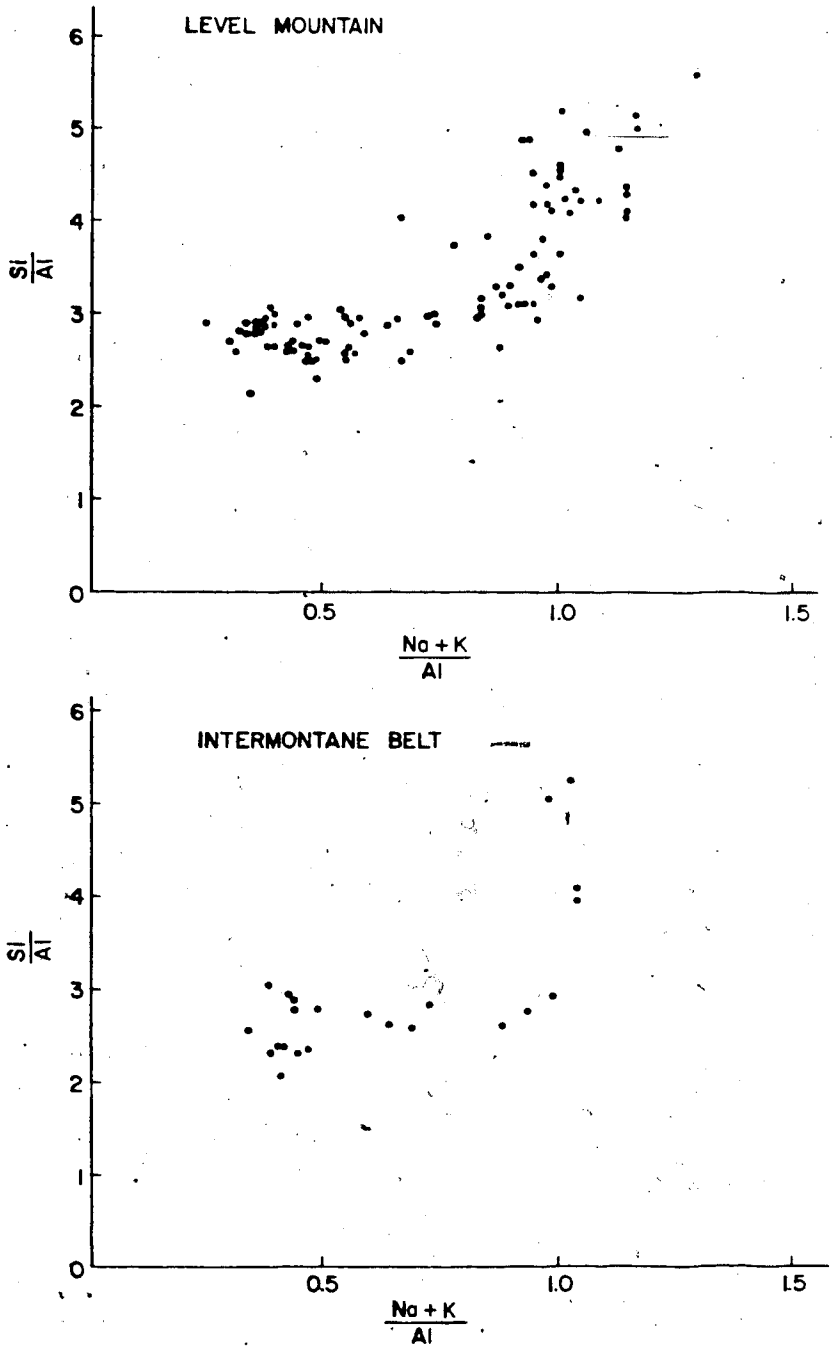

Table 7-3. LEVEL MOUNTAIN ANKARAMITE CHEMICAL ANALYSES

	H	CB	01	24/2F
SiO_2	44.9	46.8	48.5	49.3
TiO_2	1.8	1.8	1.4	1.7
Al_2O_3	14.1	13.7	7.0	4.2
Fe_2O_3	4.8	5.7	1.3	8.1
FeO	7.9	6.6	8.1	3.6
MnO	0.2	0.2	0.1	0.0
MgO	11.6	14.6	14.4	13.8
CaO	8.0	7.4	18.2	18.8
Na_2O	2.0	1.6	0.7	0.5
K_2O	0.9	0.9	0.0	0.0
P_2O_5	0.4	0.3	0.0	0.0
H_2O^+	2.0	0.1	0.0	0.0
H_2O^-	1.3	0.0	0.0	0.0
ORIGINAL TOTAL	99.60	100.00	98.84	98.45
%MELT	13.75	14.42	16.95	16.29
Q				
OR	5.6	4.3		
AB	17.7	13.7	5.8	4.2
AN	27.8	27.6	16.1	9.4
PL	45.5	41.3	21.9	13.6
WO	4.4	3.2	31.0	35.2
EN	2.9	2.3	21.5	25.4
FS	1.1	0.6	6.9	6.7
DI	8.4	5.2	59.4	67.3
EN	10.0	18.4	0.4	7.9
FS	3.7	4.8	0.1	2.1
HY	13.7	23.2	0.5	10.0
FO	11.9	11.2	9.9	0.9
FA	4.9	3.2	3.5	0.3
OL	26.6	14.4	13.4	1.2
MT	5.0	4.8	1.9	4.7
IL	3.6	3.4	2.7	3.3
AP	1.0	0.6		
Map unit	3	3	5b or younger	5b

Table 7-4. Ankaramite Chemical Analyses From Other Localities

Weight Percent	Spanish Creek QV19&QV20[1]	New Georgia[2]	New Hebrides[3]	Tahiti[4]	Hawaii[5]	Alaska[6]
SiO2	45.87	48.68	48.59	43.26	47.25	49.2
TiO2	2.32	0.43	0.67	3.40	1.61	0.2
Al2O3	13.41	12.44	11.91	9.69	9.07	2.4
Cr2O3		0.08				
Fe2O3	2.73	3.90	4.81	3.66	1.45	2.0
FeO	9.10	6.49	4.97	8.97	10.41	6.8
MnO	0.16	0.20	0.19	0.16	0.13	0.2
MgO	10.11	11.36	13.18	12.64	19.96	19.1
CaO	10.60	11.17	12.31	12.10	7.88	18.9
Na2O	3.34	1.93	2.16	1.59	1.38	0.2
H2O	1.58	1.51	0.95	1.18	0.35	0.1
P2O5	0.46	0.24	0.14	0.61	0.21	--
H2O	0.35	1.68	0.45	2.46	0.12	0.8
TOTAL	100.03	100.21	100.33	99.72	99.82	99.9

(1) D.W. Fiesinger and J. Nicholls (1975).

(2) R.L. Stanton and J.D. Bell (1969).

(3) A.J. Warden (1970).

(4) A.R. McBirney and K. Aoki (1968).

(5) G.A. MacDonald (1949).

(6) J.C. Rudnick and J.A. Noble (1959).

Spanish Creek in Well's Gray Park (Fiesinger and Nicholls, 1977). The Spanish Creek flow is higher in Ti, Na, K and P and lower in Mg than the Level Mountain ankaramites.

At Level Mountain, the older ankaramites differ from the other basalt types mainly in amount of phenocryst and possibly xenocryst olivine, or in degree of fractional crystallization of olivine. For the variation index, $(CaO+Na_2O+K_2O)/Al_2O_3$ mol, which is a measure of alkalinity, the high Al_2O_3 ankaramites are comparable to the alkali basalts at 1.3. The late ankaramites have very high contents of clinopyroxene (60%) both in thin section and in their norms. Their values of the aforementioned alkalinity index at 4.9 and 8.3 are out of character for normal basalts and even the strongly alkaline basanitoids which are generally less than two. They are spatially and temporally associated with peralkaline trachytes that sometimes are laden with nodules rich in clinopyroxene. It is interesting to note that fractionating a feldspar of any composition from these ankaramites would produce peralkaline residua. The levels of alumina in these ankaramites (5.67%), are very low for alumina in any igneous rock type. Their peculiar chemistry is somewhat akin to komatiites which are unknown from the Tertiary and not associated with alkaline suites. The peculiar circumstances of their occurence at Level Mountain in conjunction with their refractory chemical nature suggest that the low alumina ankaramites are evolved rocks.

Alkali Basalts from Level Mountain and a Comparison with B.C. and World Averages.

Chemical analyses of twenty-four primitive basalts from Level Mountain are presented in Table 7-5 along with their C.I.P.W. norms. These include both alkali basalts in the sense of Irvine and Baragar (1971) and associated lavas which are petrographically and chemically similar but contain normative hypersthene. Their order of presentation in the table is according to stratigraphic succession with examples from the plateau units 1, 2, 3, and 4 and also the stratocone units 5b, 6b or younger. Chemically primitive basalts are present for most of the eruptive history. For the basalts, the only major oxide with a bimodal distribution is MgO. Among the minor components, BaO and H_2O also showed bimodal distributions. Analyses with high and low values for MgO were grouped and averaged. The higher MgO group was found to contain significantly less Al_2O_3 and Na_2O than the low MgO group, but comparable levels of all other components. This division on MgO did not correspond to a clear division in time or space for occurrence, as the low MgO group includes both analyses from the basal plateau unit and from the stratocone cap. The high MgO group could be due to less olivine fractionation (olivine enrichment) or a higher degree of partial melting. Slight olivine enrichment is petrographically supported. Similar cluster analyses were performed on simple tests of the mean for BaO. The high BaO group, again not stratigraphically distinctive, contained

TABLE 7-5 LEVEL MOUNTAIN BASALTS

	PAY 3650	PAX 3675	PAW 3700	PAU 3815	PAR 4030	PAQ 4065	PAP 4100	PAO 4115	PAN 4125	PAM 4135	PAL 4155	PAK 4170
SiO_2	48.8	49.8	44.9	50.2	48.7	48.9	47.8	50.0	48.3	48.6	46.8	46.7
TiO_2	1.8	2.1	1.9	1.5	1.8	1.7	2.3	1.6	1.6	1.8	2.0	2.2
Al_2O_3	13.9	14.3	13.7	14.0	14.3	14.2	14.5	15.2	14.3	14.8	13.5	14.0
Fe_2O_3	4.7	4.8	4.9	4.0	1.3	4.2	4.8	3.1	3.2	5.3	2.4	1.4
FeO	6.5	7.2	4.4	6.6	9.8	7.7	7.1	7.5	8.9	7.2	9.7	11.4
MnO	0.1	0.1	0.2	0.1	0.1	0.1	0.1	0.1	0.1	0.1	0.1	0.1
MgO	8.5	6.3	6.9	10.7	9.3	9.7	10.6	9.3	10.7	10.0	10.7	9.9
CaO	7.5	8.3	11.4	8.5	9.9	9.2	8.3	8.4	8.3	8.1	9.1	9.6
Na_2O	2.9	3.5	2.6	2.7	3.3	2.6	2.2	2.6	2.7	2.5	2.6	2.5
K_2O	0.8	0.9	0.7	0.9	1.1	0.9	1.2	1.1	0.8	0.9	0.9	0.9
P_2O_5	0.2	0.4	0.3	0.2	0.3	0.2	0.4	0.2	0.1	0.1	0.3	0.5
H_2O^+	2.9	1.6	3.0	1.0	0.0	0.5	0.4	1.2	0.9	0.5	0.8	0.7
H_2O^-	1.5	0.9	2.3	0.0	0.0	0.0	0.0	0.0	0.0	0.0	1.0	0.0
CO_2			3.1				0.4	0.0				
Orig. Tot.	101.5	101.5		100.9	101.9	101.1	100.9	99.9	100.9	101.8	100.7	100.7
% MELT	16.0	13.7		15.2	12.1	14.7	11.1	11.9	15.8	14.9	13.7	12.1
Q												
OR	4.8	5.6	4.6	5.1	6.4	5.2	6.9	6.4	4.9	5.4	5.5	5.2
AB	25.4	30.1	23.7	23.1	22.8	22.4	18.4	22.2	23.0	21.3	21.8	20.4
AN	23.8	21.3	25.7	23.7	21.3	24.6	26.7	26.8	24.8	26.7	22.5	23.9
PL	49.2	51.4	49.4	46.8	44.1	47.0	45.1	49.0	47.8	47.0	44.3	44.3
NE					2.7							
WO	5.7	7.8	14.1	7.4	10.9	8.3	5.1	5.8	6.6	5.5	8.9	8.4
EN	3.8	4.7	10.0	5.1	6.4	5.4	3.6	3.9	4.3	3.5	5.6	4.8
FS	1.5	2.7	3.0	1.7	4.0	2.4	1.1	1.5	1.9	1.6	2.7	3.2
DI	11.0	15.1	27.1	14.1	21.3	16.1	9.8	11.2	12.8	10.6	17.2	16.4
EN	18.4	10.7	1.9	14.6		9.2	15.7	15.7	8.3	12.6	2.1	1.5
FS	7.4	6.1	0.6	4.9		4.0	4.8	5.9	3.5	5.6	1.0	1.0
HY	25.8	16.8	2.5	19.5		13.2	20.5	21.6	11.8	18.2	3.1	2.5
FO		0.6	4.9	5.2	11.7	6.9	5.2	2.6	10.0	6.3	13.3	12.5
FA		0.4	1.6	1.9	7.9	3.3	1.7	1.1	4.7	3.1	7.0	9.1
OL		1.0	6.5	7.1	19.6	10.2	6.9	3.7	14.7	9.4	20.3	21.6
MT	5.1	5.3	5.3	4.3	1.9	4.6	5.5	4.5	4.6	4.8	3.4	1.9
IL	3.7	4.0	3.9	2.8	3.4	3.2	4.4	3.1	3.1	3.4	3.8	4.1
AP	0.5	0.8	0.7	0.4	0.7	0.6	0.9	0.4	0.3	0.2	0.6	1.1
Classif.	T	T	AB	T	AB	T	T	T	T	T	AB	AB
Map Unit	1	1	1	2	2	3	3	3	3	3	3	3

TABLE 7-5 continued

	PAJ 4200	PAI 4230	29/IL	29/IK	29/IF Early	16/19D	PAD 4400	PAB 4505	PAA 4560	Q4	PBB 5430	PBC 5450	KD-1 DYKE
SiO_2	48.1	49.7	45.5	48.5	45.5	50.0	48.8	49.3	46.8	50.2	48.0	47.1	48.6
TiO_2	2.1	1.7	2.0	1.7	2.0	2.7	2.7	1.7	3.6	1.7	3.3	3.1	2.2
Al_2O_3	14.1	14.8	13.7	14.3	14.0	15.3	15.5	14.5	15.1	16.1	15.1	15.1	15.6
Fe_2O_3	3.4	4.7	3.4	1.1	8.2	3.9	2.5	2.7	4.5	1.4	5.5	7.6	2.6
FeO	8.4	6.3	10.2	10.7	5.4	8.3	10.2	10.6	9.0	9.9	7.4	6.2	9.9
MnO	0.1	0.1	0.2	0.1	0.2	0.1	0.1	0.0	0.1	0.1	0.1	0.2	0.2
MgO	10.5	10.3	9.1	10.2	10.1	5.9	6.3	8.6	6.7	5.4	4.3	3.7	6.0
CaO	8.5	8.0	9.7	8.2	9.1	8.2	8.0	8.9	8.8	9.6	9.9	9.4	10.2
Na_2O	2.8	2.8	2.4	2.6	2.1	3.6	3.6	3.1	3.3	3.7	3.4	3.0	3.4
K_2O	1.0	0.9	0.7	0.8	1.3	1.5	1.3	0.3	1.0	0.9	1.0	1.0	0.4
P_2O_5	0.4	0.2	0.2	0.0	0.4	0.5	0.8	0.0	0.6	0.0	0.3	0.3	0.3
H_2O^+	0.8	0.4	1.0	2.0	1.5	1.5	0.5	0.1	0.0	0.6	0.7	1.6	0.3
H_2O^-	0.0	0.0	0.6	0.0	0.0	0.7	0.3	0.2	0.1	0.4	1.1	1.7	0.3
CO_2													
Orig. Tot.	100.3	100.8	98.1	100.0	100.0	100.0	100.2	99.9	99.8	100.0	99.3	99.1	99.5
% MELT	13.5	13.7	19.1	16.6	9.8	8.6	7.5	18.4	9.1	15.1	13.4	12.9	16.6
Q											0.6	2.0	
OR	5.5	5.6	4.0	4.4	7.8	8.7	7.5	1.8	6.0	6.0	5.7	6.0	2.4
AB	23.5	23.9	20.1	21.2	17.7	30.0	30.5	26.1	28.3	31.2	29.0	26.3	28.5
AN	22.5	25.0	25.1	24.6	25.8	21.4	22.5	24.7	23.3	25.0	23.9	25.8	25.9
PL	46.0	48.9	45.2	45.8	43.5	51.4	52.9	50.8	51.5	56.1	52.9		54.3
NE										0.1			0.2
WO	6.9	5.7	9.4	6.4	7.2	6.5	5.2	8.1	7.1	9.5	10.3	8.6	9.3
EN	4.7	3.9	5.7	3.7	4.7	4.0	2.8	4.6	4.7	4.5	6.4	4.6	4.1
FS	1.7	1.3	3.2	2.3	2.1	2.2	2.2	3.1	2.0	4.9	3.3	3.7	5.2
DI	13.3	10.9	18.2	12.4	14.0	12.7	10.2	15.9	13.7	18.9	20.0	17.0	18.6
EN	6.7	13.5	5.8	7.7	5.5	2.9	2.0	8.0	3.5		4.5	5.0	
FS	2.4	4.5	3.3	4.9	2.5	1.6	1.5	5.4	1.5		2.3	4.0	
HY	9.1	18.0	9.1	12.6	8.0	4.5	3.5	13.4	5.0		6.8	9.0	
FO	9.9	5.8	8.2	9.4	10.9	5.4	7.1	6.1	5.9	6.3			7.6
FA	3.9	2.2	5.1	6.6	5.4	3.3	6.6	4.6	2.7	7.4			10.8
OL	13.9	8.0	13.3	16.0	16.3	8.7	14.3	10.6	8.6	13.7			18.4
MT	4.8	4.7	4.9	1.6	5.1	5.6	3.7	3.9	6.5	2.0	7.1	7.0	
IL	3.9	3.3	3.9	3.1	3.8	5.1	5.1	3.3	6.9	3.3	6.4	6.2	4.2
AP	0.8	0.5	0.5		1.0	1.3	1.9		1.4		0.6	0.7	0.7
Classif.	AB	T	AB	AB	T	AB	AB	AB	AB	AB	T	T	AB
Map Unit	3	3	3	3	3	3	4	4	4	4	5b	5b	8

marginally higher values of P_2O_5 and K_2O and marginally lower values of MnO. Perhaps the high $BaO+P_2O_5+K_2O$ lavas represent smaller degrees of partial melting or residual element type enrichment due to fractionation of olivine and clinopyroxene. For the H_2O division, the high total water group showed greater levels of SiO_2 and MgO with lower levels of Na_2O. Replacement of 5 to 10% of the groundmass glass by a septechlorite could account for the H_2O and MgO increase but this would cause an FeO* increase, which is not observed, and an SiO_2 decrease rather than the observed increase. Also the high H_2O group does not uniformly show more extensive groundmass alteration than the low H_2O group. Another possibility is that the high H_2O group represents slightly more hydrous melting conditions than prevailed for the majority of the basalts. For any of the three clusterings discussed, it should be emphasized that no cluster corresponds to a distinctive group of flows either in age or location. If all of the Level Mountain basalts are primary, perhaps these slight chemical differences represent local variations in source composition or differences in melt extraction and derivation. These clustering tests are summarized in Table 7-6.

Level Mountain basalts are petrographically all of alkaline affinity, but chemically some approach the subalkaline type considered to be transitional to tholeiites. Some of these lavas in fact have hypersthene as the dominant normative ferromagnesian mineral despite the

Table 7-6. LEVEL MOUNTAIN ALKALI BASALTS CLUSTER ANALYSES

	High Mg (16)		Low Mg (7)	High Ba (8)		Low Ba (15)	High H_2O (13)		Low H_2O (10)
SiO_2	49.17		49.34	48.67		49.49	49.62	>	48.67
TiO_2	1.87		2.73	2.22		2.08	2.00		2.27
Al_2O_3	14.50	<	15.58	14.59		14.94	14.73		14.94
FeO*	11.62		12.45	12.36		11.82	11.42		12.45
MnO	.09		.12	.09	<	.11	.10		.10
MgO	9.84	>	5.65	9.03		8.31	9.16	>	7.79
CaO	9.03		9.36	8.87		9.26	8.96		9.50
Na_2O	2.72	<	3.47	2.98		2.93	2.78	<	3.18
K_2O	.87		.93	.98	>	.84	.93		.84
P_2O_5	.23		.37	.39	>	.21	.26		.29
BaO				.20	>	.00	.05		.10
H_2O							1.27	>	.42
				Sem		Sem	Sem		Sem
SiO_2	1.24		1.43	.54		.27	.35		.35
TiO_2	.24		.71	.23		.15	.13		.21
Al_2O_3	.44		.48	.23		.17	.13		.27
FeO*	1.08		.79	.58		.29	.29		.25
MnO	.04		.05	.00		.01	.01		.02
MgO	.96		1.11	.58		.64	.56		.72
CaO	1.12		.85	.28		.30	.34		.28
Na_2O	.28		.21	.15		.12	.09		.14
K_2O	.20		.26	.05		.06	.03		.09
P_2O_5	.12		.26	.08		.03	.04		.08
BaO				.03		.00	.02		.04
H_2O							.25		.11

total absense of phenocryst orthopyroxene or groundmass subcalcic pyroxenes. Some of the basalts have high enough silica contents for dominant hypersthene, (silica saturation) yet have sufficient alkalis to plot above MacDonald and Katsura's (1964) alkaline/tholeiitic line. The average alkalinity index, $(mol(CaO+Na_2O+K_2O)/Al_2O3)$, of 1.42 is not appreciably different than a typical value for Level Mountain or B.C. MgO is high enough and TiO_2 low enough that these rocks do not belong with hawaiites either. The problem, given their petrographic characteristics and alkaline association on one hand versus their silica saturation seen as normative hypersthene on the other are (i) how to classify them and (ii) are they really distinctive chemically from more ordinary alkali basalts. The Level Mountain basalts were divided on normative criteria into alkaline and transitional types to see what the systematic differences were, if any. Additionally, the transitional types from Level Mountain were chemically compared to similar basalts from central B.C. Again tests of mean and standard deviation were applied. The results are presented in table 7-7. The transitional basalts from Level Mountain and Central B.C. are virtually indentical. Any differences in major element chemistry for the bona fide alkaline basalts at Level Mountain versus the transitional types are within one standard deviation. It is felt that the calculation of dominant normative hypersthene for some basalts is not statistically significant of any major

Table 7-7. Averages for transitional versus alkaline basalts.

	Level Mtn 10 Transitional basalts	Level Mtn 14 Alkali Basalts	Central BC (1) 8 Transitional
SiO2	50.06± .83	48.48±1.19	51.02±1.51
TiO2	1.71± .12	2.43± .60	1.85± .14
Al2O3	14.83± .63	14.81± .72	15.00± .65
FeO*	11.43± .89	12.29±1.08	10.69± .90
MnO	.08± .03	.12± .05	.13± .03
MgO	9.47±1.60	8.21±2.44	7.82±1.45
CaO	8.60± .57	9.52±1.10	9.25± .63
Na2O	2.83± .37	2.96± .52	3.30± .29
K2O	.82± .20	.96± .23	.76± .24
P2O5	.13± .09	.38± .16	.20± .12
	Dominant Normative Hypersthene	Normative ol or cpx dominant	
Mol (CaO+Na2O+K2O) / (Al2O3) A.I.	1.42	1.57	1.54

1. New analyses this work: Mann Creek, Redstone Hanceville, Bull Canyon
other if included in average from Fiesinger and Nicholls (1977) Wells Gray & Quesnel Lake

chemical distinction either in classification or genesis. It may relate in part to the oxidation state of the iron in the analysis and its effect on calculated normative iron bearing silicates. The alkaline basalt group does have marginally higher levels of TiO_2, K_2O and P_2O_5 with lower SiO_2 than the transitional basalts and a slightly higher alkalinity index. This may reflect a difference in the degree of partial melting, with the transitional type representative of a higher percentage of partial melting or melting at higher pH_2O. Again it should be emphasized that the two types are thoroughly interspersed stratigraphically. Even if the two types represent differences in mantle melting conditions or extent, the chemical variation between them is continous rather than discreet. Any variations in the derivation process are thus probably continous as well.

Table 7-8 presents average and representative alkali basalt analyses for the Cenozoic of B.C. The lavas and averages presented here were selected to represent alkali basalts of similar derivation and at a similar stage of evolution. Hawaiites have been excluded as these are probably derived from alkali basalts via extensive fractional crystallization. A range of $14.0<(CaO+MgO)<20.0$ weight percent was used to restrict the effect of fractionation processes. A cutoff of $1.3<(CaO+Na_2O+K_2O)/Al_2O_3$ mol ratio was applied to select lavas of undeniable alkaline affinity. Thirty four lavas were found to meet these criteria and were hierarchically

Table 7.8 Alkali Basalts, Late Cenozoic, B.C.

	1	2	3	4	5	6	7
SiO2	49.20±.26	47.27±.38	48.19±.23	48.66	48.25±.06	49.93±.46	48.46±.20
TiO2	2.13±.12	3.00±.14	2.23±.33	2.27	2.13±.01	7.00±.21	2.44±.38
Al2O3	14.82±.14	15.94±.20	16.21±1.00	16.42	13.71±.05	16.81±1.32	14.64±.40
FeO*	11.87±.22	11.68±.31	12.00±.44	11.66	10.83±.12	11.63±.14	12.04±.39
MnO	.10±.01	.16±.01	.19±.01	.16	.16±.00	.14±.01	.17±.01
MgO	8.56±.46	7.18±.46	8.08±.25	6.76	9.11±.03	6.19±.93	8.51±.23
CaO	9.23±.23	9.48±.15	8.69±.81	8.86	9.16±.40	8.26±.04	8.07±.63
Na2O	2.95±.09	3.22±.11	3.05±.15	3.75	4.34±.11	3.51±.05	3.62±.15
K2O	.89±.04	1.25±.09	1.01±.13	1.02	1.58±.20	1.15±.01	1.53±.63
P2O5	.27±.04	0.81±.06	.20±.12	.42	.74±.07	0.38±.01	.52±.02
$\frac{CaO+Na2O+K2O}{Al2O3}$	1.52	1.50	1.35	1.42	1.86	1.31	1.52

	8	9	10	11	12	13	14
SiO2	45.92	48.90±.33	50.00±1.12	49.51±.19	50.02	48.94±.88	47.18±1.44
TiO2	3.36	1.86±.02	2.00±.07	1.80±.12	1.85	2.16±.34	2.37±.54
Al2O3	14.83	14.41±.10	14.74±.62	14.28±.06	15.04	15.19±1.00	14.97±1.27
FeO*	12.70	11.19±.04	11.32±.70	11.33±.01	10.88	11.49±.42	11.48±1.35
MnO	.11	.20±.02	.18±.01	0.14±.01	.14	.16±.03	.17±.02
MgO	7.47	9.19±.02	7.44±1.22	9.46±.40	7.79	8.02±1.06	8.36±1.76
CaO	8.24	9.77±.17	9.87±.05	9.46±.04	9.33	9.11±.58	9.96±1.09
Na2O	4.42	3.79±.01	2.87±.47	2.87±.05	3.59	3.43±.42	3.10±.36
K2O	2.12	.88±.10	.68±.01	.88±.01	.92	1.07±.28	1.08±.54
P2O5	.81	.30±.02	.27±.03	.27±.01	.32	.41±.20	.58±.22
$\frac{CaO+Na2O+K2O}{Al2O3}$	1.68	1.67	1.66	1.60	1.59	1.54	1.63

1. Level Mtn (23) Hamilton, This work
2. Heart Peaks (14) Casey, thesis U of A (1980)
3. Edziza (4) Souther and Symons (1974)
4. Stikine River (1) Nicholls et al (1981) in prep
5. Atlin Lake (2) Nicholls et al (1981)
6. Rainbow Range (2) Bevier thesis UBC
7. Itchas (5) Nicholls et al (1981) in prep
8. Itchas (1) Hamilton, this work
9. Trophy Mtn (3) Fiesinger & Nicholls (1977)
10. Wells Gray (2) Fiesinger & Nicholls (1977)
11. Quesnel Lake (2) Fiesinger & Nicholls (1977)
12. Kallis Creek (1) Nicholls et al (1981) in prep
13. BC Average (11) (57)
14. World average exclusive of B.C. (15 regions 140 analyses)

B

averaged by area, for a data set of eleven averages. These were in turn used to generate a B.C. average and also as a test for source chemistry variation and differences in degree of partial melting. In a similar fashion a world average alkali basalt, exclusive of B.C., was generated from 140 analyses selected from the published literature representing fifteen sub-regions. These are presented in Table 7-9. For comparison, this world average is also presented in Table 7-8. The Level Mountain average and B.C. average are within one standard deviation for all components. The B.C. average and world average are within one standard deviation for all components. Level Mountain appears to be higher in SiO_2 than the world average but if more stringent selection criteria are used, the Level Mountain average of fourteen alkali basalts from table 7-7 is within one standard deviation of the world average for all oxides. On this basis all of the B.C. basalts are judged to be ordinary alkali basalts as they fall within the variation of continental and oceanic alkali basalts from elsewhere in the world. There is no obvious strong correlation between the B.C. analyses and alkali basalts from any specific tectonic setting or region of the world. Neither the basalts from Level Mountain nor from B.C. as a whole, are obviously "rift type" basalts or "continental margin type".

It is noteworthy that all of the B.C. plateau types have above average values for FeO* as do all of the lavas

Table 7.9 Comparative analyses of Alkali Basalts

	Recast World Avg	%var	World Avg (40)	Std Dev	Hawaii (3)	New Zealand (14)	New Zealand (13)	OFB (75)	NSW	Uganda
SiO2	47.18	1.04	47.08	±1.44	46.08	49.34	44.80	49.56	47.51	45.2
TiO2	2.17	22.88	2.36	±.54	2.79	1.17	1.96	1.42	2.82	2.3
Al2O3	14.97	8.51	14.83	±1.27	14.74	15.71	13.86	16.09	16.85	16.2
FeO*	11.48	11.79	11.45	±1.35	10.95	11.45	12.25	10.17	10.51	11.95
MnO	.17	11.76	.17	±.02	.13	0.15	0.17		0.15	0.17
MgO	8.36	23.50	8.34	±1.76	9.81	6.03	11.07	7.69	5.62	7.60
CaO	9.96	10.98	9.91	±1.09	10.54	8.38	10.16	11.14	8.28	9.30
Na2O	3.03	11.65	3.09	±.36	2.50	3.69	3.19	2.80	3.47	3.20
K2O	1.08	50.00	1.08	±.54	0.85	1.39	1.09	0.24	1.08	0.81
P2O5	0.58	37.93	.58	±.22	0.37	0.73	0.55		0.81	0.39
H2O	0.75	54.67	0.75	±.41	0.93		0.73		0.59	1.00
	100.00		99.74		100.19	99.84	99.83	100.00	99.83	99.95

	Pantelleria (3)	E Africa	Kurile (2)	Baseti (2)	Anjovan 1	Y A I 1962	Baikal Rift (2)	SRP (15)	Massif Central (6)
SiO2	47.32	48.10	48.12	47.82	46.88	46.53	47.37	46.34	44.72
TiO2	3.16	1.45	2.07	1.86	2.39	2.28	2.40	2.72	2.61
Al2O3	15.57	13.20	15.31	16.37	12.08	14.31	15.40	14.35	14.45
FeO*	11.85	10.31	9.36	10.00	12.33	12.65	11.49	13.73	10.66
MnO	0.15	0.17	0.18	0.18	0.20	0.18	.17	.19	.20
MgO	5.81	10.13	9.32	7.04	9.50	9.54	7.78	7.81	10.41
CaO	9.53	12.06	8.86	11.24	10.29	10.32	8.17	9.52	9.90
Na2O	3.64	2.45	3.02	2.92	2.92	2.85	3.13	2.84	3.51
K2O	1.31	0.35	2.33	.66	1.01	0.84	1.67	.82	1.72
P2O5	0.84	0.24	0.48	.36	0.48		.48	.80	0.81
H2O	0.81	1.04	.12	1.04	0.54	0.08	1.54	.34	1.01
	99.99	99.50	99.14	99.59	98.62	99.58	99.20	99.51	100.06

1 Hawaii alkali basalts (3) avg Poliulu Haulalai from MacDonald 1949 Mauna Kea from MacDonald to Katsura (1964)
2 New Zealand basalts (14) avg Banks Peninsula Speight 1938
Auckland (13) (1974)
3 OFB (75) Ocean Floor Basalts all MORB 42 Atlantic + (Carlsberg E Pacific Galapagos) remainder Pearce (1976)
4 NSW Nanderwar Abbot (1969)
5 Uganda Morito Varne (1968)
6 Pantelleria (3) Villari (1975) + Romano (1968)
7 E Africa Erta Ale Range (1975) Barberi et al
8 #1026 Olutorskii Progi (Koryakskoe Nagorie) ed NR Zotimova (1966)
9 Baseti (2) 152f 153 avg Brotzu et al (1975) Ethiopia
10 Anjovan East Indian Ocean Thompson + Flower 1971
11 Yoder + Tilley, (1962) Martin (1975)
12 Koselev (1977) avg 118AB Baikal Rift
13 Snake River Plain (15) Stout + Nicholls 1977
14 Massif Central Paul (1970) nodule bearing basalts (basanites)

from the Stikine. This could imply that the mantle source region beneath the Stikine (Heart Peaks, Level Mountain, Stikine River, Edziza) is enriched in FeO*. This could also imply more extensive melting from iron enriched upper mantle. If alkali basalt is a primary mantle derived magma, and if these lavas in question are related only in type but not by genetic sequence, then these chemical variations might represent vertical stratification or variation in the source region. High Ti, K, and P probably represent undepleted mantle as does high Na and Al versus Mg.

Variation diagrams have been constructed for SiO_2 versus TiO_2 and Al_2O_3 versus MgO for the B.C. data set, figure 7-7. The effect of variable source contribution for typical spinel lherzolite constituents is shown as vector subtraction from the B.C. average. Model lherzolite phases were forsterite, hypersthene, chrome diopside and spinel with a whole rock Mg/(Mg+Fe) atomic ratio between 0.93 and 0.94. This composition was chosen to approximate the B.C. nodule compositions presented in a subsequent section. Kuno and Aoki (1970) estimate the bulk Mg/Mg+Fe of the upper mantle to be close to 0.89 with olivine equal to Fo_{90} and spinel less than or equal to 0.8. Using these slightly less refractory values only affects the spinel vector's direction by about 3° without affecting its length. The other vectors are unaffected. The distribution of points in both plots is parallel with the clinopyroxene vector. The length of the field on the MgO versus Al_2O_3 plot is consistent with either

Figure 7-7.
Oxide variation diagrams for basic lavas of the IMB. Vectors demonstrate the magnitude of fractionation effects for dispersing the compositions. The point "W" is the world average alkali basalt.

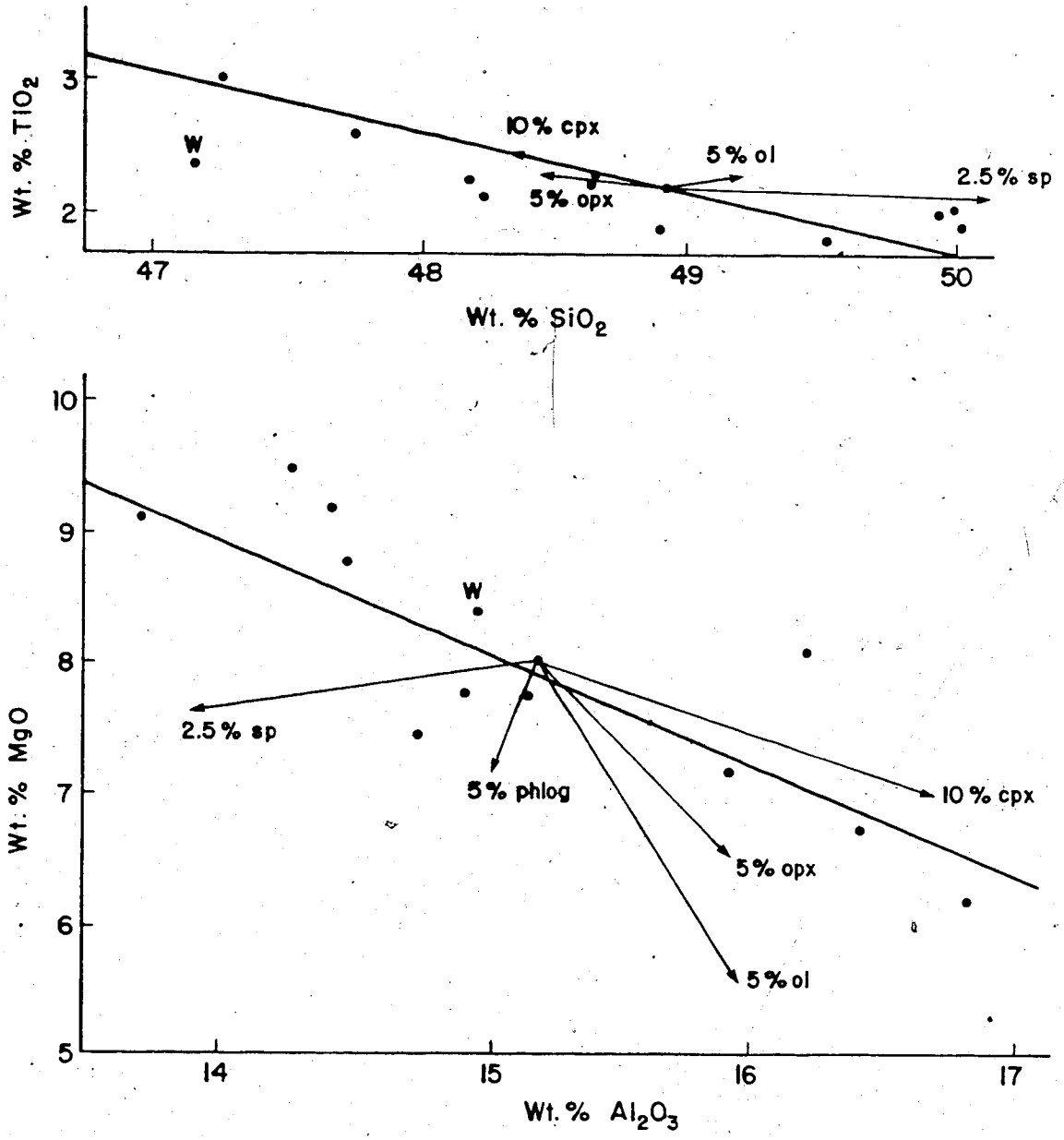

(i) a difference of 22% in the contribution of clinopyroxene to the partial melt or (ii) between 13% and 20% difference in the amount of partial melting responsible for the variation in compositions. If case two is true the major difference in percent of partial melting would still likely be related to the contribution of clinopyroxene. Model calculations for percent partial melting to derive these basalts from pyrolite range from 10% to 20% which agrees with the figures above. The variation in the TiO_2 versus SiO_2 plot is also parallel to the clinopyroxene vector but here spinel has much greater leverage such that the entire range in SiO_2 values could be explained within 6% variation of spinel contribution to the partial melt.

Variation diagrams of P_2O_5 versus TiO_2, Na_2O and K_2O have also been constructed for the B.C. data set, shown in figure 7-8.These plots are particularily useful in addressing the origin of the compositional variation. The least squares fit straight lines represent residual element models. The slopes (ratios) for K_2O and TiO_2 versus P_2O_5 are very close to unity while Na_2O/P_2O_5 is about 2. If, for instance, P_2O_5 and K_2O do not enter into any crystallizing phase and their ratio is fixed in the source region, then fractional crystallization of any non P_2O_5 and K_2O bearing phase will result in increased levels for both oxides, but still in fixed proportion. The vector corresponding to ten percent less clinopyroxene concentration is again subparallel to the trends but it is immediately obvious that

Figure 7-8.
Oxide variation diagrams for basic lavas of the IMB. Straight lines are least squares linear regression fits to the data. Curved lines are least squares exponential fits to B. C. data plus pyrolite. The point "W" is the world average. The point "B" is the B. C. alkali basalt average with the end of the arrow indicating the B.C. hawaiite average. The chemical dispersion here is probably a source variation and fractional fusion effect rather than differentiation.

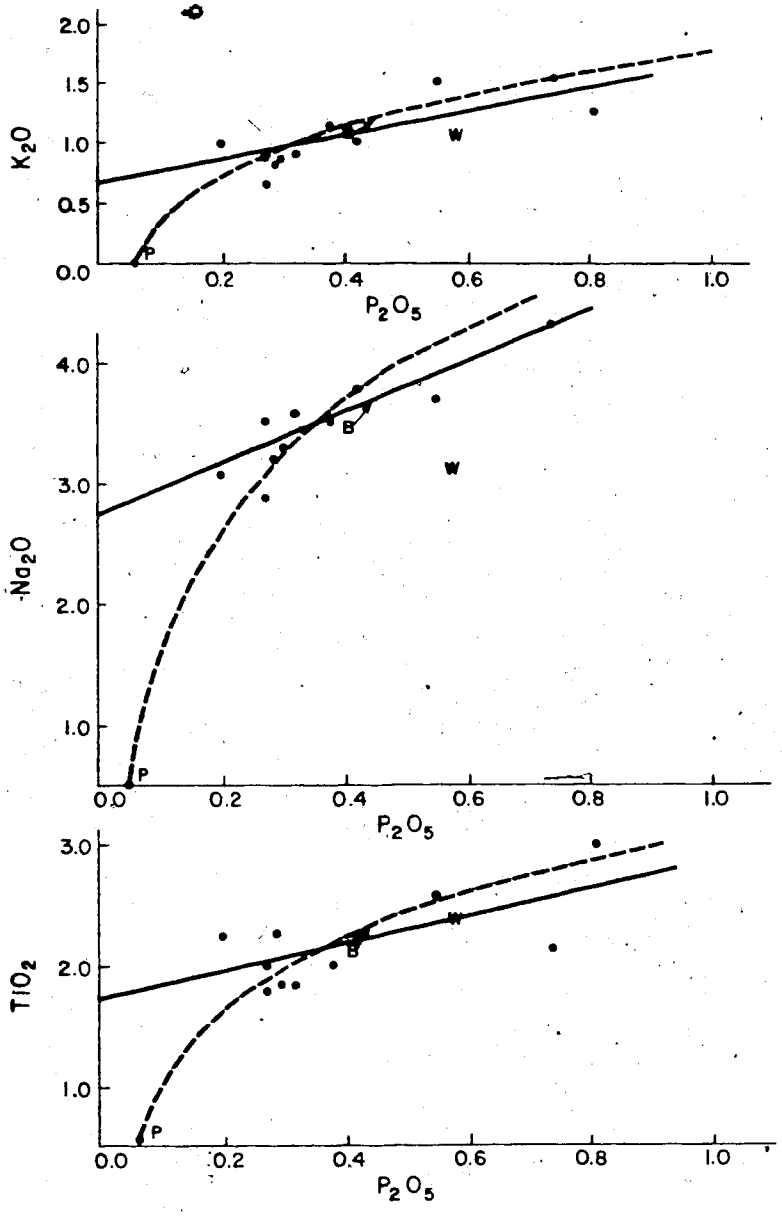

fractionation alone is inadequate to explain the variation. To explain the variation in P_2O_5 some 80% fractional crystallization would have to occur between compositions like Edziza's and those at Heart Peaks or Atlin. The variation in P_2O_5 could be explained in terms of source content or contribution of apatite. Then Edziza's partial melts would receive about 0.5% apatite while Heart Peaks would receive about 1.5% apatite. It is possible that all of the B.C. lavas represent the same degree of partial melting but that available apatite and other trace minerals are variable.

Another way to explain minor element variation is through variable degrees of partial melting of spinel lherzolite with a rather ordinary incompatible or minor element content. For this type of model, the minerals containing the minor elements melt first and further degrees of melting dilute their concentration. Na_2O and TiO_2 are also contained in several mineral phases so they will behave like diluents rather than pure residuals. For this reason expressions of the form

$$P_2O_5 = a(Na_2O)^b$$

were fit to the B.C. data set and the same hypothetical source pyrolite composition (Green and Ringwood, 1967) used in the basalt derivation calculations of ROCK. These models imply that the Heart Peaks and Atlin represent the lowest degree of partial melting and Edziza the highest. In

comparing the B.C. minor element distribution to the world average point, if we assume both have the same minor element source signatures then it can be seen that most of the B.C. lavas represent a higher degree of partial melting, implying higher heat flow or steeper geotherms for B.C. If however, we assume that all of the lavas represent the same degree of partial melting, then for their P_2O_5 levels the B.C. lavas are enriched in alkalis. This could tie into the occurrence of related peralkaline salics in B.C. Another possibility is that if melting degree and alkali contents are typical, then the mantle source region for B.C. lavas is slightly depleted in phosphorous with respect to the world average. Perhaps some additional insight can be gained in examining element ratio plot,s, figure 7-9. On the Ca/Si versus (Fe+Mg)/Si plot the olivine orthopyroxene and spinel vectors parallel the (Fe+Mg)/Si axis, while clinopyroxene has a slope of one. The scatter of points lies between these two vectors and closer to the origin than the world average point. This implies either a higher degree of partial melting or greater source depletion for the B.C. lavas than alkali basalts in general. On the Ca/Si versus P/Si plot, figure 7-10, most of the B.C. lavas plot at lower levels on both axes than the world average. This could imply, for the same degree of partial melting, that the B.C. source is depleted in both clinopyroxene and apatite. Alternatively if B.C. mantle is normal it could imply higher degrees of melting. The interesting thing about the scatter is that it occurs along

Figure 7-9.

Ca/Si versus (Fe+Mg)/Si atomic ratio plots for basic lavas of the IMB. Vectors indicate slopes for ideal mineral stoichiometry, arrows point to increased contribution, melt vector indicates direction of increased partial melting. Compared to the world average alkali basalt, the IMB compositions appear to have a reduced contribution of clinopyroxene and spinel either from source depletion or increased partial melting.

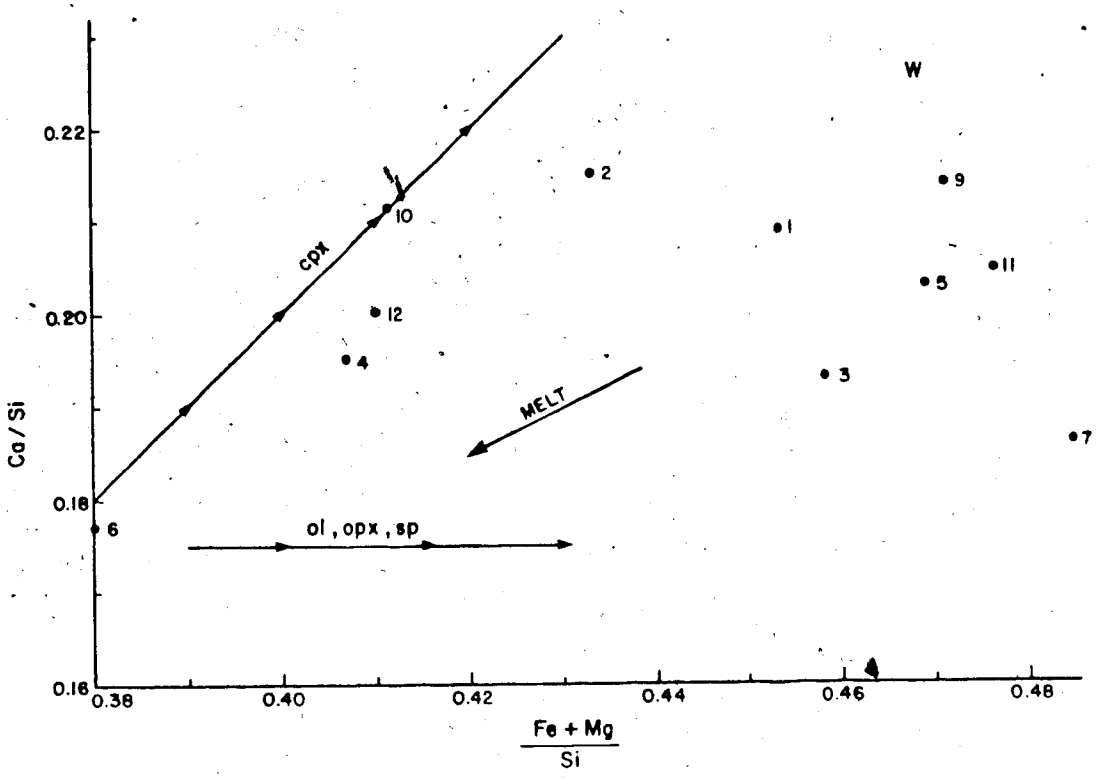

Figure 7-10.
Ca/Si versus P/Si atomic ratio plot for basic lavas of the IMB. Compared to the world average alkali basalt, the IMB compositions appear to have a reduced contribution of clinopyroxene and apatite, either due to source depletion or increased partial melting.

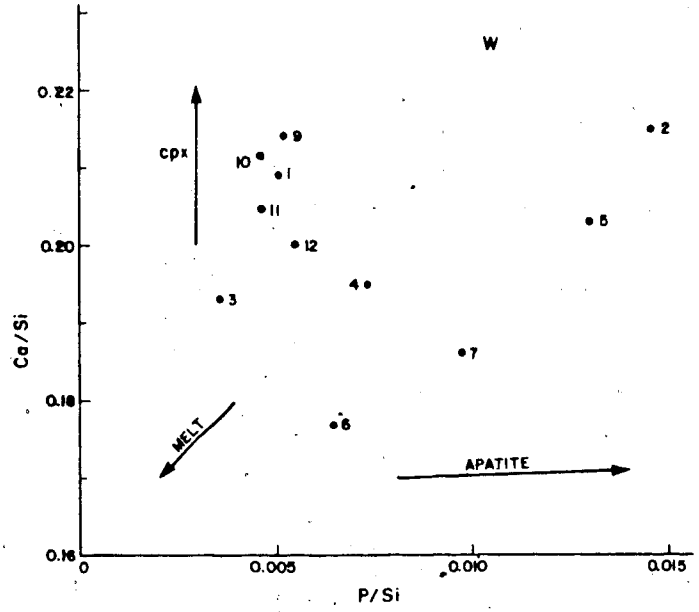

Figure 7-11.
K/Si versus (Fe+Mg)/Si atomic ratio plot for basic lavas of the IMB. Note the direction expected for increased partial melting and the scatter of IMB values in K/Si both above and below the world average. The implication is that B.C. basalts represent about the same level of partial melting as the world average but that they have considerable source heterogeneity.

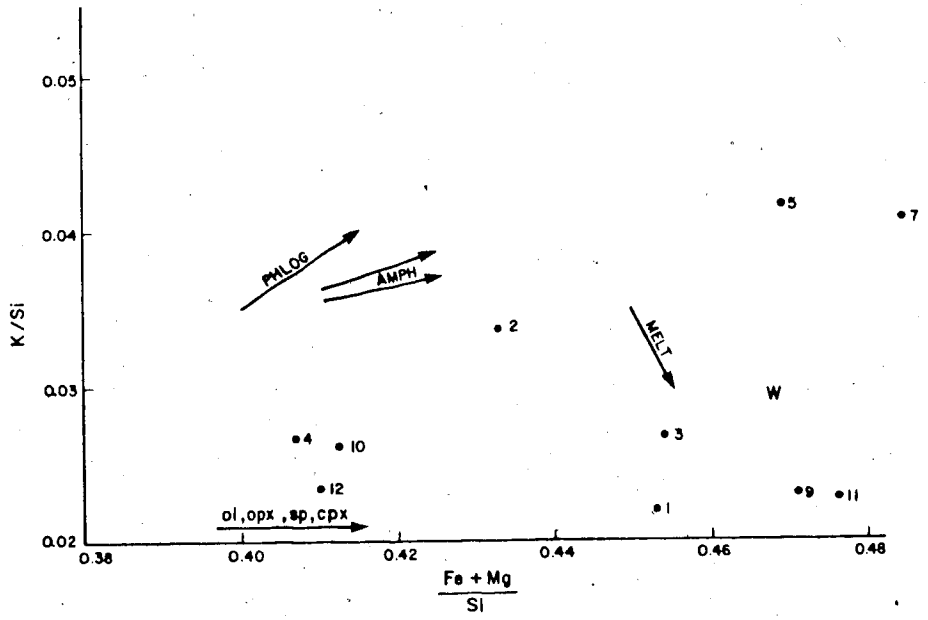

a line of constant sum. This is also perpendicular to the melting vector. This line could imply a relatively constant degree of partial melting but some source heterogeneity of the form highest source clinopyroxene content at the lowest apatite content and vice versa. The values of (Na+K)/Si scatter around the world average, refer to analyses in Table 7-8. With the low Ca/Si values for B.C. this implies a lower contribution of clinopyroxene to the melts at relatively similar source enrichment. On the K/Si versus (Fe+Mg)/Mg plot, figure 7-11, the B.C. lavas are shown to have scatter around the world K/Si value. This is also true for total alkalis. Most of the scatter is perpendicular to the melt vector and parallel to amphibole and phlogopite which are considered to be possible alkali source minerals (Best, 1974; Mysen and Boettcher, 1975; Boettcher and O'Neil, 1980). This plot can be interpreted to mean that if the range of partial melting for B.C. is on both sides of the world average, then the B.C. source is depleted in minerals like phlogopite or amphibole. Further discussion of this point is deferred to the section on lherzolites. If this plot is really showing variable source depletion for hydrous minerals and incompatible or minor elements, then there is as much mantle heterogeneity between the Rainbow range and the Itchas, which are less as 100km apart, than there is for the whole of B.C. Also, it would appear that if this plot can show variation in degree of partial melting, then Heart Peaks, Edziza and Level Mountain have fairly similar minor

mineral content in the source, but reflect as great a range in partial melting as is observed for all of B.C. From this data analysis it does not seem possible to simultaneously retain the concepts of a chemically and mineralogically homogeneous upper mantle, a constant degree of partial melting implying a narrow range of geothermal gradients and an undepleted upper mantle with high incompatible element signature as is typically assumed for alkaline lavas.

The results of this analysis indicate that most of the chemical variation for B.C. alkali basalts can be explained in terms of variable source content or contribution of clinopyroxene to the melts on the order of twenty-two percent. The contribution of clinopyroxene to the B.C. lavas is also lower than for the world average alkali basalt. The minor element variation is consistent with variable degrees of melting, with most of the B.C. basalts being formed by more extensive melting than the world average. This could be accommodated by either higher geothermal gradients, from a minimum of 21°/km by Fujii et al (1981) to 25°/km by Parrish (1981), or by a less refractory upper mantle. The latter is suspected due to the high iron and silica contents and low (Fe+Mg)/Si values.

Hawaiites and Their Relationship to the Stratigraphic Variations in Major Element Chemistry of all Basic Lavas

The hawaiites have been classified according to Irvine and Baragar (1971). They are distinguishable from the more primitive basalts and the mugearites on the basis of

normative plagioclase composition and normative colour index. The analyses are arranged in stratigraphic succession and presented in Table 7-10. The hawaiites can be chemically distinguished from the basalts on the basis of their higher TiO_2, Al_2O_3, FeO*, Na_2O, K_2O and P_2O_5 contents and lower MgO and CaO contents.

Within the hawaiite group at Level Mountain there exists a bimodal distribution for: TiO_2, Al_2O_3, MgO, CaO and P_2O_5. None of the high or low clusters for any of The test of the mean is presented for two of the clusters, Al_2O_3 and P_2O_5 in table 7-11. The low Al_2O_3 group are much more strongly alkaline. The Al_2O_3 division not only corresponds to the TiO_2, MgO and CaO division previously noted but also levels for SiO_2, FeO*, Na_2O and K_2O which were not initially apparent in the normal distributions of these oxides. The high P_2O_5 cluster also contained high TiO_2 and low MgO and CaO. This is interpreted to mean that concentration of P_2O_5 and TiO_2 proceeds with fractionation of typical basalt phenocryst phases such as olivine, clinopyroxene and plagioclase (Anderson and Greenland, 1968).

Representative hawaiite analyses for other localities of the Intermontane Belt are presented in table 7-12. The average Level Mountain hawaiite is not statistically different from the overall average for the Intermontane Belt. However there do appear to be differences from area to area.

TABLE 7-10 LEVEL MOUNTAIN HAWAIITES

	PAV 3815	PAS 3880	29/1f LATE	PAH 4300	PAG 4340	PAF 4370	PAE 4400	PAC 4465	29/1A	13-K	PBX 5385
SiO_2	47.5	48.8	46.6	48.7	49.3	47.3	47.4	52.0	50.0	48.2	47.6
TiO_2	3.0	2.7	4.2	2.9	2.6	3.5	3.1	1.9	2.7	3.2	4.4
Al_2O_3	13.3	14.1	14.1	16.4	16.3	15.7	16.2	15.8	16.2	16.3	13.8
Fe_2O_3	4.6	3.8	10.3	3.4	4.5	7.5	4.7	3.5	2.3	5.9	5.8
FeO	7.5	8.3	3.7	10.2	8.6	7.2	8.3	7.0	11.2	8.8	8.3
MnO	0.1	0.1	0.2	0.1	0.1	0.1	0.1	0.1	0.2	0.2	0.2
MgO	6.1	6.5	4.5	3.8	3.2	3.9	5.3	5.3	4.6	3.6	3.6
CaO	8.0	8.1	8.8	5.9	5.8	6.4	8.0	6.7	6.8	7.9	7.8
Na_2O	3.4	3.8	3.0	4.3	4.3	4.1	3.7	4.2	4.2	3.8	3.9
K_2O	1.5	1.4	2.2	1.8	2.2	1.7	1.3	2.1	1.9	1.3	1.5
P_2O_5	0.6	0.6	0.7	0.9	1.3	1.0	0.9	0.4	0.0	0.6	1.0
H_2O^+	1.5	1.0	1.7	1.0	1.0	1.0	0.5	0.5	0.0	0.4	0.9
H_2O^-	1.0	0.7	0.0	0.5	0.8	0.6	0.4	0.5	0.3	0.0	1.2
CO_2	2.0										
Orig. Tot.	101.8	101.8	100.0	100.1	100.9	101.0	99.9	100.2	100.0	97.2	99.3
% MELT	8.4	9.3	5.8	6.3	4.4	6.0	6.4	6.0	6.8	9.8	5.7
Q			0.2								2.1
OR	9.2	8.1	13.2	10.5	13.0	10.5	7.6	12.7	11.3	7.8	9.2
AB	29.8	31.9	26.0	36.5	36.8	35.5	31.7	36.3	31.3	32.2	33.4
AN	17.5	17.5	19.0	20.2	19.2	19.7	23.6	18.0	19.6	23.6	16.1
PL	47.3	49.4	45.0	56.7	56.0	55.2	55.3	54.3	50.9	55.8	49.5
NE									2.3		
WO	8.2	8.2	8.8	1.4	0.6	2.5	4.3	5.5	5.9	5.0	6.9
EN	5.6	5.2	6.3	0.6	0.3	1.4	2.7	3.3	2.6	2.4	4.7
FS	2.0	2.5	1.7	0.8	0.3	1.1	1.3	1.9	3.3	2.5	1.7
DI	15.9	15.9	16.9	2.8	1.2	5.0	8.4	10.6	11.8	10.0	13.3
EN	8.8	2.6	5.2	2.7	5.8	3.8	4.3	4.0	6.3	4.5	4.5
FS	3.2	1.3	1.4	3.3	6.7	3.0	2.1	2.3	8.8	4.7	1.7
HY	12.0	3.9	6.6	6.0	12.5	6.8	6.4	6.3	15.1	9.2	6.2
FO	1.0	5.9		4.3	1.4	3.3	4.3	4.2	3.3	1.4	
FA	0.4	3.2		5.6	1.8	2.8	2.3	2.6	5.1	1.6	
OL	1.4	9.1		9.9	3.2	6.1	6.6		8.4	3.0	
MT	6.8	5.4	8.4	4.9	6.0	7.4	6.9	4.9		6.8	8.6
IL	5.9	5.2	8.1	5.5	5.0	6.8	5.8	3.6		6.1	8.6
AP	1.6	1.3	1.6	2.2	3.1	2.3	2.2	0.9		1.3	2.4
Classif.	T	H-AB	H	H	H	H	H-AB	H	H	H	H
Map Unit	2	2	3	4	4	4	4	4	4	4	5b

TABLE 7-10 continued

	PBA 5420	PBD 5460	PBH 5655	PBI 5675	PBJ 5690	8/28-68 25/38	8/25-50 5815	PBQ 6397	PBR 6580	PBS 6625	PBT 7200	7250
SiO_2	48.6	48.0	49.5	49.6	48.4	49.8	49.7	47.8	46.9	46.6	46.8	46.9
TiO_2	3.5	4.1	2.6	2.9	2.1	2.4	2.6	2.9	3.8	3.8	3.9	3.8
Al_2O_3	14.4	15.7	16.8	16.1	15.4	17.1	16.6	15.4	14.8	14.7	14.7	14.7
Fe_2O_3	6.9	9.7	3.6	6.8	3.2	5.1	1.4	2.4	3.4	3.4	4.1	3.9
FeO	7.1	2.7	7.3	4.6	8.5	5.9	10.0	10.7	11.2	11.4	10.5	10.4
MnO	0.1	0.2	0.1	0.1	0.1	0.1	0.1	0.2	0.1	0.2	0.1	0.1
MgO	3.4	3.2	4.2	4.1	7.1	4.0	4.4	6.0	5.7	5.6	5.4	5.5
CaO	8.4	8.9	8.3	8.8	7.5	8.8	8.3	9.1	8.5	8.6	8.4	8.3
Na_2O	3.9	3.5	4.1	3.8	3.6	4.3	3.8	3.8	3.9	3.8	3.7	3.7
K_2O	1.5	0.9	1.4	1.5	1.2	1.1	1.3	0.9	1.0	1.0	1.1	1.1
P_2O_5	0.4	1.7	0.5	0.5	0.5	0.7	0.5	0.6	0.7	0.7	0.6	0.7
H_2O^+	0.7	1.1	0.7	1.0	0.8	0.3	0.7	0.0	0.0	0.0	0.3	0.4
H_2O^-	1.1	0.6	1.0	0.0	1.6	0.4	0.6	0.2	1.2	0.0	0.3	0.4
CO_2				0.3								
Orig. Tot.	99.9	98.7	99.8	99.6	100.8	98.4	99.9	99.9	99.8	99.8	99.9	100.6
% MELT	8.7	3.5	9.2	8.4	10.6	9.1	9.6	10.3	8.9	8.2	9.6	8.6
Q	0.3	6.5		0.1								
OR	8.8	5.4	8.2	9.2	7.0	6.4	7.9	5.1	6.2	6.0	6.4	6.7
AB	33.6	30.3	34.5	32.7	30.2	36.4	32.1	30.4	30.6	30.5	31.7	31.6
AN	17.7	24.8	23.5	22.6	22.6	24.5	24.4	22.3	19.7	20.1	20.2	20.0
PL	51.3	55.1	58.0	55.3	52.8	60.9	56.4	52.7	50.3	50.6	51.8	51.5
NE								1.0	1.3	1.0		
WO	9.3	3.6	6.0	7.5	4.7	6.5	5.6	7.9	7.6	7.4	7.4	7.1
EN	5.1	2.8	3.6	4.9	2.9	3.8	2.6	4.1	4.0	3.9	4.1	3.9
FS	3.8	0.4	2.2	2.0	1.5	2.3	3.0	3.6	3.4	3.3	2.9	2.9
DI	18.2	6.8	11.8	14.5	9.1	12.6	11.2	15.5	14.9	14.6	14.3	13.8
EN	3.5	5.2	2.4	5.4	5.4	2.6	2.3				0.4	1.0
FS	2.6	0.8	1.5	2.2	2.9	1.5	2.7				0.4	0.7
HY	6.1	6.0	3.9	7.6	8.3	4.1	4.9				0.8	1.7
FO			3.1		6.7	2.5	4.4	7.6	7.1	7.2	6.3	6.1
FA			2.1		3.9	1.6	5.7	7.4	6.6	6.8	4.9	4.9
OL			5.2		10.6	4.1	10.1	15.0	13.7	14.0	11.2	11.0
MT	7.5	8.3	5.2	6.4	4.7	5.7	2.0	3.5	4.9	4.9	5.9	5.7
IL	6.9	7.9	4.9	5.5	4.0	4.6	5.0	5.6	7.2	7.3	7.4	7.2
AP	1.0	4.0	1.2	1.3	1.3	1.5	1.1	1.4	1.6	1.7	1.5	1.6
Classif.	H	H	H	H	H-AB	H	H-AB	H-AB	H	H	H	H
Map Unit	5b	5b	6b	6b	6b	6b	6b	8	9	9	9	9

Table 7-11. L.M. Hawaiite Cluster Analyses

	High Al		Low Al	High P		Low P
SiO_2	50.02	>	48.49	49.10		49.37
TiO_2	2.87	<	3.47	3.50	>	3.02
Al_2O_3	16.55	>	14.79	16.03		15.57
FeO*	12.01	<	13.35	13.15		12.45
MnO	.12		.14	.12		.13
MgO	4.24	<	5.59	3.90	<	5.27
CaO	7.65	<	8.43	7.29	<	8.31
Na_2O	4.10	>	3.81	4.06		3.91
K_2O	1.59	>	1.24	1.60		1.36
P_2O_5	.78		.66	1.17	>	.59
	sem		sem	sem		sem
SiO_2	.38		.41	.35		.43
TiO_2	.19		.22	.31		.17
Al_2O_3	.13		.18	.39		.27
FeO*	.41		.34	.37		.39
MnO	.01		.01	.02		.01
MgO	.21		.38	.31		.28
CaO	.37		.12	.53		.18
Na_2O	.08		.04	.13		.06
K_2O	.13		.08	.18		.09
P_2O_5	.15		.05	.13		.05

Table 7-12. Hawaiite Analyses for B.C. Intermontane Belt

(54) Avg		Level Mtn (avg 21)	Heart Peaks (avg 20)	Stikine River	Edziza (3)	Mt Dunn	Alyansh	Itchas (4)	Rainbows (4)
49.17	SiO2	49.30	49.59	48.87	50.34	47.44	48.11	48.74	50.94
2.81	TiO2	3.16	2.62	2.69	2.11	2.98	3.61	2.93	2.39
16.57	Al2O3	15.71	16.47	15.84	18.91	17.25	14.92	17.01	16.45
11.90	FeO*	12.65	10.35	12.76	9.75	12.02	14.07	11.39	12.22
.16	MnO	.13	.16	.20	0.15	.13	.18	0.15	0.16
4.88	MgO	4.88	5.74	4.80	4.00	6.20	4.28	5.09	4.03
8.26	CaO	8.02	8.42	8.63	9.01	8.46	7.58	8.08	7.85
4.06	Na2O	3.97	4.06	3.95	4.02	3.89	4.22	4.35	3.98
1.57	K2O	1.43	1.79	1.55	1.45	1.24	1.81	1.67	1.59
.63	P2O5	.72	.80	.70	0.25	0.40	1.19	0.57	0.39
								0.27	0.18
1.14	SiO2	1.47	2.59		1.73			0.24	0.17
.47	TiO2	.69	.80		0.95			0.82	0.17
1.20	Al2O3	1.01	.49		1.97			0.25	0.38
1.38	FeO*	1.37	.98		2.71			0.01	0.01
.02	MnO	.05	.04		0.04			0.90	0.39
.79	MgO	1.19	1.39		0.46			0.18	0.37
.46	CaO	1.01	.80		0.45			0.17	0.22
.15	Na2O	.27	.54		0.50			0.06	0.09
.19	K2O	.37	.72		0.05			0.02	0.08
.30	P2O5	.37	.18		0.44			0.02	0.08

Oxide Variation Plots for Basaltic Lavas and Fractionation Arguments

On the basis of the correlation calculations, nine major oxide variation plots were selected to project most of the significant chemical variation. By dividing the lavas into basalts and hawaiites, very few clear trends emerged. At this point in the data analysis it was found that significant trends existed for time-map units which included both basalts and associated hawaiites. Also alkali basalts and hawaiites for the same time package were found to be chemically distinctive from subsequent and preceeding units. Consequently the variation plots were prepared for distinctive time and map units.

Major element variation diagrams for plateau units 1 and 2 (the basal two eruptive sequences of the plateau building stage) are presented in figure 7-12. The effects of fractional crystallization are shown for vectors for sample PAR which is an alkali basalt with mol ratio $(CaO+Na_2O+K_2O)/Al_2O_3 = 1.72$. The lengths of the fractionation vectors correspond to the degree of fractional crystallization and the directions depend almost entirely on the fractionated phase composition and very little on the whole rock. The fractionation vectors can be freely translated from point to point as long as their orientation and length are kept constant. This is particularily true of a vector like plagioclase on the FeO-MgO plot or olivine on the Na_2O-CaO plot. For compositions with one or more

Figure 7-12.
Oxide variation plots (anhydrous weight basis) for lower plateau lavas (units 1 and 2). Vectors denote possible effects of mineral fractionation.

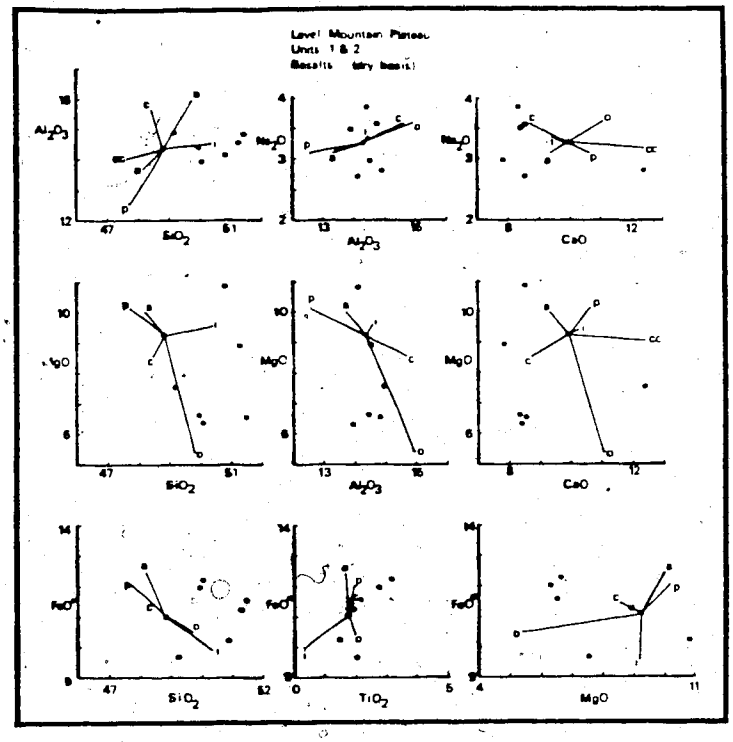

principal components in the plane of the variation diagram, such as ilmenite on FeO*-TiO_2 or olivine on FeO*-MgO, translation to another composition involves small changes in length (up to 5%) and small rotations in orientation (up to 10°). The labels correspond to: o - olivine, PAR, Fo_{83}; c - clinopyroxene, PAR, $Di_{80}Hd_{18}$; p - plagioclase, PAR, An_{60}. All three of these phenocryst vectors correspond to 10% by weight subtraction. The vector labelled i corresponds to ilmenite, PAR, and is for 3% subtraction. Vectors a and cc are alteration vectors corresponding to 10% replacement of groundmass glass by a=septechlorite, PAC, and 5% replacement by cc=calcite respectively (addition vectors). These calculations were made particularly for the oldest lavas to distinguish the effects of alteration related to chemical variation from primary igneous processes.

On examining this figure (7-12), it is apparent that most of the oxide variation can be accounted for by <10% olivine fractionation, <15% clinopyroxene fractionation and <6% ilmenite fractionation. The effect of chlorite alteration is in fact away from most of the variation trends. One flow of this set, PAW, had amygdules of calcite. This point stands apart at 12.46% on the CaO axis and its separation from the main lava group can be accounted for by 5% calcite alteration. No other lavas show this effect. Linear trends appear on MgO versus FeO*, FeO* versus TiO_2 and to a lesser extent on MgO versus Al_2O_3. It must be emphasized that the sequence of points along these trends

does not correspond to eruptive sequence. This lack of timewise order for trends on the variation diagrams is a persistent theme at Level Mountain. It would appear that the eruptive sequence samples a related suite of compositions, and while they appear to represent a fractionation sequence, the points along a given trend are not erupted in order. In most flows, appropriate degrees of fractionation of observed phenocrysts could account for the compositional variation. When sampling was performed the dense phenocryst-poor portions of flows were selected. The existence of flowage differentiation phenomena has been demonstrated by Komar (1972). The source magmas responsible for map units 1 and 2 could have been relatively uniform alkali basalts, but the existence of phenocrysts and the various flow and sampling processes, not to mention variable crystallization of the sampled flow portions, behave like dispersion vectors to string the compositions out.

Major element variation diagrams for Plateau unit 3 are presented in figure 7-13. The composition used in fractionation tests was flow PAM. It is a K-poor tholeiite in the sense of Irvine and Baragar (1971); however, the flow is petrographically an alkali basalt and has an alkalinity index of 1.35. Of the twelve compositions plotted for unit 3, five classify as K-poor tholeiites, one is a hawaiite and the other six are alkali basalts. Not only do the lavas appear out of stratigraphic order along the variation trends, but the alkali basalts and "tholeiites" are

Figure 7-13.
Oxide variation plots (anhydrous weight percent) for plateau basalts from map unit 3. The lines radiating from a common point indicate mineral fractionation directions. The two lavas joined by a common point are for (29/1f) an alkali basalt flow and its filter pressed derivative. This indicates that most of the compositional variation here is probably not related to protracted fractional crystallization of several phases.

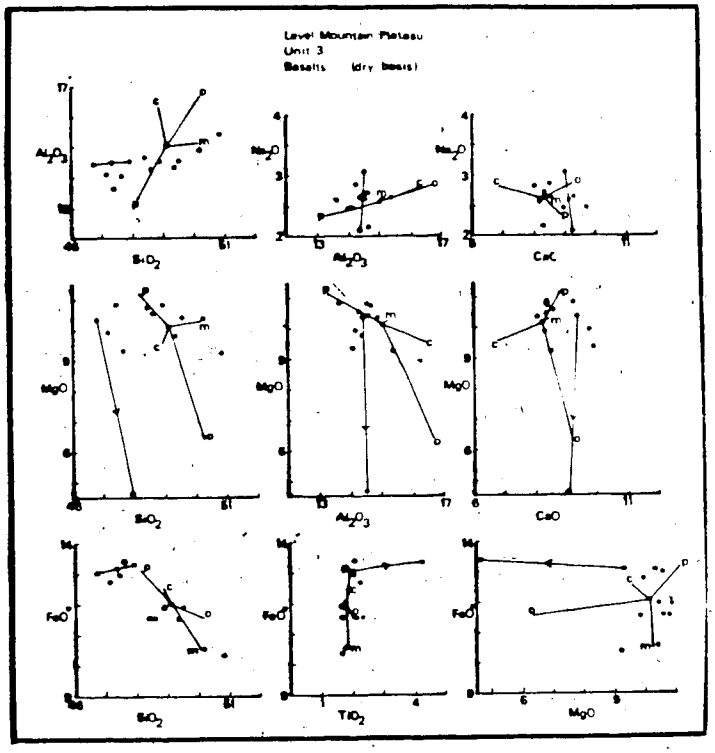

thoroughly interspersed. The fractionation vectors used were 10% for: c - clinopyroxene, PAO, $Di_{7}Hd_{1}$; o - olivine, PAR, Fo_{83}; and p - plagioclase, PAR, An_{61} and 2% for m - titanomagnetite, PAC, $Mt_{73}Ulv_{6}$. Most of the variation here can be accounted for by 15% olivine fractionation with less than 5% titanomagnetite, which is in agreement with phenocryst mineralogy. In this figure (7-13) there is an additional arrow drawn to connect alkali basalt 29/1f (an ophitic textured, ponded, columnar jointed flow) with its filter pressed derivative hawaiite (that occurred as narrow dikelets along the columnar joints). The arrow points towards the hawaiite and its length represents greater than 60% fractional crystallization of olivine, titaniferous augite and plagioclase. Crystallization (fractionation) of a single phase can usually account for most of the trend, but combined fractionation of several minerals or less produces off-trend variation. This distinction is very evident for the filter pressing case. In comparing the sequential map units another interesting twist is seen. The dispersion trends are more or less parallel and oriented along parallel mineral vectors but there is a shift in level between sequential units, compare for instance the FeO* versus SiO_2 plots or the MgO versus Al_2O_3 plots in figures 7-12 and 7-13. The shift between successive eruptive pulses is like the off-trend variation produced by protracted fractional crystallization of several phases. Perhaps sequential units are produced from different sources altogether or from the

same source which had undergone something on the order of 30 to 40% fractional crystallization between the eruption of successive map units. If this speculation has any merit then there would have to be very long lived large volume magma chambers at subcrustal depths which persist for hundreds of thousands to millions of years.

Major element variation diagrams for plateau unit 4 are presented in figure 7-14. The composition used in fractionation tests was flow PAF, a quartz normative hawaiite. Of the ten points on these diagrams, four are alkali basalts and the remainder are hawaiites. Of the hawaiites, two are nepheline normative and one is quartz normative. Two linear groups of points can be seen on the Na_2O-Al_2O_3 plot. All of the ordinary hawaiites and alkali basalts comprise the trend at the lower Na_2O level. The quartz and nepheline normative hawaiites together with the remaining ordinary hawaiites comprise the trend at high Na_2O. The lavas of unit 4 erupted nearly in timewise order along these trends. On the MgO-Al_2O_3, MgO-CaO and MgO-FeO* plots, the eruptive sequence more or less proceeds from hawaiites to alkali basalts with a steady increase in MgO. There are also lineations on SiO_2-FeO* and SiO_2-Al_2O_3 with no time For this map unit clinopyroxene, and to a lesser extent plagioclase and titanomagnetite, appear to be the controlling vectors. The vectors are 10% for: o - olivine PAF, Fo_{55}; p - plagioclase, PAF, An_{40}; c - clinopyroxene, PAF, $Di_{63}Hd_{31}$; and 2% for m - titanomagnetite, PAC,

Figure 7-14.
Oxide variation plots (anhydrous weight basis) for uppermost plateau lavas from map unit 4. Fractionation vectors are discussed in the text.

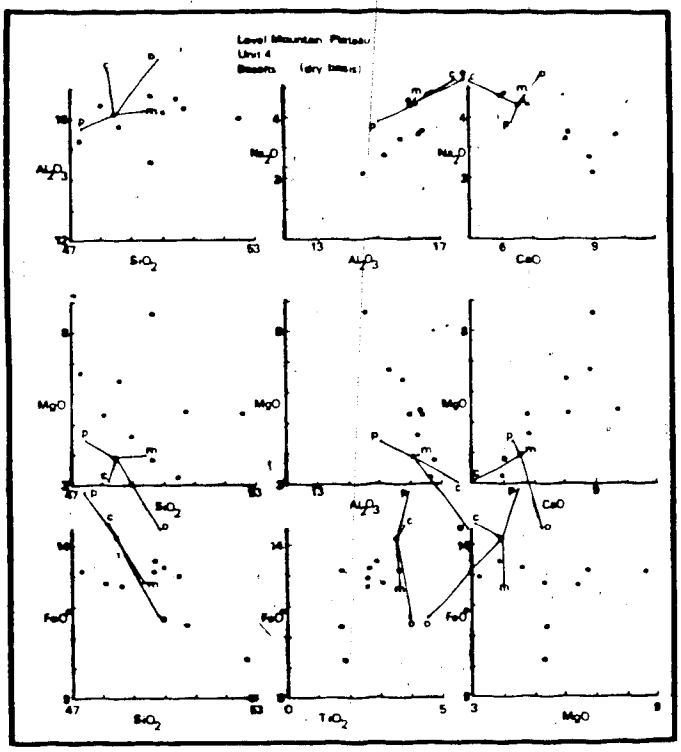

$mt_{7.3}ulv_{6}$. These lavas frequently contain large cumulophyric clots of black clinopyroxene plus plagioclase, interpreted to be cognate. Unlike the previously discussed map units, the variation cannot be explained without in excess of 40% fractional crystallization, implying longer time intervals between eruptions than for earlier units. An eruptive sequence from hawaiite going to alkali basalt could imply top to bottom emptying of a magma chamber (which had differentiated to hawaiites at the top, with related alkali basalts deeper). Alternatively, the onset of a new eruptive cycle could create a magma chamber which differentiates to hawaiite. The repeated injection of fresh related alkali basalts releases the hawaiite as injection of fresh magma proceeds, until finally the alkali basalts come out as the eruptive pace picks up and insufficient time is available for further differentation. Whichever of these possible mechanisms is responsible, the lavas of unit 4 represent the first major outpouring of hawaiites.

Figure 7-15 portrays the compositional variation for the basic lavas of the stratocone units. Because of the large variation in lava compositions represented here, the test composition used for the fractionation arguments is not a specific lava but the average of the Level Mountain hawaiites. Fractionation compositions were selected from lavas with similar element ratios to the average. The vectors used in fractionation tests are:

p - plagioclase, PBX, $An_{4.7}$, 10%

Figure 7-15.
Oxide variation plots (anhydrous weight basis) for basic lavas of the stratocone stage. For discussion of chemical variation by map unit and explanation of fractionation vectors, refer to text.

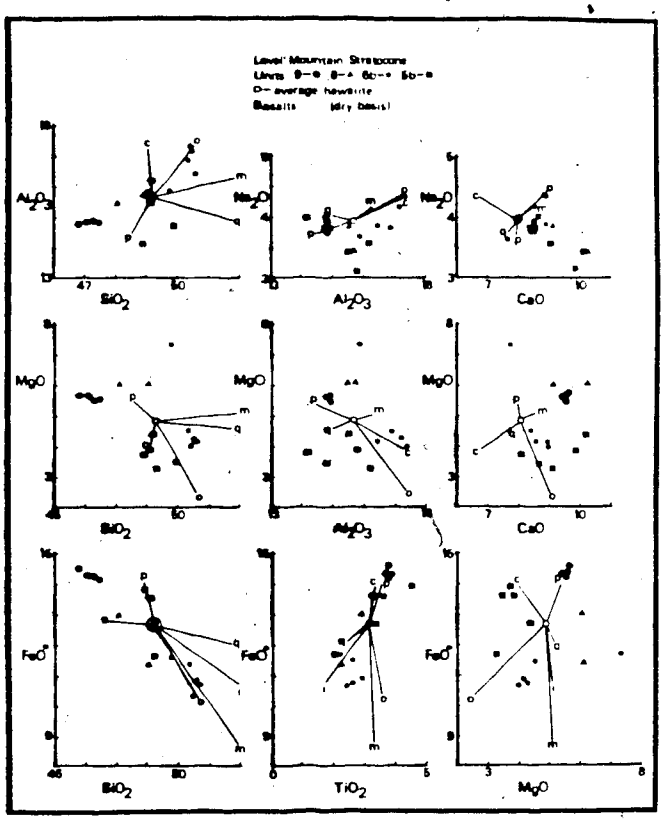

c - clinopyroxene, PBX, $Di_{..}Hd_{2.}$, 10%
o - olivine, 8/20-2/4307, $Fo_{5.}$,rim, 10%
m - titanomagnetite, PAC, $Mt_{7.}$, $Ulv_{..}$, 5%
i - ilmenite, PBX, 5% and
q - quartz, 5% addition to simulate the effect of crustal syntexis/contamination.

For many of the plots the oxide composition and vectors are orthogonal. As in the previous figures, the distinction of lava compositions between eruptive units is readily made. Again the arrangement of points along trends is not in a timewise order either within a map unit or for sequential map units.

The alkali basalts and hawaiites of map unit 5b petrographically contain phenocrysts of clinopyroxene (black augite) and plagioclase, sometimes in clots as in flows from map unit 4. The analyses plotted come only from the sequence from Meszah Peak Kakuchuya Valley. The unit commences with hawaiites, progresses to alkali basalts, then back to hawaiites. The distribution of the unit 5 points is consistent with clinopyroxene plus plagioclase fractionation each around 10%. When the map unit 5b lavas are compared to those of map unit 4b it can be seen that they are chemically distinctive and do not represent a timewise progression of the unit 4 trends.

The basic lavas of unit 6b were more widely sampled than for 5b. The sequence at Meszah Peak begins with hawaiite and progresses through quartz normative hawaiite to transitional hawaiite-alkali basalt. The other lavas sampled from Kaha-Lost Creek and Dudidontu Creek were all quartz normative hawaiites. These lavas contain olivine or

iddingsite plus titanomagnetite phenocrysts with infrequent plagioclase. Their chemical variation trends are consistent with olivine plus oxide dominated fractionation, with total range of fractionation being less than 20%. Compared to the basic lavas of 5b, the 6b lavas are all on the quartz enriched side. A vector for alkali feldspar was not plotted but for 10% addition this vector would be roughly parallel with the plagioclase fractionation vector and points the opposite direction. Contamination of basic magma with a minimum melting composition granite would be along a vector between quartz and alkali feldspar. This is also the direction for incorporation of comendite as magma mixing. The 6b basic lavas could differ from their 5b predecessors by less than 5% crustal contamination or magma mixing with a more salic melt. Both of these possibilities imply the existence of crustal level magma reservoirs as did the upward basifying trend roughly shown in the basalts of units 4, 5b, and 6b.

No basic lavas were analysed from any of the stage 7 units a, b or c. During this period basic compositions were subordinate and no well developed basic stratigraphic sequence was encountered. However in three localities marbled lavas (admixed basic and salic) were encountered. The admixed salic lava was trachyte but adjacent stratigraphic units were metaluminous phonolite ash flows, tuffs or plugs. These occurrences demonstrate the contemporaneity of basic and salic melts and lend further

credence to mixing hypotheses in the derivation of the intermediate lavas.

Only two basic lavas were analysed for unit 8, a transitional hawaiite-alkali basalt flow from Meszah Peak and an alkali basalt dyke from Egnell Creek on the southwestern plateau margin. The hawaiite contained olivine, plagioclase and titanomagnetite phenocrysts in addition to about 0.1% by volume of xenoliths. The xenoliths were dominated by two varieties: (i) a plutonic textured troctolite (olivine and plagioclase with minor clinopyroxene) and (ii) granitic gneiss. The latter crustal fragments showed disaggregation and partial melting at grain boundaries. The hawaiite is more silica-rich and iron-poor than the alkali basalt (which could be explained by less than 5% crustal contamination). The alkali basalt contained megacrysts of complexly zoned plagioclase and three or more generations of plagioclase phenocrysts. This lava is richer in CaO which is consistent with plagioclase fractionation.

The flows of map unit 9 begin as nepheline normative hawaiites and proceed to slightly more silica rich ordinary hawaiites. Their order along the trends is not their eruptive sequence. These lavas are almost totally aphyric, although one locality on the west shoulder of Meszah Peak contained sparse xenocrysts or phenocrysts of quartz, partially resorbed. The slight variation in the composition of these four flows is in keeping with either less than 5% olivine fractionation or less than 2% variable crustal

contamination. The $MgO-Al_2O_3$ and MgO-CaO plots argue strongly for olivine fractionation while $MgO-SiO_2$ and FeO^*-SiO_2 favour crustal contamination. Some combination of the two is considered most likely. As with the unit 8 lavas, these are more primitive than the basic lavas of units 5b and 6b, and 4. The unit 9 lavas are enriched in TiO_2, K_2O, and P_2O_5. The hawaiites from map unit 9 could be differentiates from a larger volume of more primitive alkali basalts having no surface manifestation.

Selected analyses were tested against a suite of hypothetical source compositions chosen from Level Mountain and other B.C. inclusions; lherzolite, troctolite, eucrite and gabbro, table 7-13. Other peridotites were also tested. Pyrolite was used as the hypothetical composition for the derivation test because the actual nodule compositions for B.C. were too depleted to give rise to most of the basalt compositions. The B.C. lherzolites, typically lacking any P_2O_5 and low in TiO_2, gave possible derivative melts less than one percent by volume. Derivation calculations were also made using LSPX, a Fortran least squares matrix calculation routine written by F. Chayes. For any of these calculations, the lava composition is related to a hypothetical source such as a peridotite, through arbitrarily selected mineral compositional vectors. Obviously the assumptions of source and phase compositions severely restrict the significance of these calculations.

Table 7-13. Model Source Compositions

	MPM	8/6-12	HP13A	TCL	GRP	TVGA
SiO_2	45.37	38.33	46.94	44.52	45.28	54.20
TiO_2	0.61	1.63	2.22	0.52	0.71	0.66
Al_2O_3	9.68	17.14	14.63	1.80	3.55	14.66
Fe_2O_3	2.23	8.64	2.38	0.0	0.0	0.0
FeO	13.05	1.57	7.95	5.36	8.47	9.04
MnO	0.16	0.09	0.11	0.16	0.14	0.15
MgO	17.74	7.10	9.94	39.76	37.57	7.48
CaO	8.55	17.44	11.57	5.10	3.09	10.40
Na_2O	1.42	0.94	2.37	0.65	0.57	2.45
K_2O	0.18	1.36	0.49	0.03	0.13	0.83
P_2O_5	0.0	2.28	0.0	0.0	0.06	0.11
H_2O+	0.56	2.15	0.84	0.0	0.0	0.0
H_2O-	0.37	1.33	0.45	0.0	0.0	0.0
Cr_2O_3	0.08		0.10	2.10	0.43	0.02
Q						1.72
OR	1.06	1.77	2.90	0.18	0.77	4.9
(AB)	12.02		20.05	5.50	4.82	20.7
(AN)	19.51	38.53	27.83	1.91	6.74	26.3
PL	31.52	38.53	47.89	7.41	11.56	47.28
LC		4.91				
NE		4.31				
(WO)	9.57	13.82	12.34	9.77	3.42	10.16
(EN)	6.05	11.94	8.34	7.99	2.65	5.34
(FS)	2.92		3.06	0.60	0.40	4.52
DI	18.53	25.76	23.75	18.36	6.47	20.01
(EN)	6.09		0.53	2.82	13.93	13.29
(FS)	2.94		0.19	0.21	2.12	11.25
HY	9.04		0.72	3.03	16.05	24.54
(FO)	22.46	4.02	11.13	61.82	53.95	
(FA)	11.95		4.50	5.13	9.07	
OL	34.41	4.02	15.63	66.95	63.02	
MT	3.23	0.63	3.45			
IL	1.16	3.10	4.22	0.99	1.35	1.25
HM		8.21				
AP		5.40			0.14	0.26
CM	0.12		0.15	3.09	0.63	0.03
Class-ifca-tion	gabbro trocto-lite	eucrite-essexite	gabbro-essexite	lherzo-lite	Perido-tite	Amphib olite

The hawaiites, and lava types transitional between hawaiite and alkali basalt, could always be distinguished from more primitive basalts on the basis of the value for maximum percent partial melting from pyrolite. The cutoff was 10.5%, with hawaiites below and alkali basalts, ankaramites and hypersthene normative basalts above. The average percent partial melting for all hawaiites was 7.7±1.9% with a total range of 4.4% to 10.3%. The average percent partial melting for all primitive basalts was 14.0±2.7% with a total range of 10.6% to 18.4%. The ranges calculated for alkali basalts are similar to the 15 to 20% range cited in Fiesinger and Nicholls (1977). Among the other source compositions tested, the Telegraph Creek lherzolite (Littlejohn and Greenwood, 1974) was so depleted that the amount of partial melting was never greater than 4% for any derivative composition, and usually the solution was zero. From this is concluded that lherzolite inclusions of this type may represent depleted or residual mantle but are not very likely basalt sources. The troctolite inclusion from Meszah Peak gave answers ranging from 18% to 32% for the Level Mountain basalts which is considered to be too high.

Fractional crystallization calculations were also performed to determine the minimum amount and proportion of subtraction of phenocryst phases which could relate two lava compositions. An example calculation was made on the Level

Mountain lavas using the average alkali basalt to yield the average hawaiite, through fractional crystallization of the same mineral vectors used in figure 7-12. The solution, presented in table 7-14, gave 7.33% Fo_{83}, 18.75% $Di_{80}Hd_{18}$, 14.4% An_{61}, and 3.5% $Mt_{73}Ulv6$ for a total fractional crystallization of 43.99, all expressed in weight fractions. While the values for some oxides of the solved hawaiite may be outside the range of one standard deviation, they are within range for the hawaiite data set. The misfit is attributed to inappropriate choice of mineral compositions. Recalling the discussion of the preceeding section, the inferred degree of fractionation within map units was generally lower than this but in fact the difference between successive eruptive pulses was of this magnitude. If fractionation of this magnitude is indeed required for hawaiite derivation, then the amount of related plutonics beneath Level Mountain and the other centers with voluminous hawaiite may approach the surficial lava volumes in magnitude. Another way of viewing this with the partial melting calculations which demonstrated that roughly half (45%) of the source amount was required to yield the hawaiites compared to the basalts.

Intermediate Lavas

It has been repeatedly stated that Level Mountain has a bimodal suite of basalts and salic lavas. There are however lavas of intermediate composition including mugearites, phonolites, benmoreites and tristanites. While never

Table 7-14. Derivation of Average Hawaiite from Average Alkali Basalt via Fractional crystallization.

	Avg Basalt x	Fo82.5 olivine	D18OHd18 augite	An60 plagioclase	Mt73Ulv6 titanomagnetite	Avg Hawaiite x	Matrix Solution Hawaiite
SiO2	49.14±.27	39.07	51.51	52.77		49.26±.31	50.50
TiO2	2.13±.12		1.13	.07	2.23	3.21±.16	3.18
Al2O3	14.81±.13	.15	2.89	29.21	7.75	15.66±.22	17.02
FeO*	11.93±.22	16.10	7.39	.62	85.75	12.68±.29	10.19
MnO	.10±.01	.20	.10		.36	.13±.01	.07
MgO	8.64±.45	43.95	15.50	.15	3.84	4.87±.24	4.11
CaO	9.14±.21	.30	21.10	2.40		8.07±.21	8.39
Na2O	2.92±.09	.23	.38	4.36		3.93±.07	3.83
K2O	.91±.05			.33		1.46±.09	1.50
P2O5	.28±.04					.72±.08	.49
Proportion		7.33	18.75	14.4	3.5		43.99%

abundant, they are best represented in the stratocone, units 5a,6b,7c,8. Not only are these lavas chemically diverse but, with one exception, they are all metaluminous or peraluminous and not obviously related (via an ordinary differentiation sequence) to the sodic alkali basalt series on one hand, or to the peralkaline trachytes and comendites on the other. The major element chemistry of these lavas is depicted by the histogram in figure 7-1 and tabulated in table 7-15. A cursory look at the range of compositions for each oxide in this group will show them to be intermediate between basalts and salics; thus the name.

The compositional variation for these lavas was presented on a set of eight variation diagrams, figure 7-16. Different symbols are used to keep track of eruptive sequence. On the variation diagrams, the effects of fractionation are shown for a transitional benmoreite, flow PBO from unit 8. The fractionation vectors are:

o - olivine, PBO, Fo_{42}, 4%
c - clinopyroxene, PBO, $Di_{78}Hd_{12}Ac_{5}$, 5%
p - plagioclase, PBP, $An_{68}Ab_{22}Or_{8}$, 10%
a - alkali feldspar, PBO, $An_{13}Ab_{68}Or_{15}$, 10%
u - ulvospinel, PBO, Mt_{2},Ulv_{66}, 5%

Linear trends appear on most plots but again there is no timewise order along the trends. Unlike in the previous diagrams, these vectors do not simply parallel the variation trends. In fact the fractionation vectors don't even satisfy the variation of unit 8 benmoreites very well. A combination of all five phases would be required to describe the existing variation for all intermediate lavas for a total of

Table 7-15. Miscellaneous Intermediate Lavas.

	8/21-6	PAT	PBV	PBU	9/1-86	25/3	26/3C
	3222	3860	5100	5220	5421		
SiO2	53.7	55.6	6 .8	59.6	60.6	59.1	57.2
TiO2	2.2	1.4	0.4	0.4	0.2	1.1	1.6
Al2O3	21.5	18.3	19.6	17.2	19.5	16.4	16.3
Fe2O3	4.6	5.1	3.1	2.9	0.0	0.5	0.9
FeO	7.0	1.9	1.6	4.8	4.8	7.0	8.7
MnO	0.0	0.1	0.1	0.1	0.1	0.0	0.1
MgO	1.1	2.5	0.1	0.0	0.0	1.2	1.5
CaO	3.1	8.0	1.4	2.2	1.4	3.4	5.4
Na2O	2.4	3.2	6.7	6.4	8.2	5.7	5.0
K2O	3.2	0.6	5.8	5.4	5.7	4.2	3.3
P2O5	1.2	0.1	0.1	0.1	0.1	0.0	0.0
H2O+	0.0	2.2	0.4	0.5	2.1	0.8	0.0
H2O-	0.0	1.2	0.0	0.6	0.2	0.7	0.0
CO2							
Original							
Total	100.1	100.3	100.3	99.2	100.5	99.0	97.9
%Melt	4.11	17.12	14.23	15.30	14.71	3.09	3.94
Q	19.9	14.6					
C	11.4						
OR	18.7	3.6	34.4	32.0	33.4	24.9	19.5
(AB)	20.8	28.1	48.8	46.6	41.4	48.7	42.4
(AN)	7.3	35.0	6.1	2.1		7.2	12.3
PL	28.1	63.1	54.9	48.7	41.4	55.9	54.7
NE			4.5	4.8	14.7		
NS					0.1		
(WO)		2.4		3.4	2.6	4.2	6.0
(EN)	2.7	1.6				1.0	1.4
(FS)	7.7	0.7		3.9	2.9	3.5	4.9
DI	10.4	4.7		7.4	5.5	8.7	12.3
(EN)		4.8				0.6	1.3
(FS)		2.0				2.1	4.6
HY		6.8				2.7	5.9
(FO)			0.2			1.0	0.7
(FA)			2.3	3.6	4.3	4.0	2.6
OL			2.5	3.6	4.3	5.0	3.3
MT	5.3	4.3	2.8	2.7		0.8	1.3
IL	4.1	2.7	0.70	0.7	0.4	2.1	3.0
HM							
AP	2.8	0.2	0.2	0.2	0.2		
PY							
CLASSIFICATION	ICELANDITE	MUGEARITE	PHONOLITE	PHONOLITE	PERALKALINE PHONOLITE	BENMOREITE	MUGEARITE
MAP UNIT	3or older	2	5A	5A	5A	5B	6B

Table 7-15. Continued

	LMI20D	LMI20C	LMI20I grey	LMI20I	LMIIIA	8/16-44 6250E DYKE	PB0 6440	PBP 6480	8/25-55 6722
SiO2	54.3	56.5	52.8	56.0	59.1	59.9	60.0	59.6	60.5
TiO2	1.6	1.5	1.4	1.5	0.2	0.5	1.2	1.3	0.9
Al2O3	15.7	16.6	14.8	15.8	20.4	19.7	16.3	16.2	17.3
Fe2O3	3.4	0.0	2.8	3.4	3.6	2.5	4.1	3.1	3.4
FeO	5.4	8.2	5.9	6.3	1.3	2.7	3.5	4.7	3.4
MnO	0.2	0.1	0.2	0.1	0.1	0.1	0.2	0.2	0.2
MgO	3.5	2.0	1.8	1.9	0.5	0.3	0.8	0.9	0.8
CaO	5.8	5.2	4.9	5.2	2.6	2.0	2.8	2.9	2.6
Na2O	4.6	5.2	4.8	5.1	5.0	5.2	6.2	6.1	5.8
K2O	2.6	3.3	4.2	4.5	4.8	4.7	4.0	3.9	4.4
P2O5	0.0	0.4	0.0	0.0	0.1	0.2	0.5	0.4	0.6
H2O+	1.6	0.2	1.5	0.2	2.1	0.9	0.1	0.1	0.0
H2O-	1.3	0.7	0.5	0.0	0.0	1.5	0.4	0.7	0.0
CO2			4.3						
Original Total	100.0	99.3	97.2	100.0	100.0	98.1	100.7	100.8	99.2
%MELT	4.79	3.86	2.88	2.89	16.69	17.23	20.51	20.83	17.40
Q	0.1				3.8	6.3	1.8	1.8	2.7
C					2.3	2.9			
OR	16.0	19.9	26.8	27.0	29.3	5.4	23.9	23.28	26.1
(AB)	40.4	44.5	36.9	41.1	43.4	9.0	53.1	51.45	49.3
(AN)	1.8	12.1	7.1	7.1	12.9	8.8	4.6	5.3	8.14
PL	55.2	56.6	44.0	48.2	56.3	53.8	57.7	57.2	57.4
NE		tr	tr	1.5					
NS									
(WO)	6.1	4.7	7.9	8.0			2.5	2.7	0.3
(EN)	3.6	1.4	3.3	0.3			0.8	0.9	0.1
(FS)	2.2	3.5	4.7	7.6			1.8	2.0	0.2
DI	11.9	9.6	15.8	14.9			5.1	5.7	0.6
(EN)	5.5	0.2			1.3	0.6	1.2	1.3	1.9
(FS)	3.4	0.6			3.5	3.5	2.9	3.1	4.7
HY	8.9	0.8			4.8		4.1	4.4	6.6
(FO)		2.4	1.3						
(FA)		6.9	1.8						
OL		9.3	3.1						
MT	4.6		4.3	4.5	2.5	2.9	4.0	4.1	3.5
IL	3.1	2.8	2.8	2.9	0.4	0.9	2.4	2.4	1.7
HM					1.33				
AP		1.0			0.1	0.4	1.1	0.9	1.5
PY									
CLASSIFICATION	MUGEARITE	PHONOLITE	PHONOLITE	PHONOLITE	TRISTANITE BENMOREITE	TRISTANITE BENMOREITE	BENMOREITE TRACHYTE	BENMOREITE TRACHYTE	BENMOREITE
MAP UNIT	7A	7A	7A	7A	7C	7C	8	8	8

Figure 7-16.
Oxide variation plots (anhydrous weight basis) for intermediate lavas of the stratocone stage. Most chemical variation for these disequibrium textured lavas fits a mixing origin from basalt plus trachyte.

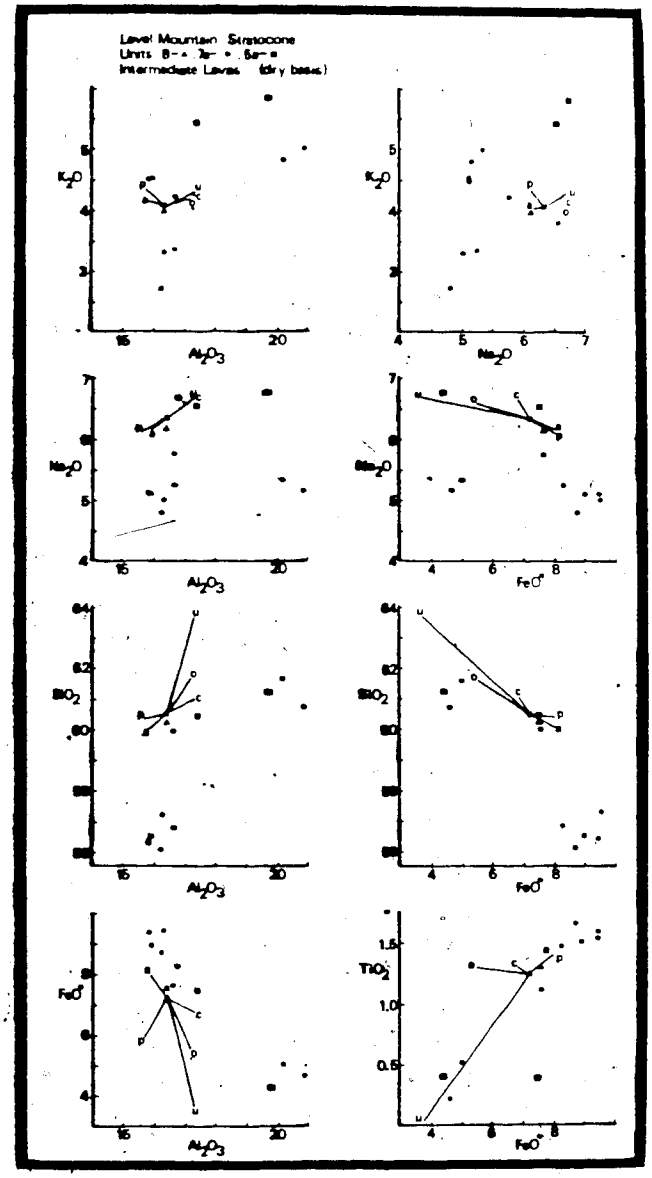

15 to 20% fractionation, with ulvospinel apparently dominant. There is an additional problem in attempting to translate these vectors to other points on the diagram. The phenocryst compositions and populations of these lavas are all different.

The mugearites 26/3c and LMI20d had two phenocryst (xenocryst) clinopyroxenes; large partially resorbed titaniferous augites and small enhedral sodic ferrohedenbergites. The unit 7a series phonolites (stratigraphic section LMI20 samples) had cumulophyric clots of anorthoclase, with or without green clinopyroxene, but always with riebeckites which sometimes occurred as mantles on fayalite cores. Most of the intermediate lavas also contained resorbed plagioclase phenocrysts of andesine composition, a feature also noted for some hawaiites. Mantled feldspars and disequilibrium multiply zoned feldspars have also been used as evidence for magma mixing, (Hibbard, 1981). Most of the phenocryst assemblages do not appear to be in equilibrium with their groundmass and regardless, they still fail to describe the variation trends on the plots.

The time-map units which contain the intermediate lavas always contain some other dominant lava type, usually basalt or trachyte. In unit 7c near the headwaters of the south fork of the Beatty Creek, basalt and trachyte lavas occur together as mixed flows. The other flows of this unit are trachyte or the intermediate types. Crustal gneiss xenoliths

have been found in trachyte of unit 7c and benmoreites of 8. Perhaps, as field evidence suggests, the intermediate lavas originate by magma mixing with variable crustal contamination.

The phonolites of unit 5a were sampled from the north wall of the Kakuchuya Valley. All were light coloured rocks with trachytic texture. 9/1-86/5421 was the thickest of such flows sampled, about 24m, with columns 1.5m across at the base that flaired toward the top of the flow. Phenocrysts included anorthoclase to 1.5cm, abundant biotite 0.9cm x 1mm thick subhedral platelets and 0.5cm prisms of black amphibole (barkevikite or basaltic hornblende). Flows PBV and PBU also contained microphenocrysts of amphibole and biotite. The only other lavas which contained phenocryst amphibole and biotite were the tristanites of unit 7. PBU and PBV are chemically similar to phonolites of the trachyte-phonolite association in general (see table 2-3 of Carmichael, Turner, and Verhoogen, 1974). Compositionally 9/1-86/5421 is distinctive in being the only peralkaline phonolite sampled, having A.I. $(Na_2O+K_2O)/Al_2O_3$ mol = 1.01 and ns calculated in the norm. Chemically this sample is very similar to phonolites from oceanic islands, see for instance the peralkaline phonolites from Tenerife, Canary Islands (eg. TC167 Edgar and Parker, 1974) and to "undersaturated trachytes" from Cinquo Picos Terceira, Azores (Self and Gunn, 1976). Two hypothesis are given for the genesis of the Tenerife Suite: fractional

crystallization or fractional melting to give two primary melts such as discussed by Yoder (1973). If bimodal fractional melting describes the genesis of alkaline volcanics like Terceira and Level Mountain, then phonolites could be the result of magma mixing or they could even be a primary melt, (Takahashi and Kushiro, 1981).

"Petrogeny's residua system" for undersaturated alkalic melts is the compositional plane Q-Ne-Ks. The Level Mountain phonolites plot along the thermal minimum through between the alkali feldspar join and the one atmosphere reaction point, see figure 7-17. The phonolites and feldspathodial trachytes of Dunedin Volcano, Price and Chappell (1975) show a similar scatter about the thermal valley but a better defined trend toward the reaction point. The one atmosphere reaction point and thermal minimum are according to Bowen and Schairer (1938) and Schairer and Bowen (1956). The one kilobar data are from Hamilton and MacKenzie (1965). The four metaluminous phonolitesof Level Mountain plot nearer to the alkali feldspar join, while the peralklaine phonolite approaches the reaction point. Once a melt reaches this system, further alkali feldspar fractionation will drive residual liquids to the reaction point. These lavas are just across the silica saturation barrier and "on trend" for the more voluminous trachytes.

The benmoreites and transitional benmoreite-trachytes of unit 8 outcrop over approximately a 100m interval on the south face of Meszah Peak. Here alkali feldspar phenocrysts

Figure 7-17.
Distribution of Level Mountain phonolites in the undersaturated portion of petrogeny's residua system (weight basis). R is the 1kbar reaction point after Hamilton and MacKenzie (1965). R' is the 1atm. reaction point after Schairer and Bowen (1935). Note that the Level Mountian phonolites plot between the one atmosphere reaction point and the thermal minimum on the alkali feldspar join. The peralkaline example is closest to the reaction point.

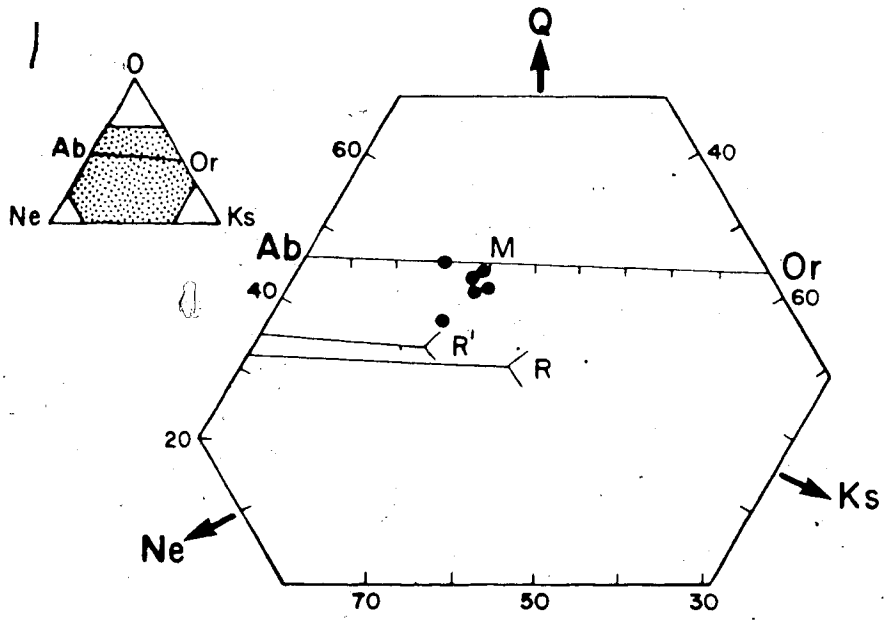

were present, as were gneiss inclusions. While the field appearance of this scoria was rather different than the aforementioned flows, the chemistry of the benmorite was virtually indentical, compare analyses PBO, PBP and 8/25-55/6722. The alternating sequence of benmoreite with trachyte is good field evidence of a mixing origin for the benmoreites. Some crustal contamination may also be involved as evidenced by the gneiss inclusion. Representative analyses of intermediate lavas from elsewhere in the IMB are presented for comparison to the Level Mountain intermediate lavas in table 7-16. The striking feature of all these analyses compared to associated basalts and trachytes, are the high levels of Al_2O_3, typically in excess of 17.0%. The mugearite from Edziza was originally described as trachybasalt. Similar mugearites from the Rainbow Range are described by Bevier (1983), as phenocryst rich (10 to 25%) thin red, grey and brown flows in sections with abundant breccias in excess of 70%. These petrographic and field descriptions are virtually identical to the mugearites and benmoreites at Level Mountain. These were also originally described as trachybasalts by Hamilton and Scarfe (1977).

The mugearites at all three centres (Level Mountain , Edziza and Rainbow Range) occur at high enough statigraphic levels to be interspersed with comendite or trachyte acid lavas. Nonetheless, a mixing hypothesis for the origin of these intermediate lavas has not been commonly invoked. At Edziza, Souther and Symons (1974) explained this chemistry

Table 7-16. Intermediate lavas from other localities in the Intermontane.

	SS4	RM	AP12	I-11A	I13	SS5	SS3	HPTA
SiO2	56.35	55.78±.38	61.72	62.74	62.10	60.13	64.52	60.99±1.47
TiO2	1.26	1.69±.10	.64	.37	.21	.20	.25	1.52± .05
Al2O3	18.45	16.59±.77	17.42	18.16	19.11	19.60	19.47	15.56± .40
FeO*	7.61	9.80±.54	5.79	4.40	4.17	5.57	2.26	5.26±1.73
MnO	.22	.14±.01	.11	.13	.08	.17	.06	.09± .02
MgO	1.94	2.31±.18	.56	.05	.11	1.12	1.20	3.20± .18
CaO	5.20	5.79±.29	2.85	1.21	1.39	1.02	1.81	5.81± .21
Na2O	5.40	4.67±.17	6.22	7.20	7.19	7.01	5.32	4.41± .21
K2O	3.57	2.57±.14	4.27	5.74	5.50	5.18	5.12	2.68± .05
P2O5	0.00	.48±.03	.42	0.00	.15	0.00	0.00	.75± .41

SS4 Mugearite, Mt. Edziza, Souther & Symons (1974)
RM Avg (4) Mugearites (R-99, R-107, R-108, R-109), Rainbow Range, Bevier (1978)
AP12 Benmoreite, Anahim Peak, Bevier (1978)
I-11A Phonolite flow from East Valley Wall north flank Itcha Mountains, Hamilton this work
I-13 Phonolite, flow from West Wall N.W. Glacial Valley Itcha Mountains, Hamilton this work
SS5 Phonolite, Mt Edziza, Souther and Symons (1974)
HPTA Avg (3) Tholeiitic Andesites, (7788-13A) Casey (1980)

to be representative of the "primary magma" for that eruptive unit. While for the Rainbows, Bevier (1978) explained their derivation by 70.71% fractional crystallization of a hawaiite parent. It is doubtful that mugearite could be a primary (unfractionated) mantle derived magma particularily for the Level Mountain and Edziza examples which are devoid of P_2O_5 and very enriched in Si, Al, Na and K relative to undeniably primitive basalts.

The three phonolite analyses presented here, all from flows rather than from tuffs, are chemically quite a coherent group. These examples from the Itcha Mountains and Mount Edziza are most similar to the flows PBU and PBV at Level Mountain. They appear to be chemically similar or transitional to tristanites. Note the small amount of difference between SS5, a corundum normative phonolite and SS3, a tristanite from Edziza, (table 7-16). At Level Mountain the tristanites have even higher levels of Al_2O_3. While there was no petrographic evidence, such as xenocrysts, to support a magma mixing hypothesis for the origin of the Itchas phonolites, the potential for crustal contamination is still there.

A single stage magma mixing model is presented in table 7-17 for each of the three intermediate lava types: mugearite, benmoreite and phonolite. These mixing models are not very sensitive to either the basaltic composition used or the trachyte composition, as the proportions work out to be almost identical. While the points for average hawaiite

Table 7-17. Magma Mixing Calculations

	Haw[1]	Trachyte[2]	Mugearite[3]	Mugearite[4]	Unit 8 Haw. 8/25-50/6397	Trachyte[2]	Benmoreite[5]	Benmoreite[6]	Haw[1]	Trachyte[2]	Phonolite[7]	Phenolite[8]
SiO_2	49.33 ±1.34	64.13 ±.21	56.67 ± .83	56.60	48.05	64.13 ±.21	60.25 ±.26	60.32	48.05	64.13 ±.21	58.27 ±2.37	61.17
TiO_2	3.16 ± .87	.61 ±.11	1.62 ± .04	1.95	2.95	0.61 ±.11	1.20 ±.10	1.16	2.95	0.61 ±.11	1.05 ± .61	1.18
Al_2O_3	15.71 ±1.03	16.30 ±.24	13.30 ± .05	16.00	15.45	16.30 ±.24	16.50 ±.14	16.10	15.45	16.30 ±.24	17.11 ±1.58	16.18
FeO*	12.65 ±1.36	5.83 ±.23	9.11 ± .53	9.30	12.97	5.83 ±.23	7.47 ±.22	7.52	12.97	5.83 ±.23	7.71 ±1.99	7.19
MnO	.13 ± .05	.16 ±.09	0.16 ± .03	.14	0.18	.16 ±.09	0.11 ±.10	0.16	0.18	.16 ±.09	0.12 ± .06	.15
MgO	4.88 ±1.13	.26 ±.03	7.58 ±1.53	2.61	6.02	.26 ±.03	0.96 ±.22	1.63	6.02	.26 ±.03	1.20 ±1.05	1.18
CaO	8.02 ± .99	1.49 ±.15	5.63 ± .46	4.81	9.10	1.49 ±.15	3.07 ±.37	3.29	9.10	1.49 ±.15	3.85 ±1.91	2.80
Na_2O	3.97 ± .33	5.97 ±.09	4.90 ± .16	4.95	3.83	5.97 ±.09	6.08 ±.30	5.46	3.83	5.97 ±.09	5.75 ± .82	5.57
K_2O	1.43 ± .42	5.07 ±.09	3.01 ± .14	3.22	0.86	5.07 ±.09	4.08 ±.11	4.07	0.86	5.07 ±.09	4.73 ± .96	4.34
P_2O_5	.72 ± .38	.10 ±.02	0.00 ± .00	.42	0.58	0.10 ±.02	0.29 ±.26	0.21	0.58	0.10 ±.02	0.12 ± .17	.22

1 Average stratocone hawaiite composition (13)
2 Average metaluminous trachytes (13)
3 Average of unit 7 mugearites (2)
4 Calculated as 51% hawaiite plus 49% trachyte
5 Average unit 8 benmoreite (4)
6 Calculated as 24% hawaiite plus 76% trachyte
7 Average stratocone phonolite (5)
8 Calculated as 20% hawaiite plus 80% trachyte

and average trachyte have not been plotted on figure 7-16, they span the dominant variation trend, with a mixing line that is nearly to it. Similar mixing relations have been discussed for alkaline volcanics by Brooks and Printzlau (1978) and by Anderson (1976).

In the case of the mugearite model, a basaltic magma and a trachyte magma must be mixed in subsequal proportions. Starting compositions of both alkali basalts and hawaiites have been used for a total range of basalt weight fraction from 0.4944 to 0.5234. The biggest discrepancies for the case shown are TiO_2, P_2O_5 and CaO. The calcium problem can be solved by varying the composition of the basaltic parent within one standard deviation. The TiO_2 and P_2O_5 excesses occur pervasively in all mugearite calculations attempted. However, they can be explained if in addition to mixing of basalt and trachyte in model proportions there is somewhere between 0.25 and 1% apatite fractionation and less than 3% fractionation of an iron titanium oxide.

Benmoreites are restricted to map units 7 and 8, so a hawaiite from that period is presented to model their derivation. Again the choice of hawaiite composition is not really that critical to the mixing proportions. The fit for the model presented here is quite good. The only discrepancies are the Na_2O and Al_2O_3 which are small enough to be accounted for by alternate choice of parent trachyte or by less than 2% of assimilation of granitic material. Because these flows contain granitic gneiss xenoliths that

are partially melted either solution is considered acceptable.

The phonolites are compositionally quite variable but the mixing proportions for basalt and trachyte vary less than 2% for any choice of parent lavas. When these calculations are made for phonolites PBU and PBV the addition of crustal material is required in the 5% range to account for their higher levels of SiO_2, Al_2O_3, Na_2O and K_2O. These particular flows are nearly as enriched in Al_2O_3 as the tristanites. There are no other magmas at Level Mountain with sufficiently high levels of Al_2O_3 to explain such products by magma mixing alone. The lack of a suitable parent composition exists for Na_2O as well, in the case of 9/1-86/5421, which is a peralkaline phonolite. Presumably this points to open system behavior for alkalis. The mixing test for phonolite genesis only partially explains their major and trace element chemistry. In addition to magma mixing there would have to be a component of crustal contamination and open system behavior for alkali and incompatible elements.

The trachyte compositions which satisfy these mixing models are all metaluminous. The Al_2O_3 and Na_2O levels of the peralkaline trachytes are too low to meet the daughter lava compositions. This presents a bit of a problem as the primary trachyte magmas at Level Mountain are thought to be peralkaline. The admixed xenocrysts in most of the phonolite lavas such as anorthoclase, sodic ferrohedenbergite and

riebeckite are all derived from peralkaline trachyte parents. There is another way to visualize the metaluminous trachyte average used in these calculations; that is a peralkaline trachyte which has experienced volatile loss and crustal contamination. These complications could accompany the magma mixing and eruptive process.

The best explanation for the low volume compositionally variable intermediate lavas is that they lie on a mixing line between the more common hawaiites and trachytes, with variable amounts of crustal contamination. When fractional crystallization models were attempted for the intermediate lavas from Level Mountain using a basaltic parent (basalt or hawaiite) and analysed phenocryst compositions there were no acceptable solutions. Additionally such fractionation models fail to explain the disequilibrium phenocryst assemblages, and they do not make allowance for crustal contamination such as the high Al_2O_3, hydrous minerals and crustal xenoliths would indicate. Mixing models presented here can account for most of the compositional variation without recourse to extensive additional fractionation or contamination.

Major Element Petrochemistry of Salic Lavas From Level Mountain and a Comparison of Similar Lavas From Other Localities in the Intermontane Belt.

Introduction

The volumetrically dominant salic lavas are peralkaline. Chemically they span a range of more than 10

weight percent in SiO_2, including types which have variously been described as comendites, comendite trachytes, pantelleritic trachytes and pantellerites. Physically they range from aphyric pitchstones, to tuffs, ignimbrites, stocks, laccolits and holocrystalline eutaxitic trachytes. Chemically their hallmark is having molecular $(Na_2O+K_2O)/Al_2O_3>1$. This agpaitic index greater than unity implies excess alkalis over the amount required to form feldspars and manifests itself as the occurrence of alkali ferromagnesian silicates.

For the purposes of minimizing the chemical variation within salic rock classifications, only four groups are recognized. Peralkaline trachyte includes the types comendite trachyte, pantelleritic trachyte and pantellerite of MacDonald (1976). Most of the Level Mountain varieties are of his pantelleritic trachyte type. These lavas lie more than 98% in the system (SiO_2, Al_2O_3, FeO*, Na_2O, K_2O) with silica content in the mid to upper 60's and more than 12.5% for normative colour index. Comendite corresponds to MacDonald's (1974) definition and is a weakly peralkaline rhyolite with silica content in excess of 70%, and total iron less than 5% which gives rise to a normative colour index less than 12.5%. In these lavas MgO and CaO are reduced to the level of minor or even trace constituents. Normative recognition of these peralkaline lavas is based on the occurrence of Ac and/or Ns, and depending on the CaO content, Wo is generally present as well.

The trachyte group includes both alkaline $(CaO+Na_2O+K_2O)/Al_2O_3>1$, and metaluminous types. They range from wollastonite to hypersthene normative and in a few cases include normative corundum. The alkaline types dominate. Petrographically and mineralogically they include types with phenocryst fayalite and hedenbergite and no unusual groundmass mineralogy in addition to lavas whose groundmass phases include the same alkali ferromagnesian minerals characteristic of the peralkaline trachyte group, aenigmatite and alkali amphiboles. The chemistry of this trachyte group contrasts slightly with the peralkaline trachytes in having lower SiO_2 and FeO*, higher Al_2O_3 and higher levels of all the minor components CaO, TiO_2, P_2O_5, MgO and MnO. These chemical characteristics for the alkaline trachytes lead to a more diverse and apparently more strongly peralkaline groundmass than in the case of some of the peralkaline trachytes.

The rhyolites are chemically quite variable, ranging between comendites and trachytes for most oxide concentrations but they are distinguished by low Na_2O. In fact the weight ratio of K_2O/Na_2O for this group is generally greater than one. This is highly peculiar compared to any other lava type at Level Mountain. These rhyolites range from metaluminous to peraluminous and have normative hypersthene with or without corundum. Rhyolites are spatially and temporally more restricted than comendites. The most comon occurrence of rhyolites is as aplitic tuffs

and partially devitrified pitchstones. Glassy commendite dykes commonly have a crystalline white rhyolite selvedge, which would seem to indicate that rhyolites are altered forms of more common comendite melts (Noble, 1967).

Peralkaline trachytes

Chemical analyses and norms of the peralkaline trachytes are presented in table 7-18. Of the thirteen analyses in this group, MacDonald's classification (1974) would call six of the rocks peralkaline trachytes of pantellerite affinity, three peralkaline trachytes of comendite affinity, and four pantellerites. The thirteen analyses represent all three salic eruptive cycles (map units 5a, 6a, and 7) of the stratocone. Most of the compositional variation can be seen in the samples from unit 6a, so no stratigraphic association or genetic sequence is inferred. Comparing the averages for the three subgroups shows them to overlap within one standard deviation for all ten oxides, table 7-19, so the three groups were subsequently combined. For the entire population, SiO_2 varied inversely as Al_2O_3, Na_2O and P_2O_5, while Al_2O_3 varied normally with Na_2O. Such variation could be explained by alkali feldspar plus apatite fractionation. A system open to SiO_2 could also partially account for these covariances. The minor components MgO and MnO vary normally with each other and with FeO*. Random variations in content of phenocryst olivine (Fa rich) and possibly clinopyroxene could account for the low and highly variable levels of MnO and MgO in

Table 7-18 Chemical Analyses for Peralkaline Trachytes

	25/7	8/2-97 5010	8/10-1 4915	8/5-8 5150	8/6-12	8/6-12 5290	25/50	25/5E	PBE 5745	PBF 5545	PBG 5580	8/7-18 5720	8/16-43 6000
SIO2	65.77	65.74	68.56	65.54	66.79	65.77	66.28	67.03	65.54	65.09	64.34	67.38	64.13
TIO2	0.40	0.31	0.46	0.50	0.58	0.54	0.46	0.45	0.48	0.45	0.52	0.48	0.59
A1203	14.63	15.26	12.13	12.80	12.45	13.16	12.91	13.44	12.96	13.49	13.41	13.09	14.85
Fe203	0.0	0.0	0.38	5.58	6.06	7.30	4.93	7.53	6.25	3.82	5.66	2.30	5.32
FeO	6.24	5.74	6.75	3.85	1.59	1.24	3.27	0.21	1.44	3.77	2.36	4.09	2.11
MnO	0.13	0.12	0.14	0.22	0.18	0.23	0.15	0.17	0.0	0.07	0.12	0.09	0.28
MgO	0.0	0.0	0.0	0.18	0.19	0.22	0.29	0.07	0.0	0.0	0.05	0.0	0.0
CaO	1.30	1.58	0.78	0.61	0.85	0.47	0.55	0.34	0.65	1.05	1.10	0.68	1.87
NA20	5.84	6.46	5.33	5.08	4.93	6.37	4.89	5.89	5.82	6.26	6.13	5.88	5.72
K20	5.25	5.29	4.63	4.66	4.13	4.28	4.61	4.59	4.95	4.90	4.97	5.00	5.14
P205	0.0	0.0	0.0	0.04	0.04	0.03	0.05	0.04	0.09	0.08	0.17	0.0	0.0
H20-	0.22	0.65	0.35	0.75	2.15	0.01	0.83	0.06	0.45	0.26	0.24	0.53	0.0
H20	0.23	0.37	0.50	0.15	0.0	0.35	0.70	0.17	1.37	0.65	0.93	0.49	0.0
ZrO2			0.01										
S			0.04	0.04	0.03	0.06	0.01						
BaO										0.12			
%MELT	15.74	15.73	17.77	17.54	19.54	19.16	17.63	17.90	16.36	16.70	16.41	16.39	16.06
Q	7.23	5.00	18.02	16.75	21.79	13.90	18.66	16.23	14.50	8.67	10.31	13.46	9.33
OR	31.02	31.26	27.36	27.54	24.94	25.41	27.24	27.12	29.25	28.96	29.37	29.55	20.37
(AB)	46.02	49.04	36.62	39.90	41.98	44.01	40.74	43.58	39.10	42.11	41.31	39.49	47.77
(AN)													
PL	46.02	49.04	36.62	39.90	41.98	44.01	40.74	43.58	39.10	42.11	41.31	39.49	47.77
AC			1.10	2.72	0.58	8.86	0.56	5.52	8.94	9.57	9.31	6.65	0.56
NS	0.79	1.31	1.68		1.10WO	0.28WO	1.00	0.34WO	1.10WO		0.19WO	0.63	3.87WO
(WO)	2.69	3.27	1.62	1.15	0.58	0.63	.32	0.20		2.05	1.62	1.41	
(EN)				0.18	0.50	0.55		0.17			0.12		
(FS)	3.06	3.72	1.84	1.08						2.33	1.69	1.60	
DI	5.75	6.99	3.45	2.41	1.07	1.18	2.04	0.38		4.37	3.43	3.01	
(EN)				0.27			40						
(FS)	7.98	6.04	10.06	1.66			89			3.56		5.29	
HY	7.98	6.04	10.06	1.93			1.30			3.56		5.29	
MT				6.73	3.99	3.04	6.87		3.25	0.74	3.54		6.00
IL	0.76	0.59	0.87	0.95	1.14	1.04	0.87	0.78	0.91	0.85	0.99	0.91	1.12
HM					3.23	2.15		5.62	0.92				0.99
TN								0.09					
AP				0.09	0.09	0.07	0.12	0.09	0.21	0.19	0.40		
PY				0.07	0.07	0.06	0.11	0.02					
Z				0.01									
CLASS-IFICA-TION	CT	CT	P	PT	P	PT	PT	P	PT	PT	PT	P	CT
MAP UNIT	5A	5A	6A	6A	6A	6A	6A	6A	6A	6A	6A	7B	7B

Table 7-19. Statistical comparison for subdivisions within the Peralkaline Trachyte Classification.

	Pantelleritic Trachyte (6)	Comenditic Trachyte (3)	Pantellerite (4)
SiO2	65.83±.98	67.65±1.10	67.98±1.34
TiO2	.49±.07	.53± .08	.49± .03
Al_2O_3	14.04±.72	13.73± .39	12.83± .52
FeO*	7.06±.50	7.39± .43	7.47±1.41
MnO	.12±.10	.20± .03	.15± .07
MgO	.01±.02	.14± .12	.06± .10
CaO	1.21±.44	.56± .27	.70± .09
Na_2O	6.03±.25	5.82± .69	5.50± .41
K_2O	5.11±.12	4.41± .21	4.82± .21
P_2O_5	.07±.07	.04± .01	.01± .02
AI	1.10	1.08	1.11
Na/K	1.79	2.15	1.73

addition to their covariance with FeO*. their covariance with FeO*. For confirmation of this, recall the enrichment of MnO in K_2O varies inversely with MgO, MnO and CaO, reflecting the variation between phenocryst populations dominated by anorthoclase, versus those dominated by phenocryst fayalite and sodic ferrohedenbergite. TiO_2 varies normally with FeO* and inversely with Al_2O_3. Sometimes there is phenocryst ulvospinel or ilmenite associated with olivine and clinopyroxene, although generally the peralkaline magmas, particularily at Level Mountain, seem to have crystallized in an oxide absent field as discussed by Ernst (1962) and Marsh (1975). The FeO*-TiO_2 covariance could indicate that some iron titanium oxide fractionation may have played a role in the genesis of the Level Mountain peralkaline trachyte magmas, while the combined effects of temperature, oxygen fugacity and peralka y preclude oxide phases during groundmass crystallization.

Comendites

Chemical analyses for representative comendites are presented in table 7-20. In reviewing the figure 7-1 histograms for comendites, the distributions appear to be normal for all oxides except SiO_2, K_2O and MnO. The population was arbitrarily divided at the means for these oxides. Means and standard deviations were calculated for high and low splits to see if any statistical differences were indicated. The results are presented in table 7-21. The high silica set was lower in Al_2O_3 and marginally lower in

Table 7-20 Chemical Analyses of Comendites

	PBW 5000	LMI20H	LMI20 Bomb	8/16-41 5960	8/11-30 6111	9/2-95 5625	9/2-99	9/2-99 6600	8/25-54 6345
SiO2	70.16	74.13	70.70	73.44	70.62	75.83	73.83	74.63	73.37
TiO2	0.33	0.15	0.19	0.13	0.27	0.0	0.15	0.08	0.17
Al2O3	14.53	13.63	14.55	12.45	13.34	12.39	12.57	11.32	12.08
Fe2O3	2.23	0.85	1.62	0.97	0.28	0.82	0.87	0.30	1.84
FeO	1.02	0.37	0.78	2.48	5.11	1.22	2.76	2.17	2.11
MnO	0.0	0.0	0.0	0.08	0.12	0.0	0.10	0.04	0.10
MgO	0.0	0.0	0.0	0.0	0.0	0.0	0.08	0.0	0.07
CaO	0.33	0.0	0.16	0.18	0.38	0.21	0.08	0.0	0.18
Na2O	5.45	5.21	5.15	6.02	5.13	4.11	5.19	5.76	5.79
K2O	5.46	4.83	5.55	4.25	4.74	5.25	4.36	4.78	4.27
P2O5	0.0	0.10	0.0	0.0	0.0	0.0	0.0	0.15	0.01
H2O+	0.0	0.44	0.70	0.0	0.0	0.17	0.0	0.26	0.0
H2O	0.49	0.29	0.59	0.0	0.0	0.0	0.0	0.52	0.0
S							0.01		0.02
ZrO2									0.01
%MELT	15.09	17.04	14.74	19.51	17.50	15.77	19.02	17.23	19.40
Q	17.62	25.54	19.29	24.88	18.42	30.93	25.52	30.47	25.37
C	32.26								
OR		28.54	32.80	25.11	28.01	31.02	25.76	28.36	25.23
(AB)	44.34	43.22	43.58	40.38	42.23	34.50	40.38	31.76	38.36
(AN)			0.19						
PL	44.34	43.22	43.77	40.38	42.23	34.50	40.38	31.76	38.36
AC	1.57	0.76		2.81	0.81	0.24	2.52	2.40	5.32
NS				1.72	0.06		0.16	3.38	1.07
WO	0.68		0.25						
(WO)				0.37	0.79	0.43	0.17		0.35
(EN)							0.01		0.02
(FS)				0.42	0.89	0.49	0.18		0.37
DI				0.80	1.68	0.93	0.35		0.73
(EN)							0.19		0.16
(FS)				4.06	8.27	1.14	4.81	3.06	3.37
HY				4.06	8.27	1.14	5.00	3.06	3.53
MT	2.33	0.76	1.96			1.07			
IL	0.63	0.28	0.36	0.25	0.51		0.28	0.15	0.32
HM	0.08	0.06	0.27						
AP									0.02
PY							0.02		0.04
Z									0.01
CLASSIFICATION	C	C	C-R	C	C	C	C	C	C
CRYSTALLINITY	CRYST	CRYST	CRYST	GLASS	CRYST	GLASS	GLASS	GLASS	GLASS
MAP UNIT	5A	7A	7A	7B	7B	7C	7C	7C	7C

Table 7-21. Chemical Variations of Comendites.

	Average High Silica Comendites (6)		Average Low Silica Comendites (3)	Average Low K20 Comendites (5)		Average High K20 Comendites (4)
SiO2	74.49±1.02	>	71.02± .63	73.36±1.67		73.29±2.51
TiO2	0.12± .07	<	.26± .07	.16± .07		.17± .14
Al2O3	12.45± .76	<	14.25± .78	12.38± .71		13.89±1.08
FeO*	2.71±1.03		3.56±1.61	3.70±1.05		2.11± .79
MnO	.05± .05		.04± .07	.09± .03	>	0.00± .00
MgO	.03± .04		0.00± .00	.03± .04		0.00± .00
CaO	.11± .09		0.29± .12	.16± .14		.18± .14
Na2O	5.37± .70		5.28± .19	5.59± .40		5.02± .61
K2O	4.64± .41		5.29± .48	4.49± .27	<	5.32± .33
P2O5	.04± .07		0.00± .00	.03± .07		.03± .05
A.I.	1.11	>	1.01	1.14	>	1.01
Na/K	1.76	>	1.52	1.89	>	1.43

TiO_2, while being more strongly peralkaline and having a higher atomic ratio of Na/K. While the high silica, high agpaitic index and low Al_2O_3 could be explained by alkali feldspar fractionation of appropriate composition, the higher Na/K ratio negates this possibility. The ratio of Na/(Na+K) for feldspar to whole rock is typically about 1.12, so that any alkali fedlspar fractionation would lower Na/K, which is in the opposite sense to the variation described. The chemical variation between the high and low silica groups is better explained by open system behavior, particularly for Si and Na, coupled to volatile loss during eruption and crystallization, or to subsolidus devitrification and alteration of groundmass glass (Noble, 1968). The clusters for low K_2O and high MnO were coincident and showed higher agpaitic index and Na/K ratios. These differences could equally well be explained by crystallization and also by glass alteration processes. Noble (1965, 1967, 1968) and Noble and Haffty (1969) have extensively described crystallization, devitrification and alteration processes in peralkaline rocks from the western U.S.A., Canary Islands and Australia. Lowering of SiO_2 and peralkalinity index (AI) are universally seen. The only elements whose levels may be unaffected by these processes are Ba, La, Nb, Rb and Zr.

Low and variable contents of phenocryst acmitic pyroxenes and iron titanium oxides have been petrographically noted for the comendite pitchstones. These

petrographic characteristics can probably account for most of the covariances involving FeO*, CaO, MgO, TiO_2 and MnO as discussed above. The direct variation of K_2O with Al_2O_3 could be explained either by feldspar fractionation, alteration or open system behavior. The inverse correlations with SiO_2 could be explained by [illegible]ation or open system behavior. While quartz fractionation is possible, the occurrence of quartz phenocrysts in comendites was rare.

Trachytes

Chemical analyses for fourteen trachytes representing map units 5a, 6a and 7, are presented in table 7-22. These lavas differ chemically from the peralkaline trachytes in having lower SiO_2 and higher Al_2O_3. They also differ from peralkaline trachytes on average in having slightly higher levels of minor elements, TiO_2, MgO and CaO, but slightly lower FeO*. They are metaluminous with an A.I. less than unity, but on the basis of alkali ratio they are virtually indistinguishable from the peralkaline trachytes. These lavas are highly variable and were not very amenable to analysis of covariance as a single set. They range from Di plus Wo normative (alkaline) to Di plus Hy normative and in the extreme Hy plus C normative. On the basis of agpaitic index, the corundum and hypersthene normative types cannot be distinguished from their diopside plus Wollastonite normative types. The more encompassing alkalinity index $(CaO+Na_2O+K_2O)/Al_2O_3$ must be used. For the trachytes, SiO_2 varied inversely with TiO_2, MgO and CaO. Unlike all of the

Table 7-22 Chemical Analyses for Trachytes.

	24/1HI	24/2C	9/2-96 5330	26/4	8/25-52 5880 STOCK	8/12-33 6140	8/26-56 6336	PBK 5745	PBY 5480	PBL 5835	PBM 6160	PBN 6340	LMIII30A	LMIII30B
SiO2	64.14	65.88	64.67	63.48	64.86	63.48	63.62	62.23	61.42	64.20	61.13	62.43	65.82	63.33
TiO2	0.40	0.38	0.46	1.88	0.41	0.59	0.64	0.66	0.74	0.43	0.54	0.98	0.44	0.57
Al2O3	17.51	15.79	14.97	17.05	16.60	15.29	15.70	16.95	16.69	16.47	15.70	15.64	14.86	16.34
Fe2O3	3.96	0.92	2.79	3.45	2.17	2.14	1.35	3.51	3.67	2.51	3.35	5.53	3.66	2.87
FeO	0.94	4.38	4.24	2.04	3.58	5.08	5.00	1.96	2.48	2.18	2.64	1.35	3.19	3.11
MnO	0.10	0.15	0.23	0.13	0.16	0.31	0.15	0.05	0.12	0.0	0.08	0.22	0.16	0.26
MgO	0.20	0.09	0.17	0.37	0.21	0.21	0.40	0.31	0.34	0.13	0.25	0.34	0.06	0.43
CaO	1.00	0.89	1.38	0.0	0.98	1.72	1.87	1.76	1.95	1.45	1.81	1.82	0.82	1.55
Na2O	6.10	5.91	5.65	5.95	6.07	5.50	6.01	6.16	6.32	6.34	5.88	5.94	5.53	5.13
K2O	5.31	5.04	4.58	4.33	6.83	4.63	5.08	5.19	5.07	5.55	5.24	5.09	4.81	5.23
P2O5	0.10	0.05	0.06	0.0	0.08	0.10	0.18	0.10	0.11	0.12	0.15	0.20	0.06	0.12
H2O+	0.06	0.45	0.37	0.91	0.04	0.34	0.0	0.33	0.31	0.0	0.32	0.05	0.24	0.21
H2O-	0.18	0.06	0.41	0.40	0.0	0.60	0.0	0.81	0.48	0.35	0.60	0.29	0.35	0.83
S		0.01	0.02		0.01	0.01						0.13	0.01	0.05
BaO									0.30	0.27	0.31			
%MELT	15.55	16.37	17.91	18.85	17.11	17.73	16.32	15.76	16.13	14.82	15.59	16.14	17.09	15.65
Q	2.63	7.75	9.96	11.75	6.97	7.88	3.37	3.62	1.99	3.82	5.83	5.96	13.04	8.80
C	0.15			2.58										
OR	31.32	29.93	27.30	25.59	28.60	27.60	30.02	30.67	29.96	32.80	30.96	30.08	28.58	30.91
(AB)	51.62	50.25	48.15	50.35	51.45	46.96	50.85	52.12	53.48	53.65	49.75	50.26	47.04	43.41
(AN)	4.31	1.68	1.99		3.74	3.42	0.86	3.27	2.20	0.09	0.82	0.98	1.56	6.11
PL	55.92	51.93	50.14	50.35	55.18	50.39	51.71	55.40	55.68	33.74	50.72	51.24	48.60	49.52
WO								1.11	1.61	1.39	1.27	1.93		
(WO)		1.01	1.91		0.25	1.90	3.02	0.89	1.44	1.45	1.90	0.98	.90	0.29
(EN)		.04	0.16		0.03	0.14	0.40	0.77	0.85	0.32	0.62	0.85	.06	0.09
(FS)		1.10	1.95		0.25	1.97	2.91		0.52	1.22	1.34	1.83	.95	0.22
DI		2.15	4.02		0.53	4.02	6.33	1.67	2.81	2.99	3.86		1.91	0.59
(EN)	0.50	.19	0.26	0.92	0.49	0.38	0.60						.09	0.99
(FS)	7.79	5.83	3.19		4.08	5.24	4.38						1.48	2.51
HY	8.29	6.02	3.45	0.92	4.57	5.62	4.98						1.57	3.49
MT		1.34	4.06	1.55	8.18	3.12	1.96	4.57	5.32	3.64	4.86	2.23	5.33	4.16
IL	0.76	0.74	0.89	3.57	0.78	1.14	1.22	1.25	1.41	0.82	1.03	1.86	0.84	1.08
HM				2.38				0.96				3.99		
AP	0.24	0.12	0.14		0.19	0.24	0.43	0.24	0.26	0.28	0.38	0.47	0.14	0.28
PY		0.02	0.04		0.02	0.02							0.02	0.09
CLASSIFICATION	T	T	T	T	T	T	T	T	T	T	T	T	T	T
MAP UNIT	5A	5A	5A	6A	7A	7A	7A	7A	7A	7A	7A	7A	7C	7C

other salic lavas, there was no negative SiO_2 - Al_2O_3 correlation. TiO_2 varied normally with CaO and P_2O_5. Al_2O_3 varied inversely with MnO. FeO* varied normally with MnO and both varied inversely with Na_2O and K_2O. The absolute levels of Na_2O and K_2O are actually higher on average for the metaluminous trachytes than for peralkaline ones. It is difficult to predict a simple fractionation, assimilation or alteration model to account for all of these variations.

Rhyolites

The chemical variation in the rhyolites is the most extensive of the salic rock types. Chemical analyses are presented in table 7-23. All examples are limited in time to statocone unit 7. No rhyolites were noted for other map units. In a normative sense, these include Hy plus Di, Hy and Hy plus C types. According to Irvine and Baragar's (1971) classification these are tholeiitic rhyolites of the potassium poor series and calc-alkaline rhyolites. For the rhyolites, SiO_2 has a particularily wide range. FeO*, Na_2O and K_2O may show bimodal distributions. High and low group averages were calculated for these four oxides. The high silica group and the low FeO* group were identical. Averages are presented in table 7-24. Averaging on the basis of SiO_2 and FeO* levels additionally revealed differences greater than one sigma for TiO_2, Al_2O_3 and A.I. such that the high SiO_2 cluster was of higher alkalinity and lower TiO_2, Al_2O_3 and FeO*. The minor elements MnO, MgO and CaO were also marginally lower (by their standard error ranges) in the

Table 7-23. Chemical Analyses of Rhyolites.

	LMI3	LMI7	8/7-19 5830	8/16-43 5990	8/16-44 6350	8/27-66 5862	8/27-63 6788	8/27-62 6890
SiO2	72.80	66.50	67.57	66.58	68.19	74.13	69.62	71.88
TiO2	0.15	0.43	0.34	0.43	0.56	0.11	0.0	0.15
Al2O3	13.68	14.79	14.96	15.07	14.36	12.93	14.17	13.86
Fe2O3	2.66	6.33	2.35	4.06	6.36	0.96	0.55	0.63
FeO	0.28	0.20	3.78	2.57	0.74	1.25	2.73	2.13
MnO	0.08	0.08	0.16	0.18	0.22	0.05	0.11	0.10
MgO	0.04	0.07	0.0	0.18	0.15	0.09	0.0	0.0
CaO	0.0	0.34	0.98	0.93	0.74	0.11	0.53	0.55
Na2O	4.78	5.49	3.90	3.57	2.90	3.91	4.33	4.71
K2O	4.76	4.92	5.81	5.49	4.49	5.14	6.28	5.39
P2O5	0.02	0.04	0.0	0.03	0.03	0.03	0.0	0.0
H2O-	0.62	0.40	0.11	0.87	1.17	1.28	1.70	0.52
H2O+	0.12	0.33	0.03	0.0	0.0	0.0	0.0	0.08
S	0.01	0.07		0.05	0.09	0.02		
%MELT	17.26	16.63	14.23	14.91	18.11	15.94	12.99	15.30
Q	26.72	15.07	18.39	22.44	32.77	31.17	16.94	21.59
C	0.66		0.47	1.64	3.50	0.80		
OR	28.13	29.07	34.33	32.74	26.89	30.73	35.87	31.85
(AB)	40.45	46.45	33.00	30.46	24.88	33.59	35.45	39.85
(AN)		1.18	4.86	4.47	3.48	0.35	0.65	0.76
PL	40.45	47.64	37.86	34.93	28.35	33.94	36.10	40.61
(WO)							0.79	0.82
(EN)								
(FS)							0.89	0.93
DI							1.68	1.76
(EN)	0.10	0.17		0.45	0.37	0.22		
(FS)			4.74	0.89		1.40	3.70	2.39
HY	0.10	0.17	4.74	1.34	0.37	1.63	3.70	2.39
MT	0.69		3.41	5.92	1.16	1.41	0.77	0.91
IL	0.28	0.43	0.65	0.84	1.08	0.21		0.28
HM	2.18	6.33			5.63			
TN		0.17						
RU		0.13						
AP		0.09		0.07	0.67	0.07		
PY	0.02	0.13		0.09	0.17	0.04		
CLASSIFICATION	R	R-T	R	R	R	R	R	R
MAP UNIT	7A	7A	7B	7B	7B	7C	7C	7C

Table 7-24 . Chemical Variation among Rhyolites.

	>70.6 (4) Hi SiO2 Low FeO < 4.21		<70.6 (4) Low SiO2 Hi FeO > 4.21	>4.36 (4) High Na2O	(4) Low Na2O	>5.41 (5) High K2O	(3) Low K2O
SiO2	72.99±1.83	>	68.07± .97	71.06±2.36	7.00±3.57	70.74±3.22	70.19±3.09
TiO2	.10± .07	<	.45± .09	.19± .18	.37± .19	.21± .18	.39± .22
Al2O3	13.83± .54	<	14.99± .26	14.30± .54	14.51± .97	14.35± .87	14.49± .61
FeO*	2.71± .46	<	6.19± .31	3.67±1.57	5.24±2.07	4.07±1.90	5.09±2.09
MnO	.09± .03	<	.16± .06	.09± .02	.15± .07	.12± .05	.13± .08
MgO	.03± .04	<	.10± .08	.03± .03	.11± .08	.05± .08	.09± .06
CaO	.30± .29		.75± .29	.36± .26	.70± .40	.62± .35	.36± .38
Na2O	4.49± .39		4.02±1.11	4.89± .49	3.62± .46	4.13± .44	4.45±1.35
K2O	5.46± .67		5.31± .46	5.41± .71	5.36± .43	5.68± .45	4.88± .09
P2O5	.01± .02		.03± .02	.02± .02	.02± .02	.01± .02	.03± .01
A.I.	.96	>	.82	.97	> .81	.90	.87
Na/K	1.25		1.15	1.37	> 1.03	1.11	< 1.39

high SiO_2 group. These chemical differences could be explained if the rhyolite classification here did not represent a single continuous related series of lavas, but rather two groups which were derived from comendites and trachytes respectively. Some of the high silica group have either phenocryst green sodic pyroxene or groundmass sodic amphiboles suggesting that they are related to comendites.

The divisions according to Na_2O and K_2O were not coincident and no significant differences in level for any other major components were noted in either case. There are two possible explanations for the Na_2O, K_2O variation. Either they are random, or there is open system behavior for these alkalis (which does not affect the other elements the same way). In that the rhyolites have the lowest Na_2O contents for salic rocks, and also the lowest Na/(Na+K) ratio, the variation is probably not random. However, the lack of correlation between Na_2O level and other oxides precludes a single mineral fractionation origin or alteration trends, as was suggested for the comendites.

Covariance and correlation coefficients were calculated for the eight rhyolites of unit 7. Silica varies inversely with Al_2O_3, FeO*, MnO and CaO. TiO_2 varies normally with Al_2O_3, FeO*, MnO, MgO, CaO and P_2O_5. Al_2O_3 varies normally with FeO* and CaO. MnO varies directly with MgO and CaO but inversely with Na_2O. MgO varies inversely with Na_2O and K_2O but normally with P_2O_5. CaO varies inversely with Na_2O. K_2O varies inversely with P_2O_5. The very unusual aspect of this

analysis is the lack of positive correlation between alkalis and any other oxide. The negative correlations all involve SiO_2, Na_2O and K_2O and may imply open system behavior (selective loss) for these components. The positive correlations for the minor components could be explained by Fe-Ti-oxide and clinopyroxene fractionation or by dilution of these components with feldspar and quartz.

Chemical Variation for all Salic Lavas

Representative chemical analyses for salic lavas from elsewhere in the Intermontane Belt are presented in table 7-25. Sample R-T from the Rainbows and HPD from the Heart Peaks are basically similar to the metaluminous trachytes of Level Mountain. For the average metaluminous trachyte from the Rainbows, all values are within the range of observed variation for Level Mountain. For the Heart Peaks dacite, the only values both out of range and beyond one standard deviation are the minor elements MgO, CaO and P_2O_5. The rhyolite from Edziza is similar to the high silica rhyolites from Level Mountain for all but the trace element MgO, which is greater for the Edziza sample. The peralkaline trachytes and pantellerites from the Rainbows and the pantellerite from Edziza fall within the variation of the peralkaline trachyte group from Level Mountain. The Edziza comendite compares favorably with the high silica comendites from Level Mountain.

A series of eight oxide variation plots are presented for all of the salic lavas from Level Mountain, figure 7-18.

Table 7-25. Chemical Analyses for Salic Lavas from other centres of the Intermontane Belt.

	RAINBOW RANGE			EDZIZA				HEART PEAKS
	R-T	R-CT	R-P	ECS1	EPS2	SS2	HPD	HPR
SiO2	66.73±.55	67.50±.46	69.18±.55	75.25	65.28	74.45	64.04±.72	76.72±1.42
TiO2	.42±.01	.38±.01	.41±.01	.16	.47	.18	.85±.01	.14± .05
Al2O3	15.43±.49	14.52±.19	12.88±.26	12.17	13.95	12.47	16.63±.04	13.00± .72
FeO*	5.67±.40	5.49±.40	6.32±.21	2.72	7.79	2.65	4.89±.14	.79± .07
MnO	.13±.02	.12±.01	.13±.01	.04	.18	.04	.20±.07	.01± .00
MgO	tr	tr	.17±.17	.40	.71	1.18	.53±.27	.08± .03
CaO	1.05±.32	.99±.11	.58±.09	.30	1.22	.29	2.00±.33	.86± .71
Na2O	5.42±.27	5.81±.15	5.33±.15	5.03	5.81	4.91	5.64±.14	4.19± .23
K2O	5.07±.20	5.12±.07	4.92±.04	3.92	4.58	3.83	4.88±.05	4.14±1.14
P2O5	.08±.01	.07±.00	.06±.00	0.00	0.00	0.00	.34±.04	.07± .03
A.I.	.93	1.04	1.09	1.03	1.04	.98	.88	.87

R-T (4)Trachyte average (R-106,R-22,R-47,R-81) both Wo and C norm types Rainbow Range Bevier (1978)
R-CT (7) Comenditic trachyte average (R-18,R-51,R-71,R-76,R-96,R-97,R-102) mildy AC or AC+NS nomative, Rainbow Range, Bevier (1978)
R-P (8) Pantellerite (pantelleritic trachyte) (R-24,R-29,R-40,R-44,R-48,R-54, R-88,R-116), mildly to strongly peralkaline high norm femics, Rainbow Range Bevier(1978)
ECS1 Edziza comendite Stage 1, Souther and Symons (1974)
EPS2 Edziza pantellerite Stage 2, Souther and Symons (1974)
SS2 Edziza Rhyolite Stage 2, Souther and Symons (1974)
HPD Avg(30,43) "Dacite", Heart Peaks, Casey (1980)
HPR Avg(19,38,39) Rhyolite, Heart Peaks, Casey (1980)

Figure 7-18.
Oxide variation plots (anhydrous weight basis) for salic lavas of the stratocone stage. No distinction is made by map unit, only by classification. For discussion of trends, refer to the text. The FeO versus Al_2O_3 plot has been used by MacDonald (1974) for the classification of peralkaline types.

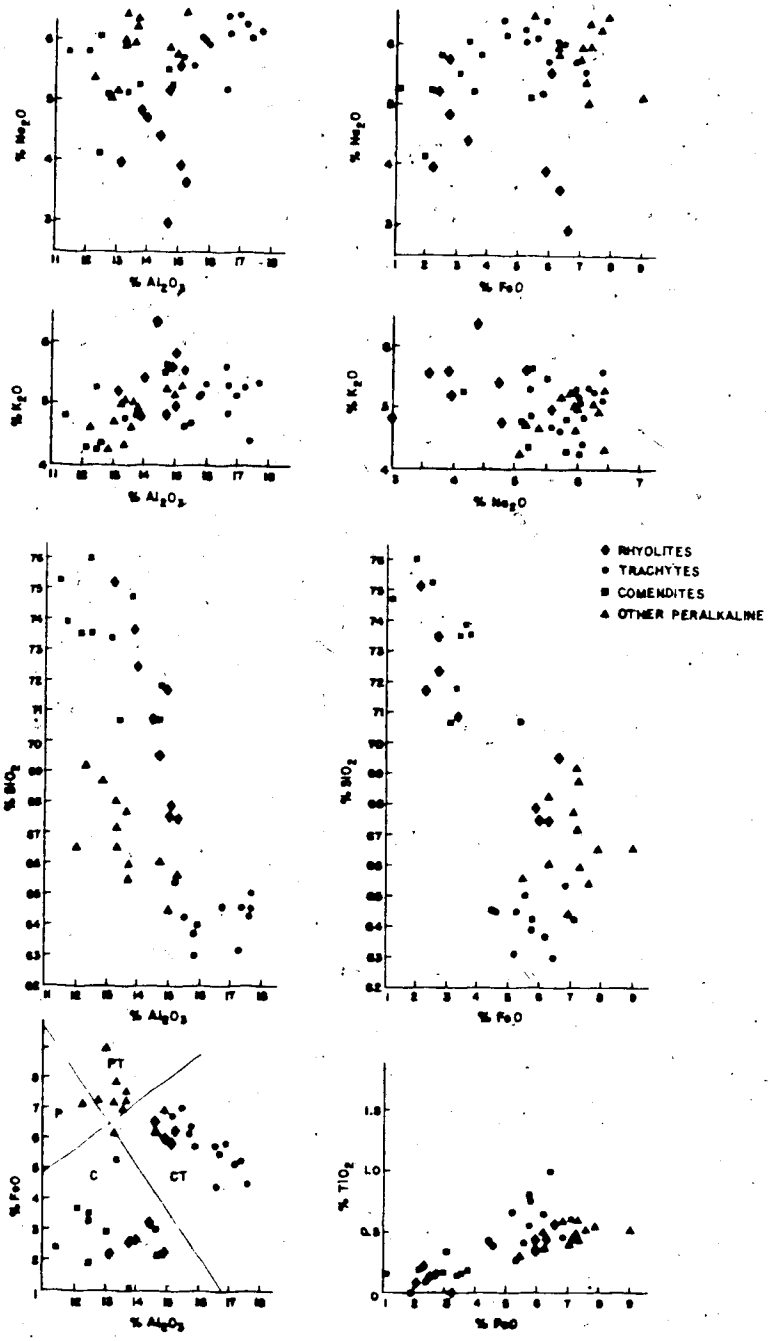

The four lava groups are easily distinguished on the basis of SiO_2, TiO_2, Al_2O_3 and FeO*. are seen between peralkaline and metaluminous trachytes and between comendites and Continuous trends peralkaline trachytes. The rhyolites plot between comendites and trachytes, generally separating into two distinct clusters. The plot of FeO* versus Al_2O_3 is the basis for MacDonald's classification (1976) of peralkaline lavas. His division boundaries and labels for comendite C pantellerite P and their related trachyte types CT and PT are also shown.

Fractionation models are presented for a typical comendite, peralkaline trachyte and metaluminous trachyte in figure 7-19. Mineral vectors correspond in direction to the removal of analysed phenocryst compositions and in length to the amount removed. The metaluminous trachyte used is flow 8/26-56/6336 with its own phenocryst analyses for clinopyroxene (5%) $Di_{41}Hd_{53}$, olivine (5%) Fo_{21} and iron titanium oxide (1%) Ulv_{93}. Plagioclase (10%) An_{26} and alkali feldspar (10%) Or_{26} come from 8/30-82/6150, another unit 7a trachyte flow. Quartz is shown as a 5% fractionation vector (rather than assimilation) for plotting ease, and for consistency so that all vectors represent the shift of composition for fractionation. Quartz does not occur as phenocryst phase in any metaluminous trachyte. Assimilation of quartz would be parallel to this direction plotted but on the opposite side of the whole rock point. The main effects of any crystal fractionation and quartz feldspar

Figure 7-19.
Mineral fractionation vectors for selected salic compositions (anhydrous oxide basis). Symbols for lava types are as in figure 7-18.

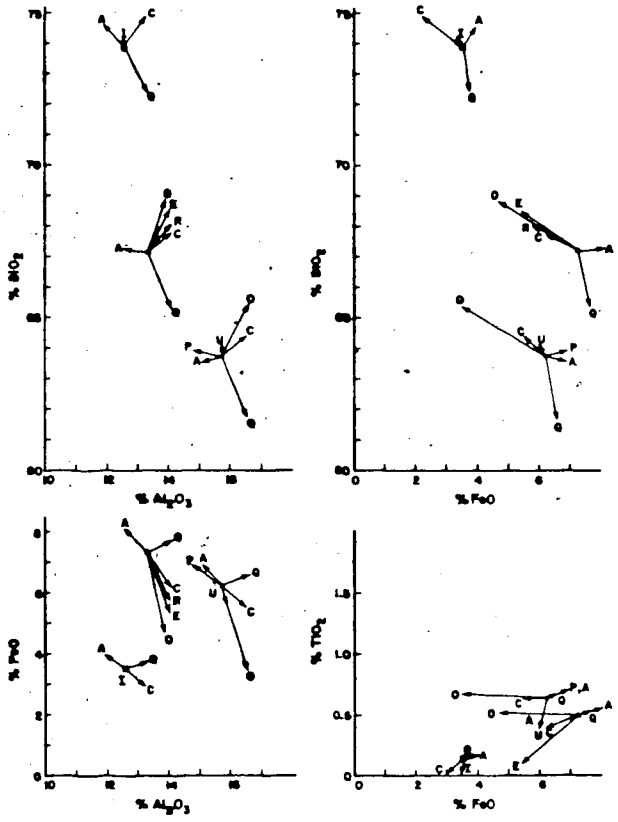

assimilation are in the direction of increasing SiO_2 and decreasing FeO*. The FeO - Al_2O_3 plot is the only one showing a reasonable lineation for metaluminous trachytes. This variation is parallel to the clinopyroxene and feldspar vectors, which matches the dominant phenocryst phases. The trend on FeO*-TiO_2 could be fit with a combination of feldspar, clinopyroxene and ulvospinel 73 as modelled, or by a more iron rich Fe-Ti oxide phase. The other variation diagrams show only a cluster of points for metaluminous trachytes. This cluster on most variation plots could be spanned in two ways, either by more than 30% combined crystal fractionation of the phases indicated or by up to 20% crustal contamination. A combination of the fractionation and contamination is also possible. For all of the variation diagrams not involving alkalis, the metaluminous trachytes are removed from the peralkaline trachytes in a direction which is inconsistent with minor amounts of crystal fractionation or crustal contamination. As little as 10% fractionation of any feldspar moves this trachyte from slightly metaluminous to slightly peralklaine and a stronger effect would be expected for the wollastonite normative members of this group. This classic "feldspar effect" has been alluded to in differentiation arguments for the origin of peralkaline rocks (Bailey and Schairer, 1964, 1966). The problem here is that feldspar fractionation alone can neither explain the variation in the metaluminous trachytes nor generate the composition of any known

peralkaline trachyte (or other peralkaline lava) for Level Mountain.

The peralkaline trachyte fractionation models used the average of the thirteen Level Mountain compositions in this group. Fractionated phases used were: alkali feldspar 25/5d (10%) Or_{32}, quartz (5%), aenigmatite (5%), riebeckite-arfvedsonite alkali amphibole (5%), olivine Fa_{35} (4%), and aegerine $Ac_{71}Hd_{29}$ (5%). All of the ferromagnesian minerals were shown to demonstrate how little difference in direction and magnitude the variation in the ferromagnesian fractionating phase can make. The trends on the variation diagrams are consistent with alkali feldspar (anorthoclase) plus alkali pyroxene or aenigmatite fractionation. This is a good match to petrography. The lineation on SiO_2-Al_2O_3 is particularly inconsistent with any significant crustal contamination. Any quartz plus feldspar assimilation would be across trend.

The only reasonable ways to reduce peralkalinity appear to be contamination by aluminous rocks or open system alkali loss. Two possible chemical statements of such a process are given below.

1) $Na_2Si_2O_5 + 2HCl = 2SiO_2 + NaCl + H_2O$

2) $2NaAlSi_3O_8 + 2HCl = Al_2SiO_5 + 2NaCl + H_2O$

In either of these cases a higher pH_2O in the adjacent wall rock would favor preservation of the peralkaline condition while higher pH_2O in the melt would result in sodium (brine) and possibly silica metasomatism at the expense of the

magma's peralkalinity. These relations also apply to crystallization at the surface where pH_2O and pTotal are low.

Two successful fractionation tests were found for deriving average comendite from average peralkaline trachyte using analysed phase compositions from Level Mountain flows. The low fO_2 case gave 40% fractional cyrstallization as (4%) Fa_{75}, (1%) clinopyroxene $Di_{55}Hd_{45}$, (28%) alkali feldspar Or_{32} and (7%) aenigmatite. The high fO_2 case gave 44% fractional crystallization as (5%) olivine, (0.1%) clinopyroxene, (30%) alkali feldspar and (7%) alkali amphibole. Both of these models provide good fits to the five major oxides SiO_2, Al_2O_3, FeO*, and Na_2O and K_2O which describe 99%+ of the beginning and ending compositions. MgO has the worst fit on both models, probably due to the choice of an olivine composition which was too magnesium rich. Use of an olivine composition with iron content greater than Fa_{75} would presumably improve the fit. This lack of real solutions for models involving fractionation of iron titanium oxide minerals matches the petrography, in that the peralkaline flows are generally devoid of opaques. In both modes the generated, P_2O_5 and CaO are slightly high for both acceptable models, but not outside the range of compositions for such peralkaline lavas at Level Mountain. The small discrepancy for these oxides could be satisfied by less than 0.2% of apatite fractionation.

An interesting feature of the fractionation models is the very small change in agpaitic index which accompained the 40% plus crystallization. The starting peralkaline trachyte had A.I. = 1.11 and the average comendite had A.I. = 1.08. The first (low fO_2) model predicted A.I. = 1.11 and the second A.I. = 1.12. These small changes in peralkalinity index match the overall distribution of Level Mountain's peralkaline compositions. Larger increases in A.I. would occur for feldspar fractionation alone and this in fact is observed for many of the peralkaline suites from elsewhere in the world for example at Pantelleria, Fant'ale, etc. At Level Mountain it would appear that the peralkalinity, (activity of ns in the melt), is effectively buffered by the crystallization of suitable alkali ferromagnesian minerals particularly sodic pyroxene, aenigmatite and alkali amphibole.

For the comendite fractionation vectors rock 9/2-99 was reasonably close to the average so that it was used as model composition. The clinopyroxene $Ac_{,,}Hd_{,}$(5%) and alkali feldspar $Or_{,,}$(10%) compositions belong to the same rock sample while ilmenite (0.25%) was from 8/27-62/6890 another glassy comendite. Quartz was 5% in length. The reason for the small ilmenite vector is the low titanium level in the rock which limits the amount of fractionation. It is interesting to note that the "feldspar effect" here is very subdued as 10% alkali feldspar fractionation produces no change in peralkalinity for the rock. The overall scatter of

the comendite compositions implies a combined fractionation of alkali feldspar, clinopyroxene and possibly quartz. Neither Fe-Ti oxide fractionation nor assimilation of quartz plus feldspar is consistent with observed variation trends.

Attempts to derive rhyolites by fractional crystallization of metaluminous trachytes failed to produce the distinctive high K/Na ratios and the metaluminous to peraluminous character. Using the average rhyolite, and an alkali feldspar 8/10-43/5990 $Or_{3,4}$ from a rhyolite ignimbrite, 10% feldspar fractionation reduced the A.I. from 0.90 to 0.89. Feldspar fractionation in this case is obviously not a very strong lever for further reducing alkalinity.

Three special projections were constructed, in the system SiO_2-Al_2O_3-Na_2O-K_2O (molecular) as a further aid to understanding the petrogenesis. All of the salic lavas lie more than 90% within this tetrahedral composition space, with the major non tetrahedral component being FeO*. The first of this series of plots, figure 7-20, is oriented perpendicular to the quartz-albite-orthoclase plane conventionally shown as 'Petrogeny's Residua System'. This plot was originally introduced by Bailey and MacDonald (1969) and has been used extensively to understand the genesis of peralkaline rocks. The compositions of the Level Mountain salic lavas diverge from the quartz-feldspar plane in such a way that the most peralkaline (most silica-rich), and most metaluminous (least silica-rich) compositions are

Figure 7-20.
Level Mountain salic lavas in special projection of Na_2O-K_2O-Al_2O_3-SiO_2 tetrahedron (molecular basis), after Bailey and MacDonald (1969). Horizontal axis corresponds to peralkalinity index, vertical axis corresponds to increasing silica saturation. Midline is trace of petrogeny's residua plane (Q-Ab-Or). The lines correspond to the quartz-feldspar cotectics.

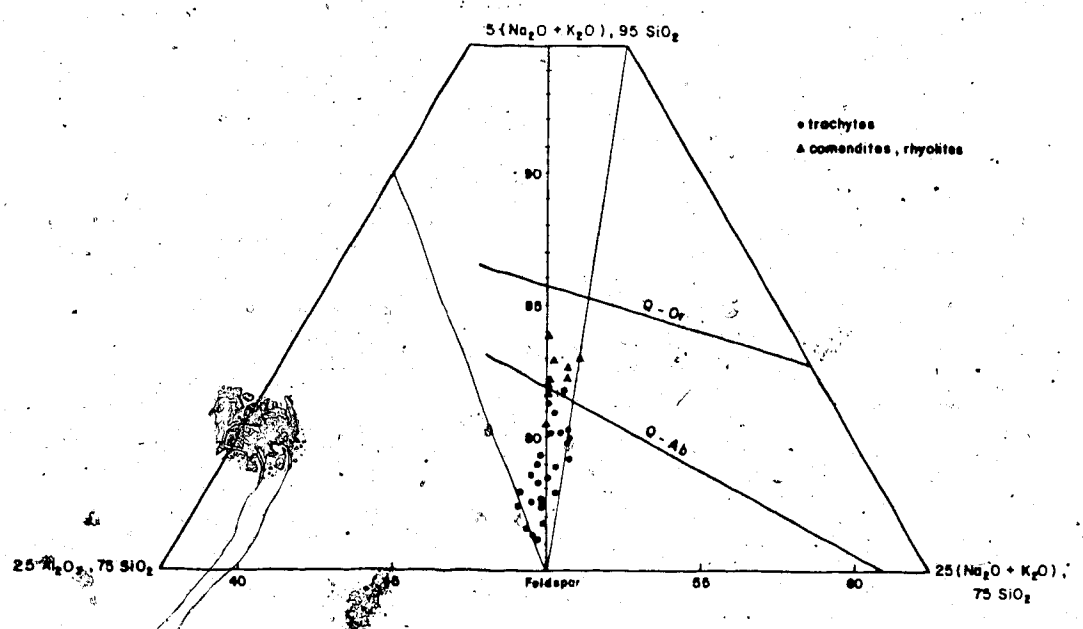

the furthest removed from the Q-Ab-Or plane. The Level Mountain lavas describe a continuous series parallel to the plane defined by the feldspar join and the chord $(Na_2O+K_2O)=5$, $SiO_2=95$ on the alkali silica face. Notice that the lavas are parallel to this plane on the silica-rich side. This means that feldspar does not lie within the plane of lava variation, so that any alkali feldspar fracitonation will not lie in the plane of the variation. Unlike many peralkaline suites which have been studied, the rock compositions here do not stem from the feldspar join. Traditionally feldspar fractionation is invoked as a dominant differentiation mechanism and means of enhancing peralkalinity. In this case, even if the variation trends were originally linear, alkali feldspar fractionation would introduce a curvature convex towards the silica apex (a positive radius of curvature about SiO_2). Such a curvature or dispersion is not seen. The location of the individual quartz-feldspar cotectics is shown as they extend from the quartz-feldspar plane into the peralkaline volume, after Bailey and MacDonald (1969). The distribution of lava compositions probably defines the two feldspar minimum as it extends toward the Q-Ab-Or eutectic.

The next figure 7-21 shows the projections of the peralkaline lavas and some of their accompanying feldspar phenocrysts. Again, this alkali ratio trapezoidal plot was introduced by Bailey and MacDonald (1969). Here the figure has been constructed for the plane parallel to the Level

Figure 7-21.
Level Mountain peralkaline salic lavas projected onto their limiting plane in the peralkaline volume of the Na_2O-K_2O-Al_2O_3-SiO_2 tetrahedron (molecular basis) after Bailey and MacDonald (1969). Light lines join whole rocks to their alkali feldspar phenocrysts.

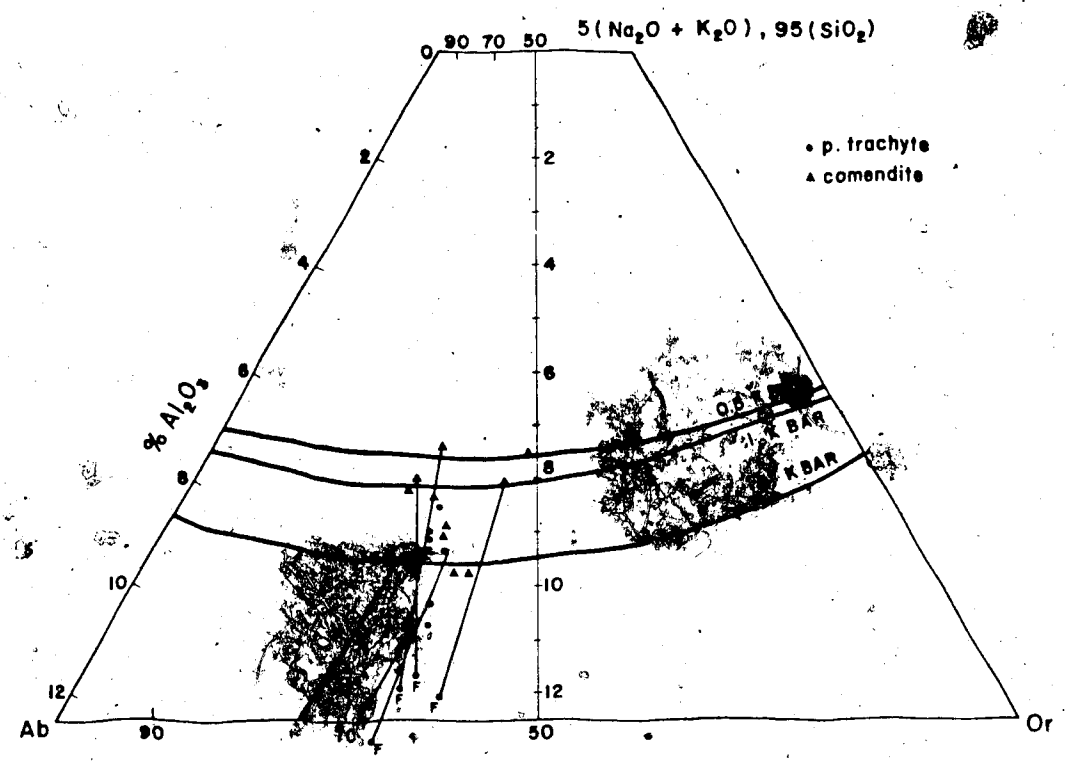

Mountain compositions. The purpose of these projections is to remove the distortion inherent in projecting compositions into the quartz-feldspar plane. The base of this trapezoid is the Ab-Or join at 12.5 mol percent Al_2O_3, but variable alkali ratio. The top of the trapezoid is in this case the 5% (Na_2O+K_2O), 95% SiO_2 chord on the alkali-silica face and thus has a value of 0% Al_2O_3. Each peralkaline suite really requires the construction of its own diagram. The important use of this figure is not to compare with other rock suites, but to compare a given suite with the quartz-feldspar water-saturated liquidus surface. Here the topology of the liquidus surface and feldspar minimum are shown as a function of pH_2O. On the 5kbar surface the quartz-feldspar minimum corresponds to a ternary eutectic, data from Carmichael et al (1974) and Tuttle and Bowen (1958). The alkali ratios, (Na 100)/(Na+K), for Level Mountain peralkaline lavas generally lie between 60 and 70. With the exception of one comendite, all of the sal[illegible] lavas contain feldspars (anorthoclase) which are more sodic yet. The majority of the lava compositions plot to the Or side of the quartz-feldspar minimum at any pressure. A similar effect is seen for granites in the Q-Ab-Or traingle. This shift towards the Or composition presumably relates to projection away from other components such as FeO, MgO and CaO, or to an actual shift of the minimum toward Or in the more complex natural systems (Naney and Swanson, 1980). The similarity in position and orientation of the Level Mountain silica

saturated peralkaline rocks to the high pressure liquidus topology and the feldspar thermal minimum in Q-Ab-Or is great enough to propose that these may be a series of equilibrium eutectic-like liquids derived by a common fractional melting process, rather than fractional crystallization of feldspars.

Figure 7-22 is an analog of Bailey and MacDonald's (1969) alkali ratio trapezoid plot as a projection into the aluminous part of the system. The plane shown here is defined by the point 10%Al_2O_3.- 90% SiO_2 on the silica alumina join with the alkali feldspar join as the base of the triangle. Note that metaluminous trachytes fall between 60 and 70 for alkali ratio (100 Na)/(Na+K), as did the peralkaline trachytes across the Q-Ab-Or plane. The rhyolites show much more scatter, with reduced alkali level and reduced Na/(Na+K) values. The alkali feldspar compositions are all more sodic than their whole rocks, and just as in the peralkaline part of the system, here too, they represent a strong lever. However, as before, the alkali feldspar does not appear to cause the variation trend for the majority of the lavas.

The plot most commonly used to assess the variation of alkalis and alumina is (Na+K)/Al versus Na/(Na+K) (atomic), which is analogous to a slice through the salic tetrahedron at a constant SiO_2 level. While it would be preferable to construct this plot at a specific SiO_2 level, it would be difficult to choose a particular SiO_2 value because of the

Figure 7-22.
Distribution of metaluminous trachytes and rhyolites with alkali ratio projected onto their limiting plane in the metaluminous volume of Na_2O-K_2O-Al_2O_3-SiO_2 (molecular basis).

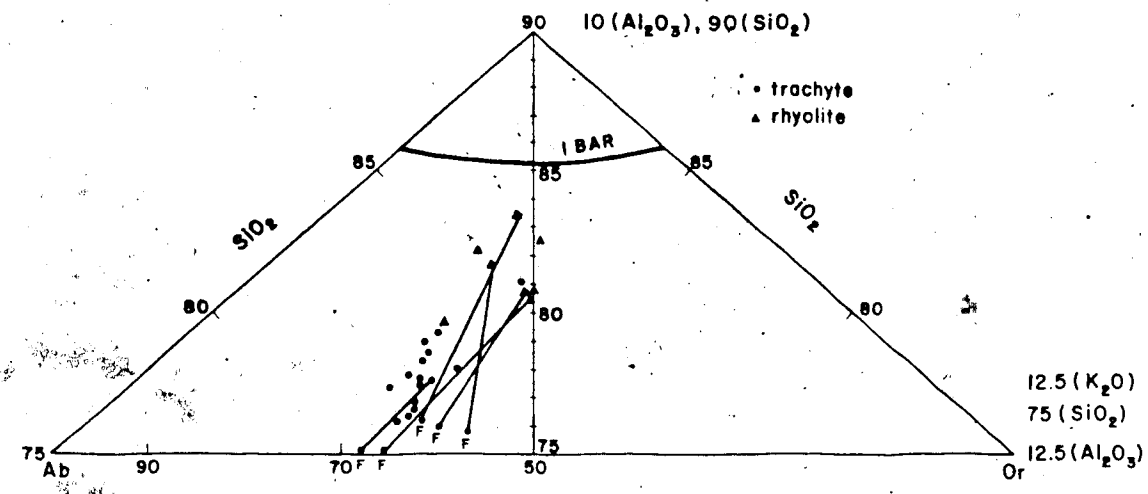

variation (8% mol or 13% weight) in, the salic lavas. For this reason the A.I. versus alkali ratio plot is retained. Plotted on this figure 7-23, are all of the salic lavas and corresponding data for alkali feldspar phenocrysts. The feldspars and whole rocks do not both lie in this plane. This figure emphasizes the leverage that the highly sodic anorthoclase phenocrysts have in any fractionation scheme. Feldspar vectors are nearly orthogonal to the trends for peralkaline trachytes and rhyolites, and in the case of the comendites they appear to generate dispersion rather than any clear trend. The only case of a feldspar vector being parallel to a rock composition trend is for the metaluminous trachytes. The straight line is the least squares fit to the 1kbar water saturated liquidus minimum given by: A.I. = 9.48 Na/(Na+K) - 4.97; r^2=.79 using data from: 1) Tuttle and Bowen (1958), 2) Thompson and MacKenzie (1967) and 3) Carmichael and MacKenzie (1963). The compositions from Carmichael and MacKenzie are (4.5%Ac + 4.5% Ns) at A.I. = 1.46 and for (8.3%Ac + 8.3% Ns) at A.I. = 1.98. The effect of indicated feldspar fractionation on metaluminous trachytes is toward the liquidus minimum plane. Apparently the peralkaline trachytes and some of the comendites straddle this plane for the liquidus minimum, which was the same deduction from the previous plots. Their dispersion along this direction is again not obviously related to anorthoclase fractionation, although such a path is possible from peralkaline trachyte to comendite. This path length was

Figure 7-23.
Plot of alkali ratio versus agpaitic index for Level Mountain salic lavas. Liquidus minimum and alkali feldspar fractionation trends after Bailey and MacDonald (1974). The Level Mountain lavas appear to originate near the liquidus minimum.

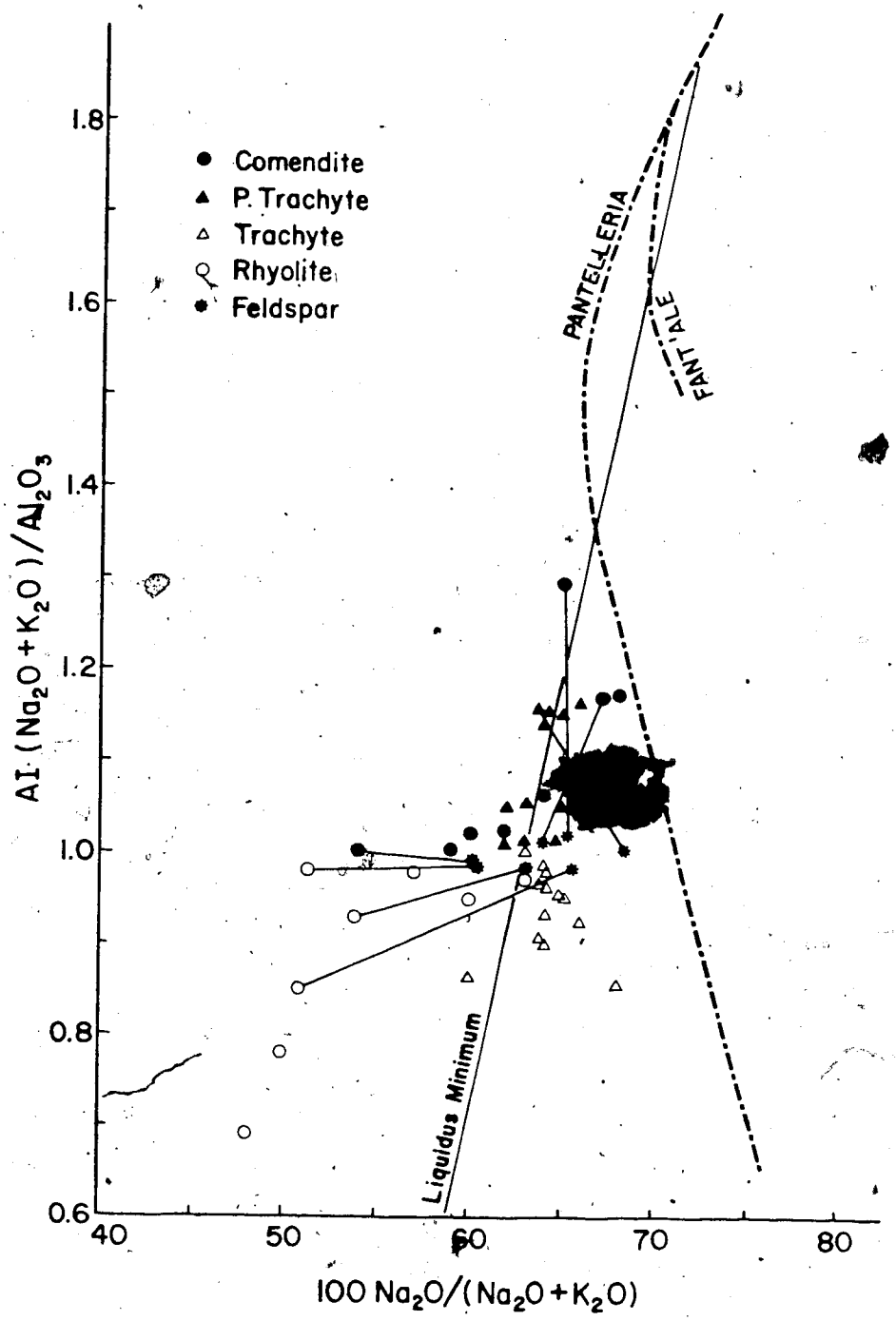

equivalent to 40% to 44% net fractionation, of which 30% was anorthoclase. The Level Mountain lavas do not lie along a single smooth curve for extensive feldspar fractionation as do most of the peralkaline suites reported in the literature. Typically, when alkali feldspar fractionation is the dominant genetic process, lava compositions should lie along smooth curves such as the examples for Pantelleria (Brotzu et al, 1974) or Fant'ale (Gibson, 1974). Note that the latter portions of these trends, at high peralkalinity index, coincide with the trace of the liquidus minimum. The Level Mountain lavas apparently attained this liquidus minimum position at a lower peralkalinity and sodium level than is typical for peralkaline suites. The Level Mountain lavas do not lie along such a singular feldspar fractionation trend. Level Mountain's peralkaline trachytes may represent a primary melt in the peralkaline part of the salic tetrahedron. Their distribution seems to match the liquidus topology between one and five kilobars pH_2O. Comendites may be derived from the peralkaline trachytes by fractional crystallization involving significant amounts of at least two mafic minerals in addition to anorthoclase.

The rhyolites lie along a trend which extrapolates to 0=Na/(Na+K) at 0=(Na+K)/Al, which would represent either contamination by aluminous rock or open system alkali loss. FeO* is their only significant non-tetrahedral component. Its effect as seen in the distribution of natural granites is to shift the composition of the thermal minimum towards

Or. This is the direction seen for the Level Mountain rhyolite trend. The strong reduction in peralkalinity seen here is not common and is not explained by the iron component (3 to 4% mol FeO* should not have such pronounced effect). The rhyolites are also not easily related to the metaluminous trachytes by feldspar fractionation and they do not follow the variation trends for the metaluminous trachytes.

TRACE ELEMENT CHEMISTRY

Introduction

Trace element concentrations for a related suite of igneous rocks can provide added insight into the controlling petrogenetic processes. The first set of models attempting to quantify the behavior of trace elements during a magmatic process was presented by Neuman, Mead and Vitaliano (1954). This work treated the process of fractional crystallization using the Nernst distribution law. The current state of quantitative trace element models for magmatic processes is reviewed by Allegre and Minster (1978). Arth's (1976) review is mathematically similar and presented in a more concise and easily understood fashion. He also presents representative and average partition coefficients for the major rock forming minerals for the range of volcanic compositions from basalt to rhyolite. More recent data of partition coefficients is given by Pearce and Norry(1979).

Interpretation of trace element patterns for suites of igneous rocks is still an "inverse problem" as discussed by Minster et al (1977) and as such does not have a single correct solution.

Aside from modelling, a great deal can still be done in a qualitative sense with trace element data. Trace element signatures provide useful comparative tests between suites with similar genetic processes. Estimates of source heterogeneity can be made in addition to using trace elements to distinguish comagmatic suites from unrelated ones (Frey, 1980). One can also compare primitive lavas between different tectonic areas to get at the fundamental differences in the upper mantle, for example White et al (1975, 1979) in their comparison of the Azores Plateau to the mid Atlantic Ridge. Comparisons of trace elements between geochemically similar magmatic suites can be used to assess the state of mantle fertility or of relative depletion from place to place (Nixon et al, 1981; Hervig et al, 1980).

Data and Analytical Methods

Trace element analyses for selected Level Mountain lavas are presented in table 7-26. Most of the analyses were performed by XRF (J.G. Holland, analyst) on whole rock powders using previously calibrated rock standards after the method of Brown et al (1977). This includes most of the values reported for Cr, Ni, Cu, Zn, Rb, Sr, Y, Zr, Nb and Ba. Additional elements and some repeats in the above set

Table 7-26. Trace Elements.

Element-Atomic No.		01	CB	h	PAP	29/1j	291f early	13-K	KD-1	16/19 D
Li	3					0		6	4	
Be	4					2		3	2	
Cr	24	132	378	288	319	363	246	38	218	129
Ni	28	77	260	231	232	195	251	29	138	129
Cu	29	43	48	66	69	96	56	36	61	51
Zn	30	108	105	98	89	128	98	133	113	127
Rb	37	21	10	15	14	9	19	22	3	24
Sr	38	576	507	540	561	510	688	862	441	934
Y	39	31	19	18	16	21	20	32	20	20
Zr	40	221	116	130	156	131	145	287	106	252
Nb	41	38	22	25	29	24	30	49	12	47
Mo	42									
Ba	56	711	330	347	344	290	433	398	174	472
Au	79					4		5	4	4
Pb	82	4			9					
Th	90	3			1			5		
U	92				0			0		

Element-Atomic No		8/21-6/3222	29/1f late	25/3b	8/28-58/5895	8/25-50/6397	LMI20d	LMIIIA	8/16-44/6250E	8/25-55/6722	LMI201
Li	3	26			5	5			40	11	7
Be	4	2			2	2	5		9	5	5
Cr	24	60	87	82	74	188		8	5	4	10
Ni	28	67	48	49	41	112		9		8	
Cu	29	44	78	43	41	153		9	44	21	30
Zn	30	188	132	93	133	119		160		160	
Rb	37	324	30	13		12		134	117		46
Sr	38		809	633	382	464	386	88	100	162	300
Y	39		30	28		30		29			
Zr	40		259	198		185		1155			
Nb	41		56	31		32		93			
Mo	42		6		6					4	
Ba	56		651	319		292		111			
Au	79					5	4		4		3
Pb	82		25		19	6				28	
Th	90					3			17		5
U	92					3			4		0

Table 7-26. Continued

Element-Atomic No		24/1H1	LMI7	9/2-96/5330	LMIII30b	8/25-52/5880	8/12-33/6140	8/26-56/6336	8/10-1/4915	8/5-8/5150	8/7-18/5720	24/2C
Li	3					20	10	14	20	25	32	
Be	4					5	5	4	9	10	9	
Cr	24	7	14	8	10	1	5	5	4	3	4	10
Ni	28	5	8	5	3	9	9	6	5	23	5	6
Cu	29	5	1	71	8	19	34	7	31	28	5	20
Zn	30	119	240	233	178	107	161	163	281	501	340	207
Rb	37	107	109	75	98	115	89			149		123
Sr	38	14	4	14	64	14	29	26	3	5	6	31
Y	39	46	60	96	54	45	54			90		84
Zr	40	895	965	740	784	637	620			1085		996
Nb	41	108	121	108	90	70	89			155		122
Mo	42						6	6	15		13	
Ba	56	323	176	330	966	723	1079			62		377
Au	79					4				3		
Pb	82		0				23	22	32	16	29	
Th	90									13		
U	92									3		

Element-Atomic No		8/6-12-5290	8/6-12n	LMIII30a	25/5d	25/5e	8/16-43cppp	9/2-95/5625	8/16-44/5960	8/25-54/6345	9/2-99	9/2-99/6600
Li	3					16	7	34	69	64	54	61
Be	4					8	6	11	13	13	11	13
Cr	24	5	3	13	15	17	5	15	3	10	9	3
Ni	28	14	3	2	5	7		8		7	1	
Cu	29	14	46	7	7	11	10	8	16	11	16	14
Zn	30	323	436	188	356	216		225		315	261	
Rb	37	124	117	116	168	154		310		275	276	
Sr	38	4	33	2	19	16	0	1	0	<1	<1	<1
Y	39	63	155	73	128	90		116		128	72	
Zr	40	1112	1122	903	1338	1306		580		1592	1617	
Nb	41	153	165	127	176	133		133		166	164	
Mo	42											
Ba	56	16	29	1085	147	127		4		23	6	
Au	79					3	3	3	4	3	3	3
Pb	82											
Th	90											
U	92											

Element-Atomic No		LMI3	8/27-66/5862	8/16-43/5990	8/16-44/6350	8/27-63/6788	8/27-62/6890
Li	3		35	7	8	30	43
Be	4		11	6	6	8	9
Cr	24	5	11	9	3	5	3
Ni	28	4	9	10	9	26	
Cu	29	5	19	12	19	30	8
Zn	30	211	223	262	221	258	
Rb	37	296	248	162	125	217	
Sr	38	0	1	5	22	1	0
Y	39	62	113	73	67	109	
Zr	40	771	566	834	766	1148	
Nb	41	126	132	116	105	138	
Mo	42					12	
Ba	56	16	3	99	945	22	
Au	79		3	4	3	3	3
Pb	82					41	
Th	90					25	
U	92					8	

were analysed by AA under the guidance of A. Stelmach. Standards were multi-element solutions. Two U.S.G.S. international geochemical powdered rock standards were analysed along with the Level Mountain samples to check laboratory methods and data reduction procedures. These were AGV-1 andesite and BCR-1 basalt referenced in Flanagan (1972). One or both of these samples had elements in the range of interest for the Level Mountain suite. Elements analysed by this method included: Li, Be, Cr, Cu, Sr and Au. For samples analysed isotopically, Rb and Sr were determined by isotope dilution. Where these values duplicated XRF or AA data, the isotope dilution measurements were reported due to their higher levels of accuracy and precision. Neutron activation analyses were performed on six selected Level Mountain samples, which spanned the compositional range of lava types, by G. Goles of the University of Oregon. Data include the rare earth elements (La, Ce, Sm, Eu, Tb, Yb and Lu), the naturally radioactive elements (Hf, Th, U, K), and analyses for Fe, Sc, Co, Cs, Sb, Br.

Comparison with Other Suites

A comparison for certain trace element abundances and element ratios in basalts is presented in Table 7-27. This compilation is intended to place Level Mountain and the other B.C. lavas in a global context. The world examples include oceanic tholeiites (MORB) and alkaline basalts, both from continental and oceanic settings. The B.C. examples are demonstrably alkaline by their overall trace element

Table 7-27. Comparison of average trace element abundances and element ratios for Basalts

	Mg / Mg+Fe2+ (atomic)	K	Ni	Nb	Rb	Sr	Ba	K/Ba	K/Rb
1) Level Mtn	.62	8100	184	27	17	614	390	22	669
2) Heart Peaks	.61	10073	87	57	25	692	703	17	487
3) Rainbow Range	.53	11415	68	26	17	573	309	26	549
4) M.O.R.B.	.68	855	44	3.5	1	103	8	110	1000
5) AZORES	.68	8450	300	---	20	450	300	21	463
6) BOINA	.62	9020	33	---	24	438	441	23	381
7) ADEN	.60	8000	49	55	24	432	420	27	470
8) DUNEDIN	.65	7994	150	63	24	671	368	28	379

	Rb/Sr	Ba/Th	Nb/Zr	Nb/Y	Ca/Sr	Mg/Ni	Ba/Ce	(La/Ce)n	(La/Sm)n
1) Level Mtn	.023	231	.225	1.3	120	428	9.75	1.89	2.14
2) Heart Peaks	.037	---	.226	2.1	97	510	----	----	----
3) Rainbow Range	.037	---	----	---	104	597	----	----	----
4) M.O.R.B.	.012	52	.027	.11	597	1166	2.08	0.73	0.67
5) AZORES	.056	---	----	---	98	288	5.12	1.24	2.46
6) BOINA	.054	142	----	---	170	1564	7.43	1.42	2.84
7) ADEN	.056	---	.298	2.0	155	587	----	----	----
8) DUNEDIN	.038	111	.260	2.5	91	351	----	----	----

References:

1) This work, Northern British Columbia, Canada
2) J. Casey, 1980 U of A unpublished Masters Thesis, Northern British Columbia, Canada
3) M.L. Bevier, 1978 UBC unpublished Masters Thesis, Central British Columbia, Canada
4) R.W. Kay and N.J. Hubbard (1978), W.M. White and W.B. Bryan (1977), L.H. Langmiur et al (1977), various oceanic tholeiites,
5) W.M. White et al (1979), Azores Islands, Ng Atlantic Ocean
6) F. Barberi et al (1974), Boina Centre, Afar Rift Ethiopia
7) K.G. Cox et al (1969), Aden Volcanic Line, South Arabia
8) R.C. Rrice and B.W. Chappell (1975), Dunedin Volcano, New Zealand

signature, particularly for the diagnostic ratios Nb/Y (Pearce and Norry, 1979) and Nb/Zr (Langmuir et al, 1977).

If one can consider these basalts at roughly the same stage of evolution or derivation, then their trace element abundances and ratios should reflect general characteristics of their mantle source regions. Note that Level Mountain has relatively typical levels of K, Ni; Sr, but low values for Rb/K, Rb/Sr, Nb/Zr, Nb/Y, Th/Ba when compared to the other alkaline basalt examples (Langmuir et al, 1977; Heinrichs et al, 1980). This probably indicates a relatively depleted mantle source with respect to the residual and incompatible elements for Level Mountain. Similar low Rb levels are seen at Heart Peaks (Casey, 1980) and in the Rainbow Range (Bevier, 1978). The only trace elements whose abundances seem disproportionately high for the Stikine are Ba and Pb.

Discussion of the Level Mountain Trace Element Variation

Selected trace element plots are shown in figures 7-24 and 7-25. The ratio Zr/Nb has been shown to be relatively constant within comagmatic suites (Weaver et al, 1972). For all of the East African volcanoes the entire lava suite basalt-benmoreite-peralkaline trachyte plots as a straight line of positive slope passing through the origin (Ferrara and Treuil, 1974). The slope varies from centre to centre. That this line passes through the origin is a prerequisite of residual element behavior. Bailey and MacDonald (1975) have shown evidence for F, Zr, Rb, Cl, Nb, Yb and Zn from Eburru of the Kenya Rift, that these are not truly residual

Figure 7-24.
Trace element variation plots for Level Mountain (Zr versus Zn, Rb and Ba). Salic compositions show considerable dispersion compared to basalts. A distinctive source composition and/or open system derivation is implied for the salic lavas.

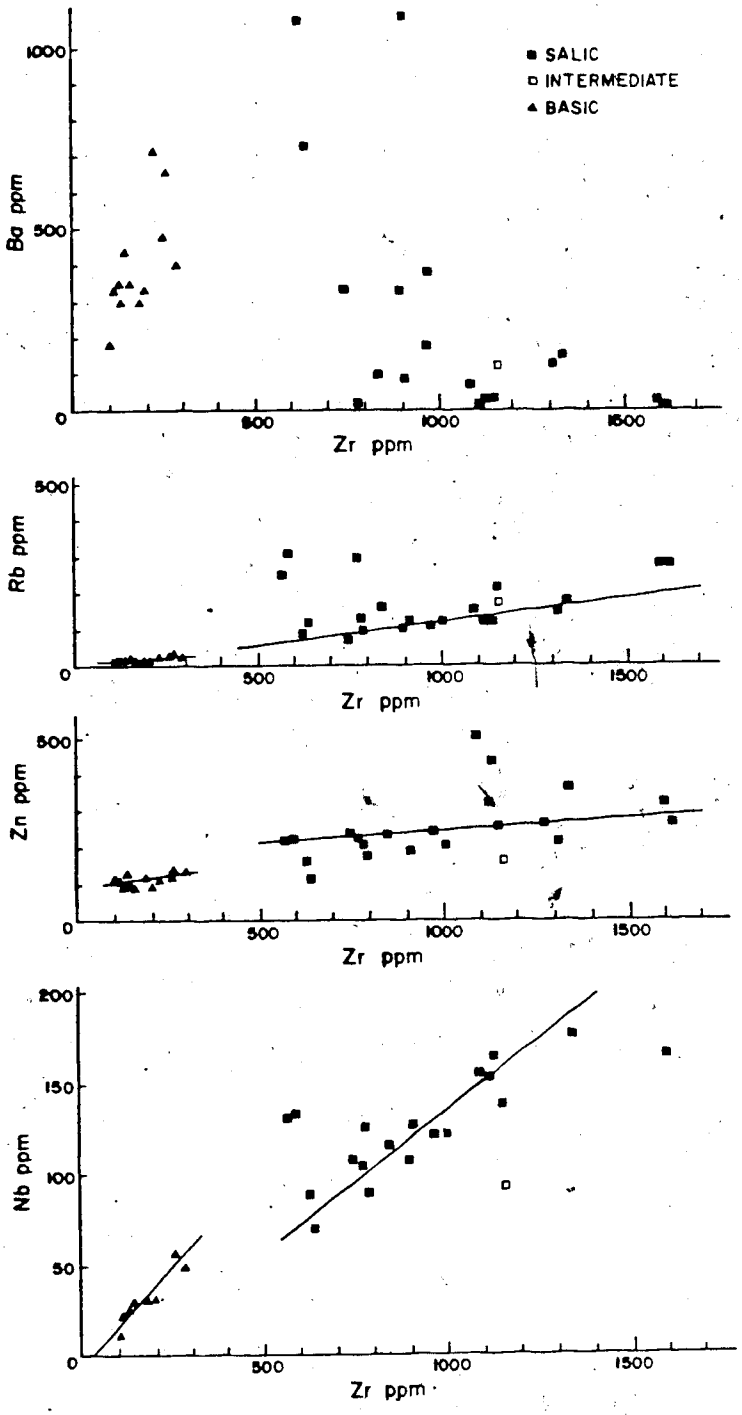

Figure 7-25.
Trace element variation plots for Level Mountain. Salic lavas and basalts generally plot in separate clusters or along distinct trends. Basalts show residual element behavior for many elements while salic lavas do not. Salic lavas do not lie along fractionation trends from basalts. A separate origin is implied.

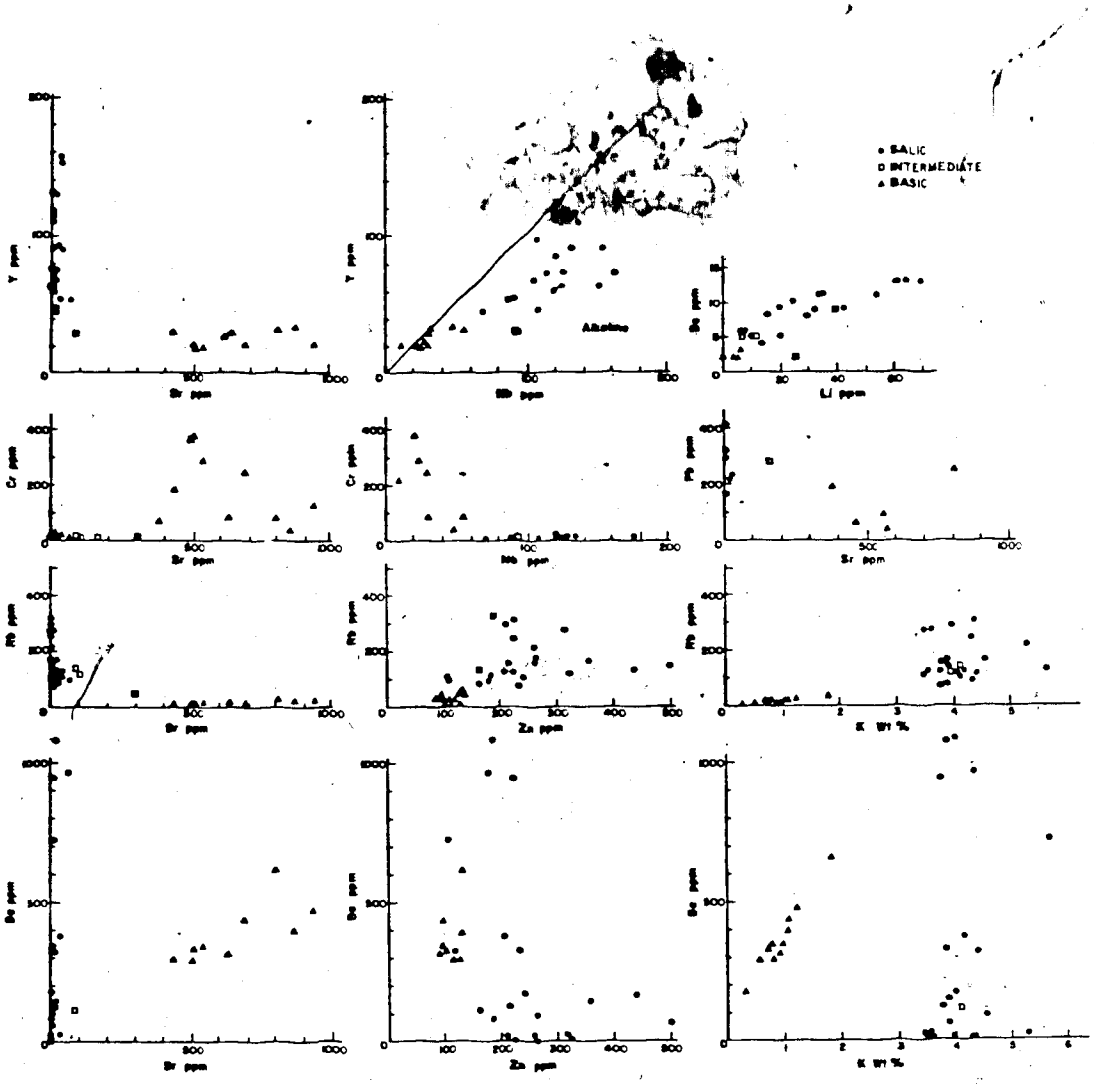

elements but evolve in an open system. When pairs of these elements are plotted, either they do not pass through the origin or they show an inflection such that the basaltic segment includes the origin but the salic does not. In the Zr versus Nb example from Level Mountain, the basic and salic segments neither extrapolate to the origin, nor do they intersect in positive concentration space. The implication using the criteria of Weaver et al (1972) is that there are two different source regions for the Level Mountain salic and basic magma series. The interpretation according to Bailey and MacDonald (1975) is that the salic magmas may require open system, perhaps with a Zr, Rb, F, Cl rich gas phase. On the Rb versus Zr plot for Level Mountain the basalts make one cluster at low values and the trachytes string out along a trend at high values. The comendites and rhyolites are removed on the high Rb side of this trend. A line can be fit to the basalt and trachyte data that passes through the origin, given by:

$$Rb = 0.125\ Zr - 3.90$$

where Rb and Zr values are in ppm. This line has a much higher Rb/Zr ratio than that from any reported alkalic volcano. If the trachytes were indeed derived by a classical alkali feldspar fractionation process, this trend would have to be flatter because Rb has a finite, positive bulk distribution coefficient for alkali feldspar, while that for Zr is zero (Bailey and MacDonald, 1975). The calculated series of possible alkali feldspar fractionation curves

(Bailey and MacDonald, 1975) have lower slopes Rb/Zr than the Eburru trend, which also makes them lower than the Level Mountain trend. They argue that no crystal-liquid process involving alkali feldspar can explain the observed trend (either melting or crystallization). This interpretation applies even more strongly to the Level Mountain data. The rhyolites and comendites were not included in the fit due to their high off-trend Rb values. This compares well with their high K/Na ratios indicating that Rb and alkalis require an open system model. On the Zr versus Zn plot, the best fit line to all data has a positive Zn intercept of 100 while for the comendites and rhyolites a parallel trend at higher Zn is seen (intercept 182 on Zn). This time the high Zn off-trend scatter is due to peralkaline trachytes. The Rb versus Zn plot shows a similar positive Zn intercept near 100 again implying open system behavior where Zn is associated with some volatile rather than crystal or liquid phases. The Li and Be data also imply an open system with Be carried in a gas phase. To fit all of the data on the Y versus Nb plot either requires two lines or an intercept that misses the origin, implying open system behavior or distinct sources or both. Most of the trace element pairs such as Sr versus Y, Sr versus Cr, sr versus Rb, etc. Show two perpendicular trends parallel to the respective element axes. This implies both separate populations and independent controls on the trace element variation. The strongly independent nature of the Rb and Sr variation at Level

Mountain contrasts markedly for centres with feldspar fractionation or fractional melting as the dominant petrogenetic process, compare for instance with Aden (Cox et al, 1970). The Sr versus Ba plot for Level Mountain is unique among alkali volcanoes in having a plagioclase-type Ba versus Sr dependence for the basalts but totally independent behavior for the salics. There is no possible single stage fractionation or fractional melting argument to explain the derivation of the salic lavas from the basalts and still satisfy the Ba and Sr data. The Ba and Sr data also deny crustal contamination of basalts as a mechanism for trachyte genesis because they fail to fit the hyperbolic mixing model of Langmuir et al (1977).

Considered as a set, the K,Rb and Ba concentrations for Level Mountain lavas portray the distinction between basalts and salics. The basalts and hawaiites lie along a single line in K-Rb-Ba space with Rb and Ba showing typical residual element behavior expected for either a fractional melting or fractional crystallization processes The projections of this line into Rb-Ba space is given by

$Rb = 0.0598\ Ba - 6.454,\ r^2 = 0.92$

and into K-Ba space by

$K = 31.7078\ Ba - 2340.97,\ r^2 = 0.96$

(where all element values are in ppm). By contrast the salic lavas have higher Rb and K values which are also too high for the projection of the basic trend. For the salic lavas K, Rb and Ba are variable and no longer correlated in any

simple fashion. The salic lava types, trachyte to rhyolite and peralkaline to metaluminous, are totally interspersed along any apparent trends. This overlap of fields precludes simple differentiation trends even within the salic group. Considering the large distribution coefficient of 6.12 for Ba into alkali feldspar versus whole rock (Philpotts and Schnetzler, 1970), a pronounced trend of Ba versus K and Ba versus Rb with onset of alkali feldspar fractionation is inevitable. The absence of such a regular trend for the Level Mountain salic lavas precludes their derivation by alkali feldspar fractionation from a basaltic parent. The scattered K-Rb-Ba data for the salic rocks suggests either open system behavior for these elements or derivation of the diverse salic lavas from source regions with variable K-Rb-Ba. This might be expected either for very small degrees of partial melting in an inhomogeneous metasomatized upper mantle or for fractional fusion of crustal rocks with variable alkali feldspar K-Rb-Ba compositions, see figure 7-26.

Rare Earth Elements in Level Mountain Lavas

Six lavas chosen to cover the compositional spectrum were analysed for rare earths, table 7-28. The chondrite normalized abundance patterns for these lavas (basalt, phonolite, tristanite, peralkaline trachyte, comendite and rhyolite) are given in figure 7-27. The enrichment for light rare earth elements (REE) is typical for alkaline lavas, but the low degree of light versus heavy enrichment is not. For

Figure 7-26.
Plot of the (K, Rb, Ba) variation for Level Mountain lavas. The K, Rb and Ba abundances vary sympathetically for the Level Mountain basalts but the salics do not follow this simple residual element behavior. When K and Rb values are normalized to Ba, all Level Mountain lavas plot on a single trend which may be due to a fractional fusion process, or to some peculiarity of evolution of salic magmas in an open system. Alkali feldspar fractionation or assimilation may cause dispersion along the trend in either direction. Comparative trends are shown for peralkaline suites from the Rainbow Range (Bevier, 1978) and Fant'ale (Gibson, 1978).

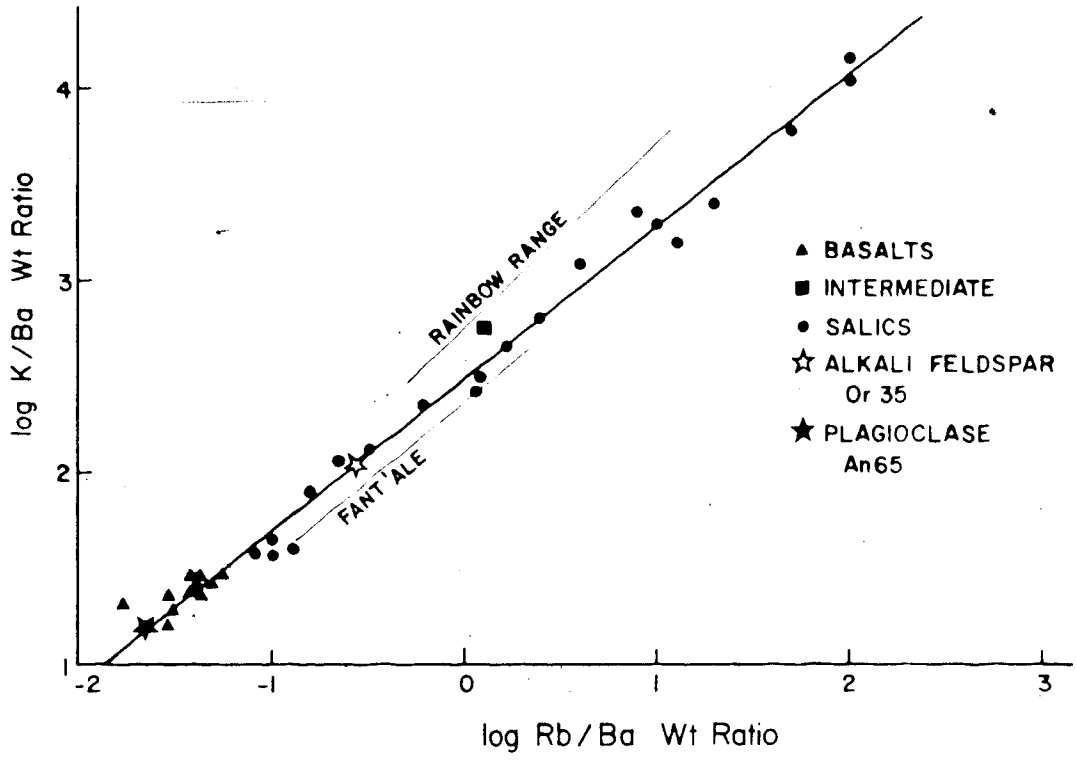

Table 7-28. Neutron activation analyses for Level Mountain lavas

Element	8/5 8/5150	13K	LMI201	44/625°E	9/2 99.6600	8-27 63.6788
Fe (%)	6.04±0.13	10.83±0.12	5.57±0.07	3.86±0.07	2.31±0.03	2.16±0.02
Sc	0.59±0.018	9.9±0.2	10.2±0.2	1.45±0.03	0.228±0.015	0.114±0.012
Co	5.24±0.16	55.1±0.8	31.8±0.4	13.8±0.4	44.8±0.6	17.0±0.3
Hf	60±4	7.6±0.6	14.1±1.1	44±3	89±7	57±4
Th	10.6±0.2	1.72±0.16	5.53±0.19	17.4±0.4	46.3±0.5	31.9±0.3
U	3.	n.d.	n.d.	4	9	7.7±0.4
K(%)	4.4±0.5	n.d.	n.d.	3.7±0.4	n.d.	n.d.
Na(%)	3.94±0.05	2.64±0.03	3.51±0.04	3.54±0.04	3.52±0.04	3.09±0.04
Cs	1.21±0.08	n.d.	n.d.	4.15±0.11	3.83±0.11	3.01±0.10
Sb	n.d.	n.d.	n.d.	0.76±0.08	n.d.	2.6±0.3
Br(??)	n.d.	209±13	630±30	159±12	940±50	780±30
La	80.5±1.2	29.9±0.6	34.9±0.7	40.3±0.6	100.3±1.4	93.8±1.2
Ce	105 ±2	40.8±1.7	46.2±0.8	57 ±2	190.5±1.9	202 ±2
Sm	18.4±1.2	8.5±0.6	9.6±0.6	5.34±0.04	18.4±1.2	20.4±1.3
Eu	3.70±0.08	3.33±0.08	2.95±0.09	0.79±0.04	1.29±0.05	1.62±0.05
Tb	1.1±0.2	n.d.	2.9±0.3	n.d.	n.d.	1.8±0.2
Yb	7.5	n.d.	2.5	2	8	7.2±0.3
Lu	1.04±0.06	0.32±0.02	0.33±0.04	0.32±0.02	1.37±0.07	1.31±0.10

Figure 7-27.
Rare earth element patterns for selected Level Mountain lavas. Normalized abundance as (1.2xsample)/LEEDY CHONDRITE.

(1) Pantellerite 8/5-8/5150
(2) Rhyolite 8/27-63/6788
(3) Comendite 9/2-99/6600
(4) Tristanite 8/16-44/6250c
(5) Phonolite LMI20i
(6) Basalt 13-k

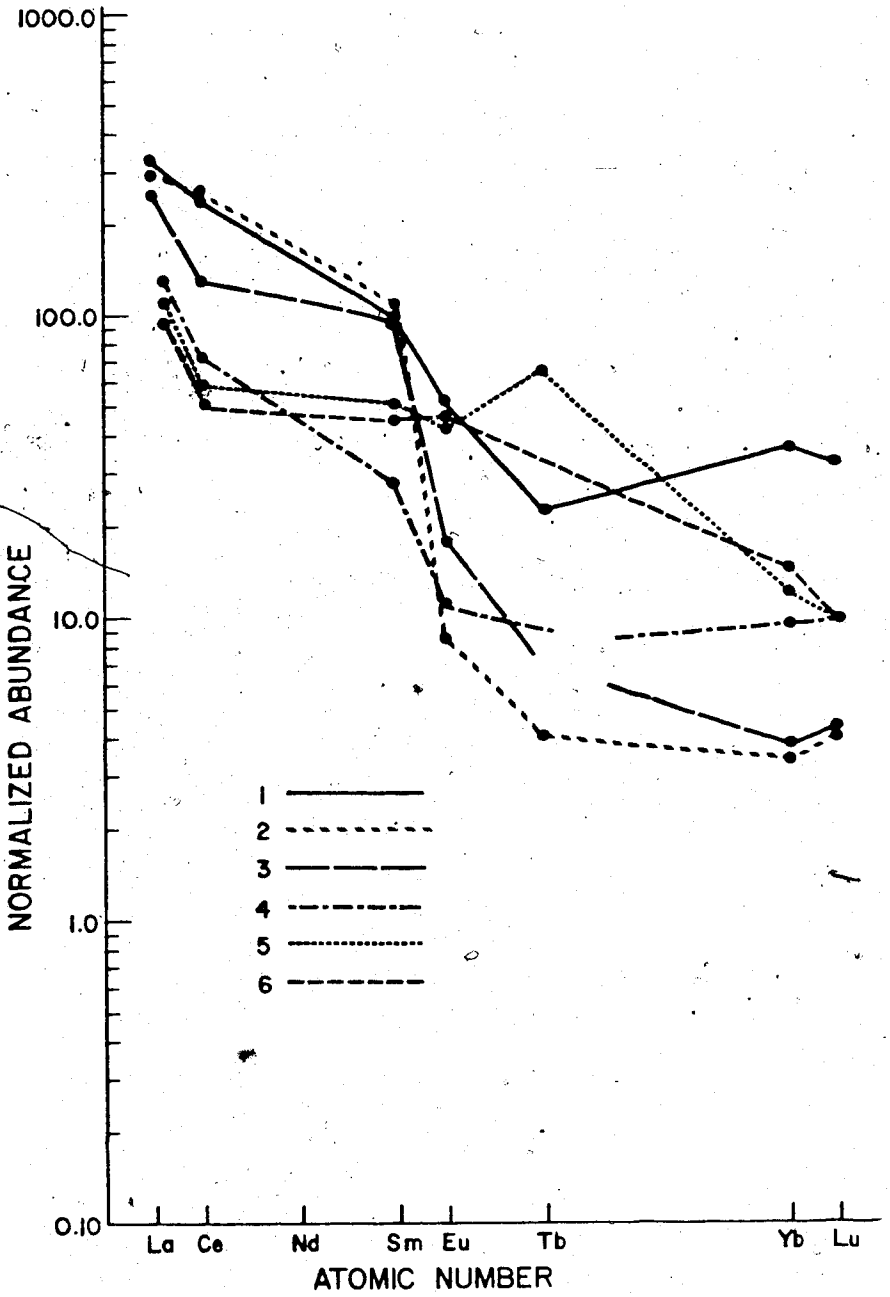

comparison see trends given by Cox et al (1969), Ferrara and Treuil (1974), and White et al (1979). Also the small difference in REE abundance levels for the range of lava types at Level Mountain is unusual. Normally the peralkaline lavas show REE abundances up by a factor of 6± 3 from the basalts whereas here the patterns cross. Compared to the other types, comendite and rhyolite have markedly lower heavy rare earth levels than the other lavas. Heavy rare earth depletion in general is characteristic of a source depleted in clinopyroxene and garnet or of suites derived by substantial fractionation of such phases. Here it probably reflects some preferential uptake of heavy rare earths by sodic clinopyroxene or other sodic ferromagnesian minerals.

The single most important feature of the rare earth patterns for the salic rocks is the total absence of a negative europium anomaly. Peralkaline salic lavas typically show strong europium depletion arising from alkali feldspar fractionation, in fact Eu depletion is documented as a characteristic of peralkaline lavas, (Ferrara and Treuil, 1974). Sometimes the concurrent or related intermediate lavas show positive europium anomalies. Here again this is not seen.

Summary

There are many distinctive features of the Level Mountain trace element signatures for salic lavas. While they show enrichment in alkalis, REE, Zn, Be, Zr, Nb, Th, Hf and depletion in V, Cr, Ni, the degree of enrichment

compared to the East African Rift, Azores and Pantelleria is subdued. In most suites U and Mo are enriched, while Sc, Cu and Eu are depleted. These aspects of the typical peralkaline trace element signature are not observed at Level Mountain. Three possible explanations for these differences are proposed: i) Level Mountain may have a partially depleted mantle source region, ii) There is the possibility for open system behavior for many of the residual elements and possibly a distinctive gas phase associated with the Level Mountain peralkaline salics and iii) Lack of pronounced alkali feldspar fractionation and development of strong peralkalinity has failed to generate the pronounced differences in trace element behavior seen for other centres.

OXYGEN ISOTOPE STUDY FOR LEVEL MOUNTAIN LAVAS AND MINERAL SEPARATES

Analytical Methods

Oxygen was extracted by fluorination reaction with bromine pentafluoride as described by Clayton and Mayeda (1963). From silicate samples O_2 gas is evolved with a residue of BrF_3 and fluoride salts. Samples were air dried and weighed, generally a 20mg sample was loaded into the nickel reaction vessels. A two hour heating to 300°C in vacuum was performed to remove absorbed water and air. The BrF_3 extraction took a nominal twelve hours at 650°C. Oxygen

was purified over in a cold trap then combusted with carbon of known isotopic composition. The yield of O_2 (CO_2) gas was determined from the pressure differential on a mercury manometer. Gas samples were transferred to glass sample tubes and and their isotopic ratios were measured. The mass spectrometer used for these determinations was a Micromass Model 602D located in the department of Soil Science. Isotope ratios were reduced on line with an HP programmable calculator. Continuous correction for instrumental drift was made by comparing each sample to preceeding and subsequent standards. The data are reported with respect to the SMOW standard assuming alpha (CO_2-H_2O) = 1.0407. Values were only accepted if their oxygen yields were within 5% of theoretically predicted amounts. Minerals were checked against ideal stoichiometry while lava yields were calculated from ten oxide anhydrous chemical analyses. Most yields are within 3%.

Level Mountain Oxygen Isotope Study

Analysis of the oxygen isotope composition for Level Mountain whole rocks and mineral separates was begun in 1976, with the assistance of Dr. Karlis Muehlenbachs. At that time, none of the Late Cenozoic volcanics in B.C. had been analysed for oxygen. The primary impetus for the study was to see if the upper mantle for B.C. and the volcanic rocks derived from it were isotopically normal or exhibited low ^{18}O character as discovered for Icelandic basalts by Muehlenbachs et al (1974). It was also anticipated that the

oxygen data would place constraints on petrogenetic and evolutionary processes within the Level Mountain suite. In a study of thirty-five samples from four Japanese Islands, oxygen isotope data were shown to monotonically increase with differentiation by fractional crystallization (Matsuhisa et al, 1973). In an another study on andesite from the Banda arc, Indonesia , oxygen and strontium isotope systems were positively correlated (Magaritz et al, 1978). For this latter example a two component mixing model was constructed for typically low ^{18}O and low $^{87}Sr/^{86}Sr$ mantle derived magma and subducted sediments. Aside from detailed interpretations such as those mentioned above, the Level Mountain samples could also be compared to other alkaline lavas of known isotopic composition. Some of these data have been previously reported by Hamilton, Baadsgard and Scarfe (1978).

A tabulation of the Level Mountain oxygen isotope data is given in table 7-29. Values are reported as $\delta^{18}O$ relative to the SMOW standard. The order of presentation is stratigraphic with most of the eruptive history having been sampled from the base of the Plateau, map unit 1, to unit 8 of the stratocone. Descriptive notes plus map location are given to the side. All of the whole rock values reported here are thought to be fresh and unaltered. For a majority of samples this is demonstrated by mineral separates. Whole rock basaltic values range from 5.7 to 6.5°/$_{oo}$ for Level Mountain.

Table 7-29 Oxygen Isotope Data for Level Mountain
Whole Rocks and Mineral Separates

Sample #	Map Unit	Whole Rock	Oxygen ‰ ^{18} SMOW				Alkali Feldspar	Qtz	Alkali Amphibole	Aenigmatite	Description/Locality
			Ol	Cpx	plag	mt					
Stratocone 8/25-50/6397	8	5.8	5.1	5.3	6.2						Transitional alkali basalt-hawaiite flow, (Ne)normative, mildly prophyritic, Meszah Peak.
MPM	8	5.7									Troctolitic inclusion, maybe cognate but has reaction rim, Fo_{80} An_{72} with brown augite and titanomagnetite.
KD-1	8	5.7			6.0	3.0					Alkali basalt dyke with plagioclase megacrysts to 3 cm. Egnell creek graben, feeder to Wrathall Plateau aa fields.
8/27-62/6890	7c	7.3									Glassy rhyolite dyke from summit of central dome at Beatty Creek-Kakuchuya Creek divide.
8/27-63/6788	7c	7.7					7.7				Glassy rhyolite dyke from central dome, anorthoclase phenocrysts.
8/27-66/5862	7c	8.9					8.1				Glassy rhyolite dyke in coll south of central dome.
9/2-95/5625	7c	10.2					8.2				Anorthoclase bearing glassy comendite dyke, SE end of ridge across wind gap to NW of central dome.
9/2-99/6600	7c	8.0									Comendite pitchstone portion of pitchstone ignimbrite flow, SE shoulder Meszah Peak.
9/2-99	7c	8.0					7.4			6.4	Comendite ignimbrite same eruptive unit as above, feldspar is low sanidine.
8/25-54/6345	7c	7.9									Comendite pitchstone flow, lower in section, foot of coll SE face of Meszah Peak.
8/16-44/6250E	7c	7.4									Tristinate dyke, ridge crest south side of south fork of Beatty Creek, disequilibrium phenocryst assemblage: Cr.cpx, bas.hbl, biotite, andesine, anorthoclase; gneiss inclusions.
8/16-44/6350	7b	10.0									Rhyolite vitric tuff, glass separate, uppermost outcrop of ridge south of south fork of Beatty Creek.

Table 7-29 (continued) Oxygen Isotope Data for Level Mountain
Whole Rocks and Mineral Separates

Sample #	Map Unit	Whole Rock	Oxygen ‰ ^{18} SMOW				Alkali Feldspar	Qtz	Alkali Amphibole	Aenigmatite	Description/Locality
			Ol	Cpx	plag	mt					
Stratocone continued											
8/12-33/6140	7b	7.4					7.2				Trachyte flow east end of Wolf Bones Ridge, peralkaline mineralogy but metaluminous chemistry.
8/16-43/6000	7b	6.5									Comenditic trachyte pitchstone flow with anorthoclase phenocrysts, N.facing cirque wall S.fork of Beatty.
8/16-43/5990	7b	5.6									Rhyolite pitchstone layer in tuff sequence, N.facing wall, S.fork of Beatty.
8/16-41/5960	7a	7.7									Comendite pitchstone flow above till horizon on central S.face of Wolf Bones Ridge.
8/25-52/5880	7a	6.0				2.0	5.9	8.1	5.5		Hypabyssal trachyte stock north edge of tarn, north of Meszah Peak, miarolitic cavities, vapour phase amethystine quartz, Q-Mt thermometer gives 614°C ±12°C subsolidus, high sanidine, perikaline mineralogy.
LMI20I	6a						7.8				Phonolite tuff with Ca-Mn-Fe carbonates (altered), SE end of graveltop ridge, feldspar is high sanidine.
LMI20D	6a	5.1									Mugearite flow/agglomerate, mixed magma 2 disequilibrium phenocryst populations.
25/6B	6a			5.6			6.7				Peralkaline trachyte flow, ridge summit separating Dudidontu and Kakuchuya valleys, anorthoclase and green sodicferrohedenbergite phenocrysts.
25/5E	6a	6.7									Peralkaline trachyte flow, prominent spire on alpine glaciated Dudidontu-Kakuchuya Ridge.
25/5A	6a						6.7				Peralkaline trachyte flow, basal flow of spire section, high sanidine.
8/6-12/5290	6a	5.8									Peralkaline trachyte flow, Wolf Bones Ridge, S.face, contains nodules.
8/6-12 nodule		8.0									Eurcrite/Essexite nodule: olivine, diopside, hornblende, phlogopite, plagioclase, nepheline, magnetite.

Table 7-29 (Continued) Oxygen Isotope Data for Level Mountain
Whole Rocks and Mineral Separates

Sample #	Map Unit	Whole Rock	Oxygen ‰ ^{18} SMOW				Alkali Feldspar	Qtz	Alkali Amphibole	Aenigmatite	Description/Locality
			Ol	Cpx	plag	mt					
Stratocone continued											
875-875150	6a	6.8					6.6		6.2		Peralkaline trachyte flow, north section Wolf Bones Ridge east end, low sanidine and Riebeckite - Arfvedsonite series amphibole.
25/1-I	5b				6.4	4.2					Transitional hawaiite-alkalibasalt, columnar flow above lahar, W.end Dudidontu-Kakuchuya Ridge.
25/1-D	5a						6.9		6.4		Peralkaline trachyte, north wall Dudidontu alpine valley, anorthoclase plus alkali amphibole.
25/1-B	5a						6.9		5.9		Peralkaline trachyte, as above, feldspar optically high sanidine.
9/2-96/5330	5a	6.9					7.0				Trachyte flow, columnar cliff former north of Wind Gap in north fork of Beatty Creek.
PBW-5000	5a						7.5			5.7	Crystalline comendite flow, basal flow on unit 5 of Meszah Peak-Kakuchuya section.
7/11-5000	5a						7.0		6.0		Peralkaline trachyte flow from western plateau surface between South Dudidontu summit and Egnell Creek; anorthoclase, Riebeckite phenocrysts.

Table 7-29 (Continued) Oxygen Isotope Data for Level Mountain
Whole Rocks and Mineral Separates, Descending Stratigraphic order, 4 digit number denotes elevation

Sample #	Map Unit	Whole Rock	Oxygen ‰ ^{18} SMOW				Alkali Feldspar	Qtz	Alkali Amphibole	Aenigmatite	Description/Locality
			Ol	Cpx	plag	mt					
Plateau											
T3-k	4	6.5									Hawaiite columnar flow of elevation summit above glacial cirque on north side of Egnell Creek.
8/9-26/4615	4			5.6	7.4						Megacryst clot (cognate xenolith?) labradorite plus black diopsidic augite, from red brown agglomeratic hawaiite flow, in stream valley cut at east and of Wolf Bones Ridge at forks of Beatty Creek.
PAC-4465	4				6.0						Hawaiite flow, Little Tahltan River, west side of canyon.
8/20-2/4426	4				6.7					An 35	Labradorite phenocryst from transitional hawaiite-alkali basalt flow, Little Tahltan Canyon, east run.
29/1-L	3	6.4									Alkali basalt, Kakuchuya Creek section at western plateau escarpment.
PAP-4100	3	6.5	5.5	5.6	7.3						Hypersthene normative basalt, Little Tahltan Canyon.
PAR-4030	2	6.5			5.9	3.7					Alkali basalt.
PAY-3650	1		5.9	6.0	6.9						Hypersthene normative basalt, Little Tahltan Canyon.
Comparative Samples											
T004-41				5.9							Telegraph Creek Lherzolite nodule from alkali basalt flow Stikine Canyon, olivine, orthopyroxene, cr-diopside, spinel sample from H. Greenwood.
217689		7.0					6.5		5.6		Pantellerite pitchstone with high sanidine and Reibeckite, Fant'ale Ethiopia sample from I. Gibson via C.M. Scarfe.
RDM		6.4									Comendite glass from perlitic dome Timor, Indonesia collected by R. Morton.
D100/26		7.0					7.1				Gold flat member Thirsty Canyon tuff, comendite, Nye Co.Nevada, ref. Taylor (1968).

The Level Mountain basalt analyses and the chrome diopside from the Telegraph Creek lherzolite nodule indicate that the mantle under the Stikine is normal with respect to its oxygen isotope composition. The basalts of the plateau are all around 6.5±0.05°/₀₀ while those of the stratocone are lighter at 5.8±0.05°/₀₀. This difference probably reflects two compositionally distinct sources, or alternatively fundamentally different processes such as the influence of gas phase or degree of partial melting. The different oxygen signature for plateau and stratocone basic lavas is not associated with "differentiation" because alkali basalts and hawiites are sampled in each case and are identical within each set. This difference would also not follow from fractional crystallization because in the basaltic compositions olivine is the dominant fractionating phase along with smaller amounts of magnetite, clinopyroxene and plagioclase. Starting from a typical plateau basalt of 6.5°/₀₀ such fractionation would drive the residual liquids to heavier oxygen compositions due to the lighter nature of most of the fractionating phases. Any fractionation which may have occurred for the plateau basalts seems to have a negligible effect in dispersing the oxygen signatures. The stratocone basalts are lower in Mg and higher in normative plagioclase. If they were plagioclase-enriched couterparts of the earlier plateau magma they would be isotopically heavier, not lighter as they turn out to be. The same increase would be expected for crustal contamination.

The salic lavas show a total range of compositions from 5.6 to 10.2°/₀₀. This range encompasses the basalts and is quite large compared to any volcanic suite which has been explained by fractional crystallization. It also spans the low, intermediate and high ^{18}O salic rock subgroups of Taylor (1968). By comparison other peralkaline glassy rocks fall in the middle of this range; see Fant'ale, Timor and Nevada values in table 7-29. The fractionation between glass and alkali feldspar inreases as the whole rock $\delta^{18}O$ increases. The largest fractionation (2.0°/₀₀) is for an anhydrous comendite, 9/2-95/5625. The $\delta^{18}O$ variation in these glassy rocks is not related to the water content. Ten hydrated obsidians, welded tuffs and perlites with corresponding feldspar values from Taylor (1968) show fractionations ranging from 2°/₀₀ to 9°/₀₀, with whole rock values all greater than 10°/₀₀. The $\delta^{18}O$ rich comendites, trachytes and rhyolites from Level Mountain clearly do not fall into this severly altered league. The pitchstones in particular are dense and optically clear. An alternate explanation of the Level Mountain salic rock variation must be sought.

The alkali ferromagnesian minerals (both riebeckite - arfvedsonite type amphiboles, aenigmatites and sodic pyroxenes) are isotopically lighter than whole rocks (glasses) and alkali feldspars. This is not just an artifact of the Level Mountain peralkaline pitchstones because the same relationship is seen for the Fant'ale pantellerite. The

alkali amphiboles fall in the general range for plutonic amphiboles of more ordinary chemistry (without peralkaline affinity), as does the sodic pyroxene fall in the range of other igneous pyroxenes. The two aenigmatite analyses, while predictably lighter than their whole rock and alkali feldspar, must stand on their own as there are no previously published values. Since all of the alkali ferromagnesian minerals and alkali feldspars are lighter than their whole rocks, it could be argued that ordinary fractional crystallization would have the effect of driving up the residual $\delta^{18}O$ value. Even for large fractionations, this effect is sufficient to explain the great variation.

From major element chemistry the derivation of the average comendite from the average peralkaline trachyte required 45% by weight fractional crystallization as 30% alkali feldspar, 7% olivine, 7% amphibole or aenigmatite and 1% clinopyroxene. This satisfies bulk oxygen balance to ± 1.25‰. When these proportions are used with respective oxygen contents and $^{18}O/^{16}O$ ratios, the mass balance can also be performed for isotopes. The following model was calculated:

	PTrach	Or_{35}	Fa_{00}	$Hd_{00}A_{10}$	Aenig	Rieb	Com.
O wt.%	46.49	47.81	32.80	37.15	41.28	41.02	48.8
$\delta^{18}O$‰	6.9	6.7	5.5	6.0	5.6	6.0	7.30
fraction	1	-.30	-.07	-.01	-.07	-.07	.55

For this example with 45% fraction crystallization, even with all of the minerals lighter than residual glass, the shift is only 0.4°/₀₀. If instead of fractionating, the alkali feldspar and other minerals crystallize at isotopic equilibrium the effect would be truly negligible. Another example was calculated for the fractional crystallization of 40% alkali feldspar from comendite 9/2-99, using tabulated values to give a shift from 8.00°/₀₀ to 8.47°/₀₀. Clearly fractional crystallization is too limited to explain the natural variation in isotopic ratios for the Level Mountain salic lavas. In the case of the basalts and hawaiites, which have minerals on both sides of the whole rock ratio, calculated fractionation effects are negligible.

Traditionally the ^{18}O values for volcanic suites have been compared to chemical differentiation indices. Matsuhisa et al (1973) used Kuno's solidification index, (SI = 100 MgO/(MgO+FeO+Na_2O+K_2O)), for the Japanese Islands while Taylor (1968) used Larsen's index, (L.I. = 1/3SiO_2 + K_2O - CaO - MgO - FeO*) for volcanics from all over the world. When these indices are calculated for the Level Mountain samples and plotted against $\delta^{18}O$, the basalts and salics plot in different clusters that are not obviously related to mixing lines or normal differentiation, see figure 7-28. The oxygen whole rock values were also plotted against percent partial melting, which was calculated from chemical analyses

Figure 7-28.
Variation plots for oxygen isotope whole rock composition of Level Mountain lavas: (1) versus Kuno's solidification index showing the trend for fractional crystallization in Oki Dogo lavs after Matsuhisa (1973), (2) versus Larsen's differentiation index showing field of all volcanic rocks after Taylor (1968), and (3) versus maximum percent partial melts for basic lavas with an amphibolite source. The trends for basic and salic lavas are distinct in all cases.

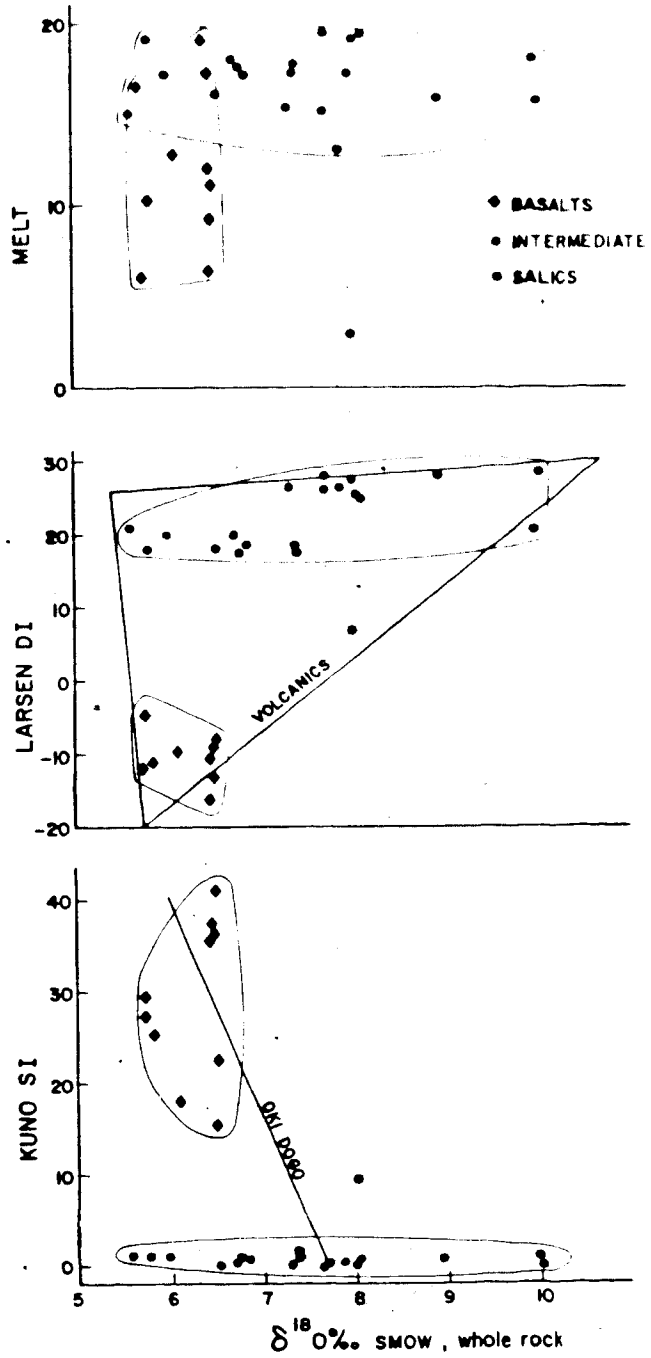

using a pyrolite source for basalts and an amphibolite source for the salics. As with the other two plots, any inferred trends for the basalts produce little or no shift, while the gross $\delta^{18}O$ variation for the salics is independent of the chemical variation index.

In attempting to find some chemical variable that correlated with $\delta^{18}O$ for the peralkaline lavas, oxide variation diagrams and element ratio plots were constructed. A weak trend was obtained for sum of alkalis with a slight improvement when reciprocal sum of the alkalis was used. This plot is shown in figure 7-29. The best fit line to the salic rock data is:

$$1/(Na_2O + K_2O) = 3.63 \times 10^{-3} \delta^{18}O + 0.0704$$

This is a weak trend, nearly horizontal, and the r^2 for all of the salic rocks is only 0.51. The basalts, as on the other variation diagrams, plot as a separate field. The salic line is not obviously a mixing trend with any known reservoir in mantle, crust or meteoric water. Local meteoric waters from Whitehorse and Fort Smith are -23°/₀₀ and -22°/₀₀ respectively. Meteoric water from Level Mountain should not be appreciably different since it is of similar latitude. For fresh water with less than 500ppm total dissolved solids the reciprocal sum of alkalis cannot be lower than 1300. Local mantle is probably 5 to 6°/₀₀ with 0.7% total alkalis at a maximum. While actual crustal compositions are unknown, they are probably higher in $\delta^{18}O$ and lower in alkalis than the peralkaline magmas, if they

Figure 7-29.
Variation plot for oxygen isotope whole rock composition versus reciprocal sum alkalis. Salic lavas from the stratocone stage define a line which may imply open system behavior. This line is not related to a crustal component, to derivation from basalt or to meteoric water. Basalts plot as a cluster showing slightly heavier oxygen for the plateau lavas than for those of the stratocone.

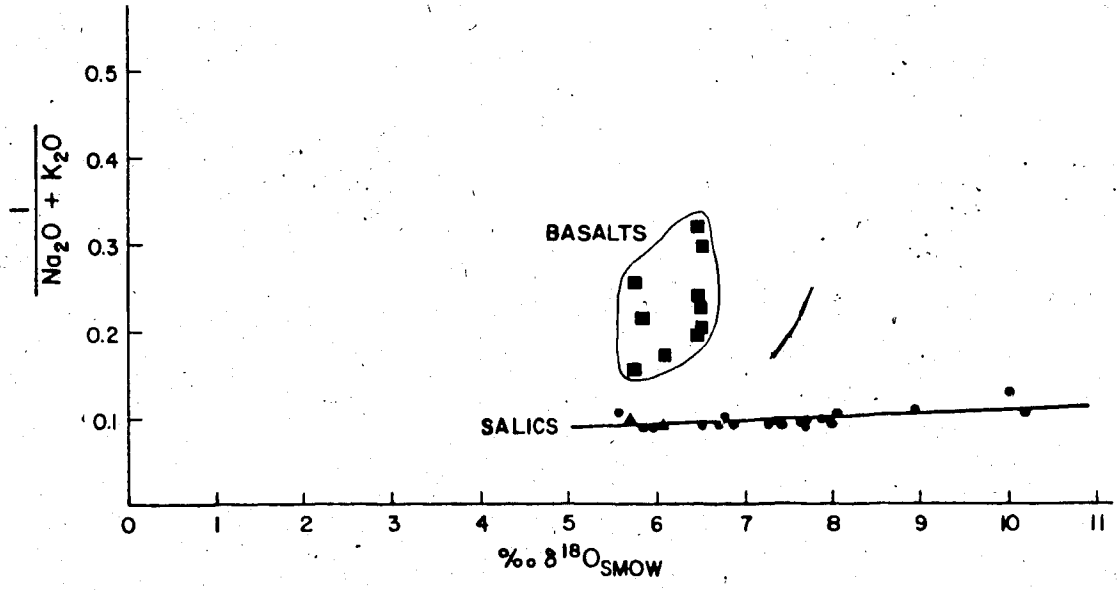

are similar to calc alkaline plutonics reported by Taylor (1968) for the western U.S.A. All of these points are well removed in their location (in $\delta^{18}O$ versus reciprocal sum alkali space) and direction from the salic lava trend for Level Mountain. Two pantellerites from the Rainbow Range have been isotopically analysed and they also fall on the trend.

There is also a linear relationship ($r^2=0.51$) for the salic lavas and Na/K ratio given by:

$$(Na/K) = -0.1668\delta^{18}O + 2.95$$

A plot of this relationship is given in figure 7-30. These relationships with oxygen and alkalis could possibly indicate an open system gaseous exchange process between peralkaline magmas and granodiorite crust. Assuming the crust to be calc-alkaline mesozoic plutonics with $\delta^{18}O$ of 13°/₀₀ and the two Level Mountain alkali lines to represent gaseous transfer type mixing, this crust could be predicted to have sum alkalis equal to 8.50% with an Na/K ratio of 0.78 or weights of Na_2O =4.49% and K_2O =4.01%. This prediction is reasonable for a typical granodiorite and the mesozoic plutonics which outcrop in the Intermontane Belt. The model would then be

$$\text{Salic Melt } 5.8+0.3‰ \quad \underset{\leftarrow [\ K,\ ^{18}O\ (H_2O)\ ]}{\overset{[\ Na,\ ^{18}O\ (CO_2,Cl,F)\ ]\rightarrow}{\rightleftharpoons}} \quad \text{Granodiorite Crust } 13.0+0.50‰$$

This type of gas-coupled alkali exchange could explain the

Figure 7-30.
Variation of oxygen isotope composition of salic rocks with Na/K ratio. Circled points are for pitchstones (comendites and rhyolites). Trend could possibly indicate open system exchange of alkalis and oxygen isotopes between a primitive comendite melt and crustal granodiorite.

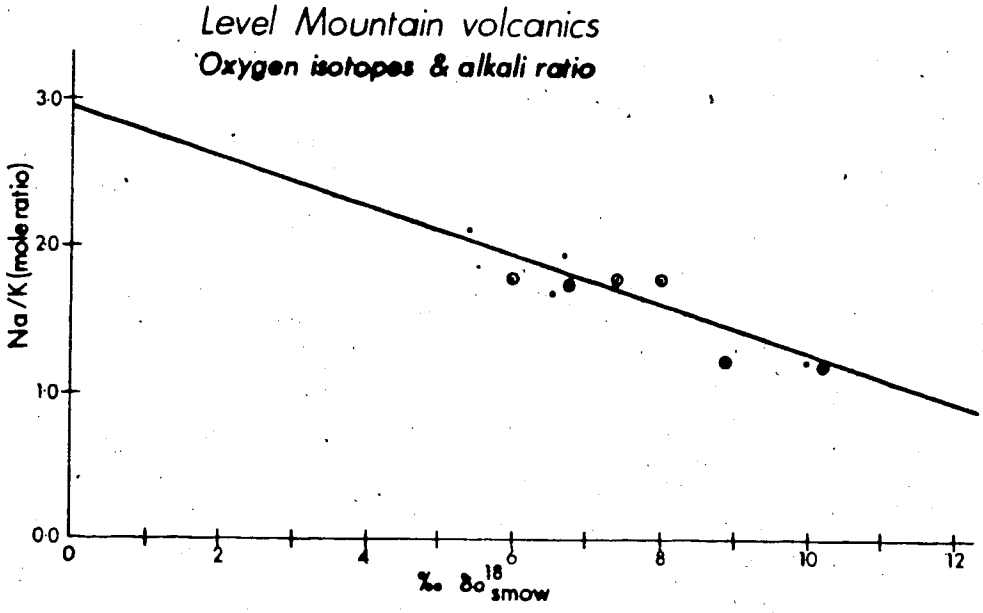

open system behaviour for Na_2O and K_2O discussed in the major element variation of the rhyolites and comendites. For granodiorites to be that heavy in oxygen implies that they are second cycle or S type granites. If an oxygen survey of the B.C. calc-alkaline plutonics shows them to be lower in $\delta^{18}O$, in the range of normal primary plutonic rocks (6‰ - 10‰; Taylor, 1968), then the model fails. The major and trace element data also support this type of open system alkali behavior, independent of the oxygen data.

The oxygen isotope data for Level Mountain's peralkaline lavas is consistent with a mantle derivation and subsequent modification by some open system higher level gaseous alkali exchange process. The oxygen data cannot eliminate either of two principal hypotheses. These are direct derivation of peralkaline melts from the mantle and derivation by protracted fractional crystallization from alkali basalts. However such derivation trends have been shown by Matsuhisa for Oki Dogo Island with a normal alkali basalt differentiation series (1973) and they do not follow the distribution of the Level Mountain data. The range of $\delta^{18}O$ values for the Level Mountain salic lavas also suggests some other process must be involved.

STRONTIUM ISOTOPE STUDY FOR LEVEL MOUNTAIN LAVAS

Introduction

A strontium isotope study was conducted during 1976-1977 with the purpose of determining the $^{87}Sr/^{86}Sr$ initial ratio for Level Mountain lavas. It was hoped that the strontium isotope ratios would verify a mantle derivation for the Level Mountain lavas and constrain the participation of crustal components in petrogenesis.

In the course of the Level Mountain study the peralkaline lavas with low levels of Sr, typically below 5ppm, and high Rb/Sr ratios were found to have a reasonably high radiogenic Sr component. The study was expanded to include accurate isotope dilution determinations of Rb and an attempt to generate Rb-Sr isochrons for these very young rocks. Due to the long half life of ^{87}Rb (1.42×10^{-11} $year^{-1}$) and the low Rb/Sr ratios for common igneous and metamorphic rocks, the accurate application of this isotope clock is usually only applicable to rocks older than 100MY. The unusual peralkaline nature of the Level Mountain salic rocks seemed amenable to such an isochron attempt despite their young age (1.2 to 4.6MY from fission track dates on glass and paleomagnetic correlation) (see discussion in subsequent sections).

The Level Mountain Rb-Sr Data

The compilation of reduced data from the Rb-Sr study is presented in table 7-30. Samples are presented in descending

Table 7-30 Strontium Isotope study for Level Mountain

Map Unit	Sample #	Type	Sr ppm	Rb ppm	Rb/Sr	weighted by 1/(STD.D)^2 87Sr/86Sr	n	87Rb/86Sr	Sr SPL/Spike Atomic	g Spike	Comments
8	8/25-50/6397	Hawaiite flow	463.572	12.381	0.027	0.70302 ±7	5	0.07688	62.90	0.6042	
8	KD-1	Alkali Basalt Dyke	441.326	(3)	0.007	0.70324 ±4	9	(0.01945)	62.54	0.6042	
7c	8/27-66/5862	Rhyolite Dyke	1.149	248.267	216.072	0.75536 ±50	2	624.48051	1.92	0.6042	unstable run Sr
7c	8/16-44/6250E	Tristanite Dyke	100.304	116.978	1.166	0.70367 ±19	4	3.37507	23.18	1.9477	
7c	8/16-44/6350	Rhyolite Tuff	21.880	(125)	5.713	0.70449 ±16	6	(16.44892)	36.00	0.6042	
7a	8/25-52/5880 (Trachyte plug)	Alkali Feldspar	13.894	103.593	7.456	0.70558 ±5	7	21.55496	6.84	1.9477	
7a	8/25-52/5880	Amphibole	6.293	56.252	8.939	0.70596 ±5	7	25.84580	3.10	1.9477	
7a	LM120 i	Phonolite Tuff	299.531	46.458	0.155	0.70347 ±3	10	0.44844	20.36	1.9477	
7a	LM120 d	Mugearite Agglomerate	386.324	-	-	0.70309 ±3	10	-	54.75	0.6042	
6a	8/5-8/5150 (P.Trachyte flow)	Alkali Feldspar	4.860	40.963	8.429	0.70890 ±50	9	24.36922	2.39	1.9477	
6a	8/5-8/5150	Amphibole	2.782	75.643	27.190	0.71282 ±8	8	78.6084	1.37	1.9477	
5b	PBC-5450	Alkali Basalt flow	586.461	(12)	0.020	0.70278 ±7	9	(0.05890)	43.52	1.9555	
5b	PBX-5385	Hawaiite flow	574.659	26.113	0.045	0.70388 ±3	4	0.13138	42.19	1.9555	small load, unstable run
5a	9/1-86/5421L	Per.Phonolite flow	46.580	109.126	2.343	0.70368 ±40	6	6.77353	22.86	1.9555	
5a	9/1-86/5421	Per.Phonolite flow	31.506	(119)	3.777	0.70506 ±22	10	(10.87462)	31.51	1.9555	unstable run
5a	PBU-5220	Phonolite flow	43.952	92.468	2.104	0.70324 ±25	7	6.08283	21.63	1.9555	
5a	PBV-5100	Phonolite flow	61.265	139.227	2.273	0.70373 ±12	5	6.60688	61.27	1.9555	
5a	9/1-87/5282L	Per.Trachyte flow	19.738	145.846	7.389	0.70764 ±234	4	21.36386	19.84	1.9555	
5a	PBW-5000 #	Comendite flow	8.349	173.973	20.838	0.70677 ±300	2	60.24783	4.11	1.9555	unstable run, high base line
5a	PBW-5000	Alkali Feldspar	17.174	67.638	3.938	0.70406 ±7	8	11.38703	8.45	1.9477	
5a	25/1-D (P.Trachyte flow)	Alkali Feldspar	6.932	38.567	5.564	0.70461 ±19	6	16.08597	3.41	1.9477	unstable run, overspiked
5a	25/1-D	Amphibole	4.975	41.251	8.292	0.70728 ±21	6	23.97431	2.45	1.9477	
4	13-K	Hawaiite flow	861.601	(22)	0.026	0.70352 ±3	9	(0.07351)	166.49	0.6042	
3	29/1-L	Alkali Basalt flow	509.749	(9)	0.018	0.70447 ±7	9	(0.05083)	65.21	0.6042	
3	PAP-4100	Basalt flow	561.158	(14)	0.025	0.70352 ±10	5	(0.07182)	27.31	1.9477	
2	PAR-4030	Alkali Basalt flow	678.115	-	-	0.70250 ±16	8	-	26.68	1.9477	
7c	8/16-44/6250	Gneiss	10.169	75	7.380	0.70512±.00003		21.236	5.00	1.9477	
8	Meszah Peak	Gneiss	710.000	69	0.097	0.70383±.00004		0.323	17.39	1.9477	
8	MPM	Troctolite	263.832	0	0.000	0.70280±.00004		0.000	19.98	1.9477	
	TCL 1004-41	Cr-Diopside	22.283	3	0.135	0.70283±.00006		0.3876	10.95	1.9477	

stratigraphic order with a brief description of rock or mineral type and any qualifying comments about the mass spectrometer run. The error quoted for $^{87}Sr/^{86}Sr$ is the standard error of the mean for n blocks (10 cycles per block) of data. The value of n is reported in the adjacent column so that sigma (the standard deviation of that measurement) may be calculated and used in place of the standard error. The Rb values in parentheses are from XRF determinations by Dr. J.G. Holland. In comparing the XRF and isotope dilution measurements on different sample aliquots, the XRF determination was generally within 10%. For these cases the $^{87}Rb/^{86}Sr$ was calculated from the natural abundance of ^{87}Rb, the XRF Rb value and the measured ^{86}Sr value all converted to atomic ratio. These examples were mostly basalts which have negligible radiogenic Sr gains since their time of eruption due to low Rb/Sr ratios. The basalts do not really figure in the isochron portion of the study, except as a comparative estimate of initial ratio.

The Level Mountain basalts have an average $^{87}Sr/^{86}Sr$ of 0.70334±.00059 which compares within the standard deviation to Dr. N. Green's determinations (unpublished) from the Gorda Ridge of 0.7028±.0002 and Armstrong's unpublished data on the Cordilleran basalts. Mount Edziza has basalt values in the range of 0.7028±.0001 Green (unpublished). The low $^{87}Sr/^{86}Sr$ values indicate the Level Mountain basalts to be primitive and mantle-derived. While the Level Mountain average is a little high for the Intermontane Belt (others

are typically 0.7031) sample PAR is as low as N. Green's Edziza sample #2902a65 at 0.7026 and is in fact the most primitive value hitherto reported for the Intermontane Belt. The diversity in $^{87}Sr/^{86}Sr$ ratios for Level Mountain basalts is from 0.7025 to 0.7045.

The intermediate lavas from Level Mountain, including the mugearite, tristanite and phonolite samples, show a similar range in $^{87}Sr/^{86}Sr$, but extend to higher values than for the basalts (0.70309 to 0.70506). These intermediate lavas also have primitive strontium values and are ultimately mantle-derived. Possible explanations for the higher Sr isotope ratios in phonolites would be: more radiogenic Sr in source, contamination by radiogenic crustal Sr, disequilibrium melting or a different degree of melting from basalts but same source, mixing between basaltic magma (primitive Sr) and a more radiogenic magma.

The trachytes, peralkaline trachytes, rhyolites and comendites have lower Sr levels than the magmas previously discussed and Rb/Sr ratios (weight) that range from 5.0 to 216.0. This lends itself to appreciable radiogenic Sr accumulation, even in the 4.5MY since the eruption of the oldest stratocone lavas at Level Mountain. The $^{87}Sr/^{86}Sr$ ratios range from 0.7041 to 0.7076 and even 0.7553 in the case of the one extremely radiogenic glassy rhyolite dyke. Assuming the initial $^{87}Sr/^{86}Sr$ ratio for this dyke to be 0.7033 a "point" age may be calculated from the slope formula of 5.886MY. Even accounting for all possible errors

this age estimate should be good to ±1.5MY. To accurately correct for this age effect and obtain true initial ratios for the Level Mountain salic lavas, isochrons were obviously needed. Before any correction for age there are rhyolites and trachytes with $^{87}Sr/^{86}Sr$ ratios in the range 0.704 to 0.705. Such low ratios could be taken to indicate: mantle origin, derivation from basalts, contamination of (low Sr) crustal melts with (high Sr) primitive basalts, partial melting of young crustal rocks (only slightly radiogenic), etc. The low values by themselves are hardly conclusive. A combination of Sr with other information is needed.

The effects of crustal contamination on the Sr isotope ratio and Sr concentration has been shown for andesite lavas of the Rio Grande Rift (Zimmerman and Kudo, 1979). On plots of Sr versus $^{87}Sr/^{86}Sr$, the contamination trend shows higher isotopic ratios at lower Sr abundance, and at higher SiO_2 content. Such a plot has been constructed for the Level Mountain data, figure 7-31. Considerable variation exists in the basalt data that could be explained by two mixing models. Line (1) is a least squares fit to the high-ratio basalts given by:

$$^{87}Sr/^{86}Sr \text{ (at.)} = 1.181 \times 10^{-5} \text{ Sr (ppm)} + 0.7103$$

with a value of $r^2 = 0.78$. This trend could indicate assimilation of crust with 20ppm Sr and 0.710 ratio by primitive basaltic magma of 650 ppm Sr and 0.7025 ratio. For this linear model, sample PAR is primitive and 29/1L represents about 25% crustal contamination. Line 2 has ten

Figure 7-31.
Variation plot of strontium versus strontium isotope ratio. Trachytes with the lowest Sr content are the easiest rocks to alter the isotope ratio either by decay of Rb, contamination with radiogenic crust or contamination from Sr rich basalts. The basalts may show 3 trends, one for crustal contaminatio and one for magma mixing with a primitive trachyte to yield phonolites. Analytical errors are plotted with bars except where they are less than the dimension of the point.

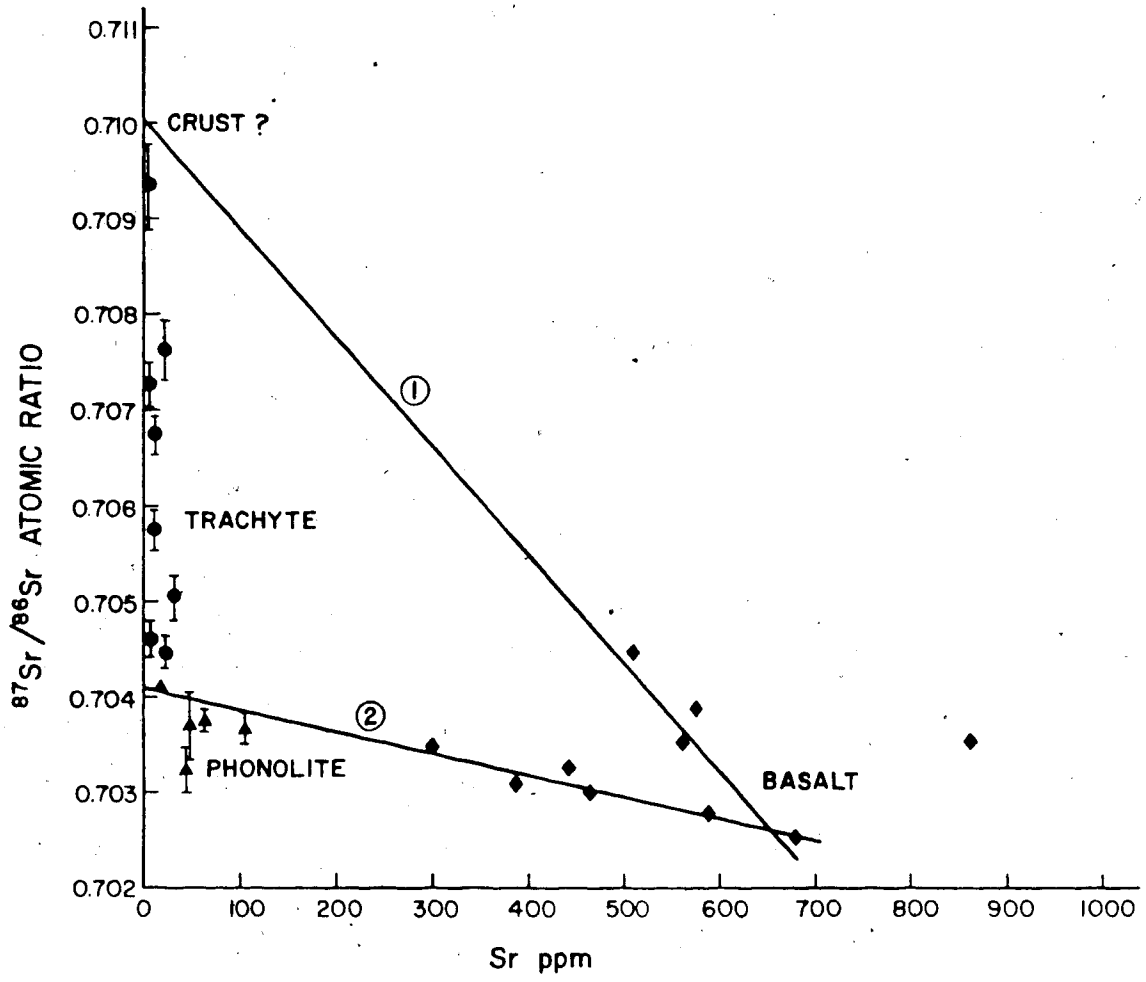

points ranging from basalts to phonolites and tristanite. The expression is given by:

$87Sr/86Sr(at.) = -2.27x10^{-4}Sr(ppm) + 0.7041$

with a value of $r^2=0.60$. The Sr ratio of the intercept is certainly not a normal crustal value. This model is thought to represent magma mixing primitive basalt with trachyte having 15ppm Sr and an initial ratio 0.704. According to this model, the phonolites scatter between 6% and 17% basalt contribution to a normal trachyte. Mugearite by this model represents about half and half basalt and trachyte. The "parent" basaltic magma may actually be hawaiite, or the hawaiites may represent contamination of alkali basalt by trachyte. This is precisely the magma mixing origin attributed to the intermediate lavas on the basis of major element chemistry. The increase in SiO_2 along with $^{87}Sr/^{86}Sr$ is considered to be coincidental, since silica as well as the other major elements fit a trachyte component just as easily as a sialic crust. The only way that this mixing line could involve crust would be for the crust to chemically resemble a trachyte and have a primitive isotope ratio. Partially melted granitic gneiss xenoliths were found in both hawaiite unit 8 from Meszah Peak and in the tristanite dyke, 8/16-44/6250. In both of these cases the isotope ratio of the inclusions were similar enough to host magmas to assume that the Sr had been partially equilibrated along with the melting. The alternative is that these granitic gneiss xenoliths with $^{87}Sr/^{86}Sr$= 0.7038 to 0.7051, could be

the primitive crustal component indicated by mixing line 2. The original magma mixing hypothesis, however, is still favored. The trachytes, peralkaline trachytes, rhyolites and comendites scatter along the isotope ratio axis at low Sr levels. No particularly good fit can be made to all of these points. It is thought that they represent variable contributions of crustal contamination or disequilibrium partial melting together with the overprint of radiogenic Sr formed since magmatism began.

Isochron Attempts and Age Estimates

If the atomic ratios $^{87}Sr/^{86}Sr$ and $^{87}Rb/^{86}Sr$ are known for contemporaneous rocks or minerals, slope ages (isochrons) can be obtained with the zero $^{87}Rb/^{86}Sr$ intercept giving the $^{87}Sr/^{86}Sr$ initial ratio. The slope formula is:

$$(\Delta^{87}Sr/^{86}Sr)/(\Delta^{87}Rb/^{86}Sr \cdot \lambda = t$$

where λ, the half life of ^{87}Rb, and t, the age, are in years. The slope of the isochron in the simplest case is determined by two points such as minerals from the same rock or one mineral and the whole rock, coeval rocks of differing Rb and Sr contents. The slope can also be the least squares best fit to a series of coeval minerals or rocks. An isochron plot has been constructed for salic and intermediate samples from stratocone map units 7, 6a, and 5a, figure 7-32. Various fits were attempted for units 7 and 5. Apparent ages increase upwards in the section. All three map units seem to have different initial ratios. Slope ages

Figure 7-32.
Rb Sr isochron plot for whole rock and mineral samples from Level Mountain stratocone. Two point isochrons give scattered ages which are generally too old compared to fission track dates. Initial ratios are quite variable.

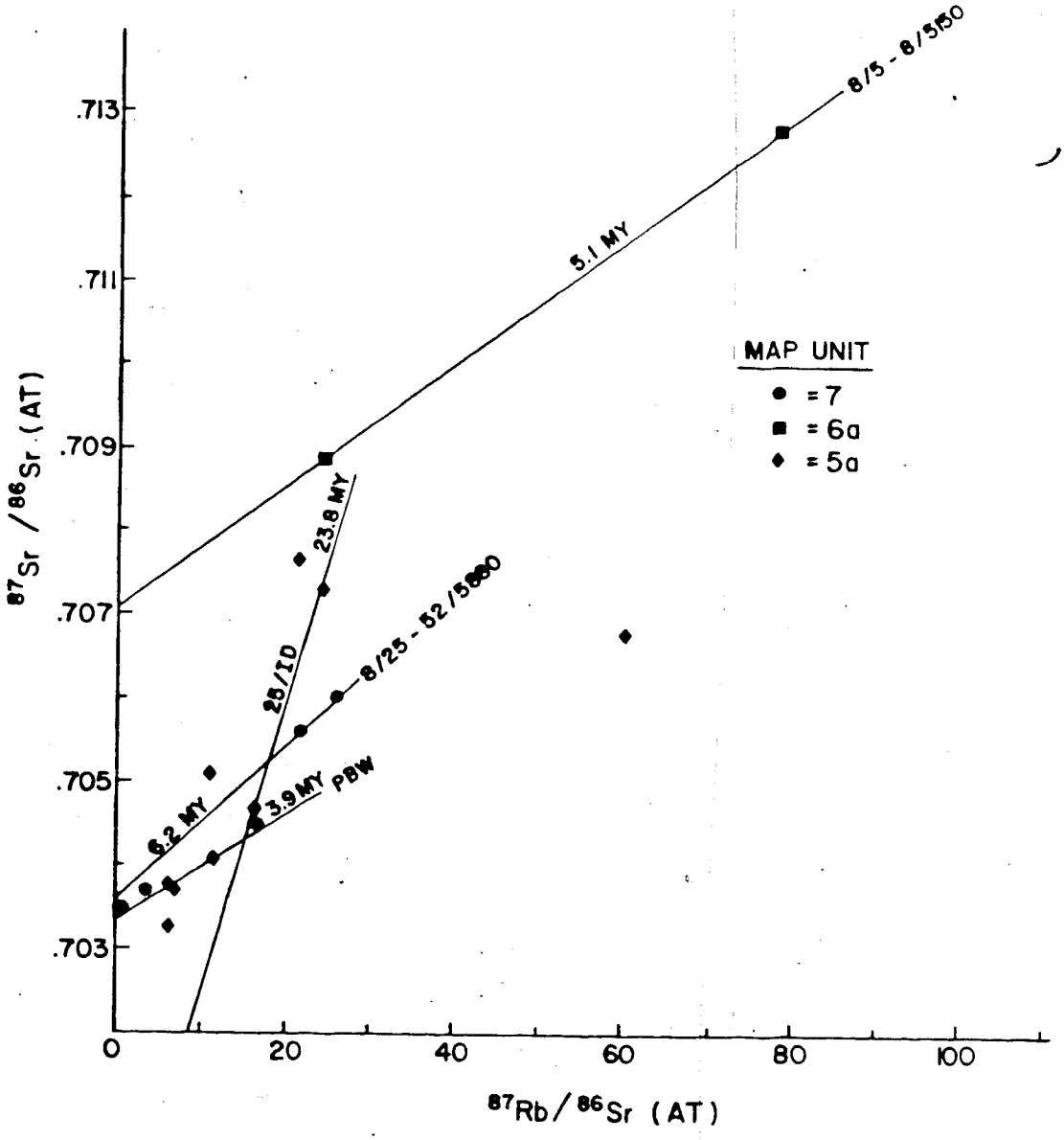

are generally in the range of 5.1±1.2MY which agree with most of the age estimates obtained from single rocks, assuming the average basalt initial ratio of $^{87}Sr/^{86}Sr$= 0.7034. The problem is that all of the ages are too old compared to age estimates from fission track dates, paleomagnetism and geomorphology. Two single flows with mineral separates from unit 5a give such divergent answers as 3.9 and 23.8MY. Lumping all of the samples from the Stratocone gives a scattered apparent isochron of slope equivalent to 9.4±1.0MY, figure 7-33. The interpretation of all these "too old" ages is problematic and is not even restricted to Level Mountain. Souther and Symons (1974) have published K-Ar dates radiocarbon and fission track ages which tie Edziza's magnetostratigraphy to a post 7MY age. Some of the Rb-Sr data on comendites and trachytes from Edziza have $^{87}Sr/^{86}Sr$ as high as 0.715 (Green, samples #SE2902a66 and SE381567a, unpublished) implying ages ranging from 2MY to 24MY. Pantellerite flows from the Rainbow Range have $^{87}Sr/^{86}Sr$ as high as 0.7293 (R-88, Bevier, 1978) implying an age of 8.55MY, which is about 1.5MY older than the oldest K-Ar dates for the Rainbow Range. These old Rb-Sr ages are not restricted to B.C. Similar peralkaline suites from Aden, South Arabia have been reported by Cox et al (1970) and Dickinson et al (1969) to give isochron ages between 20 and 30MY older than the actual eruptive age of the Aden volcanoes. These isochrons are constructed by combining samples from six volcanoes with no attention to

Figure 7-33.
Rb-Sr isochron plot showing whole rock values for salic and intermediate lavas of the stratocone. From fission track dating this sequence of lavas is younger than 4.5MY yet they give an apparent isochron age of 9.4±1.0MY. This could possibly indicate the age of a melting event in the mantle source region.

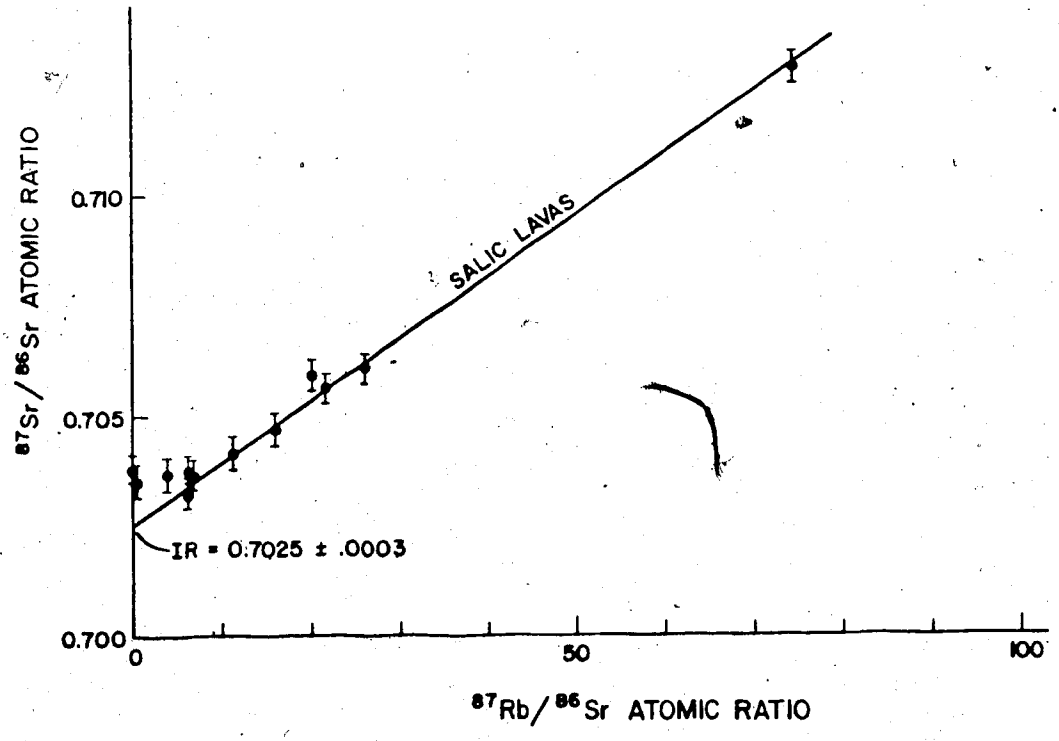

actual eruptive sequence or stratigraphy. As at Level Mountain, there is considerable variation of $^{87}Sr/^{86}Sr$ within each of the Arabian volcanic centres. In the Arabian instance, the ages are thought to reflect the previous volcanic episode of the region (a mantle melting event). In the Intermontane Belt there are no conveniently timed earlier volcanic episodes. For the Stikine (Level Mountain and Edziza) the preceeding volcanic episode was the Sloko formation at approximately 50MY. There are also no conveniently placed tectonic events, the last being the cessation of subduction off the west coast, 200 km away, at about 20MY (Grow and Atwater, 1970). Souther (1970) stressed the relation of post Miocene alkalic volcanism in the Intermontane Belt to be subsequent to the cessation of this subduction activity. The only remaining explanation is that the anomalous Rb-Sr ages for Level Mountain reflect some thermal event(s) which preceed any surface manifestation of volcanic activity. The 9.4MY lineation possibly reflects the mantle melting event responsible for voluminous plateau volcanism.

LEAD ISOTOPE GEOCHEMISTRY FOR LEVEL MOUNTAIN

Introduction

The Pb isotope systems have been used to compare rocks derived from different Pb reservoirs (Schilling, 1973; Tatsumoto, 1978) in disucssing variable depletion of the

mantle source regions for oceanic island (alkaline) versus ocean floor (tholeiitic) basalts. U and Th posess low decay rates and low diffusivities (Seitz, 1973) with respect to thermal and tectonic events. As a result, the three radiogenic Pb clocks keep time slowly and the lead isotope ratios are sensitive indicators of geochemical characteristics which persist for hundreds of millions of years or longer. Consequently, they have been extensively used in modelling convective turnover and mixing times for the mantle (mesosphere-asthenosphere) (Dupre and Allegre, 1980; Hoffman and Hart, 1978; Sun and Hanson, 1976; and Armstrong, 1968).

Of the four stable lead isotopes, ^{204}Pb is the least abundant (1.4%) and cosmogenic while ^{206}Pb, ^{207}Pb and ^{208}Pb are radiogenic. The radiogenic leads are normalized to ^{204}Pb to provide a common base for comparison. The radiogenic leads are the ultimate stable daughter isotopes of uranium and thorium decay. The lead isotope information is commonly displayed on two atomic ratio plots:

$^{208}Pb/^{204}Pb$ versus $^{206}Pb/^{204}Pb$ and

$^{207}Pb/^{204}Pb$ versus $^{206}Pb/^{204}Pb$.

The distribition of points on the first plot reflects the Th/U ratio (initial atomic isotope ratio $^{232}Th/^{238}U = K$) of the source region(s). The distribution of points on the second plot depends on the U/Pb ratio (initial atomic isotope ratio $^{238}U/^{204}Pb = U$) in the source region(s) and the joint operation of the two lead clocks. With knowledge

of, or assumptions about U and K, single or multiple stage model Pb ages may be calculated. The Pb isotope characteristics of abyssal tholeiites and oceanic islands have been reviewed by Tatsumoto (1978). He notes that all of these primitive volcanics have lead isotope ratios which correspond to negative model ages (future) for single stage growth. This feature and the wide scatter in $^{206}Pb/^{204}Pb$ he attributes to progressive U and Th enrichment with respect to Pb in the mantle source regions for basalts during much of geologic time.

Level Mountain Lead Isotope Data

The lead isotope ratio analyses are presented along with pertinent trace element data in table 7-31. There is no simple correlation of the lead isotope data with "degree" of differentiation", major and trace element abundances (including lead), $^{87}Sr/^{86}Sr$ or ^{18}O SMOW $^{o}/_{oo}$. The values and overall range in the Level Mountain lead isotope ratios is comparable to abyssal tholeiites, oceanic islands, Juan be Fuca - Gorda Ridge, East Pacific Seamount Chains (Kodiak-Bowie-Emperor), (Tatsumoto, 1978; Church and Tatsumoto, 1978), and the Mid Atlantic Ridge (Dupre and Allegre, 1980; Sun (1973). That the Level Mountain values compare to those other mantle derived suites, while failing to follow other geochemical variation, lends itself to mantle heterogeniety explanations rather than to contamination or mixing models.

Table 7-31. Lead Isotope Ratio Data and Selected Trace Element Abundances for Level Mountain Lavas.

Sample	Identification	n	$^{208}Pb/^{204}Pb$	$^{207}Pb/^{204}Pb$	$^{206}Pb/^{204}Pb$	$\delta^{18}O$SMOW
8/25-50/6397	alkali basalt-hawaiite	8	18.560 ±0.004	15.536 ±0.004	37.874 ±0.010	5.8
9/2-99/6600a	comendite	8	19.079 ±0.021	15.631 ±0.041	38.434 ±0.139	8.0
8/16-44/6250E	tristanite	7	19.023 ±0.006	15.530 ±0.005	37.992 ±0.015	7.4
LMI201	phonolite	6	19.715 ±0.020	15.625 ±0.018	38.350 ±.056	7.8
8/5-8/5150	peralkaline trachyte	5	18.804 ±.013	15.542 ±0.005	38.112 ±0.010	6.8
13-K	hawaiite	7	19.414 ±0.016	15.543 ±0.011	38.317 ±.055	6.5
Juan de Fuca/Gorda Ridge			18.5 ±0.2	15.5 ±0.1	37.8 ±0.2	

Table 7-35. Continued

Sample	Identification	$^{87}Sr/^{86}Sr$	Rb	Sr	K (%)	HF	U	TH	Pb
8/25-50/6397	alkali basalt-	0.7030	12	464	0.716	n.a.	3	3	6
9/2-99/6600	comendite	n.a.	276	4	3.619	89	9	32	56b
8/16-44/6250E	tristanite	0.7037	117	100	4.001	44	4	17	27b
LMI201	phonolite	0.7035	46	300	3.744	14	n.a.	5	7b
8/5-8/5150	peralkaline trachyte	0.7090	149	5	3.927	60	3	13	1b
13 - K	hawaiite	0.7035	22	862	1.096	8	n.a.	5	7b
Juan de Fuca/Gorda Ridge		0.7026± .0003d							

n= number of data sets averaged
n.a.= not analysed
All concentration of trace elements in ppm units except K which is weight percent
Pb= atomic ratios
a fractionated during Pb isotope determination
b Pb concentration estimated from Th value and known Pb values for samples of similar whole rock chemistry
c ref: Church + Tatsumoto, 1975
d ref: Hedge and Peterman, 1970

The lead isotope data for Level Mountain have been plotted in figure 7-34. The distribution of the Level Mountain whole rock leads is consistent with a single source. The compositions of two conformable modern Cordilleran ore leads are shown on the figure by T for the Yukon Treadwell deposit ,S for the B.C Sullivan mine, data from Russel (1972). Leeman et al (1979) analysed leads from the iron rich lavas from Craters of the Moon, (C.O.M.) Idaho, which are crustally contaminated, and from the lower crustal charnocitic xenoliths which they bear. The C.O.M. ferrolatite plots midway between the Level Mountain group and the Cordilleran ore leads, while the gneisses are extremely primitive plotting well down the concordant trend in the vicinity of $^{206}Pb/^{204}Pb = 14.5 \pm 1.5$. The purpose of pointing out these examples is to indicate the direction of crustal contamination. For the Level Mountain whole rock lead trend to represent crustal contamination, the virgin lead would have to be even more radiogenic than indicated. The only reported leads more radiogenic than those for Level Mountain are from Ross (Antartica) and St. Helena (Tatsumoto, 1978).

The bold lines through the Level Mountain data are the best fit trends for whole rock leads from the Juan de Fuca - Gorda Ridge System and the Eastern Pacific Seamount Chain after Tatsumoto (1978). The trends for MORB (Dupre and Allegre, 1980) and the Hawaiian Islands (Tatsumoto, 1978; Sun et al, 1975) are very similar. Two of the Level Mountain

Figure 7-34.
Lead isotope ratio plots for Level Mountain lavas. Lava values plot near primitive MORB trend of Tatsumoto (1978). Variations are not obviously related to differentiation or crustal contamination. Implication is fractional melting derivation from a heterogeneous but primitive mantle source.

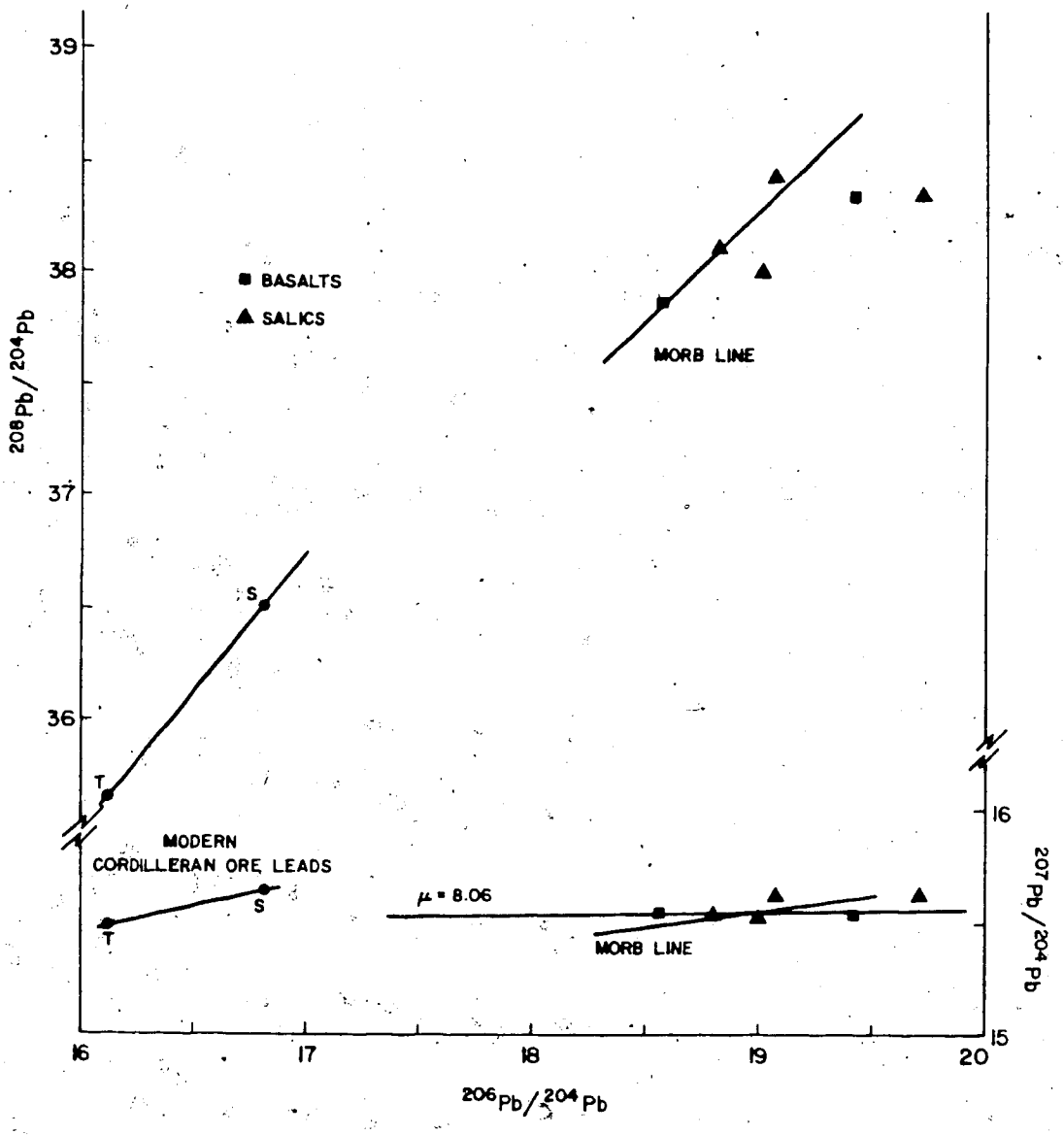

samples fall well to the right of the trend on the $^{208}Pb/^{204}Pb$ versus $^{206}Pb/^{204}Pb$ plot, indicating a lower value of kappa which is to say that there is a low Th/U ratio for the source of the hawaiite and tristanite (crustal contamination ?). Despite the fact that the Th abundances in the Level Mountain lavas are high, other incompatible elements such as U and Hf are disproportionately higher compared to MORB and abyssal basalts (Dupre and Allegre, 1980). If the Level Mountain $^{207}Pb/^{204}Pb$ versus $^{206}Pb/^{204}Pb$ data are fit with a single line, the slope is more nearly horizontal than for the Oceanic volcanics. This implies that the mantle source for the Level Mountain Leads is very young, i.e. it has been depleted and reset relatively recently.

The abundance data for the Pb, Th, and U from Level Mountain whole rocks is presented in figure 7-35, (data tabulated in preceeding section on trace elements). The plots for U-Pb, Th-Pb and U-Th indicate a single homogeneous source region for all of the Level Mountain lavas, which compares favorably with the interpretation of a single source for the Pb isotopes. This places constraints on the composition of the source region for Level Mountain. Tatsumoto (1978) has analysed the U and Th contents of mineral separates of a four phase periodite nodule (spinel lherzolite) from the strongly alkaline cinder cone at Boss Mountain (Takomkane) B.C. The spinel and Cr-diopside are enriched in U and Th relative to olivine and orthopyroxene.

Figure 7-35.
Trace element variation plots for (U, Th, Pb) of Level Mountain lavas. Here the U/Pb and Th/Pb are lower than for alkaline volcanic suites of oceanic islands and the east African rift. The U/Th ratios for lherzolite minerals are from Takomkane Mtn, B.C. (Tatsumoto, 1978).

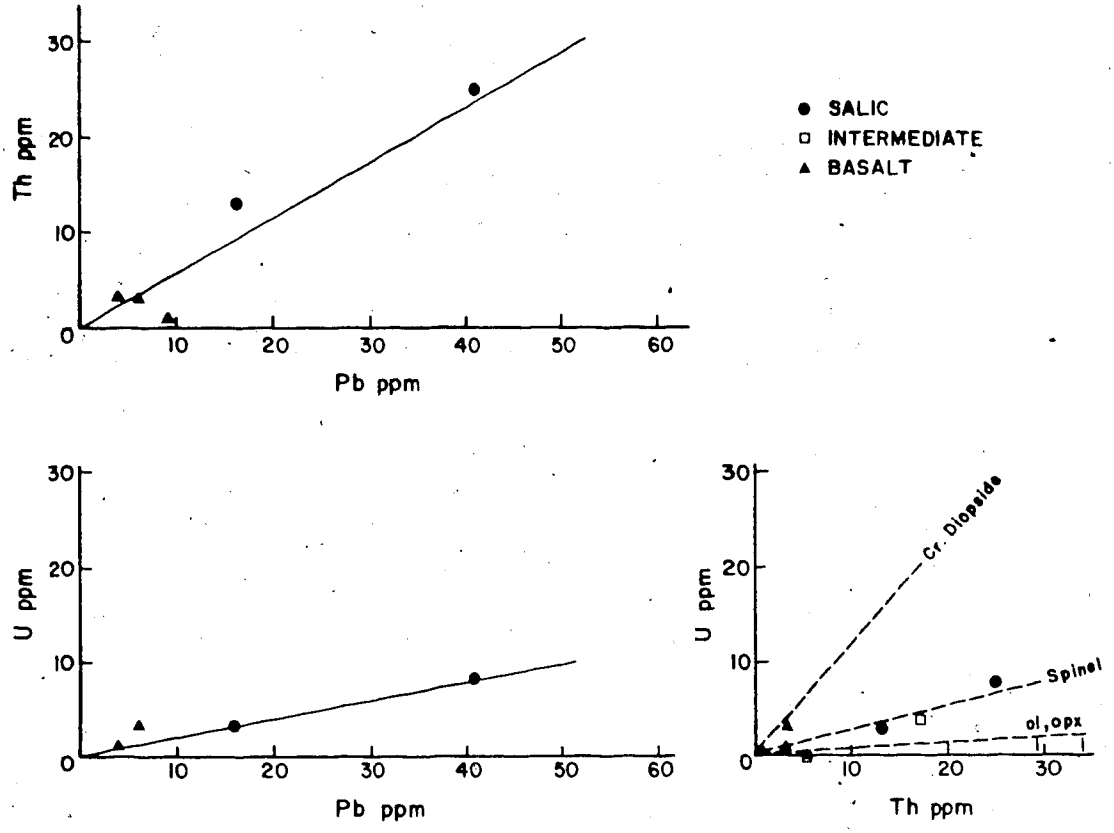

The Th/U ratios for spinel and Cr-diopside are 0.4 and 0.8 respectively. Note that the Level Mountain Th/U ratios range from about 1.0 to 5.0 but mainly fall along a line of slope 2.95. This range of Th/U ratios is typical for seamounts and oceanic islands as well. None of the aforementioned lavas, including those from Level Mountain could have been generated by melting of such depleted material as the Takomkane lherzolite. The synopsis of the lead isotope and related trace element data for Level Mountain is that the lavas were derived from a single inhomogeneous source for lead isotopes, but relatively constant in U/Pb, Th/U and Th/Pb. This source is more radiogenic than that for most primitive oceanic basalts and more heterogeneous in $^{206}Pb/^{204}Pb$.

THE UNIVERSITY OF ALBERTA

LATE CENOZOIC ALKALINE VOLCANICS OF THE LEVEL MOUNTAIN RANGE, NORTHWESTERN BRITISH COLUMBIA: GEOLOGY, PETROLOGY AND PALEOMAGNETISM

by

TARK SCOTT HAMILTON

A THESIS

SUBMITTED TO THE FACULTY OF GRADUATE STUDIES AND RESEARCH IN PARTIAL FULFILMENT OF THE REQUIREMENTS FOR THE DEGREE OF DOCTOR OF PHILOSOPHY

GEOLOGY

EDMONTON, ALBERTA

FALL 1981

ABSTRACT

Level Mountain is a Late Cenozoic shield volcano located near 131°20'W,58°31'N in the Stikine Volcanic Belt of northern British Columbia. The volcanic plateau with an average elevation of 4500',(1372m), is younger than Upper Miocene in age and is comprised of up to four sequences of alkali basalt and ankaramite flows and tuffs. The central region of peaks and ridges rises to a maximum elevation of 7200',(2195m), and has a repetitive bimodal distribution of alkali basalt and peralkaline salic lavas and tuffs that spans the period from 4.5 million years b.p. to recent times. Feeble basaltic vents with spatter, bombs and scoria apparently postdate continental glaciation. A paleomagnetic study on two stratigraphic sections that span the entire range of volcanism samples the earth's major polarity reversals for the past 6 MY.

Petrochemically the lavas belong to the sodic alkali basalt series and are of continental affinity. Oxygen isotope values near 5.6°/$_{oo}$$\delta^{18}$O SMOW have been measured for unaltered rocks including basalts, salics, and ultramafic inclusions. This would seem to indicate that the mantle under northwestern British Columbia is normal with respect to oxygen and that the Level Mountain magmas are mantle derived. Corroborating evidence is available from the whole rock strontium isotope studies which show a total range of ^{87}Sr/^{86}Sr from .7025 to .7071. The presence of basic and

salic, undersaturated and ovesaturated, peralkaline and metaluminous rocks attests to the complexity of petrogenetic processes at Level Mountain. Although the two volumetrically important lava types appear to be primary and mantle derived, the presence of some rhyolites enriched in ^{18}O, granitic gneiss inclusions in basalts and tristanites and great variation in whole rock lead isotope ratios are probably all indicative of some degree of interaction between magmas and crustal rocks. Major and trace element geochemical variations and mineralogy indicate an upper mantle origin at shallower than 15 kbar pressure from an undersaturated ultramafic source that possessed an abundance of alkalis and incompatible elements. The mineralogy and chemistry of the major rock types indicate conditions of low oxygen fugacity and a dry gas phase composition for both peralkaline flows and basalts. The field relations of some comendite flows implies flow behavior and seems to indicate a viscosity two to three orders of magnitude lower than would be predicted on the basis of silica content and whole rock chemistry. This could be partially reconciled if the gas phase had been halogen rich and dry.

Calculations of the volume and energetics of the volcanism of the Stikine Belt indicate that less than 15% of the modern heat flow is necessary to maintain the levels of volcanicity since Pliocene times.

Table of Contents

Volume II

List of Tables

List of Figures

List of Plates

List of Maps

CHAPTER 8. CRYSTALLIZATION AND MELTING EXPERIMENTS AT ONE ATMOSPHERE TOTAL PRESSURE ON SELECTED ROCKS FROM LEVEL MOUNTAIN

INTRODUCTION

A series of more than one hundred reconnaissance experiments was conducted to determine the crystallization behavior of fourteen Level Mountain lavas. Six of the lavas were peralkaline salics and five were basaltic. The remaining three were an alkaline trachyte, a tristanite and a phonolite. Additionally, thirty-five experiments were conducted to determine the solidus temperatures of six xenoliths of mafic and ultramafic composition. For these experiments, the conditions covered the temperature interval from 800°C to 1300°C with the principle range of oxygen fugacities between the FMQ and MW buffers. Twenty-nine experiments were additionally performed under more oxidizing conditions to assess the effect of variable fO_2. For the most part these experiments were rock-air buffered somewhere between FMQ and HM.

PREVIOUS WORK. CRYSTALLIZATION AND MELTING RELATIONSHIPS OF PERALKALINE ROCKS

A number of studies have been conducted on the melting characteristics of peralkaline rocks. Rather different behavior has been demonstrated for plutonic versus volcanic

undersaturated peralkaline rocks (agpaites).[1] The most prominent initial observation from experimental work was that agpaites had much longer melting intervals than common rock types (Piotrowski and Edgar, 1970; Sood et al, 1970). The large liquidus - solidus interval has been attributed in part to peralkalinity and in part to high concentrations of uncommon or incompatible geochemical elements (Ti, Zr, REE, Fe^{3+}, Cl). The halogens and water in these systems may be preferentially retained in the melt, thus affecting an abnormal depression of the solidus, particularly at higher pressures (Anderson, 1974; Manning, 1981). Edgar and Parker (1974) successfully verified this hypothesis for eight crystalline rocks, four plutonic and four volcanic. The melting intervals were typically greater for the plutonic rocks than for the volcanics of similar composition. Presumably this was due to differences in previous cooling history of samples versus incorporation of halogens into crystals and the glass. The experiments reported by Piotrowski and Edgar and by Edgar and Parker were conducted at either one atmosphere or at one kilobar water pressure, unbuffered. Their two-point hydrous liquidus curves appear to be normal, with negative slopes ($dP/dT<0$). in the determination of the liquidus for the crystalline samples,

---

[1] Peralkaline plutonic rocks have been termed agpaites (Sorenson, 1970). They are characterized by a peralkalinity index greater than unity (Ac±Ns in the norm), high concentrations of Fe, Ti, Zr, REE, F, Cl and unusual mineralogy which may include eudialite, rinkite, rosenbuschite. Typical occurences of these rocks are found at Khibina, Kola and Ilimaussaq.

For the four Tenerife phonolites the one-atmosphere liquidus temperature ranged from 1030° to 1200°C. The crystallization sequence at one atmosphere was feldspar followed by nepheline then amphibole. When pH_2O is low, clinopyroxene may crystallize before amphibole or in place of amphibole. The order of appearance of clinopyroxene on the liquidus is quite variable. The phonolites were of the mildly peralkaline type with A.I. ranging from 1.03 to 1.19. Melting intervals determined for three of the phonolites ranged from 305°C to 475°C.

The silica oversaturated peralkaline system has been studied experimentally by Bailey et al (1974). Their studies were anhydrous but unbuffered and conducted over a range of pressures from one atmosphere to approximately 1.5 kilobar. Their samples were pantellerites and pantelleritic trachytes from East Africa (Menghi, Longonot, Eburru). The work of Bailey et al (1974) was done on very peralkaline compositions with A.I. = 1.38 to 2.18. While the solidus temperature was not determined, the liquidus temperature showed a strong linear decrease with increasing peralkalinity. For all compositions studied, plagioclase was the silicate liquidus phase to one kilobar. Sample 83, Eburru Pantellerite, also had phenocryst quartz at one kilobar. There was something noteworthy and rather unusual about the liquidus curves reported in Bailey et al (1974) and Bailey and Cooper (1979), see Figure 8-1. The boundary of the liquidus line in PT space, and also the

Figure 8-1.
Liquidus curves for peralkaline trachytes (KL4, KE4) and more siliceous pantellerites (KE12, KW5) taken from Bailey et al (1974). As pressure increases the liquidus temperature goes through a minimum, then increases linearly to about 5kbar. Depending on the ascent path, such melts could develop considerable superheat. Note convergence of liquidus curves to higher P and T.

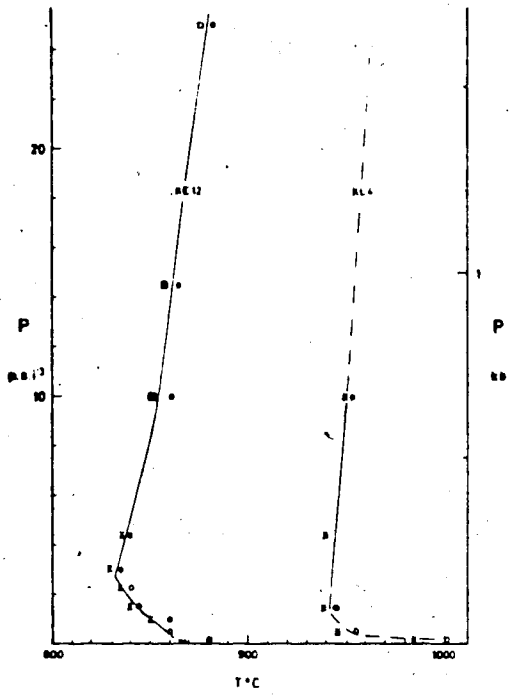

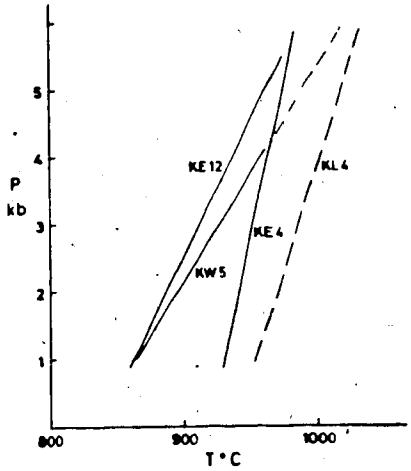

crystallization surfaces for alkali feldspar and quartz, are concave to higher temperatures with a temperature minimum at about 0.3 kilobar. If this is indeed the case, a peralkaline magma could possibly acquire some degree of superheat upon ascent (Waldbaum, 1971; Marsh and Kantha, 1978). Partially resorbed alkali feldspar and quartz phenocrysts are a common feature of sparsely crystalline and glassy peralkaline salic lavas. Comendites and pantellerites typically display flow morphologies characteristic of fluid behavior, which contrasts with the more viscous nature of calc-alkaline rhyolites of similar SiO_2 content (Shaw, 1973; Schmincke, 1974). Both of these observations might arise from such a heat input implied by the liquidus determinations of Bailey et al (1974).

EXPERIMENTAL TECHNIQUES

Experiments were cinducted on the Deltech furnace under controlled fO_2 conditions achieved by the use of known mixtures of CO and CO_2. The samples, either pressed mineral powder briquettes or glasses quenched from 1300°C, were sintered onto a Pt wire loop and suspended in the thermally uniform position of the furnace after the technique of Donaldson et al (1975). Experiment durations were generally one to three hours. Rapid quenching was achieved by severing the suspension wires so that the sample fell into a mercury filled receptacle at the base of the furnace.

RESULTS

The results of the melting experiments on Level Mountain lavas are summarized as a series of bar graphs in Figure 8-2. The basaltic lavas had the crystallization sequence oxide, olivine, clinopyroxene, plagioclase. The crystallization data is summarized in Table 8-1. An oxide phase crystallized above 1260°C. Compositionally these were magnetite - ulvospinel solid solutions. Forsterite-rich olivine was the first silicate phase on the liquidus between 1250°C and 1265°C. With the exception of Ne-normative hawaiite, 8/25-50/6397, diopsidic clinopyroxene appeared as the second silicate phase. The clinopyroxene liquidus fell in the interval 1250° to 1165°C. Towards the lower temperature end of this range an intermediate plagioclase, labradorite to andesine composition, was on the liquidus. This compares favorably with the one atmosphere crystallization experiments conducted on alkali salt by Thompson and Flower (1971) and Duke (1974). Residual phases such as alkali feldspar and nepheline did not appear until near the solidus, between 1100°C and 1050°C. Often two distinct forms were present in the crystallized phases. While the high temperature titanomagnetites tended to be well formed cubes or octahedra, a second dendritic or quench textured magnetite formed particularly in the runs quenched from the lower temperature range of the melting interval. Olivines formed as discreet prisms of equant to acicular habit, while clinopyroxenes crystallized as blades both

Figure 8-2.

Buffered crystallization sequences and melting intervals for Level Mountain lavas. Comendites: (1) 9/2-99 and (2) 8/25-54/6345; Pantellerites: (3) 25/5e and (4) 8/5-8/5150; Comenditic Trachyte: (5) 24/2 o/c and (6) 25/7; Trachyte: (7) 24/hi; Tristanite: (8) LMIIIA; Phonolite: (9) LMI20i; Hawaiite: (10) 8/25-50/6397; Alkali Basalts: (11) and (14); Ankaramites: (12) and (13). T range of experiments indicated by length of line. Highest T occurrence of a mineral plotted as appropriate symbol.

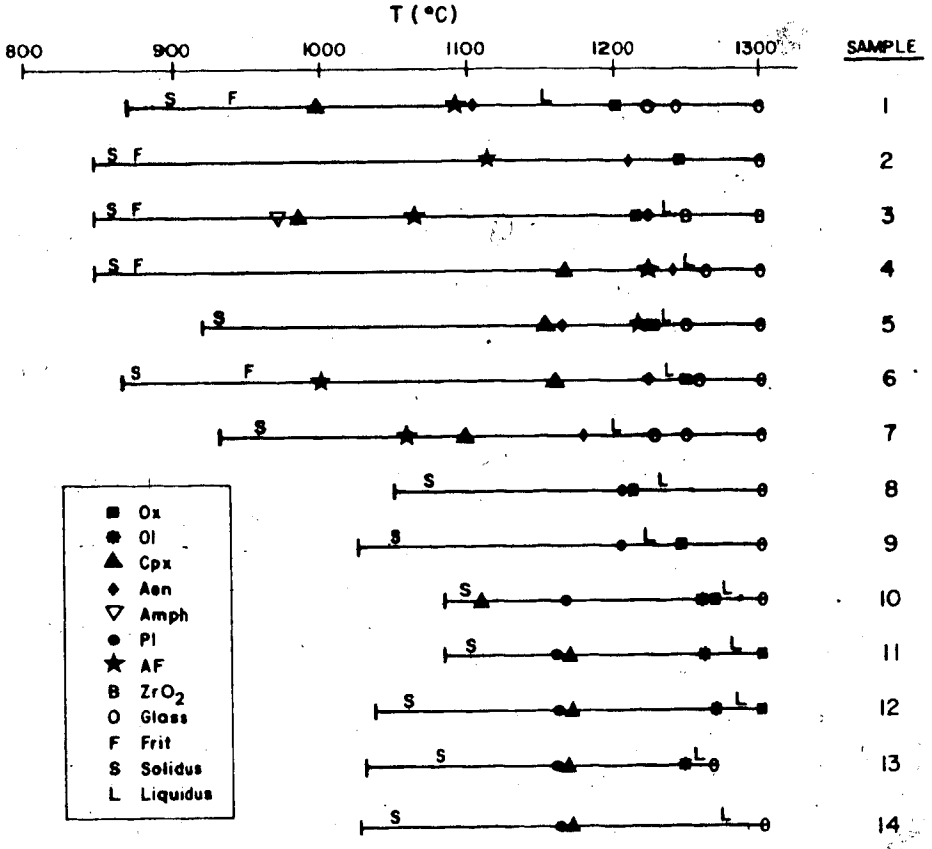

Table 8-1 Liquidus and Solidus Data for Basic and Intermediate Lavas from Level Mountain

Sample	TL°C	T_s°C	T_m°	TL°C Calc*
LMI20i phonolite	1225 ±20	1050 ±25	175 ±45	1173 pl 1086 cpx 1006 ol
LMIIIA tristanite	1230 ±25	1041 ±31	189 ±56	1364 pl 1050 cpx 876 ol
8/25-59/6397 hawaiite	1270 ±15	1080 ± 7	190 ±22	1165 ol 1140 pl 1135 cpx
PAP Alkali basalt	1275 ±15	1100 ±15	175 ±30	1210 ol 1205 cpx 1173 pl
01 Ankaramite	1250 ±10	1062 ±12	188 ±22	1327 ol 1230 cpx 1048 pl
h ankaramite	1255 ±10	1092 ± 5	163 ±15	1264 pl 1171 ol 1165 cpx
29/1-f early hawaiite	1275 ±13	1083 ±73	192 ±86	———

* French (1971)

singly and as feathery, quench textured aggregates. Plagioclase crystallized both as blades and dovetail prisms. The crystallization sequences found experimentally correspond to the natural behavior inferred from the petography of the respective lavas; however, the actual crystal forms may differ due to kinetic effects (Donaldson, 1976). The average measured silicate liquidus temperature for five Level Mountain basalts was 1265°±5°C, with a corresponding average solidus of 1083°±6°C. The average of the five basalt melting intervals was 182°±5°C.

The crystallization sequence of the phonolite and tristanite were oxide, plagioclase, alkali feldspar, clinopyroxene. The oxide appeared between 1212°C and 1247°C. Plagioclase and andesine to oligoclase composition appeared above 1205°C with the silicate liquidus temperatures for phonolite and tristanite set at 1225°±20° and 1230°±25° accordingly. The averages for these two intermediate lavas are liquidus temperature: 1228°C±3°, solidus temperature: 1045°C±5° and melting interval: 183°C±7°. The liquidus and solidus are marginally lower than for the basalts and the melting interval is the same.

The crystallization behavior of the salic lavas is summarized in Figure 8-2 with temperature data listed in Table 8-2. The average silicate liquidus temperature for the seven Level Mountain lavas was 1216° ± 13°C. The average salic solidus was 894°±15°C and the average melting interval was 308°±22°C. The largest melting range observed was for

Table 8-2 Liquidus and Solidus Data for Salic Lavas From Level Mountain

Sample	TL °C	T_s °C	T_m °	TL °C Calc*
24/1 hi trachyte	1190 ±10	965 ± 35	225 ±45	1189 1050 995
24/2 o/c	1235 ±10	930 ± 10	305 ±20	——
25/5e pantellerite	1235 ±10	862 ± 13	273 ±23	1149 1071 978
25/7	1233 ± 7	875 ± 10	358 ±17	1138 1027 986
9/2-99 comendite	1155 ±50	900 ± 30	255 ±80	1150 1056 986
8/5-8/5150 pantellerite	1250 ±10	862 ± 13	388 ±23	1147 1044 962
28/25-54/6345 comendite	1215 ±10	862 ± 13	353 ±23	1131 1060 994

* French (1971) Plagioclase; Clinopyroxene; Olivine

pantellerite 8/5 -8/5150 (388°±23°C). The liquidus determinations are somewhat higher than previously reported (Bailey et al, 1979). This is presumably due to the present study being anhydrous and buffered at lower fO_2. The long melting intervals are comparable to data on peralkaline phonolites and plutonics reported by Edgar and Parker (1974).

Aenigmatite was the first silicate to crystallize for six out of seven samples under the conditions of low fO_2. The aenigmatite crystallized as a deep reddish brown pseudo-hexagonal thin platelets both singly and in "squadron formation", where platelets in small regions of the glass were all in parallel orientation, see plates 8-1 and 8-2. This presumably indicates regions of intermediate to long range order in the glass. The aenigmatite may be preceeded by an oxide phase, although a reaction is usually indicated due to disappearance of the oxide at and below the temperature of aenigmatite crystallization. At the silicate liquidus temperature the oxide reacts with the peralkaline component (Ns) of the melt to form aenigmatite. The incongruent melting of aenigmatite has previously been reported (Lindsley, 1971; Lindsley and Haggerty, 1971). Incongruent melting has also been noted for acmite (Bailey, 1969). Aenigmatite is followed by intermediate to potassic alkali feldspar and sodic hedenbergite in either order. The pyroxenes are prismatic while the feldspars are either lathlike, in the upper end of the melting range, or a matte

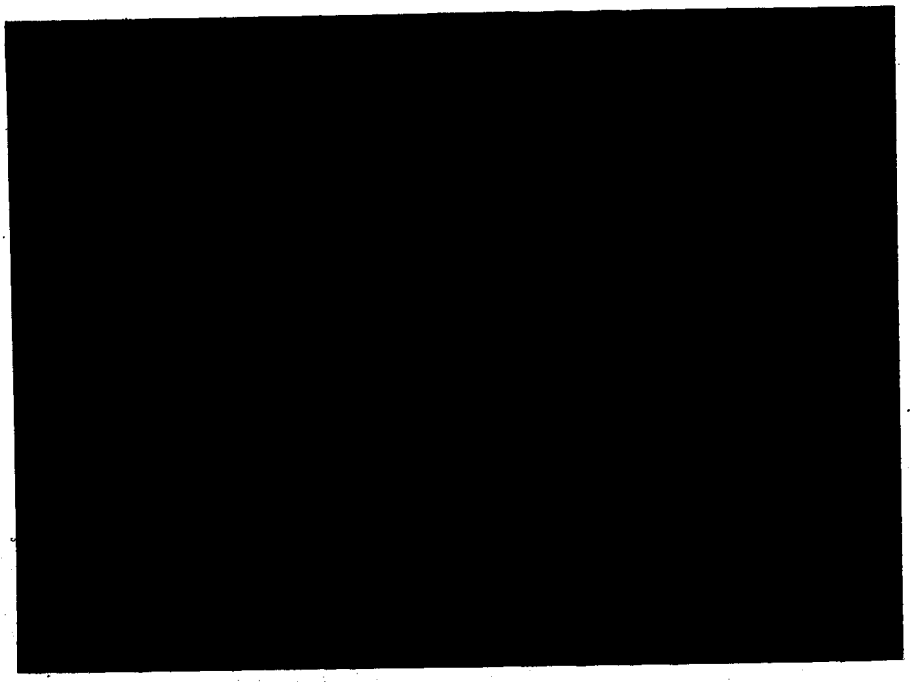

Plate 8-1.
Photomicrograph (P.P.L., 340x240microns) of a crystallization experiment on peralkaline trachyte 8/5-8/5150. Aenigmatite reddish brown pseudohexagonal platelets occur on the liquidus for T-fO_2 conditions between M-W and FMQ.

Plate 8-2.

Photomicrograph (P.P.L., 68x48microns) of a crystallization experiment on pantellerite 25/5e at 1201°C and log fO_2 = -8.78. Pseudohexagonal brown aenigmatite is followed at slightly lower temperatures by the crystallization of an oxide phase. Possibly having crossed the boundary curve for $Aen+O_2=TiMt+Nds+SiO_2$ as a result of the specific fO_2 conditions or early aenigmatite crystallization having lowered the peralkalinity sufficiently to shift the equilibria.

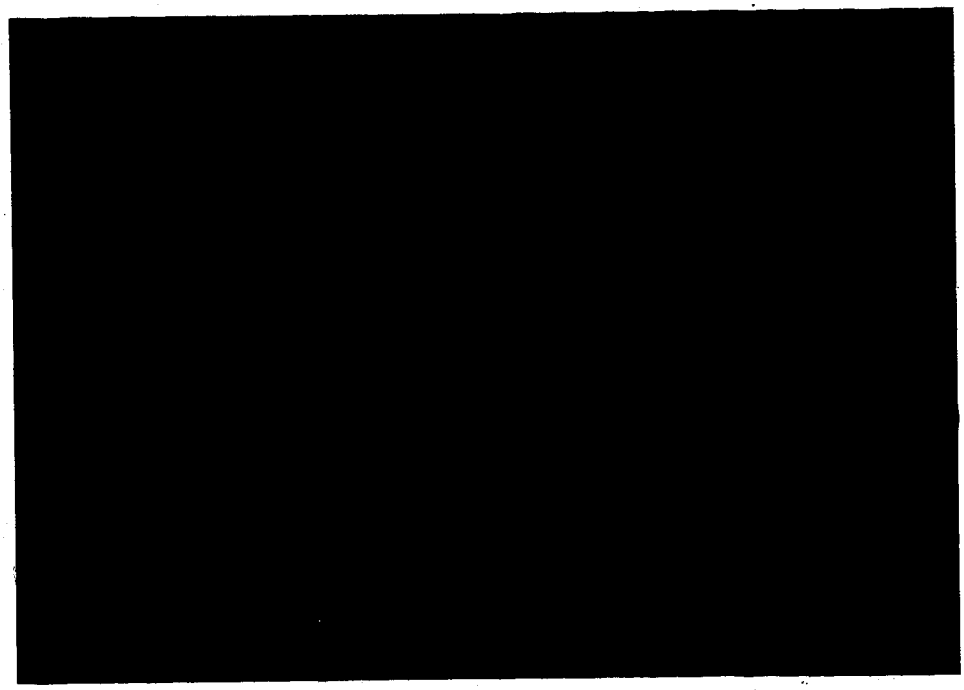

of microlites near the solidus. A bluish alkali amphibole, presumably riebeckite, was observed in one charge of pantellerite (25/5e) and in the mid-melting range of some of the earlier unbuffered experiments. The unbuffered experiments had slightly lower liquidus temperatures (average of five determinations 1138±35°C) with the sequence oxide, alkali feldspar, clinopyroxene, alkali amphibole or oxide, aenigmatite, alkali feldspar. In considering just the latter low fO_2 experiment, there is a great deal of variation in crystallization sequence and in temperature intervals between sequential appearance of the various silicate phases. This degree of variability in the crystallization behavior of these seven samples would not be expected from the small degree of compositional variation in the major element contents of these lavas.

CHAPTER 9. THE PHYSICAL BEHAVIOR OF LEVEL MOUNTAIN LAVAS

VISCOSITIES: ESTIMATED AND EXPERIMENTAL

Theoretical Viscosity Calculations

For lavas of known composition, viscosities have been predicted according to the model of Shaw (1972). These calculations were performed using a fortran computer programme supplied by J. Nicholls to give a log-linear expression of the form:

$$\ln \eta(\text{pascal-sec}) = A/T°K - B$$

which corresponds to newtonian behavior. This type of relationship has been shown to be valid above the liquidus temperature while below the liquidus the viscosities increase more rapidly due to the presence of crystals and the behavior is no longer newtonian (Shaw, 1969; Scarfe, 1973; Murase and McBirney, 1973). The conversion from SI to cgs units, which have been conventionally used is:

$$10 \text{ e } \exp(\ln \eta(\text{pascal-sec})) = \eta(\text{poise})$$

To characterize the expected variation in viscosity for Level Mountain lavas and to compare it to other British Columbia lavas, the theoretical anhydrous viscosity has been calculated at 1300°C. The range of predicted viscosities is tabulated as a function of rock type for Level Mountain and other Cordilleran lavas, table 9-1. The lowest predicted

---

[1] Throughout this chapter the symbol η is used to denote viscosity.

Table 9-1 Range of Predicted Viscosities as a Function of Rock Type

Rock Type	ln (pascal-sec)[1]	median
Alkali Basalts and Ankaramite	0.4 to 2.4	1.7
Hawaiites	1.8 to 3.4	2.7
Mugearites, Benmoreites and Phonolites	4.2 to 6.4	5.3
Trachytes and Tristanites	6.6 to 8.8	7.3
Comendites and Rhyolites	9.0 to 10.8	9.7

1. Viscosity calculated from chemical analysis on an anhydrous basis at 1300°C after the method of Shaw, 1972.

viscosities are for ankaramites and other basalts. Melts of basaltic composition have a high proportion of network modifier cations and a less polymerized polyanionic melt framework (Scarfe, 1973, 1977; Scarfe et al, 1979; Mysen et al, 1980). The highest predicted viscosities are for metaluminous rhyolites with comendites being slightly lower. The samples from Edziza and other late Cenozoic lavas in British Columbia display the same range of variation as seen at Level Mountain. For the purposes of comparison, all of these viscosities were calculated using dry chemical analyses. The effect of water is to de-polymerize the silicate melt by increasing the proportion of non-bridging oxygens. The calculated effect of this depolymerization for these relatively dry alkaline lavas is generally less than a few percent lowering in ln n and the inaccuracy introduced by comparing lavas at a single temperature of 1300°C should outweigh this. The value of 1300°C was chosen to be above, but close to, the liquidus for all of the alkaline lavas. This is about 35°C above the average basalt liquidus and 85°C above the average salic liquidus.

Experimental Viscosity Determinations

Three rocks were chosen to represent the basalt to comendite sequence at Level Mountain: hawaiite (8/25 - 50/6397), alkali basalt (PAP), and comendite (8/25 - 54/6345). For chemical analyses please see chapter on petrochemistry. Rock powders (which passed the 325 mesh screen) were prepared from these specimens. Experimental

work was performed by C.M. Scarfe at Sheffield University (Scarfe and Hamilton, 1980). Glasses free from bubbles and crystals were fused from whole rock powders, under reducing conditions, in a gas furnace at 1400° - 1600° , for two hours. Fusions were performed in alumina crucibles and the liquid was poured into a steel mold to make a glass slug whose diameter matched the internal dimensions of the outer cylinder of a concentric cylinder viscometer (Scarfe 1977). Under measurement conditions, the 8cc glass slug filled the cavity between the inner and outer platinum cylinders of the viscometer. During a measurement, shear across the silicate liquid transmits torque to the inner cylinder which results in an angular displacement. The displacement is recorded as a light spot deflection on a linear scale. At constant temperature, there is a linear relationship between rotation speed of the outer cylinder and angular displacement of the inner cylinder. This corresponds to a plot of shear stress versus shear rate, which for newtonian fluids is a straight line through the origin. All experimental determinations were performed in air. Viscosities are considered accurate to ±5°C in the range 1200°C to 1400°C. Starting glasses for the hawaiite sample were prepared under both oxidizing and reducing conditions. The resulting difference in measured viscosities was very small, with the reduced aliquot being slightly less viscous at any temperature. This could be related to enhancing the behavior of Fe as a network modifier under reducing conditions (Fe^{2+} rather than Fe^{3+}).

Results for the three Level Mountain lavas are presented in Figure 9-1. The apparatus was calibrated using NBS Standard 710, a soda-lime silica glass, for which the viscosity-temperature relationship is accurately known. Curves through experimental points are fit by hand. Dashed lines correspond to theoretically predicted viscosities. Viscosities calculated using the method of Shaw (1972) agree with experimental determinations to within 0.25 log units, with the predicted values being lower than measured values in all cases. A linear relationship exists between the logarithm of the viscosity and the reciprocal absolute temperature in the range 1300° to 1400°C. The temperature dependence of the viscosity can be described by an Arrhenius relationship of the form $n = n_0 e \exp(En/RT)$ where n_0 is constant for a given melt, and En is the activation energy for viscous flow. Activation energies for the Level Mountain lavas are in the range 98 kcal/mol for the comendite to 54 kcal/mol for the hawaiite. At any temperature above the liquidus the viscosity of the comendite is about three orders of magnitude greater than the basalts. For example, at 1300°C the comendite has $\ln n = 5.3$ poise as compared with $\ln n = 2.05$ and 2.60 for the basalts; ($\ln n = 9.4$, 3.6, 2.3 pascal - sec respectively). Despite the fact that theoretical and experimental data agree in predicting a high viscosity for comendite, this does not account for the apparent fluid nature of comendite flows at some locations on Level Mountain. Both experimental and theoretical data

Figure 9-1.
Plot of reciprocal absolute temperature versus log viscosity (in poise) comparing experimentally determined viscosities to Shaw model predictions, taken from Scarfe and Hamilton (1980).

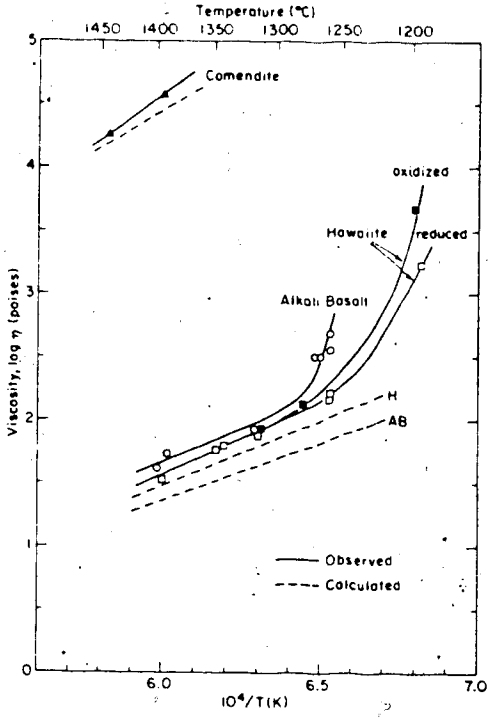

relate to a degassed dry sample. Under natural conditions of emplacement and extrusion, dissolved volatiles in the comendite melt, particulartily fluorine and chlorine (Bailey and MacDonald, 1975; Scarfe, 1977), may have reduced viscosities considerably below 10^5 poise. Degassing could eventually increase viscosity to the point where flow will cease (Nash and Evans, 1977). The other possibility is that comendite may acquire some degree of superheat (Marsh and Kantha, 1978) due to a peculiarity of the liquidus geometry in PT space and ascent path (Bailey et al, 1974). The only problem is that for the viscosity-temperature relationships presented here, an extrusion temperature of 1500°C would still give a viscosity too high to explain fluid features, lava tubes, thin flows (less than 3m thick), long low volume flows, lineations, flow folds and thin dykes (less than 1m thick) which have been observed in the field. Comendites should have a more polymerized melt than basalts due to high silica contents, high R=(Si+Al)/O (atomic) (Shaw, 1965; 1972) and low ratios of non bridging oxygens to tetrahedrally coordinated cations, principally Si and Al (NBO/T, Mysen et al, 1980). The precise effects of high Fe/(Si + Al), (Na + K), (Na/K) halogen content, and eruptive temperatures, as compared with these values in calc-alkaline rhyolites of similar silica contents, are unknown; however, all of these characteristics could contribute to a lower viscosity (Schmincke, 1974). Also there is probably a pressure effect which contributes to decreasing the

viscosity of salic melts due to a collapse of their one-atmosphere 3D polymer structure at higher pressures (Virgo et al, 1979). Characterizing the viscosities for the Level Mountain lavas is important to an understanding of their flow properties, extrusion rates and nodule transport.

CONSTRAINTS ON THE RISE TIME OF LEVEL MOUNTAIN LAVAS

Introduction

This section is devoted to placing physical and fluid mechanical constraints on the rise times and emplacement velocities of the various lava types found in the alkaline association at Level Mountain. Settling calculations have been performed for selected flow-nodule pairs. Some diapiric rise and heat transfer calculations are also presented. The data used in this section comes from a variety of places. Liquidus and solidus determinations were made on glassy charges suspended in a Deltech vertical tube quench furnace equipped for gas mixing. Oxygen fugacity was controlled to lie between FMQ and MW buffers using mixtures of CO and CO_2 after Dienes et al (1974). Viscosities are calculated at the liquidus and, when available, experimental values are used. Due to the dry nature of these lavas (see chapter on petrochemistry), the effect of wet versus dry viscosities is small, especially when compared to other assumptions made in model calculations. All of the liquidus data, eleven values covering the entire range of lava compositions, were plotted

as $10^4/T°K$ versus ln n(SI units) to give the following linear relationship at the liquidus:

$$\ln n = 18.75\ (10^4/T°K) - 117.91$$

with a coefficient of determination of $r^2 = 0.79$ as determined by least squares linear regression. This empirical expression was used along with the Shaw equation

$$\ln n = A/T°K - B$$

for each lava to predict liquidus temperature and viscosity where such data was not otherwise available. Reasonable liquidus estimates were also obtained using this expression and other B.C. alkaline lavas, the McKinney basalt, and some calc-alkaline andesites as well. It is conceivable that an expression relating viscosity and temperature should exist for a given volcano. This could be due to the mechanism of magma genesis for a related suite or perhaps due to the effect of common plumbing. Estimates of liquidus temperature and viscosity could also be made by comparison with other lavas without recourse to speculative and empirical expressions. The determination of the significance of this type of expression would require further research with additional data on viscosity and liquidus temperatures. The rational for using such empirical calculations on Level Mountain lavas was to be able to use values for actual host lava-nodule pairs.

Xenolith densities were analytically determined using a weight and volume displacement technique. Lava densities were calculated at the liquidus temperature after the method

of Bottinga and Weill (1970). The Bingham model of Sparks, Pinkerton, and MacDonald (1977) was calculated using their empirical graphs and SI units. Other calculations were done for convenience in cgs units.

Nodule Transport and the Ascent of Magmas

The majority of lava flows on Level Mountain are aphyric to fine grained and relatively free of phenocrysts. Newtonian flow models should be adequate for these lavas, however Sparks et al(1977) made a case for phenocryst laden alkaline lavas behaving as a Bingham fluid. It is conceivable that up to several flow volumes of alkali magma could be transported through the crust as crustal rich diapirs. Information relating to the physical properties of lavas used in model ascent calculations is presented in Table 9-2.

Petrographic and field relations suggest that most lavas were at or near their liquidus temperature at the time of eruption. Pleistocene basalts from Meszah Peak contain xenoliths of anorthositic gneiss, troctolite and gabbro. Of these the troctolite and gabbro are considerably denser than their host flow. Similar basalts of the adjacent Stikine canyon occasionally contain lherzolite nodules (Littlejohn and Greenwood, 1974). At three locations on Level Mountain peralkaline trachytes were found to contain armoured nodules of ultramafic composition and a positive density contrast with their host flows. A two meter wide tristanite dyke contained 5 cm long gneiss fragments with a positive density

Table 9-2. Physical Properties of Level Mountain Lavas

Sample #	Rock Type	Phenocrysts	Liquidus T°C	Solidus T°C	Density (at liquidus) g/cc **	Liquidus Viscosity Log (poise) *** Predicted	Measured
8/25-54/6345	Comendite	None (Obsidian)	1215° ± 10°	862° ± 13°	2.34	5.61	5.77
8/6-12	Comenditic Trachyte	Anorthoclase	1200°	-----	2.38	5.07	----
8/16-44/6250	Tristanite	Andesine, Barkevikite	1231°	-----	2.36	4.01	----
8/5-8/5150	Paralkaline Trachyte	Anorthoclase, Sodic Ferrohedenbergite	1250° ± 10°	862° ± 13°	2.36	3.94	----
PAP	Alkali Basalt	Forsterite	1275° ± 15°	1100° ± 15°	2.63	1.67	2.23
8/25-54/6397	Hawaiite	Labradorite	1270° ± 15°	1080° ± 7°	2.71	1.99	2.17
Hypothetical Lova	Alkali Basalt		1255°		2.70	1.00	

** Calculated after model of Bottinga & Weill (1970)
*** Calculated after model of Shaw (1972)
(Viscosities and densities are calculated using water+ of chemical analyses where any was present).

contrast. Further description of these nodule flow pairs is presented in Table 9-3 and in the chapter on petrography.

The existence of xenolith fragments in certain flows places two constraints on the rise times of these magmas. Where the nodule density is greater than the host lava and the nodule is sufficiently large, a slow ascent velocity would permit the nodule to settle out. If the solidus temperature of the nodule is below the liquidus temperature of the host magma, as it appears to be for most examples given here, the nodule should react, melt and possibly disaggregate. The rates of these phenomena depend on nodule size, relative thermal conductivities, grain size, fabric, chemical diffusivities and heat capacities of nodule and melt, as well as on the melt viscosity and flow regime. For the nodules to arrive intact at the surface, their residence time in the melt must be short enough to prevent either settling out or destruction.

For flow models involving a viscous compressible fluid and low concentration of spherical particles, the settling behavior changes as a function of frictional drag and Reynolds number. The Reynolds number is given by $Re=(ZrVe/n)$ (Bird, Stewart and Lightfoot, 1962). For $Re \leq 1.0$ the frictional drag is effectively a linear asympotic function of Re and the Stoke's Settling Law behavior is valid. For intermediate Re (1.0 to 1000.0) the relationship is a power law, where the friction factor (f) is given by $f=1.85Re\ exp(-0.6)$, reflecting the existence of a turbulent

Table 9-3. Characteristics of Xenoliths from Lavas of the Level Mountain Formation

Sample #	Rock Type	Modal Phases	T°C Solidus	(g/cc STP)	Max Size (cm)	Host Flow	Relationship
Level Mountain:							
MPM	Troctolite	Plag-ol-Cpx-Opq-Sp	1086°±8°	3.13	15 cm	Hawaiite 8/25-50/6397	CPX in Reaction W/Melt PLAG Partially Resorbed
8/6-12 N	Ultramafic	Cpx-Amph-Plag-Ne-Opg-Phlog	1078°±5	2.53	10 cm	Comenditic Trachyte 8/6-12/5290	nodules armoured by glassy reaction rinds
8/16-44 I	Gneiss	Plag-A.Flds.-Q-Amph-Opq	1080°±40	2.66	5 cm	Tristanite 8/16-44/6250	no Petrographic sign of melting
Heart Peaks:							
HP13 A	Essexite	Plag-Cpx-ol-Amph-Opq	1085°±75	2.85	> 10 cm	Hawaiite ?	no petrographic sign of melting. Sample from J. Casey
Telegraph Creek:							
TCL 1004-41	Lherzolite	ol-cpx-Cpx-Sp	1210°±22°**	3.37	5 cm	Alkali Basalt	no petrographic sign of melting. Sample from H.J. Greenwood
Hypothetical BC Lava	Lherzolite	ol-Opx-Cpx-Sp	1245°	3.3	3 cm	Alkali Basalt	CPX in Reaction W/Melt

* Hamilton 1980
* This solidus determination is comparable to the 1 bar data of Kushiro et al 1968 of 1200±5 & 1250±5 & Scarfe et al (1972) 1215±10

flow around the equator and in the lee of the particle. For high Re the friction is nearly independent f = 0.44 and the type of settling is in keeping with Newton's Law. The cutoff of Re = 2000 marks the onset of turbulent flow. Particle Reynold's numbers for relatively aphyric melts are typically smaller than 10^{-5} for salic compositions and between $2x10^{-}$ and 2x10' for basalts. For these crystal and nodule poor cases Stoke's law settling behavior should be reasonably valid. The greatest uncertainty is not the choice of the settling law, but the assumptions of viscosity and density contrast. For multiphase flow of crystal and xenolith mushes, the disperse particle theory no longer applies and particle boundary layers and particle interaction forces come into play. An alternate way of stating this is that in phenocryst laden melts there is significant crystal-crystal interaction which impedes flow. Bingham model ascent rates have been calculated for the Level Mountain examples according to the models of Sparks et al (1977). For the basaltic magmas a rapid ascent time is still implied. The Bingham model is not very informative when applied to the salic magmas. The minimum ascent velocities for nodule transport, rather than settling, imply maximum rise times on the order of tens of thousands of years. Upon consideration of cooling and crystallization processes and thermal conductivities of the materials in question, this is sufficiently long to cool salic magams by conduction alone. If ascent were this slow, plutonism rather then volcanism

would have occurred.

The model of Takeuchi et al (1972) assumes buoyant rise of melts through a lithosphere of greater density. In their model the minimum velocity for magma rise is given by

$$V = \Delta\rho g d^2/12\eta,$$

where d is the characteristic dimension of the conduit. These calculations have also been presented in Table 9-4 using an hypothetical conduit dimension of 10m, which is typical of high level vents on Level Mountain, and an assumed crustal density of 2.9g/cm^3, after the crustal model for the Intermontane Belt in Southern B.C. (Keen and Hyndman, 1979). Again the assumptions regarding geometry and viscosity have far greater effects than actual magnitude of density contrast. In all cases this buoyant magma rise model predicts velocities that are orders of magnitude faster than the minimum velocity limits set by nodule transport. This model presupposes a magma-filled conduit extending through the crust. The driving force is the magmastatic head (difference in lithostatic and magmastatic pressure at depth). For basalts this magmastatic head may be as high as a few kilobars (Maaloe, 1973). The model does not account for frictional effects or the pressure required to hold the conduit open. All limitations considered, this model should put a maximum constraint on ascent velocity. In this case the velocities calculated for the hawaiite and the "typical basalt" are 20 to 30% of the expected seismic velocities (Vp) in the crust. Velocities of this magnitude are also

Table 9-4. Model Ascent Velocities and Rise Times for Level Mountain Lavas

Sample#	Rock Type	Re	Newtonian Stokes	Bingham	r=10m Takeuchi	Maximum Residence Time (Days) Nodule Melting
8/25-50/6397	Hawaiite 7km	21.92	52.7;34.3,33.0 (1 day)	2.78×10^{-1} (3.4 yr)	1.67×10^{5} (18 sec)	(4.52×10^{-1}) 75.00 day
8/16-44/6250	Trachyte 5km	4.6×10^{-5}	4.0×10^{-2} (-145 day)	6.72×10^{-6} (2.36×10^{1} yr)	4.31×10^{3} (116 s)	(8.45×10^{-1}) 6.85 day
8/6-12/5290	Comenditic Trachyte 30km	1.4×10^{-6}	7.0×10^{-3} (13.7 yr)	1.16×10^{-6} (8.15×10^{4} yr)	3.61×10^{2} (2.3 hr)	(2.10) 16.50 day
8/25-54/6397	Comendite 30km	1.5×10^{-7}	2.5×10^{-3} (38.0 yr)	-----	1.12×10^{1} (7.4 yr)	-----
A.O.B. plus Lherzolite Nodules	Alkali Basalt 30km	3.97×10^{-1}	4.91 (7.1 days)	1.20×10^{-1} (79.2 yr)	2.59×10^{3} (12 sec)	(3.04) 11.43 day

- Velocities in cm/sec
- A depth of nodule incorporation is assumed for each sample to calculate rise times or velocity
- Re = Reynolds Number

expected from the arguments for magma emplacement in the crust governed by fracture propagation (Anderson and Grew, 1977). Using the model with its buoyancy drive mechanism, all types of magmas encountered at Level Mountain can rise from mantle depths in a matter of hours.

Rise times can also be estimated by calculating the time required to heat a nodule through its melting point. This is essentially a "Newton's Law of Cooling" calculation. Several assumptions and preliminary observations should be noted. In Clark (1966) it is shown that refractory minerals have higher thermal conductivities than melts of higher silica content. In keeping with this observation, an inclusion made up of refractory minerals will tend to have a very flat thermal profile as it heats up in a melt. Forced convection of the magma and turbulent flow will tend to transport heat to the nodule faster than assumed in these calculations, which will diminish the residence time to melting. For any positive density contrast (nodule greater than melt) some crossflow must exist so that this time estimate will be a maximum. Spherical nodules have the highest volume to surface area ratio so that any other geometry will enhance heat transfer and diminish time to melting. For this model the characteristic time is the duration of the heating process, only up until the nodule solidus is achieved. For real nodules once the solidus has been reached there will still be a finite time of melting associated with kinetic effects such as diffusion and

reactive melting. In this model, for steady state conduction, the rate of change of temperature with time is given by Tuma (1976) as

$$dT/dt = -hc\Delta TA/V\rho Cp$$

where hc = heat conduction coefficient, cal/cm²-sec-°C

ΔT = initial temperature differential, °C melt - nodule

A,V = surface area and volume of nodule, cm², cm³ respectively

ρ = density of nodule

Cp = heat capacity of nodule

The heat capacity, density and geometry of the nodule are assumed to be constant up until melting. To extend the model through melting, the heat capacity would have to be replaced by a term including the heat of melting and any excess heats of mixing associated with diffusion processes. For a spherical nodule geometry A/V = 3/r. Newton's Law of Cooling states

$$\Delta T(t) = \Delta T_o e \exp(-\alpha t)$$

where $\alpha = (dT/dt)/\Delta T_o$.

The only remaining quantity to be evaluated is hc. Kreith (1973) gives hc = kN/D where k is thermal conductivity and N is Nusselt's number, which for Reynold's numbers Re $\leq$10.0 is approximately equal to 2.0. Values of k for minerals and some rocks are published in Clark (1966). A sample calculation is presented for a general alkali basalt and a lherzolite nodule assuming the basalt to be at a liquidus

temperature of 1225°C, the lherzolite initially at 1045°, with a solidus at 1245°C (CO_2, 9.1kbar, Yoder, 1976). Then:

$$hc = (0.011)2/15 = 0.00147 \text{ cal/cm}^2\text{-sec-°C}$$

$$dT/dt = (-0.00147)3(210)/7.5(3.3)5.9(10) = 6.48\times10^{-4} \text{ °C/sec}$$

$\alpha = 3.08\times10^{-6}$, $T(t) = 10°$ and $T_o = 210°$.

Finally the heating expression can be rewritten in terms of t to give:

$$t = \ln (\Delta T(t)/\Delta T_o)/-\alpha$$

which with substitution of the appropriate values,

$$t = \ln(10/210)/-3.08\times10^{-6} \text{ gives}$$

$t = 9.87 \times 10^5$ seconds or 11.43 days.

Assuming the lherzolite to have become incorporated at a depth of 30km yields a minimum ascent velocity of 3.039 cm/sec. Depending on the assumed depths of incorporation for the inclusions the model ascent velocities are generally between those estimated by Stoke's Settling and buoyant rise, see table 9-4.

Carmichael et al (1977) present an ascent model whereby spherical magmatic diapirs rise buoyantly, yet frictionally retarded, through a very viscous upper mantle. The relationship they derive is $R^2 = 3Vn/g\Delta\rho$, where R is the effective radius of the magma diapir, V is the ascent velocity and n is the viscosity of the upper mantle. The value of n, derived from isostasy, and typically used in geodynamic arguments is 10^{21} poise (Cathles, 1975). A few trial calculations, using reasonable density contrasts and

assuming a value for either V or R to solve for the other, reveals unreasonably large radii, of hundreds to thousands of km, or unreasonably slow velocities, which for depths of 30 to 100km imply rise times of tens of millions to billions of years. The Cordilleran lithosphere is thinner and the upper mantle is softer, with lateral variations in the effective viscosity spanning two orders of magnitude at the 100km depth range (Ranalli, 1980). The diapiric transport calculation can be rearranged to estimate a viscosity for the upper mantle that would be volcanologically more reasonable. Consider a peralkaline trachyte flow, PBE from Meszah Peak. The volume of the flow is $4.8 \times 10^{-3} km^3$ for an equivalent spherical radius of 105m. Assuming a slow ascent velocity of 1.16×10^{-6} cm/sec, and densities for mantle and melt of 3.3g/cc and 2.4g/cc respectively, results in a calculated estimate for η(mantle) of 2.78×10^{16} poise. For a hypothetical diapir volume of $1km^3$, a velocity of 10^{-6} cm/sec and the same density contrast, the value of is 1.13×10^{18} poise. This begins to look plausible for the situation of a partially molten upper mantle and transport of diapirs having about 10 flow volumes worth of magma. For the ascent velocity of about 10^{-6}cm/sec, it would require approximately 42,000 years to traverse 13km of upper mantle. The evidence from age dating attempts suggests that the major eruptive periods are separated in time by tens of thousands of years. This coincidence lends support to the buoyant diapir concept and calculations discussed.

Assuming that all of the Level Mountain lavas rose as a single magma diapir from a hypothetical depth of melting and segregation of 105km to 30km. The total volume of volcanics is 1500km^3 for an equivalent diapir radius of 7.1km. As the lavas are predominantly basic, a more reasonable density contrast is 0.6g/cm^3. For a normal upper mantle viscosity (10^{21} poise), the calculated ascent velocity is 9.89 x 10^{-8}cm/sec and the traverse time to the base of the crust is 7.58 x 10^{13}sec or 2.4MY. The age for the lowest flows sampled in the Little Tahltan Canyon is interpreted from paleomagnetic evidence to be about 6.4MY. The combination of these two ages, 8.8MY, should be close to the origin time for the Level Mountain magmas. In Hamilton, Baadsgaard, and Scarfe (1978) a whole rock Rb-Sr age of 9.4±1.0MY was reported and interpreted as possibly representing some precursor thermal event in the upper mantle. The coincidence of the reported and the modelled date may lend some support to the mantle diapir model.

Carmichael et al (1977) in using the same model, and reasonable model parameters for alkali basalts and tholeiites, derived an apparent viscosity for the upper mantle of 5.3×10^{9} poise. They concluded that, while this is unlikely to represent the viscosity of the whole upper mantle, it could represent the viscosity of a thin lubricating sheath of partially fused mantle material surrounding the diapir. They also did a conductive heat loss calculation, inferring a drop of about 2°K for flow sized

bodies ascending at typical nodule settling velocities.

Carmichael et al (1977) also calculated convective heat loss for these magma diapirs with thin boundary layers. For diapirs in the volume range 0.03 to 0.185km^3, the boundary layers were all less than 40cm thick, which is one per mil of the diapir radius. The temperature losses associated with laminar boundary layer convection were 21° and 7° respectively. The losses corresponding to a turbulent boundary layer were higher, 86° and 39° respectively. Using the appropriate physical parameters for the Level Mountain hawaiite flow, 8/25-50/6397, and a model transport from 100km, the laminar convective boundary layer model gives a temperature drop of 3° while the turbulent case was 23°C. Convective heat losses offset by proportional crystallization could be a significant driving force and mechanism for differentiation even at mantle depths. This might be a means to derive large volumes of hawaiite from a more primary composition while still in the mantle depth range.

In addition to conductive and convective heat losses some other types of heat changes need to be considered. The adiabatic gradient is given by Yoder (1976) to be between 0.2 and 0.5°C/km. This is equivalent to -20° to -50° for a 100km path. For isenthalpic decompression, Waldbaum (1971) cites a value of adiabatic heating on decompression which may be as great as 22°C per kilobar. Clearly this is a mechanism to offset convective heat losses and even perhaps

to provide superheat for an ascending magma body. This mechanism could provide sufficient heat for a magma to assimilate significant quantities of wall rock, whether in the upper mantle or crust. Here the ascent velocity would be the crucial parameter. Again it is pointed out that any rising magma must undergo decompression and, if this can generate heat and drive assimilation processes, it may be difficult indeed to transport and erupt a primary magma. Thermal changes due to viscous heating and transportive friction may also be significant but their effect is thought to be less than adiabatic and convective effects (Carmichael et al, 1977).

VOLUME ESTIMATES OF LEVEL MOUNTAIN VOLCANISM

Volume estimates have been made for thirty-five typical eruptive events from Level Mountain. Estimates have been made for single eruption flows, tuffs, domes, and dykes representing the entire range of compositional types. Although estimates cover the time span of volcanic activity, the younger events are more heavily represented due to preservation and mappability. Dyke and vent pipe thicknesses were estimated at the base of the plateau as this was the volume of material added to the volcanic pile during an eruptive event. Volume estimates are presented in Table 9-5 along with characterizing information for locality, map unit = age, and composition. The entire range of volumes is 6.12×10^8 m^3 (0.612km^3) to 1.02×10^6 m^3 (0.001km^3). Typical

Table 9-5. Volume Estimates of Some Level Mountain Eruptive and Hypabyssal Events

Map Unit	Magma Type	Feature	Locality	Volume M³	(km³)	
4	Alkali Basalt	Dyke	N.E. Plateau	5.28x10⁷	0.528	
3	Alkali Basalt	Dyke	W Fork Beatty Ck.	9.25x10⁷	0.093	
9	Ankaramite	Cockscomb Dyke or Lava Field 16/19	Wrathall Plateau (NE)	3.17x10⁷	0.032	Dykes Avg (6) 0.121±0.82 km³
9	Ankaramite	Dyke	Wrathall Plateau	3.15x10⁷	0.032	
9	Ankaramite	Vent Pipe Flow	Wrathall Plateau	9.59x10⁶	0.010	
9	Ankaramite	Dykes & Flows	Wrathall Plateau (SW)	3.68x10⁷	0.368	
1	Ankaramite	Flows	Little Tahltan Canyon	6.25x10⁶	0.006	
9	Alkali Basalt	Tuya 01	Little Ketchum Lake (SW)	2.61x10⁶	0.003	
4-9	Basalt	Tuya	Eastern Plateau	1.76x10⁶	0.002	
6-9	Hawaiite	Scoria Vent 69/6178-6183	Hanging Valley S. of Meszah Peak	7.60x10⁶	0.008	
3	Ankaramite	AA Flow	Western Plateau Margin	1.02x10⁶	0.001	
2	Alkali Basalt	AA Flow 6/3240	Little Tahltan canyon	1.20x10⁷	0.012	Flows Avg (13)
3	Palagonite Tuff Breccia	------- 75/8/PT	Western Plateau Margin	5.44x10⁷	0.054	0.012±.004 km³
8-9	Alkali Basalt	Columnar Flow 24/2	South Dudidontu Ridge	7.62x10⁶	0.008	
2	Basalt	Ponded Flow	Eastern Plateau	1.94x10⁷	0.019	
8-9	Hawaiite	Columnar Flow 80/6375	North Ridge Kakuchuya Valley	3.88x10⁶	0.004	
4	Hawaiite	Columnar Flow	Western Plateau Margin	1.50x10⁷	-----	
3	Basalt	Columnar Flow PAP	Little Tahltan Canyon	1.60x10⁶	-----	
9	Hawaiite	Scoria & Ponded PBT	Meszah Peak Summit	2.01x10⁷	-----	
7a	Trachyte	Stock 8/25-52/5880	N. of Meszah Peak	6.12x10⁶	-----	
7c	Tristanite	Dyke 8/16-44,LMIIIA	Central Chain	1.44x10⁷	-----	Avg (8) cones, stocks, dykes 142±0.68 km³
6a	P. Trachyte	Flow PBE	Hanging Valley S. of Meszah Peak	4.80x10⁶	-----	
7b	Comendite	Glassy Dykes 8/25-52/6890	Divide Beatty/ Kakuchuya	4.00x10⁷	-----	
7b	Trachyte	Dome 60/6350	Divide Beatty/ Kakuchuya	8.08x10⁶	-----	
6a	Pantellerite	Tuff 8/10-1/4925	Fork of Beatty Creek	1.91x10⁶	-----	Avg (8) flows, tuffs, sills .008±.002 km³
6a	Pantellerite	Tuff 8/11-29	S. Valley Vall. N. Fork Beatty Cr	1.92x10⁷	-----	
7a	Rhyolite	Tuff & Scoria 79/6700	Ridge ESE of Meszah Peak	5.33x10⁶	-----	
7a	C. Trachyte	5 Tuff & Scoria Domes LMI20 Bomb	Beatty/ Dudidontu Divide	9.42x10⁷ each	-----	
6a	C. Trachyte	Laccolith/Sill 92/5060	Kakuchuya Valley	4.80x10⁶ 4.80x10⁶ 1.17x10⁷	-----	Basic Avg (19) Salic flows & tuffs 1.058±.78x10⁷

historic basalt flow volumes from Hawaii and elsewhere are given as 0.03 and 0.185km^3 (Carmichael et al, 1977). The average volume of five post-glacial basalt, basanite and nephelinite cinder cones from the Cariboo, Chilicotin and Stikine regions of B.C. is 0.0134 km^3. A large Pleistocene basaltic tuff cone near Jacques Lake (Campbell, 1961) has a volume of 0.126km^3. Compared to these, the Level Mountain events appear to be of ordinary size. The volume estimates have been subdivided into basic and salic types as well as into flows versus hypabyssal intrusions. It is apparent that at Level Mountain the dykes, stocks and domes are an order of magnitude larger in volume than the flows and ejecta. Flow volumes are taken to be single eruptive events, while dykes and stocks may be intermediate in size between eruptive events and eruptive episodes. There is no statistical difference in size for basic versus salic types in either the eruptive or hypabyssal group. This would seem to indicate that eruptive volumes are determined by common energetics of magma rise or by a common set of volcanic plumbing, rather than by the relative volumes of melting or differentiation events.

The volume of eruptive episodes, taken to be synonymous with the sequential map units, have been estimated using topographic maps at 1:50,000 scale for elevation control and a grid overlay for area. Volumes have been reconstructed to include materials eroded form the plateau margins and youthful alpine glacial valleys. Model densities have been

assigned to each unit on the basis of average physical and chemical properties for rock types present. Time spans for map units have been estimated from all available sources of field and laboratory data. The average time intervals between flows have been calculated for a typical flow volume of 0.01km^3 in size. This data is summarized in Table 9-6.

There have been approximately 85,000 flow sized eruptions at Level Mountain over a time period of about 6 to 7MY. The lifespan of the volcano is clearly divided into 39% initial plateau building and a 61% later stratocone development. The average time span calculated for flows of the plateau building period is 43 years while for the statocone development phase the interval is 226 years. Field mapping and geomorphology indicate that the activity was likely to have been more intense with widespread contemporaneous eruptions separated by periods of hundreds of years of quiescence. The figure of 43 years for the plateau period seems reasonable as there was insufficient time between sequential flows for extensive soil development or vegetation to have occurred.

Of the total 857.6km^3 of volcanics, 80.8% was basaltic while 19.2% was salic and dominantly peralkaline. The plateau building site was wholly basaltic. The stratocone stage, with a repeated bimodal process, was 85% salic in character.

In addition to the Level Mountain Volcanism, the volumes have been estimated for the other major centres in

Table 9-6. Volume and Mass Estimates for Level Mountain Volcanisms as a Function of Time

Map Unit or Magma Pulse	Time Span M.Y.B.P.	Duration	Dominant Composition	Volume (km^3)	Model Density	Mass in Kg.	Years/Flow
8-10	1.2 -0.0	(1.2)	basic	0.83	2.84	2.36×10^{12}	14,458
7a-c	2.4 -1.2	(1.2)	salic	55.85	2.61	146.0×10^{12}	215
6b	3.25-2.4	(1.05)	basic	14.17	2.86	40.5×10^{12}	188
6a			salic	41.68	2.56	107.5×10^{12}	
5b	4.2 -3.25	(.95)	basic	15.00	2.82	42.4×10^{12}	116
5a			salic	67.11	2.44	164.0×10^{12}	
4	4.6 -4.2	(.4)	basic	165.79	2.71	$449. \times 10^{12}$	24
3	5.6 -4.6	(1.0)	basic	165.79	2.77	$459. \times 10^{12}$	60
2	6.3 -5.6	(0.7)	basic	207.19	2.78	$576. \times 10^{12}$	34
1	7.0 -6.3	(0.7)	basic	124.18	2.73	$339. \times 10^{12}$	56
			Total	857.59	Avg 2.71	Total 2325.26×10^{12}	

for an average flow volume of 0.01 km^3
and an time span of 7×10^{4} yr.
this means an average of one flow per 82 years

the Stikine Volcanic Belt. This information is presented in Table 9-7 along with some estimates of dimensions pertaining to the source region. The total 1710km^3 of volcanics outcrops over an area of 8629km^2 in the Stikine Volcanic Belt which has a total area of 70,000km^3. The volumes and areas of the eleven major volcanic centres of the Stikine show a logarithmic distribution. Level Mountain and Mount Edziza are the largest in both area and volume. Using the total volume estimated and a time span of 5MY, it is apparent that the Stikine Volcanism is small in comparison to the Columbia River Plateau or the East African Rift and that the extrusion rates are lower by two orders of magnitude.

The volume data on the Stikine volcanism can be used to evaluate two possible source models. The two models are (i) partial melting of a slab of upper mantle and (ii) upper mantle diapirs below each of the eleven major centres. The slab hypothesis (using the surface outcrop area as an estimate of source region extent) implies the removal of a layer up to 180m thick beneath the volcanic centres. If the volume is derived over the extent of the Stikine Volcanic Belt, the removed layer may be as thin as 23m. When these slab calculations are performed for each centre, the calculated layer thickness varies from 76m to 532m with a mean of 235m and a standard deviation that is 33% of the range. Assuming that 5% to 25% partial melting accounts for the volcanics, and that this volume may be efficiently

Table 9-7. Total erupted volumes for the Major Centers of the Stikine Volcanic Belt

Center	Lat.N/Long.W	Vol (km^3)	Surface Area (km^2)	Source Region Estimates Slab Thickness (m)	Spherical diapir radius (km)
Kawdy Plateau	58°52'/131°10'	35	997	35	2.029
Heart Peaks	58°38'/132°00'	100	499	200	2.879
Level Mountain	58°25'/131°15'	860	3324	259	5.899
Tahltan Plateau	58°05'/131°35'	50	184	272	2.285
Stikine River	58°00'/131°00'	5	66	76	1.061
Mt. Edziza	57°30'/130°40'	500	1773	282	4.924
Tanzilla Plateau	58°30'/129°35'	35	166	211	2.029
Castle Rock	57°52'/130°15'	10	50	200	1.337
Klastline Plateau	57°25'/129°50'	50	1440	35	2.285
Hoodoo Mtn.	56°44'/131°20'	40	83	482	2.122
Iskut River/Mt. Dunn.	56°38'/130°45'	25	47	532	1.814
	Total	1710	Total 8629	Mean 235	Mean 2.606
				s.d. 162	s.d. 1.484

removed, implies a thickness for the melting region of between 0.94km and 4.70km for the mean figure quoted, or 0.092 to 0.460km for the minimum case of partial melting below the entire belt. When the eleven estimates are considered as a population, the distribution is normal and 85% of the entire Stikine Volcanism is accounted for within a thickness variation of ±0.5 standard deviation of the mean. All of the thickness estimates lie within ±2 standard deviations of the mean. From these model data it appears geologically reasonable that the Stikine Volcanism could originate from a thin zone of partial melting.

For the thermal model presented in this chapter, the partial melting zone could be as thick as 6km. Using this as a maximum estimate, and keeping the same levels of partial melting, an estimate of melt extraction efficiency can be made. A relatively inefficient melt extraction process has been inferred from studies of lherzolite textures (Waff and Holdren, 1980). For the case that melt generation is localized, the efficiency of melt extraction is between 78.3% and 15.7%, while for the case of a general partial melting zone beneath the entire Stikine, the melt extraction efficiency is between 7.7% and 1.5%. In either case a period of partial melting results in a considerable amount of material that may be left behind. For basaltic partial melts, the melt that stays behind could generate regions of gabbro in a more ordinary peridotite upper mantle. The idea of inefficient melt extraction is important to the concept

of upper mantle differentiation but has been proposed on other terms (Mysen and Boettcher, 1975; Lloyd and Bailey, 1975; Boettcher and O'Neill, 1980). Sufficient preconditioning of the upper mantle to generate gabbroic pods (plagioclase plus pyroxene) could result in the derivation of more salic magmas in subsequent partial melting events. It is noteworthy that the three largest centres of the Stikine have both the long spans of activity and the salic lavas one would expect from such a two stage process.

The second source model for the Stikine postulates separate diapirs below each of the centres which, successively tapped, could account for the cumulative individual volumes. For a spherical diapir model, the radii so calculated for the 11 Stikine centres are normally distributed. The mean radius is 2.61km and the range is 1.06km to 5.90km with a standard deviation that is 31% of the range. Unlike the slab calculation, only 12% by volume of the Stikine Volcanism is accounted for by average sized diapirs. Another way of stating this conclusion is that, if diapirism explains the Stikine volcanism, the diapir size is highly variable. This implies that 88% of the volcanism must be accounted for by two mega diapirs of extraordinary size. Therefore the first source mode (slab partial melting) in localized or widespread regions seems to be the more reasonable hypothesis.

THE ENERGETICS OF MELTING AND RISE

The Energetics of Volcanism at Level Mountain and for the Stikine

Volcanism can be considered as an energy dissipation process. The thermal requirements to initiate and maintain this process include mantle preheating, phase change energy associated with melting, and the work performed in magma transport to the surface. The total energy released at the surface can be considered as a contribution to the total heat flow.

As a monitor of the Level Mountain volcanism, the total energy dissipated will be considered as a function of time. The timing comes from magnetostratigraphy and limited age dating control. Mass estimates for successive units were derived from field mapping and laboratory density measurements. Three energy terms are considered. The cooling of lavas from their liquidus temperatures to surface conditions is expressed as a heat capacity intergral, using heat capacities for typical flows from each unit as calculated in ROCK. Due to the small variation (± 50°) in liquidus temperatures, regardless of lava composition, the value of 1200°C was used for all calculations. The heat of fusion values apply to liquidus temperatures for specific compositions considered representative of each unit. The transport work is expressed as a potential energy term (mgh) for the total mass of each map unit and the constant depth

of 35km. These data and calculations are summarized in Table 9-8. The largest energy contribution for each unit is the cooling term which is about five times the heat of fusion. Map units 5a, 6a, and 7a-c are dominated by salic lavas. The energy components of salic lavas are distinctive. Due to the low heats of fusion for salic lavas, the lift energy required for magma transport exceeds the phase change energy. For the remaining units, dominated by basaltic compositions, the reverse is true.

A graphical representation of the cumulative energy dissipated by Level Mountain volcanism is presented in Figure 9-2. The energy ploted is the sum of three terms discussed above. The graph should be read as: 0.979×10^{21}J was dissipated between the onset of volcanism and 6.3 MY before present, etc. Two and possibly three distinct stages are present. The shield building basaltic volcanism (units 1 to 4) has the highest rate of energy dissipation, such that 79% of the total energy expended had occurred by 4.2MY before present. The overall rate (which appears to be constant) was 1.87×10^{21}J/M.Y. For the plateau surface area of 3324 km^2, this rate is equivalent to 17.8 mW/m^2. The closest heat flow measurements in northern British Columbia are Dease and Hotailuh which average 73.5 mW/m^2 (Jessop, Souther et al, 1980 in prep.). Presuming the heat flow to be similar at Level Mountain during plateau building times, then volcanism represents 24% of the total heat flow. The next stage, roughly equal in duration, corresponds to the

Table 9-8. Energy Dissipated by Level Mountain Volcanism

Map Unit or Magma Pulse	Mass (1012 Kg)	CP (J/Kg K)	1500 SepdT cooling (1018 J)	H (1018 J)	Mgh (1018 J)	E by pulse (1018 J)
8-10	2.36	1390	4.92	0.89	0.81	6.62
7a-c	146.0	1360	299	39.7	50.1	388.80
6b	40.5	1411	85.7	15.3	13.9	114.90
6a	107.0	1381	222.	29.1	36.7	287.80
5b	42.4	1424	90.6	16.0	14.6	121.20
5a	164.0	1345	332.	44.8	56.3	433.10
4	449.0	1405	947.	169.	154.	1270.0
3	459.0	1450	999.	173.	158.	1330.0
2	576.0	1433	1240.	217.	198.	1655.0
1	339.0	1446	735.	128.	116.	979.0
						6586.42X10^{18}J

Figure 9.2.
Cumulative energy dissipated by Level Mountain volcanism.

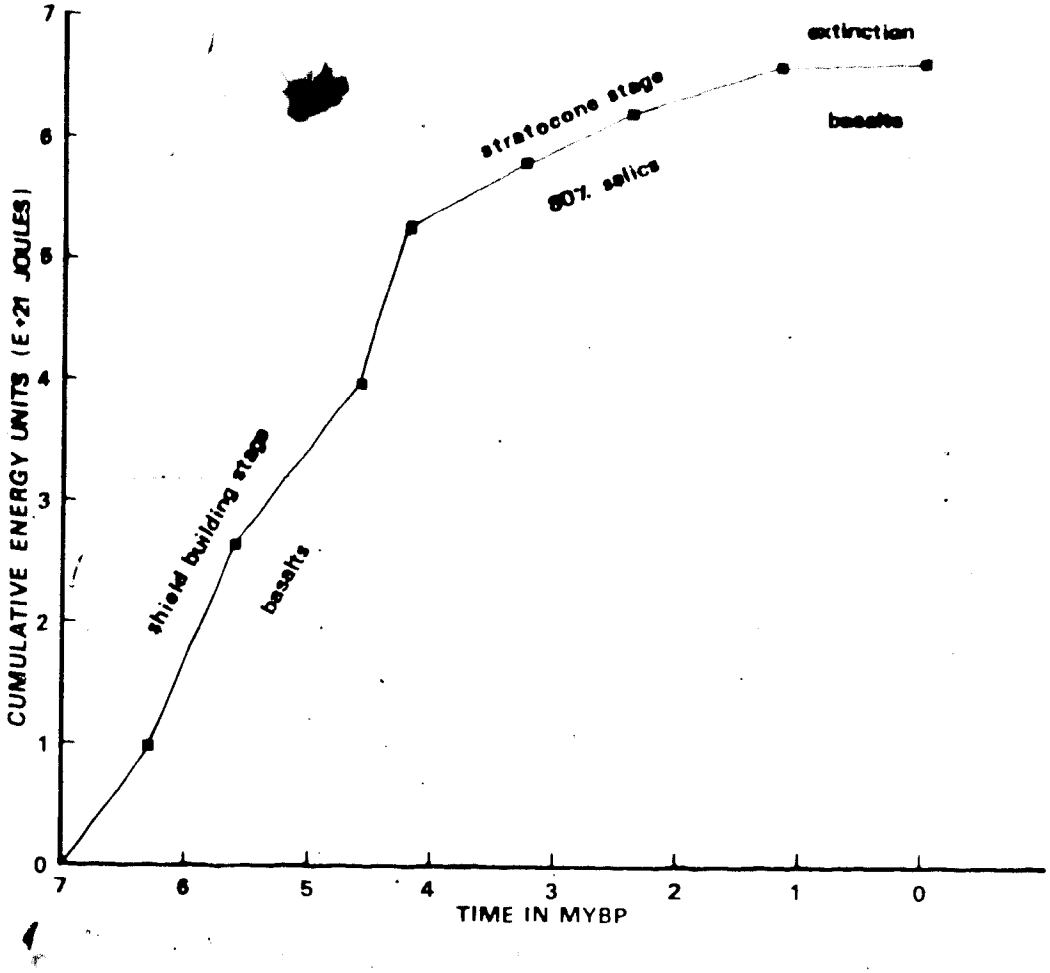

bimodal volcanism and stratocone building. Eighty two percent of the energy dissipated in this stage is by salic lavas. The rate here (also constant), is 0.45×10^{21} J/MY, which is only 25% of the previous stage. However the surface area of the stratocone cap is only 20% of the plateau as a whole; expressed in heat flow units the rate for the stratocone stage is 7.15 mW/m^2. This is still less than half of the shield rate, and only 9.7% of the modern heat flow values.

The final 1.2MY, with its low volume hawaiites and alkali basalts, represents another reduction in the rate and possibly signifies the extinction of Level Mountain. However. if the rate of the statocone stage is extrapolated to the present, the time period is about right for the release of another fifty cubic kilometers of lava. Mountain and for the Stikine as a whole. While the preceeding discussion dealt with the development of Level Mountain volcanism and the total energy dissipated by the process, the following section considers the minimum thermal requirements to initiate and maintain the volcanism. Basic data for these calculations and the results are presented in Table 9-9. Assuming the mantle source region to be at the solidus temperature, two additional energy requirements must be met: (i) the heat of fusion for the melts and (ii) the potential energy change associated with the magma transport. The energy dissipated through normal heat flow is calculated for Level Mountian and the total volcanic area within the

Table 9-9. Energy Requirements of Volcanism

	Level Mountain	Stikine Total
LAVA Volume (Km^3)	860	1710
LAVA Mass ($10^{12}Kg$)	2325	4634
Surface Area (Km^2)	3324	8629
TIME SPAN (my)	7.0	7.0
Heat of Fusion (cal/g)	85.5	86.6
SOURCE Volume * Km^3	15,623	40,556
SOURCE MASS $10^{12}Kg$	57,556	133,835
Cp J/kg°K for 1050°C 4 phase spinel peridotite	1300	1300
Modern heat flow mw/m^2		73.5
Total heat flux for 7my (J)	5.4×10^{22}	1.4×10^{23}
a) H (J)	8.32×10^{20}	1.68×10^{21}
2) Mgh (J)	7.98×10^{20}	1.59×10^{21}
I. BASE CASE HEAT (J)	1.63×10^{21}	3.27×10^{21}
$1+2$ equivalent heat flow mw/m^2	2.2 (3% of HF)	1.7 (2.3% of HF)
T from 12% of H.F. (°K) available for source heating	96	97
II. Total heat budget for 96° heating (J)	860 8.11×10^{21}	1710 2.0×10^{22}
equivalent heat flow mw/m^2	11.0(15% of HF)	10.5(14% of HF)

* Source volume has same surface area and 4.7 km thickness

Mass conversion assumes mantle source density of 3.3 g/cc

Stikine for the last 7MY. For the Stikine this value is 1.4×10^{23}J. For Level Mountain this works out to 3% while for the total Stikine Volcanic region it is 2.3% of present heat flow for northern British Columbia.

Additional energy would be required for pre-heating of the mantle source region. For this calculation model source region dimensions are estimated from the surface outcrop of volcanism and a slab thickness of 4.7km. Source region density was assumed to be 3.3g/cc. The heat capacity for a four phase spinel periodite was calculated from data in Robie, Hemingway, and Fisher (1978) to be 1300 J/kg-°K in the temperature range of interest. The heat capacity integral was solved for a temperature interval by assuming an amount of heat potentially available. Less than 40% of a surface heat flow value of 73.5 mW/m^2 probably arises from a steady state mantle contribution. A value of 12% of the total heat flow is equivalent to 30% of the mantle heat flux. This implys that less than 100° of heating can be performed over a 7MY period. Obviously heating of this type requires geologically long periods of time, or high heat fluxes, or small source regions in some combination. For the 12% pre-heat budget cited above, the pre-heat requirement is 80% and 84% of the total energy requirements for Level Mountain and the Stikine respectively. If the energy requirement for volcanism is expressed in heat flow units, these heating models represent about 15% of the modern heat flow discussed above.

The low volume alkali magmatism for the Late Cenozoic and the Stikine could be initiated and maintained by a thermal contribution equivalent to a small percentage change in the normal heat flow. If the source region must be heated to the peridotite solidus through an interval of a few hundred degrees, in the space of a few million years, an increase equivalent to 25% of the normal heat flow may be required. On the other hand, an increase in available heat as low as 2.5% could initiate and maintain alkaline volcanism from a source region already at the periodite solidus.

As a final note, the total energy dissipated through volcanism in the Stikine can be compared to a change in tectonic strain or potential energy. This can be likened to a release of mantle strain energy through subsidence of the crust over the entire Stikine Volcanic Belt. The area of the entire Stikine Volcanic Belt is estimated to be $7.19 \times 10^{10} m^2$. For 25km of crust of mean density $2800 kg/m^3$ the total mass of crust under the Stikine is $5.03 \times 10^{18} kg$. Using the expression $E = mgh$ to equate the dissipated heat and potential energy (where: $E = 1.11 \times 10^{22} J$ $m = 5.03 \times 10^{18} kg$ and $g = 9.81\ m/s^2$) h can be calculated to be 225m. The efficient release of about 0.2km of strain build up over an area the size of the Stikine Volcanic Belt is equivalent to the energy released as volcanism. Whether such tectonic strain preceeded the Late Cenozoic volcanism or actually was responsible is unknown. The release of a geologically small

amount of tectonic strain through a melting process could be responsible for this type of low volume alkaline volcanism without recourse to unusual compositions or events in the upper mantle, or large scale lateral geological movements, such as treated in plate tectonics theory. A model of strain release through volcanism is particularly appealing for the Intermontane Belt as the strain release through seismicity is anomalously low (Milne et al, 1970).

MODELLING OF A HEAT-FLOW AND A GEOTHERMAL GRADIENT FOR LEVEL MOUNTAIN AND THE STIKINE

The intent of this section is threefold, first to review existing Cordilleran heat flow data, second to calculate a steady state conduction model and third to construct a preferred PT model for the geothermal gradient under the Stikine and relate it to the origin of the Level Mountain volcanics. The steady state conduction model is in general, representative of continental geotherms. These continental geotherms are characterized by surface heat flow in equilibrium with heat flowing into the base of the lithosphere, plus a term for internally generated heat from radioactive decay (Pollack and Chapman, 1977).

A review of existing Cordilleran and Canadian heat flow measurements is presented in Table 9-10. It is noteworthy that the value of 73.5 mW/m^2, used for the Stikine in the preceeding section, is virtually identical to the Western Canadian average. The Cordilleran values are somewhat higher

Table 9-10. A summary of Cordilleran and Other Canadian Heat Flow Data

Cordillera		mW/m²	Corrected[1]	Gradient °C/km
Buckley lake		67	74	
Dease		91	100	
Hotailuh		56	62	
Penticton*		67	79	34.7
Canadian, average heat flow by region, uncorrected				
Maritimes	(3)	38.5	Eastern Canada	
Quebec	(4)	32.2		
Ontario	(12)	41.0	36 ± 2	
Manitoba	(1)	33.5		
Alberta	(2)	64.1	Western Canada	
N.W.T.	(1)	83.7	73 ± 6	
Cordillera	(4)	70.3		

data from (Jessop, Souther et al 1980 in prep.)
(Jessop and Judge, 1971)
(Lee and Clark, 1966)

1. Corrected for the effect of Pleistocene glaciation after the measurement of Jessop (1971).

than the continental average of 42 mW/m^2, but not so high as many of the circum-Pacific regions which may have values as high as 170 mW/m^2. Northern B.C. lies on the northern extension of the Western North American thermal high, with a regional heat flow of about 70mW/m^2 (Pollack and Chapman, 1977). For the Cordilleran thermal anomaly zone, there is a sharp eastward gradient of decreasing heat flow (Roy et al, 1968). Within the thermal anomaly both the crust and mantle are hotter than to the east. The corrected shallow geothermal gradient deduced for Pentiction (Jessop and Judge, 1971) is also high for a continental geotherm.

A model for heat flow at Level Mountain has been constructed assuming a simple three layer geometry. The model, in general form, is steady state conductive heat transfer through a series of arbitrarily wide parallel plates of known thickness and conductivity. The solution to Laplace's equation is given by:

$$Q/At = \Delta T/SUM(l(i)/k(i)).$$

The lefthand side of the equation is heat flux per unit area per unit time, and the right hand side is the net temperature difference across all the layers, divided by the sum of the individual layer thickness-thermal conductivity quotients. Q/At is replaced by a heat flow value and the k corresponds to geologically reasonable choices for layer compositions. With these values set, the thicknesses and temperatures are no longer independent variables so that a geothermal gradient can be calculated within acceptable

petrological and geophysical constraints.

The preferred model for steady state heat flow is 81.7 mW/m^2 with a two layer crust and one layer upper mantle characterized by:

	l (km)	k (W/m°K)
crust 1	1.50	3.14
crust 2	23.95	2.2
upper mantle	-----	3.22

The major limitation of this model is probably the steady state assumption. The model and selected solidus/liquidus data are presented in figure 9-3. Higher heat flow values would cause unrealistically high geothermal gradients that do not agree with geophysical or petrogenetic constraints. Lower heat flow values (10%) would depress the melting zone to depths below 48km which is considered unlikely. Variations at this level correspond to lateral temperature gradients of less than 0.6°C/km, which could explain the narrowness of the volcanic areas in the Intermontane Belt. Such small differences be supported by the natural variation in thermal conductivity with temperature for peridotites, by changes in proportion and composition of phases, or by very small amounts of tectonic stress (<1.0km). Caner's (1969) estimate for the Curie isotherm depth appears to be too great and his 750°C Moho isotherm appears to be too cool. The implication of this model is that the Moho under Level Mountain is about 25.4km, which would make it one of the shallowest values for the Cordillera. This model is

Figure 9-3.
Geothermal gradient for the Stikine for model calculations and assumptions as discussed in text.

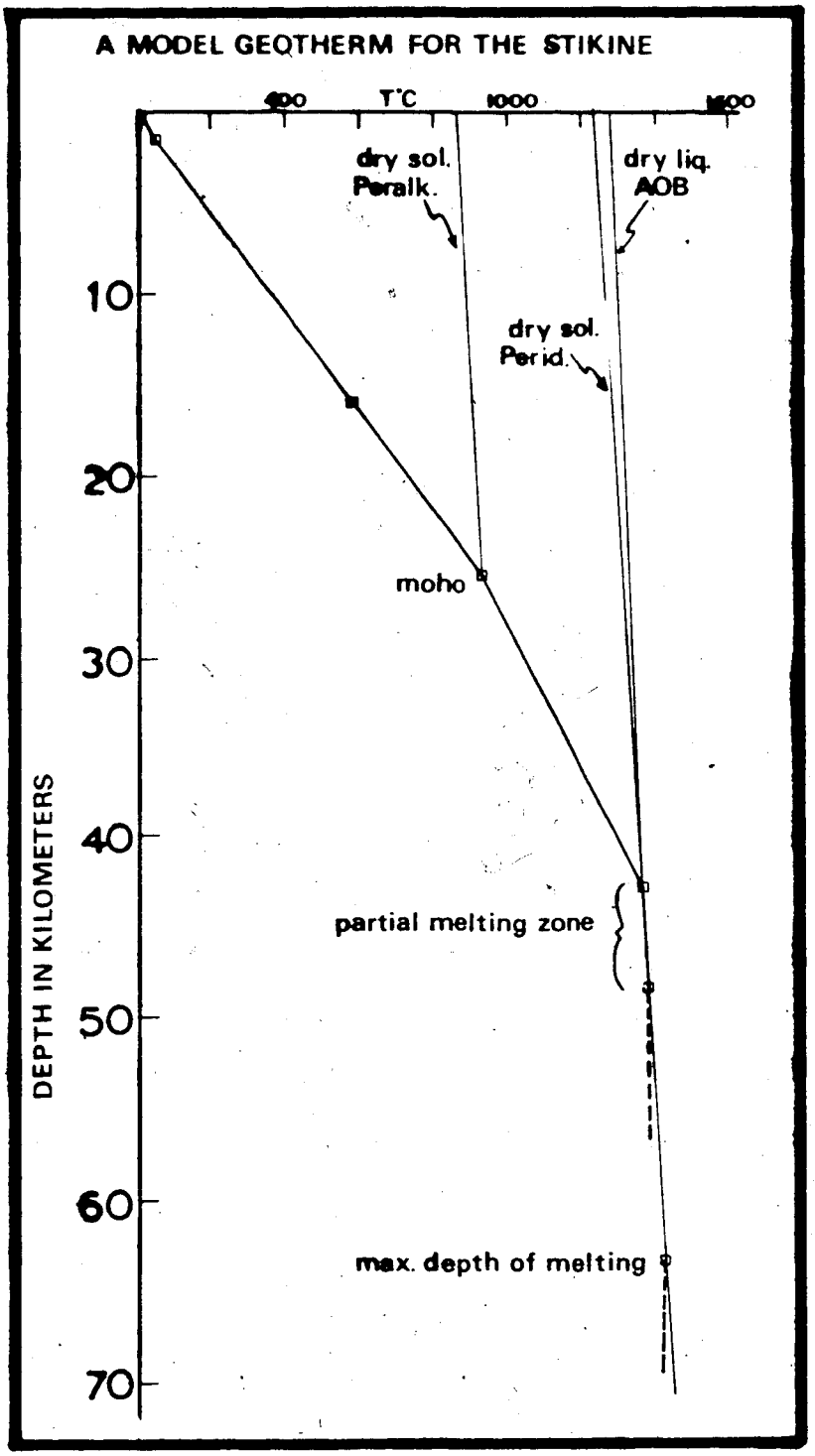

generally consistent with a mantle derivation for the Level Mountain lavas formed by the anhydrous partial fusion of spinel peridotite.

A characteristic of these steady state conduction models is a steeper geothermal gradient over most of the crust than in the upper mantle. For any reasonable choice of thermal conductivities, this geothermal gradient behavior holds for a wide range of hypothetical heat flow values (73 to 112 mW/m^2), Curie isotherm depths (16 to 18km) and crustal thicknesses (25 to 30km). The very shallow geothermal gradient is predicted to be lower in the volcanic pile as compared to adjacent areas with basement outcrop, or immediately beneath the pile in the crust. This is due to the high thermal conductivity for lavas. The Intermontane Belt in Southern and Central B.C. generally lacks a high velocity lid and the LVZ begins at the base of the crust. To more accurately fit such a constraint, the gradient in the upper mantle would probably be even more gradual. For a metasomatized alkali- and silica-rich upper mantle the thermal conductivity would be closer to lower crustal values and thus support a higher geothermal gradient. Varying the model in this direction would also lend support to a mantle derivation of peralkaline melts.

Chapter 10. GEOTHERMOMETRY AND GEOBAROMETRY ESTIMATES

INTRODUCTION

Spinel lherzolites are a common inclusion type for nodule-bearing alkaline lavas of the Intermontane Belt. Studies of phase chemistry and trace element concentrations have been reported by Littlejohn and Greenwood (1974), Fiesinger and Nicholls (1977), Fujii and Scarfe (1981) and Fujii et al (1981). Microprobe analyses of coexisting minerals from two spinel lherzolites nodules, one from Telegraph Creek and one from Grizzly Hill in Central B.C. are presented here. The various geothermometers relevant to spinel lherzolites are reviewed here. Equilibration temperatures have been estimated for the two Stikine localities: Telegraph Creek and Castle Rock (Littlejohn and Greenwood, 1974), the Selkirk material (Sinclair et al, 1977) and Grizzly Hill. The purpose of this is to estimate P,T conditions in the upper mantle beneath the Cordillera to determine the conditions of alkali basalt genesis for the Late Cenozoic, particularly at Level Mountain.

At equilibrium, the partitioning of Al, Mg, Fe etc. between the four phases olivine, orthopyroxene,, clinopyroxene and spinel, is a function of bulk composition, temperature and pressure. Considerable attention has has been given to pyroxenes as geothermometers (Boyd, 1973; Wilshire and Jackson, 1975; Presnall, 1975; Stroh, 1976). Thermodynamic models may be constructed using tabulated

information from mineral thermodynamic studies (Robie et al, 1978) and experimental data from simplified analogs of the natural peridotite system, $MgO-Al_2O_3-SiO_2$, (MacGregor 1974; Fujii and Takahashi, 1978) and the enstatite-diopside join (Mori and Green, 1977, 1976; Davis and Boyd, 1966; Lindsley and Dixon, 1975).

Consider the partition of magnesium between coexisting orthopyroxene and clinopyroxene

$$\underset{\text{opx}}{Mg_2Si_2O_6} = \underset{\text{cpx}}{Mg_2Si_2O_6}$$

At equilibrium, (P,T, composition fixed),

$$\mu^{\text{opx}}_{Mg_2Si_2O_6} = \mu^{\text{cpx}}_{Mg_2Si_2O_6}$$

the chemical potential of enstatite into both pyroxenes is equal (the sum of the $\mu(i)$ for the reaction is zero). Taking the standard state for each component to be equal to the pure phase, at some arbitrary temperature, the reaction can be rewritten as:

$$\mu^\circ_{En} + RT \ln a^{\text{opx}}_{En} = \mu^\circ_{En} + RT \ln a^{\text{cpx}}_{En}$$

and the free energy for the reaction is then given by:

$$(\Delta G^\circ)_T = -RT \ln \left[a^{\text{cpx}}_{En} / a^{\text{opx}}_{En} \right]$$

dividing through by RT and recalling the Second Law of Thermodynamics:

$$\Delta G^\circ = \Delta H^\circ - T\Delta S^\circ$$

the preceeding expression can be rewritten as

$$\frac{\Delta G^\circ}{RT} = -\ln\left(a_{En}^{cpx} / a_{En}^{opx}\right) = \frac{\Delta H^\circ}{RT} - \frac{\Delta S^\circ}{R}$$

to give the basic form of the solid assemblage geothermometry expressions. Knowledge of ΔH° and ΔS° for the particular reaction in question may come from tabulated sources for minerals (such as Robie et al, 1978). Alternatively, ΔH° and ΔS° may be estimated from P-T slopes of reaction boundaries in experimental phase equilibrium studies using the Clapeyron relation.

The general form of the solid phase assemblage geothermometers is:

$$\ln K = \frac{\Delta H^\circ}{RT} - \frac{\Delta S^\circ}{R}$$

where K is the equilibrium constant (expression of activity products) for the reaction, and ΔH° and ΔS° are the enthalpy change (heat of reaction) and entropy change (order at a given T and P). As long as the ΔH° and ΔS° are accurately known and the simple mixing approximation applies, the geothermometers should be concisely expressed as simple log-linear expressions $\ln K = A/T + B$, where A and B are constants. This is the form generally given in geothermometry papers (Wells, 1977; Mori, 1977; Herzberg and Chapman, 1976) but it is important to keep in mind that A and B are not just arbitrarily selected numbers chosen to best fit a particular collection of data, but that they have

fundamental thermodynamic significance to them. Where the ideal mixing assumptions break down, or data on simple experimental fail to fit the more complex natural assemblages, empirical formulations have been made using polynominal expressions and adding additional terms, such as Mori (1977) or Wells (1977). It should be remembered that these extra terms are really without physical meaning and have only been added to force a mathematical fit to a collection of data. The need for such modifying terms only underlines the inaccuracies in our knowledge of ΔH°, ΔS° and in the assumed solution models. Herzberg and Chapman (1976) point out their fits imply $\Delta S > 8$ cal/mol° which does not seem high in this temperature range. Mori's values (1977) imply even higher ΔS (> 9.4 cal/mol°). This probably demonstrates the oversimplification of the mixing model, rather than inaccuracy in the thermodynamic or experimental data. The familiar thermodynamic form of the geothermometer can be rewritten as an equivalent polynomial in ln K so that all geothermometers can be expressed in a common form:

$$10^4/T^\circ K = a(\ln k)^2 + b(\ln k) + c$$

where $c = 10^4 \Delta S^\circ / \Delta H^\circ$
$b = 10^4 R / \Delta H^\circ$
and a is an additional term with no thermodynamic meaning.

The state of the art in geothermometry of spinel lherzolites is summarized in Table 10-1. In addition to the magnesium partition between pyroxenes used in the derivation above, (reaction 1, Table 10-1) the two most accurate

Table 10-1. GEOTHERMOMETRY OF SPINEL LHERZOLITES

ASSEMBLAGE: Forsteritic Olivine - ol
Cr-Al Diopside - cpx
Magnesian Orthopyroxene - opx
(Mg,Fe,Al,Cr) Spinel phase - sp

REACTIONS: AT EQUILIBRIUM TO DEFINE P,T

1) $Mg_2Si_2O_6$ (opx) = $Mg_2Si_2O_6$ (cpx), $(k1)^{\circ}_{P,T} = (a^{cpx}_{En} / a^{opx}_{En})$

2) $CaMgSi_2O_6$ (cpx) + $MgAl_2O_4$ (Sp) = $CaAl_2SiO_6$ (cpx) + Mg_2SiO_4 (ol),

$$(k2)_{P,T} = \left[a^{cpx}_{CaTs} \cdot a^{ol}_{Fo} / a^{cpx}_{Di} \cdot a^{sp}_{Sp} \right]$$

3) $Mg_2Si_2O_6$ + $MgAl_2O_4$ = $MgAl_2SiO_6$ + Mg_2SiO_4 ,

$$(k3)_{P,T} = \left[a^{opx}_{MaTs} \cdot a^{ol}_{Fo} / a^{opx}_{En} \cdot a^{sp}_{Sp} \right]$$

Table 10-1. (continued)

ACTIVITY DEFINITIONS

(Pyroxenes): $M1(Al^{3+},Cr^{3+},V^{3+},Ti^{4+},Fe^{3+},Fe^{2+},Mg^{2+},Ni^{2+})$, $M2(Mn^{2+},Ca^{2+},Na^{+},Ba^{2+},Fe^{2+},Mg^{2+})$

$a^{cpx}_{En} = X^{M2}_{Mg} \cdot X^{M1}_{Mg}$

$a^{cpx}_{Di} = X^{M2}_{Ca} \cdot X^{M1}_{Mg}$

$a^{cpx}_{CaTs} = X^{M2}_{Ca} \cdot X^{M1}_{Al}$

In all cases Al^{3+} is partitioned between the tetrahedral site and M1 octahedral site on the basis of silica content in the pyroxene analysis assuming the tetrahedral site is completely filled by Si^{4+} and Al^{3+}. After assigning the site specific cations Mg^{2+}, Fe^{2+} are partitioned according to their proportions between M1 and M2, assuming ideal mixing.

$a^{opx}_{En} = X^{M2}_{Mg} \cdot X^{M1}_{Mg}$

$a^{opx}_{Mats} = X^{M2}_{Mg} \cdot X^{M1}_{Al}$

(Olivine)

$a^{ol}_{Fo} = (X^{ol}_{Fo})^2$ ideal solution $(M)_2SiO_4$

(Spinel)

$a^{sp}_{MgAl_2O_4} = X^{A}_{Mg} (X^{B}_{Al})^2$ for formula AB_2O_4 normal spinel

Table 10-1. (continued)

Calibrated Geothermometers:

Linear or polynomial regression fits of the form:

$$\frac{10^4}{T°K} = a(\ln k)^2 + b(\ln k) + c$$

P = 12 Kbar

	a	b	c
*k_1	0	-1.192	4.337
*k_2	0	-1.171	4.754

after Herzberg and Chapman (1976)

P = 16 Kbar

+k_1	0.41	0.37	5.7
*k_1	0	-1.177	4.215
+k_2	0	-1.08	5.12
*k_2	0	-1.083	4.799
†k_3	0.357	0.177	5.04
#k_3	0	-2.06	2.69

1 = Activity definitions conform to Nicholls and Carmichael (1972), Bacon and Carmichael (1973) and reference cited below
* = Herzberg and Chapman (1976), data from experimental and natural spinel peridotites
+ = Mori (1977), experimental data base
† = Mori (1977), after MacGregor (1974)
# = Mori (1977), after Obata (1976)

geothermometers are based on magnesium and aluminum partitioning between coexisting clinopyroxene spinel and olivine (reaction 2, Table 10-1) or aluminum and magnesium partitioning between coexisting orthopyroxene, spinel and olivine (reaction 3, Table 10-1). Reactions 2 and 3, involving the solubilities of alumina in pyroxenes, are not yet tested for Fe- and Cr-bearing systems. Application of theses geothermometers to the Cr bearing system may give too high a temperature estimate (Fujii and Takahashi, 1978). The definitions of activities are consistent with the geothermometry papers previously cited. Activity expressions are calculated for ideal structural formulae and using concepts of equivalent sites. For example the expression

$$a_{Fo}^{ol} = X_{Mg}^{M1} X_{Mg}^{M2} = (X_{Mg}^{M})^2 \quad \text{for M1 = M2}$$

shows the activity of the forsterite component in olivine assuming a random mixing for iron and magnesium between two octahedral sites. There is ambiguity in calculating structural formulae, particularly for pyroxenes, and several methods have been proposed (Cawthorn and Collerston, 1974; Fleet, 1974a,b). They have shown for pyroxenes of intermediate iron content, that random partitioning of Fe^{2+} between the two octahedral sites is not a very accurate assumption, because Fe^{2+} partitions in favour of Mg^{2+} into the M2 site. Magnesium and aluminum rarely exist in spinel analyses in stoichiometric proportions unbalanced by other cations. Problems arise in trying to fit data from different

laboratory studies. Additional difficulties may be encountered when fitting natural spinel lherzolites which have many additional components such as Ni, Mg, Na, Cr, Ti, V, Ba.

REVIEW OF PREVIOUS DATA FOR THE INTERMONTANE BELT

Fiesinger (1975) and Fiesinger and Nicholls (1977) performed geothermometry calculations both on solid assemblages and silica activities with coexisting lavas for spinel lherzolite and gabbroic xenoliths from Late Cenozoic lavas of the Wells Grey - Quesnel Highlands area B.C. Calculated equilibration temperatures ranged from 1050° to 1650°C with a total range of equilibration pressures from13 to 50 kbar. The larger values for P and T here lie outside the spinel lherzolite stability field even though no garnet lherzolites are reported. There is too much variation in calculated P and T to be explained by any fractionation processes at either high or low pressure or to be explained by the inaccuracy in the assumptions and calculations of the geothermometers. The implication is that the nodules have been sampled from different depths and that the geotherm varies both in time and space for the Intermontane Belt. Similar conclusions have been obtained by Fujii et al (1981) using data for two localities from central and southern B.C. Takomkane (Boss Mountain) and Clark Creek (West Kettle River). Littlejohn and Greenwood's (1974) data for Jacques Lake (Quesnel Highlands) and Castle Rock (Klastline Plateau,

Stikine Volcanic Belt) indicate high and variable equilibration temperatures according to the olivine-spinel geothermometer of Jackson (1969). These estimates should be considered with some doubt however, due to possible subsolidus reequilibration of olivine and spinel and the assumption of ideal solution in the spinels. Sinclair et al (1977) also calculated high equilibration temperatures for nodules from the Selkirk cone.

Chemical analyses of four phases were made by electron microprobe on polished block mounts of nodules from Grizzly Hill and Telegraph Creek. Data and structural formulae are reported in table 10-2. All of these analyses gave high totals between 101 and 106% due to problems with an oil film on the beryllium window on the microprobe at the time the data were collected. Despite the high totals, the recast analyses compare favorably with other mantle inclusions reported from the literature including samples from the Cordillera (Littlejohn and Greenwood, 1974).

Activities have been calculated, from the structural formula and site occupancy restrictions as summarized in Table 10-1, for these nodules and for the four Castle Rock samples from Littlejohn and Greenwood (1974), and the two samples from the Selkirk Cone (Sinclair et al, 1978). Temperatures have been calculated for the geothermometers of Herzberg and Chapman (1976), Mori (1977) and Wells (1977) for all four localities, see table 10-3. The Castle Rock and Selkirk temperatures are derived from averages based on all

Table 10-2. CHEMICAL ANALYSES OF FOUR PHASES FROM INCLUSIONS

A. OLIVINES

	TCL 1004-41	GHL
SiO_2	40.58	40.48
FeO	10.95	11.25
MnO	.09	.13
NiO	.40	.47
MgO	47.90	47.67
CaO	.09	0.0
	100.01	100.00

TCL 1004-41 also contained interstitial plagioclase <1% of An(55)Ab(43)Or(2) and mono sulfide solid solution phase approximately Py(64)Pn(36) having detectable Ni,Co,Zn and micro-inclusions of sphere

GHL additionally contained <1% of interstitial alkali feldspar of An(0.7)Ab(41.0)Or(58.3) and a similar mono-sulfide solid solution to TCL

STRUCTURAL FORMULAE PER 4 OXYGENS

Si^{4+}	1.001	1.0	1.000	1.0
Fe^{2+}	.226		.232	
Mg^{2+}	.002		.033	
Ni^{2+}	.008	2.0	.009	2.0
Mg^{2+}	1.761		1.756	
Ca^{2+}	.003		0.0	

Table 10-2. (continued)

B. Pyroxenes

	cpx		opx	
	TCL 1004-41	GHL	TCL 1004-41	GHL
SiO_2	53.58	53.49	55.64	55.14
TiO_2	0.28	0.35	0.0	0.0
Al_2O_3	5.31	5.28	4.14	4.12
Cr_2O_3	0.73	0.67	0.28	0.16
V_2O_3	0.07	0.11	0.0	0.0
FeO	2.79	2.76	7.02	7.29
MnO	0.0	0.0	0.12	0.09
MgO	14.25	14.28	32.05	32.53
CaO	22.23	22.40	0.67	0.60
NiO	0.0	0.04	0.09	0.07
Na_2O	0.69	0.63	0.0	0.0
BaO	0.06	0.0	0.0	0.0
	99.99	100.01	100.01	100.00

STRUCTURAL FORMULA PER 6 OXYGENS

Si^{4+}	1.931		1.932		1.924		1.911	
Al(IV)	.069	2.0	.068	2.0	.076	2.0	.089	2.0
Al(VI)	.157		.157		.093		.079	
Ti^{4+}	.010		.012		---		---	
Cr^{3+}	.021		.019		.008		.005	
V^{3+}	.002		.003		---		---	
Fe^{2+}	.084	1.946	.083	2.0	.203	2.0	.211	2.0
Mn^{2+}	---		---		.004		.003	
Mg^{2+}	.765		.769		1.652		1.680	
Ca^{2+}	.858		.867		.025		.022	
Ni^{2+}	---		.002		.003		.002	
Na^{+}	.048		.044		---		---	
Co^{2+}	.001		.044		---		---	

Table 10-2. (continued)

C. Spinels

	TCL 1004-41	GHL
TiO_2	0.09	0.0
Al_2O_3	54.52	59.35
Cr_2O_3	11.55	8.99
V_2O_3	0.0	0.0
Fe_2O_3	4.46	8.99
FeO	7.27	9.28
MnO	0.12	0.09
MgO	21.32	20.62
NiO	0.43	0.45
ZnO	0.10	0.05
CaO	0.14	--
	100.00	100.02

STRUCTURAL FORMULA PER 32 OXYGENS

	TCL 1004-41		GHL	
Ti^{4+}	0.02		0.0	
Al^{3+}	13.37		14.36	
Cr^{3+}	1.90	15.99	1.46	16.00
V^{3+}	---		0.0	
Fe^{3+}	0.70		0.18	
Fe^{2+}	1.26		1.59	
Mn^{2+}	0.02		0.02	
Mg^{2+}	6.61	8.00	6.31	8.00
Ni^{2+}	0.07		0.07	
Zn^{2+}	0.02		0.01	
Co^{2+}	0.02		0.0	

Table 10-3. Calculated Equilibration Temperatures (T°C) for Spinel Lherzolites from the Intermontane Belt.

	(1) SELKIRK CONE, YUKON	(2) TELEGRAPH CREEK, B.C.	(3) CASTLE ROCK, B.C.	(4) GRIZZLY HILL, B.C.
12 Kbar				
*K_1	1120	1039	1272	1041
*K_2	1304	1366	1261	1318
16 Kbar				
*K_1	1151	1066	1308	1069
+K_1	1126	1010	1301	1013
*K_2	1323	1381	1281	1336
+K_2	1246	1299	1208	1258
#†K_3	1275	1246	1324	1146
#K_3	1309	1267	1388	1137
0-40 Kbar				
#K_1	962	878	1095	878

(1) Sinclair, Tempelman-Kluit, Medaris (1977) for mineral analyses of 2 Lherzolite nodules in Pleistocene cinder cone, central Yukon

(2) Stikine region: Lherzolite nodule from Miocene or younger basalt flow at Telegraph Creek, B.C. Sample TCL *1004-41* from H. Greenwood

(3) Littlejohn and Greenwood (1974) for mineral analyses from 4 Lherzolite Nodules in Quaternary AOB breccia at Castle Rock (Stikine Region) on northern edge of Klastline Plateau

(4) Central B.C., Lherzolite nodule from Miocene basalt dyke at Grizzly Hill Hamilton (1979)

† Wells (1977)
$10^4/T°K = -1.362 \ln k + 4.570 + 3.324 Fe/Fe + Mg (opx)$
Of the natural compositions he tests this on, lherzolites and peridotites give the largest T°K discrepancies compared to other mineral geothermometers.

of the reported mineral data. The calculated temperatures fall in a tighter range than for previously reported values. Taking the Telegraph Creek, Castle Rock and Selkirk values as representative of the Upper Mantle beneath the Northern Cordillera in the vicinity of Level Mountain, the three mineral thermometers (k_2,k_3) give values in the range 1200° to 1400°C at 12 to 16 kbar, while the pyroxene thermometers give lower estimates of 875° to 1300°C. Using a surface temperature estimate (5°C), the average of all 12 kbar estimates (1219°C), and the average of all 16 kbar estimates (1228°C) for each locality, results in geothermal gradients in the range of 25°/km (82.4°/kbar) down to the intersection with the lherzolite solidus, see Figure 10-1. Owing to the Cr content of these natural samples, this geothermal gradient estimate is probably a maximum. For the simple four component experimental analog of the lherzolite system (CMAS)[1] this intersection would be at 15.8 kbar (51.8 km). Considering the effect of other components such as alkalis, iron, titanium, phosphorous and volatiles in depressing the solidus, this intersection is likely to be even shallower (see pyrolite solidus of Green and Ringwood, 1967). If some of the higher geothermometry estimates are accurate, the geotherm could be as steep as 31°/km with a solidus intersection as shallow as 41km (12.5 kbar). On the basis of trace element data, all of these spinel lherzolites appear to be high temperature refractory residua from previous

---

[1] $CaO - MgO - Al_2O_3 - SiO_2$

Figure 10-1.
P-T plot showing phase fields and solidus for mantle peridotite along with liquidus data for basaltic lavas and range of PT estimates for lherzolites from northern Cordillera.

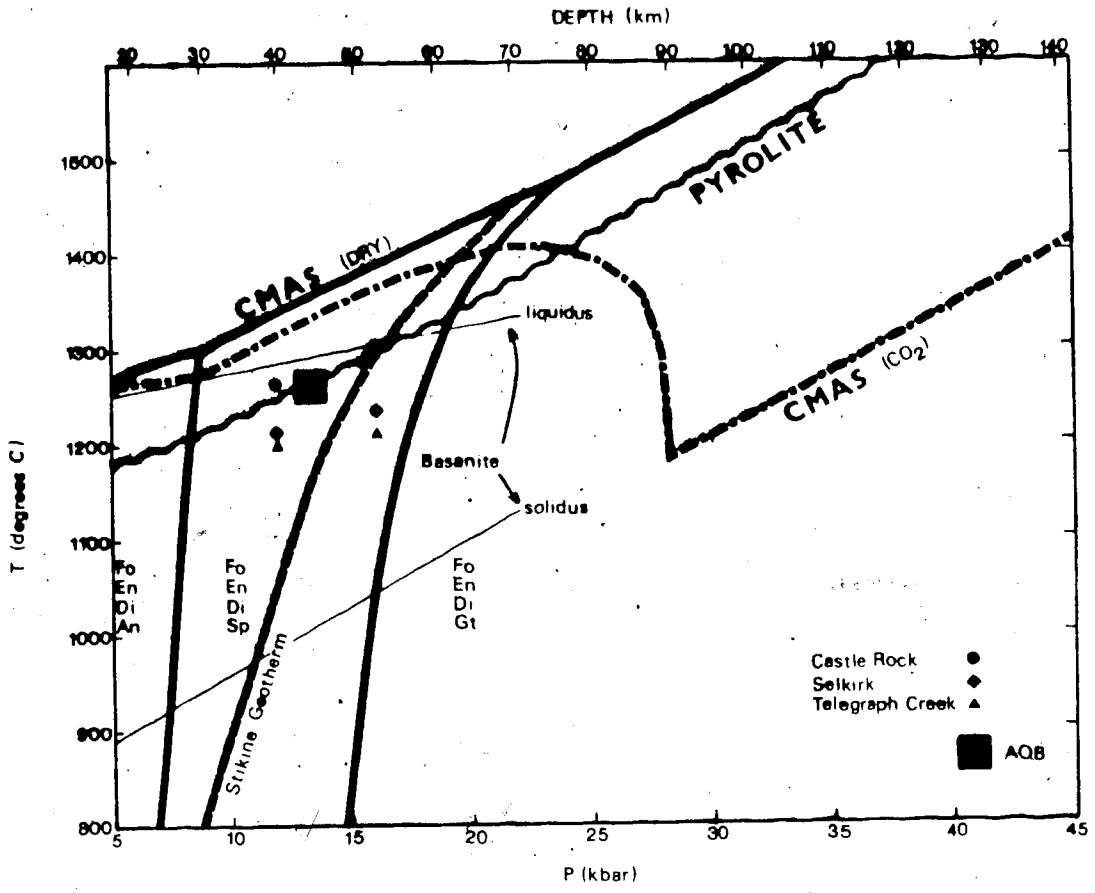

partial melting events and they are too depleted to be source rocks for normal basalt genesis.

For comparison with natural rock systems the melting relations (solidus and liquidus) of a basanite are shown in Figure 10-1. The basanite comes from Mount Shadwell, Australia (Arculus, 1975). The intersection of the basanite solidus with the hypothesized Stikine geotherm lies in the stability field of ol + Cpx + Sp + Pl + L and the liquidus - geotherm intersection is in the field of ol + L, according to the phase relations of Arculus (1975).

From the work of DePaolo (1979) the intersection of the liquidus of an AOB having log a SiO_2 = -0.4 with the anhydrous pyrolite solidus, is at 13.5kbar (44.5km). This point marking the alkali olivine basalt depth of origin lies within the field of the northern Cordilleran geothermometry estimates and slightly to the high temperature side of the hypothesized Stikine geotherm. Using these data the melting region for generating the Stikine basic lavas can be approximated to lie between 36 and 50 km depth.

GEOBAROMETRY AND GEOTHERMOMETRY FROM THE ACTIVITIES OF SILICA AND ALUMINA IN LEVEL MOUNTAIN LAVAS

Expressions for the variation of log aSiO_2 into the melt with temperature have been published by Carmichael et al (1970) and for temperature and pressure by Nicholls et al (1971), Nicholls and Carmichael (1972) and Bacon and Carmichael (1973). The basic assumption is that for the

coexistence of minerals and silicate melts at equilibrium, the compositions of the minerals define a buffer on the activity of SiO_2 into the melt. Thermodynamically this can be stated:

$$U^{\circ}_{SiO_2}(melt) + RT \ln a_{SiO_2}(melt) = U^{\circ}_{SiO_2}(minerals) + RT \ln a_{SiO_2}(minerals)$$

and for more than one solid phase the right hand size would contain additional activity terms. If the chemical potential of silica in the standard state is taken to be that of SiO_2 glass for both melt and crystals, then the activity terms are equal. The activity of silica into the melt (or solids) may be defined by:

$$\left[\log a_{SiO_2}(melt)\right]_{P,T} = \frac{\Delta G^{\circ}}{2.303RT} + \frac{\Delta V^{\circ}}{2.303RT}(P-1) + \log K$$

where $\Delta Cp = 0$ and K is the equilibrium constant for the reaction in question, defined by stoichiometry, and the activity terms are for pure mineral components into actual crystal phases, after Bacon and Carmichael (1973). Examples of such reactions that buffer silica are:

$$SiO_2(melt) = SiO_2(\beta\ Quartz)$$

and $$Mg_2SiO_4 + SiO_2(melt) = 2MgSiO_3$$

after Nicholls et al (1971). Note that in using real mineral compositions, the activity depends on both the solution model assumed and the stoichiometry. The thermodynamic form of the silica activity stated above gives rise to a unique expression for each reaction of the general form:

$$\left[\log a^{melt}_{SiO_2}\right]_{P,T} = (A/T + B) + (C/T(P-1)) + \log K$$

In keeping the same form, it can be seen that A and B come from the free energy term, while C comes from the volume change. Values of A,B and C have been calculated from existing thermodynamic data for the various silica buffering reactions. In the absence of a mineral-melt reaction which defines (buffers) the activity of SiO_2 into the melt, the following expression is used

$$\left[\log a^{melt}_{SiO_2}\right]_{P,T} = \left[\log X^{melt}_{SiO_2} + \frac{\psi(SiO2)}{T}\right] + \frac{V-V^\circ}{2.30RT}(P-1)$$

after Bacon and Carmichael (1973). The V term is evaluated using the partial molar volume data of Bottinga and Weill (1970). The other term is a function of composition

where $X^{melt}_{SiO_2}$ is the mole fraction of silica into the melt,

and the composition function is defined:

$$\phi(SiO_2)/T = \log\left[a^{melt}_{SiO_2} / X^{melt}_{SiO_2}\right]$$

The function $\phi(SiO_2)$ may be evaluated at any single temperature if the activity of SiO_2 into the melt is known Nicholls et al (1971) and Bacon and Carmichael (1973) have evaluated the activity of SiO_2 at the quench temperature of a lava. For this purpose they used T quench and log fO_2 from Buddington and Lindsley's (1964) Fe-Ti oxide data, and equilibrium groundmass mineral compositions for olivine and

titanomagnetite with the fayalite-magnetite-silica buffer. The buffer expression is:

$$\log a^{melt}_{SiO_2} = A/T + B + \log a^{ol}_{Fa} + 1/3 \log fO_2 - 2/3 \log a^{TiMt}_{Mt}$$

Note the reciprocal dependance on T and log fO_2. A small error in estimating T and/or log fO_2, while it changes the one bar activity into the melt, does not have as great an effect on estimating $\phi(SiO_2)$ for the lava. The confidence of $X(SiO_2)$ depends only on the accuracy of the bulk chemical analysis.

Alumina activities are evaluated in a parallel fashion for mineral reactions that buffer Al_2O_3. For the unbuffered case, log aAl_2O_3 into the melt must be evaluated at some known temperature to get at ϕAl_2O_3. In basic and intermediate lavas a useful defining reaction is:

$$CaMgSiO_6(cpx) + 1/2\ SiO_2(melt) + Al_2O_3(melt) = CaAl_2SiO_8(plag) + 1/2\ Mg_2SiO_4(ol)$$

where the equilibrium groundmass assemblage is used and log $aSiO_2$ into the melt must be known. The expressions

$$\log a^{melt}_{Al_2O_3} = A/T+B+\log \left[a^{pl}_{An} \left(a^{ol}_{Fo}\right)^{1/2} / a^{cpx}_{Di} \right] - 1/2 \log a^{melt}_{SiO_2}$$

and

$$\phi Al_2O_3 = \left[\log a^{melt}_{Al_2O_3} - \log X^{melt}_{Al_2O_3}\right] T$$

are evaluated using published values for A,B (Bacon and Carmichael, 1973) and compositions data for a specific basalt and its constituent mineral phases.

The variation of mineral-melt buffers for $aSiO_2$ and aAl_2O_3 are shown with temperature and pressure in figure 10-2. These diagrams have been constructed using the data of Bacon and Carmichael (1973), Nicholls and Carmichael (1972) and Nicholls et al (1971). Judging from common phenocryst assemblages, these curves likely span the $aSiO_2$ and aAl_2O_3 ranges commonly encountered for igneous melts from basalts to rhyolites. The unbuffered curves shown for basalt are for examples from Level Mountain. While the convergence of the common silica buffers at high temperature limits the applications of log $aSiO_2$ into the melt as a geothermometer, the strong pressure dependence for the mineral-melt buffers compared to unbuffered lavas lends itself to use as a geobarometer. Log $aSiO_2$ varies inversely with pressure, while log aAl_2O_3 varies directly. The use of silica and alumina buffers together improves the precision of pressure estimates.

Having defined the unbuffered variation in log $aSiO_2$ and log aAl_2O_3 into the melt as a function of P and T for a given lava, the expressions for both log $aSiO_2$ and log aAl_2O_3 may be solved simultaneously with reactions that define the activities of those components in the melt for mineral buffers, using assumed or analysed phenocryst or mantle assemblages, to give unique curves in PT space. As an example, Bacon and Carmichael (1973) solve the forsterite-enstatite buffer for SiO_2 (defined previously) and the alumina buffer given by

Figure 10-2.
Calculated alumina and silica activity mineral-melt buffer curves. Pure phases unless otherwise shown. Data from Nicholls and Carmichael (1972) and Carmichael (1973).

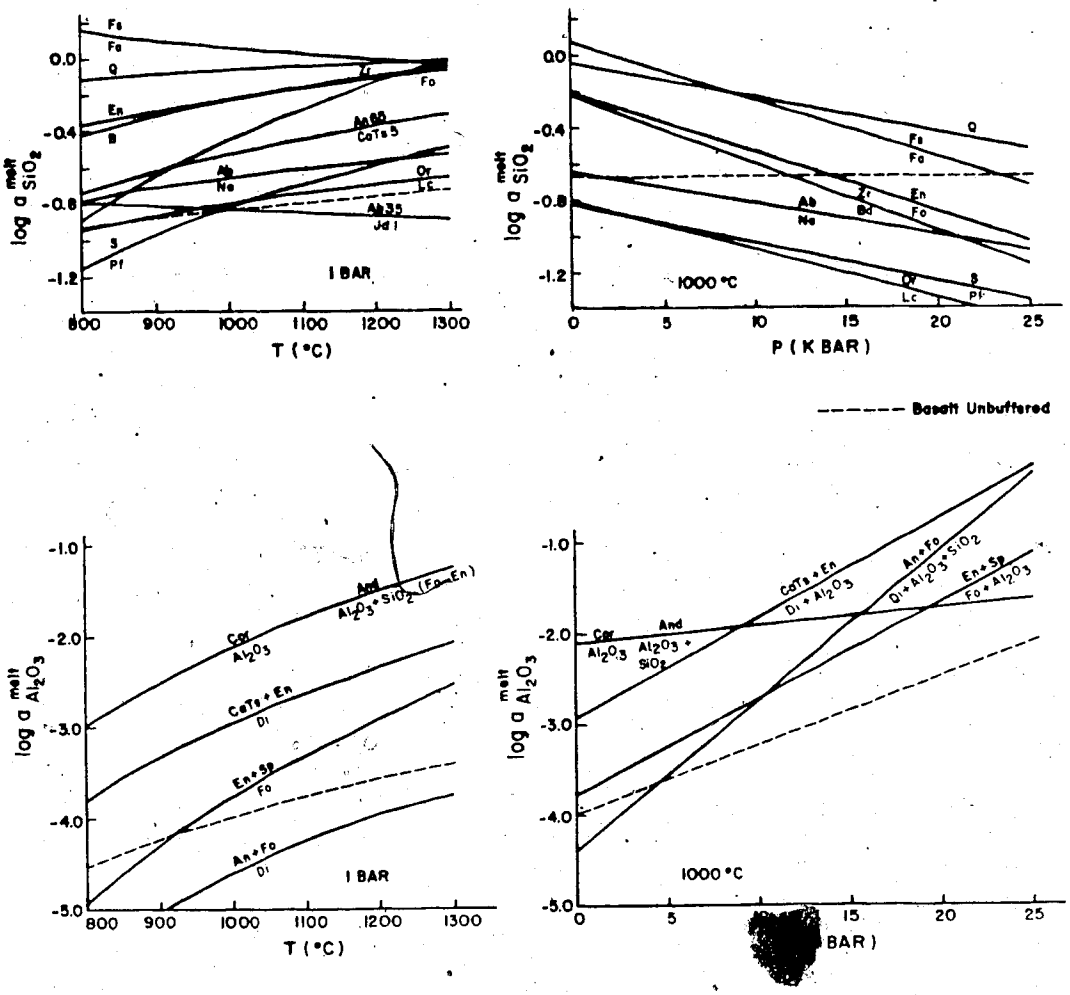

$$Mg_2SiO_4(ol) + Al_2O_3(melt) = MgAl_2O_4(sp) + MgSiO_3(opx)$$

with the unbuffered log activity expressions for the lava to give an assumed P and T of equilibration with mantle lherzolite. From the joint solution of the expressions for any mineral assemblage buffer, the general P-T curve is given by:

$$(P\text{-}1) = \frac{(B - \log X(SiO_2) + \log K)T - (\phi SiO_2 - A)}{D + ET}$$

where T is in °K, P in bars, A,B and K refer to the particular mineral-melt buffer and D+ET comes from the difference in the C coefficients for unbuffered melt and the chosen buffer reaction. In the case of the forsterite-enstatite buffer this expression is:

$$(P\text{-}1) = \frac{(0.597 - \log X(SiO_2) + \log K)T - (\phi SiO_2 + 1034)}{0.0377 + 1.34 \times 10^{-4}T}$$

where log K depends on the composition of olivine and pyroxene in the lherzolite. Similarily the olivine-orthopyroxene-spinel alumina buffer and the log alumina activity expression for the unbuffered melt can be solved to give:

$$(P\text{-}1) = \frac{(2.632 + \log K - \log X(Al_2O_3))T - (\phi Al_2O_3 + 8131)}{0.462 - 0.67002 \times 10^{-4}T}$$

where log K is given by:

$$\log K = \log a(Sp \text{ in } sp) + \log a(En \text{ in } opx) + \log a(Fo \text{ in } ol)$$

The equilibrium P-T curve for the lherzolite can also be defined by the reaction:

$$CaAl_2SiO_6 + Mg_2SiO_4 = CaMgSi_2O_6 + MgAl_2O_4$$

and $-\log K = -2156/T + 0.869 - 0.00778(P-1)$

The geobarometry of salic lavas presented in Nicholls et al (1971) depends on the simultaneous solution of two mineral-melt silica buffers. The fayalite-magnetite and quartz-silica buffers were used for a variety of acid lavas from different localities including a pantellerite from Pantelleria with P eq. > 7.3 kbar.

Following the method described above, similar geobarometry calculations have been attempted for a few representative lavas from Level Mountain. The data used in these calculations and the results are presented in table 10-4. The quench temperatures inferred here are generally less than or equal to solidus estimates for Level Mountain lavas of similar composition. The oxygen fugacity inferred is slightly greater than or equal to that of the melting experiments. buffers for FMQ and MW by gas mixing.

While no lherzolite inclusions were found in the Level Mountain lavas proper, lherzolites have been found in similar lavas from the Selkirk Cone (Sinclair et al, 1978), Castle Rock (Littlejohn and Greenwood, 1974) and at Telegraph Creek. The mineral compositions from those localities have been used with Bacon and Carmichael's data for

$$CaAl_2SiO_6 + Mg_2SiO_4 = CaMgSi_2O_6 + MgAl_2O_4$$

to give the following lines in PT space for the spinel lherzolites from the Northern Cordillera (for T in °K and P in bars).

Table 10-4 Geothermometry and Geobasometry Estimates for Level Mountain Lavas

Sample ID	T quench 1 bar °C	log fO_2	X plag An	X ol Fo	X ol Fa	X cpx Di	X cpx En	X cpx cats	X Timt mt	log a SiO_2	X SiO_2	∅ SiO_2	log a Al_2O_3	XAl_2O_3	∅ Al_2O_3	P Kbar	T °C	°C/km	Phenocryst Megacryst or Lherzolite used
8/25-50/6397 Hawaiite	985	-11.89	.599 .600	.716 .591	.274 .394	.463	.102	.095	.33	- .6875	.5184	-506 phenos	-3.883 P≤ 5.8	.0982	-3617	10.96 11.98 14.83	883 954 1028	24.56 24.28 21.13	Telegraph Creek Castle Rock Selkirk
PBP 6480 (PBO for some minerals) Hawaiite	975	-12.93	.185 .220	.338 .349 .405	.634 .627 .572	.444	.050	.022	.398 .337 .201	- .6897	.6746	-647 phenos	-4.4173 P≤10.6	.1082	-4308	9.86 9.95 12.37	805 831 900	24.9 25.5 22.2	TCL CR S
PAF 4370 Hawaiite	996	-12.06	.383	.546 .474	.439 .507	.509	.041	.061	.237	- .6109	.5481	-444 phenos	-3.955 P≤10.5	.1075	-3790	9.39 9.52 12.33	914 942 1019	29.64 30.16 25.20	TCL CR S
PAR 4030 Alkali basalt	1050	-10.91	.599	.827	.164	.612	.084	.052	.225	-1.3331	.5087	-1375 phenos	-3.6879 T >1180° P≤ 4.25 Kbar	.0883	-3485	16.54 16.59 19.30	906 932 1000	16.70 17.13 15.80	TCL CR S
PAO-4115 Basalt	1041	-10.42	.526	.773 .707	.220 .281	.607	.076	.047	.386	- .8158	.5354	-715 phenos	-4.1027 (minerals) T<1185°C P≤4.9 Kbar	.0956	-4051	14.35 14.40 17.00	803 808 896	17.06 17.11 16.07	TCL CR S
PAX 3675 Basalt	950	-13.00	.557	.762	.230	.467	.084	.052	.240	-1.2446	.5529	-1207.4 phenos	-4.1007 T<1237°C P≤9.41 Kbar	.0937	-3758	18.41 18.48 20.93	841 865 931	13.93 14.27 13.56	TCL CR S
PBX 5385 Hawaiite	980	-12.40	.457	.418	.565	.517	.066	.027	(.300)	- .4891	.5358	-273 phenos	-4.7383 T<1150°C P≤5.3 Kbar	.0931	-4645	No equil. w/ Lherzolites			
PAC 4465 Hawaiite	986	- 9.13	.457	.540	.444	(.514)	(.044)	(.053)	.819 .944	.2484	.5737	617 phenos	-4.9659 P = 23.8 Kbar	.1027	-5008	No equil. with Lherzolites or phenos?			
8/26-56/6336 Trachyte	1090	-10.00			.753				.235	.0974	.7076	337.5				6.1 Kbar Q - SiO_2/Fa Mt-SiO_2			
8/7-19/5830 C.Trachyte	1110	-10.00			.726				.15	.1074	.7500	321.3				6.5 Kbar Q - SiO_2/Fa Mt SiO_2			
8/30-82/6150	860	-13.86	.232	.394	.574	.435		Jd=.04	.436	-.3716	(.7224)	-261	-5.6133	(.0967)	-5210	6.4 Kbar Ab-Jd/Fa Mt SiO_2			

Telegraph Creek: P = 175.94 T - 277122
Castle Rock: P = 195.71 T - 277122
Selkirk: P = 187.31 T - 277122

The Castle Rock assemblage gives a very similar slope ($\Delta P/\Delta T$) to the San Quentin lherzolites of Bacon and Carmichael (1973), while the slopes for Telegraph Creek and Selkirk are slightly less. Graphical presentation of the P-T solutions for a basalt from the base of the Level Mountain plateau (unit 1) and a hawaiite from the central stratocone (unit 8) are given in Figure 10-3. Not only do these examples span most of the time of the Level Mountain volcanism, but they also span the range of depth estimates for the basaltic lavas. Two of the hawaiites presented in the table do not have real solutions (lying in positive P-T space) for lava-lherzolites or lava-phenocrysts. Those two hawaiites are assumed to be derived by substantial fractional crystallization from more primitive compositions, and in their final erupted compositions are likely to be out of equilibrium, with respect to silica and alumina activity for their phenocrysts and their presumed mantle source. As with the San Quintin lavas presented by Bacon and Carmichael, there may be some problems with the calculated pressures and temperatures. For the Level Mountain basaltic lavas all of the pressures fall into the spinel lherzolite stability field, but the temperatures seem too low for genesis of basaltic magmas. The pressures are similar to those calculated for other alkaline lavas from the

Figure 10-3.
Calculations of P-T equilibration conditions for spinel lherzolites from the northern Cordillera and two Level Mountain lavas. Upper set of 3 subparallel curves are for spinel lherzolites alone, assuming the reaction $CaTs+Fo=Di+Sp$. The plot on the left for PAX, from the lower plateau, shows the range of equilibration pressures for the unbuffered melt and lherzolite minerals, using all 3 lherzolites. Points are the intersection of $Fo+SiO_2=En$ with $Fo+Al_2O_3=Sp+En$. An estimate of pressure of equilibration for unbuffered melt and phenocrysts is given by the intersection of $Jd+SiO_2=Ab$ for the plagioclase with $Di+SiO_2+Al_2O_3=An+Fo$ for the pyroxene. The plot on the right is for stratocone hawaiite 8/25-50/6397. The pressure estimate for melt equilibration with lherzolite minerals is lower. The lower of the pairs of curves for phenocryst buffers (with negative slope) is for $CaTs+SiO_2=An$ other reactions as before. T= Telegraph Creek, S = Selkirk, CR = Castle Rock.

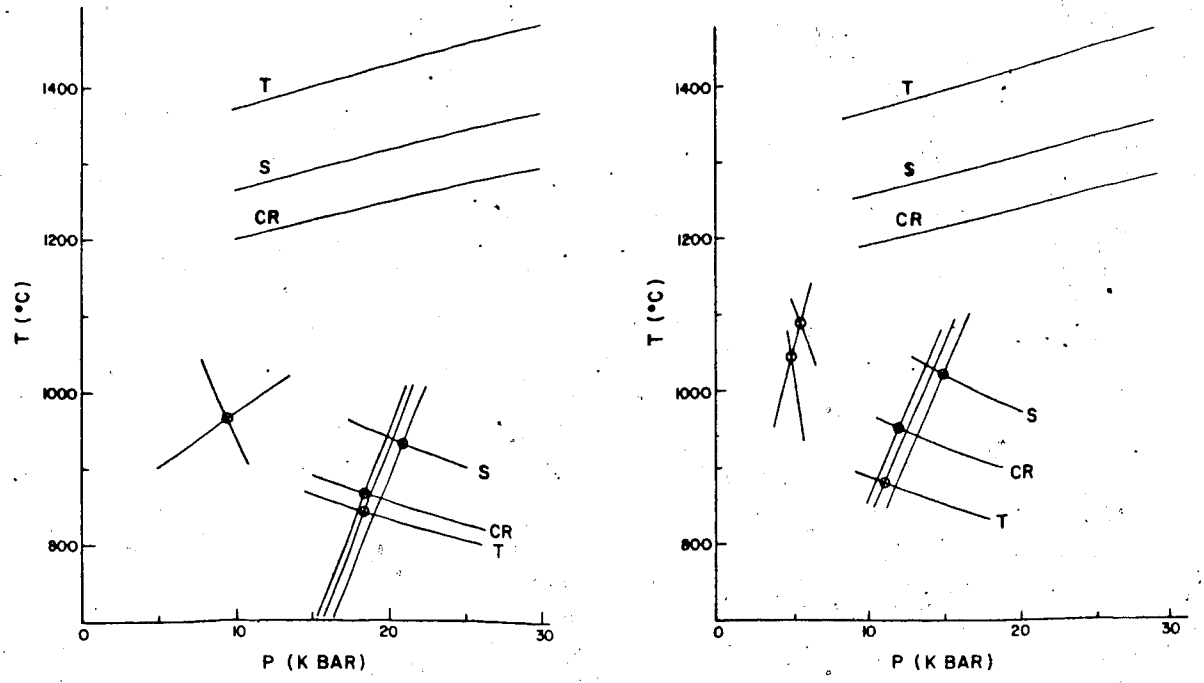

Intermontane Belt (Fiesinger and Nicholls, 1977); Nicholls et al, 1981 in prep.). The pressures calculated for three salic lavas from Level Mountain are all in the range from 6.0 to 6.5 kbar. This corresponds to the average depths calculated for diverse salic lavas in Nicholls et al (1971). The uncertainty associated with the depth (pressure) estimates for Level Mountain salic lavas is far greater than for the basalts. The two reasons for this are that the fayalites for these lavas were in reaction (petrographically) with their respective groundmass compositions (as judged by riebeckite or sodic pyroxene overgrowths), and the mineral buffers used to calculate depths were only assumed to be in equilibrium with said lavas, and this may not have been the case. The salient features of these calculations for Level Mountain are

1. that most of the basalts could have been in equilibrium with a spinel lherzolite mantle at pressures in excess of 9.4 kbar
2. that phenocryst assemblages from most basalts imply crystallization in the 4 to 6 kbar region, which could indicate the existence of crustal level magma chambers and
3. that salic lavas could have come from the lower crust or upper mantle according to the silica activity geobarometry calculations for three trachytes.

A summary of the geobarometry calculations for Level Mountain lavas is presented in Figure 10-4, with pressure

presented versus elevation (eruptive sequence) of the flows. The implication is that initial plateau volcanism originated at pressures from 18.5 to 21.0 kbar and subsequent lavas were derived from shallower depths. There is an indication of an upward migrating melting zone with time. This would be consistent with expectation from experimental studies on the spinel lherzolite system (Takahashi and Kushiro, 1981; Presnall, 1980; Ito and Kennedy, 1967). Following the reasoning of Presnall (1980), for a CO_2 bearing upper mantle, a rising geothermal gradient would intersect the lherzolite solidus cusp in the region of 20 kbar and remain there until one phase was exhausted (generally clinopyroxene). Subsequently the geotherm is constrained by the geometry of the spinel lherzolite solidus and a period of rising depth of melting could occur in a short time span, until the geotherm intersects the 10 kbar cusp on the lherzolite solidus. This sequence of events could have occurred at Level Mountain with the second cusp being reached by the time of extrusion for the basalts of the uppermost plateau (unit 4). The lavas of the stratocone could represent the further upward migration of the geotherm and melting zone into the base of the crust, or by generation of primary magmas at the 10 kbar cusp and further evolution in crustal level magma chambers.

Takahashi and Kushiro (1981) have found a partial melt of "phonolite" composition to exist in equilibrium with Fe- and K-rich spinel lherzolite (Salt Lake Crater, Oahu) at

Figure 10-4.
Geobarometry and geothermometry estimates for equilibration of Level Mountain basalts with spinel lherzolite using ($Fo-En-SiO_2$) and ($Fo-En-Sp-Al_2O_3$), imply a rising geothermal gradient and a rising zone of partial melting with time. Phenocryst equilibration conditions range from the shallow upper mantle to the lower crust. Trachyte estimates from ($Fa-Mt-SiO_2$) and ($Q-SiO_2$) imply equilibration in the lower crust.

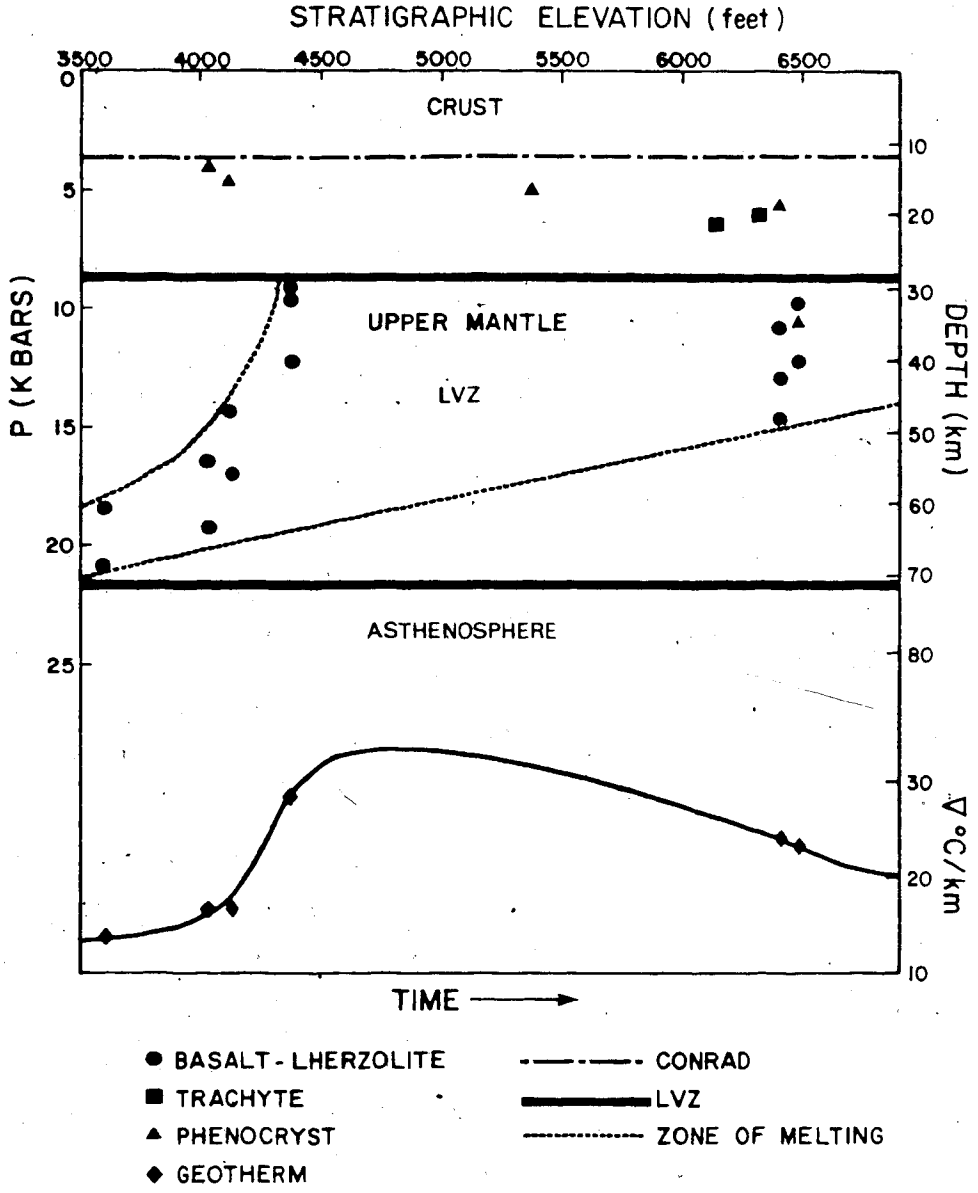

temperatures as much as 200° below the apparent lherzolite solidus (anhydrous). These melts contain in excess of 9.0% by weight K_2O and are effectively peralkaline. This is reminiscient of the bimodal melting hypothesis of Yoder (1976). As the stratocone lavas from Level Mountain include phonolites and are dominantly peralkaline, the possibility still remains that they could be directly generated at mantle depths. Takahashi and Kushiro (1981) also performed a variety of "pyrolite" type experiments involving basaltic glass sandwiched between peridotites (spinel lherzolites). They found that plagioclase - pyroxene gabbros crystallized below the lherzolite solidus and were apparently stable in the PT field for spinel lherzolite. Should significant portions of such alkaline gabbros remain behind in the upper mantle they could contribute to the mantle differentiation and to compositional variation of subsequent partial melting episodes . The existence of gabbroic compositions at mantle depths could possibly account for the peralkaline salic lavas of the stratocone stage.

CHAPTER 11. A PALEOMAGNETIC STUDY OF THE LEVEL MOUNTAIN VOLCANICS

INTRODUCTION

Paleomagnetic studies have been conducted both on Mount Edziza (Souther and Symons, 1974) and on Level Mountain (Evans and Hamilton, 1980). At Level Mountain fifty cooling units were collected from two stratigraphic sections, Figure 11-1. The composite thickness of the proximal and distal sections is greater than 1000 meters. Fourteen magnetic polarity zones are found to be present as well as several low latitude virtual geomagnetic poles (VGP's) which probably represent transitions or excursions. A combination of magnetic data, stratigraphy and fission track dates indicates that the time span of Level Mountain volcanism extends from Epoch VII (greater than 6MY) to the Brunhes Epoch (less than 1MY). These will be shown to be similar to the results from Edziza.

Most sites carry a stable remanence (TRM), which can be determined with high precision. Fisher's precision parameter k generally exceeds 100. The two stratigraphic sections include several low latitude VGP's that probably represent polarity transitions or geomagnetic excursions. Filtering out the sites with low-latitude VGP's (N=5) and high internal scatter (N=7) leaves thirty-eight site means, twenty-four of which have normal polarity and fourteen of which are reversed. The average normal direction does not

Figure 11-1.
Location of the two paleomagnetic sections are shown on the geological sketch map of the Stikine Plateau: showing Level Mountain range and location of related Late Cenozoic volcanics.

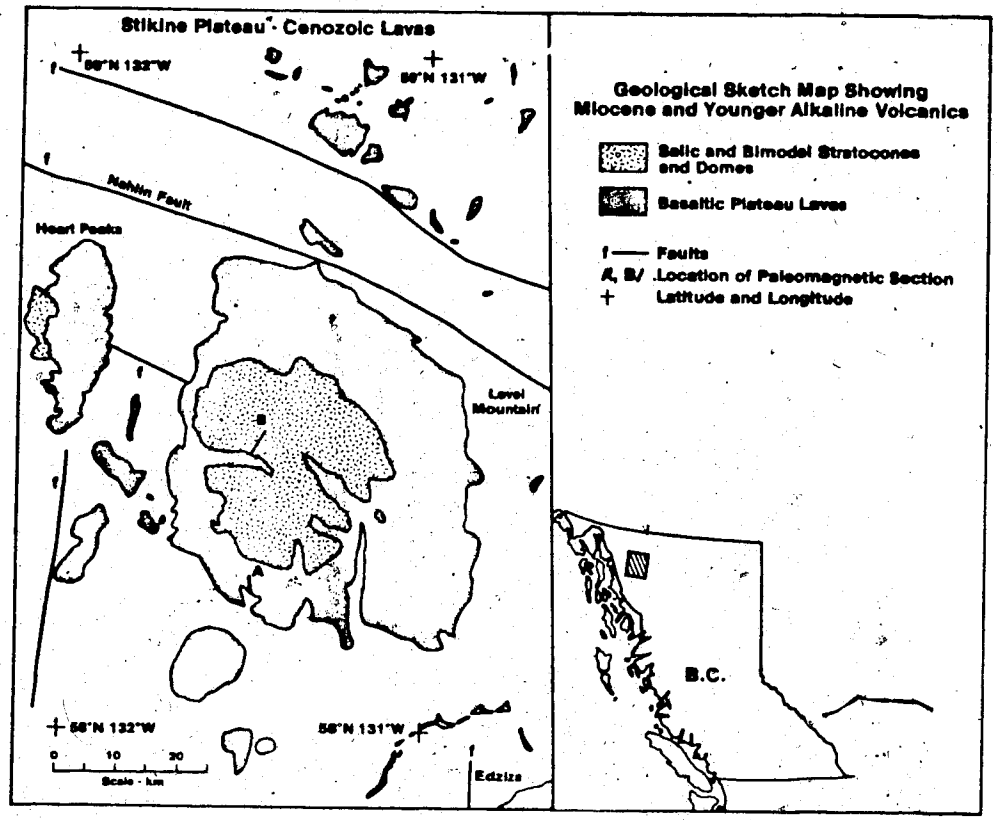

differ significantly from the inverted reverse direction, and the overall mean yields a paleopole at 85°N lat. 256°E long., with an A_{95} of 7°. The actual mean paleopole is slightly near-sided in terms of the common site longitude convention, which fails to support Wilson's eccentric dipole model (Wilson, 1972). Instead near-sidedness seems to be a persistent characteristic of paleopoles obtained from Western North America, suggesting the presence of a long term non-zonal anomaly.

The paleopole position for the best thirty-eight sites at Level Mountain includes the present spin axis as does the Edziza paleopole and the paleopole for the combined Stikine data sets. Since the circles of confidence for these paleopoles include the spin axis, any Late Cenozoic tectonic movements for the Stikine Terrane would appear to be small. The primary purpose of this study was to establish a magnetic stratigraphy for Level Mountain in hopes of correlating to the previously published magnetic stratigraphy of Edziza (Souther and Symons, 1974). An additional incentive was to seek information concerning the overall morphology of the geomagnetic field and its change with time. In this regard, the Late Cenozoic age and high latitude location of Level Mountain are particularly important. The rock magnetic properties of the samples were also investigated to document possible correlations between magnetic and petrological characteristics.

METHODOLOGY FOR THE PALEOMAGNETIC STUDY OF LEVEL MOUNTAIN

Field Procedures. Two stratigraphic sections of twenty-five flows each were collected. Five to seven cores were sampled, from each of the 50 flow-cooling units for a total of 252 cores. With three exceptions all of the flows were collected from contiguous stratigraphic sections. In these cases PBT, PBX, and PAF either exposure or access required that flows be projected "line of sight" back into the main section.

The PA section (distal and stratigraphically lower) was collected from the east facing canyon wall of the Little Tahltan River on the Southern Plateau margin at approximately 58.25°N 131.50°W, Plate 11-1. The section crosses 280 meters of vertical relief which spans the first four eruptive units (1-4) encompassing the plateau building stage at Level Mountain.

The PB section (proximal and stratigraphically higher) was collected from the South face of Meszah Peak and the south trending hanging valley which drains into the Kakuchuya Creek at approximately 58.49°N and 131.48°W, see plate 11-2. This section crosses 700m of vertical relief spanning the stratocone eruptive units 5 to 9. There is a 134m elevation gap between the two stratigraphic sections, which are separated by a lateral distance of 23km. According to field mapping there is no stratigraphic overlap between the two sections, but little or no section is inferred to be missing. The preferred interpretation is that the 134km elevation gap reflects the slope of the plateau surface

Plate 11-1.

The PA section through the basaltic flows of the Level Mountain was collected from the canyon wall of the Little Tahltan river, site PAA to upper right, site PAY lowest dark flow in stream notch above tree line. Map unit 1 extends from base of section to top of dark flows low on cliff. Map unit 2 is lighter coloured with thin flows. Map unit 3 comprises dark flows and tuffs to top of notch. Map unit 4 rests on a thick light coloured tuff unit that lies along the top of the cliff.

Plate 11-2.
View to SW along Hanging Valley from summit of Meszah Peak. The PB section through the stratocone followed the creek, down the hanging valley into the lower valley of Kakuchuya Creek.

(0.33°).

Laboratory Methods. The general measurement techniques to obtain the remanence vector for rock samples have been reviewed by McElhinny (1973) and Cox et al (1967). Pilot measurements of the magnetic vectors were made on a Princeton Applied Research Spinner magnetometer model SM-1 interfaced to a Wang 600 programmable calculator. The stability of one specimen from each flow was tested by routine alternating field (AF) techniques, mostly in peak fields of 2.5, 5, 10, 20, 40 and 80 mT. The results were used to identify regions of directional stability, and thus to select appropriate treatments for the remaining specimens. The bulk of a lab work was conducted using the Schonstedt SSM-1 interfaced to the Wang. The entire study involved about 1100 remanence measurements (presented in Appendix 3). Only one specimen from each core was measured as it has been demonstrated by Doell and Cox (1963, 1965) that very little additional accuracy is gained by multiple sampling. Each specimen was measured for natural remanent magnetization (NRM) and stepwise demagnetized to find a best estimate of D and I for each site. The stepwise demagnetization was performed in an alternating field (AF) apparatus designed and built by Murthy (1969). Due to the variation in rock types and rock magnetic properties a blanket treatment could not be prescribed for all sites. The minimum dispersion criterion (Irving et al, 1961) was applied to identify the best estimate of the mean remanence

direction at each site. Means were calculated in a hierarchial fashion. The values of D and I corresponding to the lowest value of α_{95} (highest Fisher k) were selected from among the sets of measurements at each site. In no case were fewer than three specimens from different cores finally selected to yield a D and I, and in most instances all cores could be used with no rejections. At nine sites one or two specimens exhibited anomalous behavior, either by systematically approaching the group formed by companion cores but never quite reaching this goal, or by stubbornly retaining a divergent direction. These specimens were excluded from further analysis, but it is noteworthy that they represent only 5% of the total data set. Although in part subjective, it is felt that this procedure yields the best available estimate of the true mean paleomagnetic vector at each site. A series of field and laboratory notes have been prepared site by site in descending stratigraphic order as a reference for this collection of data and to clarify any peculiarities at a given site. These notes are presented in Appendices 1 and 2.

The directional variance within each unit is generally small, with Fisher's precision parameter (Fisher, 1953) $k>100$ in 34 out of 50 flows, and $k<50$ in only 7 cases. Another convenient measure of the quality of the directional data is provided by the angular shift occurring at the demagnetization step used in the final analysis. When sites with poor internal grouping are excluded, as explained

below, these angular shifts are quite small. Sixty-seven percent of specimens undergo a shift of 3° or less, the corresponding values for <5° and <10° being 79% and 92% respectively. Thus a small fraction of the specimens have no direct evidence of end-points, and their inclusion rests on agreement with cores from the same site, as reflected by the appropriate site statistics.

MAGNETOSTRATIGRAPHY FOR LEVEL MOUNTAIN

The Stratocone Section, (PB)-Meszah Peak

The essential magnetostratigraphic information for Level Mountain is summarized in Table 11-1. The variation of VGP latitude as a function of elevation is presented as a magnetogram in Figure 11-2.

It is evident that the stratocone section (PB) spans at least three polarity zones. In order of increasing age these are normal, reversed, normal. The uppermost normal magnetozone, stratigraphically map unit 9, comprising hawaiite flows at the summit of Meszah Peak, can confidently be regarded as sampling the Brunhes (Epoch 1). These flows are the most recent on Level Mountain and field relations indicate that they postdate Quaternary continental glaciation (according to field mapping performed by the author and observations of Ostensoe, 1960).

Sites PBP down through PBL are clearly reversed. The most straightforward correlation with the established

Table 11-1 Level Mountain Paleomagnetic Remanence Data by Sites

Unit	Site	Elev	Dens	% NRM	AF	n	R	k	α95	D	I	LAT	LONG
9	PBT	7250	2.89	8.8	400	3(2)	2.9881	168	9.5	32.7	78.9	72.2	270.3
9	PBS	7200	2.96	0.5	800	3(2)	2.9932	294	7.2	46.5	55.1	52.7	336.7
9	PBR	6625	3.00	12.9	200	5	4.9378	64	9.6	51.7	61.9	55.0	322.1
9	PBQ	6580	2.94	4.1	400	3(2)	2.9886	175	9.3	30.4	54.0	59.0	355.9
8	PBP	6480	2.52	83.9	200	5	4.9656	116	7.1	216.0	-73.8	-71.6	119.0
8	PBO	6440	2.54	95.4	100	5	4.9387	65	9.5	184.0	-86.2	-65.5	51.3
7	PBN	6340	2.54	61.0	200	5	4.9983	2352	1.6	262.0	-78.3	-54.3	90.5
7	PBM	6160	2.60	101.0	50	5	4.9891	367	4.0	221.2	-62.3	-60.9	151.5
7	PBL	5835	2.62	79.1	200	5	4.9571	93	8.0	172.3	-65.6	-78.8	257.6
7	(PBY)	5780	2.58	16.4	100	5	4.7744	18	18.7	19.7	30.7	46.0	22.3
7	(PBK)	5745	2.54	100.0	0	5	4.7136	14	21.2	358.4	1.0	32.5	51.9
6b	PBJ	5690	2.80	35.0	100	5	4.9651	115	7.2	28.1	74.1	75.5	298.9
6b	PBI	5675	2.80	38.6	200	5	4.9709	138	6.6	20.2	80.8	73.7	252.3
6b	PBH	5655	2.75	51.8	50	5	4.9917	482	3.5	1.6	79.5	78.3	232.7
6a	PBG	5580	2.48	79.7	200	5	4.9867	301	4.4	19.2	-1.2	(29.4	27.8)
6a	PBF	5545	2.58	57.0	200	5	4.9621	106	7.5	12.4	5.1	(33.7	35.1)
6a	PBE	5475	2.50	78.3	200	5	4.9775	178	5.8	19.3	4.3	(32.1	27.0)
5b	PBD	5460	2.42	98.8	50	6	5.9849	331	3.7	18.7	14.5	(37.3	26.4)
5b	(PBC)	5450	2.78	98.8	100	5	4.8212	22	16.5	353.4	48.8	61.4	62.0
5b	PBB	5430	2.86	9.5	200	5	4.9167	48	11.2	331.8	66.0	70.7	122.1
5b	PBA	5420	2.80	76.2	50	4(1)	3.9968	937	3.0	4.3	53.9	66.3	41.2
5b	(PBX)	5385	2.87	35.8	50	5	4.6887	13	22.2	197.5	-76.8	-79.2	93.1
5a	PBU	5220	2.64	21.1	100	5	4.9351	62	9.8	348.9	72.6	84.1	144.0
5a	PBV	5100	2.26	100.0	0	4(1)	3.9908	326	5.1	8.9	61.8	74.0	25.8
5a	PBW	5000	2.34	46.7	100	5	4.9781	183	5.7	68.4	85.9	60.1	245.4
4	(PAA)	4560	2.87	11.5	400	5	3.9924	4	44.1	167.3	-64.0	-75.5	267.7
4	PAB	4505	2.64	235.4	100	5	4.9884	345	4.1	42.9	81.7	67.3	259.7
4	PAC	4465	2.66	70.4	200	5	4.9841	251	4.8	189.3	-67.3	-80.4	191.5
4	(PAD)	4440	2.63	9.8	400	2(2)	1.9869	76	29.0	169.5	-75.0	-83.5	0.4
4	PAE	4400	2.78	65.6	100	5	4.9978	1818	1.8	313.0	69.3	63.4	149.5
4	PAF	4370	2.58	25.5	100	5	4.9773	176	5.8	294.2	81.7	61.0	198.2
4	PAG	4340	2.66	54.9	100	5	4.9894	377	3.9	280.4	76.9	54.0	185.1
4	PAH	4300	2.56	42.2	100	5	4.9886	351	4.1	15.8	66.7	77.2	356.4
3	PAI	4230	2.70	39.1	200	5	4.9940	667	3.0	63.0	86.2	60.7	243.9
3	PAJ	4200	2.72	19.2	200	5	4.9878	328	4.2	310.1	80.0	66.0	191.3
3	PAK	4170	2.82	24.3	200	5	4.9346	61	9.9	330.7	83.6	68.2	213.2
3	PAL	4155	2.92	15.5	100	5	4.9804	204	5.4	308.6	70.1	61.7	154.6
3	PAM	4135	2.74	46.2	200	5	4.9744	156	6.1	163.2	-45.6	-56.9	258.1
3	PAN	4125	2.82	88.4	200	5	4.9294	57	10.3	169.4	-46.2	-58.6	248.3
3	PAO	4115	2.78	77.0	100	4(1)	3.9986	2141	2.0	167.0	-75.0	-82.5	355.8
3	PAP	4100	2.64	30.1	200	5	4.9317	59	10.1	173.4	-84.4	-69.0	46.5
2	PAQ	4065	2.70	33.1	200	5	4.9916	476	3.5	349.8	60.8	72.6	76.2
2	PAR	4030	2.88	47.1	100	4(1)	3.9957	698	3.5	44.7	57.8	55.3	334.5
2	PAS	3880	2.79	66.5	50	4(1)	3.9914	349	4.9	18.7	69.7	78.6	335.2
2	(PAT)	3860	2.40	108.1	200	4(1)	3.6531	9	33.1	156.6	-77.8	-76.2	8.3
2	PAU	3815	2.80	86.0	200	5	4.9910	444	3.6	154.6	-60.7	-67.2	285.6
2	PAV	3780	2.80	106.0	100	5	4.9259	54	10.5	178.8	-71.8	-88.5	256.5
1	PAW	3700	2.62	54.4	100	5	4.9698	133	6.7	0.0	21.3	(43.0	50.0)
1	PAX	3675	2.78	97.5	100	5	4.9955	889	2.6	147.5	-87.0	-62.9	42.9
1	PAY	3650	2.64	20.4	400	5	4.9770	174	5.8	65.5	-87.5	-55.7	41.9

Notes:
- Elev = elevation above sea level (feet)
- Dens = mean density in g/cc for cores from site
- % NRM = % of NRM intensity remaining upon reaching endpoint
- AF = field strength of last demag step upon reaching endpoint
- n = number of cores accepted (rejected)
- R = vector resultant of n unit vectors
- k = Fisher's precision parameter
- α95 = half-angle of cone of 95% confidence
- D = declination
- I = inclination
- LAT = latitude of equivalent VGP
- LONG = longitude of equivalent VGP

Figure 11-2.
Magnetogram for Level Mountain lavas showing polarity (VGP Lat) versus absolute stratigraphic elevation for the two Level Mountain sections. Lines are broken for erosional interval or other indicated time hiatus.

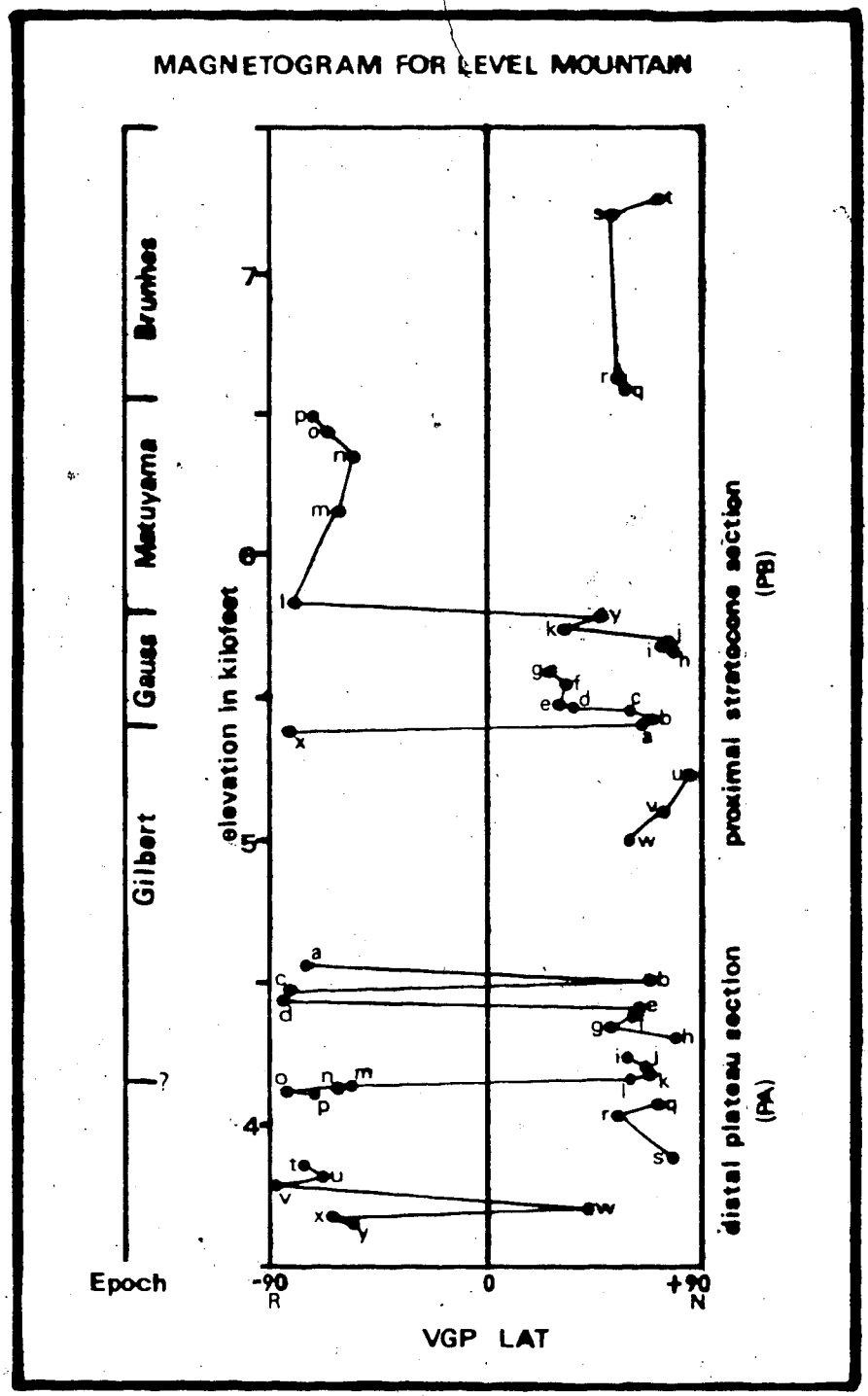

geomagnetic polarity time scale, Figure 11-3, is that these belong to the Matuyama (Epoch 2). It is uncertain whether this sequence of five reversed sites at Level Mountain lies above, below or misses the Jaramillo event entirely. It is not unreasonable to suppose that the short term normal events (Jaramillo, Gilsa, Olduvai) comprising less than 0.3MY (McDougall and Chamalaun, 1966; Cox, 1969) could be missed by a random sampling of only a few flows spread over the length of the Matuyama (some 1.75MY).

Sites PBY and PBK at the base of map unit 6 are normal, but of low precision, and have somewhat shallow inclinations, possibly representing a transition or excursion of the geomagnetic field. Flows at the base of map unit 6 have been dated (by fission track on pitchstones) at two locations on Level Mountain near the head of the Kakuchuya Valley. The dates are 2.61 ±0.12 and 2.46 ±0.12MY (N. Briggs, pers. comm., 1978). These dates coincide within error to the Matuyama/Gauss boundary. It appears that the sequence of flows from PBL down through PBJ samples this transition, with sites PBY and PBK actually lying in the transition itself.

Sites PBJ, PBI and PBH most likely lie in the upper portion of the Gauss (Epoch 3). Below these basalts is a stratigraphic break and a lithological change to peralkaline trachytes. The next four flows have very shallow remanence directions, but the corresponding within- and between-site grouping is good. This group of flows (PBD, PBE, PBF, PBG)

Figure 11-3.
Reference geomagnetic polarity time scale adapted from Mankinen and Dalrymple (1979) down to the base of the Thvera, and from MacDougall et al. (1977) down into Epoch 7.

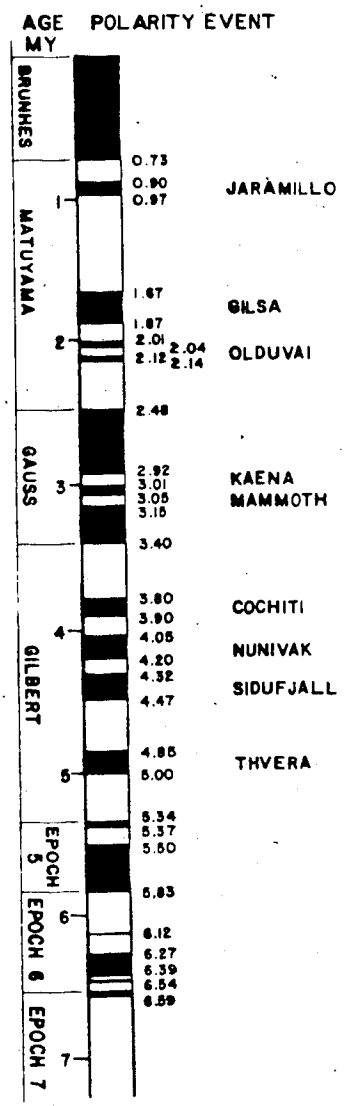

represents either an excursion or a transition from an underlying normal to an unrecorded reversed polarity event lying between PBG and PBH. This could be the transition from the lower Gauss into the Mammoth event, the transition into the base of the Kaena, the transition out of the top of the Cochiti or the transition out of the top of the Nunivak. Without additional sampling or radiometric dating, this ambiguity cannot be resolved. The underlying three flows, PBC, PBB and PBA give normal directions, if somewhat shallow. Despite the shallow nature, the distribution of directions at PBA at least is very tight. Stratigraphically and petrochemically, site PBX belongs with map unit 5b and the sequence of basalts above, but is reversed. This site has no clear endpoint[1] but neither does it display random behavior to AF demagnetization. It is tentatively assigned to the top of the Gilbert (Epoch 4) implying that the base of map unit 5b samples the Gilbert to Gauss transition at 3.40MY (Mankinen and Dalrymple, 1979). The reason that this second interpretation is not favored is that the overlying sequence of seven flows would all have to fit into the 40,000 year normal interval between the Mammoth and the Kaena. These possibilities could be further assessed with

---

[1] On AF demagnetization as the softer (and usually random) components of remanence are progressively removed, the remanence direction changes systematically approaching the true TRM. Once the TRM has been reached, further demagnetization produces no change in direction until all of the remanence has been removed. Sister specimens and other cores from the same site also approach this common TRM direction, which is termed the endpoint.

another stratigraphic section. There is unsampled stratigraphy adjacent to PBX but it would have to be picked up laterally (westwards) along the northern Kakuchuya valley wall. The problem in the vicinity of the PB section is the morainal cover at this stratigraphic interval where the hanging valley enters the Kakuchuya.

The underlying map unit 5a is the basal unit of the stratocone. Sites PBU and PBV (phonolites) and site PBW (comendite) are all normal. This fact, and the foregoing discussion, would place the three flows in one of the short-lived normal events of the Gilbert reversed epoch. Another pitchstone fission track date of 4.51 ±0.26MY was obtained from this unit 5a further to the south across the Kakuchuya-Dudidontu ridge (N. Briggs, pers. comm.). Assuming this date to correspond to PBW, this site (within error) could correspond to the Sidufjall normal event between 4.47 and 4.32MY (Mankinen and Dalrymple, 1979), or possibly the underlying Thvera. One other possibility is that the sequence of sites is not quite as old as unit 5a laterally, and that those flows of the PB section are younger than the date given, possibly placing them during either the Nunivak or the Cochiti event.

In summary, for the stratocone section, stratigraphic and map unit divisions correspond fairly well to magnetic breaks. There are many possible correlations between the PB section and the geomagnetic polarity time scale. The favored interpretation is that this sequence of twenty-five lavas

spans most of the recent four geomagnetic polarity epochs, commencing during the Gilbert at about 4.5MY and continuing up into the Brunhes, younger than 0.73MY. Alternatively, assuming that all of the normal and reversed polarity zones in the lower part of the stratocone have been sampled results in a minimum age estimate for the base of the stratocone between 3.40 and 3.15MY. In the favored interpretation, this sequence catches: the Gauss/Matuyama transition, the beginning of the transition into the Kaena or Mammoth event, and the transition from the Gilbert into the base of the Gauss. Eruptive activity appears to have been sparse and sporadic because the sampling indicates no evidence for the various events in the Brunhes and Matuyama Epochs.

The Plateau Section (PA)-Little Tahltan Canyon

The section of 25 flows sampled from the Little Tahltan Canyon crosses one of the best exposures of basalts which comprise the Level Mountain shield. This section is lower both in elevation and stratigraphic position than the stratocone section described above.

There is no radiometric data at all for the PA section and thus any correlation with the standard time-scale must be regarded as rather tentative. Furthermore, Mankinen and Dalrymple (1979) do not carry their polarity time scale beyond about 5MY. Taking the base of the PB section as representing the Sidufjall event, and simply matching the sequence of normal and reversed intervals determined by

McDougall et al (1977), see figure 11-3, leads to the conclusion that the lowest sites (PAX and PAY) fall near the middle of Epoch 6 (about 6MY). This is a minimum estimate for the onset of volcanism in the area. If "events" within the Gilbert epoch or Epochs 5 and 6 have been missed in this sampling, which seems probable, the base of the section will be correspondingly older. In this context it is reasonable to suppose that the eight flows (PAE to PAL) represent the lower part of Epoch 5 (5.50-5.83MY), not the very short normal interval at the top of Epoch 5 (5.34-5.37MY) which one-to-one matching implies. It also seems probable that the extremely short events at 6.12 and 6.39MY would not be recorded at Level Mountain. If this is so then sites PAQ to PAS may represent the normal interval 6.27 to 6.39MY, with sites PAX and PAY consequently having an age of about 6.6MY.

The frequency of volcanism during the plateau building is apparently greater than during the subsequent stratocone stage. For the minimum estimate of the onset of volcanism in the area of about 6MY, the duration of plateau building is about 1.5MY and possibly as long as 2.1MY for the case of missed events. This translates to an average time interval between eruptions of sixty to eighty thousand years, or about one order of magnitude more frequent activity than during the stratocone stage. However both the field relations and the remanence vectors indicate that eruptive activity during plateau time was more clustered. From this viewpoint, the four plateau units may have been short lived

intense periods of activity separated by quiescent periods of about half a million years in duration. For this second interpretation the quiescent periods during the plateau and stratocone stages are of about the same length, but the volumes of erupted material are more than an order of magnitude different.

A Comparison of the Paleomagnetic Sections from Level Mountain and Mount Edziza

Magnetograms for the three paleomagnetic sections from Mount Edziza (Souther and Symons, 1974) are shown in Figure 11-4. Tentative correlations of Level Mountain and Mount Edziza eruptive sequences to the geomagnetic polarity-time scale are given in Figure 11-5. The directions for sites PBS, PBR and PBQ agree with the uppermost flows of stratigraphic sections A and C on Edziza. The uppermost flows at both centres are basaltic in nature.

Sites PBP, PBO (map unit 8) and PBN (map unit 7) have steeper inclinations and more westerly declinations than most of the sites from map units 5, 7 and 9 of Edziza which are also interpreted to be of Matuyama age. While Souther and Symons (1974) have apparently caught the Jaramillo normal event at their site A6, no similar intervening normal event has been sampled at Level Mountain.

The directions for sites PBP, PBO and PBN are tentatively likened to the direction at Edziza's site A5 which is placed below the Jaramillo, while the intermediate chemistry of flows PBP and PBO (benmoreites) is similar to

Figure 11-4.
Magnetograms for the three Edziza stratigraphic sections. Data from Souther and Symons (1974). Elevation referenced to base of each section. Bar scale indicates map unit designation. Connecting lines are broken for time hiatus (or sampling gap) as inferred from stratigraphic notes.

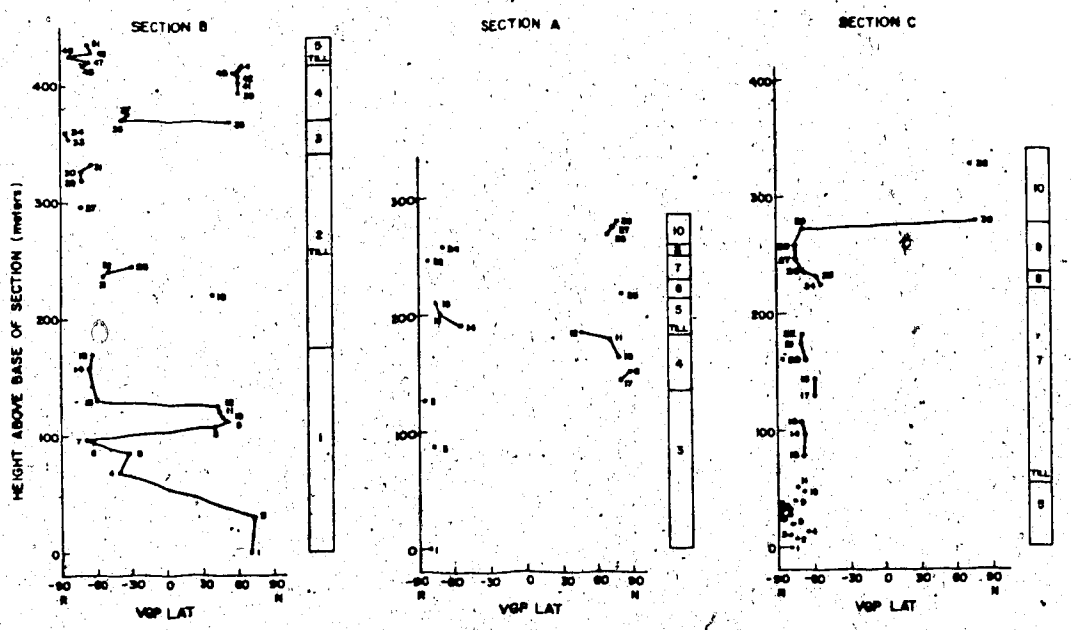

Figure 1.1-5.
Suggested correlation for volcanism at Level Mountain and Mount Edziza with the reference polarity time scale.

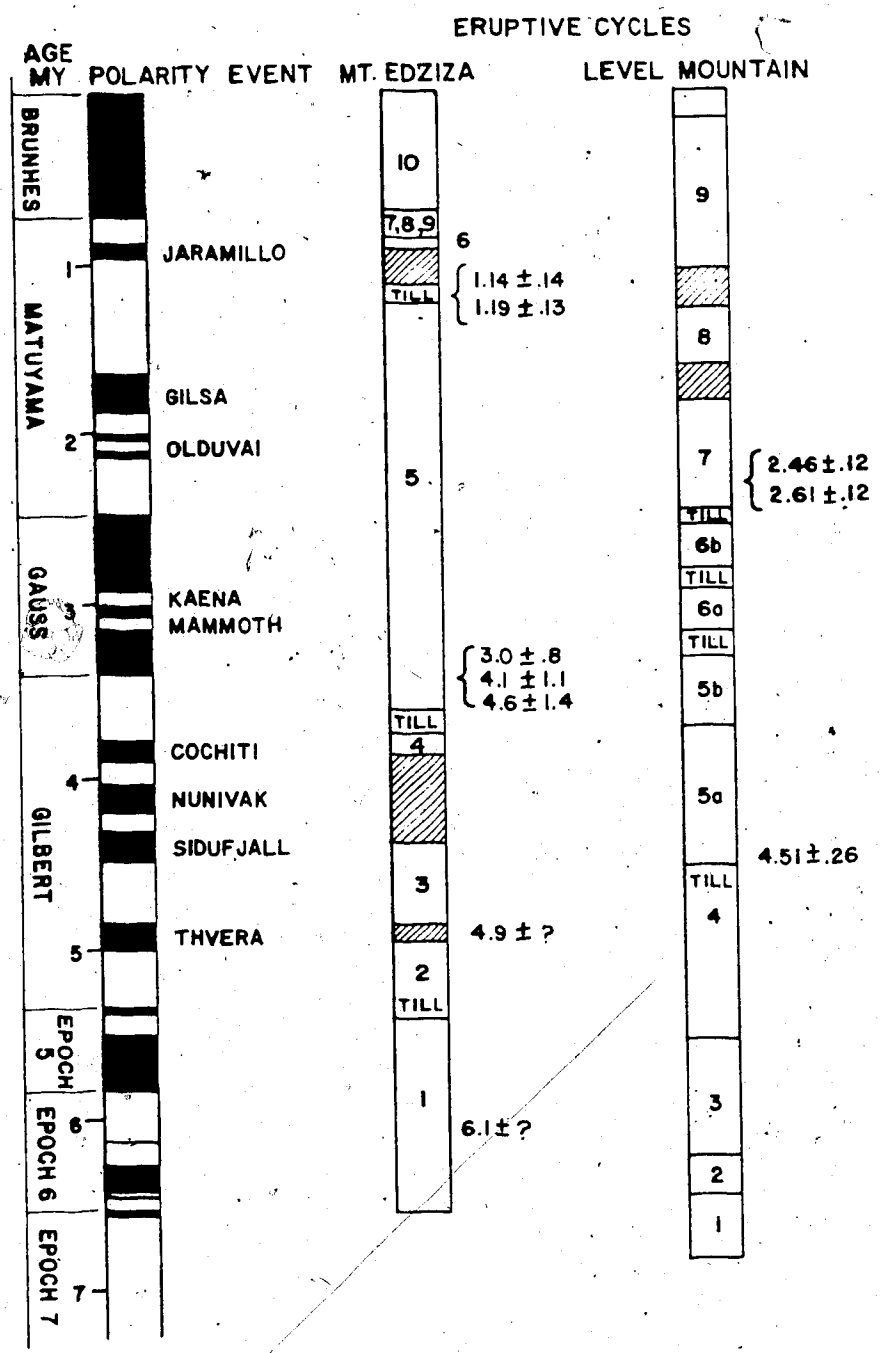

trachybasalts of unit 7 in sections A and C at Edziza.

The eruptive activity of map unit 6 (Level Mountain) appears to have been contemporaneous with glacial activity, as it is underlain by and includes tills, and is overlain by fluvioglacial sands and gravels. While the overlying unit could be Pleistocene, the underlying till implies a glaciation in the region at or prior to 2.5MY. The combination of information on glaciation at Level Mountain and Mount Edziza indicates that 3 or more episodes of continental galciation occurred between the Pleistocene and about 5MY.

The stratigraphic interval including map units 5 and 6 at Level Mountain is lithologically most similar to the sequence from B16 to B32 (Edziza unit 2). These sections are both characterized by abundant peralkaline flows and tuffs. It appears that the bimodal volcanism and stratocone stage at Edziza may preceed its equivalent at Level Mountain by as much as 0.5MY, with such activity beginning at Edziza during the reversed magnetozone of Epoch 5 or at the base of the Gilbert. It is also interesting to note that salic volcanics are included in the Edziza plateau, while at Level Mountain they are restricted to the Stratocone cap. There is a general age, magnetic and lithologic similarity for the stratocone section at Level Mountain and the younger portions of the 3 sections on Edziza.

The lower plateau section (B) at Edziza is bracketed by K-Ar dates as having been erupted between 6.1 and 4.9MY

(Souther and Symons, 1974). The best estimate from combined paleomagnetic and radiometric information is that the Edziza plateau building commences sometime during the lowest normal event of Epoch 6 sampling all three polarity zones of that epoch and the overlying reversed magnetozone of Epoch 5. The low latitude VGP site (PAW) could possibly represent a transition to the short normal zone at the top of Epoch 7. This indicates the possibility that the lowest sampled stratigraphy at Level Mountain is older by at least 0.4MY than the age cited for the base of the Edziza plateau.

CHAPTER 12. SUMMARY AND CONCLUSIONS REGARDING THE PETROGENESIS OF THE LEVEL MOUNTAIN VOLCANICS AND THEIR RELATIONSHIP TO THE TECTONICS OF THE INTERMONTANE BELT.

The most salient geological feature of the Stikine region of northwestern British Columbia is the Late Cenozoic volcanic activity. Since upper Miocene time more than 1700km^3 of lavas have been erupted both as isolated flows and major volcanic edifices covering about 12% of the land area in the Stikine Volcanic Belt (Souther,1977b). Within this region are eleven major volcanic centres of which Level Mountain and Mount Edziza are the largest. Most of the Stikine lavas belong to the sodic alkali basalt series and are of continental affinity. At level Mountain there are two volumetrically dominant lava types. Alkali basalt flows and related basic lavas (sub-alkaline basalt, hawaiite, ankaramite) comprise an oval shield approximately 50km in diameter with an average thickness of 600m. The shield-building stage lasted 2MY or more, ending during the Pliocene at about 4.5MY ago. At that time a fundamental change occurred both in the chemistry of the erupted lavas and their physiographic expression. This second stage of volcanism at level Mountain, with much greater variability in the eruptive style (including flows, pyroclastics, domes, cupolas, dykes and hypabyssal stocks), resulted in the construction of a complex centrally-placed stratocone cap approximately 25km in diameter with a thickness of about 750m. While the entire classic sodic alkali basalt

differentiation series is present, the dominant lavas of the stratocone stage were peralkaline trachytes. Other compositions in decreasing order of abundance are: comendites, rhyolites, hawaiites, benmoreites, phonolites and mugearites.

A variety of models for magma transport were calculated using one-atmosphere viscosity and liquidus determinations for the range of lava compositions. Basic magmas had very rapid ascent velocities in the range of 1 to 10cm/sec with salic magmas being about two orders of magnitude slower. The volumes of typical flows and other single eruption features were on the order of 10^{-1} to $10^{-2}km^3$. That the Level Mountain range is comprised of many such low volume and low viscosity flows argues for low overall rates of volcanicity and the relatively efficient transport of small aliquots of magma directly from the upper mantle.

The isotopic and chemical evidence for the origin of the Level Mountain volcanics is straightforward. Basalts and inclusions with primitive $^{87}Sr/^{86}Sr$ values (0.7025 to 0.70440) and primitive Pb isotope ratios (in the range of typical values for MORB and oceanic islands) argue for an upper mantle derivation from a heterogeneous source. Oxygen isotope values for basalts and inclusions (5.5 to 5.9‰ $\delta^{18}O$ SMOW) confirm that the upper mantle beneath Level Mountain is normal with respect to oxygen. The shift to lighter isotopic compositions for the stratocone basalts, with respect to those on the shield stage,

indicates some heterogeneity for oxygen in the source region as well, and may indicate a shift in the depth of the melting zone as volcanism proceeded. Considering all of the Late Cenozoic lavas from the IMB, scatter in the O and Sr isotope signatures, along with the variation in major and trace element ratios for lavas of similar evolution, argues for a very local scale heterogeneity in their upper mantle source regions. Somewhat lower abundances of K, Rb, U, Th and light rare earths for lavas of the IMB, compared to those from the source regions of alkalic magmas in general (White et al, 1979), may indicate that the upper mantle beneath the Cordillera has been depleted by prior melting events. Such depletion might have occurred through volcanism and plutonism accompanying the Mesozoic emplacement of allochthonous Cordilleran terranes (Monger and Price, 1979).

The major and trace element chemical variations for all of the Level Mountain lavas are inconsistent with the derivation of the volumetrically important peralkaline lavas of the Stratocone stage via the classical fractional crystallization processes from an alkali basalt primary magma. All of the chemical variation is typified by two clusters which are interpreted to indicate that there are two principle magma types, basalt and peralkaline trachyte. The peralkaline salic magmas have some equally primitive lead, strontium and oxygen isotope values to the basalts, but the range in oxygen and strontium extends to higher values indicating a combination of secondary processes

including crustal contamination and selective open system behavior. The peralkaline salic magmas are traditionally interpreted to be derived by substantial fractional crystallization of a wollastonite-normative intermediate or basaltic parent (the orthoclase effect of Bailey and Schairer, 1966). At Level Mountain the major element variation of these peralkaline lavas (principally Na and K) is inconsistent with a derivation via any extensive alkali feldspar fractionation. This interpretation is also born out in the normalized rare earth patterns which are totally lacking in europium anomalies. The distribution of salic lavas about the thermal minimum in the liquidus surface indicates that they may be a related series of partial melts. Geobarometry estimates for trachytes using silica activities give equilibration depths below 20km, in the lower crust. It is uncertain whether this reflects a depth of origin or rest point on the ascent path for the salic magmas. The high one-atmosphere temperatures determined in this study and the expected shape of the liquidus with increasing pressure (Bailey et al, 1974) suggest that the melting probably does not occur within the crust.

The source compositions and P, T conditions for the origin of the basaltic and peralkaline magmas are not very well constrained. Geothermometry and geobarometry calculations on lherzolite inclusions from the Stikine Volcanic Belt indicate equilibration depths in the range from 30 to 70 kilometers. Geobarometry estimates from silica

and alumina activities on Level Mountain lavas gives a similar depth range. This agrees with data for central B. C. reported by Fiesinger and Nicholls (1977) and Fujii et al, 1981. According to the recent synthesis of P and S wave residuals for the Cordillera, the upper mantle lacks a seismically resolvable high velocity lid, and these aforementionned depth estimates correspond to a range from the base of the crust down through the upper half of the low velocity zone (Wickens and Buchbinder, 1980). While the geobarometry estimates place the likely source region in the stability field for spinel lherzolite, the lherzolite compositions from the IMB are too geochemically depleted (Tatsumoto, 1978) to give rise to extractable quantities of basaltic partial melts. Matrix calculations give maximum partial melts of 4% but less than 1% is far more common. Similar calculations using Level Mountain basalts and a pyrolite source give partial melts in the range from 5% to 10% which is high enough for melt extraction. The salic lavas require either a more enriched source or a different derivation mechanism. Peralkaline partial melts can only be derived from peralkaline bulk compositions, which is an unlikely situation in the crust or the mantle. One possibility is that the upper mantle or portions of it become metasomatized by such processes as gase us transfer of incompatible elements from deeper in the mantle or by a series of partial melting episodes with inefficient melt extraction (Boettcher and O'Neil, 1980). This differentiated

upper mantle could contain pods of compositions approaching granulite and gabbro, which is what the partial melting calculations for deriving salic melts require.

The cause of the Level Mountain and related Late Cenozoic volcanics of the IMB is an open question. Alkaline magmas are associated with extensional tectonics such as continental rift and oceanic fracture zones but they also occur on oceanic islands, seamount chains and in continental margin environments (MacDonald, 1974; Bailey, 1977). Some of the structural characteristics of the IMB, as deduced from regional geophysics, resemble a continental rift setting. This structural similarity and the presence of alkaline volcanism, led Souther (1977b) to hypothesize an incipient continental rift. A drawback to this model is the lack of active seismicity in the IMB (Milne et al, 1978) and that the magnitude and rates of volcanism for the SVB are lower than East Africa by two orders of magnitude. The related alkaline volcanism of the Anahim Volcanic Belt led Bevier et al (1979) to point out a possible association with a tear fault in the subducted Juan de Fuca plate. There has been no subduction activity in the vicinity of the northern Canadian Pacific margin since approximately 20MY ago (Grow and Atwater, 1970). This lack of a clear cut tectonic association led to a critical assessment the energy requirements for Level Mountain and the Stikine. Calculations on the amount of energy dissipated by volcanism indicate that the Late Cenozoic volcanism of the SVB could

be initiated and maintained by small changes (15%) in the total heat flux for the region. Changes of this magnitude could arise from the small tectonic stresses associated with the modern shear geometry of the adjacent continental margin (slip on the Queen Charlotte fault is about 6cm/yr) or from the re-equilibration of the thermal structure for the underlying upper mantle, with uplift and rebound of the geotherm following the completion of the subduction for the Kula plate in Mid-Tertiary time.

BIBLIOGRAPHY

Allegre, C. J., and Minster, J. F., 1978. Quantitative models of trace element behavior in magmatic processes. Earth and Planetary Science Letters, 38, pp.1-25.

Anderson, A. T. 1968. The oxygen fugacity of alkaline basalt and related magmas, Tristan de Cunha. American Journal of Science, 266, pp.704-727.

Anderson, A. T. 1974. Chlorine, sulfur and water in magmas and oceans. Geological Society of America Bulletin, 85, pp.1485-1492.

Anderson, A. T. 1976. Magma mixing: petrological process and volcanological tool. Journal of Volcanology and Geothermal Research, 1, pp.3-33.

Anderson, O. L., and Grew, P. C. 1977. Stress corrosion theory of crack propagation with applications to geophysics. Reviews of Geophysics and Space Physics, 15, pp.77-104.

Arculus, R. J. 1975. Melting behavior of two basalts in the range 10 to 35 kilobars. Carnegie Institute of Washington Yearbook, 74, pp.512-515.

Armstrong, R. L. 1968. A model for the evolution of strontium and lead isotopes in a dynamic earth. Reviews of Geophysics, 6, pp.175-200.

Armstrong, R. L., Green, N.L., and Watters, B.R. 1977. Strontium isotope study of Late Cenozoic volcanic rocks of the Canadian Cordillera. Geological Association of Canada Programme with Abstracts, 2, p.5.

Arth, J. G. 1976. Behavior of trace elements during processes and a summary of theoretical models and their applications. U. S. G. S. Journal of Research, 4, pp.41-47.

Ashby, M. E., and Verrall, R. A. 1978. Micromechanisms of flow and fracture and their relevance to the rheology of the upper mantle. Philosophical Transactions of the Royal Society London Series A, 288, pp.59-95.

Bacon, C. R., and Carmichael, I. S. E. 1973. Stages in the P-T Path of ascending basalt magma: an example from San Quintin, Baja California. Contributions

to Mineralogy and Petrology, 41, pp.1-22.

Bailey, D. K. 1969. The stability of acmite in the presence of H_2O. American Journal of Science, 267 A, (Schairer Volume) pp.1-16.

Bailey, D. K. 1974. Experimental petrology relating to oversaturated peralkaline volcanics. Bulletin Volcanologique, 38, pp.637-653.

Bailey, D. K. 1977. Continental rifting and mantle degassing. *In* Petrology and Geochemistry of Continental Rifts. *Edited by* E. R. Neuman and I. M. Ramberg. Reidel, Dordrecht.

Bailey, D. K., Cooper, J. P., and Knight, J. L. 1974. Anhydrous melting and crystallization of peralkaline obsidians. Bulletin Volcanologique, 38, pp.653-658.

Bailey, D. K., and Cooper, J. P. 1979. Comparison of the crystallization of pantelleritic obsidian under hydrous and anhydrous conditions. Fourth NERC Report, London. pp.230-233.

Bailey, D. K., and MacDonald, R. 1969. Alkali feldspar fractionation trends and the derivation of peralkaline liquids. American Journal of Science 267, pp.242-248.

Bailey, D. K., and MacDonald, R. 1970. Petrochemical variations among mildly peralkaline (comendite) obsidians from the oceans and continents. Contributions to Mineralogy and Petrology, 28, pp.340-5.

Bailey, D. K., and MacDonald, R. 1975. Fluorine and chlorine in peralkaline liquids and the need for magma generation in an open system. Mineralogical Magazine, 40, pp.405-414.

Bailey, D.K., and Schairer, J. F. 1964. Feldspar liquid equilibrium in peralkaline liquids - the orthoclase effect. American Journal of Science, 262, pp.1198-2006.

Bailey, D. K., and Schairer, J.F. 1966. The system Na_2O-Al_2O_3-Fe_2O_3-SiO_2 at one atmosphere and the petrogenesis of alkaline reactions. Journal of Petrology, 7, pp.114-170.

Baker, B. H., Goles, G. G., Leeman, W. P., and Lindstrom, M. M. 1977. Geochemistry and petrogenesis of a basalt-benmoreite-trachyte suite from the

southern part of the Gregory Rift, Kenya. Contributions to Mineralogy and Petrology, 64, pp.303-322.

Baker, I. 1969. Petrology of the volcanic rocks of St. Helena Islands, South Atlantic. Bulletin of the Geological Society of America, 80, pp.1283-1310.

Banks, R. J., and Ottey, P. 1974. Geomagnetic depth sounding in and around the Kenya Rift valley. Geophysical Journal of the Royal Astronomical Society, 36, pp.321-335.

Basu, A. R. 1979. The mantle sample: inclusions in kimberlites and other volcanics. *In* Geochemistry of ultramafic xenoliths from San Quentin Baja California, pp.391-400. *edited by* F. R. Boyd and H. O. A. Meyer, *publisher* American Geophysical Union.

Basu, A. R., and MacGregor, I. D. 1975. Chromite spinels from ultramafic xenoliths. Geochimica et Cosmochimica Acta, 39, pp.937-945.

Berry, M. J., and Forsyth, A. 1975. Structure of the Canadian Cordillera from seismic refraction and other data. Canadian Journal of Earth Sciences, 12, pp.187-208.

Bevier, M. L. 1977. Structure, petrology and geochemistry of a peralkaline shield volcano. Rainbow range, British Columbia. Abstracts, Geological Society of America meeting, Seattle, p.897.

Bevier, M. L. 1978. Field relations and petrology of the Rainbow Range shield volcano, West-Central British Columbia. M.Sc. thesis, Department of Geology, University of British Columbia, Vancouver.

Bevier, M. L., Armstrong, R. L., and Souther, J. G. 1979. Miocene peralkaline volcanism in West-Central British Columbia - Its temporal and plate tectonics setting. Geology, 7, pp.389-392.

Birch, F. 1966. Compressibility; elastic constants. *In* Handbook of Physical Constants. Geological Society of America Memoir No.97. *edited by* S. P. Clark Jr.

Bird, R. B., Stewart, W. E., and Lightfoot, E. N. 1960. Transport Phenomena. Wiley, New York.

Boettcher, A. L., and O'Neil, J. R. 1980. Stable isotope,

chemical and petrographic studies of high pressure amphiboles and micas: evidence for metasomatism in the mantle source regions of alkali basalts and comendites. American Journal of Science, 280 A, pp.594-621.

Bostock, H. S. 1948. Physiography of the Canadian Cordillera, with special reference to the area north of the fifty-fifth parallel. Geological Society of America Memoir 247.

Bottinga, Y., and Weill, D. F. 1970. Densities of liquid silicate systems calculated from partial molar volumes of oxide components. American Journal of Science, 269, pp.169-182.

Bowman, H. R., Asaro, F., and Perlman, J. 1973. On the uniformity of composition in obsidians and evidence for magmatic mixing. Journal of Geology, 81, pp.312-327.

Bowen, N. L. 1938. Lavas of the African rift valleys and their tectonic setting. American Journal of Science, Series 5, 35 A, pp.19-33.

Bowen, N. L., and Schairer, J. F. 1938. Crystallization equilibrium in nepheline-albite-silica mixtures with fayalite. Journal of Geology, 46, pp.397-411.

Boyd, F. R. 1973. A pyroxene geotherm. Geochimica et Cosmochimica Acta, 37, pp.2533-3576.

Brooks, C. K., and Printzlau, I. 1978. Magma mixing in mafic alkaline volcanic rocks: the evidence from relict phenocryst phases and other inclusions. Journal of Volcanology and Geothermal Research, 4, pp.315-331.

Brotzu, P., Morbidelli, L., Piccirillo, E. M., and Traversa, G. 1974. Petrological Features of the Boseti Mountains, a complex volcanic system in the axial portion of the main Ethiopian Rift. Bulletin Volcanologique, 38, pp.206-234.

Brousse, R., and Varet, J. 1966. Les trachytes du Mont-Dore et du Cantal septentrional et leurs enclaves. Bulletin Societe Geologique de France, 8, pp.246-262.

Brown, G. M., Holland, J. G., Sigurdsson, H., Tomblin, J. F., and Arculus, R. J. 1977. Geochemistry of the Lesser Antilles volcanic island arc. Geochimica et Cosmochimica Acta, 41, pp.785-802.

Bryan, W. B. 1964. Relative abundance of intermediate members of oceanic basalt - trachyte association: evidence from Clarion and Socorro Islands, Revillagigedo Islands, Mexico. Journal of Geophysical Research, 69, pp.3047-3049.

Bryan W. B. 1966. History and Mechanism of eruption of soda rhyolite and alkali basalt, Socorro Island, Mexico. Bulletin Volcanologique, 29, pp.453-480.

Bryan, W. B. 1976. A basalt-pantellerite association from Isla Socorro, Islas Revillaggedo, Mexico. *In* Volcanoes and Tectonosphere. Tokai U. Press.

Bryan, W. B., Finger, L. W., and Chayes, F. 1969. Estimating proportions in petrographic mixing equations by least squares approximation. Science, 163, pp.926-927.

Buchbinder, G., and Poupinet, G. 1977. P-wave residuals in Canada. Canadian Journal of Earth Science, 14, pp.1292-1304.

Buddington, A. F., and Lindsley, D. H. 1964. Iron titanium oxide minerals and synthetic equivalents. Journal of Petrology, 5, pp.310-357.

Bullard, E. C. 1949. Electromagnetic induction in a rotating sphere. Proceedings of the Royal Society of London, Series A, 199, p.413.

Bullard, E. C., Freedman, C., Gellman, H., and Nixon, J. 1950. The westward drift of the geomagnetic field. Philosophical Transactions of the Royal Society of London, Series a, 243, p.67.

Butterman, W. C., and Foster, W. R. 1967. Zircon stability and the ZrO_2-SiO_2 phase diagram. American Mineralogist, 52, pp.880-885.

Campbell, R. B., 1961. Quesnel Lake map-area, west half, British Columbia. Geological Survey of Canada.

Campbell, R. B., and Tipper, H. W. 1971. Geology of the Bonaparte Lake map-area; Geological Survey of Canada, Memoir No. 363.

Caner, B. 1969. Long aeromagnetic profiles and crustal structure in Western Canada. Earth and Planetary Science Letters, 7, pp.3-11.

Caner, B. 1970. Electrical conductivity structure in Western Canada and petrological interpretation. Journal of Geomagnetism and Geoelectricity, 22,

pp.113-129.

Caner, B., Camfield, P. A., Anderson, F., and Niblett, E. R. 1969. A large scale magneto-telluric survey in Western Canada. Canadian Journal of Earth Science, 6, pp.1245-1261.

Carmichael, I. S. E., and MacKenzie, W. S. 1963. Feldspar - liquid equilibrium in pantellerites, an experimental study. American Journal of Science, 261, pp.382-396.

Carmichael, I. S. E., and Nicholls, J. 1967. Iron - titanium oxides and oxygen fugacities in volcanic rocks. Journal of Geophysical Research, 72, pp.4665-4687.

Carmichael, I. S. E., Nicholls, J., and Smith, A. E. 1970. Silica activity in igneous rocks. American Mineralogist, 55, pp.246-263.

Carmichael, I. S. E., Nicholls, J., Spera, F. J., Wood, B. J., and Nelson, S. A. 1977. High temperature properties of silicate liquids, applications to the equilibration and ascent of basaltic magma. Philisophical Transactions of the Royal Society, London, Series A, 286, pp.[illegible]

Carmichael, I. S. E., [illegible], F. J., Verhoogen, J. 1974. Igneous P[illegible]gy. McGraw-Hill, New York.

Carslaw, H. S., and [illegible], J. C. 1973. Conduction of heat in solids. Oxford Clarendon, London.

Casey, J. 1980. Geology of the Heart Peaks Volcanic Centre. M.Sc. thesis, Department of Geology, University of Alberta, Edmonton.

Cathles, L. M. 1975. The Viscosity of the Earth's Mantle. Princeton University Press.

Cawthorn, R. G., and Collerson, K. D. 1974. The recalculation of pyroxene n-member parameters and the estimation of ferrous and ferric iron content from electron microprobe analysis. American Mineralogist, 59, pp.1203-1208.

Chayes, F. 1963. Relative abundance of intermediate members of the oceanic basalt - trachyte association. Journal of Geophysical Research, 68, pp.1519-1534.

Chayes, F. 1964. A petrographic distinction between Cenozoic volcanics in and around the open ocean. Journal

of Geophysical Research, 69, pp.1573-1588.

Church, S. E., and Tatsumoto, M. 1975. Lead isotope relations in oceanic basalts from the Juan de Fuca - Gorda Ridge area, N.E. Pacific ocean. Contributions to Mineralogy and Petrology, 53, p.253.

Clague, P. A. 1978. The oceanic basalt - trachyte association: an explanation of the Daly Gap. Journal of Geology, 86, pp.739-743.

Clark, S. P. 1966. Thermal Conductivity. Geological Society of America Memoir No. 97, pp.459-483.

Clayton, R. N., and Mayeda, T. K. 1963. The use of bromine pentafluoride in the extraction of oxygen from oxides and silicates for isotopic analysis. Geochimica et Cosmochimica Acta, 22, p.43.

Clowes, R. M. 1981. Geophysics and the Canadian Cordillera. Programme with abstracts, Geological Association of Canada, Vancouver.

Cockfield, W. E., 1925. Explorations between Atlin and Telegraph Creek, B.C. Geological Survey of Canada, Summer report, Part A, pp.37-74.

Cohen, L. H., Ito, K., and Kennedy, G. C. 1967. Melting and phase relations in an anhydrous basalt to 40 kilobar. American Journal of Science, 265, pp.475-518.

Cohn, S., and Ahrens, T. 1977. Dynamic tensile fracture of basic igneous rock. EOS Transactions of the American Geophysical Union, 58, p.1229.

Cooper, J. P., and Bailey, D. K. 1979. Oxidation state in anhydrous experiments of peralkaline obsidians. Fourth NERC Report (London), pp.234-241.

Cox, A. 1968. Lengths of geomagnetic polarity reversals. Journal of Geophysical Research, 73, pp.3247-3260.

Cox, A. 1969. Geomagnetic reversals. Science, 163, pp.237-245.

Cox, A., Dalrymple, G. B., and Doell, R. R. 1967. Reversals of the earth's magnetic field. Scientific American, 216, pp.44-54.

Cox, A., and Doell, R. R. 1960. Review of Paleomagnetism. Bulletin of the Geological Society of America,

71, pp.645-768.

Cox, K. G., Gass, I. G., and Mallick, D. I. J. 1969. The evolution of the volcanoes of Aden and Little Aden, South Arabia. Quarterly Journal of the Geological Society (London), 124, pp.283-308.

Cox, K. G., Glass, I. G., and Mallick, D. I. J. 1970. The peralkaline volcanic suite of Aden and Little Aden, S. Arabia. Journal of Petrology, 7, pp.433-461.

Craig, H. 1961. Standard for reporting the concentration of deuterium and ^{18}O in natural waters. Science, 133, p.1833.

Daly, R. A. 1933. Igneous Rocks and the Depths of the Earth. McGraw-Hill, New York.

Davis, B. T. C., and Boyd, F. R. 1966. The join $Mg_2Si_2O_6$-$CaMgSiO_6$ at 30 kilobar pressure and its application to pyroxenes from kimberlites. Journal of Geophysical Research, 71, pp.3567-3576.

Deer, W. A., Howie, R. A., and Zussman, J. 1978. Rock Forming Minerals, Volume 2A; Single Chain Silicates. Longman, London.

Deines, P., Nafziger, R. H., Ulmer, G. C., and Woerman, E. 1974. Temperature-oxygen fugacity tables for selected gas mixtures in the system C-H-O at one atmosphere total pressure. Bulletin of the Earth and Mineral Sciences Experiment Station, No. 88, Pennsylvania State University.

DeLong, S. E., Fox, P. J., and McDowell, F. W. 1978. Subduction of the Kula Ridge at the Aleutian Trench. Geological Society of America Bulletin, 89, pp.83-95.

DePaolao, D. J. 1979. Estimate of the depth of origin of basic magmas: a modified thermodynamic approach and a comparison with experimental melting studies. Contributions to Mineralogy and Petrology, 69, pp.265-278.

Dey-Sarkar, S. K., and Wiggins, R. A. 1976. Upper mantle structure in western Canada. Journal of Geophysical Research, 81, pp.3619-3632.

Dickinson, D. R., Dodson, M. H., Gass, I. G., and Rex, D. C. 1969. Correlations of initial $^{87}Sr/^{86}Sr$ with Rb/Sr in some late tertiary rocks of S. Arabia.

Earth and Planetary Science Letters, 6, pp.84-90.

Doell, R. R., and Cox, A. 1961. Paleomagnetism. Advances in Geophysics, 8, pp.221-313.

Doell, R. R., and Cox, A. 1963. The accuracy of the paleomagnetic method as avaluated from the historic Hawaiian lava flows. Journal of Geophysical Research, 68, pp.1997-2009.

Doell, R. R. and Cox, A. 1965. Paleomagnetism of Hawaiian lava flows. Journal of Geophysical Research, 70, pp.3377-3405.

Donaldson, D. H. 1976. An experimental investigation of olivine morphology. Contributions to Mineralogy and Petrology, 57, pp.187-213.

Donaldson, C. H., Williams, R. J., and Lofgren, G. 1975. A sample holding technique for study of crystal growth in silicate melts. American Mineralogist, 60, pp.324-326.

Duke, J. M. 1974. The effect of oxidation on the crystallization of an alkali basalt from the Azores. Journal of Geology, 82, pp.524-528.

Dupre and Allegre, 1980. Isotopic composition of lead and strontium and development of Azores Islands.

Eaton, J. P., and Murata, J. K. 1960. How volcanoes grow. Science, 132, pp.925-938.

Edgar, A. D., Parker, L. M. 1974. Comparison of melting relationships of some plutonic and volcanic peralkaline undersaturated rocks. Lithos, 7, pp.263-273.

Epstein, S. 1957. The variations of $^{18}O/^{16}O$ in nature and some geologic implications. *In* Researches in Geochemistry, *Edited by* Abelson, pp.217-240.

Ernst, W. G. 1962. Synthesis, stability relations and occurrence of riebeckite. Journal of Geology, 70, pp.689-736.

Evans, M. E., and Hamilton, T. S. 1980. Paleomagnetic results from a Late Tertiary-Quaternary volcano in northern British Columbia. EOS, Transactions of the American Geophysical Union, 61, p.218.

Fengor, M. 1981. Pedology, Fauna and Climate of the Level Mountain Range, northern British Columbia. In

preparation.

Ferrara, G., and Treuil, M. 1974. Petrological implications of trace element and strontium isotope distributions in basalt-pantellerite series. Bulletin Volcanologique, 88, pp.548-574.

Fiesinger, D. W. 1975. Petrology of the Quaternary volcanic centres in the Quesnel Highlands and Garibaldi provincial park areas, British Columbia. Ph.D. thesis, Department of Geology, University of Calgary, Calgary.

Fiesinger, D. W., and Nicholls, J. 1977. Petrography and Petrology of Quaternary volcanic rocks, Quesnel Lake region, east-central British Columbia. *In* Volcanic Regimes in Canada. Geological Association of Canada Special paper no.16 pp.25-38. *Edited by* W. R. A. Barager, L. C. Coleman and J. M. Hall.

Fisher, R. A. 1953. Dispersion on a sphere. Proceedings of the Royal Society of London, Series A, 217, pp.295-305.

Fitton, J. G., and Gill, R. C. O. 1970. The oxidation of ferrous iron in rocks during mechanical grinding. Geochimica et Cosmochimica Acta, 34, pp.518-524.

Flanagan, F. J. 1973. Values for international geochemical reference samples (1972). Geochimica et Cosmochimica Acta, 37, pp.1189-1200.

Fleet, M. E. 1974. Mg and Fe^{2+} site occupancies in coexisting pyroxenes. Contributions to Mineralogy and Petrology, 44, pp.207-214.

Fleet, M. E. 1974. Partition of Mg and Fe^{2+} in coexisting pyroxenes. Contributions to Mineralogy and Petrology, 44, pp.251-257.

French, W. J. 1971. The correlation between anhydrous crystallization temperatures and rock compositions. Contributions to Mineralogy and Petrology, 31, pp.154-158.

Frey, F. A. 1980. Evidence for heterogeneous primary MORB and mantle sources, NW Indian Ocean. Contributions to Mineralogy and Petrology, 74, pp.387-403.

Fudali, R. F. 1965. Oxygen fugacities of basaltic and andesite magmas. Geochimica et Cosmochimica

Acta, 29, pp.1063-1075.

Fujii, T., and Takahashi, E. 1978. On the solubility of alumina in orthopyroxene coexisting with olivine and spinel in the system $MgO-Al_2O_3-SiO_2$. Mineralogical Journal, 8, pp.122-128.

Fujii, T., and Scarfe, C. M. 1981. Petrology of ultramafic nodules from Boss Mountain, central British Columbia. Geological Association of Canada/Mineralogical Association of Canada, abstracts of Calgary meeting.

Fujii, T. Scarfe, C. M., and Hamilton, T. S. 1981. Geochemistry of ultramafic nodules from southern British Columbia: evidence for banding on the upper mantle. Geological Association of Canada/Mineralogical Association of Canada, abstracts of Calgary meeting.

Fulton, R. J. 1975. Quaternary geology and geomorphology, Nicola-Vernon area, British Columbia. Geological Survey of Canada, Memoir no.380.

Gabrielse, H., and Wheeler, J. O. 1961. Tectonic framework of southern Yukon and northwestern British Columbia. Geological Survey of Canada, paper no. 60-24.

Gabrielse, H., and Souther, J. G. 1962. Dease Lake, British Columbia map-area. Geological Survey of Canada Map 21-1962.

Garland, G. D., and Tanner, J. G. 1957. I[redacted]gations of gravity and isostasy in the S[redacted]n Canadian Cordilleria. Publications of t[redacted]oyal Dominion Observatory, 19, part5, pp.69-222.

Gass, I. G., and Mallick, D. I. J. 1968. Jebel Khariz: an upper Miocene strato volcano of comenditic affinity on the S. Arabian coast. Bulletin Volcanologique, 32, pp.33-38.

Ghent, E. D., Nicholls, J., Stout, M. Z., and Rotenfusser, B. 1977. Clinopyroxene amphibolite boudins from Three Valley Gap, B.C. Canadian Mineralogist, 15, pp.269-282.

Ghiorso, M.S., and Carmichael, I. S. E. 1980. A regular solution model for met-aluminous silicate liquids. Contributions to Mineralogy and Petrology, 71, pp.323-343.

Gibson, I. L. 1972. The chemistry and petrogenesis of a

suite of pantellerites from the Ethiopian Rift. Journal of Petrology, 13, pp.31-44.

Gibson, I. L. 1974. A review of the geology, petrology and geochemistry of the volcano Fant'ale. Bulletin Volcanologique, 38, pp.791-803.

Gilbert, M. C. 1969. High pressure stability of acmite. American Journal of Science (Schairer volume), 267 A, pp.145-159.

Goldich, S. S., Ingamells, C. O., Thaemletzd, p. 1959. The chemical composition of Minnesota Lake marl: a comparison of rapid and conventional chemical methods. Economic Geology, 54, pp.285-300.

Goldschmidt, V. M. 1937. The principle of distribution of chemical elements in minerals and rocks. Journal of the Chemical Society, pp.655-672.

Goles, G. G. 1976. Some constraints on the origin of the phonolites from the Gregory Rift, Kenya and inferences concerning basaltic magmas in the rift system. Lithos, 9, pp.1-8.

Gornostayev, V. P. 1972. On the deep geoelectric model of Pribaikalye. Geol. Geofiz., 6, pp.98-101.

Grant, F. S., and West, G. F. 1965. Interpretation Theory and Applied Geophysics. McGraw-Hill, New York.

Green, D. H., and Ringwood, E. A. 1967. The genesis of basaltic magmas. Contributions to Mineralogy and Petrology, 15, pp.103-190.

Green, H. W. 1976. Plasticity of olivine in peridotites. *In* Electron microscopy in mineralogy. *Edited by* H. R. Wenk, Springer-Verlag, New York.

Green, N. L. 1977. Multistage andesite genesis in the Garibaldi Lake area, southwestern B.C. Ph.D. thesis, Department of Geology, University of British Columbia, Vancouver.

Grow, J. A., and Atwater, T. 1970. Mid-Tertiary tectonic transition in the Aleutian ARC. Geological society of America Bulletin, 81, pp.3715-3722.

Hakli, T. A., and Wright, T. L. 1967. The fractionation of nickel between olivine and augite as a geothermometer. Geochimica et Cosmochimica Acta, 31, pp.877-884.

Halley, E. 1692. An account of the cause of the change of

the variation of the magnetic needle; with an hypothesis of the structure of the internal part of the earth. Philosophical Transactions of the Royal society, 17, pp.563-578.

Hamilton, D. L., and MacKenzie, W. S. 1965. Phase equilibration studies in the system Ne-Kal-Qtz-H_2O. Mineralogical Magazine, 34, pp.214-231.

Hamilton, T. S. 1979. The geology of claim blocks Fission 100-1000, Grizzly Hills Provincial forest. B.C. Department of Mines open file report for 1977.

Hamilton, T. S. 1981. The Level Mountain range and late Cenozoic volcanism in the Stikine. Abstract, February Geological Association of Canada Cordilleran Section Meeting, pp.22-23.

Hamilton, T. S., and Baadsgaard, H., and Scarfe, C. M. 1978. Petrogenesis of late Cenozoic volcanics, Level Mountain, northern British Columbia. Geological Association of Canada/Mineralogical Association of Canada/Geological Society of America programme abstracts, 10, pp.414-415.

Hamilton, T. S., and Muehlenbachs, K. 1977.The ^{18}O geochemistry of Cenozoic lavas from the Level Mountain volcanic centre, British Columbia. EOS, America Geophysical Union Transactions, 58, p.1248.

Hamilton, T. S., and Scarfe, C. M. 1976. Cenozoic alkaline lavas from the Level Mountains volcanic centre. Abstracts, Geological Association of Canada/Mineralogical Association of Canada Annual Meeting, 1, p.47.

Hamilton, T. S., and Scarfe, C. M. 1977. Preliminary Report on the Petrology of the Level Mountain volcanic centre, northwestern British Columbia. Geological Survey of Canada, Paper no.77-1A, Report of activities, part A, pp.429-434.

Handin, J. 1966. Strength and Ductility. *In* Handbook of physical constants, Geological Society of America Memoir No.17, *Edited by* S. P. Clark.

Harris, N. B. W. 1981. The role of fluorine and chlorine in the petrogenesis of a peralkaline complex from Saudi Arabia. Chemical geology, 31, pp.303-311.

Heinricks, H., Schultz, B., Dobrick, J., and Wedepolil, K. H. 1980. Terrestrial geochemistry of Cd, Bi, Tl,

Pb, Zn, Rb. Geochimica et Cosmochimica Acta, 44, pp.1519-1535.

Hertogen, J., and Gijbels, R. 1976. Calculation of trace element fractionation during partial melting. Geochimica et Cosmochimica Acta, 40, pp.312,322.

Hervig, R. L. 1981. Dolomite-apatite inclusions in chrome diopside crystal, Bellsbrook kimberlite, South Africa. American Mineralogist, 66, pp.346-350.

Herzberg, C. T., and Chapman, N. A. 1976. Clinopyroxene geothermometry of spinel lherzolites. American Mineralogist, 61, pp.626,637.

Heirtzler, J. R., Dickson, G. D., Herron, E. M., Pitman, W. C., and LePichon, X. 1968. Marine magnetic anomalies, geomagnetic field reversals and motions of the ocean floor and continents. Journal of Geophysical Research, 73, pp.2119-2136.

Hibbard, M. J. 1981. The magma mixing origin of mantled feldspars. Contributions to Mineralogy and Petrology, 76, pp.158-170.

Hofmann, A. W., and Hart, S. R. 1978. An assessment of local and regional isotopic equilibrium in the mantle. Earth and planetary Science Letters, 38, pp.44-62.

Hofmann, A. W., and Margaritz, M. 1977. Diffusion of Ca, Sr, Ba and Co in a basalt melt: implications for the geochemistry of the mantle. Journal of Geophysical Research, 82, pp.5432-5440.

Holland, H. D. 1972. Granites, solutions and base metal deposits. Economic Geology, 67, p.281.

Huebner, J. S. 1971. Research techniques for high pressure and high temperature. *In* Solid Phase oxygen Buffers. *edited by* G. C. Ulmer.

Hurley, P. M. 1977. Estimates of possible diffusional effects in trace element separations. Earth and Planetary Science Letters, 34, pp.225-230.

Irvine, T. N., and Baragar, W. R. A. 1971. A Guide to the Chemical Classification of the Common Volcanic Rocks. Canadian Journal of Earth Science, 8, pp.523-549.

Irving, E. 1964. Paleomagnetism and its applications to geological and geophysical problems. John Wiley,

New York.

Irving, E. 1966. The great paleozoic reversal of the geomagnetic field. EOS Transaction of the American Geophysical Union, 47, p.78.

Irving, E., Stott, P. M., and Ward M. A. 1961. Demagnetization of igneous rocks by alternating magnetic fields. Philosophical Magazine, 6 pp.225-241.

Ito, K., and Kennedy, G. C. 1967. Melting and phase relations in a natural peridotite to 40 kilobar. American Journal of Science, 265, pp.519-538.

Jacobs, J. A. 1975. The Earth's Core. Academic Press, New York.

Jackson, E. D. 1969. Chemical variation in coexisting chromite and olivine in the chromite zones of the stilliwater complex. Economic Geology Monographs, 4, pp.41-71.

Jessop, A. 1971. The distribution of glacial perturbation of heat flow in Canada. Canadian Journal of Earth Science, 8, pp.162-166.

Jessop, A., and Judge, A. 1971. Five heat flow measurements from Southern Canada. Canadian Journal of Earth Science, 8, pp.711-716.

Jessop, A., and Souther, J. G. 1980. Geothermal measurements in northern B.C. and the southern Yukon. in preparation.

Johnson, S. H., Couch, R. W., Gemperle, M., and Banks, E. R. 1972. Seismic redfraction measurements in southeast Alaska and western British Columbia. Canadian Journal of Earth Science, 9, pp.1756-1765.

Johnson, W. A. 1926. The Pleistocene of Cariboo and Cassiar districts, B. C. Royal Society of Canada, 3rd series, 20, pp.137-147.

Kanasewich, E. R. 1966. Deep crustal structure under the plains and Rocky Mountains. Canadian Journal of Earth Science, 3, pp.932-945.

Kawada, K. 1966. Studies of the thermal state of the earth: variation in the thermal conductivity of rocks. Bulletin of Earthquake Research Institute, Tokyo University, 44, pp.1071-1091.

Keen, C. E., and Hyndman, R. D. 1979. Geophysical review of the continental margins of eastern and western Canada. Canadian Journal of Earth Science, 16, pp.712-747.

Kelley, K. K., and King, E. G. 1961. Contributions to the data on theoretical metallurgy. XIV. Entropies of the elements and inorganic compounds. United States Bureau of Mines Bulletin, 592, 149pp.

Kelsey, C. H. and McKie, D. 1964. The unit cell of aenigmatite. Mineralogical Magazine, 33, pp.986-1001.

Kerr, F. A. 1936. The physiography of the Cordilleran region of northern B. C. Royal Society of Canada, 3rd series, 30.

Kiselev, A. I., Golovko, H. A., and Medvedev, M. E. 1978. Petrochemistry of Cenozoic basalts and associated rocks in the Baikal Rift zone. Tectonophysics, 45, pp.49-54.

Klein, C. 1968. Coexisting Amphiboles. Journal of Petrology, 9, pp.281-330.

Komar, P. D. 1972 (a). Mechanical interactions of phenocrysts and flow differentiation of igneous dykes and sills. Geological Society of America Bulletin, 83, pp.973-988.

Komar, P. D. 1972 (b). Flow differentiation in igneous dykes and sills: profiles of velocity and phenocryst concentration. Geological Society of America Bulletin, 83, pp.3443-3448.

Kuno, H., and Aoki, K. I. 1970. Chemistry of ultramafic nodules and their bearing on the origin of basaltic magmas. Physics of Earth and Planetary Interiors, 3, pp.273-301.

Kuno, M. 1973. Geomagnetic polarity changes and the duration of volcanism in successive lava flows. Journal of Geophysical Research, 78, pp.5972-5982.

Kushiro, I., Yono, Y. S., and Akimoto, S. 1968. Melting of a peridotite nodule at high pressures and high water pressures. Journal of Geophysical Research, 73, pp.6023-6029.

Lambert, A., and Caner, B. 1965. Geomagnetic depth-sounding and the coast effect in western Canada. Canadian Journal of Earth Science, 2, pp.485-509.

Langmuir, C. H., Bender, J. F., Bence, A. E., Hanson, G. N., and Taylor, S. R. 1977. Petrogenesis of basalts from the Famous area: Mid Atlantic ridge. Earth and Planetary Science Letters, **36**, pp.133-156.

Lee, W. H. K., and Clark, S. P. 1966. Heat flow and volcanic temperatures. *In* Handbook of Physical Constants. Geological Society of America Memoir No. 97. pp.483-513.

Leeman, W. P., and Dasch, E. J. 1978. Strontium, lead and oxygen isotope investigation of the Skaergard Intrusion, E. Greenland. Epsel, **41**, pp.47-59.

Leeman, W. P., Vitaliano, C. J., and Prinz, M. 1976. Evolved lavas from the Snake River Plain, Craters of the Moon National Monument, Idaho. Contributions to Mineralogy and Petrology, **56**, pp.35-60.

LePichon, X., and Heirtzler, J. R. 1968. Magmatic anomalies in the Indian Ocean and sea floor spreading. Journal of Geophysical Research, **73**, pp.2101-2117.

Lindsley, D. H. 1971. Synthesis and preliminary results on the stability of aenigmatite. Carnegie Institute of Washington Yearbook, **70**, pp.188-190.

Lindsley, D. H., and Dixon, S. A. 1976. Diopside - enstatite equilibria at 850-1400°C, 5 to 35 kilobars. American Journal of Science, **276**, pp.1285-1301.

Lindsley, D. H., and Haggerty, S. E. 1971. Phase relations of Fe-Ti oxides and aenigmatite; oxygen fugacity of the Pegmatoid zones. Carnegie Institute of Washington Yearbook, **70**, pp.278-284.

Lloyd, F. E., and Bailey, D. K. 1975. Light element metasomatism of the continental mantle: The evidence and the consequences. Physics and Chemistry of the Earth, **9**, pp.389-416.

Liotard, J. M., Verniers, J., and Duquy, C. 1979. Variabilite des valeurs de coefficient de partage: influence de la structure des liquides magmatiques. Chemical Geology, **26**, pp.237-247.

Littlejohn, A. L., and Greenwood, H. J. 1974. Lherzolite nodules in basalts from British Columbia, Canada. Canadian Journal of Earth Science, **11**, pp.1288-1308.

Lovering, J. F. 1966. Electron microprobe analysis of chlorine in two pantellerites. Journal of

Petrology, 7, pp.65-67.

Lowry, R.K. 1981. Comment concerning experimental data on diffusion of major elements between glasses or liquids with basaltic rhyolitics and phenolitic compositions. Earth and Planetary Science Letters, 52, pp.221-222.

Maaloe, S. 1973. T-P relations of ascending primary magmas. Journal of Geophysical Research, 78, p.6877.

MacDonald, G. A., and Katsura, T. 1964. Chemical composition of Hawaiian lavas. Journal of Petrology, 5, pp.82-113.

MacDonald, R. 1974 (a). Tectonic settings and magma associations. Bulletin Volcanologique, 38, pp.575-594.

MacDonald, R. 1974 (b). Nomenclature and petrochemistry of the peralkaline oversaturated extrusive rocks. Bulletin Volcanologique, 38, pp.498-517.

MacDougall, K., Saemundsson, K., Johannesson, H., Watkins, N. D., and Kristjansson, L. 1977. Extension of the geomagnetic polarity time scale to 6.5MY. K-Ar dating, geological and paleomagnetic study of a 3,500m lava succession in W. Iceland. Geological Society of America Bulletin, 88, pp.1-15.

MacGregor, I. D. 1974. The system $MgO-Al_2O_3-SiO_2$: the solubility of Al_2O_3 in enstatite for spinel and garnet peridotite compositions. American Mineralogist, 59, pp.110-119.

Malkus, W. V. R. 1968. Precession of the earth as a cause of geomagnetism. Science, 160, pp.259-264.

Mankinen, E. A., and Dalrymple, B. G. 1979. Revised geomagnetic polarity time scale for the interval 0-5MYBP. Journal of Geophysical Research, 84, pp.615-626.

Manning, D. A. C. 1981. The effect of fluorine on liquidus phase relationships in the system Qz-Ab-Orwith excess water at one kilobar. Contributions to Mineralogy and Petrology, 76, pp.206-215.

Manning, D. A. C., Hamilton, E. L., Henderson, C. M. B., and Dempsey, M. J. 1980. The probable occurrence of interstitial Al in hydrous fluorine bearing and fluorine free aluminosilicate melts. Contributions to Mineralogy and Petrology, 75,

pp.257-262.

Margaritz, M., Whitford, D. J., and James, D. E. 1978. Oxygen isotopes and the origin of high $^{87}Sr/^{86}Sr$ andesites. Earth and Planetary Science Letters, **40**, pp.220-230.

Marsh, J. S. 1975. Aenigmatite stability in silica undersaturated rocks. Contributions to Mineralogy and Petrology, **50**, pp.134-144.

Marsh, B. D., and Kantha, L. H. 1978. On heat and mass transfer from an ascending magma. Earth and Planetary Science Letters, **39**, pp.435-443.

Mathez, E. A. 1973. Refinement of the Kudo-Weill plagioclase thermometer and its application to the basaltic rocks. Contributions to Mineralogy and Petrology, **41**, pp.61-72.

Matsuhisa, Y. 1973. Oxygen isotope variation in magmatic differentiation processes of volcanic rocks of Japan. Contributions to Mineralogy and Petrology, **39**, pp.277-288.

Matsuhisa, Y., Goldsmith, J. R., and Clayton, R. N. 1979. Oxygen isotope fractionation in the system $Q-Ab-An-H_2O$. Geochimica et Cosmochimica Acta, **43**, pp.1131-1140.

Matsui, Y., Onuma, N., Nagasawa, H., Higuchi, H., and Banno, S. 1977. Crystal structure control in trace element partition among crystals and magma. Bulletin of the Society of Mineralogy and Crystallography

McBirney, A. R. 1963. Conductivity variations and terrestrial heat flow variation. Journal of Geophysical Research, **68**, pp.6323-6329.

McBirney, A. R. 1969. Proceedings of the andesite conference. Oregon Department of Mines Bulletin, **65**, pp.175-184.

McBirney, A. R., and Williams, H. 1969. Thermal aspects of the generation and rise of magmas. *In* Geology of Galapagos Islands. Geological Society of America Memoir No. 118, pp.180-194.

McDougall, I., and Chamalaun, F. H. 1966. Geomagnetic polarity scale of time. Nature, **5060**, p.1415.

McDougall, I., Saemundsson, K., Johannesson, H., Watkins, N. D., and Kristjansson, L. 1977. Extension of the

geomagnetic polarity time scale to 6.5MY: K-Ar dating, geological and paleomagnetic study of a 3500m lava succession in W. Iceland. Geological Society of America Bulletin, 88, pp1-15.

McElhinney, M. W. 1973. Paleomagnetism and Plate Tectonics. Cambridge University Press.

McElhinney, M. W., and Merrill, R. T. 1975. Geomagnetic secular variation over the past 5MY. Reviews of Geophysics and Space Physics, 13, pp.687-708.

McIntire, W. L. 1963. Trace element partition coefficients, a review of theory and applications to geology. Geochimica et Cosmochimica Acta, 27, pp.1209-1264.

Mercier, J. C. C., and Nicolas, A. 1975. Textures and fabrics of upper mantle peridotites as illustrated by xenoliths from basalts. Journal of Petrology, 16, pp.454-487.

Millhollen, G. L. Irving, I. J., and Wyllie, P. J. 1974. Melting interval of peridotite with 5.7% H_2O to 30kilobars. Journal of Geology, 82, pp.575-587.

Milne, W. G. 1963. Seismicity of Western Canada. Boletin Bibliografico de Geofisica y Oceanographia Americanas, 3, pp.17-40.

Milne, W. G., Rogers, G. C., Riddihough, R. P., McMechan, G. A., and Hyndman, R. D. 1978. Seismicity of Western Canada. Canadian Journal of Earth Science, 15, pp.1170-1193.

Milne, W. G., Smith, W. E. T., and Rogers, G. C. 1970. Canadian seismicity and micro-earthquake research in Canada. Canadian Journal of Earth Science, 7, pp.591-601.

Minster, J. F., Minster, J. B., Allegre, C. J., and Treuil, M. 1977. Systematic use of trace elements in igneous processes. II. Inverse problem of the fractional crystallization process in volcanic suites. Contributions to Mineralogy and Petrology, 61, p.49.

Monger, J. W. H. 1968. Early Tertiary stratified rocks. Greenwood map area (82 E/2). Geological Survey of Canada paper no.67-42.

Monger, J. W. H., and Irving, E. 1980. Northward displacement of north-central British Columbia. Nature, 285, pp.289-293.

Monger, J. W. H., and Price, R. A. 1979. Geodynamic evolution of the Canadian Cordillera - progress and problems. Canadian Journal of Earth Science, 16, pp770-791.

Monger, J. W. H., Souther, J. G., and Gabrielse, H. 1972. Evolution of the Canadian Cordillera. American Journal of Science, 272, pp.577-602.

Mori, T. 1977. Geothermometry of spinel lherzolites. Contributions to Mineralogy and Petrology, 59, pp.261-279.

Mori, T., and Green, D. H. 1975. Pyroxenes in the system Mg_2SiO_4-$CaMgSi_2O_6$ at high pressure. Earth and Planetary Science Letters, 25, pp.277-286.

Mori, T., and Green, D. H. 1976. Sub-solidus equilibria between pyroxenes in the CaO-MgO-SiO_2 system at high pressures and temperatures. American Mineralogist, 61, pp.616-625.

Mori, T., and Green, D. H. 1978. Laboratory duplication of phase equilibria observed in natural garnet lherzolites. Journal of Geology, 86, pp.83-97.

Muehlenbachs, K., Anderson, A. T., and Sigvaldason, G. E. 1974. Low-^{18}O basalts from Iceland. Geochimica et Cosmochimica Acta, 38, pp577-588.

Muehlenbachs, K., and Clayton, R. N. 1972. Oxygen isotope studies of fresh and weathered basalts. Canadian Journal of Earth Science, 9, pp.172-184.

Muehlenbachs, K., and Stone, G. T. 1973. Oxygen isotope compositions of some basaltic lavas from the Snake River plain. Carnegie Institute of Washington Yearbook, 72, pp.598-601.

Murase, T., and McBirney, A. R. M. 1973. Properties of some common igneous rocks and their melts at high temperatures. Geological Society of America Bulletin, 84, pp.3563-3592.

Murthy, G. S. Paleomagnetic studies in the Canadian shield. Ph.D. thesis, Department of Physics, University of Alberta, Edmonton.

Mysen, B. O. 1975. Partitioning of Fe and Mg between crystals and partial melts in a peridotite upper mantle. Contributions to Mineralogy and Petrology, 52, pp.69-76.

Mysen, B. O., and Boettcher, A. L. 1975. Melting of a

hydrous mantle I and II. Journal of Petrology, 16, pp.520-593.

Mysen, B. O., and Kushiro, I. 1979. Pressure dependance of Ni partitioning between forsterite and aluminous silicate melts. Earth and Planetary Science Letters, 42, pp.383-388.

Mysen, B. O., Virgo, D., and Scarfe, C. M. 1980. Relations between the anionic structure and viscosity of silicate melts - a raman spectroscopic study. American Mineralogist, 65, pp.690-710.

Nagata. T. 1961. Rock Magnetism. Mazuren press, Tokyo.

Naney, M. T., and Swanson, S. E. 1980. The effect of Fe and Mg on crystallization in granitic systems. American Mineralogist, 65, pp.639-654.

Nash, W. P., Carmichael, I. S. E., and Johnson, R. W. 1969. The mineralogy and petrology of Mount Suswa, Kenya. Journal of Petrology, 10, pp.409-439.

Nash, W. P., and Evans, J. H. 1977. Natural silicate liquids, fugacities and flow. Abstracts, Geological Association of America meeting, Seattle, p.110.

Neir, A. O. 1947. A mass spectrometer for isotope and gas analyses. Review of Scientific Instruments, 18, pp.398-411.

Neumann, H., Mead, J., and Vitaliano, C. J. 1954. Trace element variation during fractional crystallization as calculated from the distribution law. Geochimica et Cosmochimica Acta, 6, pp.90-00.

Nicholls, J. 1980. A simple thermodynamic model for estimating the solubility of H_2O in magmas. Annales de Geophysique, 36, p.211.

Nicholls, J., and Carmichael, I. S. E. 1969. Peralkaline acid liquids: a petrologic study. Contributions to Mineralogy and Petrology, 20, pp.268-294.

Nicholls, J., and Carmichael, I. S. E. 1972. The equilibration temperature and pressure of various lava types with spinel and garnet peridotite. American Mineralogist, 57, pp.941-959.

Nicholls, J., Carmichael, I. S. E., and Stormer, J. C. 1971. Silica Activity and P(total) in igneous rocks. Contributions to Mineralogy and Petrology, 33,

pp.1-20.

Nicholls, J., Stout, M. Z., and Fiesinger, D. W. 1981. Petrologic variations in Quaternary volcanic rocks, British Columbia, and the underlying upper mantle. In press.

Nicholls, J., Stout, M. Z., and Ghent, E. D. 1976. Petrology and basanite and trachy basalt lavas, western Brithish Columbia. EOS American Geophysical Union Transactions, 57, p.1018.

Nixon, P. H., Rogers, N. W., Gibson, I. L., and Grey, A. 1981. Depleted and fertile mantle xenoliths from South African kimberlites. Annual Reviews of Earth and Planetary Science, 9, pp.285-309.

Noble, D. C. 1965. Gold Flat member of Thirsty Canyon Tuff - a pantellerite ash flow sheet in southern Nevada. U.S.G.S.Professional paper 525-B, pp.85-90.

Noble, D. C. 1967. Sodium, potassium and ferrous iron contents of some secondarily hydrated natural silicic glasses. American Mineralogist, 52, pp.280-286.

Noble, D. C. 1968. Systematic variation of major elements in comendite and pantellerite glass. Earth and Planetary Science Letters, 4, pp.167-172.

Noble, D. C., and Haffty, J. 1969. Minor element and some revised major element content of some Mediterranean pantellerites and comendites. Journal of Petrology, 10, pp.502-509.

Noble, D. C., and Parker, D. F. 1974. Peralkaline silicic volcanic rocks of the western United States. Bulletin Volcanologique, 38, pp.803-828.

Obata, M. 1976. The solubility of Al_2O_3 in orthopyroxenes in spinel and plagioclase peridotites and spinel pyroxenite. American Mineralogist, 61, pp.804-816.

O'Neill, J. R. 1977. Stable isotopes in mineralogy. Physics and Chemistry of Minerals, 2, pp.105-123.

O'Neill, J. R., and Taylor, H. P. 1967. Oxygen isotope and cation exchange chemistry of feldspars. American Mineralogist, 52, pp.1414-1437.

Onuma, N., Higuchi, H., Wakita, H., and Nagasawa, H. 1968. Trace element partition between two pyroxenes

and the host lava. Earth and Planetary Science Letters, 5, pp.47-51.

Osborn, E. F. 1942. The system $CaSiO_3$-diopside-anorthite. American Journal of Science, **240**, pp.751-788.

Ostensoe, E. 1960. Level Mountain, northwestern British Columbia. B.Sc. thesis, Department of Geology, University of British Columbia, Vancouver.

Parrish, R. 1981. Cenozoic uplift history of the coast mountains of British Columbia. Abstract, Geological Association of Canada, Cordilleran section meeting, Vancouver, p.30.

Pearce, J. A., and Cann, J. R. 1973. Tectonic setting of basic volcanic rocks determined using trace element analyses. Earth and Planetary Science Letters, **19**, pp.290-300.

Pearce, J. A., and Norry, M. J. 1979. Petrogenetic implications of Ti, Zr, Y, and Yb variations. Contributions to Mineralogy and Petrology, **69**, pp.33-47.

Peters, L. J. 1949. The direct approach to magnetic interpretation and its practical implications. Geophysics, **14**, pp.290-320.

Philpotts, J. A., and Schnetzler, C. C. 1970. Phenocryst-matrix partition coefficients for K, Rb, Sr and Ba with applications to anorthosite and basalt genesis. Geochimica et Cosmochimica Acta, **34**, pp.307-322.

Philpotts, J. A. 1978. The law of constant rejection. Geochimica et Cosmochimica Acta, **42**, pp.909-920.

Pinsent, R. H., and Smith, D. G. W. 1975. The development of carbonate bearing biotite isograd assemblages from Tete Jaune Cache, B.C. Canadian Mineralogy, **13**, pp.151-161.

Piotrowski, J. M., and Edgar, A. D. 1970. Melting relations on undersaturated alkaline rocks from Greenland, Africa, and Canada. Medd. om. Gronland, **181**, p.66.

Piwinski, A. J. 1973. Experimental studies of igneous rock series central Sierra Nevada batholith, California, Part II. N. Jb. Miner. Mh. pp.193-215.

Pollack, H. N., and Chapman, D. S. 1977. Mantle heat flow.

Earth and Planetary Science Letters, **34**, pp.174-184.

Presnall, D. C. 1976. Alumina content of enstatite as a geobarometer for plagioclase and spinel lherzolites. American Mineralogist, **61**, pp.582-588.

Presnall, D. C. 1980. A double partial melt zone in the mantle beneath Mid ocean Ridge. Physics of Earth and Planetary Interiors, **23**, pp.103-111.

Price, R. C,, and Chappell, B. W. 1975. Fractional crystallization and the petrology of Dunedin volcano. Contributions to Mineralogy and Petrology, **53**, pp.157-182.

Ranalli, G. 1980. Rheological properties of the upper mantle in Canada from olivine microrheology. Canadian Journal of Earth Sciences, 17, pp.1499-1505.

Reed, S. J. B., and Ware, N. G. 1975. Quantitative electron microprobe analysis of silicates using energy dispersive X-Ray spectrometry. Journal of Petroloogy, **16**, pp.499-519.

Reitmayr, G. 1975. An anomaly of the upper mantle below the Rhinegraben studied by the inductive response of natural electromagnetic fields. Journal of the Royal Astronomical Society, **41**, pp.651-658.

Riddihough, R. P. 1977 A model for recent plate interactions off Canada's west coast. Canadian Journal of Earth Science, **14**, pp.384-396.

Riddihough, R. P. 1981. Major plate interactions affecting the Canadian Cordillera over the last 100 Ma: constraints and uncertainties. Abstracts, Geological Association of Canada, Cordilleran section meeting, Vancouver, p.33.

Ridley, K. J. 1975. The non-reproducibility of chemical analyses on reference rock standards and an evaluation of the cause of the problem. M.Sc. thesis, Department of Geology, University of Windsor, Windsor, Ontario.

Ridley, W. I. 1970. The petrology of Las Canadas volcanoes, Tenerife, Canary Islands. Contributions to Mineralogy and Petrology, **26**, pp.124-160.

Robie, R. A., Hemmingway, B. S., and Fisher, J. R. 1978. Thermodynamic properties of minerals and related substances at 298.15°K and 1Bar (10^5pascals)

pressure and at higher temperatures. Geological Survey Bulletin 1452.

Roebroeck, E. J., and Nyland, E. 1975. P Wave residuals in western Canada. Canadian Journal of Earth Science, **12**, pp.174-181.

Roedder, E. 1965. Liquid CO_2 inclusions in olivine bearing nodules and phenocrysts from basalts. American Mineralogist, **50**, pp.1746-1782.

Roy, R. F., Blackwell, D. D., and Birch, F. 1968. Heat generation of plutonic rocks and continental heat flow provinces. Earth and Planetary Science Letters, **5**, pp.1-12.

Rucklidge, J. C., Gibb, F. G., Fawcett, J. J., and Gasparrini, E. L. 1970. Rapid rock analysis by microprobe. Geochimica et Cosmochimica Acta, **34**, pp.245-247.

Russell, R. D. 1972. Evolutionary model for lead isotopes in conformable ores and in ocean volcanics. Reviews of Geophysics and Space Physics, **10**, p.529.

Scarfe, C. M. 1973. Viscosity of basic magmas at varying pressure. Nature, **241**, pp.101-102.

Scarfe, C. M. 1977. Viscosity of a pantellerite melt at one atmosphere. Canadian Mineralogist, **15**, pp.185-189.

Scarfe, C. M., and Hamilton, T. S. 1980. Viscosity of lavas from the Level Mountain volcanic centre, northern British Columbia. Carnegie Institute of Washington Institute Yearbook, **79**, pp.318-320.

Scarfe, C. M., Mysen, B. O., and Rai, C. S. 1979. Invariant melting behavior of mantle material: partial melting of two lherzolite nodules. Carnegie Institute of Washington Yearbook, **78**, pp.498-501.

Scarfe, C. M., Paul, D. K., and Harris, P. G. 1972. Melting experiments at one atmosphere on two ultramafic nodules. N. Jb. Min. Mb., **10**, pp.469-476.

Schairer, J. F., and Bowen, N. L. 1955. The system K_2O-Al_2O_3-SiO_2. American Journal of Science, **253**, pp.681-746.

Schairer, J. F., and Bowen, N. L. 1956. The system Na_2O-Al_2O_3-SiO_2. American Journal of Science, **254**, pp.129-195.

Schilling, J. G. 1973. Iceland mantle plume: geochemical study of Reykjanes Ridge. Nature, 242, pp.565-575.

Schimann, K., and Smith, D. G. W. 1980. The optical fusion of whole rock powder and their analysis by an electron microprobe technique. Canadian Mineralogist, 18, pp.131-143.

Schmincke, H. U. 1974. Volcanological aspects of peralkaline silicic welded ash flow tuffs. Bulletin Volcanologique, 38, pp.594-637.

Seitz, M. G. 1973. U and Th partitioning in diopside melt and whitlockite melt systems. Carnegie Institute of Washington Yearbook, 72, p.581.

Self, S., and Gunn, B. M. 1976. Petrology, volume and age relations of alkaline and saturated peralkaline volcanics from Terceria, Azores. Contributions to Mineralogy and Petrology, 54, pp.293-313.

Shand, S. J. 1927. The Eruptive Rocks. Wiley, New York.

Shandley, P. D., and Bacon, L. O. 1963. Abstracts, Society of Exploration Geophysicists New Orleans meeting.

Shaw, D. M. 1961. Element distribution laws in geochemistry. Geochimica et Cosmochimica Acta, 23, p.116.

Shaw, H.R. 1963. Obsidian - H_2O viscosities at 1000 and 2000 bars in the temperature range 700 to 900°C. Journal of Geophysical Research, 68, pp.6337-6343.

Shaw, H. R. 1965. Comments on viscosity, crystal settling and convection in granitic magmas. American Journal of Science, 263, pp.120-152.

Shaw, H. R. Rheology of basalt in the melting range. Journal of Petrology, 10, pp.510-535.

Shaw, H. R. 1972. Viscosity of magmatic silicate liquids. American Journal of Science, 272, pp.870-893.

Sinclair, P. D., Templeman-Kluit, D. J., and Medaris, L. G. 1977. Lherzolite nodules from a Pleistocene cinder cone in central Yukon. Canadian Journal of Earth Science, 15, pp.220-226.

Skiles, D. D. 1972. The laws of reflection and refraction of incompressible magnetohydrodynamic waves in a fluid-solid interface. Physics and Chemistry of

Planetary Interiors, 5 p.90.

Skinner, B. J. 1962. Thermal expansion of ten minerals. U. S. G. S. Professional paper 450D, pp.109-112.

Skinner, B. J. 1966. Thermal expansion. *In* Handbook of Physical Constants. Geological Society of America Memoir No.97, pp.75-97.

Sleep, N. H. 1974. Separation of magma from a mostly crystalline mush. Bulletin of the Geological Association of America, 85, pp.1225-1232.

Smith. D. G. W. 1976. Mineralogical Association of Canada Short Course in Microbeam Techniques.

Smith, D. G. W., and Gold, C. M. 1979. EDATA2: A Fortran IV computer program for processing wavelength and/or energy dispersive electron microprobe analyses. *In* Microbeam Analyses. *Edited by* D. E. Newbury, San Francisco Press.

Smith, P. J., and Needham, J. 1967. Magnetic declination in medieval China. Nature, 214, p.1213.

Sobolev, N. V. 1977. Deep-seated inclusions in kimberlites and the problem of the compositions of the upper mantle.

Soga, N. 1967. Elastic constants of garnet under pressure and temperature. Journal of Geophysical Research, 72, pp.4227-4234.

Sorenson, H. 1970. Internal structures and geological setting of three agpaitic intrusions: Khibina and Lovozero of the Kola Peninsula and Ilimaussaq, S. Greenland. Canadian Mineralogist, 10, pp.299-334.

Souther, J. G. 1967. Acid volcanism and its relationship to recent crustal movements in the Canadian Cordillera. Bulletin Volcanologique, 40, pp.161-176.

Souther, J. G. 1970. Volcanism and its relationship to recent crustal movements in the Canadian Cordillera. Canadian Journal of Earth Science, 7, pp.553-568.

Souther, J. G. 1971. Geology and mineral deposits of Tulsequah map-area, British Columbia, Geological Survey of Canada, Memoir no.362.

Souther, J. G. 1977 (a). Volcanism and tectonic environments

in the Canadian Cordillera - a second look. *In* Volcanic regimes in Canada. Geological Association of Canada Special Paper, volume 16, pp.3-24.

Souther, J. G. 1977 (b). Late Cenozoic volcanism and tectonics of the west central Cordillera of North America. Abstracts, Geological Association of America, Seattle meeting, p.1185.

Souther, J. G., and Armstrong, J. E. 1966. North-central belt of the Cordillera of British Columbia. Canadian Institute of Mining Special, 8, pp.171-184.

Souther, J. G., and Symons, D. T. A. 1974. Stratigraphy and paleomagnetism of Mount Edziza volcanic complex, northwestern British Columbia. Geological Survey of Canada Paper 73-32.

Sparks, R. S. J., and Pinkerton, H. 1978. Effect of degassing on rheology of basaltic lava. Nature, 276, pp.385-386.

Sparks, R. S. J., Pinkerton, H., and MacDonald, R. 1977. The transport of xenoliths in magmas. Earth and Planetary Science Letters, 35, pp.234-238.

St.Armand, P. 1957. Geological and geophysical synthesis of the tectonics of portions of British Columbia, the Yukon and Alaska. Bulletin of Geological Society of America, 68, pp.1343-1370.

Stacey, R. A. 1973. Gravity anomalies, crustal structure and plate tectonics in the Canadian Cordillera. Canadian Journal of Earth Science, 10, pp.615-628.

Stacey, R. A. 1974. Plate tectonics, volcanism and the lithosphere in British Columbia. Nature, 250, pp.133-134.

Stanton, R. L., and Bell, J. D. 1969. Volcanic and associated rocks of the New Georgia group, British Islands Protectorate. Overseas Geological and Mineralogical Research, 10, pp.113-145.

Stocker, R. L., and Gordon, R. B. 1975. Velocity and internal friction in partial melts. Journal of Geophysical Research, 80, pp.4828-4836.

Stroh, J. M. 1975. Late Cenozoic volcanism, Baja California Norte, Mexico. Ph.D. thesis, Geology Department,

University of Washington, Seattle.

Stroh, J. M. Solubility of alumina in orthopyroxene plus spinel as a geobarometer in complex systems: applications to spinel bearing alpine type peridotites. Contributions to Mineralogy and Petrology, 54, pp.173-188.

Stull, D. R., and Prophet, H. 1971. JANAF thermochemical tables. National Standard Reference Data Service, U. S. National Bureau of Standards, 37, p.1141.

Sun, S. S. 1973. Lead isotope studies of young volcanic rocks from Oceanic islands, Mid Ocean Ridges and Island Areas. Ph.D. thesis, Department of Geology, Columbia University, New York.

Sun, S. S., and Hanson, G. N. 1976. Rare earth element evidence for differentiation of McMurdo volcanics, Ross Island, Antarctica. Contributions to Mineralogy and Petrology, 54, pp.139-155.

Sun, S. S., Tatsumoto, M.,and Schilling, J. G. 1975. Mantle mixing along the Reykjanes Ridge axis: Pb isotope evidence. Science, 190, p.143.

Sutherland, D. S. 1974. Petrography and mineralogy of peralkaline silicic rocks. Bulletin Volcanologique, 38, pp.517-548.

Symons, D. T. A. 1978. Paleomagnetism of Mesozoic plutons in the western most complex of British Columbia., Canadian Journal of Earth Science, 14, pp.2127-2139.

Takahashi, E., and Kushiro, I. 1981. Melting of a dry peridotite at high pressures and basalt magma genesis. In press.

Takeuchi, H., Fujii, N., and Kikuchi, M. 1972. Mechanism of magma ascent. Zishim. Ser.2 25, pp.266-268.

Tatsumoto, M. 1978. Isotopic composition of lead in Oceanic basalt and its implication to mantle evolution. Earth and Planetary Science Letters, 78, pp.63-87.

Taylor, H. P. 1968. The oxygen isotope geochemistry of igneous rocks. Contributions to Mineralogy and Petrology, 19, pp.1-71.

Thompson, R. N. 1972. Melting behavior of two Snake River

lavas at pressures up to 35kbar. Carnegie Institute of Washington Yearbook, 71, pp.406-410.

Thompson, R. N., and Chisholm, J. E. 1969. Synthesis of Aenigmatite. Mineralogical magazine, 37, pp.253-255.

Thompson, R. N., and Flower, M. F. J. 1971. One atmosphere melting and crystallization relations of lavas from Anjouan, Comores Archipelago, Western Indian Ocean. Earth and Planetary Science Letters, 12, pp.97-107.

Thompson, R. N., and MacKenzie, W. S. 1967. Feldspar-liquid equilibria in peralkaline acid liquids, an experimental study. American Journal of Science, 265, pp.714-734.

Tilley, C. E., Yoder, H. S., and Schairer, J. F. 1964. New relations on melting of basalts. Carnegie Institute of Washington Yearbook, 63, pp.92-97.

Tuma, J. J. 1976. Handbook of Physical Calculations. McGraw-Hill, New York.

Tuttle, O. F. 1958. Origin of granite in the light of experimental studies in the system $NaAlSi_3O_8$ - $KAlSiO_3O_8$ - SiO_2 - H_2O. Geological Society of America memoir No.74.

Urey, H. C. 1947. The thermodynamics of Isotopic Substances. Journal of the Chemical Society, London, pp.562-581.

Vacquier, V., Steenland, N., Henderson, R., and Zeitz, I. 1951. Interpretation of Aeromagnetic maps. Geological Society of America Memoir No. 47.

Varet, J. 1969. Les phonolites agpaitiques et miaskitiques du Cantal septentrional (Auvergne France). Bulletin Volcanologique, 33, pp.621-656.

Varne, R. 1970 Hornblende lherzolite and the upper mantle. Contributions to Mineralogy and Petrology, 27, pp.45-51.

Vestine, E. H. 1967. Main Geomagnetic Field. *In* Physics of Geomagnetic Phenomena. *Edited by* S. Matsushita and W. H. Campbell. Academic Press, New York.

Vine, F. J., and Hess, H. H. 1970. Sea floor spreading. *In* The Sea. *Edited by* A. E. Maxwell. Volume 4, pp.587-622.

Vine, F. J., and Mathews, D. H. 1963. Magnetic anomalies over Oceanic Ridges. Nature, **199**, p.947.

Virgo, D., Mysen, B. O., Scarfe, C. M., and Sharma, S. K. 1979. Contrasting pressure dependence of the viscosity of silicate melts. EOS Transactions of the American Geophysical Union, Spring meeting.

Volfinger, M., and Robert, J. L. 1980. Structural control of the distribution of trace elements between silicates and hydrothermal solutions. Geochimica et Cosmochimica Acta, **44**, pp.1455-1463.

Waff, H. S., and Bulau, J. R. 1979. Equilibrium fluid distribution in an ultramafic partial melt under hydrostatic conditions. Journal of Geophysical Research, **84**, pp.6109-6114.

Waff, H. S., and Holdren, G. R. 1980. The nature of grain boundaries in Dunite and lherzolite xenoliths: implications for magma transport in refractory upper mantle material. EOS Transactions of the American Geophysical Union, **61**, p.1239.

Waldbaum, D. R. 1971. Temperature changes associated with adiabitic decompression in geological processes. Nature, **232**, pp.545-547.

Washington, H. S. 1896. Volcanic rocks of central Italy. Journal of Geology, **4**, pp.547-554.

Washington, H. S. 1913. The volcanoes and rocks of Pantelleria. Journal of Geology, **21**, pp.653-713.

Washington, H. S. 1914. The volcanoes and rocks of Pantelleria. Part III. Petrology. Journal of Geology, **22**, pp.16-27.

Wass, S. Y., and Rogers, N. W. 1980. Mantle metasomatism - precursor to continental alkaline volcanism. Geochimica et Cosmochimica Acta, **44**, pp.1811-1823.

Watkins, N. D. 1973. Brunhes epoch geomagnetic secular variation on Reunion Island. Journal of Geophysical Research, 78, p.7763.

Watson, K. D., and Mathews, W. H. 1944. The Tuya-Teslin area, northern British Columbia. British Columbia Department of Mines, bulletin No. 19.

Weaver, S. D., Scleal, J. S. C., and Gibson, J. L. 1972. Trace element data relevant to the origin of trachytic and pantelleritic lavas in the East

African Rift system. Contributions to Mineralogy and Petrology, **36**, pp.181-194.

Wells, P. R. A. 1977. Pyroxene geothermometry in simple and complex systems. Contributions to Minerology and Petrology, **62**, pp.129-139.

Wheeler, J. O., and Gabrielse, H. 1972. The Cordilleran structural province. *In* Variations in Tectonic Styles in Canada. *Edited by* R. A. Price and R. J. W. Douglas, Geological Association of Canada, special paper no.11, pp.1-81.

White, W. M. 1979. The petrology and geochemistry of the Azores Islands. Contributions to Mineralogy and Petrology, **69**, pp.201-214.

White, W. M., Hart, S. R., and Schilling, J. G. 1975. Geochemistry of the Azores and the Mid Atlantic Ridge. Carnegie Institute of Washington Yearbook, **74**, pp.224-234.

White, W. M., Tappin, M. D., and Schilling, J. G, 1979. The petrology and geochemistry of the Azores Islands. Contributions to Mineralogy and Petrology, **69**, pp.201-213.

White, W. H. 1959. Cordilleran tectonics in British Columbia. Bulletin of the American Association of Petroleum Geologists, **43**, pp.60-100.

White, W. H., Bone, M. N., and Milne, W. G. 1968. Seismic refraction surveys in British Columbia, a preliminary interpretation. *In* The crust and the upper mantle under the Pacific area. American Geophysical Union Monograph no.12, pp.81-93.

White, W. H., and Savage, J. C. 1965. A seismic refraction and gravity study of the earth's crust in British Columbia. Bulletin of the Seismological Society of America, **55**, pp.463-486.

Wickens, A. J. 1971. Variations in lithosphere thickness in Canada. Canadian Journal of Earth Science, **8**, pp.1154-1162.

Wickens, A. J. 1977. The upper mantle of southern British Columbia. Canadian Journal of Earth Science, **14**, pp.1100-1115.

Wickens, A. J., and Buchbinder, G. G. R. 1980. S-wave residuals in Canada. Bulletin of the Seismological Society of America, **70**, pp.809-822.

Wilshire, H. G., and Jackson, E.D. 1975. Problems in determining mantle geotherms from pyroxene compositions. Journal of geology, 83, pp.313-329.

Wilshire, H. G., and Shervais, J. W. 1974. Al-augite and Cr-diopside ultramafic xenoliths in basaltic rocks from western U. S.: structural and tectonic relationships. Physics and Chemistry of the Earth, 9, pp.257-272.

Wilshire, H. G., and Trask, N. J. 1971. Structural and textural relationships of amphiboles and phlogopite in peridotite inclusions, Dish Hill, California. American Mineralogist, 56, pp.240-255.

Wilson, R. L. 1970. Permanent aspects of the earth's non-dipole magnetic field over upper Tertiary times. Geophysical Journal of the Royal Astronomical Society, 19, pp.417-438.

Wilson, R. L. 1970. Paleomagnetic stratigraphy of Tertiary lavas from northern Ireland. Geophysical Journal of the Royal Astronomical Society, 20, p.1

Wilson, R. L. 1971. Dipole offset- the time average paleomagnetic field over the past 25MY. Geophysical Journal of the Royal Astronomical Society, 22, pp.491-504.

Wilson, R. L. 1972. Paleomagnetic differences between normal and reversed field sources, and the problem of far sided and right handed pole positions. Geophysical Journal of the Royal Astronomical Society, 28, pp.295-304.

Wilson, R. L., Dagley, P., and McCormack, A. G. 1972. Paleomagnetic evidence about the source of the geomagnetic field. Geophysical Journal of the Royal Astronomical Society, 28, p. 213.

Wones, D. R., and Gilbert, M. E. 1969. The fayalite - magnetite - quartz assemblage between 600°C and 800°C. American Journal of Science (Schairer volume), 267A, pp.480-488.

Wright, J. B. 1971. The phonolite - trachyte spectrum. Lithos, 4, pp.1-5.

Wright, T. L., and Doherty, P. C. 1970. A linear programming and least squares computer method for solving petrologic mixing problems. Bulletin of the Geological Society of America, 81, pp.1995-2008.

Wyllie, P. J. 1971. The Dynamic Earth, a textbook in Geosciences. John Wiley and Sons, New York.

Yagi, K. 1966. The system acmite - diopside - and its bearing on the stability relation of natural pyroxenes of the acmite - hedenbergite diopside series. American Mineralogist, 51, pp.976-1000.

Yagi, K., and Souther, J. G. 1974. Aenigmatite from Mount Edziza, British Columbia. American Mineralogist, 59.

Yoder, H. S. 1965. Diopside - anorthite - water at 5 and 10 kilobars and its bearing on explosive volcanism. Carnegie Institute of Washington Yearbook, 64, pp.82-89.

Yoder, H. S. 1973. Contemporaneous basaltic and rhyolitic magmas. American Mineralogist, 58, pp.153-171.

Yoder, H. S. 1976. Generation of basaltic magma. Publication of the National Academy of Science, Washington.

Yoder, H. S., and Tilley, C. E. 1962. Origin of basaltic magmas: an experimental study of natural and synthetic rock systems. Journal of Petrology, 3, pp.342-532.

Yorath, C. J., and Chase, R. L. 1981. Tectonic history of allochthonous terranes: northern Canadian Pacific continental margin. Abstracts, Geological Association of Canada, Cordilleran section meeting, Vancouver.

Zimmerman, C., and Kudo, A. M. 1979. Geochemistry of andesites and related rocks, Rio Grande Rift, New Mexico. *In* Rio Grande Rift: Tectonics and Magmatism. *Edited by* R. E. Riecker, American Geophysical Union Publication, pp.355-382.

APPENDIX 1. FIELD AND REMANENCE NOTES ON LEVEL MOUNTAIN STRATOCONE SECTION

SITE COMMENTS (PB section decreases in elevation to south)

PBT Hawaiite summit of Meszah Peak, map unit 9. Magnetic declination very erratic in site vicinity, possibility of lightening strikes, directions approach selected at different rates from different directions, inhomogeneous magnetization between cores, sister specimens often disagree until cleaned to >800 oersteds. The chosen direction is not a stable endpoint for all cores. The rejected ones were still coming in. Cores 2 through 5 topographically oriented on Nuttlitude cone.

PBS Hawaiite next to highest flow on west shoulder of Meszah Peak between crater and dyke, map unit 9. While three cores approach a common endpoint, cores 4 and 5 do not, indicating the site to be inhomogeneously magnetized.

PBR Hawaiite highest prominent cliff outcrop on West shoulder of Meszah Peak as seen from south side, map unit 9. Abundant xenoliths, all cores approach a common endpoint in 200 to 400 oersted range. Restricting choice to cores 1,2 and 5 at 400 oersteds would improve statistics without changing direction.

PBQ Hawaiite cliff former below PBR map unit 9, abundant xenoliths, all cores approach common endpoint at 200 to 400 oersteds. Restricting choice to cores 1,2 and 5 improves statistics without changing direction. Below this elevation steep slopes, talus and scoria limit available outcrop. Additional section between Q and P could be collected on East face of Meszah Peak with aid of rope work.

PBP Benmoreite map unit 8. Narrow outcrop <3m wide in creek-snow chute on South face of Meszah Peak. Flows at this level are all thin and aside from a few blocky outcrops like this are scoriaceous, many thin trachytes interspersed, frequency decreasing upsection. All cores approach a common endpoint and stay there between 25 and 400 oersteds.

Appendix 1. continued.

PBO Benmoreite map unit 8, lowest blocky outcrop in snow chute, abundant mafic inclusions, below this point talus and scree cover resumes, all cores are stable at a common endpoint from NRM to 800 oersteds. Restricting choice to cores 1,2 and 3 improves statistics without changing direction.

PBN Trachyte lava tube low on south face of Meszah Peak, map unit 7A. All specimens are stable and coincident from NRM to 400 oersteds.

PBM Trachyte ledge, unit 7A at break in slope between lava tubes and tarn, all cores coincident from NRM to 400 oersteds.

PBL Trachyte ledge unit 7A. Site inhomogeneously magnetized probably due to low and variable magnetic mineral content. Cores come in from different directions at different rates. Endpoint somewhat scattered. statistics can be improved without affecting direction by restricting choice to cores 1,2,3 and 4 at 400 oersteds.

PBY Trachyte flow massive columnar jointing, flow 46m thick, unit 7A, cores sampled from separate columns 2/3 of the way up the flow, site is transitional and scattered. No obvious stable endpoint is achieved. Intensity is low and remnance is soft. Statistics can't be much improved unless sample is dropped to 2 cores.

PBK Basal trachyte flow of unit 7A, near base of cliff outcrop formed by PBY. Laterally unit 6 is overlain by fluvioglacial/volcanofluvioglacial sands and gravels. Site is scattered and transitional. Some of scatter could be due to poor coring as all specimens were either in three pieces, short, or hole oriented.

PBJ Basalt, unit 6B. Columnar jointed outcrop forms waterfall, good agreement of all specimens from NRM to 400 oersteds.

PBI Hawaiite, unit 6B. Weathering light grey very abundant phenocrysts of plagioclase and black augite, good agreement of all specimens from NRM to 400 oersteds.

PBH Hawaiite, unit 6B, with very abundant plagioclase and black augite. Direction chosen as stable endpoint, statistics can be markedly improved without changing direction by eliminating core 3, which comes in more slowly than the others and shows some disagreement between sister specimens, possible hematite and CRM component in core 3.

Appendix 1. continued.

PBG Peralkaline trachyte, unit 6A. Uppermost of three similar flows, all cores agree with good statistics but inclination is very shallow, transitional site.

PBF Peralkaline trachyte, unit 6A. Forms ledge and holds up flat profile in stream valley, phenocrysts of anorthoclase, fayalite and green pyroxene, all specimens agree from NRM to 800 oersteds with shallow inclination, transitional direction.

PBE Peralkaline trachyte flow, unit 6A. Holds up prominent waterfall, peculiar exfoliation textures, good agreement of all specimens but shallow inclination, transitional direction. From this point down only the prominent resistant flows are sampled, tuffs and agglomerates are omitted. Laterally in several places a till is present at this stratigraphic level.

PBD Vesicular browm weathered hawaiite, unit 5B, with plagioclase and augite phenocrysts. All specimens coincide at a shallow inclination transitional direction. These cores all contain appreciable maghemite both as phenocryst alteration and as veins and amygdules.

PBC Amygdaloidal alkali basalt flow, unit 5B. All cores achieve stable endpoints but site is somewhat scattered. Statistics can be improved without affecting direction by eliminating core 3 which was hole oriented.

PBB Alkali basalt with plagioclas and black pyroxene phenocrysts, unit 5B. Site somewhat scattered. Core 2 was eliminated due to inhomogeneity inferred from disagreement between sister specimens.

PBA Hawaiite flow, unit 5B, stable endpoint for four specimens

PBX Hawaiite rubbly outcrop west of stream cut, unit 5B. No exposure in creek at this point due to lateral moraine of Kakuchuya valley, site is definitely reversed. Eliminating core 2 improves statistics but does not affect direction.

PBU Phonolite flows cooled as a single unit. Slight primary (?) dip down 11° to N230°E, unit 5A, site is somewhat scattered.

Appendix 1. continued

PBV Phonolite flows, unit 5A. Weak site, all specimens but one have common NRM direction but scatter away randomly by 100 oersteds indicating a soft remnance.

PBW Crystalline comendite flow, unit 5A. Stable direction for all cores from NRM to 100 oersteds.

APPENDIX 2. FIELD AND REMANENCE NOTES ON LEVEL MOUNTAIN PLATEAU SECTION

SITE COMMENTS (Little Tahltan section decreases in elevation to south along E facing cliff)

PAA Alkali basalt flow, map unit 4. Columnar outcrop, local topographic high back from cliff edge, possible lightening strikes, inhomogeneous site all cores approach the chosen endpoint but at different rates. Cores 3 and 5 were rejected as they were still coming in at 400 oersteds but became random by 600.

PAB Alkali basalt flow, map unit 4, 3m thick columnar flow sampled 1m up from base. This was the next prominent outcrop 150m south of PAA, very coherent site, stable from NRM to 400 oersteds.

PAC Hawaiite flow, map unit 4, abundant phenocrysts of plagioclase and black clinopyroxene, good site, all cores agree from NRM to 200 oersteds.

PAD Alkali basalt, map unit 4. Site is reversed but scattered, while individual cores attain stable endpoints (1 and 4), there is no common direction. Each core came from a different column and the flow was sampled over a distance of 15m laterally but this is not atypical.

PAE Hawaiite map unit 4, very tight site. All cores agree from NRM to 400 oersteds.

PAF Hawaiite, map unit 4. No safe acess at this point in section so PAF was sampled 300m line of site to the south, good endpoint for all cores 100 to 200 oersteds.

PAG Hawaiite, map unit 4. Good endpoint. All specimens stable and coincident from 50 to 400 oersteds.

PAH Hawaiite basal columnar flow of map unit 4 rests on yellowish green tuff horizon that delimits units 3 and 4 over much of the southern plateau, stable direction, all cores agree from NRM to 200 oersteds.

PAI Basalt highest major cooling unit of continous exposure and thickness of unit 3, spheriodially weathering coarse ophitic texture. The five cores here were sampled from only two columns, good site, all cores agree in 100 to 200 oersted range.

APPENDIX 2. continued.

PAJ Alkali basalt, map unit 3, good site, all specimens agree in 100 to 200 oersted range.

PAK Alkali basalt, map unit 3, calcite and zeolites present, rejecting core 5 improves statistics without significantly changing direction.

PAL Alkali basalt, basal flow of 3 that comprises a single columnar cooling unit, forms promontory north of stream notch in cliff. While the overlying section was sampled along 2km of cliff margin, the underlying section follows the stream notch in this cliff and is nearly vertical. All cores for this suite attain a good common endpoint between 100 and 200 oersteds.

PAM Basalt flow with thompsonite and chabazite in fractures. This is third flow down from PAL due to poor acess, map unit 3. The intervening flows may contain the transition from the reverse polarity of PAL. The stable endpoint is achieved by all cores at 200 oersteds, the direction is a little shallow making this a transitional site.

PAN Alkali basalt unit 3, lower flow of pair that comprises a single columnar cooling unit immediately below PAM, site somewhat scattered similar shallow reversed direction to PAM, statistics can be improved by restricting choice to cores 2,3 and 5 but direction does not change.

PAO. Basalt unit 3, xenocrysts of forsterite and brown spinel, , good site tight distribution for 25 to 400 oersteds on all but core 4, which is consequently rejected.

PAP Basalt columnar outcrop, unit 3, overlies carbonized wood and peat, site reversed and somewhat scattered best agreement in direction at 200 oersteds but core 4 still coming in.

PAQ Alkali basalt, lowest flow in unit 3, upwards to PAP there are two flows and a rubbly Lahar which were not sampled due to poor access on cliff face, this sampling gap coincides with a polarity change, this site is normal with good agreement for all cores above 200 oersteds despite the fact that PAQ is mapped in unit 3 and seems to belong there chemically as well, its magnetic orientation appears to go better with underlying PAR and PAS. The time interval between units 2 and 3 is probably small.

APPENDIX 2. continued

PAR Alkali basalt separated from PAQ by an orange-buff tuff horizon mapped as the unit 2-3 boundary. There is good agreement for all cores by 200 oersteds except #2 which did not have a sun bearing and the two topographic sitings disagreed. This core also did not achieve an endpoint so it should be rejected.

PAS Transitional hawaiite-basalt map unit 2, Two flows between here and PAR were omitted due to cover inside the notch and no access on the cliff face, core 5 had to be rejected because it disagreed with all other cores and was more intensely magnetized by 2 to 3 orders of magnitude, otherwise this is a good site.

PAT Vesicular altered hawaiite (?) flow map unit 2, two flows omitted between here and PAS. From here down cliff exposure required that safety ropes be used during drilling and orientation. This site is quite scattered, all cores achieve endpoints but only 1 and 2 coincide, the site is reversed but probably has a later CRM component related to maghematite alteration as seen petrographically, and in failure of core to saturate even by 5 kilogauss in IRM test.

PAU Basalt, map unit 2, massive columnar flow >5m thick, one flow between here and PAT not sampled, most cores coincide from NRM to 400 oersteds.

PAV Basalt lowest massive flow in map unit 2. This columnar cooling unit is comprised of four individual flows, one cooling unit between here and PAU not sampled. Cores 2 and 3 were drilled through fractures and became broken in several pieces and had to be hole oriented. They scatter somewhat from other 3 cores which show good agreement by ~200 oersteds.

PAW Alkali basalt highest cooling unit in map unit 1, the 1 to 2 boundary, mapped at the top of PAW because of distinctive colour and massive appearance of underlying flows. However there is no tuff horizon, paleosol or other obvious time break here. This site has an unusual shallow inclination but is normal compared to adjacent flows above and below. It is also low intensity for basalts, probably represents an excursion since long time break is not inferred.

APPENDIX 2. continued.

PAX Transitional basalt massive cooling unit typical of map unit 1, good agreement for all cores from NRM to 200 oersteds.

PAY Basalt massive basal flow of map unit 1. Below this level there is no further outcrop nearby, only several hundred feet of rubbly cold agglomerates (volcano-fluviatile). The Little Tahltan River here appears to be resequent to a Tertiary stream valley of moderate proportions. Bedrock is porphyry similar to outcrop on Kaketsa Mtn. and of the Sloko volcanics. Although all cores agree with high Fisher k the best direction is probably given by cores 1 and 4 at 100 to 400 oersteds as other cores approach and pass through this region.

APPENDIX 3. REMANENCE DATA FOR LEVEL MOUNTAIN LAVAS

SITE	DENS	ELEV.	TREAT	EMU	INC	DEC
PBT01A	3.1	7250	0	3.52E-03	62.6	-5.1
PBT01A	3.1	7250	25	3.08E-03	61.6	-17.0
PBT01A	3.1	7250	50	2.40E-03	59.1	-1.9
PBT01A	3.1	7250	100	1.04E-03	56.2	8.4
PBT01A	3.1	7250	200	9.92E-03	69.1	19.1
PBT01A	3.1	7250	400	8.06E-03	50.0	42.4
PBT01A	3.1	7250	800	3.71E-03	60.0	50.0
PBT01A	3.1	7250	1000	2.27E-03	62.1	51.6
PBT02B	2.9	7250	0	4.46E-03	196.5	13.4
PBT02B	2.9	7250	25	4.39E-03	197.5	14.7
PBT02B	2.9	7250	50	3.89E-03	202.1	20.1
PBT02B	2.9	7250	100	2.76E-03	196.0	63.1
PBT02B	2.9	7250	200	1.16E-03	59.7	86.8
PBT02B	2.9	7250	400	5.06E-04	3.0	84.1
PBT02B	2.9	7250	800	1.59E-04	70.0	44.5
PBT03A	3.0	7250	0	4.24E-03	331.9	59.5
PBT03A	3.0	7250	25	4.09E-03	333.8	57.2
PBT03A	3.0	7250	50	4.35E-03	333.9	56.9
PBT03A	3.0	7250	100	4.26E-03	332.2	58.9
PBT03A	3.0	7250	200	3.23E-03	357.0	73.4
PBT03A	3.0	7250	400	1.56E-03	9.8	73.7
PBT03A	3.0	7250	800	4.53E-04	19.4	77.8
PBT03C	3.0	7250	0	3.53E-03	334.9	55.7
PBT03C	3.0	7250	25	3.52E-03	334.8	55.8
PBT03C	3.0	7250	50	3.22E-03	325.1	65.1
PBT03C	3.0	7250	100	3.53E-03	334.9	55.7
PBT03C	3.0	7250	200	2.47E-03	19.1	63.6
PBT03C	3.0	7250	400	1.51E-03	34.9	65.9
PBT03C	3.0	7250	800	4.59E-06	68.6	74.2
PBT03T	3.1	7250	0	3.55E-04	42.8	87.1
PBT03T	3.1	7250	25	3.27E-04	63.7	83.6
PBT03T	3.1	7250	50	2.41E-04	63.5	78.7
PBT03T	3.1	7250	100	9.81E-05	53.1	74.6
PBT03T	3.1	7250	200	3.36E-05	44.8	73.3
PBT03T	3.1	7250	400	1.51E-05	40.1	73.4
PBT03T	3.1	7250	700	4.59E-06	44.0	76.6
PBT03T	3.1	7250	1000	1.62E-06	72.6	76.7
PBT04B	2.4	7250	0	1.87E-03	253.9	61.5
PBT04B	2.4	7250	25	1.82E-03	255.2	56.3
PBT04B	2.4	7250	50	1.84E-03	260.2	35.0
PBT04B	2.4	7250	100	1.66E-03	248.8	20.5
PBT04B	2.4	7250	200	1.05E-03	224.5	31.3
PBT04B	2.4	7250	400	4.45E-03	274.5	54.3
PBT04B	2.4	7250	800	3.38E-03	223.1	71.0
PBT04B	2.4	7250	1000	2.06E-03	276.0	68.2
PBT05B	2.9	7250	0	1.57E-01	72.9	40.9
PBT05B	2.9	7250	200	1.36E-02	11.6	83.0
PBT05B	2.9	7250	400	4.95E-03	36.9	78.4
PBT05B	2.9	7250	800	1.97E-03	43.3	68.4
PBT05B	2.9	7250	1000	1.29E-03	40.5	72.3
PBS01C	3.0	7200	0	9.48E-03	11.8	51.7
PBS01C	3.0	7200	100	5.16E-03	22.0	49.9
PBS01C	3.0	7200	200	1.92E-03	21.0	52.6
PBS01C	3.0	7200	400	5.58E-04	15.6	56.5
PBS01C	3.0	7200	800	1.84E-04	50.0	57.0
PBS02A	2.9	7200	0	1.06E-02	54.5	8.6
PBS02A	2.9	7200	100	5.53E-03	22.9	26.8
PBS02A	2.9	7200	200	1.94E-03	25.5	35.7
PBS02A	2.9	7200	400	7.67E-04	33.6	41.7
PBS02A	2.9	7200	800	2.62E-04	40.3	50.8
PBS03C	3.0	7200	0	1.26E-02	52.4	-18.8
PBS03C	3.0	7200	25	1.13E-02	43.2	-10.1
PBS03C	3.0	7200	50	8.79E-03	32.5	2.1
PBS03C	3.0	7200	100	5.19E-03	26.0	14.2
PBS03C	3.0	7200	200	1.42E-03	24.9	26.8
PBS03C	3.0	7200	400	5.66E-04	21.6	35.2
PBS03C	3.0	7200	800	1.76E-04	47.3	57.4
PBS04A	2.9	7200	0	2.55E-01	354.4	6.2
PBS04A	2.9	7200	100	5.54E-02	7.6	17.9
PBS04A	2.9	7200	200	5.29E-03	8.1	11.3
PBS04A	2.9	7200	400	1.22E-03	6.7	4.4
PBS05B	3.0	7200	0	4.12E-01	58.6	-7.1
PBS05B	3.0	7200	100	8.98E-02	50.2	-9.9
PBS05B	3.0	7200	200	2.19E-02	51.4	-8.7
PBS05B	3.0	7200	400	1.00E-02	51.7	-5.9
PBR01B	3.0	6625	0	8.73E-03	130.0	62.8
PBR01B	3.0	6625	100	3.16E-03	50.6	63.7
PBR01B	3.0	6625	200	1.12E-03	51.8	60.8
PBR01B	3.0	6625	400	5.38E-04	37.7	58.7
PBR01B	3.0	6625	800	5.69E-04	22.8	10.4
PBR02B	3.0	6625	0	8.72E-03	41.6	54.1
PBR02B	3.0	6625	100	4.37E-03	29.2	61.3
PBR02B	3.0	6625	200	2.35E-03	29.1	62.5
PBR02B	3.0	6625	400	9.06E-04	28.7	62.3
PBR02B	3.0	6625	800	1.42E-04	18.2	60.2
PBR03B	3.0	6625	0	4.82E-02	105.2	21.5
PBR03B	3.0	6625	100	5.55E-03	80.7	47.0
PBR03B	3.0	6625	200	2.24E-03	69.7	53.8
PBR03B	3.0	6625	400	7.98E-04	73.3	50.8
PBR03B	3.0	6625	800	7.97E-04	71.7	50.7
PBR04B	3.0	6625	0	2.01E-02	112.1	39.2
PBR04B	3.0	6625	100	4.10E-03	68.7	65.1
PBR04B	3.0	6625	200	1.61E-03	70.0	64.5
PBR04B	3.0	6625	400	3.85E-04	99.8	69.6
PBR04B	3.0	6625	800	1.05E-04	134.4	52.2
PBR05B	3.0	6625	0	8.63E-03	38.2	52.9
PBR05B	3.0	6625	100	4.87E-03	32.7	61.2
PBR05B	3.0	6625	200	2.42E-03	34.0	62.4
PBR05B	3.0	6625	400	1.03E-03	35.2	63.0
PBR05B	3.0	6625	800	2.34E-04	24.2	61.5
PBQ01A	3.0	6580	0	9.35E-03	39.9	56.1
PBQ01A	3.0	6580	100	3.75E-03	26.5	58.8
PBQ01A	3.0	6580	200	1.11E-03	29.4	55.3
PBQ01A	3.0	6580	400	5.14E-04	37.1	55.2
PBQ02B	3.0	6580	0	9.03E-03	35.3	55.2
PBQ02B	3.0	6580	100	3.88E-03	36.3	54.1
PBQ02B	3.0	6580	200	1.21E-03	41.0	54.8
PBQ02B	3.0	6580	400	5.41E-04	38.6	46.8
PBQ03B	3.0	6580	0	2.68E-02	143.8	12.4
PBQ03B	3.0	6580	25	2.09E-02	142.8	13.2
PBQ03B	3.0	6580	50	1.07E-02	135.2	21.9
PBQ03B	3.0	6580	100	3.27E-03	117.4	40.8
PBQ03B	3.0	6580	200	7.79E-04	79.0	61.4
PBQ03B	3.0	6580	400	3.75E-04	54.6	57.5
PBQ03B	3.0	6580	800	1.46E-04	66.7	54.5
PBQ04B	2.9	6580	0	2.67E-02	104.2	17.5
PBQ04B	2.9	6580	100	6.16E-03	89.9	28.6
PBQ04B	2.9	6580	200	1.68E-03	78.6	37.3
PBQ04B	2.9	6580	400	5.84E-04	79.9	38.9
PBQ04B	2.9	6580	800	1.56E-04	68.3	46.1
PBQ05B	2.8	6580	0	7.61E-03	18.6	32.6
PBQ05B	2.8	6580	100	2.79E-03	21.1	48.0
PBQ05B	2.8	6580	200	1.47E-03	21.8	51.3
PBQ05B	2.8	6580	400	8.80E-04	20.9	51.5
PBP01B	2.6	6480	0	8.27E-04	224.5	-58.6
PBP01B	2.6	6480	100	9.47E-04	225.3	-66.9
PBP01B	2.6	6480	200	7.18E-04	225.4	-66.4
PBP02A	2.5	6480	0	8.41E-04	146.9	-71.6
PBP02A	2.5	6480	100	9.22E-04	182.2	-76.2
PBP02A	2.5	6480	200	6.79E-04	188.5	-76.0
PBP03A	2.5	6480	0	8.06E-04	242.4	-86.2
PBP03A	2.5	6480	100	9.29E-04	198.2	-76.4
PBP03A	2.5	6480	200	6.76E-04	202.0	-75.8
PBP04B	2.5	6480	0	7.08E-04	295.7	-71.2
PBP04B	2.5	6480	25	9.30E-04	260.7	-79.1
PBP04B	2.5	6480	50	1.01E-03	244.9	-80.8
PBP04B	2.5	6480	100	8.70E-04	220.4	-82.3
PBP04B	2.5	6480	200	6.24E-04	233.8	-79.8
PBP04B	2.5	6480	400	3.44E-04	235.6	-76.0
PBP04B	2.5	6480	800	8.55E-05	343.1	-68.7
PBP05A	2.5	6480	0	7.40E-04	235.7	-49.6
PBP05A	2.5	6480	100	8.55E-04	217.7	-68.4
PBP05A	2.5	6480	200	5.93E-04	223.9	-68.2
PBO01B	2.6	6440	0	2.24E-03	202.7	-85.0
PBO01B	2.6	6440	50	2.33E-03	222.0	-85.0
PBO01B	2.6	6440	100	2.11E-03	230.3	-85.4
PBO02C	2.5	6440	0	1.74E-03	228.6	-75.6
PBO02C	2.5	6440	25	1.73E-03	228.3	-76.0
PBO02C	2.5	6440	50	1.73E-03	227.7	-76.6
PBO02C	2.5	6440	100	1.72E-03	226.2	-77.5
PBO02C	2.5	6440	200	1.76E-04	210.3	-83.4
PBO02C	2.5	6440	400	8.45E-04	174.6	-86.2
PBO02C	2.5	6440	800	8.57E-04	223.3	-79.3
PBO03C	2.4	6440	0	4.52E-03	87.6	-86.4
PBO03C	2.4	6440	100	4.28E-03	50.8	-87.7

SITE	DENS	ELEV	TREAT	EMU	INC	DEC
PBO03C	2.4	6440	200	3.35E-03	45.1	-86.4
PBO04A	2.6	6440	0	1.74E-03	80.4	-73.1
PBO04A	2.6	6440	50	1.80E-03	68.8	-79.4
PBO04A	2.6	6440	100	1.65E-03	63.6	-79.3
PBO05A	2.6	6440	0	1.20E-02	178.3	-76.7
PBO05A	2.6	6440	50	1.18E-02	179.4	-76.3
PBO05A	2.6	6440	100	1.14E-02	180.5	-76.7
PBN01B	2.5	6340	0	1.01E-02	275.9	-79.4
PBN01B	2.5	6340	100	8.95E-03	270.4	-79.6
PBN01B	2.5	6340	200	6.31E-03	260.6	-79.3
PBN02A	2.7	6340	0	1.12E-02	262.2	-78.2
PBN02A	2.7	6340	100	9.91E-03	260.3	-77.9
PBN02A	2.7	6340	200	6.73E-03	257.6	-77.4
PBN03C	2.5	6340	0	1.04E-02	268.5	-77.0
PBN03C	2.5	6340	100	9.20E-03	264.0	-76.8
PBN03C	2.5	6340	200	6.51E-03	260.4	-76.8
PBN04A	2.5	6340	0	1.10E-02	267.7	-77.8
PBN04A	2.5	6340	100	9.91E-03	262.6	-77.8
PBN04A	2.5	6340	200	6.72E-03	262.1	-77.6
PBN05A	2.5	6340	0	1.26E-02	280.0	-80.1
PBN05A	2.5	6340	100	1.12E-02	277.1	-79.3
PBN05A	2.5	6340	200	7.31E-03	270.8	-80.0
PBM01A	2.6	6160	0	2.21E-03	223.3	-62.3
PBM01A	2.6	6160	50	2.20E-03	222.9	-63.6
PBM01A	2.6	6160	100	2.14E-03	223.0	-63.4
PBM02B	2.6	6160	0	2.03E-03	234.0	-62.8
PBM02B	2.6	6160	25	2.03E-03	234.6	-62.8
PBM02B	2.6	6160	50	2.05E-03	235.1	-62.8
PBM02B	2.6	6160	100	2.02E-03	235.3	-62.9
PBM02B	2.6	6160	200	1.86E-03	235.5	-63.0
PBM02B	2.6	6160	400	1.17E-03	229.7	-64.0
PBM02B	2.6	6160	800	3.01E-04	146.7	-56.5
PBM03A	2.6	6160	0	1.70E-03	218.1	-63.2
PBM03A	2.6	6160	50	1.71E-03	216.7	-62.9
PBM03A	2.6	6160	100	1.68E-03	216.6	-63.3
PBM04A	2.6	6160	0	1.71E-03	218.3	-62.7
PBM04A	2.6	6160	50	1.75E-03	216.1	-62.1
PBM04A	2.6	6160	100	1.72E-03	218.1	-62.2
PBM05A	2.6	6160	0	2.18E-03	216.0	-58.7
PBM05A	2.6	6160	50	2.19E-03	216.0	-58.9
PBM05A	2.6	6160	100	2.14E-03	215.4	-58.5
PBL01A	2.6	5835	0	2.40E-04	77.7	49.1
PBL01A	2.6	5835	50	1.17E-04	92.0	48.7
PBL01A	2.6	5835	100	4.86E-05	162.4	-15.3
PBL01A	2.6	5835	200	2.39E-05	169.4	-55.5
PBL01A	2.6	5835	400	2.70E-05	114.6	-40.1
PBL02B	2.7	5835	0	1.99E-04	100.9	4.5
PBL02B	2.7	5835	50	1.41E-04	120.6	-36.7
PBL02B	2.7	5835	100	1.71E-04	143.0	-61.7
PBL02B	2.7	5835	200	1.61E-04	151.8	-67.1
PBL02B	2.7	5835	400	4.76E-04	99.1	-59.9
PBL03C	2.6	5835	0	7.04E-05	224.9	59.9
PBL03C	2.6	5835	25	5.38E-05	205.4	39.8
PBL03C	2.6	5835	50	6.33E-05	194.6	-19.8
PBL03C	2.6	5835	100	1.38E-04	190.0	-54.8
PBL03C	2.6	5835	200	1.60E-04	189.2	-61.9
PBL03C	2.6	5835	400	1.27E-04	193.6	-65.6
PBL03C	2.6	5835	800	7.06E-05	182.5	-67.2
PBL04A	2.6	5835	0	1.33E-04	148.0	-66.9
PBL04A	2.6	5835	50	1.66E-04	165.6	-67.8
PBL04A	2.6	5835	100	1.75E-04	169.4	-68.7
PBL04A	2.6	5835	200	1.58E-04	166.6	-68.5
PBL04A	2.6	5835	400	1.86E-04	270.0	-69.8
PBL05A	2.6	5835	0	1.87E-04	168.3	-37.5
PBL05A	2.6	5835	50	2.08E-04	171.2	-51.5
PBL05A	2.6	5835	100	2.26E-04	174.1	-58.4
PBL05A	2.6	5835	200	2.64E-04	266.0	-66.5
PBL05A	2.6	5835	400	1.14E-04	180.8	-68.5
PBY01A	2.6	5780	0	5.78E-04	56.5	62.9
PBY01A	2.6	5780	50	2.95E-04	50.6	57.4
PBY01A	2.6	5780	100	8.64E-05	27.9	39.3
PBY01A	2.6	5780	200	2.19E-04	43.9	18.0
PBY01A	2.6	5780	300	6.32E-05	28.4	12.1
PBY01A	2.6	5780	400	2.83E-05	15.2	21.6
PBY02B	2.6	5780	0	5.60E-04	10.1	53.2
PBY02B	2.6	5780	50	2.47E-04	359.9	48.0
PBY02B	2.6	5780	100	1.01E-04	11.1	27.7
PBY02B	2.6	5780	200	3.82E-05	9.6	-3.5
PBY02B	2.6	5780	300	6.43E-05	35.7	19.2
PBY02B	2.6	5780	400	2.58E-05	2.3	12.8
PBY03C	2.6	5780	0	8.94E-04	43.1	75.5
PBY03C	2.6	5780	25	7.48E-04	44.3	75.4
PBY03C	2.6	5780	50	1.74E-04	72.6	61.9
PBY03C	2.6	5780	100	6.51E-05	36.7	38.9
PBY03C	2.6	5780	200	3.89E-05	17.6	12.5
PBY03C	2.6	5780	300	7.13E-05	37.2	19.9
PBY03C	2.6	5780	400	1.40E-05	22.4	-30.1
PBY04C	2.6	5780	0	7.11E-04	104.8	42.6
PBY04C	2.6	5780	25	5.33E-04	106.0	46.9
PBY04C	2.6	5780	50	2.06E-04	88.0	47.2
PBY04C	2.6	5780	100	6.92E-05	30.8	35.5
PBY04C	2.6	5780	200	5.46E-05	359.9	-7.2
PBY04C	2.6	5780	400	1.58E-05	321.3	-20.3
PBY04C	2.6	5780	800	7.32E-06	14.5	-29.1
PBY05B	2.5	5780	0	4.14E-04	11.9	45.7
PBY05B	2.5	5780	50	3.27E-04	1.9	26.8
PBY05B	2.5	5780	100	2.54E-04	358.2	7.3
PBY05B	2.5	5780	200	1.94E-04	355.7	-3.4
PBY05B	2.5	5780	400	8.89E-05	297.4	-16.9
PBK01A	2.5	5745	0	3.54E-04	55.7	61.2
PBK01A	2.5	5745	50	1.66E-04	56.2	50.3
PBK01A	2.5	5745	100	7.25E-05	22.8	41.7
PBK01A	2.5	5745	200	6.53E-05	17.3	22.6
PBK01A	2.5	5745	400	3.01E-05	350.4	30.4
PBK02A	2.5	5745	0	4.68E-04	344.7	73.2
PBK02A	2.5	5745	25	3.38E-04	349.6	71.6
PBK02A	2.5	5745	50	1.77E-04	346.1	63.9
PBK02A	2.5	5745	100	7.52E-05	343.3	47.7
PBK02A	2.5	5745	200	4.75E-05	348.5	23.1
PBK02A	2.5	5745	400	1.79E-05	349.1	8.3
PBK02A	2.5	5745	800	3.11E-05	9.0	-6.3
PBK03A	2.6	5745	0	2.12E-04	200.2	85.2
PBK03A	2.6	5745	50	6.10E-05	353.9	21.4
PBK03A	2.6	5745	100	6.60E-05	351.4	-16.9
PBK03A	2.6	5745	200	4.86E-05	5.0	-15.7
PBK03A	2.6	5745	400	2.67E-05	5.2	0.7
PBK04A	2.6	5745	0	3.56E-04	12.2	34.5
PBK04A	2.6	5745	50	2.99E-04	5.4	18.6
PBK04A	2.6	5745	100	2.53E-04	360.0	1.0
PBK04A	2.6	5745	200	2.12E-04	355.5	-10.9
PBK04A	2.6	5745	400	7.98E-05	356.4	-13.9
PBK05A	2.5	5745	0	3.66E-04	4.8	12.5
PBK05A	2.5	5745	50	3.30E-04	8.8	2.1
PBK05A	2.5	5745	100	2.97E-04	10.6	-6.2
PBK05A	2.5	5745	200	2.47E-04	10.1	-15.3
PBK05A	2.5	5745	400	1.30E-04	10.2	-20.1
PBJ01A	2.8	5690	0	1.97E-03	37.7	77.5
PBJ01A	2.8	5690	50	1.08E-03	22.6	69.8
PBJ01A	2.8	5690	100	6.41E-04	24.2	71.6
PBJ02B	2.8	5690	0	2.24E-03	25.2	66.8
PBJ02B	2.8	5690	50	1.11E-03	33.1	74.0
PBJ02B	2.8	5690	100	6.78E-04	26.6	71.4
PBJ03C	2.7	5690	0	1.91E-03	346.7	71.0
PBJ03C	2.7	5690	50	9.65E-04	297.4	85.9
PBJ03C	2.7	5690	100	5.23E-04	56.7	71.8
PBJ04C	2.9	5690	0	1.53E-03	45.6	73.9
PBJ04C	2.9	5690	25	1.00E-03	43.9	78.3
PBJ04C	2.9	5690	50	8.33E-04	26.9	74.5
PBJ04C	2.9	5690	100	6.05E-04	346.8	81.6
PBJ04C	2.9	5690	200	4.02E-04	25.3	71.4
PBJ04C	2.9	5690	400	1.49E-04	28.2	72.8
PBJ04C	2.9	5690	800	2.65E-05	62.5	35.8
PBJ05B	2.8	5690	0	1.49E-03	32.1	69.1
PBJ05B	2.8	5690	50	1.00E-03	20.8	69.9
PBJ05B	2.8	5690	100	7.46E-04	24.4	69.9
PBI01A	2.8	5675	0	5.05E-03	329.8	79.0
PBI01A	2.8	5675	100	4.54E-03	338.1	80.6
PBI01A	2.8	5675	200	3.54E-03	347.3	79.8
PBI02B	2.9	5675	0	6.50E-03	20.2	77.3
PBI02B	2.9	5675	25	6.89E-03	30.9	78.2
PBI02B	2.9	5675	50	6.58E-03	24.3	78.3
PBI02B	2.9	5675	100	6.15E-03	23.9	79.2
PBI02B	2.9	5675	200	4.79E-03	20.8	80.0
PBI02B	2.9	5675	400	2.09E-03	13.8	81.6
PBI02B	2.9	5675	800	3.44E-04	3.6	66.6
PBI03C	2.8	5675	0	4.90E-03	51.6	66.0
PBI03C	2.8	5675	100	1.63E-03	12.9	84.9
PBI03C	2.8	5675	200	1.02E-03	320.1	86.5
PBI04B	2.8	5675	0	3.32E-03	65.6	77.0
PBI04B	2.8	5675	100	1.75E-03	35.3	81.6
PBI04B	2.8	5675	200	9.39E-04	32.8	80.3
PBI05B	2.7	5675	0	3.85E-03	44.3	63.6

SITE	DENS	ELEV	TREAT	EMU	INC	DEC
PBI05B	2.7	5675	100	1.82E-03	40.3	68.1
PBI05B	2.7	5675	200	1.04E-03	41.7	72.5
PBH01A	2.7	5655	0	3.19E-03	33.7	73.0
PBH01A	2.7	5655	50	2.53E-03	7.3	80.0
PBH01A	2.7	5655	100	2.38E-03	4.3	81.7
PBH01B	2.8	5655	0	2.48E-02	91.2	36.4
PBH01B	2.8	5655	50	1.73E-02	94.0	34.4
PBH01B	2.8	5655	100	7.82E-03	94.3	39.7
PBH01B	2.8	5655	200	2.25E-03	86.8	57.8
PBH01B	2.8	5655	400	6.51E-04	70.2	66.9
PBH02B	2.7	5655	0	4.21E-03	5.8	71.6
PBH02B	2.7	5655	50	2.94E-03	357.6	77.5
PBH02B	2.7	5655	100	1.88E-03	357.8	78.6
PBH03B	2.8	5655	0	2.17E-02	13.6	39.0
PBH03B	2.8	5655	50	3.81E-03	4.6	53.1
PBH03B	2.8	5655	100	1.70E-04	352.5	74.3
PBH03C	2.8	5655	0	5.10E-02	24.9	-45.5
PBH03C	2.8	5655	100	1.35E-03	347.4	19.5
PBH03C	2.8	5655	200	8.28E-04	298.5	30.0
PBH03C	2.8	5655	400	5.36E-04	281.9	26.9
PBH03D	2.8	5655	0	8.34E-02	281.3	-1.0
PBH03D	2.8	5655	25	4.63E-02	280.0	2.3
PBH03D	2.8	5655	50	1.82E-02	276.8	8.0
PBH03D	2.8	5655	100	4.01E-03	273.0	27.1
PBH03D	2.8	5655	200	1.86E-03	275.1	43.6
PBH03D	2.8	5655	400	7.85E-04	276.8	48.0
PBH03D	2.8	5655	800	1.42E-04	306.3	53.0
PBH03D	2.8	5655	1000	1.46E-04	294.6	48.0
PBH03D	2.8	5655	1200	2.88E-05	339.3	0.3
PBH04B	2.8	5655	0	4.17E-03	56.5	72.4
PBH04B	2.8	5655	50	2.39E-03	26.1	82.4
PBH04B	2.8	5655	100	1.51E-03	22.7	81.2
PBH05A	2.7	5655	0	4.46E-03	318.5	75.6
PBH05A	2.7	5655	50	2.76E-03	335.6	80.2
PBH05A	2.7	5655	100	1.91E-03	349.6	80.9
PBG01A	2.5	5580	0	2.83E-04	21.6	3.1
PBG01A	2.5	5580	100	2.71E-04	21.0	1.2
PBG01A	2.5	5580	200	2.41E-04	21.2	0.5
PBG02B	2.5	5580	0	3.19E-04	17.4	0.2
PBG02B	2.5	5580	100	2.97E-04	18.6	-4.1
PBG02B	2.5	5580	200	2.50E-04	18.7	-4.7
PBG03A	2.5	5580	0	2.32E-04	17.8	6.4
PBG03A	2.5	5580	100	2.17E-04	19.3	-1.3
PBG03A	2.5	5580	200	1.77E-04	19.4	-2.7
PBG04A	2.5	5580	0	3.88E-04	27.0	9.8
PBG04A	2.5	5580	100	3.57E-04	23.7	4.7
PBG04A	2.5	5580	200	3.11E-04	23.3	2.8
PBG05C	2.4	5580	0	2.99E-04	14.0	4.6
PBG05C	2.4	5580	25	3.03E-04	13.7	3.0
PBG05C	2.4	5580	50	2.97E-04	13.9	1.0
PBG05C	2.4	5580	100	2.90E-04	13.5	-0.2
PBG05C	2.4	5580	200	2.36E-04	13.5	-1.9
PBG05C	2.4	5580	400	1.74E-04	14.5	-4.0
PBG05C	2.4	5580	800	1.26E-04	13.2	2.4

SITE	DENS	ELEV	TREAT	EMU	INC	DEC
PBF01A	2.5	5545	0	2.82E-05	28.1	62.8
PBF01A	2.5	5545	100	7.77E-06	20.3	47.9
PBF01A	2.5	5545	200	4.57E-06	0.6	10.9
PBF01A	2.5	5545	400	1.38E-06	43.5	18.1
PBF02C	2.7	5545	0	3.00E-04	11.1	10.9
PBF02C	2.7	5545	25	3.00E-04	11.3	10.2
PBF02C	2.7	5545	50	2.95E-04	10.9	8.9
PBF02C	2.7	5545	100	2.78E-04	10.8	6.2
PBF02C	2.7	5545	200	2.46E-04	10.7	3.8
PBF02C	2.7	5545	400	1.58E-04	9.7	3.0
PBF02C	2.7	5545	800	5.37E-05	10.8	4.3
PBF03A	2.5	5545	0	1.18E-04	10.8	12.6
PBF03A	2.5	5545	100	1.08E-04	18.3	6.2
PBF03A	2.5	5545	200	8.15E-05	18.4	4.8
PBF04B	2.6	5545	0	2.29E-04	16.4	13.3
PBF04B	2.6	5545	100	2.21E-04	17.6	4.0
PBF04B	2.6	5545	200	1.99E-04	17.6	2.8
PBF05B	2.6	5545	0	2.41E-04	11.2	8.6
PBF05B	2.6	5545	100	2.09E-04	13.6	4.4
PBF05B	2.6	5545	200	1.84E-04	14.3	3.2
PBE01C	2.5	5475	0	2.05E-04	22.9	-0.3
PBE01C	2.5	5475	25	2.09E-04	23.1	-1.1
PBE01C	2.5	5475	50	2.07E-04	22.9	-2.3
PBE01C	2.5	5475	100	1.98E-04	23.2	-2.9
PBE01C	2.5	5475	200	1.61E-04	21.4	-2.6
PBE01C	2.5	5475	400	1.20E-04	22.1	-3.0
PBE01C	2.5	5475	800	8.04E-05	23.0	-3.5
PBE02B	2.5	5475	0	1.98E-04	13.7	3.2
PBE02B	2.5	5475	100	1.89E-04	17.4	1.0
PBE02B	2.5	5475	200	1.55E-04	18.5	0.5
PBE03B	2.5	5475	0	2.19E-04	22.8	10.7
PBE03B	2.5	5475	100	1.98E-04	22.8	9.1
PBE03B	2.5	5475	200	1.63E-04	22.4	8.0
PBE04B	2.5	5475	0	1.73E-04	17.1	12.9
PBE04B	2.5	5475	100	1.64E-04	17.3	9.1
PBE04B	2.5	5475	200	1.33E-04	15.1	10.6
PBE05B	2.5	5475	0	2.47E-04	18.3	8.4
PBE05B	2.5	5475	100	2.29E-04	18.7	7.1
PBE05B	2.5	5475	200	2.04E-04	19.1	4.9
PBD01B	2.7	5460	0	2.80E-03	21.6	22.6
PBD01B	2.7	5460	50	2.76E-03	21.3	21.5
PBD01B	2.7	5460	100	1.70E-03	351.6	10.8
PBD02A	2.1	5460	0	2.58E-03	20.3	16.5
PBD02A	2.1	5460	50	2.53E-03	20.2	15.8
PBD02A	2.1	5460	100	2.38E-03	19.2	15.1
PBD03B	2.6	5460	0	2.80E-03	21.1	12.6
PBD03B	2.6	5460	25	2.76E-03	21.0	12.3
PBD03B	2.6	5460	50	2.73E-03	21.0	11.9
PBD03B	2.6	5460	100	2.63E-03	21.4	11.3
PBD03B	2.6	5460	200	2.09E-03	21.4	9.8
PBD03B	2.6	5460	400	1.19E-03	22.5	5.4
PBD03B	2.6	5460	800	4.75E-04	22.1	-25.2
PBD04A	2.4	5460	0	1.85E-03	14.4	12.2
PBD04A	2.4	5460	50	1.82E-03	14.9	12.1

SITE	DENS	ELEV	TREAT	EMU	INC	DEC
PBD04A	2.4	5460	100	2.73E-03	21.5	19.6
PBD05A	2.2	5460	0	2.61E-03	16.4	11.9
PBD05A	2.2	5460	50	2.65E-03	17.9	12.4
PBD05A	2.2	5460	100	2.49E-03	16.7	8.9
PBD06A	2.5	5460	0	2.67E-03	17.0	14.0
PBD06A	2.5	5460	50	2.66E-03	17.0	13.4
PBD06A	2.5	5460	100	2.59E-03	16.6	12.4
PBC01B	2.8	5450	0	2.06E-03	355.6	54.2
PBC01B	2.8	5450	25	2.01E-03	352.5	53.9
PBC01B	2.8	5450	50	1.99E-03	351.4	53.5
PBC01B	2.8	5450	100	1.81E-03	350.2	53.8
PBC01B	2.8	5450	200	1.41E-03	346.5	51.1
PBC01B	2.8	5450	400	6.01E-04	350.6	50.3
PBC01B	2.8	5450	800	1.99E-04	304.8	22.2
PBC02B	2.8	5450	0	1.72E-03	6.2	43.8
PBC02B	2.8	5450	100	1.45E-03	2.7	41.2
PBC02B	2.8	5450	200	9.39E-04	358.8	38.3
PBC03B	2.7	5450	0	2.52E-03	313.7	48.9
PBC03B	2.7	5450	100	2.22E-03	316.4	51.4
PBC03B	2.7	5450	200	1.86E-03	312.7	50.5
PBC04B	2.6	5450	0	1.33E-03	11.2	33.3
PBC04B	2.6	5450	100	1.13E-03	8.2	32.3
PBC04B	2.6	5450	200	8.85E-04	7.9	28.1
PBC05B	3.0	5450	0	1.03E-03	33.5	7.6
PBC05B	3.0	5450	100	1.74E-03	1.0	57.9
PBC05B	3.0	5450	200	1.44E-03	359.7	56.9
PBB01A	2.9	5430	0	5.60E-03	128.6	80.7
PBB01A	2.9	5430	100	1.25E-03	340.1	62.5
PBB01A	2.9	5430	200	1.19E-03	340.6	62.2
PBB01A	2.9	5430	400	4.87E-04	189.2	84.8
PBB01A	2.9	5430	600	1.95E-04	344.7	62.5
PBB02A	2.9	5430	0	6.01E-02	307.7	36.4
PBB02A	2.9	5430	100	5.27E-03	306.4	61.0
PBB02A	2.9	5430	200	1.17E-03	321.5	77.5
PBB02A	2.9	5430	400	3.15E-04	283.0	79.3
PBB02A	2.9	5430	600	1.73E-04	268.7	67.1
PBB02A	2.9	5430	800	1.03E-03	55.9	48.2
PBB02B	2.8	5430	0	4.10E-02	147.2	-4.6
PBB02B	2.8	5430	100	2.88E-03	149.1	7.2
PBB02B	2.8	5430	200	5.50E-04	154.7	43.1
PBB02B	2.8	5430	400	1.61E-04	214.0	69.0
PBB02B	2.8	5430	600	9.57E-05	292.9	61.2
PBB02B	2.8	5430	800	6.60E-05	90.7	57.8
PBB03A	2.9	5430	0	4.65E-03	314.7	46.2
PBB03A	2.9	5430	100	2.97E-03	313.0	53.7
PBB03A	2.9	5430	200	2.10E-03	306.1	56.0
PBB03A	2.9	5430	400	1.05E-03	304.8	56.9
PBB03A	2.9	5430	600	4.25E-04	302.5	53.0
PBB04A	2.8	5430	0	4.12E-02	96.0	-31.1
PBB04A	2.8	5430	100	9.56E-04	60.9	-11.1
PBB04A	2.8	5430	200	2.99E-04	358.8	65.2
PBB04A	2.8	5430	400	1.56E-04	325.4	43.9
PBB04A	2.8	5430	600	1.75E-04	254.3	76.2
PBB05A	2.8	5430	0	6.14E-03	20.8	55.8

SITE	DENS	ELEV	TREAT	EMU	INC	DEC
PBB05A	2.8	5430	25	4.99E-03	15.7	59.4
PBB05A	2.8	5430	50	3.70E-03	5.3	61.9
PBB05A	2.8	5430	100	1.74E-03	348.9	63.7
PBB05A	2.8	5430	200	7.08E-04	334.7	63.7
PBB05A	2.8	5430	400	2.78E-04	321.3	60.1
PBB05A	2.8	5430	800	7.61E-05	41.3	62.4
PBB05B	2.9	5430	0	6.28E-03	352.3	63.1
PBB05B	2.9	5430	400	3.49E-04	313.2	55.4
PBB05B	2.9	5430	600	2.25E-04	299.2	45.3
PBA01A	2.8	5420	0	6.32E-03	356.6	55.3
PBA01A	2.8	5420	50	4.75E-03	6.9	51.0
PBA01A	2.8	5420	100	3.72E-03	1.9	52.3
PBA02A	2.8	5420	0	6.24E-03	201.6	43.9
PBA02A	2.8	5420	50	5.37E-03	190.0	47.7
PBA02A	2.8	5420	100	2.70E-03	185.3	50.8
PBA03C	2.8	5420	0	7.76E-03	15.2	47.3
PBA03C	2.8	5420	25	6.72E-03	5.7	54.4
PBA03C	2.8	5420	50	5.74E-03	1.9	56.1
PBA03C	2.8	5420	100	2.80E-03	357.1	58.7
PBA03C	2.8	5420	200	6.66E-02	331.4	57.4
PBA03C	2.8	5420	400	2.72E-04	280.4	3.3
PBA03C	2.8	5420	800	1.19E-04	356.0	51.7
PBA04A	2.8	5420	0	5.18E-03	20.3	62.0
PBA04A	2.8	5420	50	3.76E-03	2.2	54.8
PBA04A	2.8	5420	100	1.06E-03	351.1	54.5
PBA05A	2.8	5420	0	5.89E-03	22.9	57.3
PBA05A	2.8	5420	50	4.94E-03	6.1	53.8
PBA05A	2.8	5420	100	2.08E-03	2.2	52.9
PBX01A	2.9	5385	0	1.89E-03	184.9	-73.8
PBX01A	2.9	5385	50	3.02E-04	214.9	-53.0
PBX01A	2.9	5385	100	8.49E-05	211.2	-8.3
PBX01A	2.9	5385	200	4.82E-05	224.5	21.2
PBX01C	2.9	5385	0	3.23E-03	199.9	-47.2
PBX01C	2.9	5385	25	7.42E-04	209.4	-33.4
PBX01C	2.9	5385	50	3.03E-04	198.4	-40.2
PBX01C	2.9	5385	100	7.70E-05	202.6	-16.9
PBX01C	2.9	5385	200	1.13E-04	204.6	10.5
PBX01C	2.9	5385	400	5.57E-05	236.2	50.4
PBX02A	2.9	5385	0	2.09E-03	90.4	-17.6
PBX02A	2.9	5385	50	1.43E-03	85.4	-66.6
PBX02A	2.9	5385	100	1.68E-05	47.3	-82.4
PBX02A	2.9	5385	100	1.68E-04	25.1	-76.9
PBX02A	2.9	5385	200	3.83E-05	124.4	-53.1
PBX02B	2.8	5385	0	1.68E-03	93.2	-36.8
PBX02B	2.8	5385	50	1.35E-03	85.2	-69.7
PBX02B	2.8	5385	100	7.35E-05	316.7	-58.9
PBX02B	2.8	5385	200	1.31E-04	304.6	-27.3
PBX03A	2.8	5385	0	3.28E-03	169.7	-74.6
PBX03A	2.8	5385	50	3.82E-03	169.2	-81.1
PBX03A	2.8	5385	100	1.59E-03	176.6	-85.9
PBX03A	2.8	5385	200	1.97E-04	244.1	-75.8
PBX04B	2.9	5385	0	5.46E-03	152.7	-68.2
PBX04B	2.9	5385	50	1.17E-03	215.1	-79.7
PBX04B	2.9	5385	100	1.54E-04	279.2	-39.6
PBX04B	2.9	5385	200	4.73E-05	258.0	-27.3
PBX05B	2.9	5385	0	4.53E-03	168.9	-74.5
PBX05B	2.9	5385	50	1.17E-03	207.5	-77.0
PBX05B	2.9	5385	100	1.61E-04	250.9	-56.4
PBX05B	2.9	5385	200	5.27E-05	252.3	-56.8
PBU01C	2.6	5220	0	4.69E-04	353.1	44.6
PBU01C	2.6	5220	50	1.79E-04	345.2	59.0
PBU01C	2.6	5220	100	9.17E-05	343.0	64.0
PBU01C	2.6	5220	200	4.14E-05	333.9	62.1
PBU01C	2.6	5220	400	1.53E-05	31.6	84.6
PBU01C	2.6	5220	800	7.10E-06	91.2	66.9
PBU02C	2.7	5220	0	4.51E-04	321.5	63.6
PBU02C	2.7	5220	50	1.86E-04	337.8	66.7
PBU02C	2.7	5220	100	1.17E-04	343.0	67.5
PBU02C	2.7	5220	200	5.09E-05	351.7	68.6
PBU02C	2.7	5220	400	2.58E-05	9.2	69.7
PBU02C	2.7	5220	800	9.37E-06	61.8	57.7
PBU03B	2.6	5220	0	2.98E-04	43.3	41.2
PBU03B	2.6	5220	50	1.30E-04	16.0	51.8
PBU03B	2.6	5220	100	7.47E-05	9.9	66.5
PBU03B	2.6	5220	200	3.51E-05	331.9	71.7
PBU03B	2.6	5220	400	1.25E-05	262.9	85.9
PBU04B	2.7	5220	0	4.45E-04	199.6	50.5
PBU04B	2.7	5220	25	1.83E-04	268.8	82.9
PBU04B	2.7	5220	50	1.43E-04	304.0	82.0
PBU04B	2.7	5220	100	7.96E-05	322.2	76.7
PBU04B	2.7	5220	200	3.68E-05	308.6	76.2
PBU04B	2.7	5220	400	1.82E-05	108.0	53.0
PBU04B	2.7	5220	400	1.81E-05	101.0	43.4
PBU04B	2.7	5220	800	2.59E-06	263.2	1.4
PBU05A	2.6	5220	0	4.68E-04	79.9	78.3
PBU05A	2.6	5220	50	2.00E-04	43.7	81.5
PBU05A	2.6	5220	100	8.46E-05	17.3	84.5
PBU05A	2.6	5220	200	4.20E-05	226.2	81.8
PBU05A	2.6	5220	400	1.27E-05	109.8	76.1
PBV01A	2.2	5100	0	2.96E-04	5.5	57.5
PBV01A	2.2	5100	100	7.87E-05	6.8	60.7
PBV01A	2.2	5100	200	3.96E-06	138.2	-23.5
PBV02A	2.3	5100	0	2.90E-04	1.9	63.8
PBV02A	2.3	5100	100	5.34E-05	0.5	71.2
PBV02A	2.3	5100	200	1.70E-06	68.8	18.1
PBV03B	2.2	5100	0	4.87E-04	12.6	64.9
PBV03B	2.2	5100	25	4.43E-04	8.2	65.9
PBV03B	2.2	5100	50	3.56E-04	7.1	66.9
PBV03B	2.2	5100	100	9.83E-05	346.1	72.4
PBV04A	2.2	5100	0	2.47E-04	15.8	60.7
PBV04A	2.2	5100	100	5.02E-05	18.1	61.4
PBV04A	2.2	5100	200	1.36E-05	335.4	27.9
PBV05A	2.3	5100	0	2.57E-04	324.2	56.8
PBV05A	2.3	5100	100	7.66E-05	320.3	51.6
PBV05A	2.3	5100	200	1.81E-05	315.8	24.5
PBW01B	2.4	5000	0	1.04E-04	214.3	85.1
PBW01B	2.4	5000	50	8.32E-05	209.6	86.7
PBW01B	2.4	5000	100	5.21E-05	231.0	88.6
PBW01B	2.4	5000	200	2.22E-05	205.4	47.7
PBW02B	2.3	5000	0	1.23E-04	141.0	81.8
PBW02B	2.3	5000	50	1.00E-04	146.5	83.2
PBW02B	2.3	5000	100	5.87E-05	140.6	82.9
PBW02B	2.3	5000	200	1.82E-05	61.3	86.3
PBW03B	2.4	5000	0	1.08E-04	0.1	80.1
PBW03B	2.4	5000	50	8.36E-05	18.8	79.3
PBW03B	2.4	5000	100	4.84E-05	14.4	82.1
PBW03B	2.4	5000	200	1.80E-05	26.0	83.6
PBW04B	2.3	5000	0	1.23E-04	98.0	82.2
PBW04B	2.3	5000	50	9.48E-05	72.7	81.5
PBW04B	2.3	5000	100	5.32E-05	72.1	82.3
PBW04B	2.3	5000	200	1.55E-05	18.7	76.8
PBW05B	2.3	5000	0	1.27E-04	67.6	78.8
PBW05B	2.3	5000	25	1.17E-04	58.9	78.7
PBW05B	2.3	5000	50	1.02E-04	59.8	79.3
PBW05B	2.3	5000	100	6.19E-05	58.1	82.8
PBW05B	2.3	5000	200	2.08E-05	82.4	83.5
PBW05B	2.3	5000	400	7.80E-06	306.2	82.1
PBW05B	2.3	5000	800	1.90E-06	355.2	35.7
PAA01B	2.8	4560	0	1.18E-03	283.5	-61.2
PAA01B	2.8	4560	400	7.74E-04	208.9	-76.6
PAA01C	2.9	4560	0	1.28E-03	280.8	-54.7
PAA01C	2.9	4560	200	1.76E-03	230.1	-73.6
PAA01C	2.9	4560	400	9.39E-04	231.2	-77.0
PAA01C	2.9	4560	600	4.44E-04	238.5	-76.2
PAA01D	2.9	4560	0	1.51E-03	309.6	-38.1
PAA01D	2.9	4560	25	1.49E-03	253.3	-59.6
PAA01D	2.9	4560	50	1.52E-03	238.8	-60.2
PAA01D	2.9	4560	100	1.54E-03	230.6	-60.7
PAA01D	2.9	4560	200	9.57E-04	235.2	-47.7
PAA01D	2.9	4560	400	2.06E-04	236.5	-43.8
PAA01D	2.9	4560	800	1.61E-04	200.2	-60.5
PAA02A	2.9	4560	0	2.41E-02	97.7	4.9
PAA02A	2.9	4560	200	1.12E-03	120.4	-61.0
PAA02A	2.9	4560	400	6.35E-04	140.5	-71.5
PAA02A	2.9	4560	600	3.70E-04	163.7	-47.3
PAA02C	2.9	4560	0	2.31E-02	98.5	2.3
PAA02C	2.9	4560	100	3.59E-03	100.0	-16.1
PAA02C	2.9	4560	200	1.26E-03	106.1	-47.0
PAA02C	2.9	4560	400	5.20E-04	125.5	-58.7
PAA02C	2.9	4560	600	2.56E-04	102.1	-55.3
PAA02C	2.9	4560	800	1.68E-04	98.6	-51.2
PAA03B	2.9	4560	0	9.82E-02	91.8	11.5
PAA03B	2.9	4560	200	5.53E-03	94.2	4.1
PAA03B	2.9	4560	400	1.10E-03	103.2	-5.7
PAA03B	2.9	4560	600	5.25E-04	101.7	-9.6
PAA03C	2.8	4560	0	8.97E-02	90.7	11.6
PAA03C	2.8	4560	100	2.19E-02	90.0	10.7
PAA03C	2.8	4560	200	3.38E-03	93.8	-1.2
PAA03C	2.8	4560	400	7.45E-04	102.1	-26.0
PAA03C	2.8	4560	800	2.91E-04	94.1	-47.8
PAA04B	2.9	4560	0	6.81E-03	257.4	-23.5
PAA04B	2.9	4560	400	1.06E-03	204.5	-70.6

SITE	DENS	ELEV	TREAT	EMU	INC	DEC
PAA04C	2.8	4560	0	6.61E-03	257.4	-20.3
PAA04C	2.8	4560	100	1.90E-03	197.5	-56.7
PAA04C	2.8	4560	200	1.34E-03	196.6	-65.3
PAA04C	2.8	4560	400	1.03E-03	208.6	-70.9
PAA04C	2.8	4560	600	3.49E-04	204.5	-65.2
PAA04C	2.8	4560	800	1.94E-04	166.1	-64.6
PAA05B	2.9	4560	0	9.02E-03	212.0	18.5
PAA05B	2.9	4560	200	1.07E-03	205.1	-25.6
PAA05B	2.9	4560	400	4.73E-04	210.2	-43.0
PAA05B	2.9	4560	600	1.81E-04	195.9	-31.6
PAA05C	2.9	4560	0	1.21E-02	204.6	18.5
PAA05C	2.9	4560	100	2.85E-03	200.4	1.8
PAA05C	2.9	4560	200	1.09E-03	203.6	-21.4
PAA05C	2.9	4560	400	3.76E-04	211.5	-30.5
PAA05C	2.9	4560	800	6.42E-05	50.2	-12.4
PAB01C	2.7	4505	0	2.97E-03	21.2	70.2
PAB01C	2.7	4505	25	2.94E-03	23.9	71.2
PAB01C	2.7	4505	50	2.90E-03	23.1	73.2
PAB01C	2.7	4505	100	2.84E-03	28.8	76.4
PAB01C	2.7	4505	200	1.47E-03	22.6	71.2
PAB01C	2.7	4505	400	1.28E-03	35.8	79.2
PAB01C	2.7	4505	800	5.75E-04	34.7	78.2
PAB02D	2.6	4505	0	6.97E-05	21.5	83.1
PAB02D	2.6	4505	50	6.78E-03	18.7	82.5
PAB02D	2.6	4505	100	6.78E-03	22.0	82.4
PAB02D	2.6	4505	200	4.71E-03	24.8	82.0
PAB02D	2.6	4505	400	3.08E-03	13.4	81.1
PAB02D	2.6	4505	400	3.08E-03	13.3	81.1
PAB02D	2.6	4505	401	2.30E-03	11.2	74.4
PAB02D	2.6	4505	410	2.74E-03	30.1	83.6
PAB02D	2.6	4505	800	1.41E-03	32.9	83.3
PAB03C	2.6	4505	0	2.09E-03	345.1	86.3
PAB03C	2.6	4505	50	2.09E-03	345.1	86.3
PAB03C	2.6	4505	81	2.11E-03	7.7	86.0
PAB03C	2.6	4505	100	1.98E-03	353.6	85.9
PAB03C	2.6	4505	200	1.81E-03	344.1	86.2
PAB03C	2.6	4505	400	1.39E-03	336.2	86.6
PAB03C	2.6	4505	410	1.19E-03	30.5	86.1
PAB03C	2.6	4505	800	6.23E-04	53.2	87.6
PAB04D	2.7	4505	0	1.63E-03	58.7	79.1
PAB04D	2.7	4505	50	1.63E-03	58.6	78.4
PAB04D	2.7	4505	100	1.61E-03	57.0	78.3
PAB04D	2.7	4505	200	1.50E-03	60.3	77.8
PAB04D	2.7	4505	400	1.23E-03	58.3	77.8
PAB04D	2.7	4505	410	1.05E-03	62.4	80.0
PAB04D	2.7	4505	800	6.11E-04	61.5	80.3
PAB05B	2.6	4505	0	8.62E-04	9.8	78.3
PAB05B	2.6	4505	50	7.88E-04	27.8	77.2
PAB05B	2.6	4505	100	7.06E-04	25.6	76.9
PAB05B	2.6	4505	200	5.43E-04	23.3	77.2
PAB05B	2.6	4505	400	3.47E-04	21.5	77.3
PAB05B	2.6	4505	410	3.00E-04	32.3	79.0
PAB05B	2.6	4505	800	1.28E-04	39.5	78.3
PAC01A	2.6	4465	0	5.54E-03	184.8	-65.8
PAC01A	2.6	4465	100	5.38E-03	184.6	-68.9
PAC01A	2.6	4465	200	3.84E-03	177.8	-70.9
PAC01B	2.6	4465	0	3.83E-03	223.9	-56.9
PAC01B	2.6	4465	25	3.90E-03	225.5	-57.3
PAC01B	2.6	4465	50	3.90E-03	225.6	-57.6
PAC01B	2.6	4465	100	3.77E-03	223.6	-59.3
PAC01B	2.6	4465	200	3.49E-03	215.9	-63.8
PAC01B	2.6	4465	400	1.77E-03	217.8	-62.2
PAC01B	2.6	4465	800	8.42E-04	221.6	-60.8
PAC02B	2.6	4465	0	8.30E-03	189.7	-68.7
PAC02B	2.6	4465	100	7.65E-03	187.1	-69.7
PAC02B	2.6	4465	200	4.89E-03	186.6	-69.8
PAC03B	2.7	4465	0	1.94E-03	198.5	-60.7
PAC03B	2.7	4465	100	1.73E-03	186.3	-65.1
PAC03B	2.7	4465	200	1.17E-03	187.5	-64.8
PAC04B	2.7	4465	0	6.33E-03	186.5	-63.2
PAC04B	2.7	4465	100	6.20E-03	185.6	-64.6
PAC04B	2.7	4465	200	5.15E-03	184.8	-64.9
PAC05B	2.7	4465	0	7.63E-03	190.2	-68.6
PAC05B	2.7	4465	100	6.92E-03	187.7	-68.2
PAC05B	2.7	4465	200	5.78E-03	188.7	-68.3
PAD01B	2.7	4440	0	3.71E-03	195.2	-29.0
PAD01B	2.7	4440	100	1.78E-03	189.8	-45.4
PAD01B	2.7	4440	200	1.04E-03	189.9	-47.5
PAD01B	2.7	4440	400	5.17E-04	193.5	-47.1
PAD01B	2.7	4440	600	2.58E-04	199.3	-43.7
PAD01B	2.7	4440	800	1.29E-04	196.4	-44.0
PAD03B	2.7	4440	0	1.84E-02	116.7	-24.5
PAD03B	2.7	4440	100	6.73E-03	117.2	-23.3
PAD03B	2.7	4440	200	2.53E-03	124.4	-14.3
PAD03B	2.7	4440	400	1.04E-03	130.7	-11.2
PAD03B	2.7	4440	800	2.62E-04	134.4	-12.8
PAD04A	2.7	4440	0	3.55E-02	86.7	-55.1
PAD04A	2.7	4440	100	1.59E-02	95.1	-59.9
PAD04A	2.7	4440	200	4.72E-03	106.0	-66.9
PAD04A	2.7	4440	400	1.43E-03	134.3	-67.2
PAD04A	2.7	4440	600	8.85E-04	127.9	-68.0
PAD04A	2.7	4440	800	4.83E-04	131.7	-67.4
PAD04B	2.7	4440	0	2.28E-02	117.7	-74.2
PAD04B	2.7	4440	25	2.17E-02	112.9	-74.3
PAD04B	2.7	4440	50	1.38E-02	125.1	-67.5
PAD04B	2.7	4440	100	8.64E-03	123.6	-74.5
PAD04B	2.7	4440	200	3.52E-03	135.3	-74.5
PAD04B	2.7	4440	400	1.15E-03	147.8	-72.5
PAD04B	2.7	4440	800	2.41E-04	144.4	-72.5
PAD04B	2.7	4440	1000	1.61E-04	140.0	-75.0
PAD05B	2.4	4440	0	3.79E-03	182.1	-72.9
PAD05B	2.4	4440	100	1.72E-03	184.6	-73.9
PAD05B	2.4	4440	200	1.10E-03	186.4	-73.4
PAD05B	2.4	4440	400	5.72E-04	195.3	-75.1
PAD05B	2.4	4440	800	1.13E-04	242.3	-83.6
PAE01B	2.8	4400	0	1.05E-02	319.4	69.8
PAE01B	2.8	4400	25	1.01E-02	315.7	69.7
PAE01B	2.8	4400	50	9.64E-03	313.7	69.9
PAE01B	2.8	4400	100	8.69E-03	312.6	69.0
PAE01B	2.8	4400	200	6.55E-03	311.1	70.1
PAE01B	2.8	4400	400	3.13E-03	308.9	69.2
PAE01B	2.8	4400	800	1.05E-03	303.4	69.9
PAE02C	2.7	4400	0	5.90E-03	325.2	69.5
PAE02C	2.7	4400	100	2.67E-03	317.8	67.6
PAE02C	2.7	4400	200	2.03E-03	315.9	67.1
PAE03B	2.8	4400	0	9.04E-03	310.4	69.8
PAE03B	2.8	4400	100	8.28E-03	308.2	69.9
PAE03B	2.8	4400	200	6.46E-03	308.6	69.8
PAE04B	2.8	4400	0	6.12E-03	320.7	72.5
PAE04B	2.8	4400	100	3.02E-03	309.5	68.9
PAE04B	2.8	4400	200	1.99E-03	308.1	68.9
PAE05B	2.8	4400	0	7.20E-03	324.6	69.4
PAE05B	2.8	4400	100	5.16E-03	316.8	70.7
PAE05B	2.8	4400	200	3.68E-03	318.4	69.3
PAF01A	2.6	4370	0	6.41E-03	49.1	71.5
PAF01A	2.6	4370	100	2.14E-03	297.9	83.6
PAF01A	2.6	4370	200	1.59E-03	281.0	83.7
PAF02B	2.6	4370	0	6.23E-03	308.2	79.9
PAF02B	2.6	4370	100	2.59E-03	317.4	79.0
PAF02B	2.6	4370	200	1.98E-03	297.6	77.6
PAF03A	2.5	4370	0	1.48E-02	243.5	83.0
PAF03A	2.5	4370	100	1.38E-02	263.5	81.8
PAF03A	2.5	4370	200	9.82E-03	245.3	82.6
PAF04A	2.6	4370	0	1.04E-02	325.7	77.6
PAF04A	2.6	4370	100	9.46E-03	325.8	77.3
PAF04A	2.6	4370	200	7.14E-03	326.7	77.2
PAF05B	2.6	4370	0	1.01E-02	241.9	80.7
PAF05B	2.6	4370	25	1.00E-02	251.4	79.7
PAF05B	2.6	4370	50	9.82E-03	249.8	80.1
PAF05B	2.6	4370	100	9.20E-05	247.5	80.1
PAF05B	2.6	4370	200	6.92E-03	251.6	80.1
PAF05B	2.6	4370	400	3.52E-03	263.7	79.0
PAF05B	2.6	4370	800	1.80E-03	236.3	77.6
PAG01B	2.6	4340	0	1.20E-02	304.6	78.8
PAG01B	2.6	4340	25	1.08E-02	286.9	79.8
PAG01B	2.6	4340	50	1.00E-02	289.5	79.7
PAG01B	2.6	4340	100	8.71E-03	277.3	78.0
PAG01B	2.6	4340	200	5.82E-03	278.8	80.2
PAG01B	2.6	4340	400	2.28E-03	270.8	79.0
PAG01B	2.6	4340	800	4.53E-04	263.8	75.2
PAG02B	2.6	4340	0	1.18E-02	258.2	74.6
PAG02B	2.6	4340	100	9.10E-03	260.2	73.9
PAG02B	2.6	4340	200	5.44E-03	233.0	78.8
PAG03B	2.7	4340	0	5.96E-03	329.6	69.8
PAG03B	2.7	4340	100	2.65E-03	299.7	77.5
PAG03B	2.7	4340	200	1.64E-03	300.9	76.7
PAG04A	2.7	4340	0	5.14E-03	296.7	84.3
PAG04A	2.7	4340	100	1.56E-03	282.5	79.1
PAG04A	2.7	4340	200	9.74E-04	289.5	78.8
PAG05B	2.7	4340	0	1.48E-02	293.0	73.8
PAG05B	2.7	4340	100	9.74E-03	286.2	74.1
PAG05B	2.7	4340	200	6.19E-03	285.8	74.8

SITE	DENS	ELEV	TREAT	EMU	INC	DEC
PAH01B	2.7	4300	0	7.37E-03	16.7	68.9
PAH01B	2.7	4300	25	5.55E-03	13.5	68.4
PAH01B	2.7	4300	50	3.84E-03	18.9	69.1
PAH01B	2.7	4300	100	2.94E-03	17.5	68.1
PAH01B	2.7	4300	200	1.65E-03	19.7	68.0
PAH01B	2.7	4300	400	5.72E-04	26.9	69.2
PAH01B	2.7	4300	800	1.57E-04	22.0	60.3
PAH02B	2.4	4300	0	6.74E-03	17.7	63.5
PAH02B	2.4	4300	100	1.90E-03	20.9	65.6
PAH02B	2.4	4300	200	1.85E-03	21.1	66.3
PAH03B	2.3	4300	0	7.32E-03	17.6	61.2
PAH03B	2.3	4300	100	1.61E-03	23.1	62.8
PAH03B	2.3	4300	200	9.12E-04	20.2	61.6
PAH04B	2.7	4300	0	9.21E-03	1.2	67.2
PAH04B	2.7	4300	100	8.11E-03	1.5	66.5
PAH04B	2.7	4300	200	7.76E-03	3.0	66.4
PAH05A	2.7	4300	0	3.43E-03	10.3	72.5
PAH05A	2.7	4300	100	2.13E-03	14.3	69.8
PAH05A	2.7	4300	200	1.30E-03	13.8	70.2
PAI01C	2.7	4230	0	1.06E-03	323.4	62.5
PAI01C	2.7	4230	25	8.36E-04	344.8	76.8
PAI01C	2.7	4230	50	7.45E-04	23.8	82.0
PAI01C	2.7	4230	100	5.14E-04	35.5	84.0
PAI01C	2.7	4230	200	2.82E-04	44.9	85.4
PAI01C	2.7	4230	400	1.36E-04	21.2	85.0
PAI01C	2.7	4230	800	4.27E-05	176.5	82.1
PAI02C	2.7	4230	0	1.05E-03	34.8	78.6
PAI02C	2.7	4230	100	4.77E-04	53.6	81.5
PAI02C	2.7	4230	200	2.52E-04	55.0	82.1
PAI03A	2.7	4230	0	1.24E-03	259.6	82.6
PAI03A	2.7	4230	100	5.61E-04	47.9	87.8
PAI03A	2.7	4230	200	3.55E-04	36.5	87.4
PAI04C	2.7	4230	0	3.46E-03	60.5	87.6
PAI04C	2.7	4230	100	3.19E-03	82.0	88.0
PAI04C	2.7	4230	200	2.43E-03	78.4	88.2
PAI05B	2.7	4230	0	3.36E-03	110.1	85.8
PAI05B	2.7	4230	100	3.10E-03	104.2	85.3
PAI05B	2.7	4230	200	2.38E-03	114.2	85.9
PAJ01A	2.9	4200	0	6.33E-03	281.9	7.6
PAJ01A	2.9	4200	100	1.18E-03	304.5	72.2
PAJ01A	2.9	4200	200	6.26E-04	301.0	75.3
PAJ02A	2.8	4200	0	2.77E-03	314.4	67.9
PAJ02A	2.8	4200	100	9.73E-04	306.4	76.3
PAJ02A	2.8	4200	200	4.39E-04	288.9	80.2
PAJ03B	2.5	4200	0	9.56E-03	336.3	80.6
PAJ03B	2.5	4200	100	4.38E-03	342.8	80.3
PAJ03B	2.5	4200	200	2.35E-03	338.4	81.8
PAJ04A	2.7	4200	0	9.39E-03	300.8	80.2
PAJ04A	2.7	4200	100	9.39E-03	300.8	80.2
PAJ04A	2.7	4200	200	2.14E-03	299.4	80.2
PAJ05B	2.7	4200	0	7.51E-03	333.4	78.5
PAJ05B	2.7	4200	100	3.99E-03	332.5	79.2
PAJ05B	2.7	4200	200	2.24E-03	332.3	79.9
PAK01A	2.9	4170	0	9.65E-03	305.6	75.3

SITE	DENS	ELEV	TREAT	EMU	INC	DEC
PAK01A	2.9	4170	100	2.90E-03	300.9	78.8
PAK01A	2.9	4170	200	1.35E-03	298.1	79.2
PAK02A	2.8	4170	0	1.27E-02	307.3	82.1
PAK02A	2.8	4170	100	5.57E-03	306.0	81.5
PAK02A	2.8	4170	200	2.64E-03	309.0	80.7
PAK03B	2.8	4170	0	7.31E-03	324.1	77.0
PAK03B	2.8	4170	25	6.93E-03	322.0	77.2
PAK03B	2.8	4170	50	6.52E-03	318.0	78.9
PAK03B	2.8	4170	100	5.59E-03	322.2	76.6
PAK03B	2.8	4170	200	3.57E-03	319.3	77.3
PAK03B	2.8	4170	400	2.03E-03	316.0	77.8
PAK03B	2.8	4170	800	9.23E-04	330.2	73.5
PAK04A	2.8	4170	0	5.42E-03	0.2	76.4
PAK04A	2.8	4170	100	2.25E-03	12.0	75.7
PAK04A	2.8	4170	200	8.25E-04	17.2	76.0
PAK05A	2.8	4170	0	2.61E-03	104.3	76.3
PAK05A	2.8	4170	100	1.07E-03	139.5	81.5
PAK05A	2.8	4170	200	1.03E-03	139.4	81.6
PAL01B	2.9	4155	0	7.84E-04	276.1	67.6
PAL01B	2.9	4155	100	8.88E-05	287.9	67.3
PAL01B	2.9	4155	200	4.88E-05	307.7	62.8
PAL02B	3.0	4155	0	1.02E-03	281.9	80.0
PAL02B	3.0	4155	25	4.43E-04	303.1	79.5
PAL02B	3.0	4155	50	2.80E-04	313.3	74.7
PAL02B	3.0	4155	100	1.39E-04	315.3	68.6
PAL02B	3.0	4155	200	7.57E-05	303.9	71.2
PAL02B	3.0	4155	400	3.36E-05	302.2	67.1
PAL02B	3.0	4155	800	1.34E-05	305.1	31.2
PAL03B	2.9	4155	0	9.46E-04	351.6	68.5
PAL03B	2.9	4155	100	1.26E-04	321.3	69.1
PAL03B	2.9	4155	200	7.11E-05	330.3	60.2
PAL04B	2.9	4155	0	5.79E-04	264.9	61.5
PAL04B	2.9	4155	100	1.50E-04	298.5	73.8
PAL04B	2.9	4155	200	9.29E-05	299.5	75.7
PAL05C	2.9	4155	0	8.18E-04	297.8	79.6
PAL05C	2.9	4155	100	1.37E-04	318.9	69.2
PAL05C	2.9	4155	200	8.57E-05	317.8	62.2
PAM01B	2.7	4135	0	1.51E-03	165.2	-38.8
PAM01B	2.7	4135	100	1.45E-03	167.3	-38.3
PAM01B	2.7	4135	200	1.03E-03	167.3	-38.9
PAM02B	2.7	4135	0	4.13E-04	344.9	33.0
PAM02B	2.7	4135	25	1.58E-04	129.9	-38.1
PAM02B	2.7	4135	50	2.65E-04	143.8	-42.6
PAM02B	2.7	4135	100	2.37E-04	155.9	-47.6
PAM02B	2.7	4135	200	1.56E-04	165.4	-49.4
PAM02B	2.7	4135	400	1.53E-04	100.7	-83.8
PAM02B	2.7	4135	800	1.30E-05	146.1	-37.7
PAM03C	2.8	4135	0	5.07E-04	111.2	30.6
PAM03C	2.8	4135	100	4.47E-04	158.8	-46.3
PAM03C	2.8	4135	200	2.81E-04	160.2	-47.9
PAM04C	2.8	4135	0	1.56E-03	160.4	-50.1
PAM04C	2.8	4135	100	1.52E-03	164.4	-51.8
PAM04C	2.8	4135	200	1.06E-03	162.8	-52.3
PAM05B	2.7	4135	0	6.87E-04	70.4	11.2

SITE	DENS	ELEV	TREAT	EMU	INC	DEC
PAM05B	2.7	4135	100	2.77E-04	155.8	-32.2
PAM05B	2.7	4135	200	1.48E-04	160.3	-39.4
PAN01B	2.9	4125	0	2.50E-04	206.9	7.5
PAN01B	2.9	4125	100	2.71E-04	165.3	-32.6
PAN01B	2.9	4125	200	1.23E-04	168.6	-33.0
PAN02C	2.8	4125	0	4.62E-04	187.3	-3.1
PAN02C	2.8	4125	100	4.92E-04	172.7	-47.7
PAN02C	2.8	4125	200	3.04E-04	173.0	-49.3
PAN03B	2.8	4125	0	1.47E-04	130.9	-14.8
PAN03B	2.8	4125	100	2.73E-04	152.2	-40.3
PAN03B	2.8	4125	200	2.35E-04	158.2	-46.9
PAN04B	2.7	4125	0	2.07E-04	149.5	-12.9
PAN04B	2.7	4125	100	4.63E-04	185.4	-42.7
PAN04B	2.7	4125	200	2.37E-04	183.8	-44.5
PAN05C	2.9	4125	0	1.97E-04	87.4	-33.6
PAN05C	2.9	4125	25	3.50E-04	139.1	-51.4
PAN05C	2.9	4125	50	3.55E-04	152.0	-52.1
PAN05C	2.9	4125	100	2.83E-04	158.3	-52.8
PAN05C	2.9	4125	200	1.76E-04	161.6	-55.5
PAN05C	2.9	4125	400	7.29E-05	152.1	-50.7
PAN05C	2.9	4125	800	4.16E-05	229.3	-37.0
PAO01C	2.9	4115	0	3.38E-03	181.3	-75.9
PAO01C	2.9	4115	100	1.68E-03	175.1	-74.6
PAO01C	2.9	4115	200	5.28E-04	178.9	-73.2
PAO02C	2.8	4115	0	3.43E-03	162.9	-77.5
PAO02C	2.8	4115	100	2.65E-03	166.9	-75.3
PAO02C	2.8	4115	200	1.28E-03	163.9	-75.8
PAO03C	2.8	4115	0	6.81E-03	165.6	-74.7
PAO03C	2.8	4115	100	4.53E-03	166.8	-74.4
PAO03C	2.8	4115	200	1.58E-03	171.8	-74.2
PAO04A	2.8	4115	0	4.03E-03	296.2	-23.3
PAO04A	2.8	4115	100	3.36E-03	295.4	-22.8
PAO04A	2.8	4115	200	1.60E-03	295.4	-23.1
PAO05B	2.6	4115	0	9.30E-05	184.4	10.4
PAO05B	2.6	4115	25	2.62E-04	154.7	-74.9
PAO05B	2.6	4115	50	2.60E-04	161.2	-75.0
PAO05B	2.6	4115	100	1.31E-04	159.0	-75.5
PAO05B	2.6	4115	200	5.30E-05	174.3	-67.8
PAO05B	2.6	4115	400	1.72E-05	178.1	-71.8
PAO05B	2.6	4115	800	1.05E-05	128.5	-29.5
PAP01B	2.6	4100	0	6.43E-04	227.0	-42.0
PAP01B	2.6	4100	100	2.43E-04	163.9	-76.1
PAP01B	2.6	4100	200	1.27E-04	158.3	-75.7
PAP02B	2.6	4100	0	2.26E-04	310.4	-56.8
PAP02B	2.6	4100	100	1.84E-04	153.2	-86.8
PAP02B	2.6	4100	200	8.97E-05	121.9	-85.0
PAP03B	2.8	4100	0	3.09E-04	344.5	-20.3
PAP03B	2.8	4100	100	1.50E-04	357.3	-75.1
PAP03B	2.8	4100	200	8.75E-05	358.8	-83.7
PAP04B	2.7	4100	0	2.37E-04	276.2	-38.7
PAP04B	2.7	4100	100	1.48E-04	266.4	-77.4
PAP04B	2.7	4100	200	1.01E-04	250.8	-79.5
PAP05B	2.5	4100	0	1.47E-03	305.2	-35.7
PAP05B	2.5	4100	25	8.79E-04	259.9	-78.3

SITE	DENS	ELEV	TREAT	EMU	INC	DEC
PAP05B	2.5	4100	50	7.84E-04	194.6	-83.3
PAP05B	2.5	4100	100	4.52E-04	170.0	-80.7
PAP05B	2.5	4100	200	1.81E-04	165.6	-75.0
PAP05B	2.5	4100	400	4.34E-05	173.9	-62.9
PAP05B	2.5	4100	800	2.36E-05	207.3	48.1
PAQ01A	2.8	4065	0	2.71E-03	319.5	57.1
PAQ01A	2.8	4065	100	8.45E-04	331.2	59.7
PAQ01A	2.8	4065	200	3.79E-04	341.3	58.6
PAQ02A	2.7	4065	0	2.68E-03	325.4	61.6
PAQ02A	2.7	4065	100	1.10E-03	332.9	62.9
PAQ02A	2.7	4065	200	5.47E-04	346.7	61.1
PAQ03B	2.6	4065	0	3.70E-03	311.9	41.4
PAQ03B	2.6	4065	100	3.77E-03	333.8	58.1
PAQ03B	2.6	4065	200	2.73E-03	349.5	63.4
PAQ04B	2.6	4065	0	2.12E-03	332.9	46.4
PAQ04B	2.6	4065	100	4.52E-03	344.7	55.6
PAQ04B	2.6	4065	200	9.82E-04	353.3	59.8
PAQ05C	2.8	4065	0	2.62E-03	347.2	40.7
PAQ05C	2.8	4065	25	2.06E-03	345.9	42.8
PAQ05C	2.8	4065	50	1.91E-03	347.3	46.0
PAQ05C	2.8	4065	100	1.67E-03	353.1	54.9
PAQ05C	2.8	4065	200	1.06E-03	358.5	60.2
PAQ05C	2.8	4065	400	3.55E-04	1.6	62.4
PAQ05C	2.8	4065	800	5.75E-05	34.5	59.3
PAR01B	2.9	4030	0	1.44E-03	37.0	67.2
PAR01B	2.9	4030	100	5.17E-04	46.1	55.5
PAR01B	2.9	4030	200	3.21E-04	48.1	54.4
PAR01B	2.9	4030	400	1.12E-04	48.9	54.1
PAR02B	2.8	4030	0	2.25E-03	146.9	42.6
PAR02B	2.8	4030	100	5.11E-04	153.6	80.8
PAR02B	2.8	4030	200	2.94E-04	283.3	82.2
PAR02B	2.8	4030	400	1.58E-04	302.6	59.8
PAR03B	2.9	4030	0	1.39E-03	31.5	65.0
PAR03B	2.9	4030	100	9.11E-04	44.0	61.8
PAR03B	2.9	4030	200	6.00E-04	42.8	60.5
PAR04B	2.8	4030	0	1.15E-03	71.9	76.4
PAR04B	2.8	4030	100	7.03E-04	43.9	56.6
PAR04B	2.8	4030	200	4.90E-04	41.4	57.6
PAR05B	3.0	4030	0	1.65E-03	50.3	68.9
PAR05B	3.0	4030	25	1.42E-03	49.7	65.0
PAR05B	3.0	4030	50	1.31E-03	47.4	62.3
PAR05B	3.0	4030	100	1.18E-03	46.6	61.0
PAR05B	3.0	4030	200	9.27E-04	46.1	58.8
PAR05B	3.0	4030	400	4.24E-04	43.7	60.0
PAR05B	3.0	4030	800	8.61E-05	110.8	36.5
PAS01B	2.9	3880	0	1.94E-03	345.3	67.1
PAS01B	2.9	3880	50	8.00E-04	15.6	67.7
PAS01B	2.9	3880	100	4.17E-04	18.1	66.8
PAS01B	2.9	3880	200	2.24E-04	21.6	71.5
PAS02A	2.7	3880	0	6.81E-04	14.3	69.0
PAS02A	2.7	3880	50	5.16E-04	19.0	69.6
PAS02A	2.7	3880	100	4.12E-04	20.7	69.4
PAS02A	2.7	3880	200	2.96E-04	17.3	69.8
PAS03A	2.7	3880	0	1.91E-03	29.0	67.0
PAS03A	2.7	3880	50	1.44E-03	27.3	66.5
PAS03A	2.7	3880	100	1.13E-03	29.1	65.7
PAS03A	2.7	3880	200	7.45E-04	25.6	64.9
PAS04B	2.9	3880	0	1.39E-03	21.1	78.0
PAS04B	2.9	3880	25	1.25E-03	13.0	75.5
PAS04B	2.9	3880	50	1.16E-03	10.0	74.6
PAS04B	2.9	3880	100	1.04E-03	8.3	74.9
PAS04B	2.9	3880	200	9.21E-04	346.4	75.1
PAS04B	2.9	3880	400	3.90E-04	315.7	9.4
PAS04B	2.9	3880	800	2.16E-04	78.4	-64.8
PAS05B	2.8	3880	0	4.61E-02	119.6	3.6
PAS05B	2.8	3880	50	3.77E-02	119.3	2.8
PAS05B	2.8	3880	100	2.44E-02	118.9	3.1
PAS05B	2.8	3880	200	7.96E-03	114.5	6.5
PAS05B	2.8	3880	400	1.07E-03	98.5	31.7
PAS05B	2.8	3880	800	3.52E-04	76.1	52.1
PAS05C	2.7	3880	0	9.31E-02	152.0	-11.5
PAS05C	2.7	3880	50	8.19E-02	152.4	-11.5
PAS05C	2.7	3880	100	5.88E-02	152.0	-12.2
PAS05C	2.7	3880	200	2.03E-02	150.8	-11.6
PAS05C	2.7	3880	400	2.04E-03	143.0	-3.9
PAS05C	2.7	3880	800	9.90E-04	118.0	-81.1
PAT01B	2.7	3860	0	9.73E-05	134.0	-10.0
PAT01B	2.7	3860	100	1.57E-04	164.9	-56.8
PAT01B	2.7	3860	200	1.43E-04	164.9	-56.2
PAT01B	2.7	3860	400	9.46E-05	164.9	-59.0
PAT01B	2.7	3860	800	4.12E-05	158.7	-59.8
PAT02B	2.5	3860	0	1.06E-03	158.9	-50.9
PAT02B	2.5	3860	100	1.11E-03	169.9	-51.6
PAT02B	2.5	3860	200	1.02E-03	160.1	-52.9
PAT02B	2.5	3860	400	8.32E-04	159.5	-53.0
PAT02B	2.5	3860	800	6.30E-04	161.7	-54.3
PAT03A	2.7	3860	0	7.14E-05	248.0	-63.0
PAT03A	2.7	3860	100	7.11E-05	248.1	-63.0
PAT03A	2.7	3860	200	6.45E-05	246.9	-63.4
PAT03A	2.7	3860	400	3.84E-05	279.5	-79.0
PAT03A	2.7	3860	800	2.65E-05	253.0	-73.3
PAT04B	1.8	3860	0	5.12E-05	339.7	-11.3
PAT04B	1.8	3860	100	5.59E-05	339.0	-17.6
PAT04B	1.8	3860	200	5.77E-05	338.5	-20.6
PAT04B	1.8	3860	400	5.18E-05	341.5	-17.8
PAT04B	1.8	3860	800	4.06E-05	341.9	-19.5
PAT05C	2.3	3860	0	1.09E-03	39.7	-63.5
PAT05C	2.3	3860	25	1.15E-03	41.1	-61.8
PAT05C	2.3	3860	50	1.10E-03	35.7	-62.4
PAT05C	2.3	3860	100	1.04E-03	27.2	-63.3
PAT05C	2.3	3860	200	1.12E-03	35.8	-63.3
PAT05C	2.3	3860	400	1.20E-03	24.4	-69.1
PAT05C	2.3	3860	800	9.01E-04	37.6	-64.4
PAU01A	2.8	3815	0	7.48E-04	152.7	-57.4
PAU01A	2.8	3815	100	7.37E-04	155.3	-57.3
PAU01A	2.8	3815	200	6.11E-04	154.3	-57.5
PAU02A	2.7	3815	0	1.71E-03	155.8	-57.3
PAU02A	2.7	3815	100	1.68E-03	156.5	-57.5
PAU02A	2.7	3815	200	1.69E-03	156.0	-57.4
PAU03B	3.1	3815	0	5.43E-04	144.3	-63.7
PAU03B	3.1	3815	25	5.60E-04	146.4	-61.4
PAU03B	3.1	3815	50	5.61E-04	146.4	-61.5
PAU03B	3.1	3815	100	5.51E-04	147.4	-61.1
PAU03B	3.1	3815	200	4.75E-04	147.6	-61.8
PAU03B	3.1	3815	400	3.51E-04	149.0	-62.1
PAU03B	3.1	3815	800	2.15E-04	133.4	-75.5
PAU04B	2.7	3815	0	1.02E-03	154.7	-62.4
PAU04B	2.7	3815	100	9.82E-04	154.6	-61.4
PAU04B	2.7	3815	200	7.75E-04	155.9	-61.5
PAU05B	2.7	3815	0	7.87E-04	160.4	-64.8
PAU05B	2.7	3815	100	7.86E-04	159.7	-65.1
PAU05B	2.7	3815	200	6.91E-04	159.6	-65.0
PAV01B	2.8	3780	0	1.49E-03	176.4	-72.8
PAV01B	2.8	3780	100	1.46E-03	179.7	-72.8
PAV01B	2.8	3780	200	1.34E-03	180.2	-73.3
PAV02B	2.8	3780	0	1.51E-03	200.0	-65.1
PAV02B	2.8	3780	25	1.54E-03	200.7	-64.1
PAV02B	2.8	3780	50	1.54E-03	200.9	-64.1
PAV02B	2.8	3780	100	1.50E-03	200.0	-65.2
PAV02B	2.8	3780	200	9.20E-04	191.8	-59.1
PAV02B	2.8	3780	400	8.16E-04	199.0	-62.4
PAV02B	2.8	3780	800	5.25E-04	196.6	-68.3
PAV02B	2.8	3780	1000	3.42E-04	192.1	-60.5
PAV03A	2.8	3780	0	2.22E-04	213.8	-76.1
PAV03A	2.8	3780	100	2.72E-04	215.6	-70.8
PAV03A	2.8	3780	200	1.75E-04	215.1	-72.0
PAV04B	2.8	3780	0	2.65E-04	152.0	-75.9
PAV04B	2.8	3780	100	2.61E-04	143.3	-65.8
PAV04B	2.8	3780	200	1.67E-04	146.1	-67.9
PAV05B	2.8	3780	0	4.05E-05	186.9	-42.9
PAV05B	2.8	3780	100	4.61E-05	154.2	-73.8
PAV05B	2.8	3780	200	3.45E-05	157.8	-76.9
PAW01B	2.6	3700	0	4.22E-04	1.7	21.1
PAW01B	2.6	3700	25	3.33E-04	357.1	23.3
PAW01B	2.6	3700	50	3.23E-04	359.1	21.5
PAW01B	2.6	3700	100	3.04E-04	2.3	18.9
PAW01B	2.6	3700	200	1.63E-04	5.1	12.0
PAW01B	2.6	3700	400	6.38E-05	352.3	11.4
PAW01B	2.6	3700	800	3.91E-05	331.9	39.1
PAW02A	2.5	3700	0	4.00E-04	339.3	22.4
PAW02A	2.5	3700	25	3.55E-04	343.3	20.9
PAW02A	2.5	3700	50	3.26E-04	350.4	20.2
PAW02A	2.5	3700	100	2.89E-04	353.3	19.9
PAW02A	2.5	3700	200	1.13E-04	1.5	4.7
PAW02A	2.5	3700	400	7.22E-05	343.1	-4.9
PAW02A	2.5	3700	800	5.60E-05	335.6	-17.8
PAW02B	2.5	3700	0	3.07E-04	330.3	5.2
PAW02B	2.5	3700	25	2.85E-04	340.9	18.7
PAW02B	2.5	3700	50	3.06E-04	348.1	24.5
PAW02B	2.5	3700	100	2.42E-04	352.1	26.4
PAW02B	2.5	3700	200	1.20E-04	354.0	20.8
PAW02B	2.5	3700	400	4.23E-05	4.3	60.8

SITE	DENS	ELEV	TREAT	EMU	INC	DEC
PAW02B	2.5	3700	800	3.58E-07	255.3	7.0
PAW03A	2.7	3700	0	3.76E-04	4.9	10.3
PAW03A	2.7	3700	50	3.20E-04	4.3	13.7
PAW03A	2.7	3700	100	2.48E-04	2.9	16.3
PAW04A	2.7	3700	0	1.01E-03	5.3	20.0
PAW04A	2.7	3700	25	7.37E-04	3.4	29.1
PAW04A	2.7	3700	50	5.71E-04	1.6	30.0
PAW04A	2.7	3700	100	2.72E-04	0.3	31.8
PAW04A	2.7	3700	200	8.64E-05	353.1	38.6
PAW04A	2.7	3700	400	3.11E-05	356.4	45.2
PAW04A	2.7	3700	800	1.15E-05	318.5	-17.3
PAW05B	1.8	3700	0	3.59E-04	333.8	37.3
PAW05B	1.8	3700	25	2.52E-04	357.5	30.0
PAW05B	1.8	3700	50	2.37E-04	0.5	24.6
PAW05B	1.8	3700	100	1.75E-04	1.2	19.7
PAW05B	1.8	3700	200	5.46E-05	10.0	21.0
PAW05B	1.8	3700	400	1.87E-05	105.3	6.2
PAW05B	1.8	3700	800	4.07E-05	32.0	-73.6
PAX01B	2.7	3675	0	6.38E-04	105.0	-69.3
PAX01B	2.7	3675	50	6.69E-04	107.5	-83.0
PAX01B	2.7	3675	100	5.85E-04	108.7	-84.6
PAX01B	2.7	3675	200	5.83E-04	107.3	-85.1
PAX01B	2.7	3675	400	1.52E-04	123.4	-84.4
PAX02B	2.8	3675	0	9.64E-04	181.0	-79.5
PAX02B	2.8	3675	50	1.03E-03	160.9	-85.5
PAX02B	2.8	3675	100	7.68E-04	141.6	-86.1
PAX02B	2.8	3675	200	3.88E-04	139.0	-86.2
PAX02B	2.8	3675	400	3.75E-04	240.7	-88.2
PAX03B	2.9	3675	0	1.08E-03	216.9	-82.1
PAX03B	2.9	3675	50	1.16E-03	194.3	-85.1
PAX03B	2.9	3675	100	1.03E-03	179.0	-85.6
PAX03B	2.9	3675	200	5.62E-04	179.7	-86.1
PAX04B	2.7	3675	0	6.37E-04	196.5	-80.0
PAX04B	2.7	3675	50	8.08E-04	186.6	-84.8
PAX04B	2.7	3675	100	5.54E-04	190.5	-86.9
PAX04B	2.7	3675	200	2.01E-04	191.0	-86.2
PAX05B	2.8	3675	0	2.56E-04	140.6	-78.4
PAX05B	2.8	3675	25	4.59E-04	115.5	-86.2
PAX05B	2.8	3675	50	5.08E-04	114.6	-87.2
PAX05B	2.8	3675	100	3.71E-04	112.2	-88.9
PAX05B	2.8	3675	200	1.55E-04	36.2	-88.5
PAX05B	2.8	3675	400	3.38E-05	314.7	-49.9
PAX05B	2.8	3675	800	9.91E-06	261.2	-3.8
PAY01B	2.5	3650	0	3.14E-04	306.7	-68.0
PAY01B	2.5	3650	100	4.06E-04	79.6	-89.1
PAY01B	2.5	3650	200	2.04E-04	106.3	-87.7
PAY02A	2.7	3650	0	3.20E-04	299.0	-53.2
PAY02A	2.7	3650	100	3.10E-04	10.3	-84.5
PAY02A	2.7	3650	200	1.60E-04	324.0	-86.3
PAY03B	2.6	3650	0	3.31E-04	337.3	-50.1
PAY03B	2.6	3650	100	3.18E-04	8.4	-82.1
PAY03B	2.6	3650	200	1.62E-04	27.4	-83.8
PAY03B	2.6	3650	400	5.68E-05	64.3	-85.1
PAY03B	2.6	3650	800	1.89E-05	253.1	-79.9

SITE	DENS	ELEV	TREAT	EMU	INC	DEC
PAY04B	2.7	3650	0	3.63E-04	350.7	-65.3
PAY04B	2.7	3650	25	4.12E-04	358.9	-78.5
PAY04B	2.7	3650	50	4.26E-04	357.9	-83.5
PAY04B	2.7	3650	100	3.77E-04	311.3	-87.7
PAY04B	2.7	3650	200	1.90E-04	255.0	-87.8
PAY04B	2.7	3650	400	6.19E-05	145.4	-87.3
PAY04B	2.7	3650	800	1.53E-05	186.7	-55.2
PAY05B	2.7	3650	0	4.96E-04	81.2	-64.5
PAY05B	2.7	3650	100	5.23E-04	93.4	-78.7
PAY05B	2.7	3650	200	2.47E-04	100.7	-79.0
PAY05B	2.7	3650	400	1.12E-04	99.6	-80.2
PAY05B	2.7	3650	800	1.12E-04	84.3	-81.4

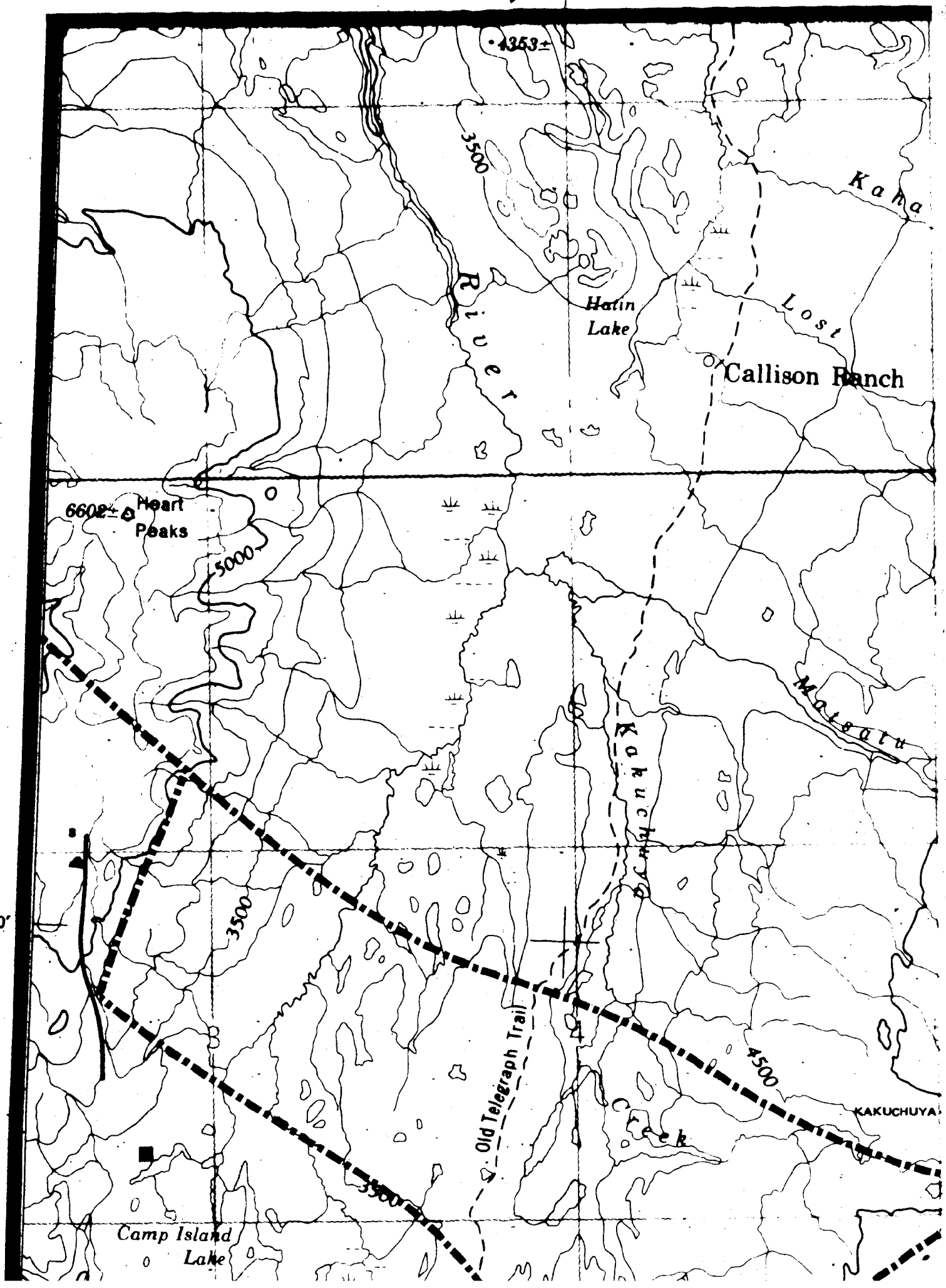
4353±
3500
Kaka
River
Hatin Lake
Lost
Callison Ranch
6602±
Heart Peaks
5000
Matsaru
Kakuchuya
58° 30'
3500
4500
Old Telegraph Trail
Creek
KAKUCHUYA
3500
Camp Island Lake

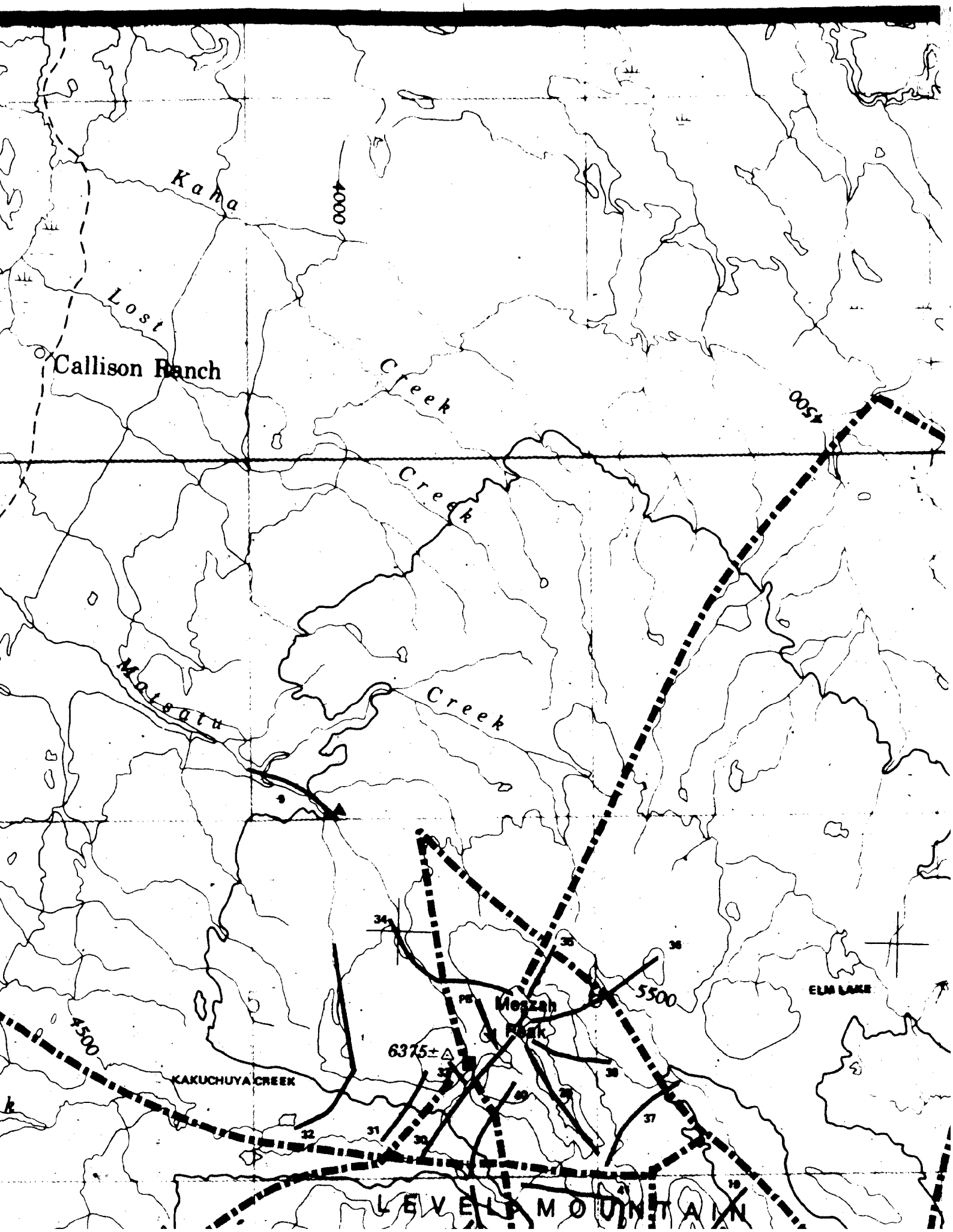
Kaha
Lost
Callison Ranch
Creek
Creek
Creek
Matsatu
4000
4500
4500
5500
ELM LAKE
Mazeh
Peak
6375±△
KAKUCHUYA CREEK
LEVELA MOUNTAIN

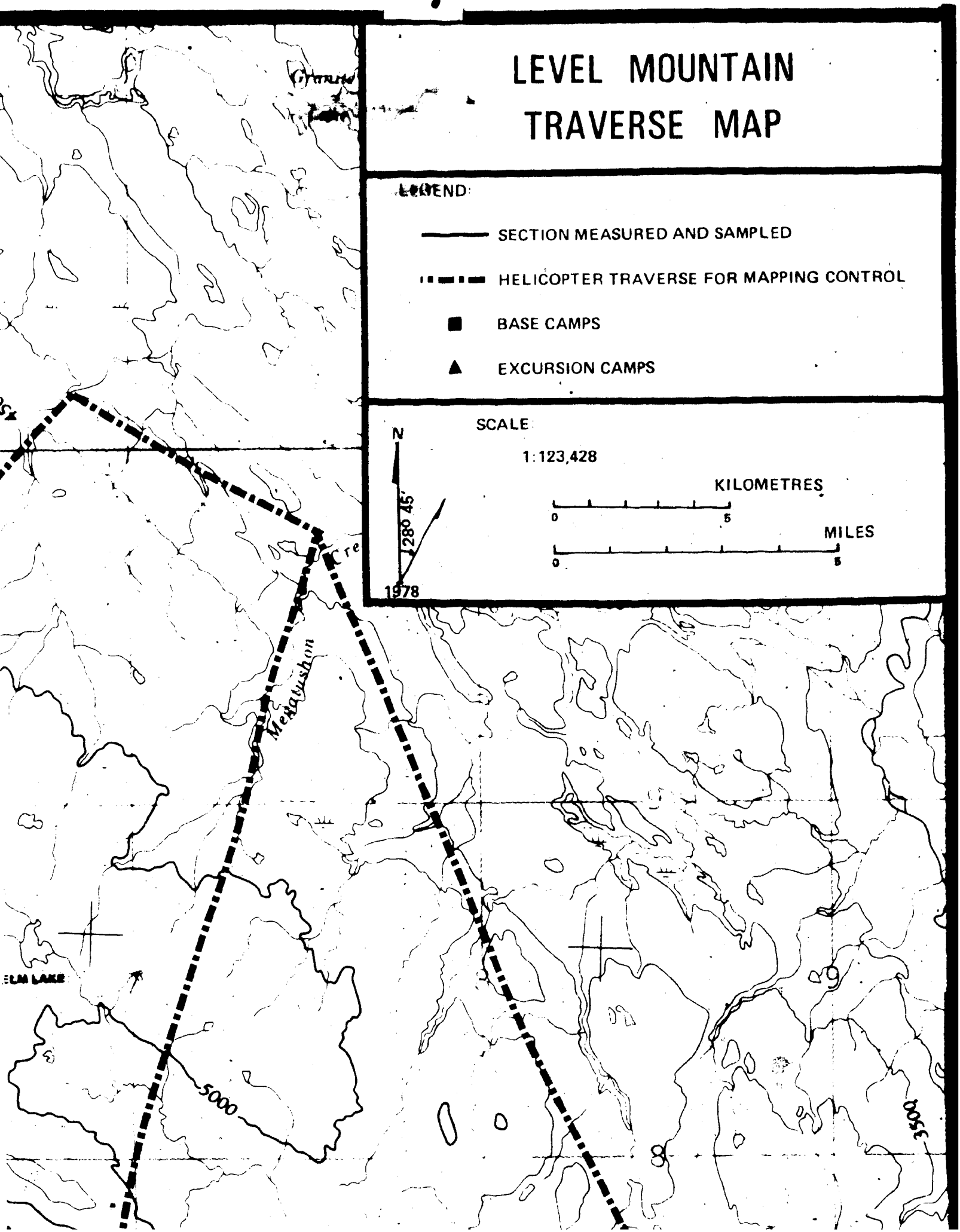
LEVEL MOUNTAIN
TRAVERSE MAP
LEGEND
SECTION MEASURED AND SAMPLED
HELICOPTER TRAVERSE FOR MAPPING CONTROL
BASE CAMPS
EXCURSION CAMPS
SCALE
1:123,428
KILOMETRES
0
5
MILES
0
5
N
280° 45'
1978
Metaboshon
5000
3500

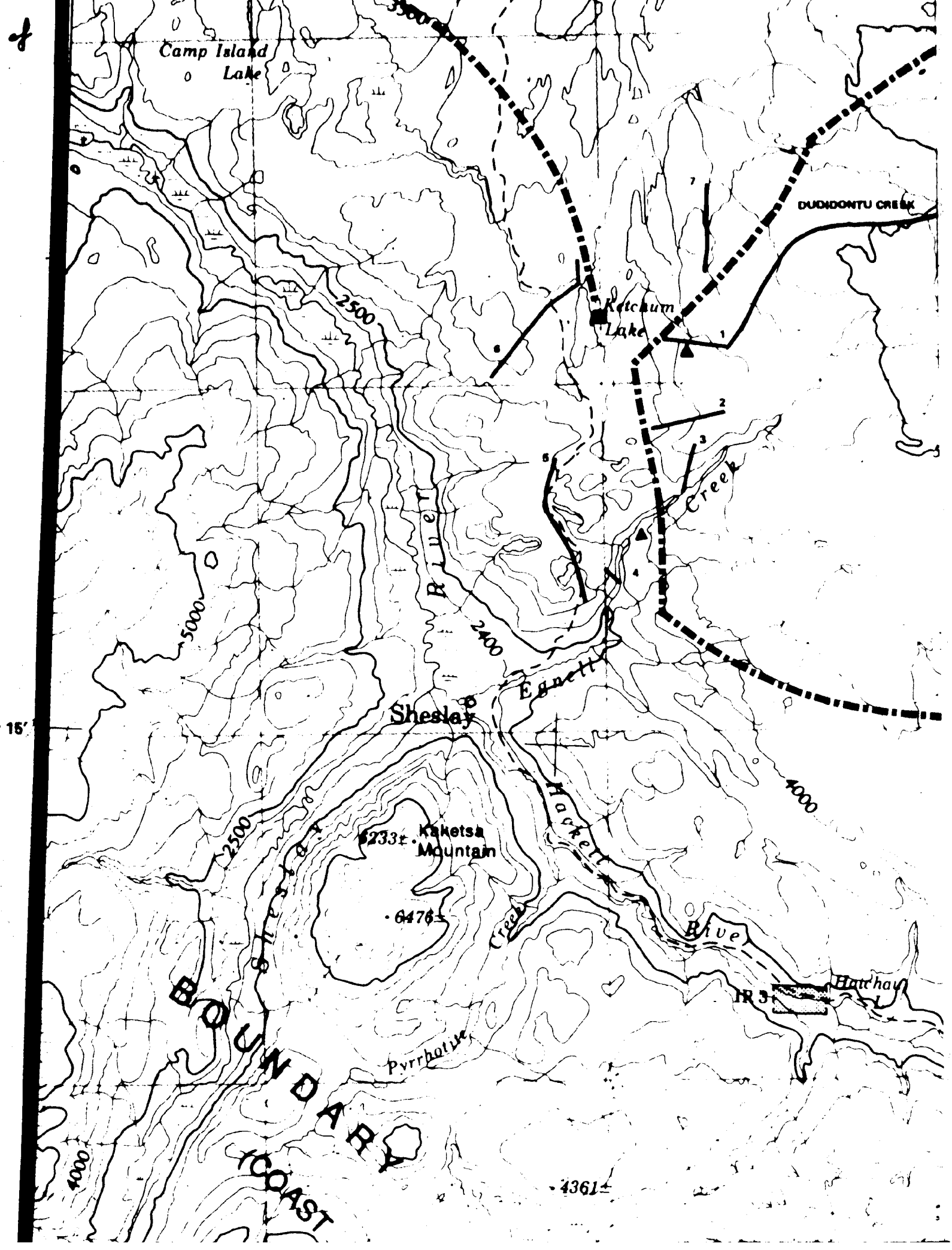
Camp Island Lake
DUDIDONTU CREEK
Ketchum Lake
2500
5000
2400
4000
Shesley
Creek
River
Hackett
Creek
Kaketsa Mountain
6233±
6476±
4361±
BOUNDARY
COAST
Pyrrhotite
Hatchay
HR 3

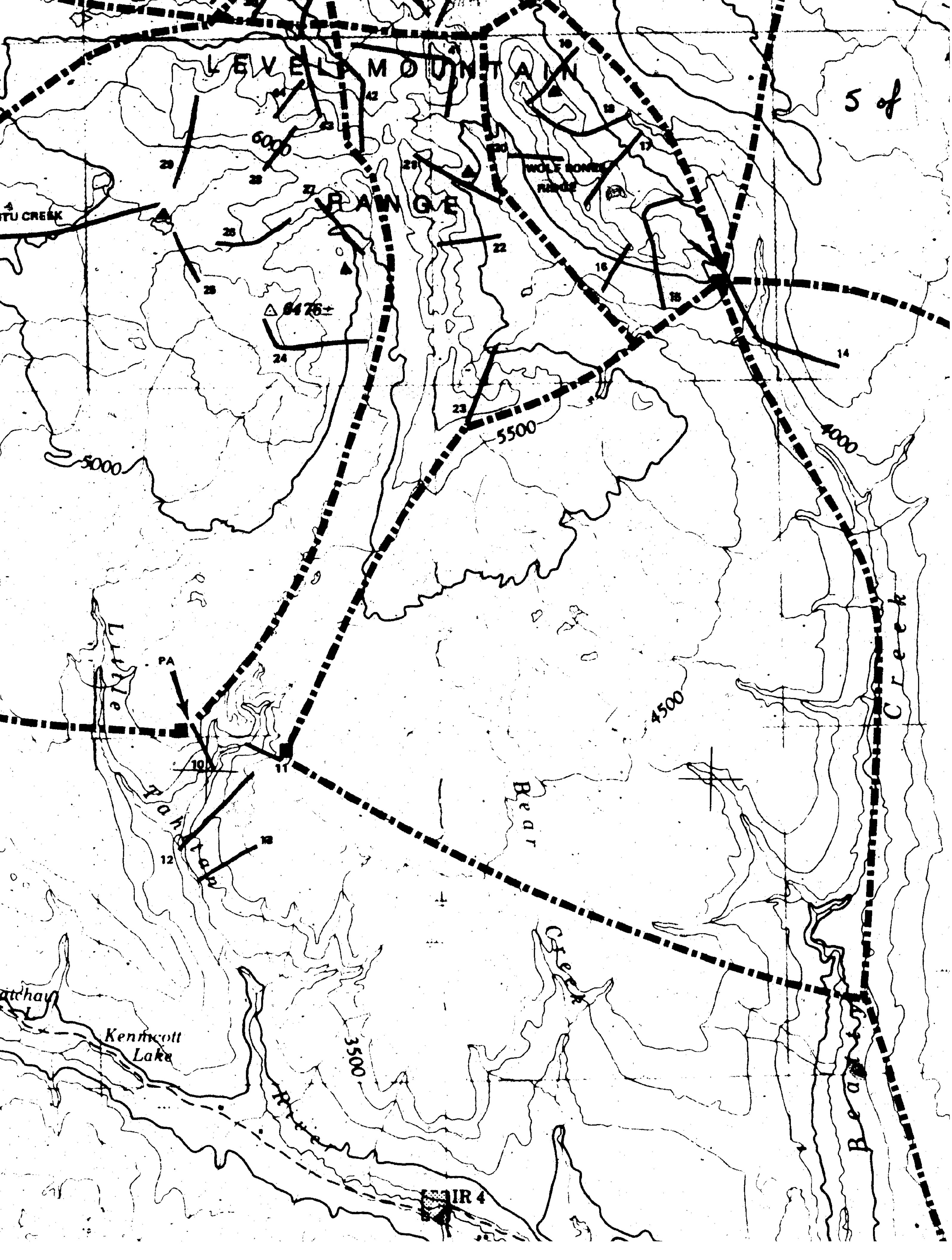
5 of
LEVEL MOUNTAIN
RANGE
6000
5000
5500
4000
4500
3500
Little
Tahltan
Bear
Creek
Creek
Kennicott
Lake
IR 4
PA
10
11
12
13
14
15
16
17
18
19
20
22
23
24
25
26
27
28
29
41
42
43
44

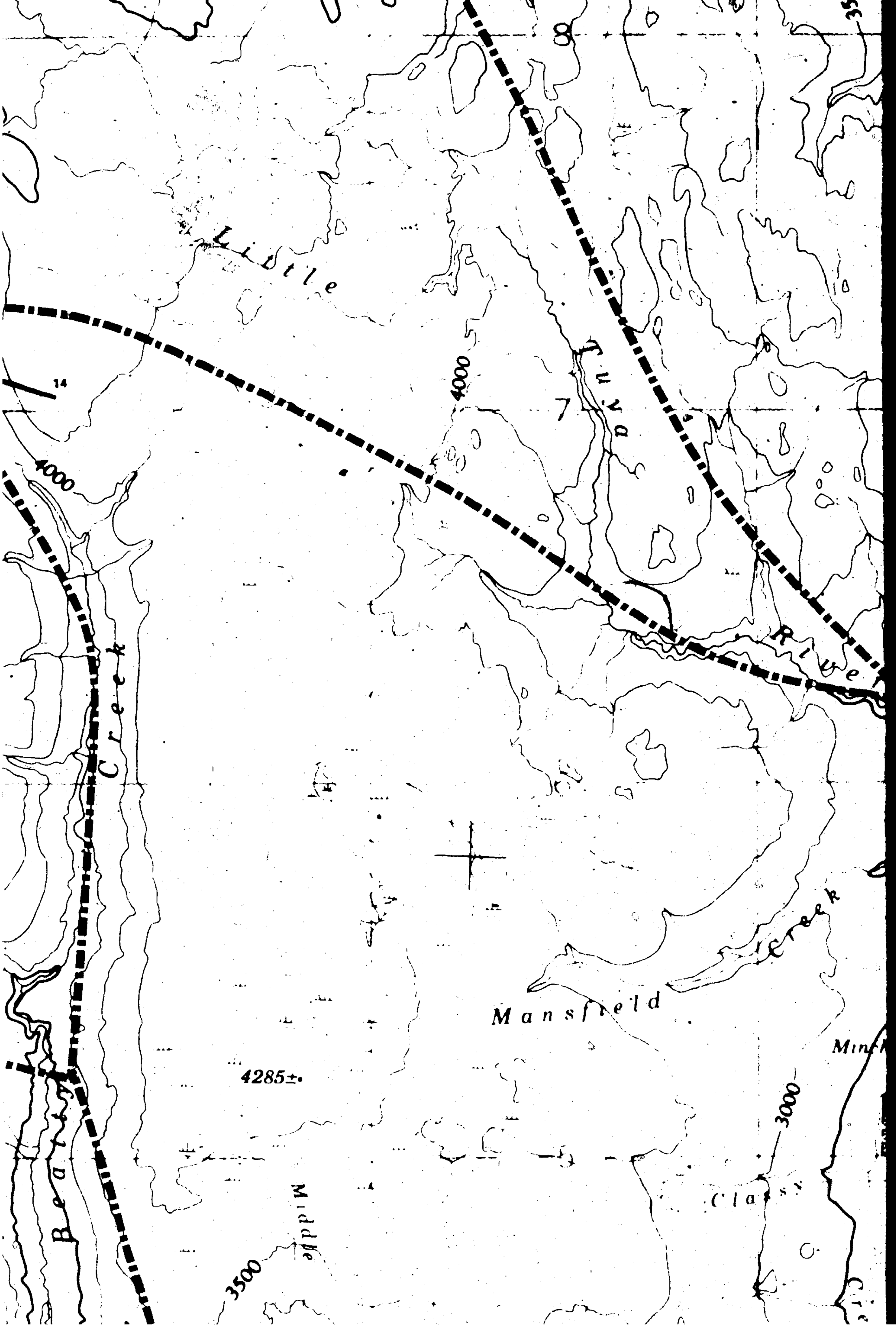
Little
Tuva
7
4000
14
4000
River
Creek
Creek
Mansfield
Mink
4285±
3000
Beatty
Middle
3500
Class

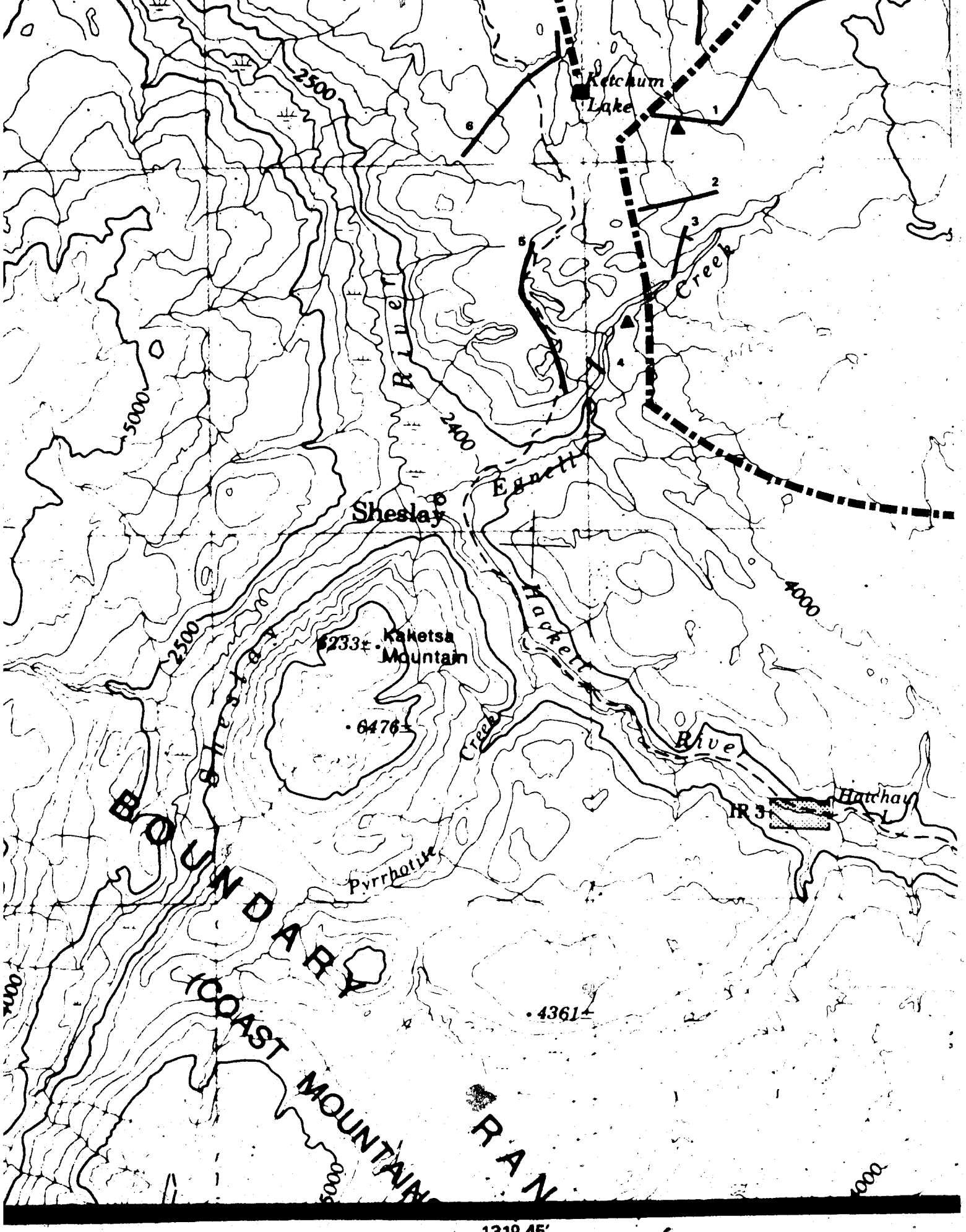
Ketchum Lake
Sheslay
Eaglet
Hackett
Creek
River
Kaketsa Mountain
6233±
6476±
4361±
Pyrrhotite
Creek
Hatchan
IR 3
BOUNDARY
COAST MOUNTAIN
RANGE
2500
5000
2400
4000
131° 45'

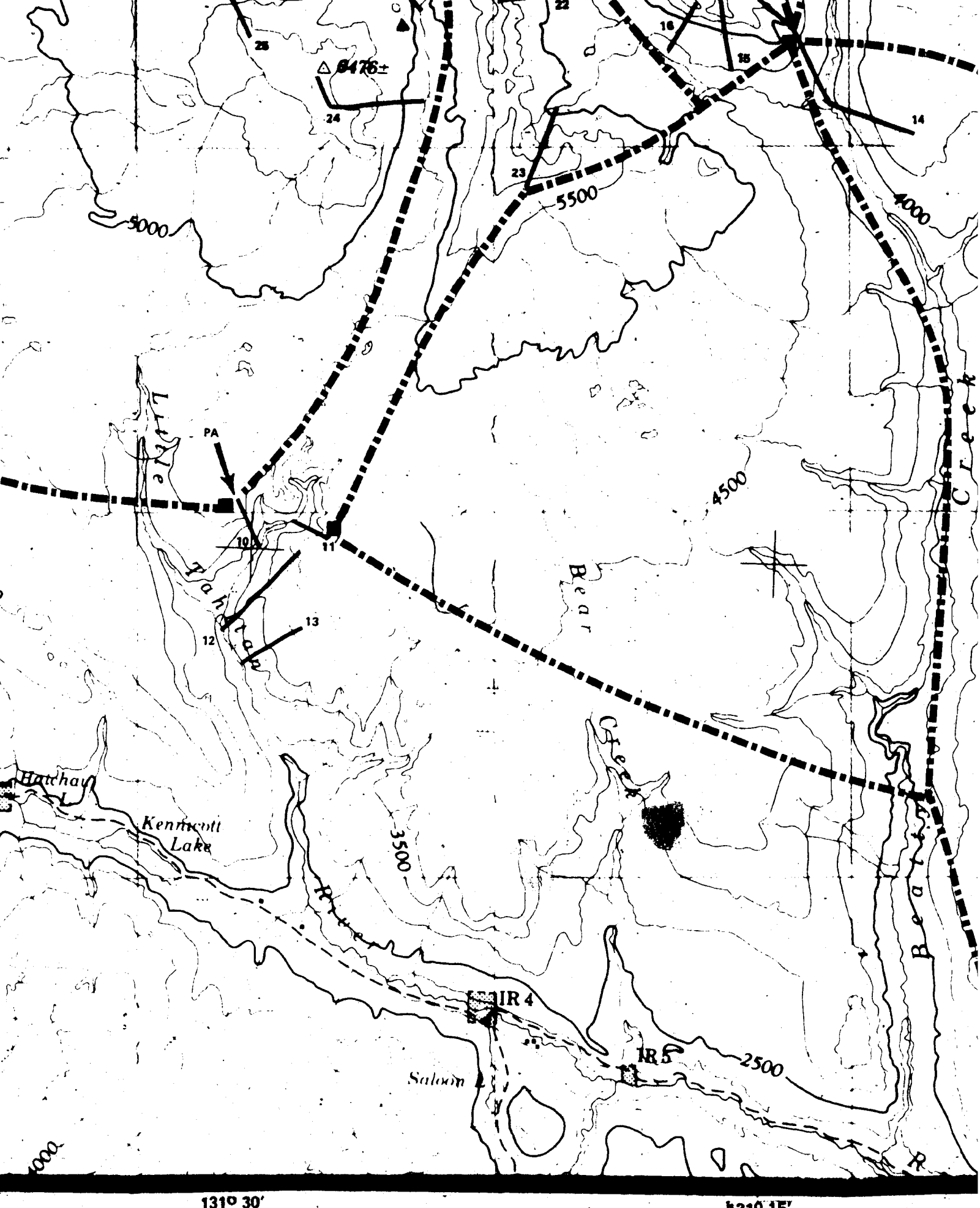
△6476±
5000
5500
4000
4500
3500
2500
PA
Little Rabbit
Rabbit Creek
Bear Creek
Kennicott Lake
Hatchau
Saloon
IR 4
IR 5
10
11
12
13
14
15
16
22
23
24
25
131° 30'
131° 15'

8 f

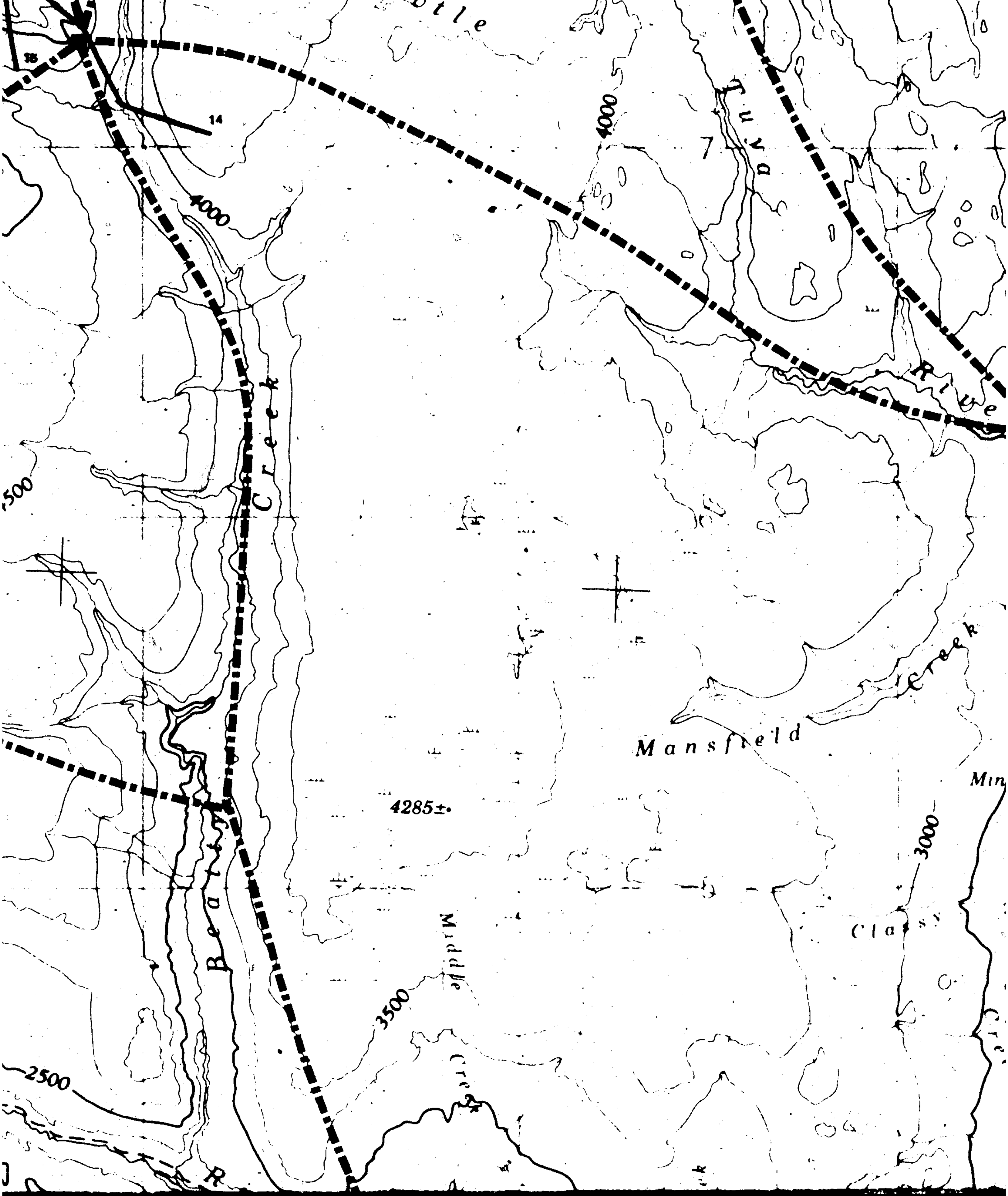
4000
4000
7
Tuya
River
Beatty
Creek
Mansfield
Creek
4285±
3500
3000
2500
14
131° 15′
131° 00′

1 of 1

GEOLOGIC MAP

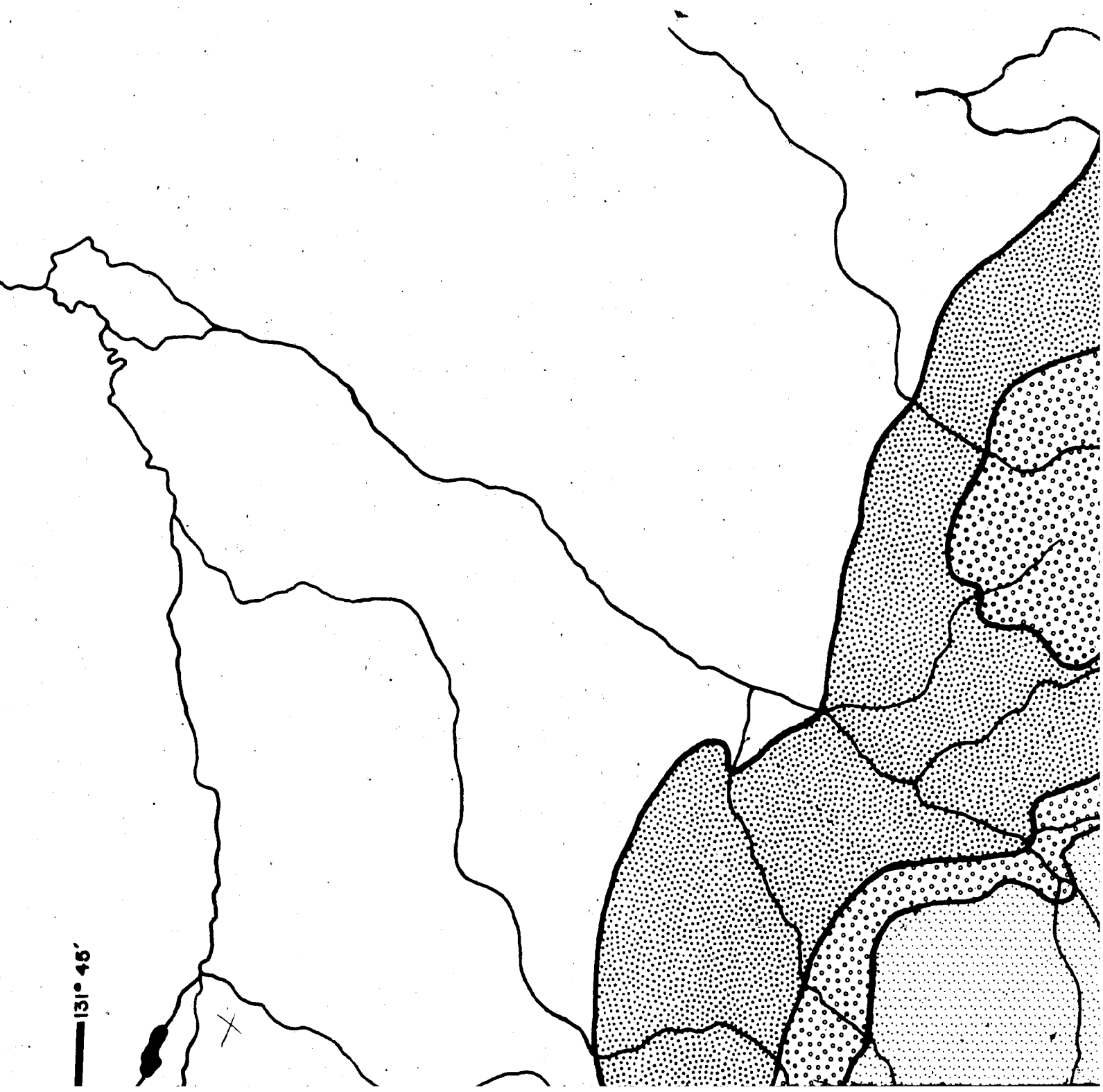

OLOGIC MAP OF THE LEVEL MOUNTAIN VOLCANICS, NORTH

2 of

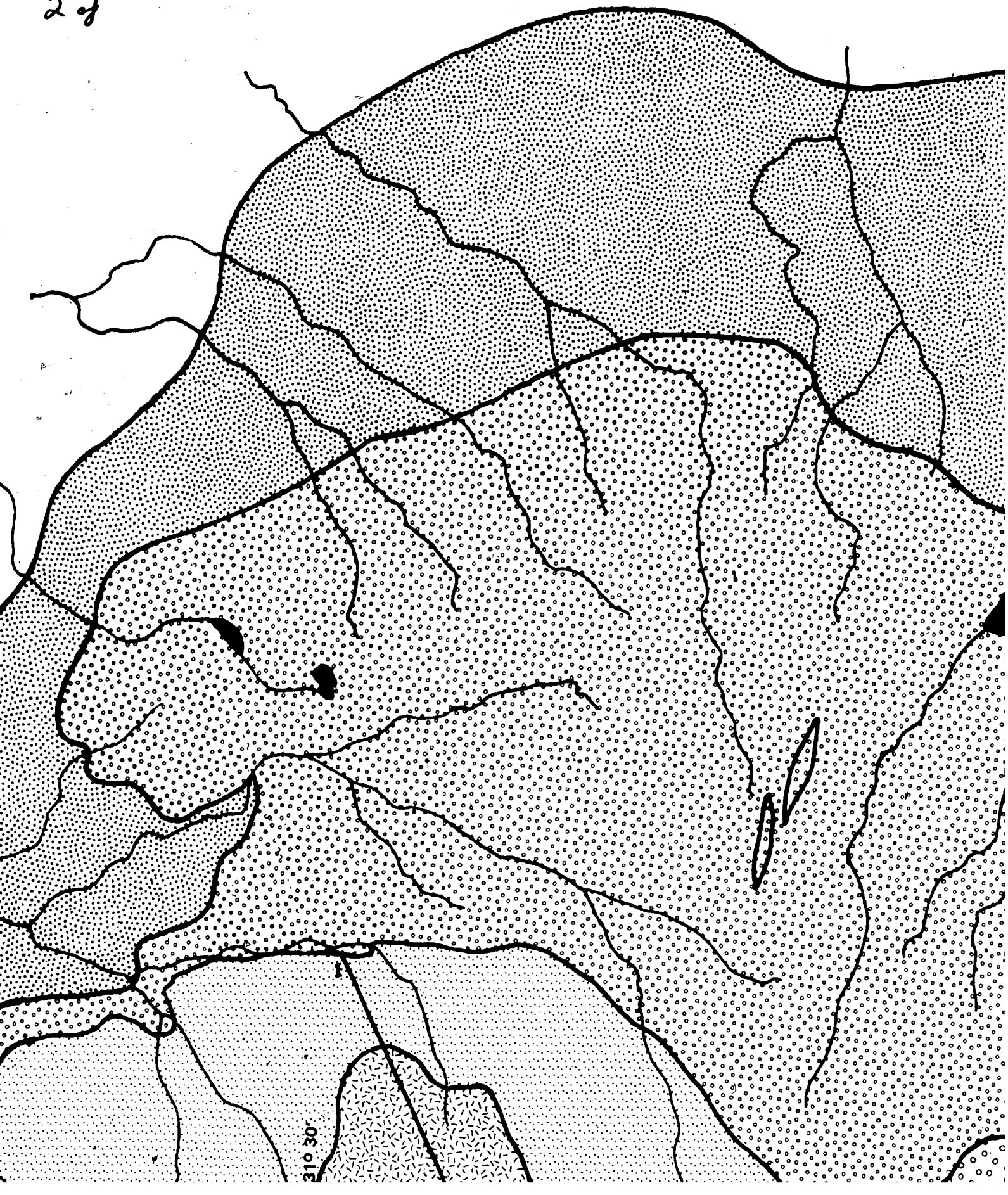

ORTHWESTERN BRITISH COLUMBIA

3 of

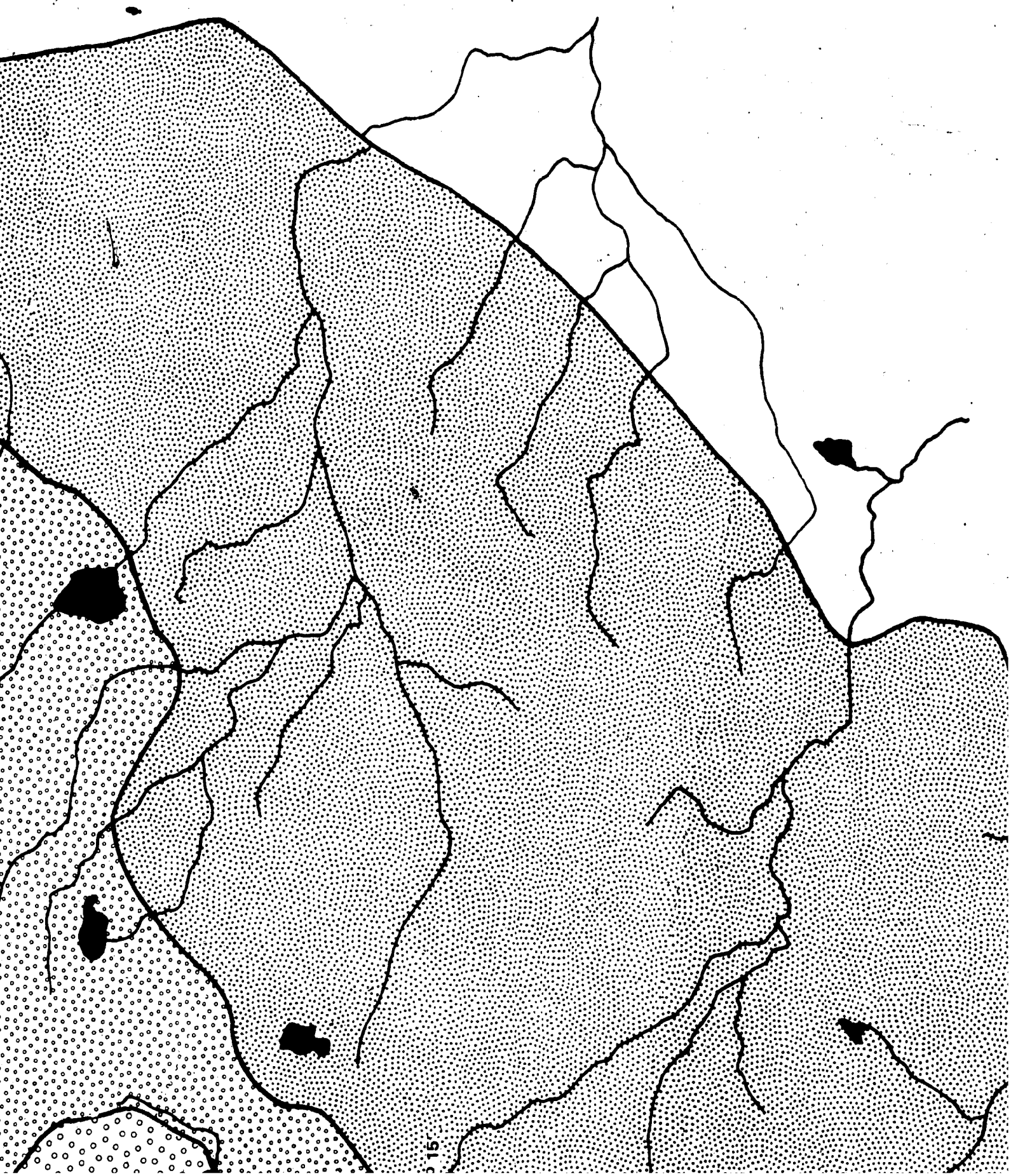

TISH COLUMBIA

4 of

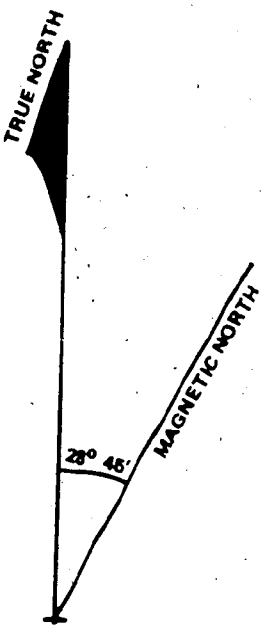
TRUE NORTH
MAGNETIC NORTH
23°
45'

6 f

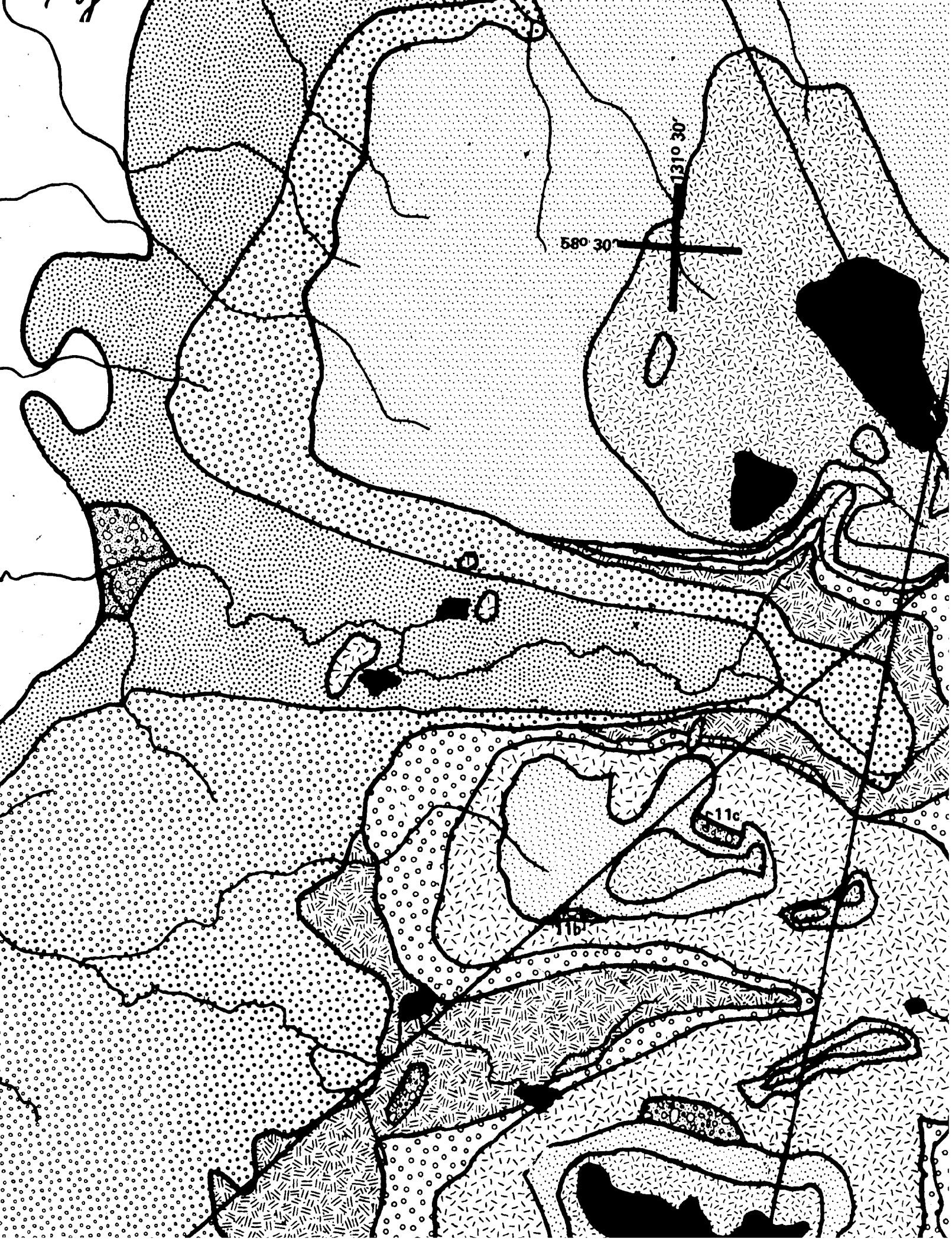
131° 30'
58° 30'
11c
11b

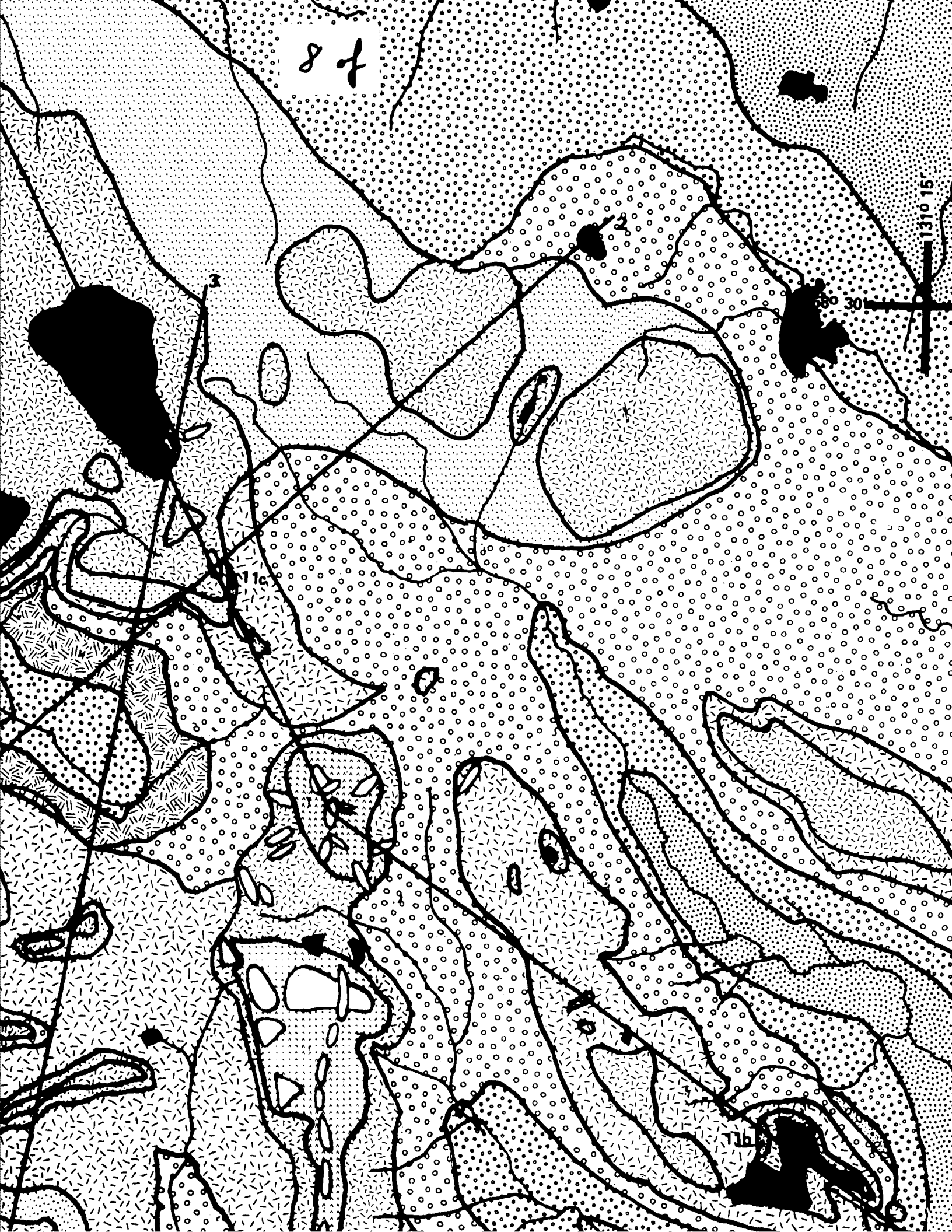
87
3
2
1310 15'
30
11c
11b

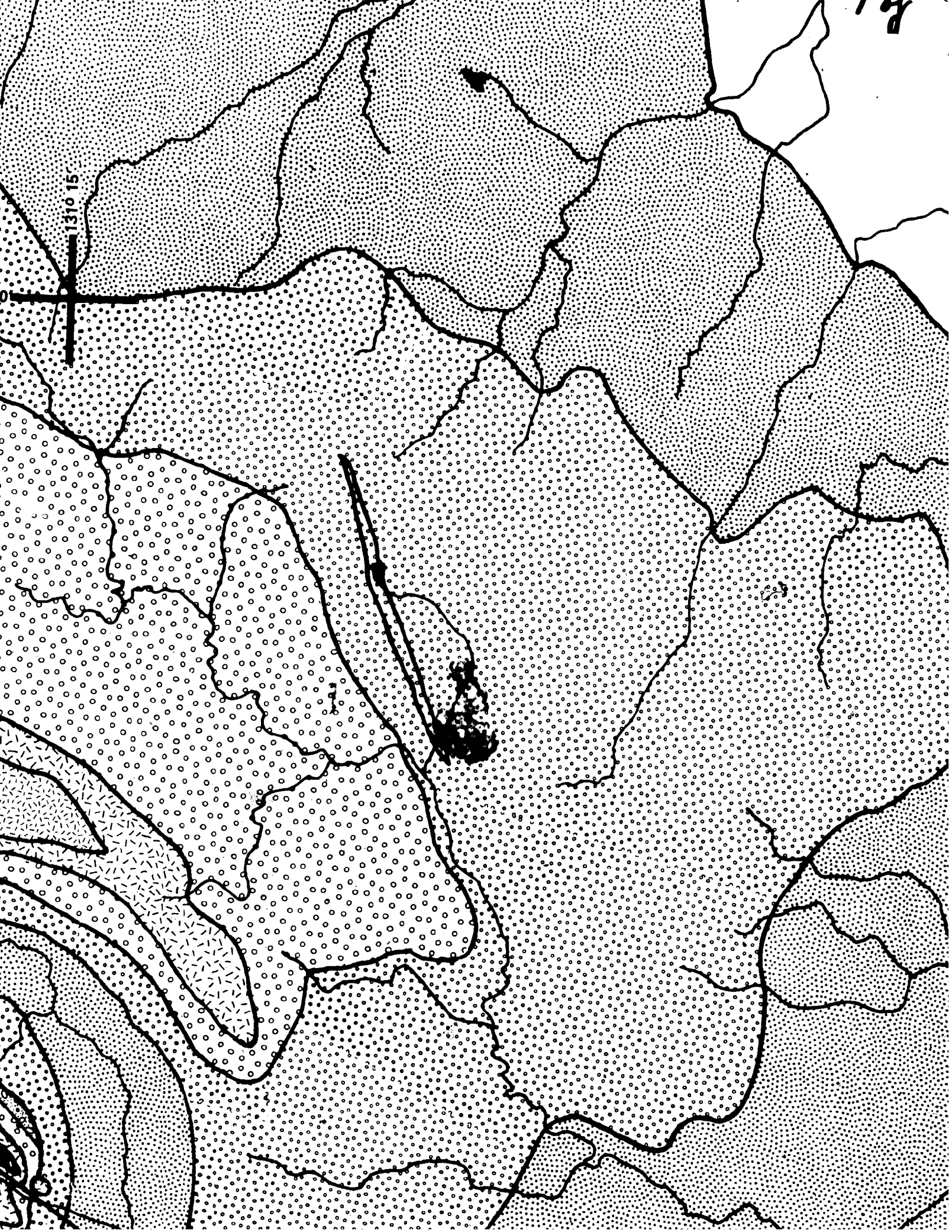
131° 15'

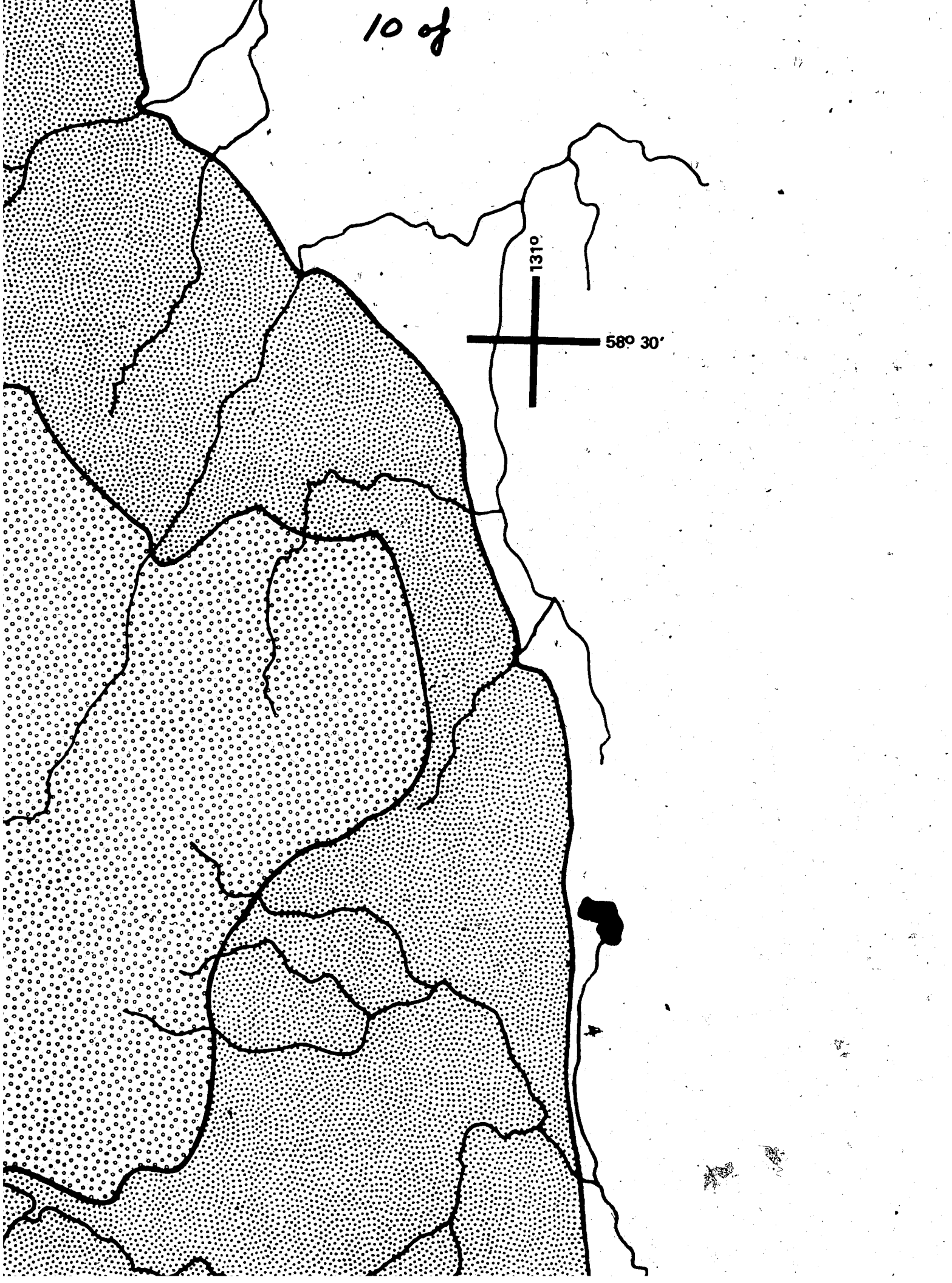
10 of
131°
58° 30'

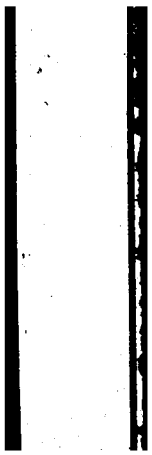

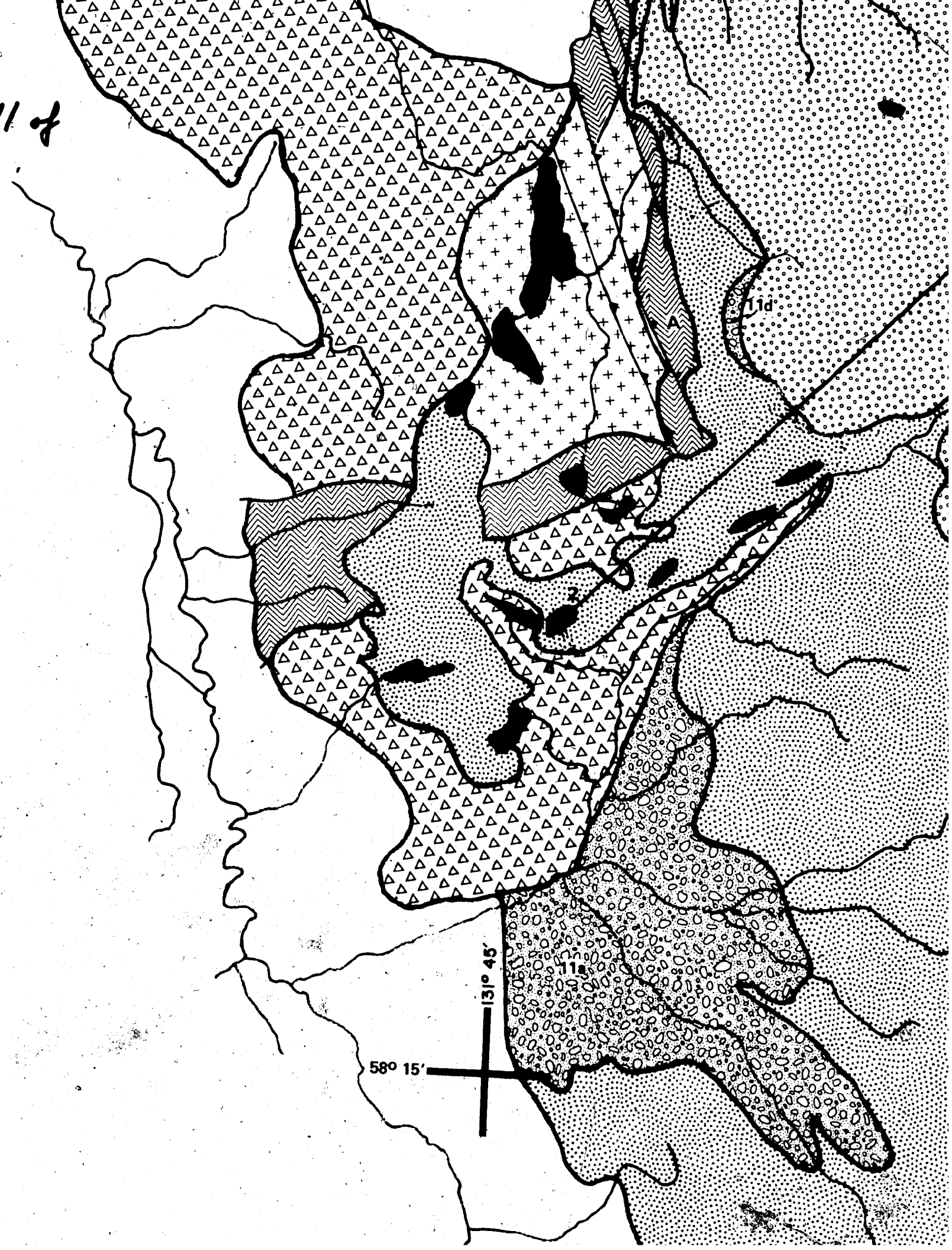
11d
A
2
131° 45'
11a
58° 15'

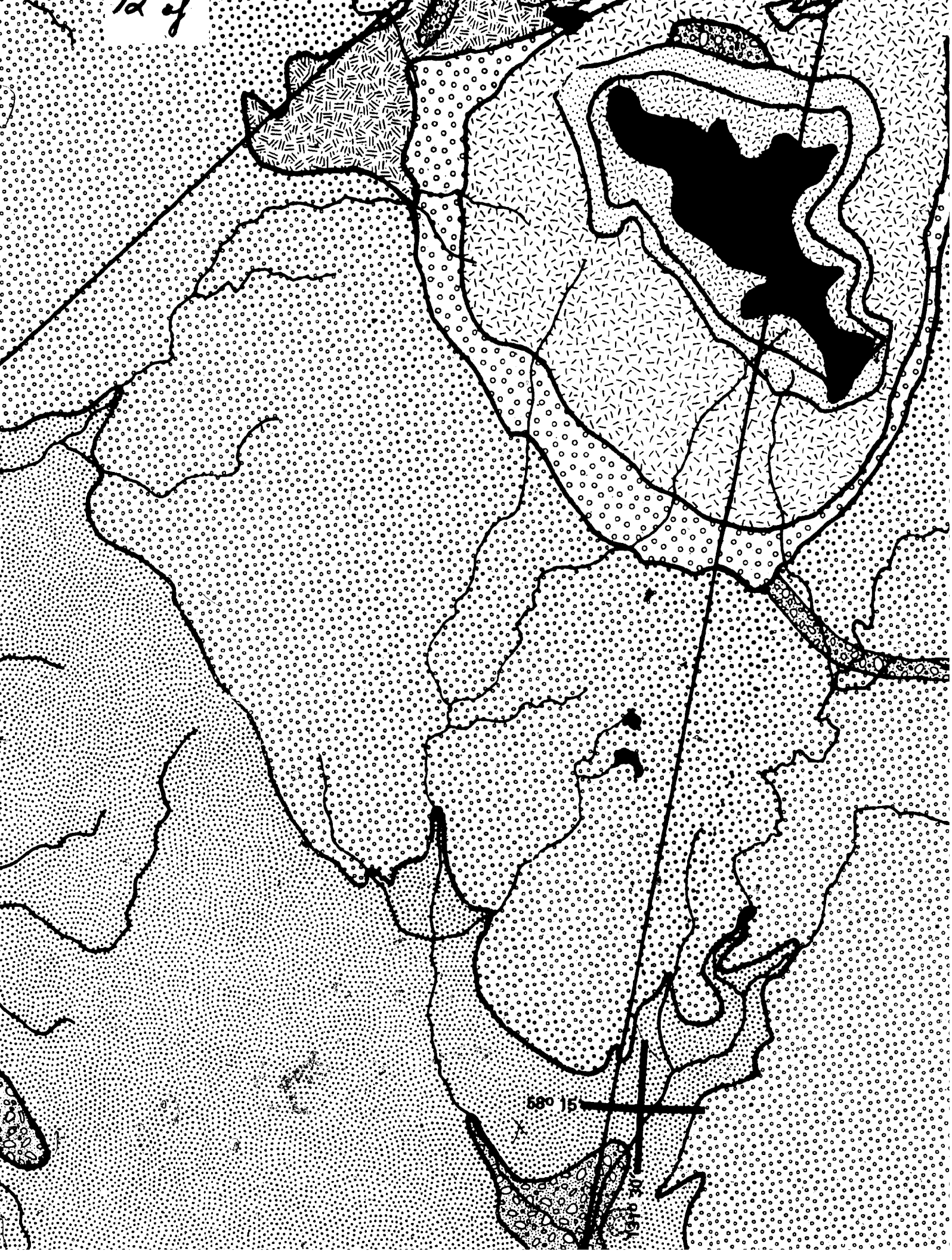
58° 15'

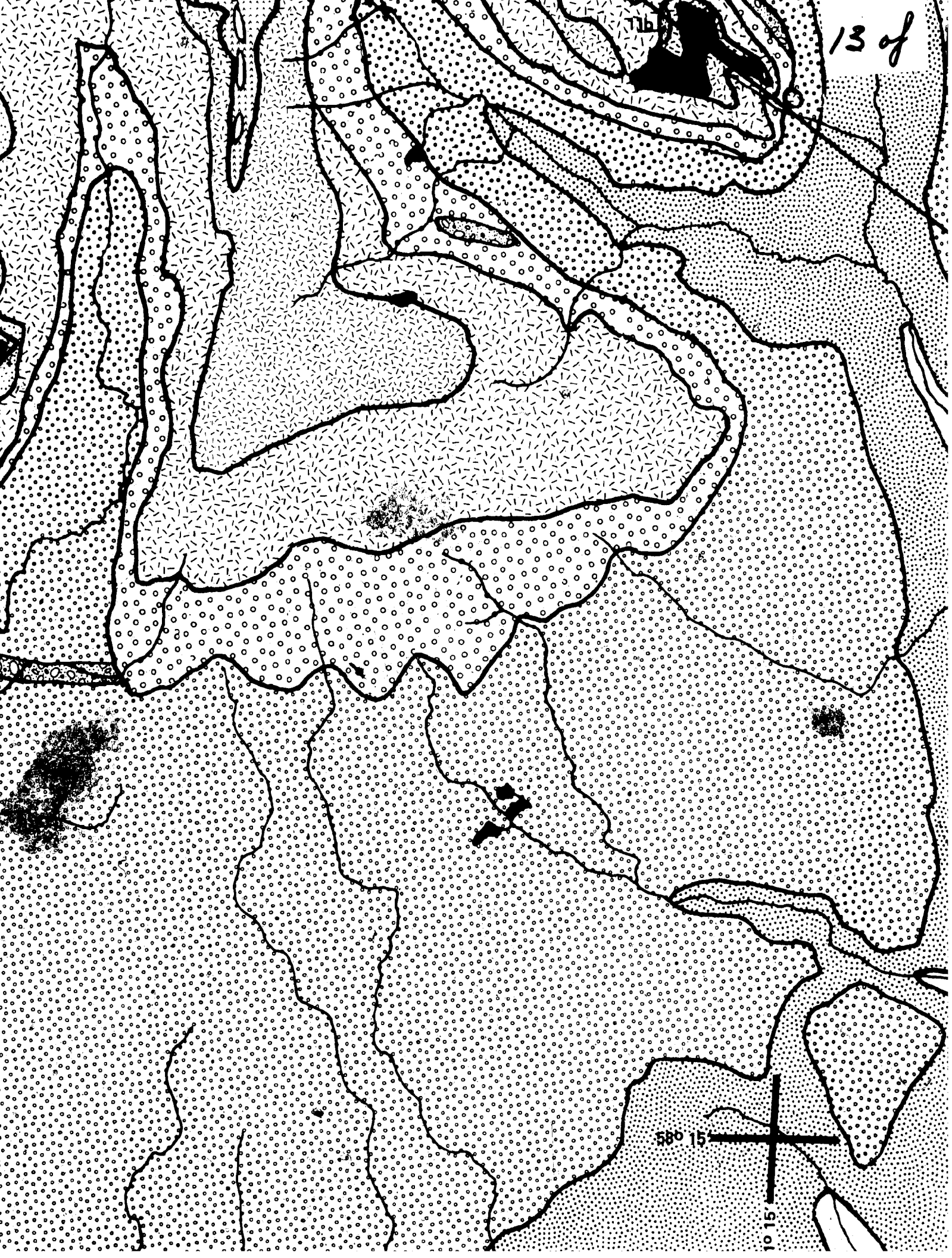
Tjb
13 of
58° 15
10 15

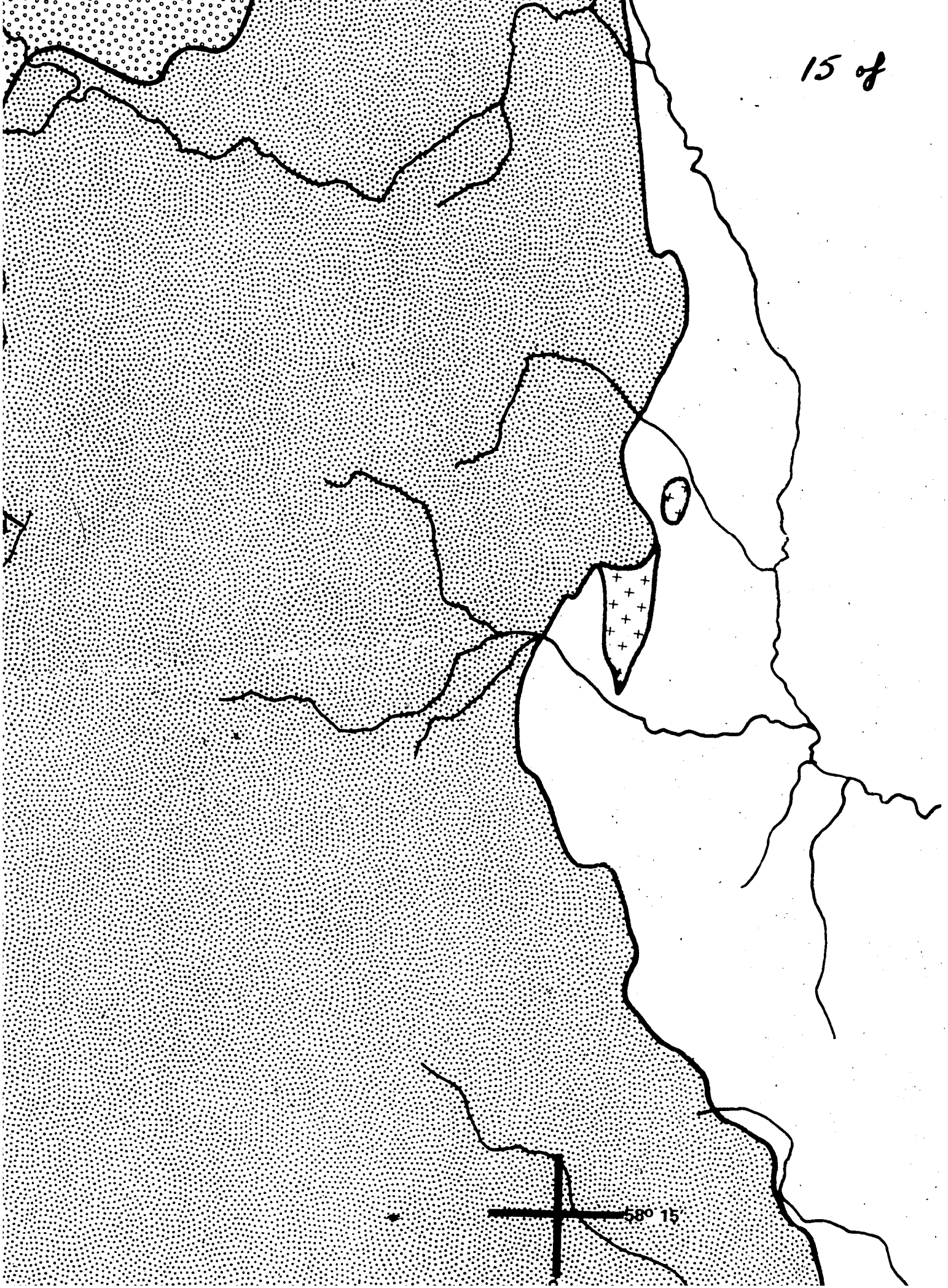
15 of
58° 15

16 f

58° 15'

GEOLOGICAL CROSS SECTIONS

(VERTICAL EXAGGERATION 2x)

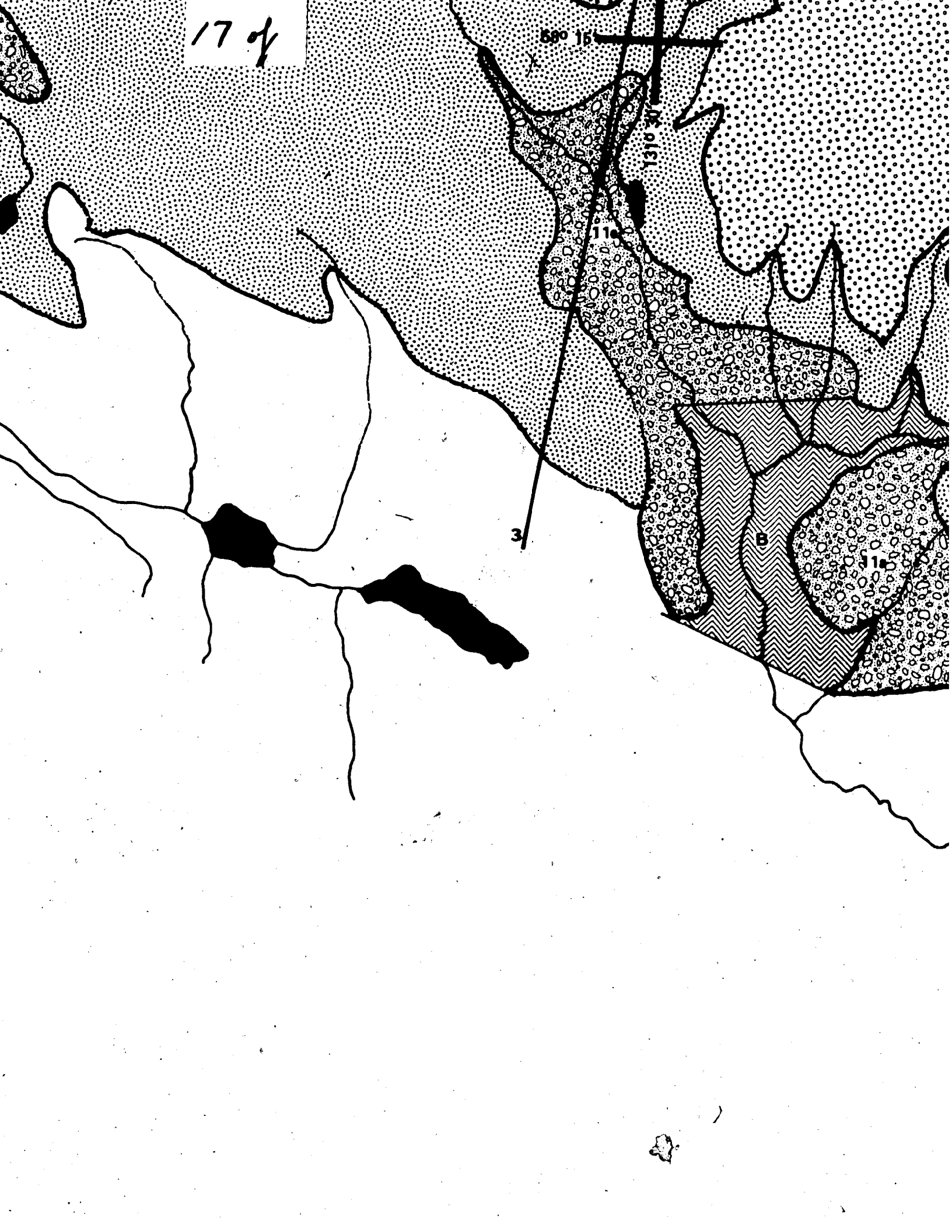
17 y
58° 15
J 1a
3
B
J 1a

58° 15'
131° 15'

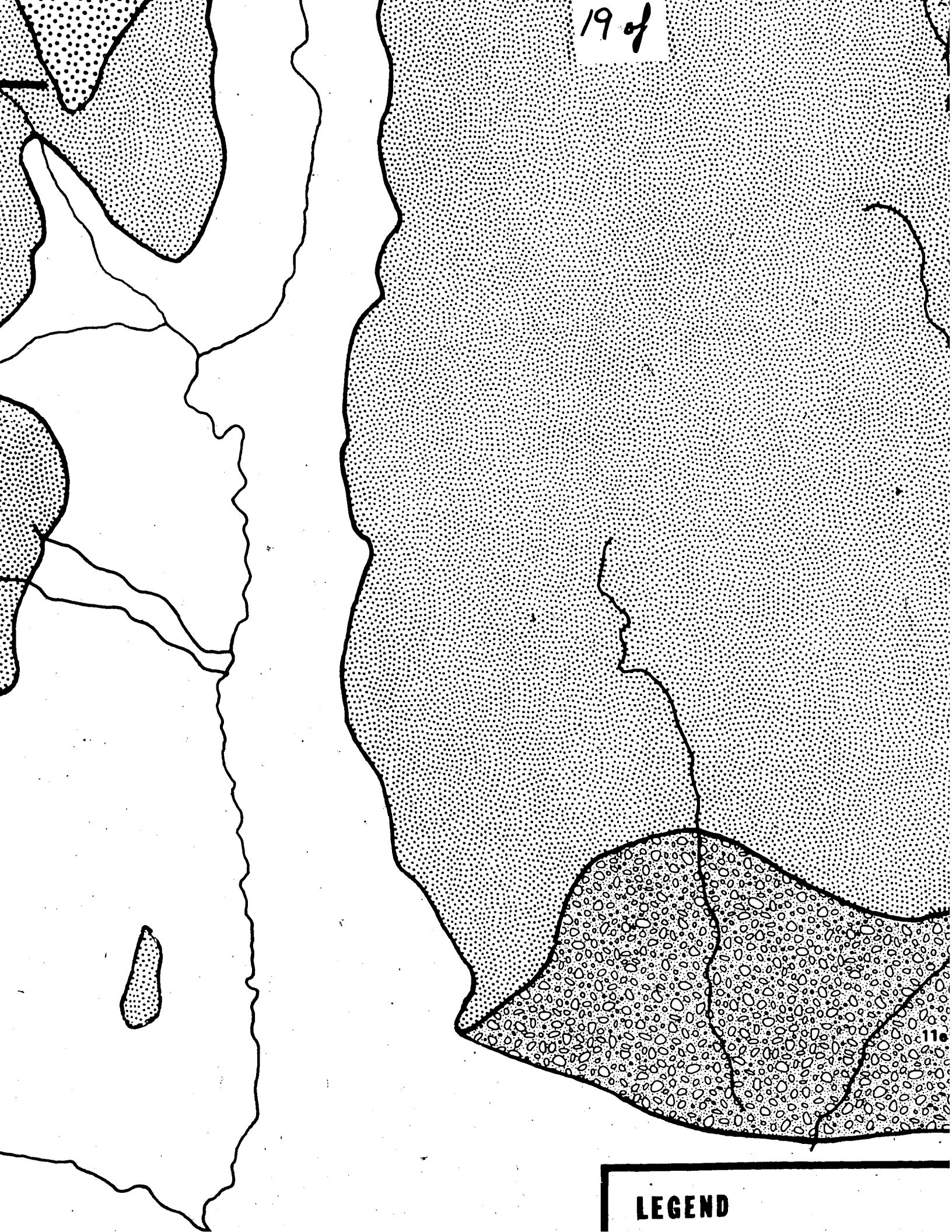
19 of
11e
LEGEND

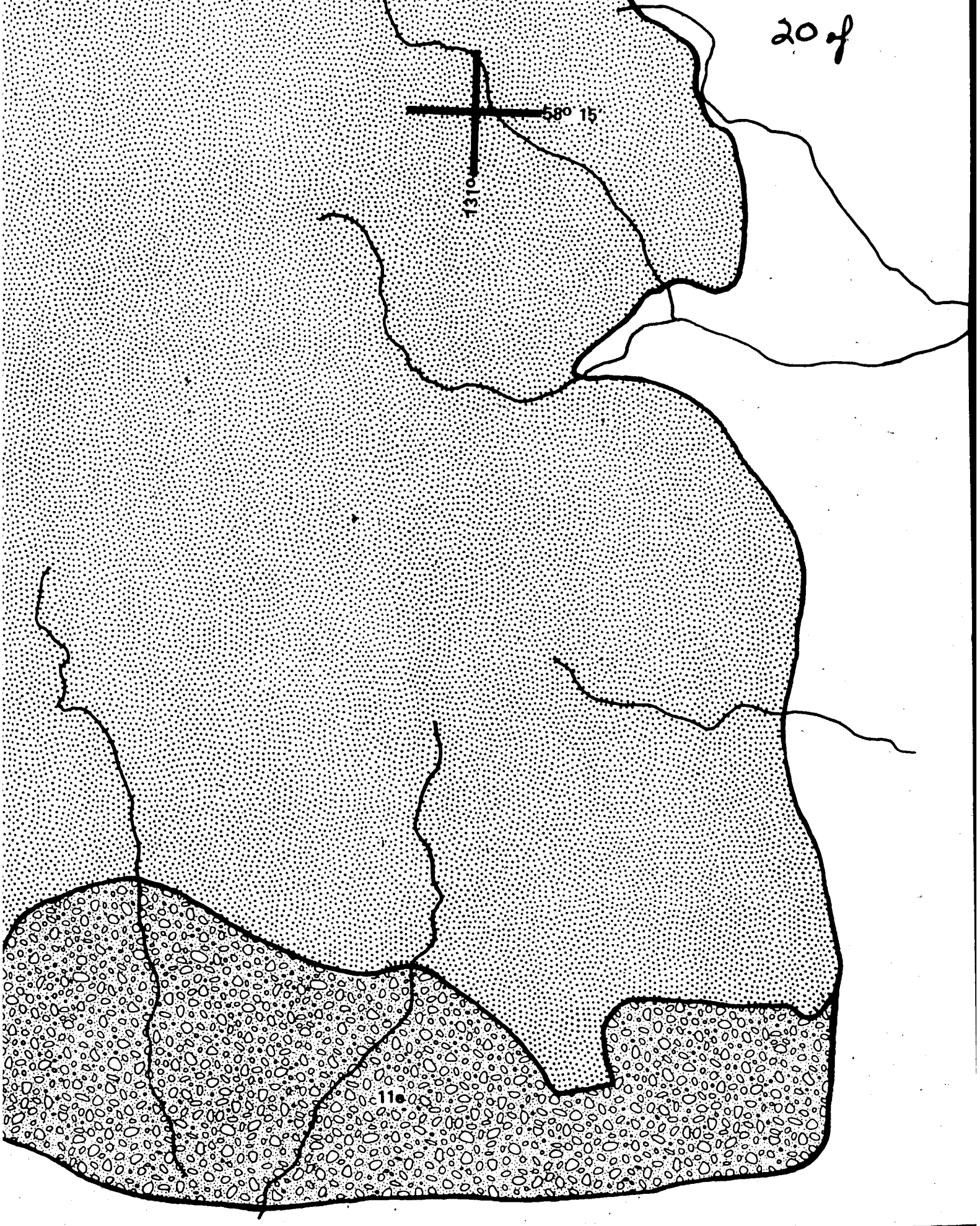

LEGEND

SECTION #1 - NNW

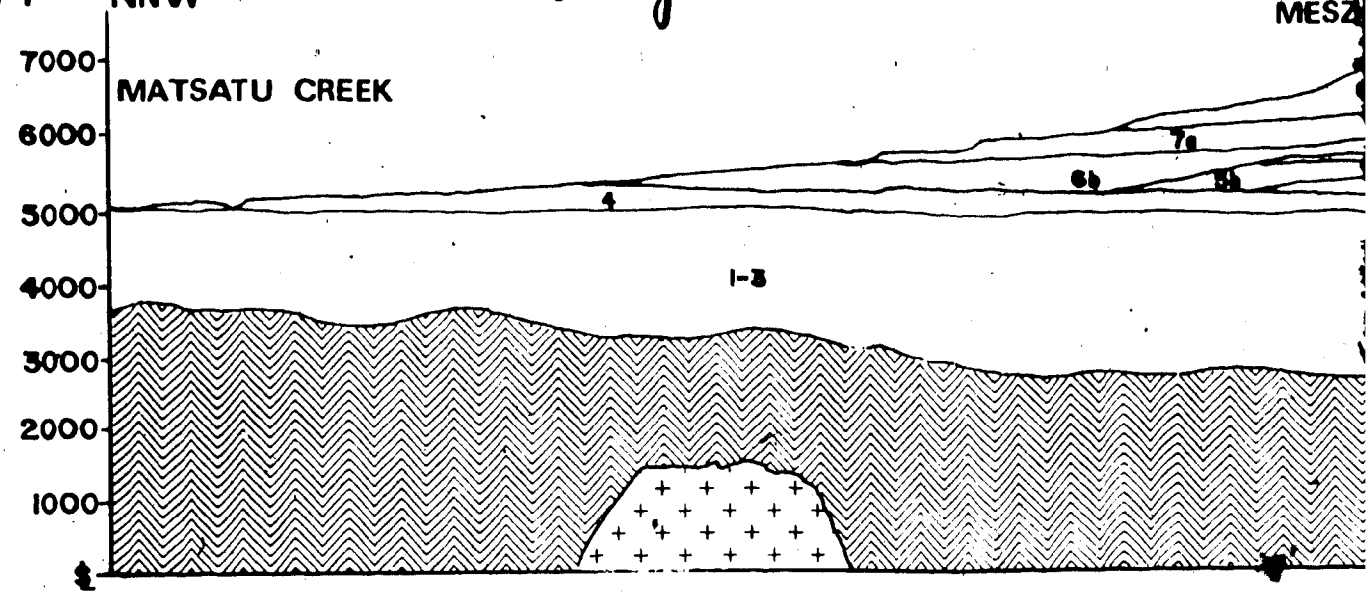

SECTION #2 - SW

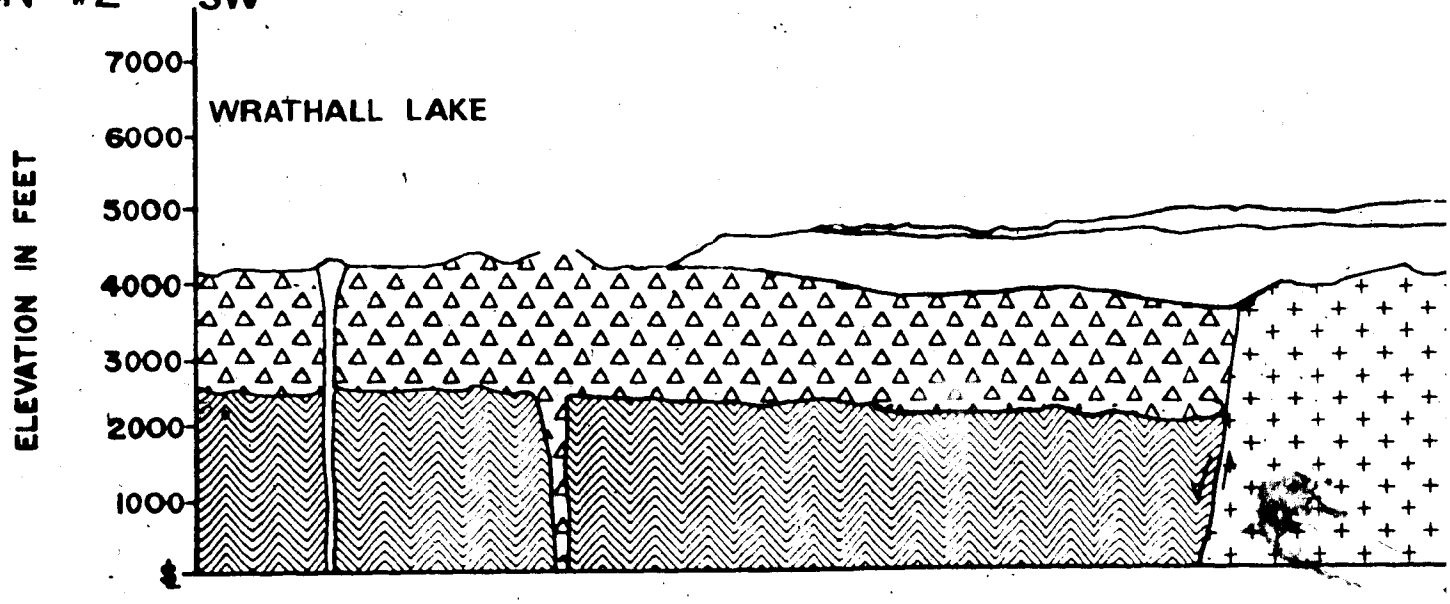

SECTION #3 - S

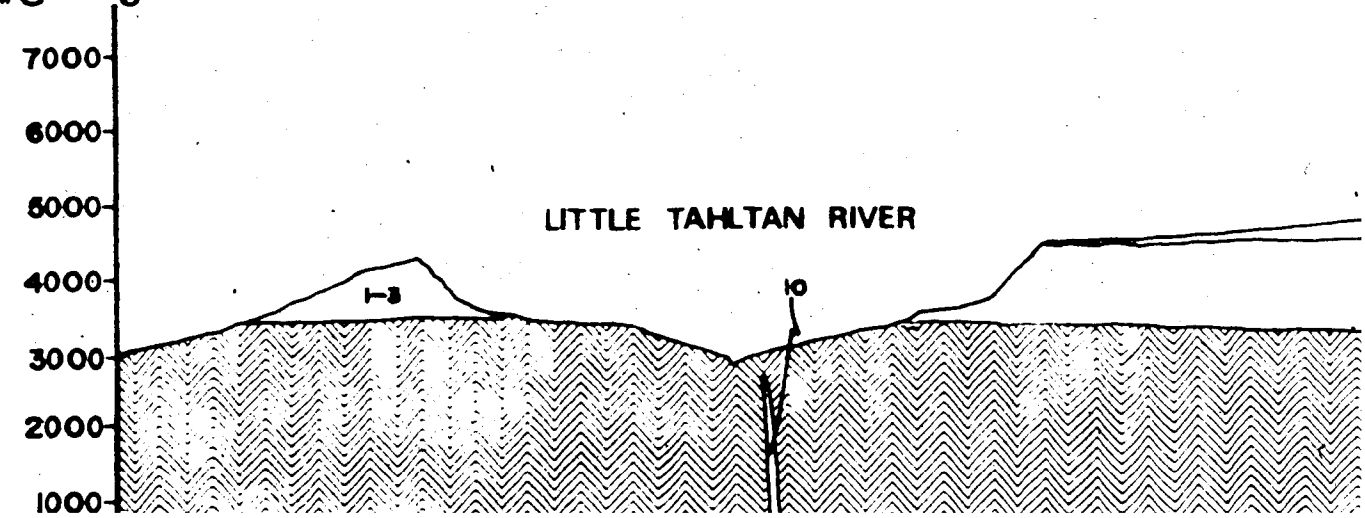

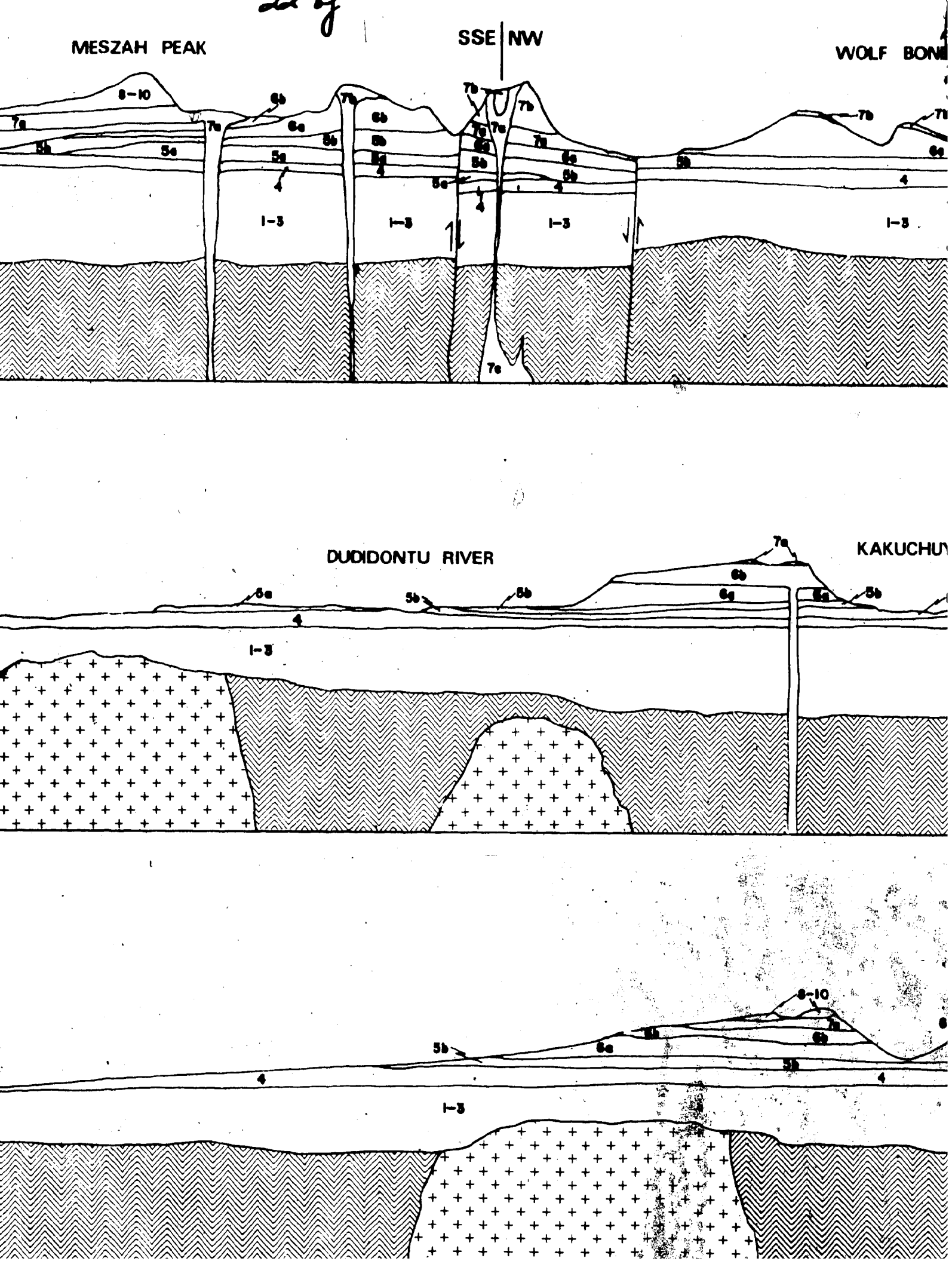
MESZAH PEAK
SSE
NW
WOLF BONE
8–10
7a
7b
6a
6b
5a
5b
4
1–3
DUDIDONTU RIVER
KAKUCHU

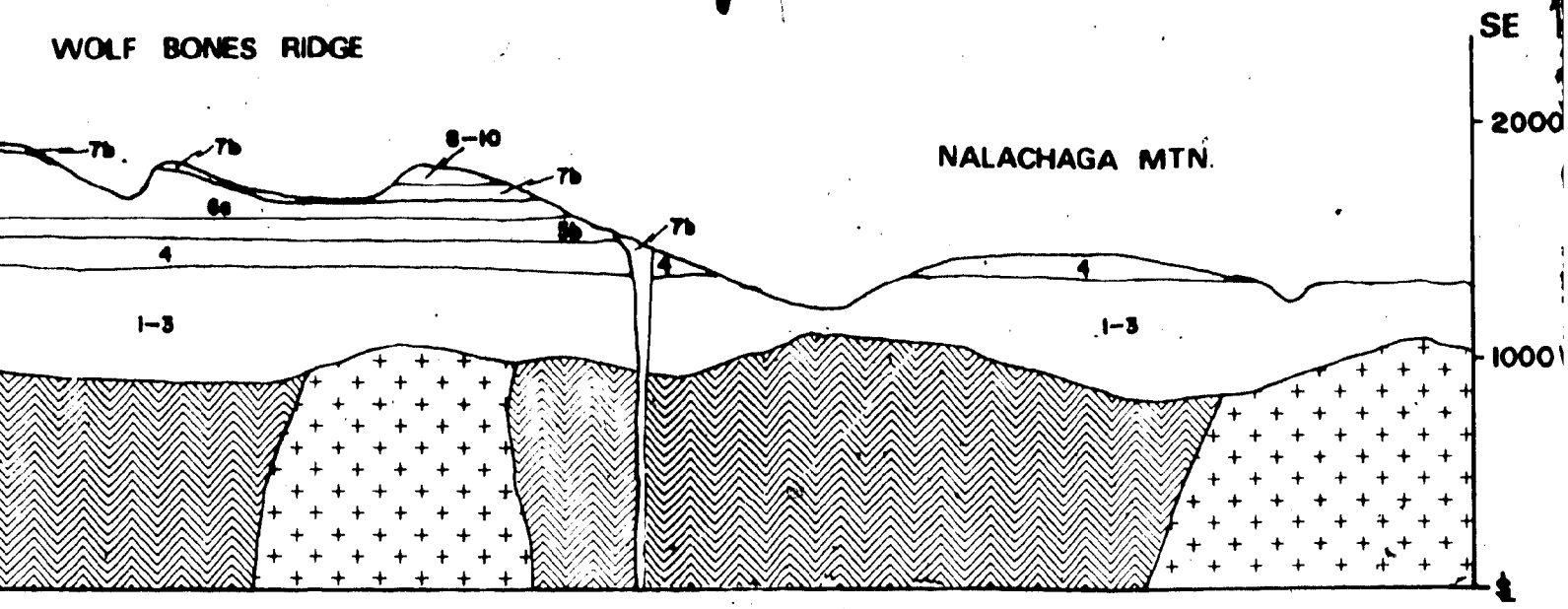
WOLF BONES RIDGE
SE
NALACHAGA MTN.
2000
1000
7b
8-10
6a
5b
4
1-3

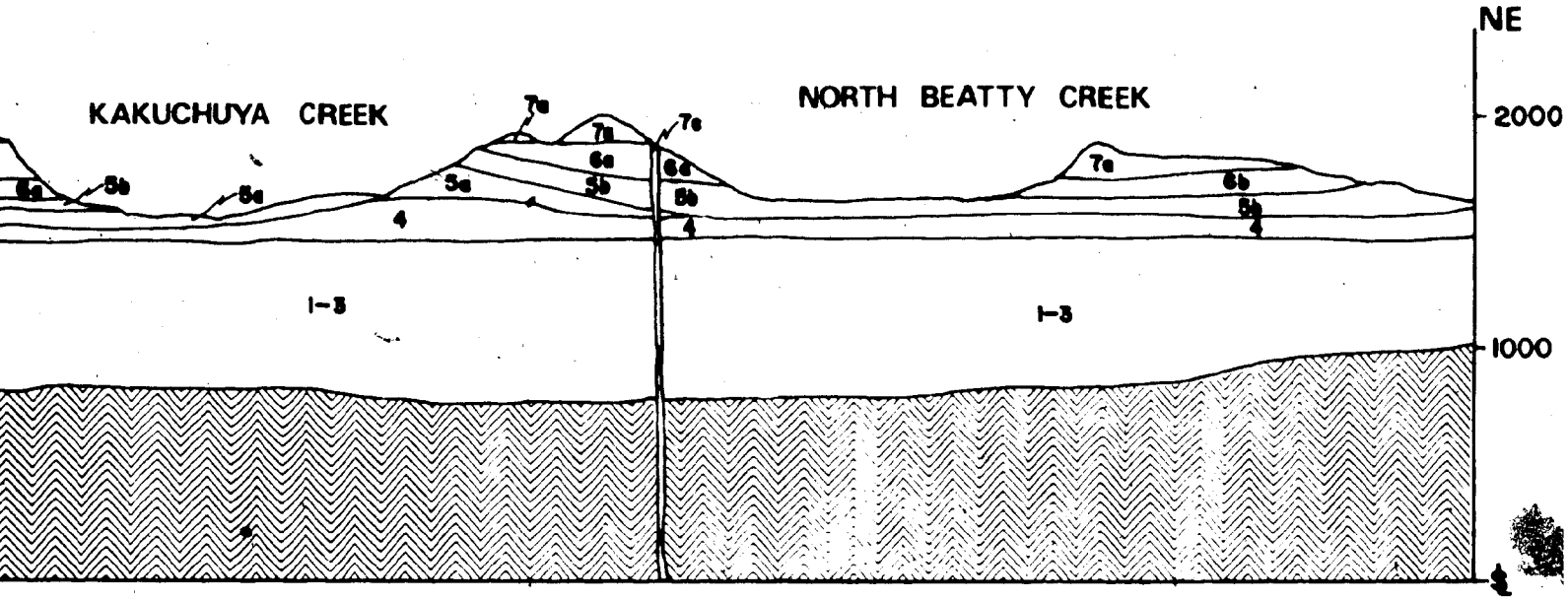
NE
KAKUCHUYA CREEK
NORTH BEATTY CREEK
2000
1000
7a
6a
5b
5a
4
1-3

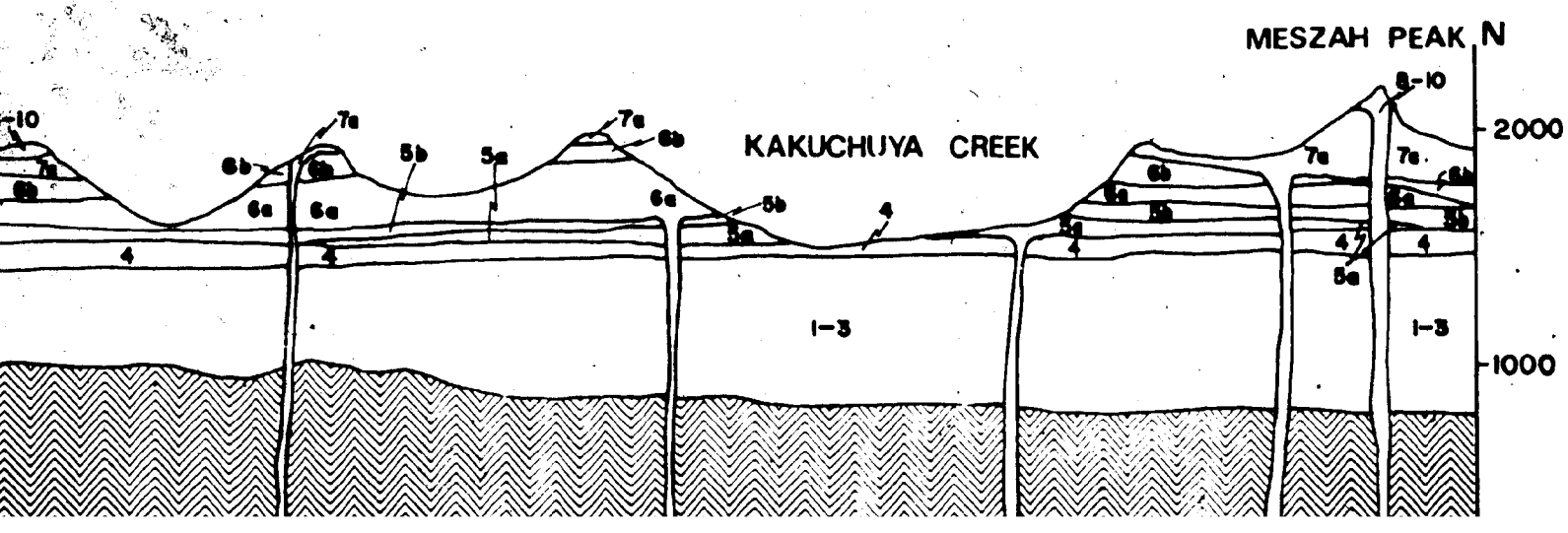
MESZAH PEAK
N
KAKUCHUYA CREEK
2000
1000
8-10
7a
6b
6a
5b
5a
4
1-3

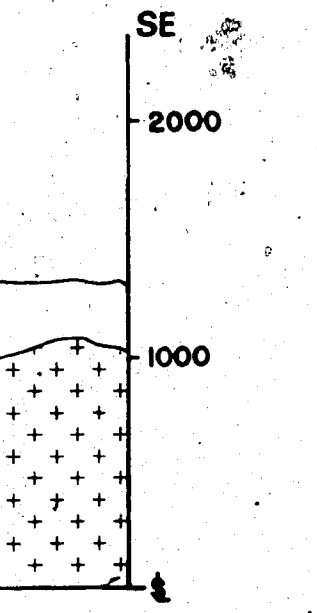

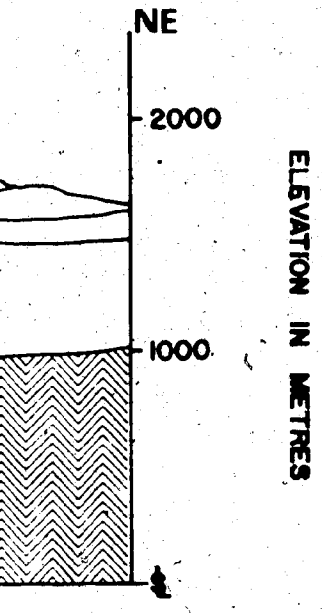

ELEVATION IN METRES

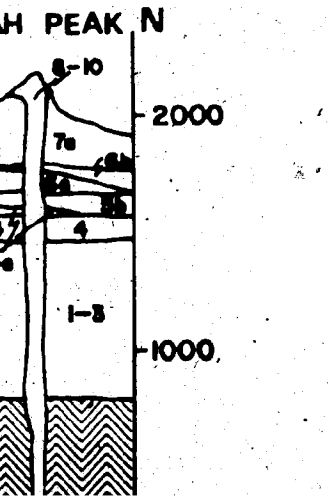

LEGEND

PLEISTOCENE AND EARLIE

11

LEVEL MOUNTAIN VOLCAN

9-10 PLEISTOCENE AI

8 PLEISTOCENE

7c

7b

7a PLIOCENE (2.5 M

6b

6a

5b

5a UPPER MIOCENI

4

3
2
1 MIDDLE ? TO UI

SLOKO VOLCANICS

D UPPER CRETAC

MESOZOIC PLUTONICS

C JURASSIC ?

TAKWAHONI FM.

B JURASSIC ?

META-PELITES

A UPPER PALEOZ

SCALE:

LEGEND

PLEISTOCENE AND EARLIER SEDIMENTS

11		a-Till, b-Lahar, c-Fluvial, d-Lacustrine, e-Outwash

LEVEL MOUNTAIN VOLCANICS

9–10	PLEISTOCENE AND RECENT ?	Hawaiite, flows, dykes, blocky aa, bombs and spatter, pelagonite tuff breccia
8	PLEISTOCENE	Mugearite and Trachybasalt; flows, agglomerates,
7c		Tristanite dykes, Rhyolite domes
7b		ndite, Rhyolite, Phonolite; flows
7a	PLIOCENE (2.5 MY)	Comendite, flows, ash flow tuffs, lava tubes
6b		Alkali Basalt, flows, agglomerates
6a		Peralkaline Trachyte (pantelleritic) flows
5b		Ankaramite and Alkali Basalt, flows and agglomerates
5a	UPPER MIOCENE (4.0 - 4.5 MY)	Comendite, Trachyte, Phonolite, flows and dykes
4		Alkali Basalt, flows, pillow basalts, pelagonite tuffs
3		Ankaramite, flows, tuffs, agglomerates
2		Transitional Basalts Alkaline to Tholeiitic, flows, tuffs
1	MIDDLE ? TO UPPER MIOCENE	Ankaramite flows

SLOKO VOLCANICS

D	UPPER CRETACEOUS OR PALEOCENE ?	Subaerial Calc Alkaline Volcanics, Pyroxene + Hornblende Andesite flows and dykes, Basaltic Andesite flows, Rhyodacite and Rhyolite domes, dykes, breccias

MESOZOIC PLUTONICS

C	JURASSIC ?	Calc Alkaline Intermediate to Acid Plutonics, Hornblende Biotite Granodiorite, Quartz Monzonite, Granite Pegmatite

TAKWAHONI FM.

B	JURASSIC ?	Shales, Silty Shales, Greenstones

META-PELITES

A	UPPER PALEOZOIC ?	Biotite Chlorite Schist, possibly metamorphosed equivalent of B

SCALE:

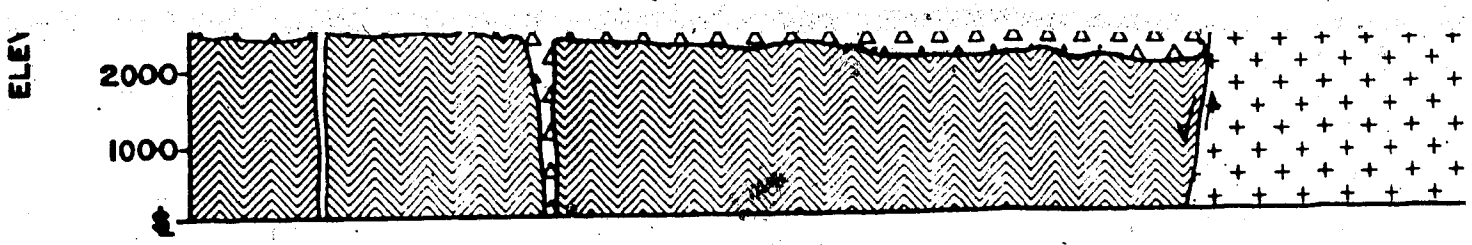
ELEV
2000
1000

SECTION #3 - S

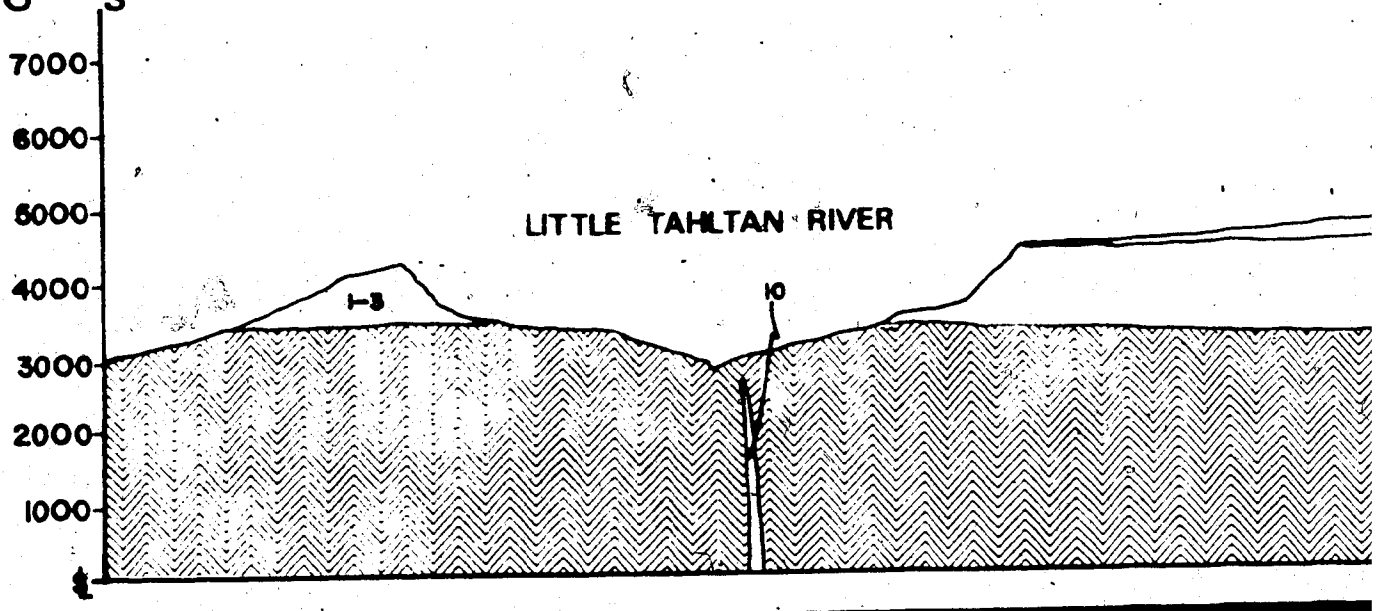
7000
6000
5000
4000
3000
2000
1000
LITTLE TAHLTAN RIVER
I-3
10

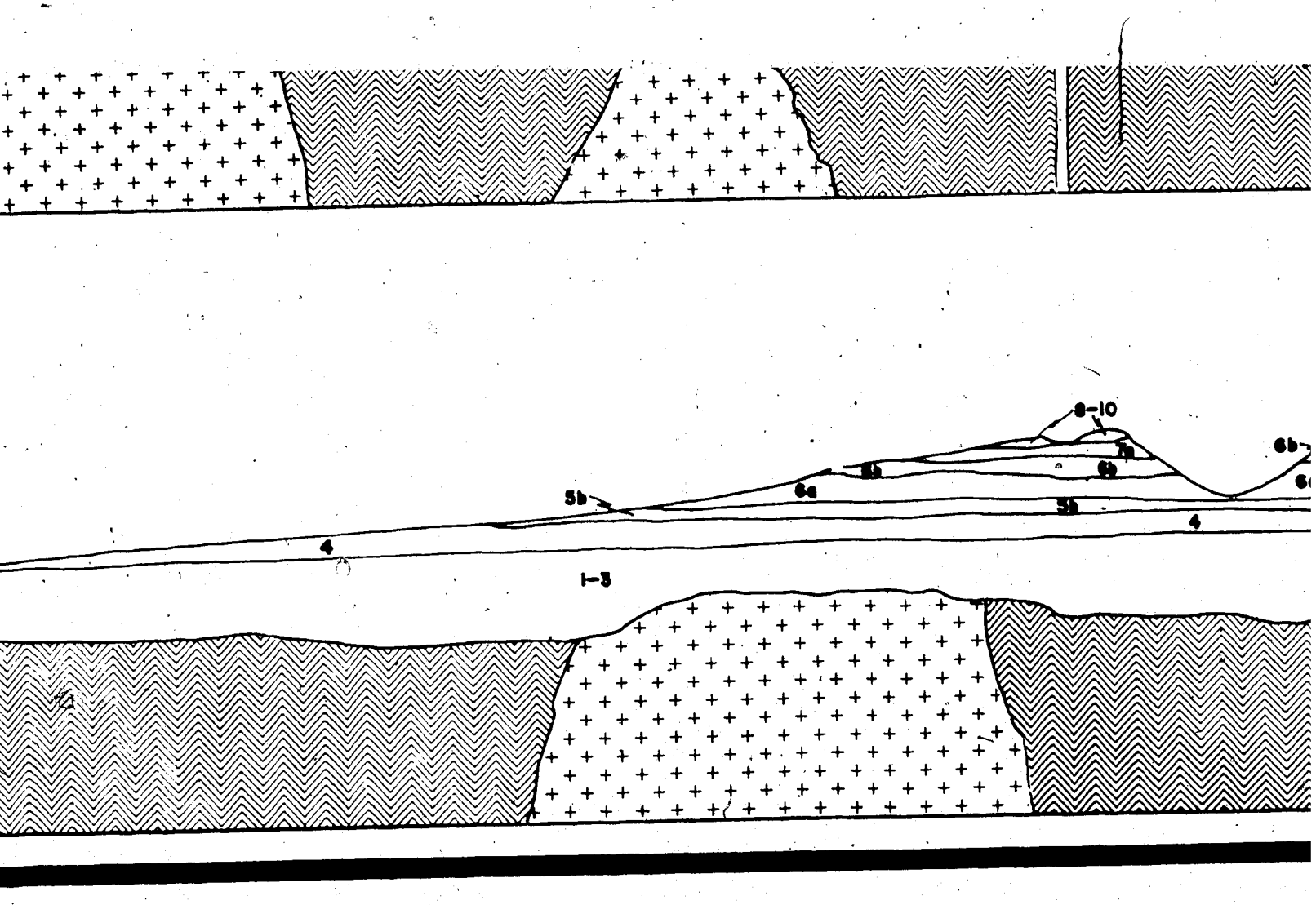
8–10
6b
5b
6a
5b
4
4
1–3

28 y

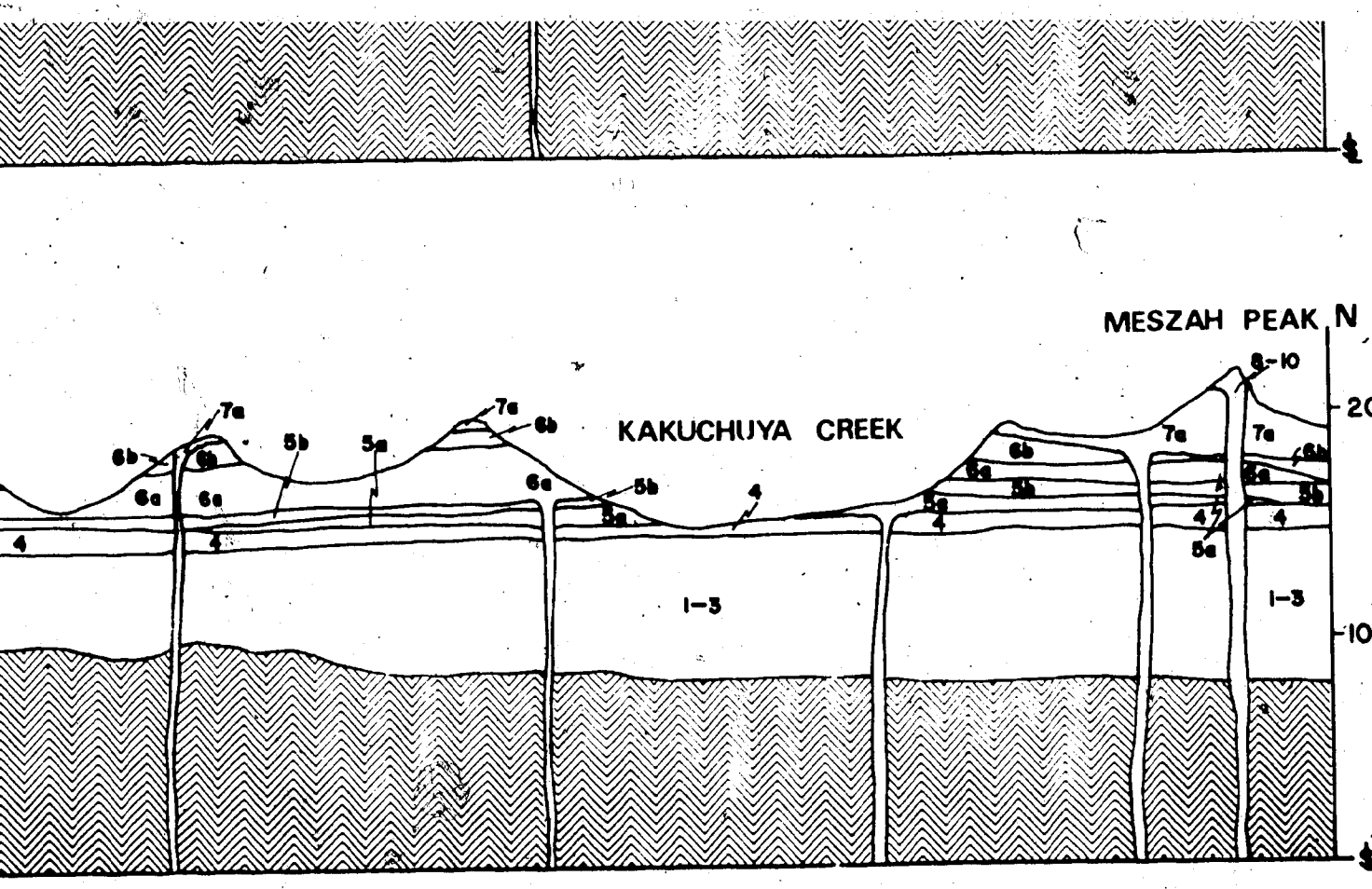

E3

29 of 29

SLOKO VOLCANICS

D — UPPER CRETACEOUS OR PALEOCENE ?

Subaerial Calc Alkaline Volcanics, Pyroxene + Hornblende Andesite flows and dykes, Basaltic Andesite flows, Rhyodacite and Rhyolite domes, dykes, breccias

MESOZOIC PLUTONICS

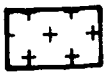

C — JURASSIC ?

Calc Alkaline Intermediate to Acid Plutonics, Hornblende Biotite Granodiorite, Quartz Monzonite, Granite Pegmatite

TAKWAHONI FM.

B — JURASSIC ?

Shales, Silty Shales, Greenstones

META-PELITES

A — UPPER PALEOZOIC ?

Biotite Chlorite Schist, possibly metamorphosed equivalent of B

SCALE: